REACTIONS OF IRON-SULFUR CLUSTERS IN PROTEINS

SARAH E. J. FAWCETT

ST JOHN'S COLLEGE

A thesis submitted to the Board of the Faculty of Physical Sciences for the degree of Doctor of Philosophy, University of Oxford

TRINITY, 1998

THESIS ABSTRACT

REACTIONS OF IRON-SULFUR CLUSTERS IN PROTEINS

S.E.J. FAWCETT, ST JOHN'S COLLEGE

D. PHIL., TRINITY 1998

This thesis describes the investigation of reactions of iron-sulfur clusters in proteins using direct electrochemistry. The influence of potential on metal uptake to generate the [M3Fe-4S] cluster from the [3Fe-4S] cluster of *Desulfovibrio africanus* Fd III is studied. The influence of potential was complex: rapid and reversible interconversions (M = Fe and Zn) occurred only between the states $[M3Fe\text{-}4S]^{2+}$ and $[3Fe\text{-}4S]^{0}$, with $[3Fe\text{-}4S]^{1+}$ having little affinity for M. The $[M3Fe\text{-}4S]^{1+}$ cubanes and the hyper-reduced $[3Fe\text{-}4S]^{2-}$ were relatively unreactive.

The reactivity of the transformed cluster, [M3Fe-4S] (M = Fe, Zn, Co), from the 7Fe Fd of *Desulfovibrio africanus* was studied and was found to react with a number of small thiol molecules, indicating that either ligand addition or exchange takes place at the transformed M site of the cluster. No reaction was observed with oxygenic ligands. In all cases, with the exception of imidazole, negative shifts in reduction potentials were observed.

Reactions of the [2Fe-2S] cluster from the ferredoxin of *Clostridium pasteurianum* and a number of site-directed mutants of this ferredoxin are studied. The cysteine ligands of the cluster were identified and evidence was obtained for serinate ligation of the cluster in a number of mutants. The reduction potentials of these serinate-ligated clusters were found to have a notable dependence on pH. A mutant ferredoxin containing only three cysteine ligands was investigated, which was found to interact with an exogenous thiolate ligand and, in addition, displayed a second reduction couple, indicating the formation of the $[2Fe\text{-}2S]^{0}$ state.

Reactions of the [3Fe-4S] cluster and various [M3Fe-4S] adducts, from the ferredoxin of the hyperthermophile *Pyrococcus furiosus,* are studied. The [3Fe-4S] cluster exhibited a complex pH dependence over a wide pH range. The formation of the hyper-reduced $[3Fe\text{-}4S]^{2-}$ state was observed, which required $3H^{+}$ for the overall $3e^{-}$ reduction from $[3Fe\text{-}4S]^{1+}$. Metal uptake reactions for M = Fe, Zn, Cd, were found to be slower than for its mesophilic counterpart, the 7Fe Fd III from *Desulfovibrio africanus*. Conversely, Tl uptake was found to be rapid, suggesting that co-ordination of Tl does not require reorganisation of the protein structure.

ACKNOWLEDGEMENTS

Firstly, I would like to thank my supervisor Fraser Armstrong for his enthusiasm on iron-sulfur chemistry and for the help and support given throughout the course of this thesis.

I would like to thank the people who I have collaborated with including, Prof. Andrew Thomson and Dr. Jacques Breton at the Centre for Metalloprotein Studies, University of East Anglia for the MCD spectroscopy, many thanks must go to Dr. Jacques Meyer and his group, CEA-Départment de Biologie Moléculaire et Structurale, France, for provision of the *Clostridium pasteurianum* protein samples. Thanks must also go to Dr. Julea Butt for providing the foundation and starting point for the work in *Chapters 3* and *4*. I would like to acknowledge the financial support I received from the UK EPSRC and St. John's College.

Thanks to the Armstrong Group, and the ever changing list of faces which have provided me with friendship and encouragement throughout the course of this thesis. A big thank you must go to Judy who has answered my questions about chemistry with much wisdom and patience, as well as being an excellent proof reader 'across the water'. Thanks also to Jill Duff for her endless optimism in the lab and Kerensa Heffron for being not only an excellent chemist and proof reader but also a marvellous chef. Thanks also to Dr. Dirk Heering for his help with pK's and the indispensable 'base-line' programme. To the others - too many to mention all - but I would like to thank, Harsh Pershad, David Davis, Helen Harper and Philip Miller.

For providing endless friendship and support, throughout the years in which I have known them, thanks must go to Kath Cotton, Carolyn Palmer and Marion Lawson.

And finally I would like to thank Mick for many things but not least the many hours spent proof reading on the train. This thesis is dedicated to my parents who have supported me, without question, for the last twenty-six years and for this I am extremely grateful.

'Is there anybody there?' said the Traveller,
Knocking on the moonlit door;
And his horse in the silence champed the grasses
Of the forest's ferny floor

The Listeners 1912, Walter de la Mare

TABLE OF CONTENTS

CHAPTER 6

REACTIONS OF THE FERREDOXIN FROM THE HYPERTHERMOPHILE *Pyrococcus furiosus* 267

LIST OF FIGURES

CHAPTER 1

CHAPTER 2

CHAPTER 3

CHAPTER 4

CHAPTER 5

CHAPTER 6

LIST OF TABLES

CHAPTER 1

CHAPTER 2

CHAPTER 3

CHAPTER 4

CHAPTER 5

CHAPTER 6

SYMBOLS AND ABBREVIATIONS

A	electrode area
A	solution $[3Fe\text{-}4S]^{1+/0}$ couple
A'	film $[3Fe\text{-}4S]^{1+/0}$ couple
a	anodic
A_λ	absorbance at wavelength λ
a_{H+}	activity of protons
ATP	adenosine triphosphate
Av Fd I	*Azotobacter vinelandii* ferredoxin I
B	solution $[4Fe\text{-}4S]^{2+/1+}$ couple
B'	film $[4Fe\text{-}4S]^{2+/1+}$ couple
C	solution $[3Fe\text{-}4S]^{0/2-}$ couple
C'	film $[3Fe\text{-}4S]^{0/2-}$ couple
c	cathodic
C	concentration
ca.	circa - approximately
CE	counter electrode
CoM	Coenzyme M
Cp	*Clostridium pasteurianum*
Cyt *c*	Cytochrome *c*
Cv	*Chromatium vinosum*
D	diffusion coefficient
D'	film $[M3Fe\text{-}4S]^{2+/1+}$ couple
Da Fd III	*Desulfovibrio africanus* ferredoxin III
DEAE	diethylaminoethyl
DTNB	5,5'-dithio*bis*(2-nitrobenzoic acid)
DTT	dithiothreitol
Dx	Desulforedoxin
E	potential
$E^{\circ\prime}$, E'_m	reduction potential

$E^{\circ\prime}_{acid}$	reduction potential in the limit of acid pH
$E^{\circ\prime}_{alk}$	reduction potential in the limit of alkali pH
E. coli	*Escherichia coli*
EDTA	Ethylene-diamine-*tetra*-acetic acid
EGTA	ethene glycol-*O,O′-bis*(2aminoethyl)-*N,N,N′,N′-tetra*-acetic acid
E_{pa}	anodic peak potential
E_{pc}	cathodic peak potential
ESEEM	Electron Spin Echo Envelope Modulation
EPR	Electron Paramagnetic Resonance
ET	electron-transfer
F	Faraday constant (96 484 C mol^{-1})
F'	film L-[4Fe-4S]$^{2+/1+}$ couple (where L is an exogenous ligand (*Chapter 4*))
Fd	ferredoxin
3Fe Fd_A	[3Fe-4S] cluster of *Pf* Fd, with disulfide bridge oxidised
3Fe Fd_B	[3Fe-4S] cluster of *Pf* Fd, with disulfide bridge reduced
FeS	Iron-sulfur (cluster/protein etc.)
FNR	regulator of fumarate or nitrate reduction
FTIR	Fourier Transform Infra-red spectroscopy
h	hour(s)
h	Planck constant (6.626×10^{-34} J Hz^{-1})
Hepes	*N*-[2-hydroxyethyl]piperazine-*N*-[2-ethanesulfonic acid]
HiPIP	high potential iron-sulfur protein
i	current
i_p	peak current
i_{pa}	anodic peak current
i_{pc}	cathodic peak current
IRP	iron regulatory protein
IRE	Iron responsive element
IRE-BP	Iron responsive element binding protein
IRP	Iron regulatory protein
kDa	kilodaltons
k_{obs}	observed rate constant

K_{ox}	equilibrium dissociation constant for proton binding to the *oxidised* state
K_{red}	equilibrium dissociation constant for proton binding to the *reduced* state
k_s	heterogeneous electron transfer rate (s^{-1})
l	path length of cell
LHS	Left hand side
LPC	Low Potential Couple
m	mass of particle
MCD	Magnetic Circular Dichroism
Mes	2-[*N*-morpholino]ethanesulfonic acid
mRNA	messenger RNA
n	number of electrons
n.d.	data not determined
NADH	reduced nicotinamide adenine dinucleotide
NifS	
NMR	Nuclear Magnetic Resonance
Ox, O	oxidised species
p	peak
ppm	parts per million
Pf Fd	*Pyrococcus furiosus* ferredoxin
PGE	pyrolytic graphite 'edge'
pI	isoelectric point
R	molar gas constant (8.314 J $mol^{-1}K^{-1}$)
Rd	Rubredoxin
RE	reference electrode
Red, R	reduced species
RHS	Right hand side
RNA	
RNR	ribonucleotide reductase

S	spin
s	second(s)
Sa Fd	*Sulfolobus acidocaldarius* ferredoxin
SCE	standard calomel electrode
SDS	sodium dodecylsulfate
SHE	standard hydrogen electrode
t	time (s)
T	temperature (K)
Ta	*Thermoplasma acidophilum*
Taps	*N*-tris[hydroxymethyl]methyl-3-amino-propanesulfonic acid
Tris	tri[hydroxymethyl]aminomethane, Trizma base
UV/Vis	Ultraviolet/Visible
vs.	Versus
VTMCD	Variable temperature magnetic circular dichroism
WE	working electrode
WT	wild-type
XAS	X-ray absorption spectroscopy

Γ	total surface concentration
ν	scan rate
ε	molar extinction coefficient
λ	wavelength
δ	peak width at half-height
μ_B	Bohr magneton (9.2740×10^{-24} J T^{-1})
ΔE_p	anodic-to-cathodic peak separation
ΔG°	standard Gibbs free energy change
2Fe	[2Fe-2S] cluster
3Fe	[3Fe-4S] cluster
4Fe	[4Fe-4S] cluster
7Fe Fd	[3Fe-4S][4Fe-4S]-containing ferredoxin

AMINO ACIDS

A, Ala	alanine
C, Cys	cysteine
D, Asp	aspartic acid
E, Glu	glutamic acid
F, Phe	phenylalanine
G, Gly	glycine
H, His	histidine
I, Ile	isoleucine
K, Lys	lysine
L, Leu	leucine
M, Met	methionine
N, Asn	asparagine
P, Pro	proline
Q, Gln	glutamine
R, Arg	arginine
S, Ser	serine
T, Thr	threonine
V, Val	valine
W, Trp	tryptophan
Y, Tyr	tyrosine

CHAPTER 1

INTRODUCTION

CHAPTER 1

INTRODUCTION

1.1 FeS CLUSTERS IN BIOLOGY

In 1960 iron-sulfur clusters were discovered as a new functional group in biological systems.[1] Since then, the diversity of proteins which contain these clusters and the variety of their function have become increasingly apparent.[2] Iron-sulfur (FeS) proteins are present in almost all known organisms, ranging from the most primitive and ancient members of the biosphere to the most advanced. FeS clusters are represented in the most complex enzyme systems known, for example the multi-subunit, membrane-bound mitochondrial complexes (responsible for energy transduction) and ribonucleotide reductase (necessary for the synthesis of DNA). So far there have been well over one hundred different types of FeS proteins isolated and this list continues to grow.[2-6]

FeS clusters are often found along with other redox-active centres in proteins such as in the mitochondrial complexes, in which their role is likely to be the efficient transfer of electrons across large distances of insulating protein matrix. Many FeS proteins, such as ferredoxins, contain one or more FeS clusters as their only prosthetic group. Initially the role of such proteins was believed to be simply electron transfer, but whilst this is likely to be the case in many systems, the ability of some simple clusters to catalyse complex, non-redox chemistry has been demonstrated. The best known example of a cluster operating in a non-redox role is aconitase, which converts citrate to isocitrate, and is an enzyme of the citric acid cycle.[7] Subsequently further members of the dehydratase group (as aconitase is) were discovered e.g. serine dehydratase.[8-10] Two further systems, in which FeS clusters are implicated as the active-site, are the Fe-only hydrogenases[11] and nitrogenase,[12,13] which also contains a complex Mo/Fe/S cluster.

The more recent discovery that some DNA/RNA binding proteins contain FeS clusters in a regulatory role, rather than a redox capacity, has once again extended the domain of these ubiquitous metal centres. Two important examples are the iron regulatory protein (IRP),[14,15] and the fumarate nitrate reduction (FNR) protein, a redox responsive regulator that activates and represses genes enabling anaerobic or aerobic metabolism in *Escherichia coli*.[16-18] Indeed, the disassembly and reassembly of FeS clusters as a result of changes in the levels of O_2 (FNR) or iron (IRP) may be a common mechanism by which gene expression is regulated.[15] A further example of the regulatory function of FeS proteins is provided by the SoxR protein of *E. coli*. Although its mechanism of action is unknown, it is thought that the oxidation $[2Fe\text{-}2S]^{1+}$ to $[2Fe\text{-}2S]^{2+}$ by dioxygen provides the signal for activation of a defence mechanism against superoxide (O_2^-).[19-21]

The diversity of function of FeS clusters does not end here: FeS clusters are implicated in the formation and stabilisation of radicals in proteins such as ribonucleotide reductase (RNR),[22] lysine 2,3 amino mutase,[23] biotin synthase,[24] and ferredoxin-thioredoxin reductase.[25,26] Ferredoxins containing as many as 12 [4Fe-4S] clusters have been isolated from archae and these have been suggested to be Fe-storage proteins.[27] Further to this, there are also a number of FeS proteins whose *in vivo* role has yet to be discovered e.g. rubrerythrin[28] and nigerythrin.[29]

It is therefore clear that the expanding field of biological FeS cluster chemistry requires a concerted effort, using a variety of techniques (EPR, MCD, ^1H NMR and electrochemistry) in order to understand their varied chemistry and function. The work in this thesis will combine the use of voltammetric methods with site-directed mutagenesis (SDM) and spectroscopy in order to answer, at a fundamental level, some of the questions which still surround FeS cluster chemistry.

1.2 CLUSTER STRUCTURE AND LIGATION

The term 'ferredoxin' (Fd), 'redox protein containing iron', was first used by Mortenson *et al.* in 1962 when they reported the isolation of a low molecular weight, brown protein, containing an unusually high concentration of non-haem iron, from the bacterium *Clostridium pasteurianum*.[30] Subsequently it was found that a considerable number of other organisms also contained a similar protein, and that in addition to the unusually high iron content, these proteins contained inorganic sulfide, since they released H_2S upon acidification.[31] Chemical assays showed that the ratio of iron to acid-labile sulfur was close to unity, and always indicated that at least two or more iron atoms were present - so initiating the first thoughts of iron 'clusters' in these proteins.[31] Electron Paramagnetic Resonance (EPR) spectroscopy at cryogenic temperatures revealed a signal, ($g = 1.94$) which was unprecedented for iron proteins at the time and it was proposed that the signal resulted from non-haem iron.[1,32] By 1966 the EPR signal from a [2Fe-2S] centre was shown to be consistent with tetrahedral co-ordination of the iron centre by sulfur (either inorganic or cysteine sulfur), with antiferromagnetic coupling between high spin Fe^{3+} and Fe^{2+} within the cluster.[33]

It was not until two decades later that the first structures of proteins containing FeS clusters were solved by X-ray crystallography. The structures, a mononuclear Fe centre,[34] a dinuclear [2Fe-2S] centre[35] and a cubane [4Fe-4S] cluster[36,37] are illustrated in Figure 1.1. In each case inorganic sulfide and cysteinyl complete tetrahedral co-ordination of the Fe centres. More recently, further types of FeS clusters have been identified by X-ray crystallography, including the important [3Fe-4S] cluster,[a] (in both cubic and linear forms)[39-42] and several higher nuclearity clusters[43 12,44,45]

[a] The [3Fe-4S] cubane cluster was initially incorrectly identified as a novel ring structure linked by labile sulfide atoms[38]

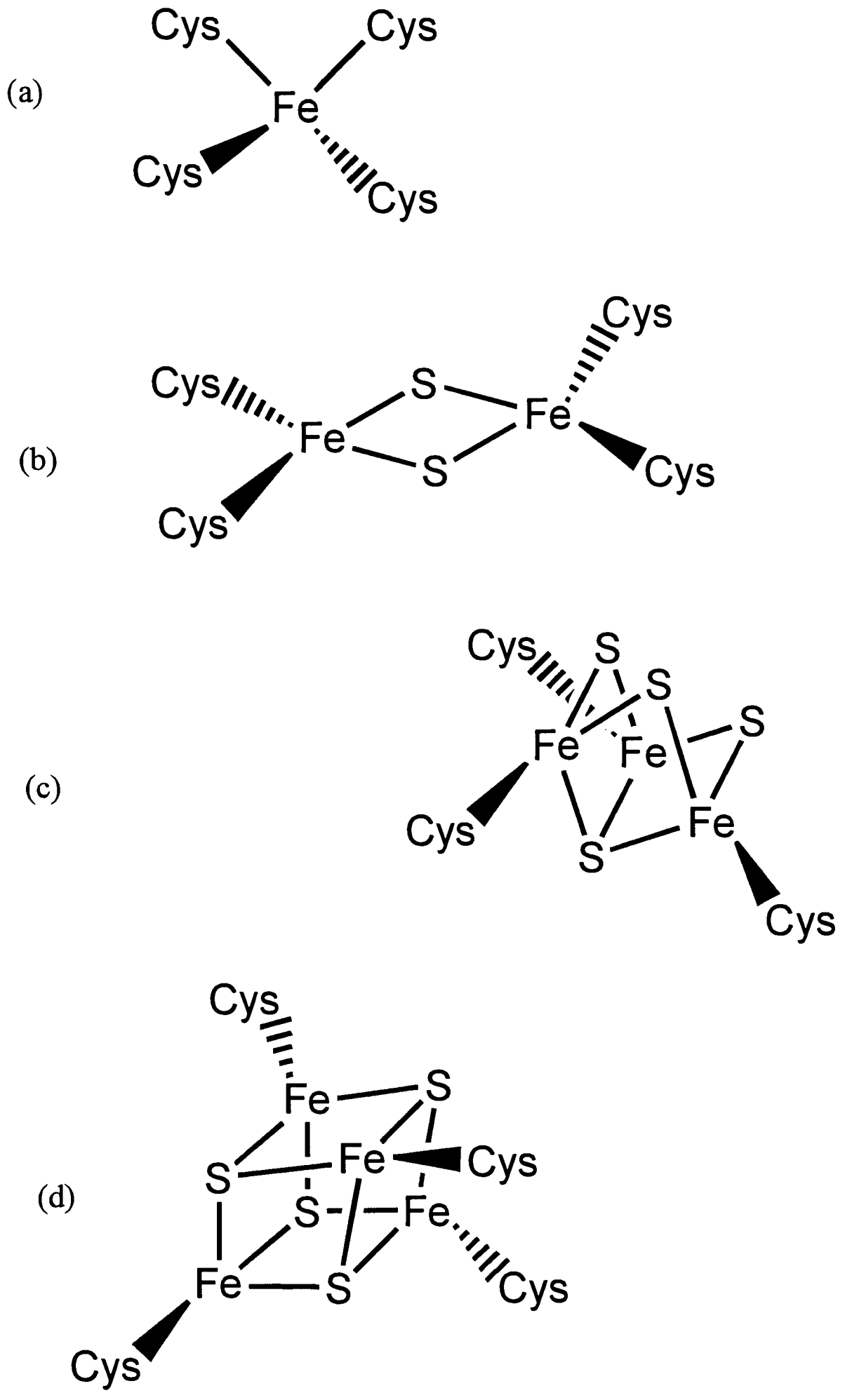

Figure 1.1 Structures of biological FeS clusters

(a) a mononuclear centre (b) [2Fe-2S] (c) [3Fe-4S] (d) [4Fe-4S]

1.2.1 Mononuclear Centres

Mononuclear Fe centres are known as 'rubredoxin-type' centres and are found in a variety of different bacterial proteins. Although strictly speaking rubredoxins (Rds) are not FeS clusters, since they contain only one Fe atom and no inorganic sulfide, they are included here for discussion because the central iron is tetrahedrally surrounded by four cysteinyl S atoms. They may therefore be regarded as a core unit, from which the more complex clusters are composed. The mononuclear centre may be found either on its own, as in rubredoxins and desulforedoxins (Dxs), or together with a hemerythrin-type dinuclear Fe centre, as in rubrerythrin[28] and nigerythrin.[29] Reduction potentials for the $Fe^{3+/2+}$ couple vary between +20 and -60 mV in Rds and Dxs, but may be as high as 281 mV and 213 mV, for rubrerythrin and nigerythrin respectively.[2] Specific roles for Rds have not been identified, except as electron-transfer agents in the hydroxylation of fatty acids or as electron donors to nitrate reductase.[2]

The arrangement of co-ordinating cysteine residues, the **-Cys-X_2-Cys-** motifs[b] near the C- and N-terminus, is highly conserved in all Rds and similar motifs are observed in rubrerythrin. Desulforedoxin, however, is co-ordinated with the motifs **-Cys-X_2-Cys-** and **-Cys-Cys-**. This imposes considerable distortion upon the FeS_4 core unit because of the adjacent cysteines.[46]

1.2.2 [2Fe-2S] Clusters

[2Fe-2S] clusters have a $Fe_2(\mu_2\text{-}S)_2$ core,[c] normally with four cysteine residues completing the tetrahedral co-ordination of the two iron atoms. A variation of this is presented by the Rieske subclass of 2Fe ferredoxins, in which the ligation is not confined to cysteine, instead two histidines and two cysteines co-ordinate each of the two iron atoms respectively. The core charge of [2Fe-2S] clusters may be either 2+ or 1+, thus in the oxidised state, $[2Fe\text{-}2S]^{2+}$, the two Fe atoms are both Fe^{3+}. These two Fe^{3+}, $S = 5/2$ centres are antiferromagnetically coupled to give a diamagnetic ground state ($S = 0$). In the reduced state the irons are also antiferromagnetically coupled (Fe^{2+}; $S = 2$ and Fe^{3+};

---

[b] Where Cys is the three letter code for the amino acid cysteine, X denotes *any* amino acid, the subscript numbers denote the number of 'X' amino acids between the cysteines. A complete list of the three and single letter codes for the amino acid residues is given in the *Abbreviations* section.

[c] μ_2 implies that the sulfur is bridging two atoms, similarly μ_3 implies the sulfur is bridging three atoms.

$S = 5/2$), but give a paramagnetic $S = 1/2$ ground state. Furthermore, Mössbauer spectroscopy indicates that $[2Fe\text{-}2S]^{1+}$ clusters tend to contain a valence localised Fe^{3+} site and a valence-localised Fe^{2+} site.[6] The reduction potentials for the 2+/1+ couple are widespread, covering a range from 300 mV to -460 mV. [2Fe-2S] clusters occur in a wide range of both simple and complex proteins and their function is generally electron transfer. One notable exception is the regulatory protein SoxR which is a homodimer, contains two [2Fe-2S] clusters and controls the expression of several genes whose products are made in response to O_2^{-}.[20]

There are many different types of [2Fe-2S] containing proteins which can be arranged into several smaller sub-classes. The 'plant-type' or 'chloroplast-type' ferredoxins are extremely similar to each other and all have reduction potentials between -300 mV and -460 mV, with uniform spectroscopic properties. The arrangement of the co-ordinating residues, **-Cys-X_4-Cys-X_2-Cys-X_{29}-Cys-**, and NMR studies indicate that the first two cysteines co-ordinate the Fe^{2+} site in the reduced cluster.[47] Similar to the clusters of the plant-type ferredoxins are those which are found in photosynthetic bacteria and halobacteria, differing only in the spacing between the third and fourth cysteine residues in the motif above.

There are numerous examples of other sub-classes of [2Fe-2S] clusters, having different spectroscopic properties to the plant-type ferredoxins, however, due to the lack of X-ray crystallography data these are difficult to characterise. For example, the hydroxylase class includes adrenal ferredoxin (adrenodoxin) and *Pseudomonas putida* ferredoxin (putidaredoxin). The [2Fe-2S] ferredoxins from *Clostridium pasteurianum* (*Cp*) and *Azotobacter vinelandii* (*Av*), both nitrogen fixing bacteria, provide examples of other sub-classes. The *Cp* Fd (see *Chapter 5*) has a highly unusual amino acid sequence, and its function at present is unknown, although it has been suggested to be involved in nitrogen fixation, since it displays a highly specific electrostatic interaction with the nitrogenase MoFe protein of *Cp*.[48]

Rieske clusters, also a subclass of [2Fe-2S] clusters, are prominent in both photosynthetic and respiratory chains, and are most obviously different from other [2Fe-2S] clusters in that their reduction potentials are markedly higher, ranging from

140 mV to 350 mV.[d] In addition to this they display anomalous EPR properties, $g_{av} = 1.90$ compared to $g_{av} = 1.96$ for Fd-type $[2Fe\text{-}2S]^{1+}$ centres.[49] Mössbauer, ^{14}N-ENDOR, ESEEM and resonance Raman studies all indicate that these characteristic properties are a result of non-cysteinyl ligation at the Fe^{2+} site. The cluster is co-ordinated by two cysteines and two nitrogenous residues. Studies upon phthalate dioxygenase from *Pseudomonas cepacia* have provided strong evidence that one of the ligands, co-ordinated to the Fe^{2+} site is a histidine.[50] The use of consensus sequence alignments also indicates that all Rieske-type [2Fe-2S] clusters are ligated by a **-Cys-X-His-$X_{16/17}$-Cys-X_2-His-** motif. A summary of sequences, showing binding motifs for a number of different 2Fe clusters, is shown in Table 1.1.

[d] Bacterial dioxygenases, contain mononuclear non-haem Fe in addition to the Rieske cluster, have reduction potentials ranging from -155 mV to 0 mV for the Rieske centre.

LIGATING SEQUENCE	FERREDOXIN
NH^{3+}-X_n-**Cys** -X_4-**Cys**-X_2-**Cys**-X_{29}-**Cys**-X_n-CO_2^-	Plant-type Fds[4]
NH^{3+}-X_n-**Cys**-X_5-**Cys**-X_2-**Cys**-$X_{36/37}$-**Cys**-X_n CO_2^-	Hydroxylase-type Fds[4]
NH^{3+}-X_n-Cys-X_3-Cys-X_2-Cys-X_{36}-Cys- $X_{30/31}$-Cys-X_{59}-Cys-X_n-CO_2^-	Biotin synthases[51]
NH_3^+-X_n-**Cys**-X_2-Cys-X_9-**Cys**-X_{31}-**Cys**-X_3-**Cys**-X_n-CO_2^-	*Clostridium pasteurianum* Fd[52]
NH_3^+-X_n-**Cys**-X-**His**-X_{16} -**Cys**-X_2-**His**-X_n-CO_2^-	Benzene dioxygenase Fd[53]
NH_3^+-X_n-**Cys**-X-**His**-X_{17}-**Cys**-X_2-**His**-X_n-CO_2^-	Dioxygenases[53]
NH_3^+-X_n-**Cys**-X-**His**-X_2-Cys-X_{14}-**Cys**-X-Cys-**His**-X_n-CO_2^-	Rieske proteins[53]

Table 1.1 Binding motifs of [2Fe-2S] clusters found in biology

Those residues in ***bold*** *are established to be ligating residues to the cluster, based upon X-ray crystallography, sequence homology, site-directed mutagenesis or spectroscopic evidence.* NH_3^+ *and* CO_2^- *represent the amino and carboxylic terminal functionalities of the protein chain.*

1.2.3 [4Fe-4S] Clusters

Iron-sulfur clusters containing 4Fe atoms, existing in the 'cubane' form (Figure 1.1(d)), are one of the most common electron-transfer groups in biology. Clusters in which all the Fe atoms are co-ordinated by cysteine residues are the most common type of 4Fe ferredoxins, and are principally electron-transfer agents. A minority of 4Fe cubane clusters which have one of the iron atoms co-ordinated by a residue other than cysteine are thought to take part in more complicated reactions other than electron transfer, as discussed in *Section 1.2.4*.

Redox States

[4Fe-4S] clusters can theoretically occur in any one of five oxidation states (0, 1+, 2+, 3+, 4+) but the most frequently found electron-transfer reactions are the $[4Fe\text{-}4S]^{2+/1+}$ and $[4Fe\text{-}4S]^{3+/2+}$ couples. However, no individual cluster is known to cycle through

both of these redox reactions under physiological conditions. Two types of 4Fe cluster exist in nature. 'Ferredoxin' type clusters are confined to the $[4Fe\text{-}4S]^{2+/1+}$ couple and have reduction potentials covering a range between +80 and -700 mV.[2] The 'HiPIP' clusters (**Hi**gh **P**otential **I**ron **P**rotein) cycle between the 3+ and 2+ oxidation states and have reduction potentials in the range +100 to +450 mV.[2] Factors determining which reduction couple the cubane is confined to are not clearly understood, despite the existence of several high resolution X-ray crystal structures. Crystallographic and resonance Raman studies of bacterial ferredoxins and HiPIPs have shown that the structures of the clusters are very similar but that there are major differences in their local environments. These include the amino acid sequence, folding pattern, location and position of cysteines and the hydrogen bonding network. It is thought that the number of hydrogen bonds from the peptide (between the amide N-H and sulfur ligands) to the [4Fe-4S] cluster (five in HiPIPs compared to eight in Fds) may be crucial, since the NH...S bonds will help to stabilise the less positively charged (1+) reduced states.[54-57] Other factors to consider include hydrophobic interactions, solvent exposure and the electric field gradient close to the cluster. Clusters in HiPIPs are known to be totally inaccessible to water and surrounded by hydrophobic residues, causing a further decrease in the reduction potentials, whilst ferredoxin clusters are generally in a more hydrophilic environment and more accessible to water.[57,58] These differences in the local environment of the two different clusters result in a shift of the reduction potentials of both the 3+/2+ and the 2+/1+ transitions. As a result the second transition, which is observed in bacterial ferredoxins, is shifted out of the biologically useful potential range for HiPIPs, whilst the first transition becomes feasible.

The third, only recently identified, redox transition of cubane clusters, is the $[4Fe\text{-}4S]^{1+/0}$ couple, which generates an all-Fe^{2+} 4Fe cluster. Other examples of biological FeS clusters which have been generated in the all-Fe^{2+} state include the Rieske $[2Fe\text{-}2S]^{0}$ centre of complex III,[59] the $[2Fe\text{-}2S]^{0}$ centre in *Anabaena variabilis* ferredoxin[60] and the all-ferrous $[3Fe\text{-}4S]^{2-}$ cluster, as observed in a number of 7Fe Fds. The latter example is discussed further in *Section 1.2.4*.[61] The $[4Fe\text{-}4S]^{0}$ cluster from the iron protein in nitrogenase was tentatively reported in 1994,[62] but has only recently been more carefully characterised by Burgess *et al.*[63] A synthetic all-ferrous [4Fe-4S] cluster with phosphine

ligands has also been recently reported.[64] Similarities can be drawn between this species and the $[3Fe\text{-}4S]^{2-}$ state - both have very low reduction potentials and were thought originally not to exist because of inherent instability as a result of the excess negative charge localised over the cluster. As described in *Section 1.2.4,* this effect may be offset by proton binding at or near to the cluster as indicated by a well-defined pH dependence of the reduction potential. However, this is unlikely to be the case for the [4Fe-4S] cluster from the iron protein in nitrogenase, since the reduction potential is apparently independent of pH.[63]

Structure

The [4Fe-4S] core (illustrated in Figure 1.1) has been described as two interlocking tetrahedra of 4Fe and 4S, with the Fe tetrahedron being smaller than that of the S atoms (the average Fe-Fe distance is 2.75 Å and the S-S distance is 3.55 Å). The magnetic and electronic properties of [4Fe-4S] clusters are understandably more complex than those of 2Fe Fds, and the Mössbauer and EPR data have often been rationalised in terms of antiferromagnetic interactions between pairs of Fe atoms:

$[4Fe\text{-}4S]^{3+}$ **($S = 1/2$)** *from* $\{Fe^{3+}/Fe^{3+}$ **($S = 5$)**$\}$ *coupled to* $\{Fe^{2+}/Fe^{3+}$**($S = 9/2$)**$\}$

$[4Fe\text{-}4S]^{2+}$ **($S = 0$)** *from* $\{Fe^{2+}/Fe^{3+}$ **($S = 9/2$)**$\}$ *coupled to* $\{Fe^{2+}/Fe^{3+}$ **($S = 9/2$)**$\}$

$[4Fe\text{-}4S]^{1+}$ **($S = 1/2$)** *from* $\{Fe^{2+}/Fe^{2+}$ **($S = 4$)**$\}$ *coupled to* $\{Fe^{2+}/Fe^{3+}$ **($S = 9/2$)**$\}$.

Both $[4Fe\text{-}4S]^{1+}$and $[4Fe\text{-}4S]^{3+}$ clusters are $S = 1/2$ but they are readily distinguished by EPR. $[4Fe\text{-}4S]^{3+}$ clusters give rise to axial EPR signals (typically $g_{\|} = 2.12$ and $g_{\perp} = 2.04$) with $g_{av} > 2$, whereas $[4Fe\text{-}4S]^{1+}$ clusters give rise to (usually) rhombic EPR signals (typically g = 2.06, 1.92, 1.88) with $g_{av} < 2$.[2] As listed above, $[4Fe\text{-}4S]^{1+}$ clusters exhibit the $S = 1/2$ ground state, but there are several cases of $[4Fe\text{-}4S]^{1+}$ clusters which exist in both $S = 1/2$ and 3/2 ground states. The nitrogenase Fe-protein provided the first example,[65] but further studies have documented a number of other examples including *Pyrococcus furiosus* Fd,[66] CO-dehydrogenase and glutamine 5-phosphoribosyl-1-pyrophosphate amidotransferase from *Bacillus subtilis*.[67] A further

example of a [4Fe-4S]$^{1+}$ cluster existing in the S = 3/2 ground state is the transformed cluster [Fe3Fe-4S]$^{1+}$ (*Section 1.3.3*) from *Desulfovibrio africanus* Fd III.[68]

Ligating Patterns

Some of the known arrangements of cysteines involved in co-ordinating [4Fe-4S] clusters are shown in Figure 1.2. For 8Fe ferredoxins there is a consensus sequence involving two **-Cys-X_2-Cys-X_2-Cys-X_3-Cys-Pro-** groupings. Each cluster is co-ordinated by three cysteines from one group and one from the other e.g. *Peptococcus aerogenes* Fd, (Figure 1.2). On the basis of sequence/structure comparisons it has been postulated that 8Fe Fds are the common ancestor of all 4Fe or 3Fe Fds.[69] Fds which only contain one cluster e.g. *Bacillus thermoproteolyticus* Fd (see Figure 1.2) contain an α-helix which has been proposed to replace the second cluster in the sequence.

1.2.4 [3Fe-4S] Clusters

The [3Fe-4S] cluster type is the most recently established of all the simple core ferredoxin structures. FeS clusters containing only 3Fe atoms were first identified in 1980 as a result of Mössbauer studies of *Azotobacter vinelandii* Fd I by Münck and co-workers.[70] Initially the X-ray crystal structure of this 7Fe Fd was misinterpreted as a cyclic [3Fe-3S] core for one cluster, in addition to the cubane [4Fe-4S] cluster. However, the cyclic structure was completely at variance with the spectroscopic evidence, in particular EXAFS data for [3Fe-4S] and [4Fe-4S] clusters were extremely similar and showed no evidence for the long Fe-Fe distances (> 4 Å) that the cyclic [3Fe-4S] cluster would require. Subsequent re-investigation of this Fd at 1.9 Å resolution[40] and the solution of the X-ray crystal structures of inactive aconitase (2.1 Å resolution)[71] and *Desulfovibrio gigas* Fd II (1.7 Å resolution)[72] showed that a [3Fe-4S] core stoichiometry with a $Fe_3(\mu_3\text{-}S)(\mu_2\text{-}S)_3$ structure was in fact correct. This can be visualised as a cubane cluster with one of the corner Fe atoms missing (Figure 1.1(c)). Apart from the linear [3Fe-4S] cluster in partially unfolded aconitase, all [3Fe-4S] cluster cores examined to date can be assumed to take up this configuration, as evidenced by their homologous spectroscopic properties.

Originally it was thought that [3Fe-4S] clusters were only formed *via* oxidative degradation of [4Fe-4S] clusters - generally as a result of aerobic purification.[73] This is certainly the case for aconitase and a number of [4Fe-4S] ferredoxins. However, examination of amino acid sequences, and investigation of systems purified anaerobically and *in vivo* detection with EPR has shown that [3Fe-4S] clusters are native to a number of proteins. Notable examples are found in succinate dehydrogenase,[74] fumarate reductase,[74] nitrate reductase,[75] hydrogenase,[11] glutamate synthase[76,77] and many other simple ferredoxins.[4]

Redox States

Under physiological conditions, [3Fe-4S] clusters may undergo a one electron transfer (1+/0), with reduction potentials covering the range +70 to -420 mV. In the oxidised state, $[3Fe\text{-}4S]^{1+}$, three Fe^{3+} ions ($S = 5/2$) are antiferromagnetically coupled to give an $S = 1/2$ ground state, which gives rise to an isotropic or axial EPR signal with g_{av} usually between 1.96 and 2.01 and the low-field g-value close to 2.02. In the reduced state, $[3Fe\text{-}4S]^{0}$, MCD, Mössbauer, EPR and saturation magnetisation studies indicate an $S = 2$ ground state that arises from antiferromagnetic interaction between a valence delocalised Fe^{2+}/Fe^{3+} pair ($S = 9/2$) and a valence-trapped Fe^{3+} site $S = 5/2$.[78]

More recently, a further two-electron reduction couple to give the $[3Fe\text{-}4S]^{2-}$ state has been reported for a number of 7Fe Fds containing 3Fe clusters. This fully reduced state, the 'hyper-reduced' state contains three Fe^{2+} subsites, and has been partially characterised by EPR, MCD and UV/Vis spectroscopy in the 7Fe Fd from *Sulfolobus acidocaldarius*.[61,79,80] It has also been observed in the 7Fe Fds of *Desulfovibrio africanus*,[61] and *Azotobacter vinelandii*.[61] Protein film voltammetry over a wide pH range shows that in all three examples, the reversible $2e^-$ reduction of the 3Fe cluster is pH dependent - there is a net uptake of three protons, concomitant with reduction from $[3Fe\text{-}4S]^{1+}$ to the all-Fe^{2+} state. It is not yet known where the protons are bound, whether at or near to the cluster, but they are likely to help to stabilise the cluster, by neutralising the high negative charge density produced by adding $3e^-$. The observed reduction potentials at equilibrium are very negative, for the 7Fe Fds mentioned above the reduction potential $[3Fe\text{-}4S]^{0/2-}$ is < -700 mV at pH 7.3, 0 °C.[61]

Ligating Patterns

In Figure 1.2 some common ligating patterns of both 3Fe and 4Fe clusters are illustrated. The cysteine pattern which accompanies the [3Fe-4S] cluster in proteins is varied but has a common theme: the arrangement contains two closely spaced cysteines and one other remote cysteine. These have been found to be **-Cys-X_2-Cys-** in aconitase, **-Cys-X_5-Cys-** in *Desulfovibrio gigas* Fd II, *Pyrococcus furiosus* Fd, *Sulfolobus acidocaldarius* Fd, succinate dehydrogenase, fumarate reductase, nitrate reductase, and **-Cys-X_7-Cys-**, as in *Azotobacter vinelandii* Fd I and *Thermus thermophilus* Fd. Since facile interconversion between [3Fe-4S] and [4Fe-4S] clusters may occur in aconitase and a number of ferredoxins (*Section 1.3.3*) it is useful to compare these [3Fe-4S] binding motifs with the co-ordination of a typical [4Fe-4S] cluster. The motif for a typical 4Fe cluster is, **-Cys-X_2-Cys-X_2-Cys-X_n-Cys-**, whilst for a 3Fe Fd, the ligating sequence may simply differ by the replacement of the second cysteine, in this group, by another amino acid residue. If this residue can co-ordinate an Fe atom, a 4Fe cluster may be formed. Such a cluster, with a non-cysteinyl ligand, is likely to show different chemical reactivity to conventional all-cysteine ligated clusters (*Section 1.3.3*). In the case where an aspartate is believed to be the co-ordinating residue, as for *Pyrococcus furiosus* Fd and *Desulfovibrio africanus* Fd III, a [4Fe-4S] cluster can be assembled, but it is readily converted, under oxidising conditions, to a [3Fe-4S] cluster. Alternatively, if the replacement residue is unable to co-ordinate an Fe atom - for example alanine, as in *Streptomyces griseolus* Fd I (**-Cys-X_2-Ala-X_2-Cys-X_n-Cys-**) - a 3Fe cluster is formed, and conversion to a 4Fe cluster does not occur. An alternative cluster ligation pattern which produces 3Fe cluster assembly is the insertion of two additional residues between the second and third cysteines in the sequence above, such that the second cysteine is moved to a position remote from the cluster, as in *Azotobacter vinelandii* Fd I (Figure 1.2). It is necessary, however, to exercise caution when comparing sequences and cluster ligation patterns - there are further variations possible to those that have been mentioned: proline (often found directly after the fourth cysteine in 7Fe Fds and expected to confer rigidity) may be absent, or there may be five or six additional residues between the second and third cysteines of the second grouping - as in photosynthetic 8Fe Fds. Furthermore, different arrangements are known to exist for the [4Fe-4S] clusters in HiPIPs, *E. coli* endonuclease III and for aconitase.[2]

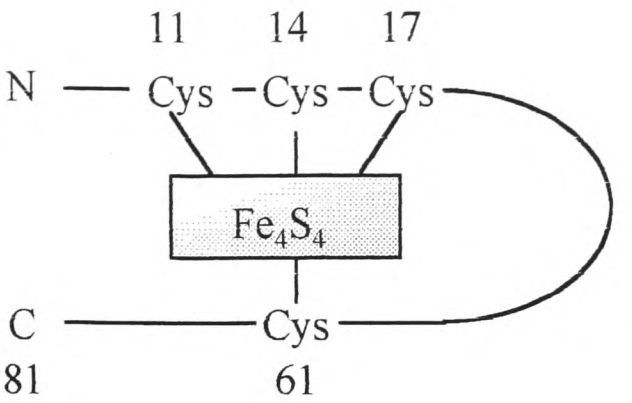

***Bacillus thermoproteolyticus* Fd**

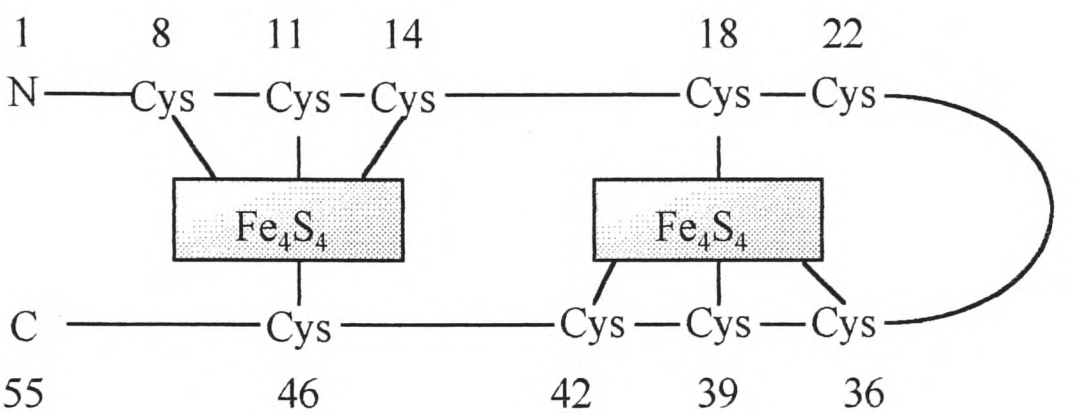

***Peptococcus aerogenes* Fd**

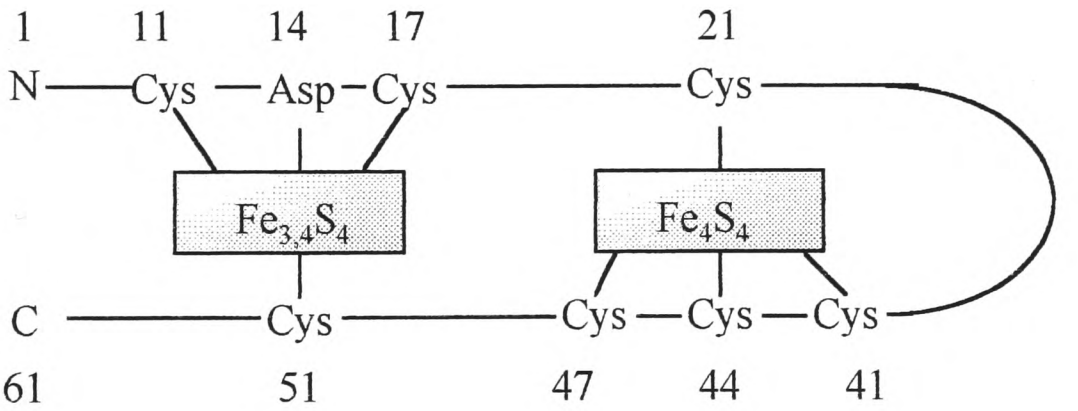

***Desulfovibrio vulgaris* Fd I**
***Desulfovibrio africanus* Fd III**
***Sulfolobus acidocaldarius* Fd (7 Cys, 103 residues)**
***Thermaplasma acidophilum* Fd (9 Cys, 142 residues)**

Figure 1.2 Cluster binding patterns in proteins containing [4Fe-4S] and [3Fe-4S] clusters *(continued overleaf)*

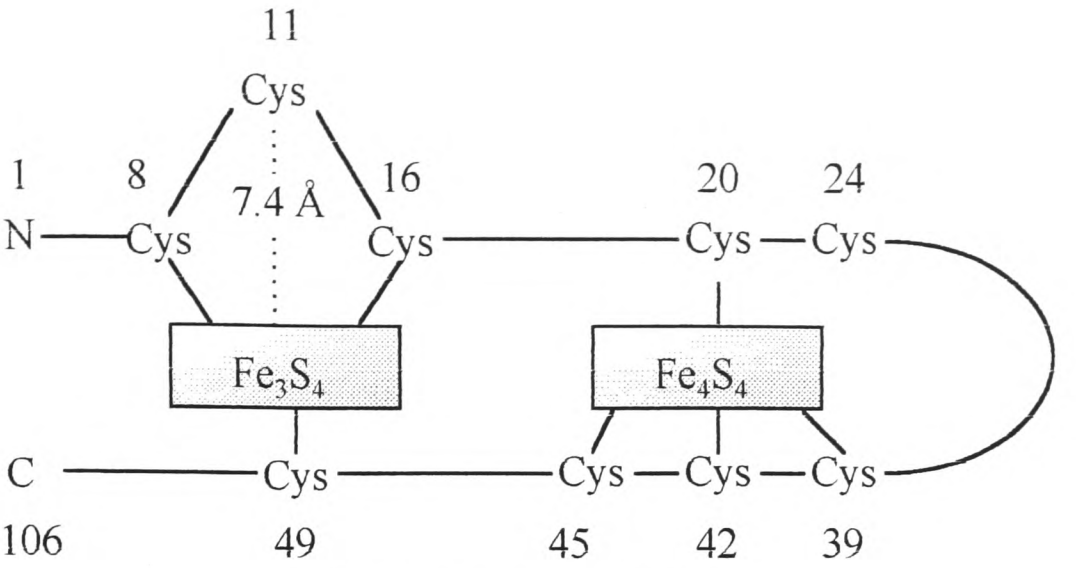

***Azotobacter vinelandii* Fd I**

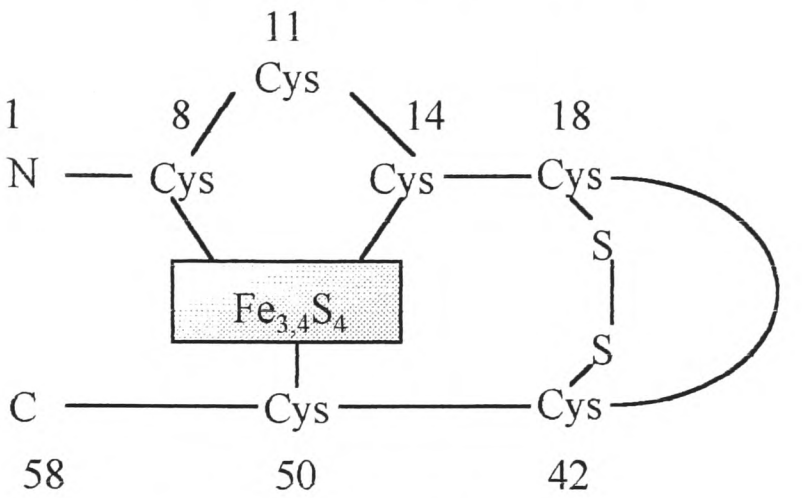

***Desulfovibrio gigas* Fd II**

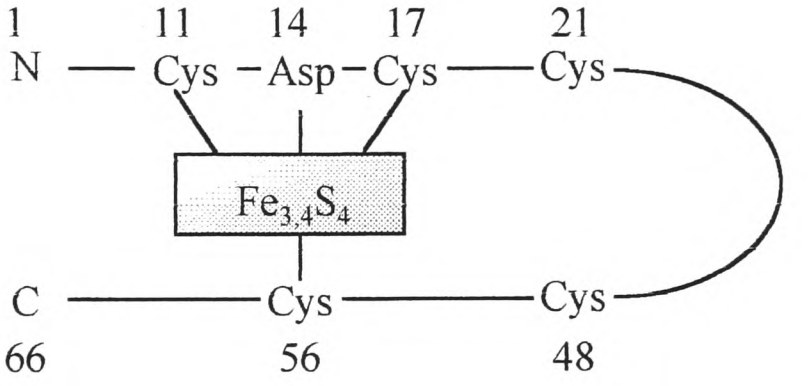

***Pyrococcus furiosus* Fd**

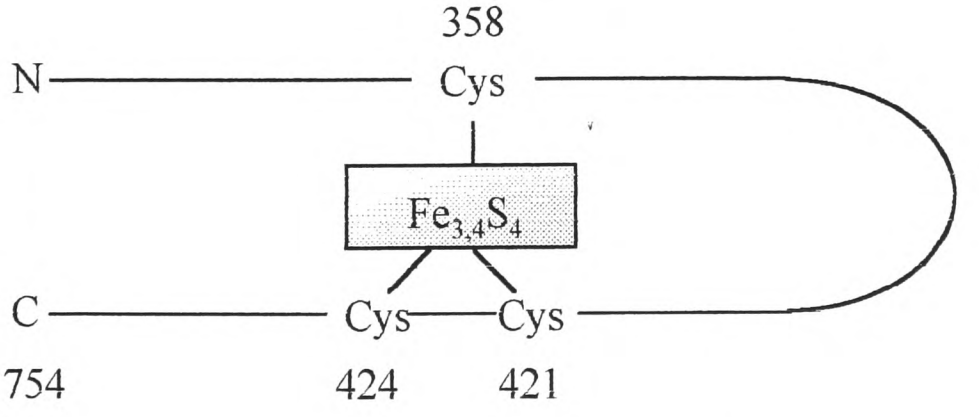

Porcine Mitochondrial Aconitase

1.2.5 Higher Nuclearity Clusters

Higher nuclearity FeS clusters, which contain more than four Fe atoms, are found in biology. One of the best characterised examples of this class of cluster is in the enzyme nitrogenase, which catalyses the reduction of dinitrogen to ammonia.

$$N_2 + 8H^+ + 8e^- + 16MgATP \rightarrow 2NH_3 + H_2 + 16MgADP + 16\ P_i \quad \textbf{Equation 1.1}$$

Molybdenum-containing nitrogenase is composed of two separate proteins - the Fe-protein and MoFe-protein. Dinitrogen reduction is catalysed by the MoFe protein following electron transfer (ET) from the Fe-protein. X-ray structures of both proteins, from *Azotobacter vinelandii*[12,43,44,81] and from *Clostridium pasteurianum*[82] have been reported. The Fe-protein contains a single [4Fe-4S] cubane cluster bridging two identical subunits and the MoFe-protein contains two metallo clusters: the FeMo-cofactor (Figure 1.3(a)) and the P-cluster (Figure 1.3(b)).

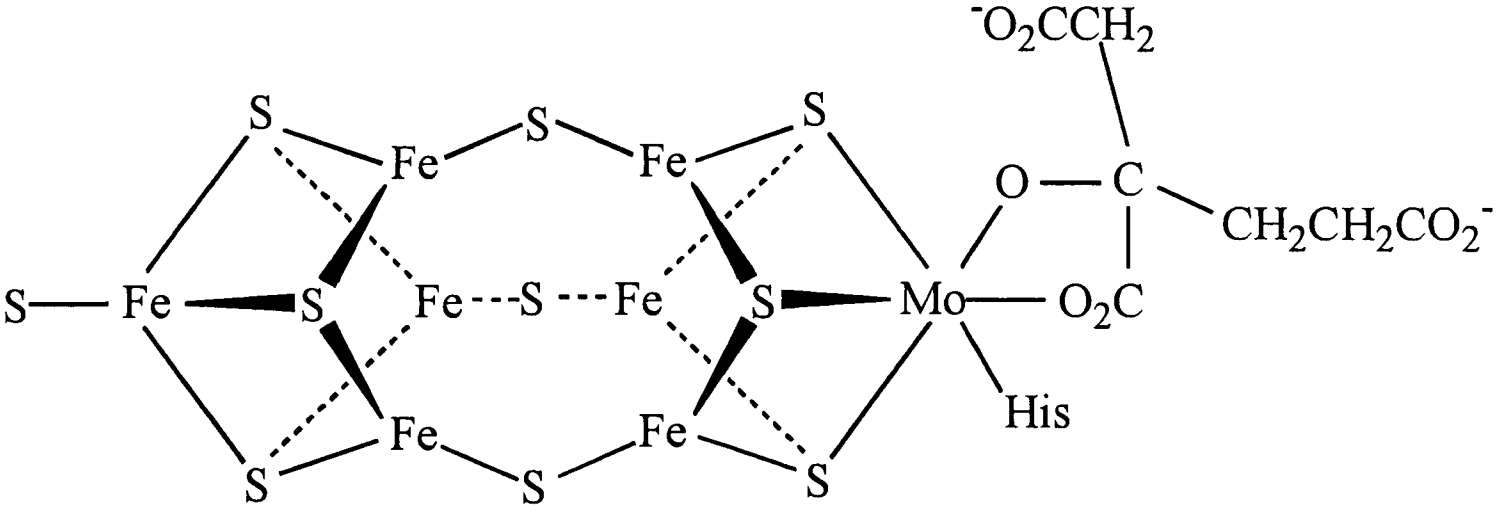

Figure 1.3(a) The FeMo-cofactor of nitrogenase[12]

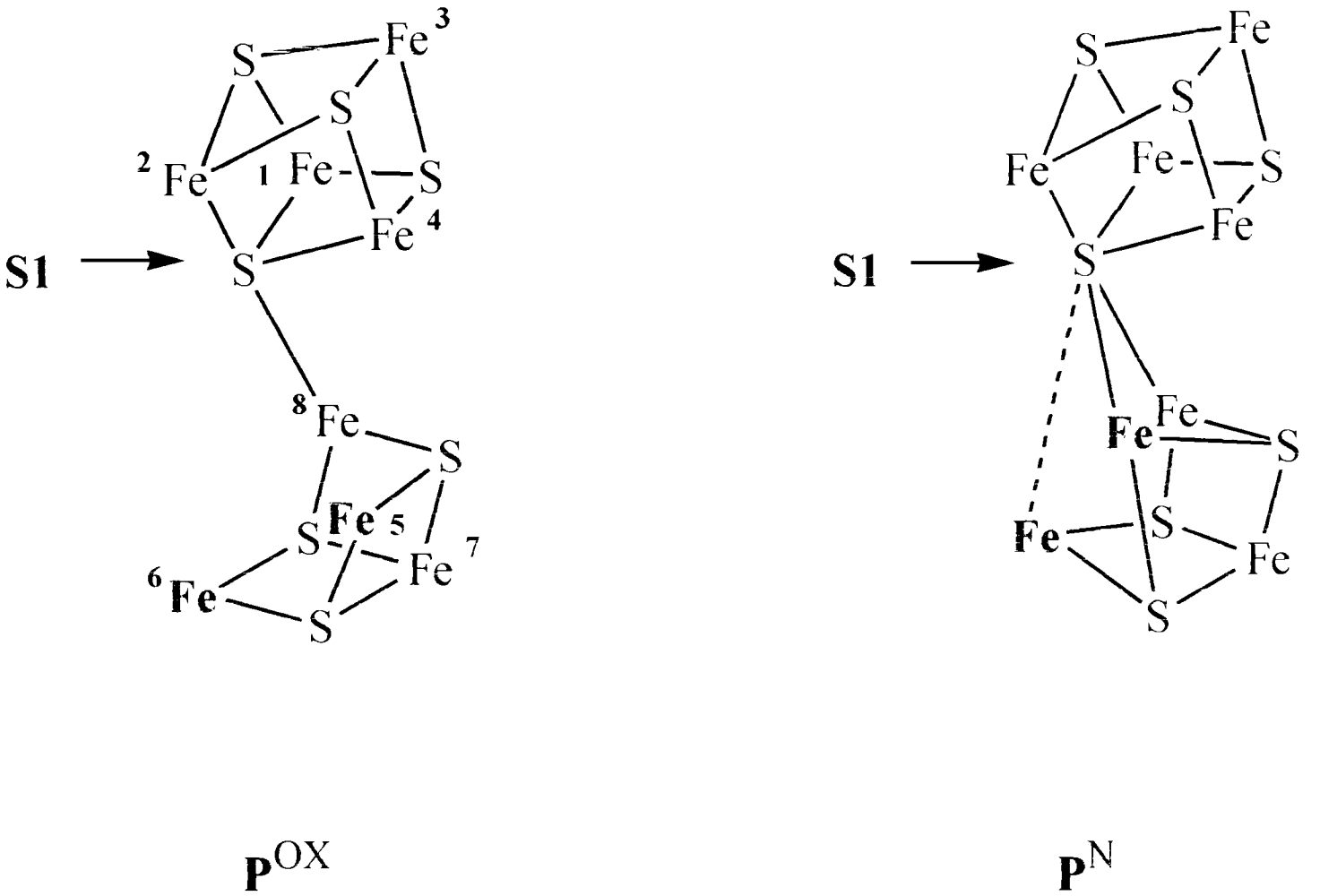

$\mathbf{P}^{OX}$ $\mathbf{P}^{N}$

Figure 1.3(b) A structural representation of the P^{OX} and P^{N} forms of the P-cluster from nitrogenase

The bonding of the central sulfur (S1) to the Fe atom furthest away is shown as a dotted line, because the S1-Fe distance (2.92 Å) is longer than the normal Fe-S bond distance.[12] *($\boldsymbol{P}^{N}$ denotes the P-cluster in the dithionite-reduced state or native state.)*

The refined structure of the P-cluster has recently been amended, and is now believed to be composed of an [8Fe-7S] cluster rather than a [8Fe-8S] cluster.[12] The most significant changes occurring during oxidation or reduction of the MoFe-protein are confined to the P-cluster.[12] In the oxidised state the P-cluster contains a bridged [4Fe-4S] and [4Fe-3S] cluster. In this form, the central sulfur (S1) is four-co-ordinate: three Fe atoms from the cubane and one Fe atom from the partial cubane (Figure 1.3(b)). Reduction of the P-cluster involves movement of *two* Fe atoms, coloured red in Figure 1.3(b). Thus, in the reduced state P^{N}, the central sulfur adopts a distorted octahedral environment, with six surrounding Fe atoms. The large difference between the oxidised and reduced forms of the P-cluster may explain why this protein was riginally proposed to contain a [8Fe-8S] cluster - a 'combination' structure from P^{OX} and P^{N}.

In the oxidised state the P-cluster is co-ordinated to the MoFe-protein by six cysteinyl ligands - Cys62 and Cys154 co-ordinate Fe3 and Fe2 respectively, whilst Cys88 is a bridging cysteinyl ligand which co-ordinates both Fe4 and Fe5. Similarly, Cys70 and Cys153 co-ordinate Fe7 and Fe6 respectively, with Cys95 a bridging ligand which binds both Fe1 and Fe8. In addition to these aforementioned cysteinyl ligands two further protein ligands complete the Fe co-ordination: Cys88 co-ordinates Fe5 through a backbone amide nitrogen ligand and the Oγ of Ser188 co-ordinates Fe6. In the reduced state these latter ligands (of Fe5 and Fe6) are replaced by interactions with the central S1 sulfur (Figure 1.3(b)) Thus in both the P^{OX} and P^{N} forms of the P-cluster all the Fe atoms remain four-co-ordinate.

These redox-mediated structural changes of the P-cluster ligands suggest a possible role in coupling electron and proton transfer in nitrogenase. Oxidation of the P-cluster is accompanied by co-ordination of Ser188 and the amide nitrogen of Cys88 to cluster Fe atoms. Both of these ligands will be protonated in their free states and may be deprotonated in their bound states. This therefore suggests that two-electron oxidation of the P-cluster will simultaneously release two protons. Hence, the observed ligand exchange reaction may be enforcing unidirectional electron flow through the P-cluster, by controlling protonation of the exchangeable ligands.[12] This complex reaction, composed of both structural and redox-dependent changes, is rare in FeS clusters, but demonstrates their ability to function in multiple roles.

1.3 CLUSTER FUNCTION AND REACTIVITY

1.3.1 Cluster Oxidation States

As described in Section 1.2, each cluster type is able (in principle at least) to exist in a number of different oxidation states, and it is this ability which is the fundamental basis of cluster reactivity. A summary of cluster oxidation states for 1, 2, 3 and 4Fe clusters is given in Table 1.2 and the ranges of the corresponding reduction potentials are shown in Figure 1.4.

Fully Reduced.....Fully Oxidised				
Fe^{2+}	**Fe^{3+}**			
$[2Fe\text{-}2S]^{0}$	**$[2Fe\text{-}2S]^{1+}$**	**$[2Fe\text{-}2S]^{2+}$**		
$[3Fe\text{-}4S]^{2-}$	*$[3Fe\text{-}4S]^{1-}$*	**$[3Fe\text{-}4S]^{0}$**	**$[3Fe\text{-}4S]^{1+}$**	
$[4Fe\text{-}4S]^{0}$	**$[4Fe\text{-}4S]^{1+}$**	**$[4Fe\text{-}4S]^{2+}$**	**$[4Fe\text{-}4S]^{3+}$**	*$[4Fe\text{-}4S]^{4+}$*

Table 1.2 Oxidation states for iron-sulfur clusters

Bold - is typical

Plain - is rare

Italic - undetected in biological FeS clusters

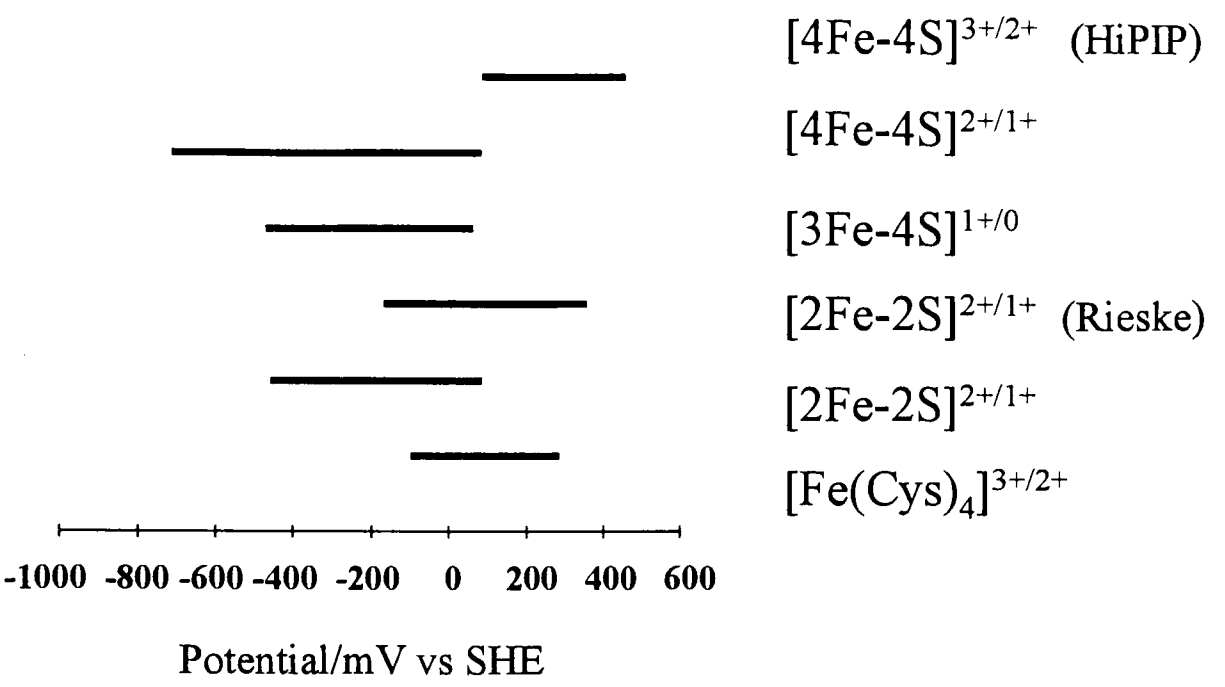

Figure 1.4 Reduction potentials of biological FeS clusters

(Reduction potentials of $[4Fe\text{-}4S]^{0}$ and $[3Fe\text{-}4S]^{2-}$ are not shown since these are not yet proved to be universal oxidation states.)

1.3.2 Electron Transfer

Ferredoxins are small mobile electron-carrier proteins, typically of mass 6-12 kDa, and generally containing $[Fe(Cys)_4]^{2-/1-}$, $[2Fe\text{-}2S]^{2+/1+}$, $[3Fe\text{-}4S]^{1+/0,}$ $[4Fe\text{-}4S]^{3+/2+/1+}$ centres, i.e. Rds, Dxs, 2Fe-, 3Fe-, 4Fe, 7Fe- and 8Fe Fds, and HiPIPs. They are electron donors/acceptors for a tremendous range of plant, mammalian and bacterial enzymes. Some are thought to be specific to a single system, others may be able to transfer electrons to or from more than one centre - as for example the Chloroplast 2Fe Fds which accept electrons from photosystem I and can transfer them to nitrite reductase, sulfite reductase, glutamate synthase, thioredoxin reductase or $NADP^+$ reductase.[83]

FeS clusters are also important for intra-molecular electron transfer in complex enzymes such as membrane bound respiratory enzymes - for example in mitochondrial Complexes I, II and III.[2] FeS clusters, however, play a similar role in many soluble redox enzymes and are able to function as one-electron donors/acceptors to many different active site co-factors - for example, binuclear Fe-oxo centres, Mo/W-pterin, Ni and flavin. An excellent example of the complexity of the electron-transfer properties of multiple FeS

clusters is provided by the NiFe hydrogenase of *Desulfovibrio gigas*. In the small subunit there are three FeS clusters (two 4Fe and one 3Fe cluster), with the 3Fe cluster being placed halfway between the two 4Fe clusters (Figure 1.5). These three clusters appear to form an obvious 'wire' through the protein matrix,[84,85] but the reduction potential of the 3Fe is much higher than that of the other two clusters. Alternative suggestions for the roles of the 3Fe cluster include a structural function,[86,87] or with such a high reduction potential, the role of the 3Fe cluster may be defensive, i.e. protection against oxidative damage by O_2.[86,88]

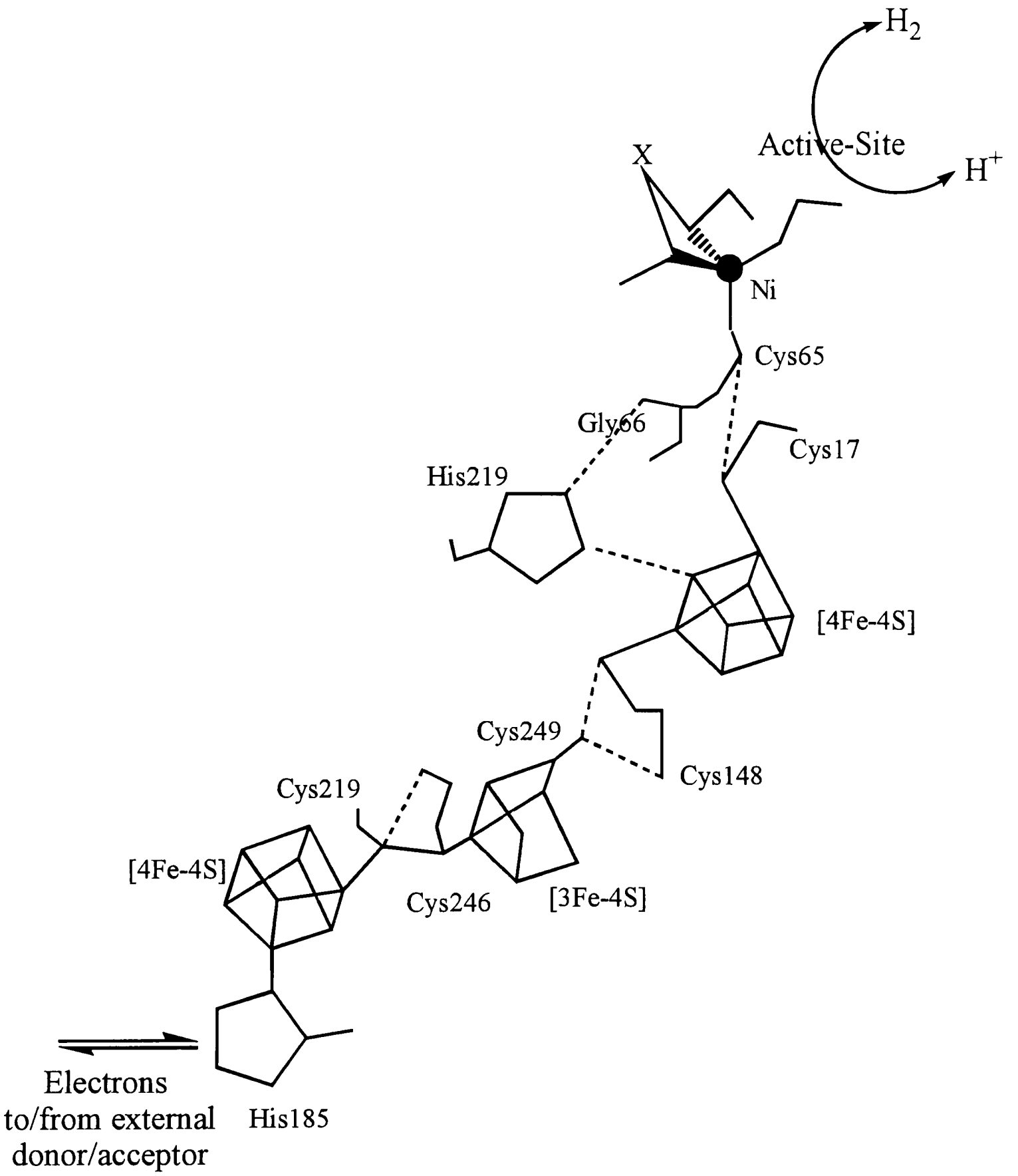

Figure 1.5 The proposed electron-transfer pathway in the nickel-iron hydrogenase from *Desulfovibrio gigas*[84]

1.3.3 Cluster Interconversions

Over the last decade it has been reported that some FeS clusters have the innate ability to change their structural type, as a response to environmental factors such as exposure to air, chemical oxidation or reduction, pH changes, or changes of the ligating residues to

the cluster (by site directed mutagenesis). The first example of cluster transformation was the interconversion of $2[Fe_2S_2]^{1+}$ to $[Fe_4S_4]^{2+}$ in synthetic complexes,[6] whilst other examples include, $[4Fe\text{-}4S]^{2+}$ and $[3Fe\text{-}4S]^{1+}$ interconversion in *Desulfovibrio gigas* Fd II[89] and aconitase.[90] This latter interconversion (Equation 1.2), between the 3Fe and 4Fe forms of the cubane cluster, has been found in a number of different cases, both biological and synthetic.

$$[3Fe\text{-}4S]^{0} + Fe^{2+} \rightarrow [Fe3Fe\text{-}4S]^{2+} \qquad \textbf{Equation 1.2}$$

The primary example of this interconversion is found in the FeS enzyme, aconitase. Aerobically purified, aconitase is inactive and contains a [3Fe-4S] cluster.[90] However, if it is then placed under reducing conditions with an excess of Fe^{2+}, the cluster is converted to the active [4Fe-4S] form. Many other proteins which contain a [4Fe-4S] cluster, including dehydratases and ferredoxins which have non-cysteinyl ligation of an Fe atom in the cluster, are particularly susceptible to this type of reversible cluster interconversion. Notable examples include *Desulfovibrio africanus* Fd III and *Pyrococcus furiosus* Fd, both of which are considered in greater detail in the following chapters of this thesis. These 'labile' clusters have been exploited to synthesise a number of mixed metal clusters in biologically viable systems. A wide range of metals, other than Fe^{2+}, have been successfully incorporated into such receptive [3Fe-4S] clusters including: Zn,[91-95] Co,[91,96,97] Ni,[92,97,98] Cd,[94,95,97,99] Tl,[100,101] Cu,[99,102] Mn,[91] Cr[99] and Ga.[103] Other 4Fe Fds which *do* have complete cysteinyl ligation to all Fe atoms are susceptible to oxidative degradation, which gives the apoprotein. This usually requires more extreme measures than brief exposure to O_2, e.g. prolonged exposure to air and/or treatment with ferricyanide, as is the case for the [4Fe-4S] cluster of the 7Fe Fd I from *A. vinelandii*.[104,105]

Alternatively, interconversion between 3Fe/4Fe clusters may be accomplished with the use of site directed mutagenesis. Altering a critical residue in the binding domain of the FeS cluster can result in structural changes as seen in both *Escherichia coli* fumarate reductase[106] and dimethyl sulfoxide reductase (DMSO) reductase.[107] If the residue **[Z]** in **-Cys-X_2-[Z]-X_2-Cys-X_3-Cys-Pro-** is changed from valine to cysteine, the 3Fe cluster

in *E. coli* fumarate reductase is converted into a 4Fe cluster. Conversely in DMSO reductase, if the residue **[Z]** in the same sequence is changed from a cysteine to one of either Trp/Ser/Phe/Tyr, the native 4Fe cluster is converted to a 3Fe cluster.

Aconitase, additionally, undergoes a further structural transformation as shown in Figure 1.6. If the inactive protein is placed in highly alkaline conditions (pH 9-10.5) or urea is added, the $[3Fe\text{-}4S]^{1+}$ form is converted into a linear $[3Fe\text{-}4S]^{1+}$ species, known as the 'purple form'(Figure 1.6). This has unique electronic and magnetic properties, with a ground state of $S = 5/2$. The major protein rearrangement, from cuboidal to linear form, involves cysteine ligand swapping. The linear form retains two of the original cysteines, two 'new' cysteines are recruited from a distant α-helix and the third 'original' cysteine ligand is released. Reduction of the purple aconitase in the presence of Fe^{2+} leads to the formation of $[4Fe\text{-}4S]^{2+/1+}$ clusters, but without Fe^{2+} present only breakdown products are observed which include $[2Fe\text{-}2S]^{2+/1+}$ clusters. There are no known linear [3Fe-4S] clusters functionally active in biology.

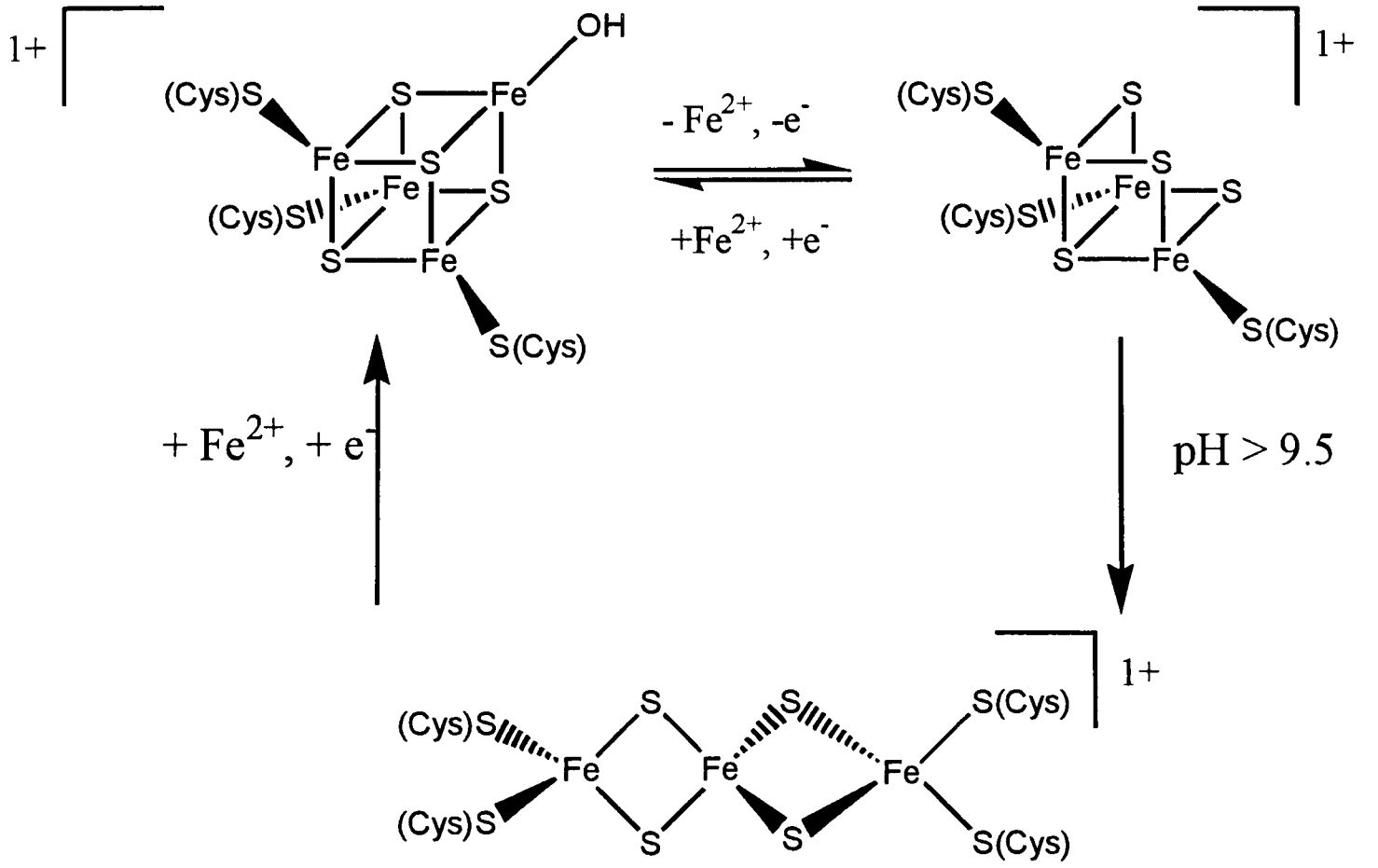

Figure 1.6 Cluster transformations in aconitase

Conversion from [4Fe-4S] to [2Fe-2S] clusters is rare, but does occur in the iron protein from nitrogenase. $[4Fe\text{-}4S]^{2+}$ to $[2Fe\text{-}2S]^{2+}$ conversion follows binding of MgATP to the oxidised protein in the presence of iron chelators such as α,α–bipyridyl.[108,109] A similar reaction is observed in the regulatory protein FNR: upon exposure to air the yellow/green active form of FNR turns deep red, as an almost quantitative conversion of the cuboid cluster to the dinuclear centre occurs.[110] As in the case of the nitrogenase Fe-protein, the conversion of the FNR protein is reversible - addition of cysteine, Fe^{2+}, DTT and the NifS protein restores the absorption spectrum and DNA binding capabilities associated with the presence of a $[4Fe\text{-}4S]^{2+}$ cluster.[110] This type of cluster conversion is relatively uncommon in comparison to the [4Fe-4S] ↔ [3Fe-4S] cluster conversions discussed previously. Recently it has been proposed that sub-unit bridging $[4Fe\text{-}4S]^{2+/1+}$ clusters, which undergo oxidative degradation to $[2Fe\text{-}2S]^{2+}$ clusters during purification, are a common feature of FeS enzymes that function using a radical mechanism (homolytic cleavage of C-H or C-C bonds) such as biotin synthase, anaerobic ribonucleotide reductase, pyruvate formate lyase, lysine 2,3-aminomutase and lipoic acid synthase.[111] It has also been proposed that oxidative cluster conversion to $[2Fe\text{-}2S]^{2+}$ clusters may play a physiological role in these radical enzymes, by providing a method of regulating enzyme activity in response to oxidative stress, without irreversible cluster degradation.[111]

1.3.4 Proton Transfer

In biology it is through the translocation of protons across membranes, concomitant with the movement of electrons that energy is converted, and the coupling of electron transfer to proton transfer is an area of intense current interest. Whilst FeS clusters are well known agents of electron transfer they have not, until recently, been implicated in coupled proton transfer. A centre involved in coupling must be able to undergo redox transitions, as well as protonation, and one of the main ways in which coupling is brought about is through the addition or loss of an electron, changing the pK of a centre and causing protonation or deprotonation. A further result is that the change in charges is compensated for, allowing further reduction or oxidation to occur.

Although FeS clusters are frequently found in nature in cases where both electron and proton transfer events occur (most obviously in the transmembrane proteins of the mitochondrial respiratory chain) suggestions that FeS clusters may themselves facilitate proton transfer have been speculative.[112] In cases where H^+ exchange does occur, there is direct evidence for the involvement of FeS clusters in proton transfer activity in catalysis e.g. at the FeMo cofactor of nitrogenase ($N_2 + 8H^+ + 8e^- \rightarrow 2NH_3 + H_2$)[12,113] and the H-cluster of Fe-only hydrogenases ($2H^+ + 2e^- \rightarrow H_2$).[11] Both these enzymes facilitate the coupling of protons and electrons when FeS clusters are the only prosthetic groups available.

In model studies of nitrogenase, reducing the dinitrogen molecule at either the Fe-S or Mo-S sites of the cofactor in nitrogenase requires prior protonation of S donors.[114] Proton uptake coupled to electron transfer has been monitored,[115] but the precise mechanism of this process is not well understood. Recent evidence has shown that structural and redox-dependent changes of the P-cluster may dictate the coupling of proton and electron transfer (see *Section 1.2.5*). Similar processes may also be relevant in other FeS cluster containing enzymes, e.g. Ni-hydrogenases,[86] CO dehydrogenase[116] and sulfite reductase (Table 1.3).[117] These proteins contain additional prosthetic groups which may also be involved in coupling proton and electron transfer.

Reaction	FeS Enzyme	Prosthetic Group
$2H^+ + 2e^- \rightarrow H_2$	Ni-hydrogenase	Ni
$CO_2 + 2H^+ + 2e^- \rightarrow CO + H_2O$	CO dehydrogenase	Ni
$SO_3^{2-} + 6H^+ + 6e^- \rightarrow S^{2-} + 3H_2O$	Sulfite reductase	Haem

Table 1.3 Enzymes containing FeS clusters

There are likely to be many more reactions which use FeS clusters to couple electron and proton transfer. In-depth studies have proved to be difficult due to the complex nature of these reactions but as discussed below, electrochemistry is proving to be particularly amenable to the study of coupled reactions.[118,119]

There are several reports of protonation accompanying electron transfer in simple, non catalytic 2Fe and 4Fe centres, including non-protein analogues, ferredoxins and the Rieske [2Fe-2S] cluster from Complex III.[120-123] However, almost all protein-bound clusters show only weak interactions between protons and clusters or, alternatively, protonation of a nearby amino-acid residue in the protein occurs instead. In the Rieske clusters, which are ligated by two cysteine and two histidine residues, the ligating histidine residues are able to be protonated and hence the reduction potential of these clusters is pH dependent.[124,125] In contrast, extensive studies on the [3Fe-4S] clusters of various 7Fe ferredoxins suggest that one distinguishing factor of [3Fe-4S] clusters is their ability to undergo protonation.[61,80] Reduced $[3Fe\text{-}4S]^0$ clusters were first observed (MCD spectroscopy) to undergo a one-proton uptake reaction when a sample of *Azotobacter chroococcum* 7Fe Fd was shown to exhibit two pH-dependent forms for the reduced $[3Fe\text{-}4S]^0$ cluster.[126] This was followed by similar reports for the 7Fe Fd from *Azotobacter vinelandii*[127-130] and also the $[3Fe\text{-}4S]^0$ from the 7Fe Fd of *Sulfolobus acidocaldarius*.[79]

The ability of [3Fe-4S] clusters to accept protons can be partly rationalised in terms of the electronic structure. The large number of electrons and the weak interactions between the transition metals in a cluster means that gaining an accurate picture of the electronic structure of a cluster is not easy. In the fully oxidised state the five d-electrons on each iron are only slightly delocalised amongst the metal sites. In contrast, there is significant delocalisation for the S atoms.[131] Upon reduction of the cluster most of the added charge (56 to 70 %) migrates onto the sulfur atoms, as a result of changes in the orbitals which formally accept the extra electron.[132,133] Thus the orbitals on the sulfide groups, in a simple FeS cluster, have the capability to act as electron pair donors and acceptors. It is clear that this acid/base behaviour will depend on the redox state of the FeS cluster.

The bonding model, as described above, is only very generalised. For 2Fe, 3Fe and 4Fe clusters, the varying geometries of these clusters, i.e. if there is more than one bonding type of sulfur atom: μ_2 and μ_3, means that there will be a considerable difference in cluster basicity. The μ_2-S atoms are more basic due to their higher electron density, and

will therefore be more likely to undergo protonation reactions. The cluster with the greatest possibility for protonation is therefore the [3Fe-4S] cluster, which has a 'crown' of three μ_2-S atoms, providing possible site(s) for protonation. Indeed, in a number of well-documented examples, this 'crown' of S atoms is well known to co-ordinate a metal atom and hence exhibit Lewis basicity - examples include aconitase, *Desulfovibrio africanus* Fd III, *Desulfovibrio gigas* Fd II, *Pyrococcus furiosus* Fd and the non-protein cluster analogue $[Fe_3S_4(LS_3)]^{3-}$, where (LS_3) is a tripodal ligand[134-136].

1.3.5 Substrate Binding and Activation

If an FeS cluster is to perform effectively as an enzyme's active site then it is required to selectively bind substrate. Functionalisation of FeS centres for substrate binding requires special cluster composition and/or different ligation patterns. Two notable ways in which this is achieved are non-cysteinyl metal ligation and/or replacement of Fe by another metal. Heterometallic clusters contained in enzymes which are able to bind substrates include CO dehydrogenase and nitrogenase. The nitrogenase enzyme contains a Mo-Fe-S cluster but, although it has been studied for many years, the actual mechanism is still under debate (*Section 1.2.5*).[12]

Homometallic FeS centres are found in the active sites of Fe-hydrogenases and a number of (de)hydratases. This latter class of FeS cluster enzyme is known to bind its substrates at the FeS cluster which features a unique Fe site serving as a Lewis acid catalyst for binding and activating the substrate. Many different types of (de)hydratases are known including those with mononuclear Fe, [2Fe-2S] and [4Fe-4S] active sites.[2] Spinach dihydroxy acid dehydratase[137] contains a [2Fe-2S] cluster which displays significant changes in its EPR spectrum upon substrate binding - indicative of binding of the substrate at or very near to the cluster.

(De)hydratases which contain [4Fe-4S] centres are much more common and include aconitase, phosphogluconate dehydratase, maleate hydratase, serine dehydratase, isopropylmalate isomerase and fumarase.[10] Aconitase is the most thoroughly characterised[7] and is a citric acid cycle enzyme which catalyses the stereospecific isomerization of citrate to isocitrate *via* the intermediate *cis*-aconitate. The active site

contains a [4Fe-4S] cluster which readily loses a specific Fe upon oxidation. As deduced from Mössbauer, EPR and ENDOR studies in the absence of substrate this unique Fe site is four co-ordinate with the fourth ligand a solvent hydroxyl. Substrate binding occurs with protonation of the bound hydroxyl, and involves co-ordination *via* the hydroxyl and the β-carboxyl (for citrate) or the α-carboxyl (for isocitrate), resulting in a six-co-ordinate Fe site (Figure 1.7).

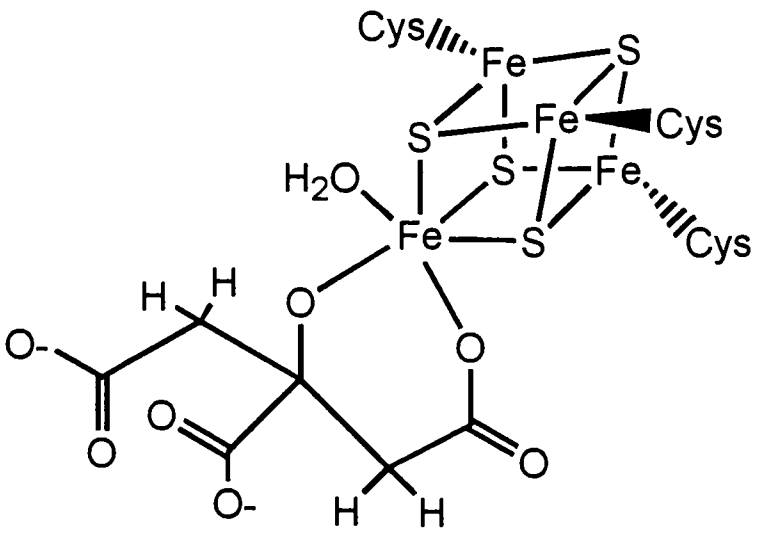

Figure 1.7 Citrate co-ordinated to the [4Fe-4S] cluster in aconitase[7]

1.3.6 Regulatory Processes

The possibility that FeS centres may participate in regulating gene expression was suggested following the discovery that the mammalian iron regulatory protein (IRP, formerly the iron responsive element binding protein, IRE-BP) was actually cytoplasmic aconitase. IRP regulates the synthesis of the iron-storage protein ferritin and the transferrin receptor which are involved in the storage and uptake of Fe respectively. Translational regulation of these proteins in the cytoplasm is due to the following control system. The messenger RNAs (mRNAs) for the transferrin receptor and for ferritin, contain iron-responsive elements (IREs), these are stem-loop structures that occur in the un-translated regions. The IREs bind with high affinity to the IRP. IRP is a ca. 100 kDa protein which is found in all higher forms of life from molluscs to insects and vertebrates. IRP is activated during an iron deficiency and is inactivated when plentiful iron is found in the cytoplasm.

The inactive form of IRP is identical to the cytoplasmic form of aconitase which lacks its $[4Fe\text{-}4S]^{2+/1+}$ cluster.[7] The FeS cluster participates in the regulation of iron uptake by undergoing cluster changes according to the Fe concentration in the cell.[15] When the iron concentration is high a [4Fe-4S] cluster is formed in the IRP, resulting in the blockage of any interaction with IREs. This has the result that when the cellular iron content is high, iron uptake is decreased and iron storage is increased. When the complete FeS cluster is present, the protein also has aconitase activity.

When the iron concentration is low, the [4Fe-4S] cluster is lost and the IRP protein is able to bind to the IREs - having the net effect that iron storage is decreased and the iron uptake increased. In this case, it appears that the cluster must be completely disassembled rather than just losing one Fe atom before the IRP acquires the capacity to bind RNA with the affinity seen *in vivo*, although the mechanism of assembly/disassembly is not known.[7,14] Flint has suggested that the transformation may perhaps be due to oxidation with O_2 or O_2^- or a NO derivative.[10] A similar role, involving DNA binding in response to cellular Fe concentration, was subsequently proposed for *Azotobacter* 7Fe Fds.[138]

A further example of the regulatory role of FeS clusters is provided by the *E. coli* FNR protein (fumarate nitrate reduction), a redox-responsive transcription regulator which activates and represses a family of genes required for anaerobic and aerobic metabolism.[16] When anaerobically purified the active form of the FNR protein is dimeric and contains two $[4Fe\text{-}4S]^{2+}$ clusters per dimer.[17] On exposure to air these clusters are rapidly converted to $[2Fe\text{-}2S]^{2+}$ clusters; these are more stable to oxygen but unable to sustain biological activity (e.g. DNA binding).[18,110] The presence of the 4Fe cluster in the anaerobically purified form of FNR is associated with an increase in specific DNA binding compared with the aerobically purified form, which lacks the 4Fe cluster.[139] The loss of this cluster, as well as the loss of specific DNA binding, upon exposure of FNR to oxygen, suggests that the [4Fe-4S] cluster serves as an oxygen sensor.

An oxygen sensing role has also been proposed for the [4Fe-4S] cluster in *Bacillus subtilis* glutamine phosphoribosylpyrophosphate amidotransferase. This enzyme catalyses the first step in purine nucleotide biosynthesis and contains a [4Fe-4S] cluster. The FeS cluster is essential for enzymatic activity and has a low reduction potential at E^{o} < -600 mV. Under limiting growth conditions, the internal concentration of O_2 increases, and the need for the *de novo* synthesis of purines declines. The increased O_2 levels tend to oxidise and destroy the FeS cluster, making the enzyme susceptible to proteolysis, since the structural support is lost. Loss of activity when the protein is exposed to O_2, correlates with the degradation of the cluster - hence the effect of O_2 on the cluster regulates the rate of purine synthesis. In this way the cluster is acting as a 'fuse', i.e. the weak link which can be removed when there is no further need for the fully functioning enzyme.

1.4 ELECTROCHEMICAL TECHNIQUES

1.4.1 Cyclic Voltammetry

Electrochemical techniques have been employed for over a century to investigate the kinetics and thermodynamics of electron transfer and associated reactions. The most important aspect is the ability to control the electrochemical potential - in cyclic voltammetry this is varied either continuously or in steps or pulses, and the current response is recorded. In this way an immediate picture of the redox processes is obtained, including both the thermodynamics and kinetics of the electron transfer, and whether any chemical or other processes are occurring. Cyclic voltammetry is the simplest method and, as a result, the most clearly understood electrochemical procedure.[140,141]

In a cyclic voltammetry experiment the potential is swept linearly with time, forward and backward between two previously set limits, as shown in Figure 1.8, and the current is recorded simultaneously as a function of time. The applied potential at time, t, is defined by,

$$E(t) = E_i + \nu t(-1)^{(s+1)} \qquad \textbf{Equation 1.3}$$

where ν is the scan rate in V sec^{-1}, t is the time (in seconds) from the starting potential E_i and *s* is the segment number.

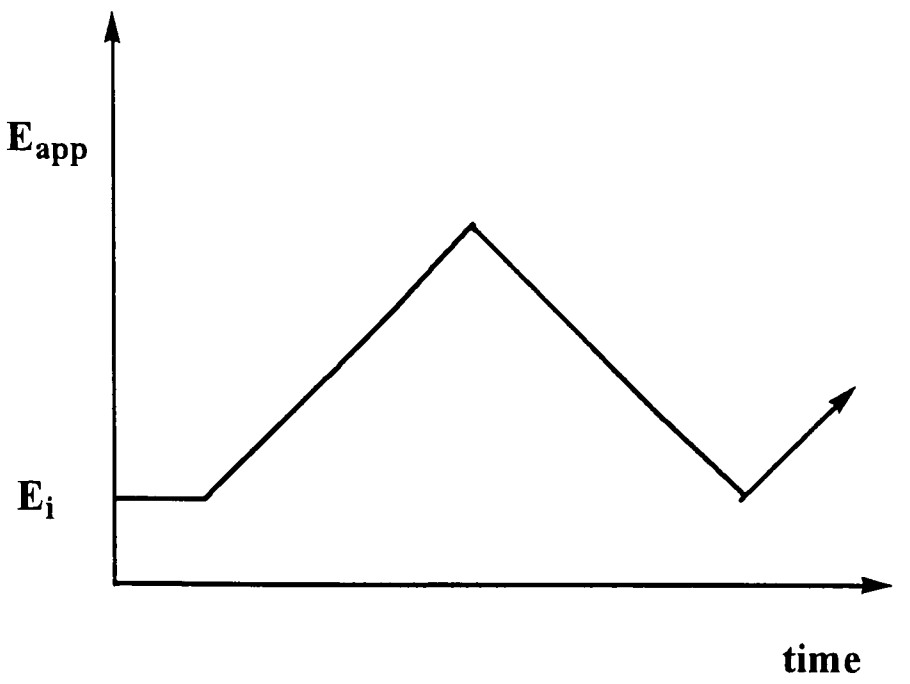

Figure 1.8 The variation of potential with time for analogue cyclic voltammetry
Defined by Equation 1.3

Typically a three-electrode cell is used for cyclic voltammetry, as shown in Figure 1.9. The current measured must be characteristic of only the processes of interest which occur at the working electrode (WE). Current flows though the WE/counter electrode (CE) circuit - the CE is designed to allow free electron flow and thus not limit reactions occurring at the WE. The three electrode cell thus avoids passing current through the reference electrode (RE), and thus the RE is unaffected by electrolysis and maintains its constant potential. The potential of the working electrode is controlled, relative to the reference electrode (typically a calomel electrode Hg/Hg_2Cl_2), by a potentiostat.

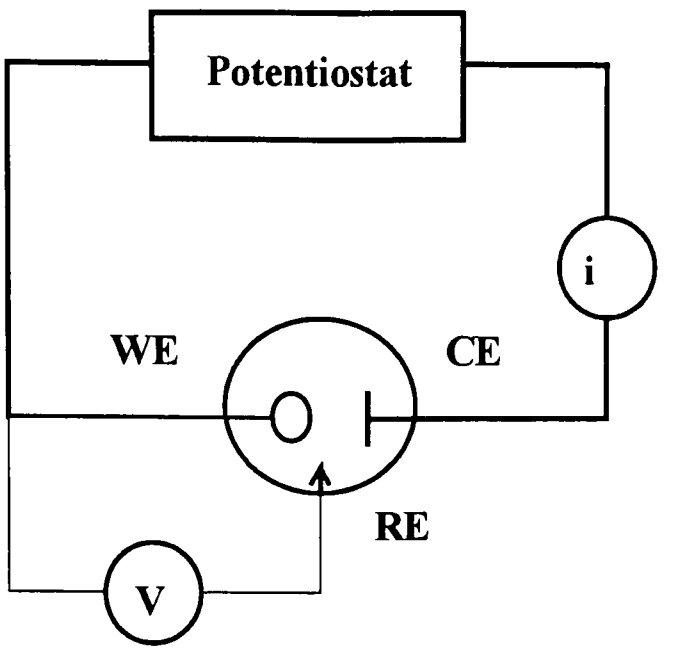

Figure 1.9 A three electrode cell

For the reversible reduction of the species Ox by *n* electrons, to the species Red, as represented by the half-cell reaction,

$$Ox + ne^- \rightarrow Red \qquad \textbf{Equation 1.4}$$

the relationship between the concentration of Ox and Red and the potential of the solution E, under equilibrium conditions (i.e. no current) is defined by the **Nernst Equation** (Equation 1.5).

$$E = E^\circ + \frac{RT}{nF} \ln\left\{\frac{[Ox]}{[Red]}\right\} \qquad \textbf{Equation 1.5}$$

where the Faraday constant, F, is the charge per mole of electrons, R is the universal gas constant and T the absolute temperature. The reduction potential, E°, at which [Red]=[Ox], is a direct measure of the Gibbs free energy for the reduction reaction:

$$\Delta G^\circ = -nFE^\circ \qquad \textbf{Equation 1.6}$$

When a cyclic voltammetric experiment is carried out, there are two contributions to the observed current, the non-faradaic current and the faradaic current.[142]

1. **Non-faradaic current** - this originates from the charging of the double layer at the electrode-solution interface. It is analogous to charging a capacitor (and is also called the capacitance or charging current) and is termed non-faradaic because no electrons actually cross the electrode-solution interface (Figure 1.10(i)).

2. **Faradaic current** - this is due to the oxidation or reduction of molecules at the electrode - electrons are exchanged between the electrode and molecules either in solution or confined to the electrode surface (Figure 1.10(ii)).

(i)

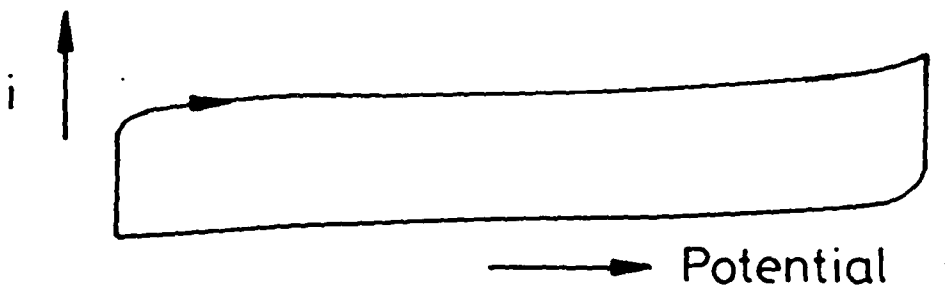

(ii)

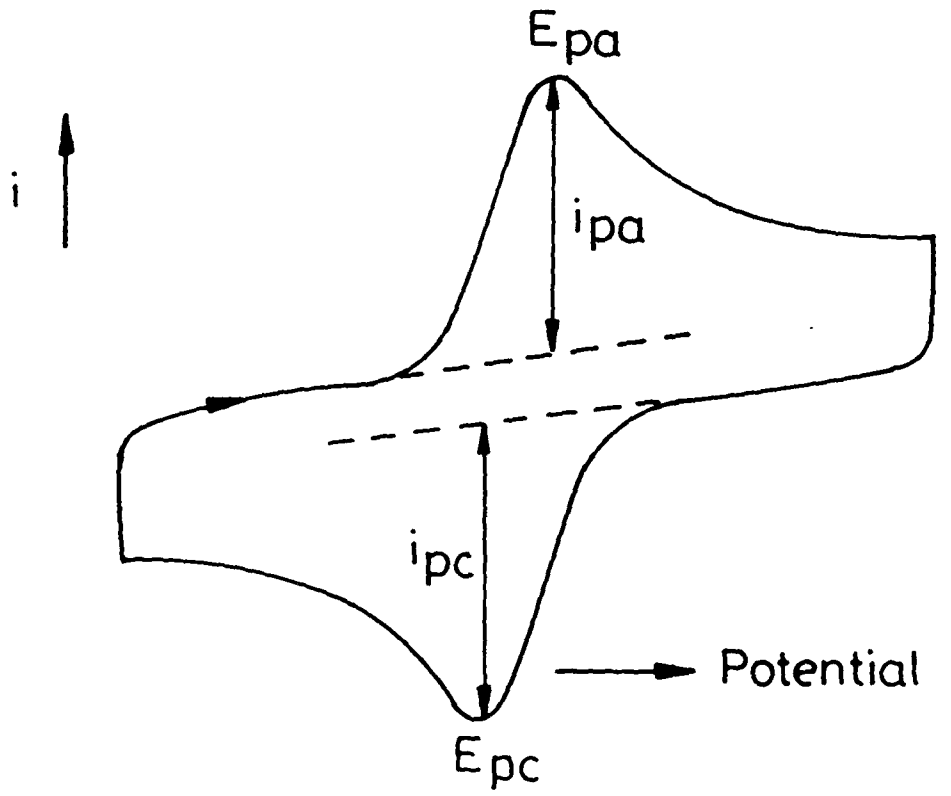

Figure 1.10 The potential and current profiles of a cyclic voltammetric sweep

(i) A typical non-faradaic response ('buffer blank')

(ii) A cyclic voltammogram of a freely diffusing, redox active species. The reduction potential is given by the average of the oxidation and reduction peaks i.e. $(E_{pa}+E_{pc})/2$.

1.4.1.1 The Free Diffusion Configuration

When a working electrode (WE) is placed into a protein solution the current response, as the potential is changed, is due to the reversible transfer of electrons between the electrode and redox centre in the protein molecule. It is likely that before this can happen protein molecules must be transiently adsorbed onto the electrode surface, and then desorb after the electron transfer has occurred. This is illustrated in Figure 1.11, where k_s is the rate of heterogeneous electron transfer between Ox/Red and the electrode, (dependent on potential), while k_{ads} and k_{des} are the rates of adsorption and desorption.

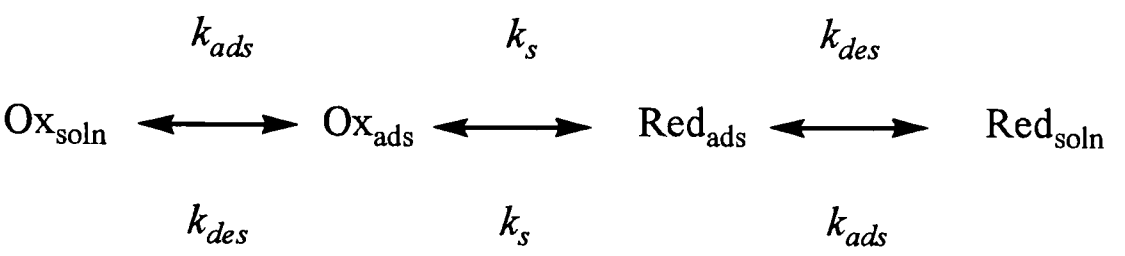

Figure 1.11 The free diffusion configuration

Cyclic voltammetry on a simple redox couple in solution (with a stationary planar electrode) gives a characteristic current-voltage profile as shown in Figure 1.10(ii). The measured reduction potential (E^o) is usually given by the average of the oxidation (E_{pa}) and reduction peaks (E_{pc}). If the solution contains the oxidised form (*A*) and the scan starts at a more positive potential (E_1) than the formal reduction potential for the reaction, E^o, only a non-faradaic current will be initially observed. As the electrode potential approaches E^o a faradaic current will then begin to flow, and *A* will gradually begin to be reduced (*B*). This current response grows to a peak i_p as the rate of heterogeneous electron-transfer increases with potential, and will then diminish (but not to zero) as the concentration of the redox-active form becomes depleted at the electrode surface (for a macroelectrode). However, on reaching E_2, the potential is then swept back, re-oxidising the reduced species previously formed and current in the opposite sense is thus observed.

The theoretical response of a freely diffusing Nernstian system in a voltammetric experiment is well established.[142] The peak current for the oxidative sweep, i_p in amperes, is given by the **Randles-Sevcik** equation:

$$i_p = 0.4463nFAC_o\left(\frac{nF}{RT}\right)^{1/2}\nu^{1/2}D_o^{1/2} \qquad \textbf{Equation 1.7}$$

where A is the electrode area (cm^2), D_o the diffusion coefficient for oxidised species (cm^2s^{-1}), C_o the concentration of oxidised species (mol cm^{-3}), ν the scan rate ($V\ s^{-1}$) and R, T and F take their usual meanings.

The peak separation, ΔE_p is

$$E_{pa} - E_{pc} = 1.109\frac{RT}{nF} = 59/n \quad \text{mV at 298 K} \qquad \textbf{Equation 1.8}$$

where E_{pa} and E_{pa} are the anodic and cathodic peak heights respectively, and the reduction potential, E^o, is defined as,

$$E^o = \frac{\left(E_{pa} + E_{pc}\right)}{2} \qquad \textbf{Equation 1.9}$$

Equations 1.7 to 1.9 describe an ideal voltammetric response when the dominant mode of transport to the electrode is linear diffusion - a macroplanar electrode. The following conditions for the system must be assumed:

1. The rate of heterogeneous electron transfer, k_s, between Ox_{ads} and Red_{ads} and the electrode is fast.
2. The reactants and products do not undergo chemical changes during the lifetime of the experiment.
3. The diffusion coefficients for the oxidised and reduced forms are similar.

If these conditions are not met, or the system is more complicated than a straightforward electron transfer, deviations will occur in the shape of the voltammogram. If adsorption is strong then the waveform will appear more symmetrical - the extreme case of this is the immobilised configuration as discussed in the next section. A slower electron transfer rate constant will result in a larger peak separation. If there is a gross change in the shape or form of the voltammogram this indicates that the reactants or products are undergoing a chemical change (or catalytic) reaction.

1.4.1.2 The Immobilised Configuration

In the immobilised configuration, the protein is strongly adsorbed to the electrode surface, ideally as a monolayer or submonolayer. Therefore electron transfer does not involve adsorption and desorption or transport of the protein to the electrode, because the redox active molecule is already 'semi-permanently' bound.

$$Ox_{ads} \xleftarrow{k_s} Red_{ads}$$

Figure 1.12 The immobilised configuration

For simplicity, adsorption upon the electrode is assumed to behave as described by the Langmuir isotherm,[143,144] which assumes that strong adsorption of the redox-active species gives rise to a coverage, (monolayer or less) which consists of a *non-interacting*, and homogeneous ensemble of molecules.

Using the Nernst equation (Equation 1.5) to generate the current-potential profile is straight-forward since the current is the result of maintaining the equilibrium population of the oxidised and reduced species, as a function of potential (Figure 1.13).

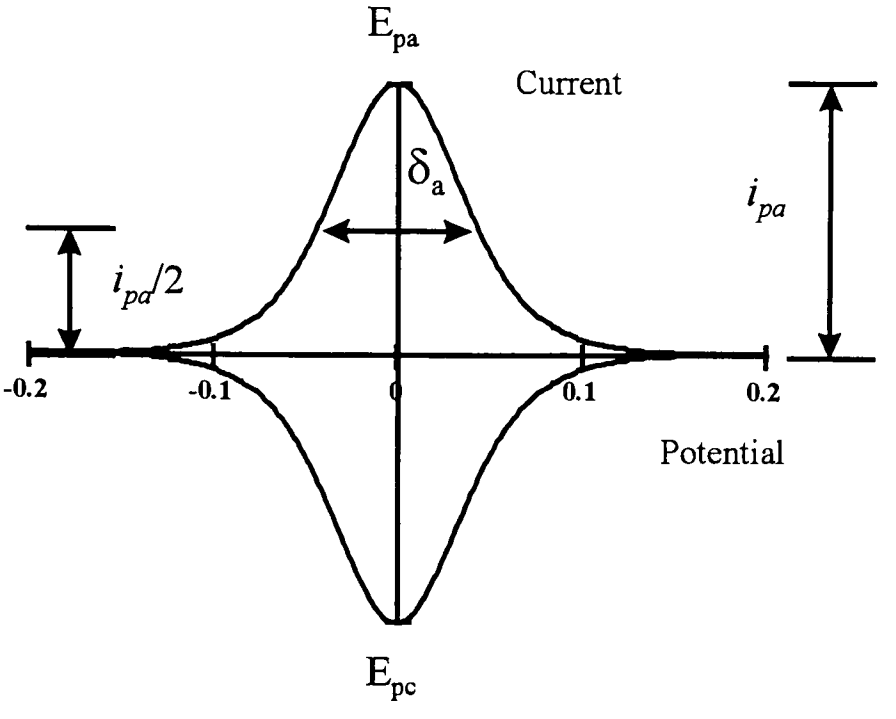

Figure 1.13 Cyclic voltammogram of a species immobilised on an electrode
A reversible voltammogram. The non-faradaic response has been omitted for clarity.

The peak current i_p is given by

$$i_p = \frac{n^2F^2}{4RT}\nu A\Gamma^* \qquad \textbf{Equation 1.10}$$

where Γ^* is the total surface concentration of redox-active species, other terms are as defined previously and the ratio of anodic to cathodic peak currents (i_{pa}/i_{pc}) is equal to 1. The direct proportionality between the peak current and ν for an adsorbed species (Equation 1.10) can be contrasted with the $\nu^{1/2}$ relationship observed in molecules diffusing linearly to the electrode (Equation 1.7) and can be used diagnostically in this way. Several further idealised differences are also apparent:

1. There is zero peak separation for an adsorbed species at equilibrium, i.e.

$$\Delta E_p = E_{pa} - E_{pc} = 0 \qquad \textbf{Equation 1.11}$$

2. The peak width at half-height, δ, is given by

$$\delta = 3.53\frac{RT}{nF} = \frac{0.083}{n} \text{ mV at } 273 \text{ K} \qquad \textbf{Equation 1.12}$$

Thus, it can be seen that co-operative multi-electron transfer reactions ($n > 1$) will result in both peaks having a narrower half-height peak width and the peak height will be correspondingly greater because i_p is proportional to n^2 (Equation 1.10).

3. The area under the *i*-E curve, corrected for any background (i.e. non-faradaic) current, corresponds to the charge passed in reducing (or oxidising) the layer of adsorbed species Ox (or Red). Therefore the number of electroactive centres can be calculated from the area under the *i*-E curve.

$$\frac{\text{Area under peak}}{\nu} = nFA\Gamma^* \qquad \textbf{Equation 1.13}$$

1.5 BIOELECTROCHEMISTRY

1.5.1 Introduction

The major technique used in this thesis to probe and explore biological iron-sulfur cluster chemistry is *dynamic electrochemistry* - monitoring the current flowing through a system as the driving force is varied with time.[142,145] Although this is a relatively new method of studying biological systems it offers unusual and unique insights which are often difficult to gain by conventional methods.[146-149]

Despite the fact that dynamic electrochemistry has long been successfully applied to study the thermodynamics and kinetics of small molecule systems, the general opinion was that it would be of little use for biological systems. Biological redox electrochemistry has therefore often been confined to the status of a static technique i.e. potentiometry - a well-used method of measuring a reduction potential. Here, small molecules (usually organic redox-active dyes) are used to facilitate attainment of equilibrium between the solution and the electrode during spectroscopically monitored redox titrations.[150] This method is however, restrictive in several ways: it is available only to stable species with a spectroscopic signal; the potential window is confined to the redox dyes; large quantities of protein are required, which is then contaminated with the redox dyes and it is time consuming. Also it gives only thermodynamic, and not kinetic information. Since biological redox processes do not occur at equilibrium, a technique which is able to interrogate systems in 'real' time is invaluable. In this respect dynamic electrochemistry (voltammetry) is an essential tool, because the time as well as the potential dependence of reactions can also be easily observed. There are two variations of direct voltammetry, both of which have been used in this thesis: the diffusion configuration (*Section 1.4.1.1*) and the immobilised configuration (*Section 1.4.1.2*).

1.5.2 A Historical Perspective

Hill and Kuwana and their co-workers were the first to achieve reversible, diffusion-controlled voltammetry of a protein (cytochrome *c*) at a solid electrode without mediators and with no sign of denaturation.[151-153] This work has lead to investigators being able to directly observe the protein interacting with the electrode, being able to control and monitor the redox status both in the time and potential domains, which in turn can lead to deconvolution of both the thermodynamic and kinetic data.[146,154]

Previously it had been the general belief that reversible and direct electrochemistry would be unfeasible due to slow rates of diffusion and the buried redox centres, although these argument have since been dispensed with as the course of research has progressed.[146] Denaturation of protein at the electrode surface has however proved an ongoing problem, especially in the case of early experiments. Hence the dropping mercury electrode was introduced because the surface of the electrode (crucial for success) was continually renewed and therefore kept clean.[142,145] Voltammograms, however, did not produce results which were consistent with the reduction potentials of the native species[155-158] and were often complicated by the appearance of large signals, attributed to strongly adsorbing species, most frequently denatured proteins.[146] Strong adsorption of the electroactive species is not itself a problem and, in fact aids the biological electrochemist. However, if this is accompanied by denaturation and serious changes to the protein active site it is disadvantageous, as the true mechanism of the protein will be obscured.

As mentioned above, the first major breakthrough in direct protein electrochemistry was achieved by two groups who separately reported reversible electron transfer between cytochrome *c* (cyt *c*) and an electrode. Eddowes and Hill observed electrochemistry at a gold electrode[151,152] using 4,4'-bipyridyl to modify the electrode surface. As the reduction potential of this organic molecule is much lower than that of cyt *c*, it was argued that it takes no part in the electron-transfer mechanism. At the same time, Yeh and Kuwana reported the reversible electrochemistry of cyt *c* at a Sn-doped indium oxide electrode, without a mediator.[153] Although this electrode was naturally functionalised at

the surface by its stable oxide groups, it neatly demonstrated that the use of a mediator was not required for direct reversible protein interaction.

From these early beginnings the search began for improved electrode surfaces and electrochemical promoters. The term *promoter*[e] was introduced for compounds which enhance the electrochemical response but do not take part in the redox reaction in contrast to mediators.[151] Hill and co-workers suggested that the success of gold electrodes in combination with 'XY' promoters was due to the group X having a high affinity for the electrode surface and the Y moiety having a weakly basic group which is able to interact with the protein. Alternatively, it was found that unpromoted electrochemistry of cyt *c* was possible at a carbon surface, and that the response was improved by creating a high density of oxide groups on the surface.[159]

1.5.3 Carbon Electrodes

Carbon electrodes are suitable for protein film voltammetry for the following reasons,

1. The large potential window over which the electrodes can be used means that carbon electrodes may access potentials which are well outside the limits obtainable with chemical reductants in aqueous solution
2. They allow a large variation of pH to be used
3. Varied surface functionalities are available for experiments

Pyrolytic graphite is formed by deposition of carbon from the vapour phase, and ideally is a single 'crystal' of graphite - it therefore provides two different types of electrode surface - either basal or edge plane. A basal plane electrode is produced by cleaving *parallel* to the layers of aromatic carbon, whereas an edge plane electrode is produced by cleaving *across* the aromatic rings. Cleaving the basal plane produces few C-O functionalities (conduction between planes is poor) and the resulting surface is hydrophobic - this often results in poor electrochemistry.[159] Edge cut graphite produces highly reactive carbon atoms (with unsaturated valence) which react with dioxygen or

[e] In this thesis, the term 'co-adsorbate' is used in place of promoter, as this more accurately describes the process occurring. Large positively charged molecules such as polymyxin and neomycin are used to promote the co-adsorption of the negatively charged ferredoxins.

water to form a layer of C-O functionalities including: carboxylates, alcohols, aldehydes, ketones and quinones, and is also a much better conductor.[159-161] To produce an active and clean electrode surface pyrolytic graphite edge (PGE) plane electrodes are polished using alumina powder and then sonicated extensively before use. The negative surface of a PGE electrode means that positively charged proteins, like cyt *c*, are more likely to interact, for purely electrostatic reasons. When the pH of the cyt *c* solution is lowered, the electrode surface groups are protonated and the electrochemical response from cyt *c* is attenuated. The opposing effect is observed when $Fe(CN)_6^{3-}$ was added.[159]

In contrast to cyt *c*, most proteins possess an overall negative charge on their surface, and so their electrostatic interaction with pyrolytic graphite edge electrodes is limited.[162] The electrochemical response of these systems can be improved by the addition of promoters, which are positively charged, to combat the repulsive forces between the negatively charged protein and the negative electrode surface. Addition of cationic reagents ($M^{4+} > M^{3+} > M^{2+} >> M^{+}$ in order of effectiveness) induces stable, well defined voltammetry for bacterial and chloroplast ferredoxins, rubredoxin, flavodoxin and plastocyanin.[159,163-165] Much stronger interactions can be produced if complex polyamines (which possess a rigid spatial array of $-NH_3$ groups) are used as promoters.[166,167] These include the amino glycosides neomycin and tobramycin and also the polyamine, polymyxin. However, not all protein/promoter combinations work as well as might be predicted from this simplistic electrostatic model - this is indicative of other forces also playing a significant role in protein/electrode interactions, for example lateral protein-protein interactions.[159,168]

This directed use of promoters was originally used to facilitate electrochemistry of molecules freely diffusing in solution. Indeed, many studies have been carried out using this method. However, the use of promoters to help adsorption of protein molecules on the surface, has lead to the development of the immobilised configuration.

1.6 THE IMMOBILISED CONFIGURATION AND ITS ADVANTAGES

When a protein is adsorbed on the surface of the electrode in the immobilised configuration, it is possible to extract more information than with the diffusing system. The ideal scenario is as follows:

1. Redox-active protein molecules are adsorbed strongly at the surface of an electrode.
2. Adsorption occurs with minimal disruption of the native conformation.
3. Electron transfer between the electrode and protein active sites is reversible and Nernstian equilibrium is maintained at each value of the applied potential.
4. The protein forms up to, but not more than, a monolayer on the electrode surface. Each active site behaves independently of, but identically to, those in neighbouring proteins.

A schematic representation of the immobilised configuration is shown in Figure 1.14.

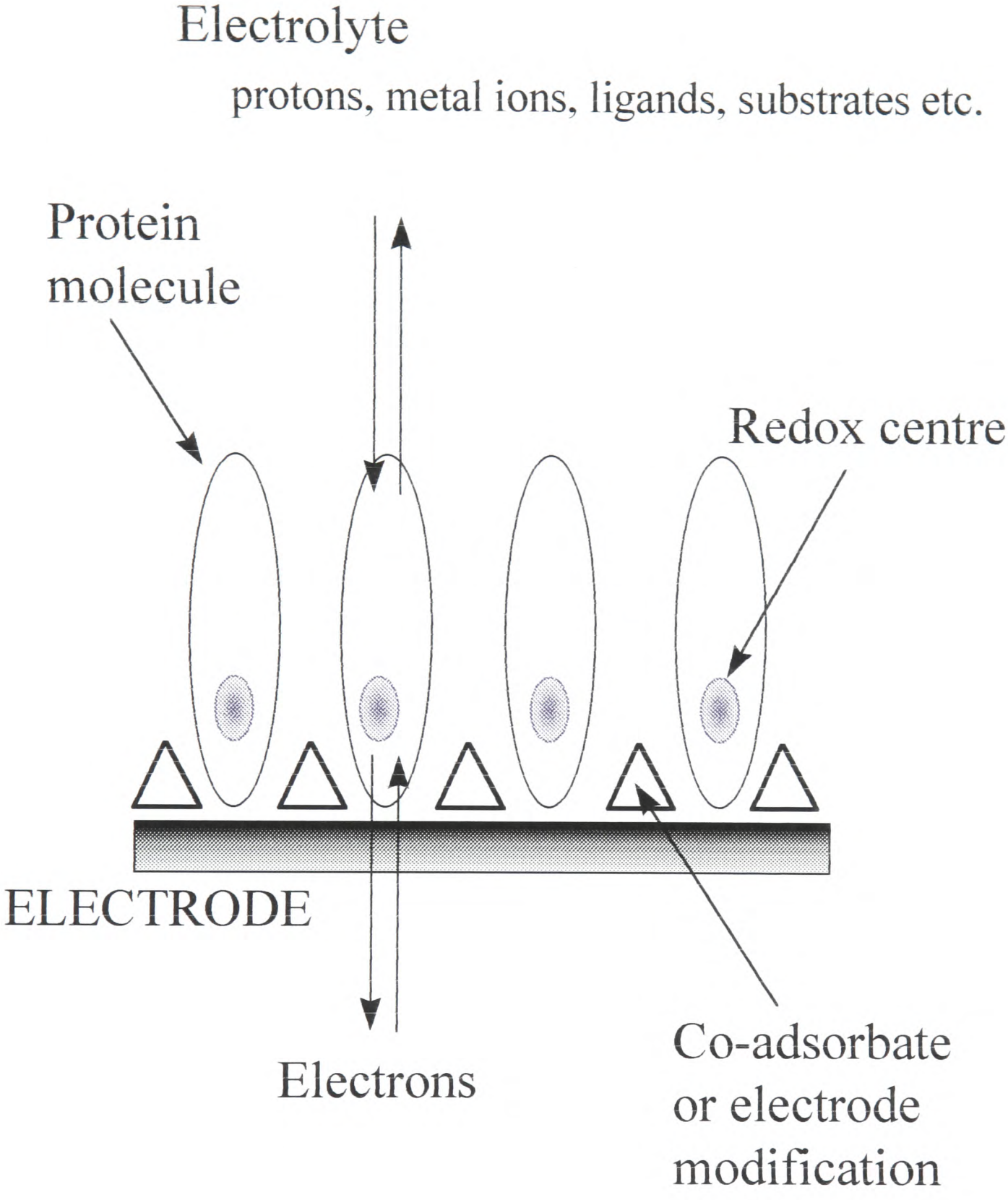

Figure 1.14 Schematic representation of a monolayer

Protein molecules immobilised on the surface - the 'idealised configuration'

The advantages of all protein molecules being confined to the electrode surface are described below.

1. Wave form analysis

With the protein freely diffusing in solution, information contained in the voltammetric wave-form is very often too convoluted to be of any help. However, for the immobilised configuration the information is easily accessible: the number of actual electroactive molecules can be derived by integration; the peak height and width give information to determine the number of electrons which are involved in the transition state (Equation 1.12); and the cooperativity of the reaction can be determined, i.e. if more than one electron is involved. Additionally the peak separation, ΔE_p, and its dependence on scan rate can be used to derive rate constants for electron exchange between the electrode and the redox sites.[144] Furthermore, if asymmetry is seen in the voltammetry this can indicate the presence of coupled reactions and the voltammetry can be analysed to obtain rates of these.

2. Sample economy

Protein film voltammetry is a useful technique for samples which are only available in limited quantities. A typical protein film at a standard electrode (ca. 0.2 cm^2) requires only about 10^{-12} mole of protein. This is approximately 0.5 % of the amount which is required for an EPR measurement.

3. Control of the redox status of all the centres in the sample

Since it is possible to control the redox status of all the centres exactly, any chemical activity which is dependent upon the redox state of the protein can be carefully monitored in the time domain through changes in the applied electrode potential.

4. Instantaneous change of environment

Strong adsorption of the film onto the electrode surface allows the protein to be directly transferred from one electrolyte solution to another. These solutions may have a different chemical environment - and thus the effect which this has upon the sample can be readily seen. This technique has been used extensively in this thesis. An example, in which the technique of protein film voltammetry excels, is the investigation of biological

systems at extremes of pH. Many samples would not survive a macro dialysis into a solution at pH 2, but an experiment under these conditions becomes possible with protein film voltammetry.

5. Sensitivity and stoichiometry

The very small sample size being examined means that reactions which occur between the protein active site and reagents from the electrolyte can be quantified at a very low concentration level e.g. thallium co-ordination to a [3Fe-4S] cluster, as discussed in *Chapter 6*.

1.7 COUPLED ELECTRON TRANSFER

1.7.1 Square Schemes

Many redox reactions in biology involve more than just electron-transfer, and often conformational change, proton binding or substrate binding and catalysis can be dependent on the redox state of the bio-active centre. In some cases a chemical reaction or a conformational change may be required *before* electron transfer can occur. Such processes which are both electron-transfer reactions and chemical reactions are said to be *coupled* processes. Coupled reactions can, like 'pure' electron-transfer reactions, be observed and studied in cyclic voltammetry experiments. They can be identified using electrochemistry, because of the characteristic differences which they display compared to an idealised 'electron-only-transfer' reaction. A simple scheme of a coupled reaction is shown in Figure 1.15.

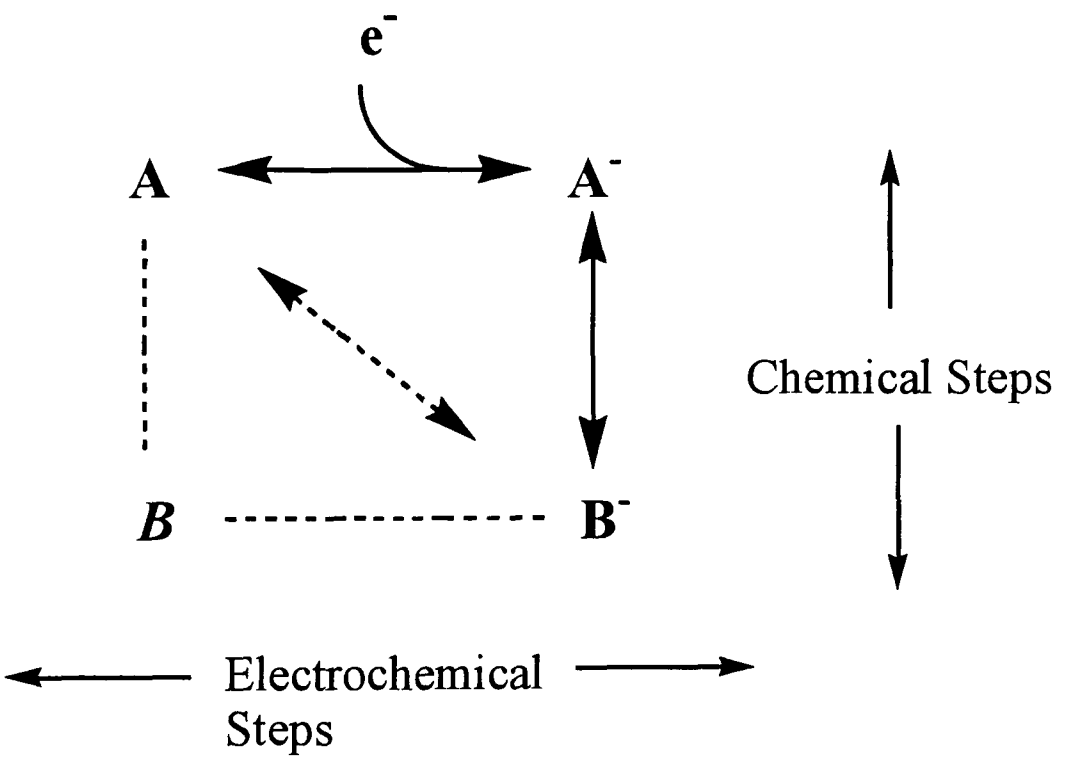

Figure 1.15 A 'square scheme'

A square scheme illustrating how a chemical reaction (A^- to B^-) follows reduction of the species A. For the re-oxidation, B^- must first undergo a chemical reaction to A^-.

The figure above (Figure 1.15) shows a generalised 'square scheme',[169,170] where the electrochemical and chemical reactions are assumed to occur separately (horizontal and vertical reactions respectively). A redox reaction is said to be 'gated' if its rate is controlled by a chemical reaction, i.e. $B^- \rightarrow A$, rather than an electrochemical reaction

$A^{\cdot} \rightarrow A$. With cyclic voltammetry, it is possible to separate out the kinetics of these reactions by altering the timescale over which the experiment is carried out, i.e. by varying the potential scan rate. Thus voltammetry is ideally suited to investigation of coupled reactions. In Figure 1.16, an example of the voltammetry of a coupled reaction is shown.

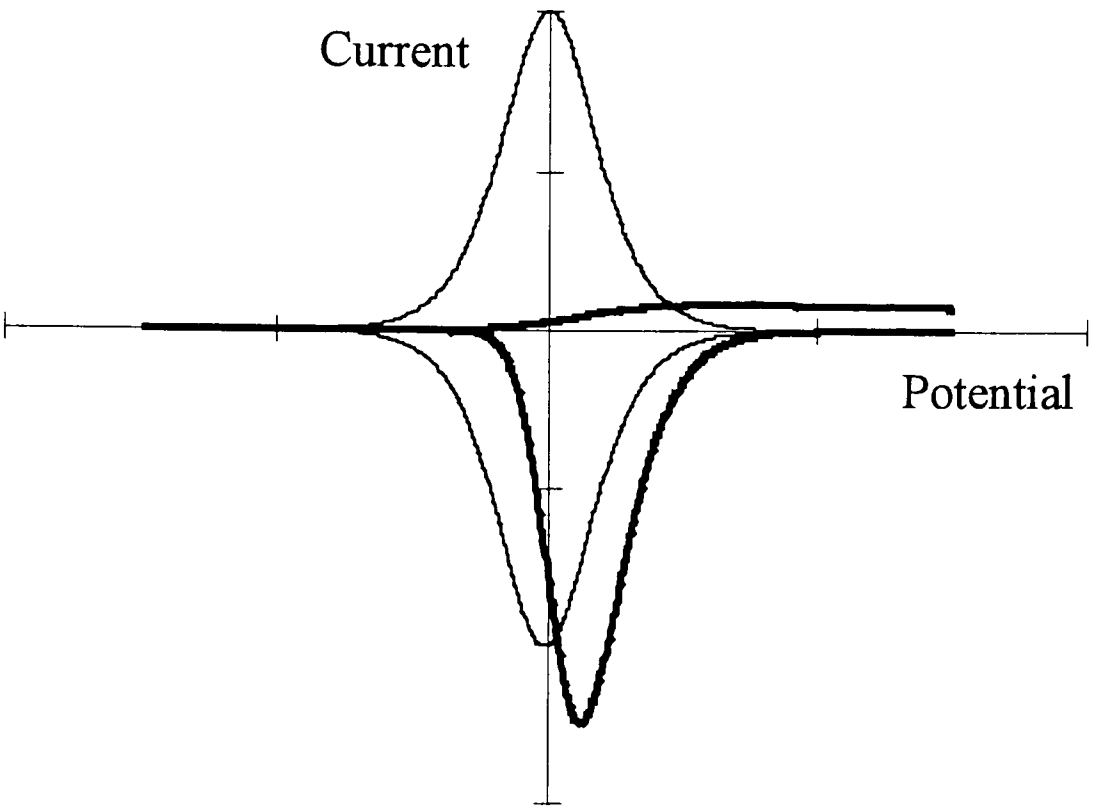

Figure 1.16 Example of the voltammetry of a gated redox reaction

*A typical response of a gated redox reaction (**bold**) compared to a non-gated redox reaction. The reductive electron-transfer of the gated reaction is followed by conversion to an electrochemically inactive form ($B^{\cdot}$ in Figure 1.15). The reductive wave is sharper and at a higher potential due to the ET equilibrium being 'pulled across'. The oxidative scan is considerably broadened as ET cannot occur before a chemical or conformational conversion occurs i.e. it is 'gated'.*

In the above example (Figure 1.16) an electron-transfer reaction is coupled to a non-catalytic chemical reaction e.g. proton transfer. It is clear from Figure 1.16 that the reduction process is facilitated (peak is sharp) while the oxidative process is retarded (peak is broad). Thus the oxidative reaction is 'gated' i.e. a chemical reaction is required before oxidation can occur.

In Figure 1.15, the time for interconversion between the reduced state A^- and the more stable B^- is comparable with the timescale of the experiment. If B^- is electroinactive, then the reductive and oxidative scans will be no longer symmetrical (as for the ideal case of electron-transfer only). The reduction potential will be characteristic of the diagonal interconversion between A and B^- instead of the simple $A \rightarrow A^-$ reaction. As a direct result of this, the re-oxidation of B^- is gated because it must first convert to A^- before oxidation can proceed. Thus the species A^- is said to be *transient,* similar transient states in biology may occur and be functionally relevant, though it is apparent that their detection with conventional methods may be difficult.[171]

If the scan rate of this system is slowed down, the oxidative and reductive waves become symmetrical and the reduction potential reflects the thermodynamic distribution of species. Alternatively if the scan rate is increased further then the voltammetry will revert to that expected for electron-transfer alone, $A \rightarrow A^-$ i.e. as shown in Figure 1.13, where the oxidation and reduction waves are symmetrical. Thus, any deviation from total symmetry of the oxidative or reductive peaks can be indicative of a coupled electron-transfer reaction.

1.7.2 Redox Coupled Ligand Transfer

If a chemical reaction of an electroactive species depends upon the oxidation state of that species, then it will be manifested in the observed voltammetry. An example of this is the rapid and reversible, redox-coupled binding of an exogenous ligand to an FeS cluster. As described in *Section 1.3.3* a number of [4Fe-4S] Fds do not have all cysteinyl ligated clusters and in some instances one cysteine is replaced by an aspartate residue. It has been shown that it is possible to observe an interaction between these specific clusters (with aspartate ligation) and exogenous ligands, in particular thiolate ligands.[172] On introducing an adsorbed Fd film to a solution containing the ligand, changes are observed in the voltammetry. Most noticeably, an interaction with many of the ligands is not seen until the cluster is reduced, $[M3Fe\text{-}4S]^{1+}$. It is not known whether the reaction is a substitution of a cluster ligand (e.g. the aspartate) or an additive reaction, but many ligand interactions impose a change of reduction potential on the cluster and these

reactions are thus dependent on the redox state of the cluster. These reactions are explored and commented on in *Chapter 4*.

1.7.3 Redox Coupled Proton Transfer

Electron transfer can be represented by the simple half-cell reaction

$$Ox + ne^- \rightarrow Red$$

However, if this reaction is coupled with the transfer of y protons, the situation can be represented pictorially as a square scheme as shown in Figure 1.13.

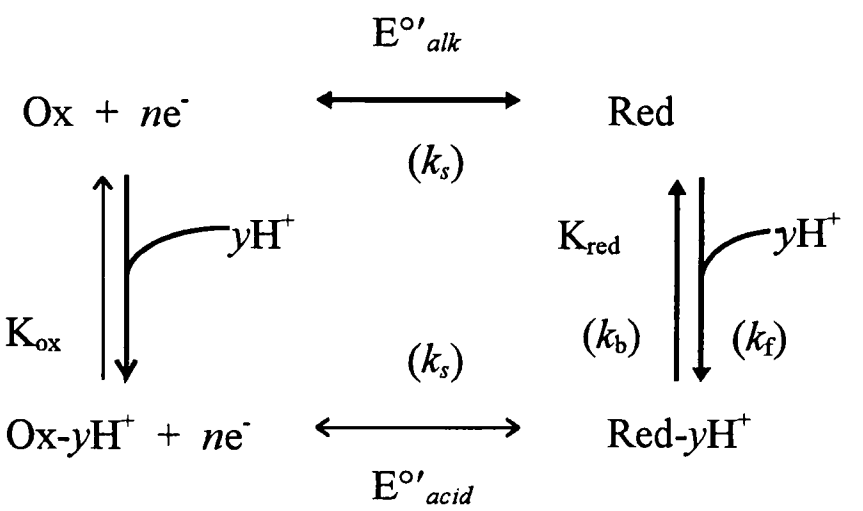

Figure 1.17 A square scheme for redox coupled proton transfer

K_{ox} and K_{red} are the equilibrium dissociation constants for proton binding to the oxidised and reduced species respectively; $E^{o'}_{alk}$ and $E^{o'}_{acid}$ are the reduction potentials in the limit of high and low pH; k_s is the heterogeneous electron transfer rate; and k_f and k_b are the rates of the forward and backward reactions in the proton dissociation equilibrium and are defined such that $K_{red} = k_b / k_f$

1.7.3.1 Thermodynamics

Proton transfer, if coupled to a redox reaction, can be detected by voltammetry as a variation in the reduction potential with pH. Protonation on or near the redox-active group in the protein means that the relative energy difference between the oxidised and reduced state (*i.e.* Ox and Red-yH^+) is influenced by the positive charge of the proton (or the negative charge of the deprotonated acid). If the Nernst equation is applied to the redox-equilibria in the square scheme (Figure 1.17) the variation of the reduction

potential with pH (and also K_{red}, K_{ox}, n, and y) can be quantified. The derivations of these equations are given in *Appendix A*.

Relative to reduction potential in the acid limit, $E°'_{acid}$,

$$E° = E°_{acid} + \frac{RT}{nF}\ln\left(\frac{[H^+]^y + K_{red}}{[H^+]^y + K_{ox}}\right) \qquad \textbf{Equation 1.14}$$

or relative to the reduction potential in the alkali limit, $E°'_{alk}$.

$$E° = E°_{alk} + \frac{RT}{nF}\ln\left(\frac{1 + {[H^+]^y}/{K_{red}}}{1 + {[H^+]^y}/{K_{ox}}}\right) \qquad \textbf{Equation 1.15}$$

A schematic plot of the reduction potential *versus* pH is shown in Figure 1.18 where $pK_{ox} = -\log_{10}K_{ox}$ and $pK_{red} = -\log_{10}K_{red}$.

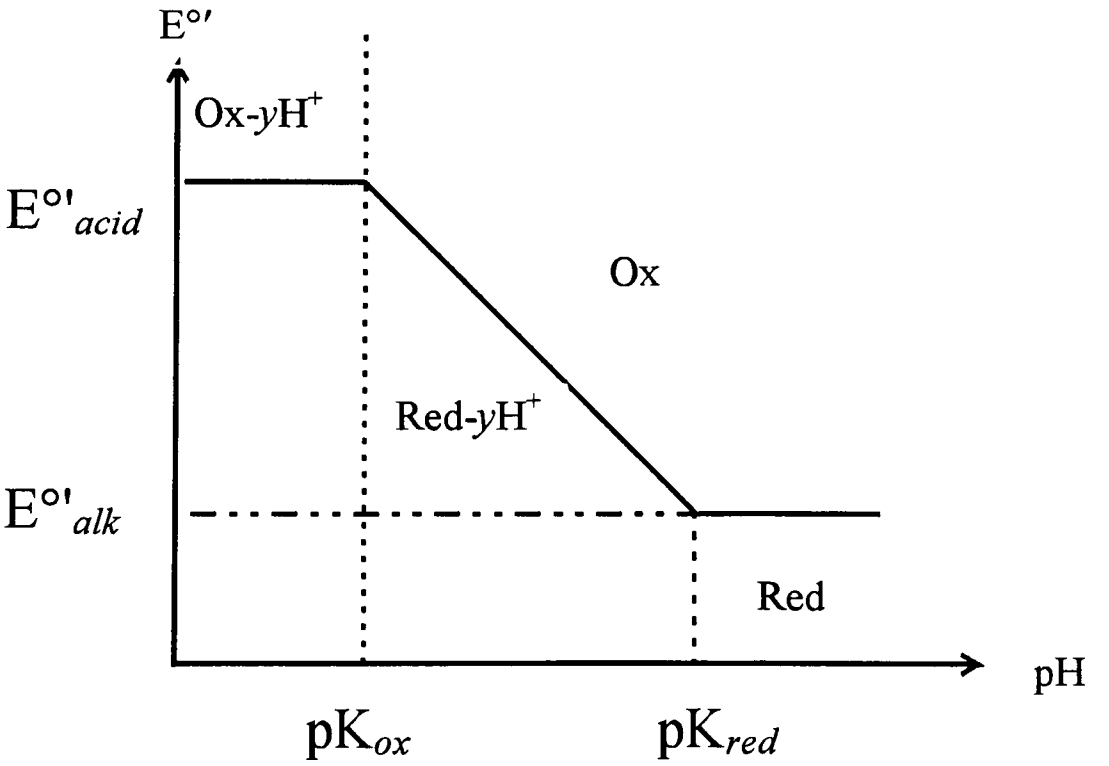

Figure 1.18 Schematic plot of E°' *versus* pH

From the gradient of this plot (in between pK_{ox} and pK_{red}) the proton to electron ratio can be estimated as follows (at 0 °C):

$\Delta E/\Delta pH$ = -54.2 mV per pH unit for one proton per electron (y/n = 1.0)

(i.e. $dE/dpH = -2.303RTy/nF$)

These calculations apply when there is strong coupling between the protonation and electron transfer. If the coupling is weaker, for example if the protonation site is far from the redox centre, then the gradients will not follow this idealised scheme, because pK_{ox} and pK_{red} may be very similar.

1.7.3.2 Kinetics

The kinetics of redox-coupled proton transfer can also be resolved by direct voltammetry and modelled to determine the kinetic parameters k_s, k_f, and k_b. If the rate of proton transfer becomes slower than the voltammetric scan rate applied, the coupled reactions of the square scheme can be resolved within the timescale of the voltammetry. Electron-transfer rates can be modelled according to Butler-Volmer theory[144] or, more recently using Marcus theory.[173,174] Consideration of the immobilised film configuration with respect to Marcus theory has recently been investigated by Armstrong *et al.*[118,175]

1.7.4 Summary

As described, the techniques of immobilised film voltammetry enable very detailed studies of complex biological molecules to be undertaken. They are especially useful when the protein is in short supply, and for observing redox centres which lie beyond the potential boundaries of commonly used chemical reductants and oxidants. The method is also useful for centres which are normally labile, and allows the kinetics of coupled reactions to be examined.

1.8 OTHER TECHNIQUES

1.8.1 EPR

A universal technique in bioinorganic chemistry today is Electron Paramagnetic Resonance (EPR) spectroscopy. Although not used directly as a tool in this thesis a short descriptive section is included here because EPR is so widely used in discussions, not only on FeS clusters, but on almost all bioinorganic molecules. EPR measures the interaction between a paramagnet and an applied magnetic field. Classically, the electron in a vacuum spins on its own axis creating a moving electric field and causing a magnetic moment. When an external magnetic field is applied the paramagnet can align either parallel or anti-parallel to the applied field. This energy difference between the two states is proportional to the field strength.

$$\Delta E = h\nu = g\,\mu_B B \qquad \textbf{Equation 1.16}$$

where, ΔE is the separation of the two Zeeman levels, ν, the frequency of radiation, μ_B is the Bohr magneton, B is the applied field and g is the 'g factor'.

A free electron in a vacuum exhibits an EPR resonance with a g value of 2.0023. Differences from this value are due to the spin-orbit interactions between the paramagnet and the environment, which are inherently dependent upon the chemical environment, and on the symmetry of the system. By comparisons and theoretical considerations g values obtained from experimental observations can enable identification of compounds.

Proteins containing FeS clusters possess broad and ill-defined UV/Vis spectra which makes elucidation and characterisation difficult. However they are ideal candidates for EPR investigation because they contain paramagnetic centres. The first example was carried out in 1960, by Beinert and Sands who detected a 'g = 1.94' signal in frozen biological samples and proposed this to come from non-haem iron.[1] Since then EPR has become an extremely useful technique for studying FeS cluster containing proteins.[176]

The EPR transitions of a compound are determined by the quantum mechanical spin (S) of the paramagnet. Thus the EPR signal of FeS clusters is dependent upon the oxidation

state, i.e. the number of unpaired electrons. The paramagnetism of a FeS cluster is due to spin coupling of high spin d^5 Fe^{3+} ions (S = 5/2) and d^6 Fe^{2+} ions (S = 2). This can occur in two ways: *ferromagnetically* (with parallel aligned spins) or *antiferromagnetically* (anti-parallel spins) and, hence, when there are more than two iron atoms the situation can be complex. It has been found by Mössbauer spectroscopy, NMR studies and theoretical calculations that the magnetic substructures of 4Fe and 3Fe clusters are made up of ferromagnetically coupled dimers.[78,133,177] These are then coupled *antiferromagnetically* to give the total spin of the cluster. Some typical values for FeS clusters are given in Table 1.4.

Species	**g_{obs} value**	**Spin of dimers**		**Spin of cluster**
[4Fe-4S]$^{2+}$	EPR silent	S = 9/2 (Fe^{2+}-Fe^{3+})	S = 9/2 (Fe^{2+}-Fe^{3+})	S = 0
[4Fe-4S]$^{1+}$	g ≈ 1.94	S = 9/2 (Fe^{2+}-Fe^{3+})	S = 4 (Fe^{2+}-Fe^{2+})	S = 1/2
[3Fe-4S]$^{1+}$	g ≈ 2.01	S = 2 (Fe^{3+}-Fe^{3+})	S = 5/2 Fe^{3+}	S = 1/2
[3Fe-4S]^{0}	g ≈ 8 -12	S = 9/2 (Fe^{3+}-Fe^{2+})	S = 5/2 Fe^{3+}	S = 2
[2Fe-2S]$^{2+}$	EPR silent	S = 5/2 Fe^{3+}	S = 5/2 Fe^{3+}	S = 0
[2Fe-2S]$^{1+}$	g ≈ 1.96	S = 5/2 Fe^{3+}	S = 2 Fe^{2+}	S = 1/2

Table 1.4 Spin states of FeS clusters

For the reduced [2Fe-2S]$^{1+}$ cluster, the two iron atoms are not equivalent and can be described as one Fe^{3+} and one Fe^{2+} ion (i.e. valence localised). In the oxidised cluster [2Fe-2S]$^{2+}$, the sulfur bridge allows for magnetic interaction between the two iron atoms.

1.8.2 MCD

As for EPR, magnetic circular dichroism (MCD) exploits the Zeeman splitting of electronic levels which occur when a paramagnetic sample is placed in a magnetic field. It is an optical technique which measures the differential absorption of left and right circularly polarised light by molecules in a magnetic field - a phenomenon first observed by Faraday in 1846. MCD is much more informative about FeS proteins than UV/Vis spectroscopy and can provide an informative fingerprint of the cluster type.[178] MCD signals are field and temperature dependent - a property that can be used to gain information about the ground-state g-values and spin values in the form of magnetisation curves (a record of signal intensity whilst the field or temperature is varied). The generation of magnetisation curves from frozen protein solutions did not routinely take place until 1980 due to limitations in electro-magnet design.

Although EPR has been the most convenient method of observing the presence of FeS clusters in proteins, the MCD magnetisation properties have provided an alternative way of characterising the spin and zero-field parameters of electronic ground states. The MCD spectra of FeS clusters are complex because of the range of electronic states and also the exchange coupling of the spin, on two or more centres, may relax the spin selection rules. If a cluster contains both high-spin Fe^{2+} and high-spin Fe^{3+} this means that a multitude of *d* states will be generated by exchange coupling, and with three or four Fe ions involved, the density of *d* states becomes very high. However, the allowed optical transitions from an exchange-coupled ground state will be minimal at very low temperatures, when the cluster is frozen into a single ground state component. Thus, at low temperature the MCD spectra of FeS clusters contains reasonably well resolved features - these will be due to thiolate-to-Fe^{3+} and S^{2-}-to-Fe^{3+} transitions. MCD spectra of all FeS clusters generally show features (i.e. optical transitions) across the whole spectrum from 200 to 2000 nm.[178]

MCD has been used to identify a pH-dependent form of both *Azotobacter chroococcum* Fd and the closely related ferredoxin I from *Azotobacter vinelandii*. Both of these proteins have been shown to take up one proton when reduced to the n = 0 oxidation level.[126,179] The exact position of protonation has not yet been established although an inorganic sulfur atom was proposed to be the site of protonation on the basis of the

changes observed in the MCD spectrum.[126,128] More recently the $[3Fe\text{-}4S]^{0}$ cluster present in the 7Fe Fd from *Sulfolobus acidocaldarius* (*Sa*) has also been shown to undergo redox-linked protonation.[79] In addition, the fully reduced cluster, $[3Fe\text{-}4S]^{2-}$, from *Sa* has also been characterised by MCD spectroscopy.[61] The spectrum of $[3Fe\text{-}4S]^{2-}$ shows little intensity at wavelengths longer than ca. 400 nm, which is consistent with the UV/Vis absorption spectrum, and the spectrum is similar to that of the Fe^{2+} state of the rubredoxin centre. Thus, the MCD transition of the hyper-reduced cluster lies in the region expected for Fe^{2+}-thiolate complexes and indeed, charge-transfer transitions involving Fe^{2+} and S^{2-} are also expected to be at similar wavelengths.

1.9 AIMS OF WORK

Since the discovery of FeS clusters in proteins, their varied forms together with their ability to encompass a wide range of oxidation states, means that they are an essential part of many biochemical redox reactions. Their growing role in more complicated reactions, other than simple electron-transfer, has meant that the study of the simpler cluster species, and understanding how these react and can change within their protein framework, has become essential in understanding how the more complex systems work. The work in this thesis encompasses FeS cluster chemistry and in particular the investigation of reactions other than simple electron transfer in 2Fe, 3Fe and 4Fe clusters.

1.9.1 The influence of cluster potential upon heterometal cluster formation

Although a number of studies have been carried out on heterometal clusters (e.g. [M3Fe-4S]) - in particular their spectroscopic characteristics - no previous work has investigated the mechanism of formation of these intriguing clusters. Understanding the factors which determine the formation of these clusters will help to explain why they are formed readily *in vitro* but are rarely (as yet) detected *in vivo* e.g. the FeMo cofactor of nitrogenase. Protein film voltammetry allows the potential, and hence redox state of the cluster, to be precisely controlled: *Chapters 3* and *6* describe the use of this technique to investigate the potential dependence of metal uptake in both *Desulfovibrio africanus* Fd III and *Pyrococcus furiosus* Fd.

1.9.2 The transient nature of exogenous ligand binding to *Desulfovibrio africanus* Fd III

Ligand transfer is a recognised function of a number of FeS proteins e.g. aconitase, but is not a universal trait of FeS clusters. Recently the discovery that ligand exchange occurs at the P-cluster of nitrogenase, and is likely to be directing the coupled electron/proton transfer, has increased the prominence of these reactions.[12] However, because of the transient nature of ligand transfer the reactions are often difficult to study. Protein film voltammetry is an ideal method because of the ease of transfer of an adsorbed protein film between different solutions. The direct redox control which is imposed can also be used to investigate the redox 'coupled' nature of these chemical reactions.

1.9.3 The influence of the protein co-ordination sphere of a 2Fe ferredoxin

The [2Fe-2S] ferredoxin from *Clostridium pasteurianum* belongs to an unusual subclass of 2Fe Fds and its function is unknown, although it has been proposed to interact with *Cp* nitrogenase.[48] When this study was initiated the residues ligating the cluster were not known, and a series of site directed mutants were therefore constructed to determine which residues co-ordinate the cluster. This provided a unique opportunity to investigate the influence of the different co-ordination spheres upon the cluster electrochemically.

1.9.4 Characterisation and investigation of the 4Fe Fd from *Pyrococcus furiosus*

The hyperthermophilic archaeon *Pyrococcus furiosus* exists at very high temperatures (T_{opt} = 100 °C) and consequently its proteins are adapted to an extreme environment.[180] *Pyrococcus furiosus* contains a 4Fe ferredoxin and comparisons can therefore be made between those 4Fe Fds obtained from mesophilic organisms and *Pf* Fd. *Pyrococcus furiosus* 4Fe Fd is also unusual in that it contains a convertible 4Fe cluster, which readily loses an Fe atom to become a 3Fe cluster. The absence of any other clusters which would complicate the response add to the suitability of this protein for electrochemical investigation. Thus, the $[3Fe\text{-}4S]^0$ cluster previously observed in 7Fe Fds[61] can be investigated in a protein which does not contain the additional [4Fe-4S] cluster. In addition, metal uptake reactions can be investigated in a hyperthermophilic protein and comparisons made with its mesophilic counterpart (*Section 1.9.1*).

1.10 REFERENCES

1) Beinert, H.; Sands, R. H. *Biochem. Biophys. Res. Commun.* **1960**, 41-46.

2) Johnson, M. K. *Encyclopedia of Inorganic Chemistry*; Wiley: Chichester:, **1994**; Vol. 4.

3) Beinert, H. *Faseb Journal* **1990**, *4*, 2483-2491.

4) Cammack, R. *Advances in Inorganic Chemistry*, **1992**; Vol. 38.

5) Matsubara, H.; Saeki, K. *Adv. Inorg. Chem.* **1992**, *38*, 223-280.

6) Beinert, H.; Holm, R. H.; Munck, E. *Science* **1997**, *277*, 653-659.

7) Beinert, H.; Kennedy, M. C.; Stout, C. D. *Chemical Reviews* **1996**, *96*, 2335-2373.

8) Grabowski, R.; Hofmeister, A. E. M.; Buckel, W. *TIBS* **1993**, 297-300.

9) Hofmeister, A. E. M.; Albracht, S. P. J.; Buckel, W. *Febs Letters* **1994**, *351*, 416-418.

10) Flint, D. H.; Allen, R. M. *Chemical Reviews* **1996**, *96*, 2315-2334.

11) Adams, M. W. W. *Biochim. Biophys. Acta* **1990**, 115-145.

12) Peters, J. W.; Stowell, M. H. B.; Soltis, S. M.; Finnegan, M. G.; Johnson, M. K.; Rees, D. C. *Biochemistry* **1997**, *36*, 1181-1187.

13) Burgess, B. K.; Lowe, D. J. *Chemical Reviews* **1996**, *96*, 2983-3011.

14) Haile, D. J.; Rouault, T. A.; Harford, J. B.; Kennedy, M. C.; Blondin, G. A.; Beinert, H.; Klausner, R. D. *Proceedings of the National Academy of Sciences of the United States of America* **1992**, *89*, 11735-11739.

15) Beinert, H.; Kiley, P. *Febs Letters* **1996**, *382*, 218-219.

16) Spiro, S.; Guest, J. R. *FEMS Microbiol. Rev.* **1990**, 399-428.

17) Khoroshilova, N.; Beinert, H.; Kiley, P. J. *Proceedings of the National Academy of Sciences of the United States of America* **1995**, *92*, 2499-2503.

18) Green, J.; Bennett, B.; Jordan, P.; Ralph, E. T.; Thomson, A. J.; Guest, J. R. *Biochem.J.* **1996**, *316*, 887-892.

19) Gaudu, P.; Weiss, B. *PNAS* **1996**, *89*, 10094.

20) Hidalgo, E.; Bollinger, J. M.; Bradley, T. M.; Walsh, C. T.; Demple, B. *Journal of Biological Chemistry* **1995**, *270*, 20908-20914.

21) Hildalgo, E.; Demple, B. *EMBO Journal* **1994**, *13*, 138-146.

22) Mulliez, E.; Fontecave, M.; Gaillard, J.; Reichard, P. *J. Biol. Chem.* **1993**, 2296-2299.

23) Petrovich, R. M.; Ruzicka, F. J.; Reed, G. H.; Frey, P. A. *J. Biol. Chem.* **1991**, 7656-7660.

24) Sanyal, I.; Cohen, G.; Flint, D. H. *Biochemistry* **1994**, 3625-3631.

25) Staples, C. R.; Ameyibor, E.; Fu, W. G.; Gardetsalvi, L.; Strittetter, A. L.; Schurmann, P.; Knaff, D. B.; Johnson, M. K. *Biochemistry* **1996**, *35*, 11425-11434.

26) Staples, C. R.; Gaymard, E.; StrittEtter, A. L.; Telser, J.; Hoffman, B. M.; Schurmann, P.; Knaff, D. B.; Johnson, M. K. *Biochemistry* **1998**, *37*, 4612-4620.

27) Hedderich, R.; Albracht, S. P. J.; Linder, D.; Koch, J.; Thauer, R. K. *FEBS Letters* **1992**, 65-68.

28) LeGall, J.; Prickril, B. C.; Moura, I.; Xavier, A. V.; Moura, J. J. G.; Huynh, B.-H. *Biochemistry* **1988**, 1636-1642.

29) Pierik, A. J.; Wolbert, R. B. G.; Portier, G. L.; Verhagen, M. F. J. M.; Hagen, W. R. *Eur. J. Biochem.* **1993**, 237-245.

30) Mortenson, L. E.; Valetine, R. C.; Carnahan, J. E. *Biochem. Biophys. Res. Commun.* **1962**, 448-452.

31) Buchanan, B. B.; Lovenberg, W.; Rabinowitz, J. C. *Proc. Nat. Acad. Sci. USA* **1963**, 345-353.

32) Beinert, H.; Lee, W. *Biochem. Biophys. Res. Commun.* **1961**, 40-45.

33) Gibson, J. F.; Hall, D. O.; Thornley, J. H. M.; Whately, F. R. *Proc. Nat. Acad. Sci. USA* **1966**, 987-990.

34) Herriott, J. R.; Sieker, L. C.; Jensen, L. H.; Lovenberg, W. *J. Mol. Biol.* **1970**, 391-406.

35) Fukuyama, K.; Hase, T.; Matsumoto, S.; Tsukihara, T.; Katsube, Y.; Tanake, N.; Kakudo, M.; Wada, K.; Matsubara, H. *Nature* **1980**, 522-524.

36) Adman, E. T.; Sieker, L. C.; Jensen, L. H. *J. Biol. Chem.* **1972**, 3987-3996.

37) Fukuyama, K.; Nagahara, Y.; Tsukihara, T.; Katsube, Y.; Hase, T.; Matsubara, H. *J. Mol. Biol.* **1988**, 183-193.

38) Cammack, R. *Nature* **1980**, *286*, 442.

39) Stout, C. D. *J. Biol. Chem.* **1988**, 9256-9260.

40) Stout, C. D. *J. Mol. Biol.* **1989**, 545-555.

41) Kissinger, C. R.; Adman, E. T.; Sieker, L. C.; Jensen, L. H.; Legall, J. *Febs Letters* **1989**, *244*, 447-450.

42) Kennedy, M. C.; Kent, T. A.; Emptage, M.; Merkle, H.; Beinert, H.; Münck, E. *J. Biol. Chem.* **1984**, 14463-14471.

43) Kim, J.; Rees, D. C. *Nature* **1992**, 553-560.

44) Kim, J.; Rees, D. C. *Science* **1992**, *257*, 1677-1682.

45) Chan, M. K.; Kim, J.; Rees, D. C. *Science* **1993**, 792-794.

46) Moura, I.; Huynh, B. H.; Hausinger, R. P.; LeGall, J.; Xavier, A. V.; Munck, E. *J. Biol. Chem* **1980**, *255*, 2493.

47) Dugad, L. B.; LaMar, G. N.; Banci, L.; Bertini, I. *Biochemistry* **1990**, *29*, 2263.

48) Golinelli, M. P.; Gagnon, J.; Meyer, J. *Biochemistry* **1997**, *36*, 11797-11803.

49) Trumpower, B. L. *Microbiol. Rev.* **1990**, *54*, 101.

50) Gurbiel, R. J.; Batie, C. J.; Sivaraja, M.; True, A. E.; Fee, J. A.; Hoffman, B. M.; Ballou, D. P. *Biochemistry* **1989**, *28*, 4861-4871.

51) Ohsawa, I.; Speck, D.; Kisou, T.; Hayakawa, K.; Zinsius, M.; Gloeckler, R.; Lemoine, Y.; Kamogawa, K. *Gene* **1989**, *80*, 39.

52) Meyer, J.; Fujinaga, J.; Gaillard, J.; Lutz, M. *Biochemistry* **1994**, *33*, 13642-13650.

53) Davidson, E.; Ohnishi, T.; Atta-Asafo-Adjei, E.; Daldal, F. *Biochemistry* **1992**, *31*, 3342.

54) Adman, E. T.; Watenpaugh, K. D.; Jensen, L. H. *Proc. Natl. Acad. Sci. U.S.A.* **1975**, 4854-4858.

55) Jensen, G. M.; Warshel, A.; Stephens, P. J. *Biochemistry* **1994**, *33*, 10911-10924.

56) Langen, R.; Jensen, G. M.; Jacob, U.; Stephens, P. J.; Warshel, A. *Journal of Biological Chemistry* **1992**, *267*, 25625-25627.

57) Backes, G.; Mino, Y.; Loehr, T. M.; Meyer, T. E.; Cusanovich, M. A.; Sweeney, W. V.; Adman, E. T.; Sanders-Loehr, J. *J. Am. Chem. Soc.* **1991**, 2055-2064.

58) Orme-Johnson, N. R.; Mims, W. B.; Orme-Johnson, W. H.; Bartsch, R. G.; Cusanovich, M. A.; Peisach, J. *Biochim. Biophys. Acta* **1983**, *748*, 68.

59) Verhagen, M. F. J. M.; Link, T. A.; Hagen, W. R. *FEBS Lett.* **1995**, 75-78.

60) Im, S.-C.; Lam, K.-Y.; Lim, M.-C.; Ooi, B.-L.; Sykes, A. G. *J. Am. Chem. Soc.* **1995**, 3635-3636.

61) Duff, J. L. C.; Breton, J. L. J.; Butt, J. N.; Armstrong, F. A.; Thomson, A. J. *Journal of the American Chemical Society* **1996**, *118*, 8593-8603.

62) Watt, G. D.; Reddy, K. R. N. *Journal of Inorganic Biochemistry* **1994**, *53*, 281-294.

63) Angove, H. C.; Yoo, S. J.; Burgess, B. K.; Munck, E. *Journal of the American Chemical Society* **1997**, *119*, 8730-8731.

64) Goh, C.; Segal, B. M.; Huang, J.; Lang, S. R.; Holm, R. H. *J. Am. Chem. Soc.* **1996**, *118*, 11844-11853.

65) Lindahl, P. A.; Day, E. P.; Kent, T. A.; Orme-Johnson, W. H.; Munck, E. *J. Biol. Chem.* **1985**, *260*, 11160.

66) Conover, R. C.; Kowal, A. T.; Fu, W.; Park, J. B.; Aono, S.; Adams, M. W. W.; Johnson, M. K. *Journal of Biological Chemistry* **1990**, *265*, 8533-8541.

67) Vollmer, S. J.; Switzer, R. L.; Debrunner, P. G. *Journal of Biological Chemistry* **1983**, *258*, 4284-4293.

68) George, S. J.; Armstrong, F. A.; Hatchikian, E. C.; Thomson, A. J. *Biochemical Journal* **1989**, *264*, 275-284.

69) Bruschi, M.; Guerlesquin, F. *FEMS Microbiol. Rev.* **1988**, 155-176.

70) Emptage, M. H.; Kent, T. A.; Huynh, B. H.; Rawlings, J.; Orme-Johnson, W. H.; Münck, E. *J. Biol. Chem.* **1980**, 1793-1796.

71) Robbins, A. H.; Stout, C. D. *Proteins* **1989**, *5*, 289.

72) Kissinger, C. R.; Adman, E. T.; Sieker, L. C.; Jensen, L. H. *Journal of the American Chemical Society* **1988**, *110*, 8721-8723.

73) Beinert, H.; Thomson, A. J. *Archives of Biochemistry and Biophysics* **1983**, *222*, 333-361.

74) Ackrell, B. A. C.; Johnson, M. K.; Gunsalus, R. P.; Cecchini, G. *Chemistry and Biochemistry of Flavoenzymes*; Ackrell, B. A. C.; Johnson, M. K.; Gunsalus, R. P.; Cecchini, G., Ed.; CRC Press: Boca Raton, **1992.**

75) Guigliarelli, B.; Asso, M.; More, C.; Augier, V.; Blasco, F.; Pommier, J.; Giordano, G.; Bertrand, P. *European Journal of Biochemistry* **1992**, *207*, 61-68.

76) Knaff, D. B.; Hirasawa, M.; Ameyibor, E.; Fu, W. G.; Johnson, M. K. *Journal of Biological Chemistry* **1991**, *266*, 15080-15084.

77) Vanoni, M. A.; Edmondson, D. E.; Zanetti, G.; Curti, B. *Biochemistry* **1992**, *31*, 4613-4623.

78) Papaefthymiou, V.; Girerd, J.-J.; Moura, I.; Moura, J. J. G.; Münck, E. *J. Am. Chem. Soc.* **1987**, 4703-4710.

79) Breton, J. L.; Duff, J. L. C.; Butt, J. N.; Armstrong, F. A.; George, S. J.; Petillot, Y.; Forest, E.; Schafer, G.; Thomson, A. J. *European Journal of Biochemistry* **1995**, *233*, 937-946.

80) Duff, J. L. C. *Ph. D. Thesis*; University of Oxford:, **1996.**

81) Georgiadis, M. M.; Komiya, H.; Chakrabarti, P.; Woo, D.; Kornuc, J. J.; Rees, D. C. *Science* **1992**, *257*, 1653-1659.

82) Kim, J.; Woo, D.; Rees, D. C. *Biochem.* **1993**, *32*.

83) Knaff, D. B.; Hirasawa, M. *Biochimica Et Biophysica Acta* **1991**, *1056*, 93-125.

84) Volbeda, A.; Charon, M.-H.; C., P.; Hatchikian, E. C.; Frey, M.; Fontecilla-Camps, J. C. *Nature* **1995**, 580-587.

85) Fontecilla-Camps, J. C. *J. Biol. Inorg. Chem.* **1996**, 91-98.

86) Albracht, S. P. J. *Biochim. Biophys. Acta* **1994**, 167-204.

87) Teixeira, M.; Moura, I.; Xavier, A. V.; Moura, J. J. G.; LeGall, J.; DerVartanian, D. V.; Peck, H. D.; Huynh, B.-H. *J. Biol. Chem.* **1989**, 16435-16450.

88) Przybyla, A. E.; Robbins, J.; Menon, N.; Peck, H. D. *FEMS Microbiol. Rev.* **1992**, 109-136 and references therein.

89) Moura, J. J. G.; Moura, I.; Kent, T. A.; Lipscomb, J. D.; Huynh, B. H.; Legall, J.; Xavier, A. V.; Munck, E. *Journal of Biological Chemistry* **1982**, *257*, 6259-6267.

90) Kent, T. A.; Dreyer, J. L.; Kennedy, M. C.; Huynh, B. H.; Emptage, M. H.; Beinert, H.; Munck, E. *Proceedings of the National Academy of Sciences of the United States of America-Biological Sciences* **1982**, *79*, 1096-1100.

91) Finnegan, M. G.; Conover, R. C.; Park, J. B.; Zhou, Z. H.; Adams, M. W. W.; Johnson, M. K. *Inorganic Chemistry* **1995**, *34*, 5358-5369.

92) Srivastava, K. K. P.; Surerus, K. K.; Conover, R. C.; Johnson, M. K.; Park, J. B.; Adams, M. W. W.; Munck, E. *Inorganic Chemistry* **1993**, *32*, 927-936.

93) Surerus, K. K.; Munck, E.; Moura, I.; Moura, J. J. G.; Legall, J. *Journal of the American Chemical Society* **1987**, *109*, 3805-3807.

94) Butt, J. N.; Armstrong, F. A.; Breton, J.; George, S. J.; Thomson, A. J.; Hatchikian, E. C. *Journal of the American Chemical Society* **1991**, *113*, 6663-6670.

95) Butt, J. N.; Fawcett, S. E. J.; Breton, J.; Thomson, A. J.; Armstrong, F. A. *Journal of the American Chemical Society* **1997**, *119*, 9729-9737.

96) Moura, I.; Moura, J. J. G.; Munck, E.; Papaefthymiou, V.; Legall, J. *Journal of the American Chemical Society* **1986**, *108*, 349-351.

97) Moreno, C.; Macedo, A. L.; Moura, I.; Legall, J.; Moura, J. J. G. *Journal of Inorganic Biochemistry* **1994**, *53*, 219-234.

98) Conover, R. C.; Park, J. B.; Adams, M. W. W.; Johnson, M. K. *Journal of the American Chemical Society* **1990**, *112*, 4562-4564.

99) Staples, C. R.; Dhawan, I. K.; Finnegan, M. G.; Dwinell, D. A.; Zhou, Z. H.; Huang, H. S.; Verhagen, M.; Adams, M. W. W.; Johnson, M. K. *Inorganic Chemistry* **1997**, *36*, 5740-5749.

100) Butt, J. N.; Sucheta, A.; Armstrong, F. A.; Breton, J.; Thomson, A. J.; Hatchikian, E. C. *Journal of the American Chemical Society* **1991**, *113*, 8948-8950.

101) Fu, W. G.; Telser, J.; Hoffman, B. M.; Smith, E. T.; Adams, M. W. W.; Finnegan, M. G.; Conover, R. C.; Johnson, M. K. *Journal of the American Chemical Society* **1994**, *116*, 5722-5729.

102) Butt, J. N.; Niles, J.; Armstrong, F. A.; Breton, J.; Thomson, A. J. *Nature Structural Biology* **1994**, *1*, 427-433.

103) Vo, E.; Wang, H. C.; Germanas, J. P. *Journal of the American Chemical Society* **1997**, *119*, 1934-1940.

104) Morgan, T. V.; Stephens, P. J.; Devlin, F.; Stout, C. D.; Melis, K. A.; Burgess, B. K. *Proceedings of the National Academy of Sciences of the United States of America-Biological Sciences* **1984**, *81*, 1931-1935.

105) Stephens, P. J.; Morgan, T. V.; Devlin, F.; Pennerhahn, J. E.; Hodgson, K. O.; Scott, R. A.; Stout, C. D.; Burgess, B. K. *Proceedings of the National Academy of Sciences of the United States of America* **1985**, *82*, 5661-5665.

106) Manodori, A.; Cecchini, G.; Schroder, I.; Gunsalus, R. P.; Werth, M. T.; Johnson, M. K. *Biochemistry* **1992**, *31*, 2703-2712.

107) Rothery, R. A.; Weiner, J. H. *Biochemistry* **1991**, *30*, 8296-8305.

108) Anderson, G. L.; Howard, J. B. *Biochemistry* **1984**, *23*, 2118-2122 To:.

109) Ryle, M. J.; Lanzilotta, W. N.; Seefeldt, L. C.; Scarrow, R. C.; Jensen, G. M. *J. Biol.Chem.* **1996**, *271*, 1551-1557.

110) Khoroshilova, N.; Popescu, C.; Munck, E.; Beinert, H.; Kiley, P. J. *Proceedings of the National Academy of Sciences of the United States of America* **1997**, *94*, 6087-6092.

111) Duin, E. C.; Lafferty, M. E.; Crouse, B. R.; Allen, R. M.; Sanyal, I.; Flint, D. H.; Johnson, M. K. *Biochemistry* **1997**, *36*, 11811-11820.

112) Mitchell, R.; Rich, P. R. *Biochem. Biophys. Acta* **1994**, 19-26.

113) Smith, B. E.; Eady, R. R. *Eur. J. Biochem.* **1992**, 1-15.

114) Sellman, D.; Mahr, G.; Knoch, F.; Moll, M. *Inorg. Chim. Acta* **1994**, 45-59.

115) Duyvis, M. G.; Wassink, H.; Haaker, H. *Eur. J. Biochem.* **1994**, 881-890.

116) Shin, W.; Stafford, P. R.; Lindahl, P. A. *Biochemistry* **1992**, 6003-6011.

117) Crane, B. R.; Siegel, L. M.; Getzoff, E. D. *Science* **1995**, 59-67.

118) Armstrong, F. A.; Heering, H. A.; Hirst, J. *Chemical Society Reviews* **1997**, *26*, 169-179.

119) Hirst, J.; Duff, J. L. C.; Jameson, G. N. L.; Kemper, M. A.; Burgess, B. K.; Armstrong, F. A. *Journal of the American Chemical Society* **1998**, 120, 7085-7094

120) Tsai, H.; Sweeney, W. V.; Coyle, C. L. *Inorg. Chem.* **1985**, 2796-2798.

121) Henderson, R. A.; Oglieve, K. E. *Journal of the Chemical Society-Chemical Communications* **1994**, 377-379.

122) Nakamoto, M.; Tanaka, K.; Tanaka, T. *Bull. Chem. Soc. Japan* **1988**, 4099-4105.

123) Magliozzo, R. S.; McIntosh, B. A.; Sweeney, W. V. *Journal of Biological Chemistry* **1982**, *257*, 3506-3509.

124) Anemuller, S.; Schmidt, C. L.; Schafer, G.; Bill, E.; Trautwein, A. X.; Teixeira, M. *Biochemical and Biophysical Research Communications* **1994**, *202*, 252-257.

125) Link, T. A.; Hagen, W. R.; Pierik, A. J.; Assmann, C.; Vonjagow, G. *European Journal of Biochemistry* **1992**, *208*, 685-691.

126) George, S. J.; Richards, A. J. M.; Thomson, A. J.; Yates, M. G. *Biochem. J.* **1984**, 247-251.

127) Johnson, M. K.; Bennett, D. E.; Fee, J. A.; Sweeney, W. V. *Biochim. Biophys. Acta.* **1987**, 81-94.

128) Stephens, P. J.; Jensen, G. M.; Devlin, F. J.; Morgan, T. V.; Stout, C. D.; Martin, A. E.; Burgess, B. K. *Biochemistry* **1991**, 3200-3209.

129) Stout, C. D. *J. Biol. Chem.* **1993**, 25920-25927.

130) Shen, B. H.; Martin, L. L.; Butt, J. N.; Armstrong, F. A.; Stout, C. D.; Jensen, G. M.; Stephens, P. J.; Lamar, G. N.; Gorst, C. M.; Burgess, B. K. *Journal of Biological Chemistry* **1993**, *268*, 25928-25939.

131) Noodleman, L.; Case, D. A.; Aizman, A. *J. Am. Chem. Soc.* **1988**, 1001-1005.

132) Noodleman, L.; Norman, J. G., Jr.; Osborne, J. H.; Aizman, A.; Case, D. A. *J.Am. Chem. Soc.* **1985**, 3418-3426.

133) Noodleman, L.; Case, D. A. *Adv. Inorg. Chem.* **1992**, 423-470.

134) Zhou, J.; Holm, R. H. *Journal of the American Chemical Society* **1995**, *117*, 11353-11354.

135) Zhou, J.; Hu, Z. G.; Munck, E.; Holm, R. H. *Journal of the American Chemical Society* **1996**, *118*, 1966-1980.

136) Zhou, J.; Raebiger, J. W.; Crawford, C. A.; Holm, R. H. *Journal of the American Chemical Society* **1997**, *119*, 6242-6250.

137) Flint, D. H.; Emptage, M. H. *Journal of Biological Chemistry* **1988**, *263*, 3558-3564.

138) Thomson, A. J. *FEBS Lett.* **1991**, 230-236.

139) Lazazzera, B. A.; Beinert, H.; Khoroshilova, N.; Kennedy, M. C.; Kiley, P. J. *Journal of Biological Chemistry* **1996**, *271*, 2762-2768.

140) Nicholson, R. S.; Shain, I. *Anal. Chem.* **1964**, 706-723.

141) Nicholson, R. S. *Anal. Chem.* **1965**, 1351-1355.

142) Bard, A. J.; Faulkner, L. R. *Electrochemical Methods; Fundamentals and Applications*; Wiley: New York, **1980.**

143) Laviron, E. *J. Electroanal. Chem.* **1974**, 355-393.

144) Laviron, E. *J. Electroanal. Chem.* **1979**, 19-28.

145) Southampton Electrochemistry Group *Instrumental Methods in Electrochemistry*; Ellis Horwood: Chichester, **1985.**

146) Armstrong, F. A. *Structure and Bonding* **1990**, *72*, 137-230.

147) Bond, A. M.; Hill, H. A. O. *Metal Ions in Biological Systems*; Bond, A. M.; Hill, H. A. O., Ed.; Marcel Dekker: New York, 1991; Vol. 27, pp 431-494.

148) Hill, H. A. O.; Hunt, N. I. *Methods in Enzymology* **1993**, 501-522.

149) Armstrong, F. A.; Butt, J. N.; Sucheta, A. *Methods in Enzymology* **1993**, *227*, 479-500.

150) Wilson, G. S. *Methods in Enzymology* **1978**, 396-410.

151) Eddowes, M. J.; Hill, H. A. O. *J. Chem. Soc. Chem. Commun.* **1977**, 771-772.

152) Eddowes, M. J.; Hill, H. A. O. *J. Am. Chem. Soc.* **1979**, 4461-4464.

153) Yeh, P.; Kuwana, T. *Chem. Lett.* **1977**, 1145-1148.

154) Armstrong, F. A. *Bioelectrochemistry of Biomacromolecules*; Birkhauser: Basel, **1997**; Vol. 5.

155) Weitzman, P. D. J.; Kennedy, I. R.; Caldwell, R. A. *FEBS Lett.* **1971**, 241-244.

156) Kuznetzov, B. A.; Mestechkina, N. M.; Shumankovich, G. P. *Bioelectrochem. Bioenerg.* **1977**, 1-17.

157) Ikeda, T.; Toriyama, K.; Senda, M. *Bull. Chem. Soc. Japan* **1979**, 1937-1943.

158) Bianco, P.; Haladjian, J. *Biochem. Biophys. Res. Commun.* **1977**, 323-327.

159) Armstrong, F. A.; Cox, P. A.; Hill, H. A. O.; Lowe, V. J.; Oliver, B. N. *Journal of Electroanalytical Chemistry and Interfacial Electrochemistry* **1987**, *217*, 331-366.

160) Panzer, R. E.; Elving, P. J. *Electrochim. Acta* **1975**, 635-647.

161) Kamou, G. N.; Willis, W. S.; Rusling, J. F. *Anal. Chem.* **1985**, 545-551.

162) Armstrong, F. A.; Cox, P. A.; Hill, H. A. O.; Oliver, B. N.; Williams, A. A. *Journal of the Chemical Society-Chemical Communications* **1985**, 1236-1237.

163) Armstrong, F. A.; Hill, H. A. O.; Oliver, B. N. *Journal of the Chemical Society-Chemical Communications* **1984**, 976-977.

164) Armstrong, F. A.; Hill, H. A. O.; Walton, N. J. *Febs Letters* **1982**, *145*, 241-244.

165) Armstrong, F. A.; Hill, H. A. O.; Oliver, B. N.; Whitford, D. *Journal of the American Chemical Society* **1985**, *107*, 1473-1476.

166) Armstrong, F. A.; Lannon, A. M. *Journal of the American Chemical Society* **1987**, *109*, 7211-7212.

167) Armstrong, F. A.; Lannon, A. M. *Biochemical Society Transactions* **1988**, *16*, 842-843.

168) Armstrong, F. A.; Hill, H. A. O.; Walton, N. J. *Accounts of Chemical Research* **1988**, *21*, 407-413.

169) Brunschwig, B. S.; Sutin, N. *J. Am. Chem. Soc.* **1989**, 7454-7465.

170) Bond, A. M.; Oldham, K. B. *J. Phys. Chem.* **1983**, 2492-2502.

171) Armstrong, F. A. *Journal of Biological Inorganic Chemistry* **1997**, *2*, 139-142.

172) Butt, J. N.; Sucheta, A.; Armstrong, F. A.; Breton, J.; Thomson, A. J.; Hatchikian, E. C. *Journal of the American Chemical Society* **1993**, *115*, 1413-1421.

173) Chidsey, C. E. D. *Science* **1991**, 919-922.

174) Weber, K.; Creager, S. E. *Anal. Chem.* **1994**, 3164-3172.

175) Hirst, J.; Armstrong, F. A. *Submitted* **1998**.

176) Hagen, W. R. *Adv. Inorg. Chem.* **1992**, 165-222.

177) Bertini, I.; Ciurli, S.; Luchinat, C. *Structure and Bonding Vol. 83*; Bertini, I.; Ciurli, S.; Luchinat, C., Ed.; Springer-Verlag: Berlin Heidelberg, **1995**, pp 1-54.

178) Thomson, A. J.; Cheeseman, M. R.; George, S. J. *Meth. Enzym.* **1993**, 199-231.

179) Armstrong, F. A.; George, S. J.; Thomson, A. J.; Yates, M. G. *Febs Letters* **1988**, *234*, 107-110.

180) Fiala, G.; Stetter, K. O. *Archives of Microbiology* **1986**, *145*, 56-61.

CHAPTER 2

EXPERIMENTAL METHODS

CHAPTER 2

EXPERIMENTAL METHODS

This chapter details the experimental methods and procedures which were used in this thesis. Where particular experiments required specific procedures, these are detailed in the relevant chapters.

2.1 PROTEIN PREPARATION AND PURIFICATION

2.1.1 Sources of Protein

Cells of *Pyrococcus furiosus* (*Pf*) (strain vc1) DSM 3638 were supplied by Drs. N. Raven and R. Sharp (Centre for Applied Microbiology and Research, Porton Down, UK).[1] The ferredoxin was isolated and purified (*Section 2.1.4*) using a similar methodology to that which had been used successfully to purify similar ferredoxins e.g. the 7Fe Fd from *Sulfolobus acidocaldarius*.[2,3] The 7Fe ferredoxin (Fd III) from *Desulfovibrio africanus* (*Da*), strain Benghazi (NCIB 8401), was provided by Dr. E. C. Hatchikian (Laboratoire de Chimie Bacterienne, CNRS, Marseilles, France) and had been purified as described in the literature.[4] The recombinant 2Fe ferredoxin and various mutants, from *Clostridium pasteurianum* (*Cp*) were provided by Dr. J. Meyer (CEA, Grenoble, France) and these were prepared and purified as described in the literature.[5,6] All proteins were stored as concentrated 'beads' in liquid nitrogen until required.

2.1.2 Diafiltration

For all experiments in this thesis, protein samples were dialysed into the desired buffer-electrolyte solution using an Amicon 8MC unit. For small sample volumes (< 1 ml) this unit was equipped with a microvolume assembly, for large volumes (> 5 ml), an Amicon 8010 unit was used. Diafiltration of samples was achieved using a YM3 membrane

(excluding molecular weights > 3 kDa) for all the ferredoxins studied. The system was operated at 2 bar nitrogen gas in a refrigerator at 4 °C. Buffer exchange was assumed to be complete when a volume of fresh buffer equivalent to five times the initial volume, had passed through the membrane.

2.1.3 Protein Concentration

Protein concentration of the ferredoxins was determined from the UV/Vis absorption spectrum, using the published extinction coefficients quoted in Table 2.1. Spectra were recorded using a Hitachi U-3210 spectrophotometer fitted with 1 cm, (1 ml) quartz cuvettes (Hellma).

	Extinction Coefficient	
Ferredoxin	**λ (nm)**	**ε ($M^{-1}cm^{-1}$)**
Desulfovibrio africanus Fd III[7]	408	28,600
Pyrococcus furiosus 4Fe Fd[8]	390	17,000
Pyrococcus furiosus 3Fe Fd[8]	408	18,000

Table 2.1 Extinction coefficients of the ferredoxins investigated

Extinction coefficients for the oxidised forms of the cluster, $[3Fe\text{-}4S]^{1+}$ and $[4Fe\text{-}4S]^{2+}$

2.1.4 Purification of *Pyrococcus furiosus* Ferredoxin

The ferredoxin was isolated and purified using a similar methodology to that which had been used successfully to purify similar ferredoxins e.g. the 7Fe Fd from *Sulfolobus acidocaldarius*.[2,3] After each stage the protein sample containing the ferredoxin was concentrated in an Amicon using a YM3 membrane and dialysed into the buffer required for the next stage.

2.1.4.1 Primary Purification of *Pf* Fd[a]

Preparation of cell-free extract

The cells were suspended in 50 mM Tris/HCl buffer (Sigma) at pH 7.6, containing 2 mM dithiothreitol (Sigma), 5 mM $MgCl_2$ (BDH), 0.1 mg ml^{-1} DNase I (Sigma), 20 μM pepstatin (Sigma) and 20 μM leupeptin (Sigma). Lysozyme (Sigma) 1 mg ml^{-1} was added to the cell suspension and the resultant mixture was agitated on a shaker for 2 hours at 37 °C. This mixture was then centrifuged at 30,000 g for 30 minutes at 4 °C, to separate the insoluble matter from the soluble proteins. The supernatant was subsequently decanted and ultracentrifuged at 150,000 g for 3 hours.

Anion exchange chromatography

The supernatant was loaded onto a column (2 × 40 cm) of DE-52 DEAE-cellulose (Whatman) which had been pre-equilibrated with 50 mM Tris-HCl buffer pH 7.6, 2 mM dithiothreitol. The ferredoxin was eluted with a linear gradient of NaCl (0-0.6 M in 50 mM Tris-HCl, pH 7.6). Fractions were assayed, and those with a A_{390}/A_{280} ratio greater than 30 % of the maximum A_{390}/A_{280} ratio were retained.

Gel filtration

The retained fractions from the anion exchange chromatography were concentrated and subjected to chromatography on a column (2 × 100 cm) of Sephacryl S100HR (Pharmacia). The column was equilibrated and eluted using a pump (Pharmacia; flow rate 0.6 - 0.8 ml min^{-1}) with 50 mM Tris/HCl buffer, containing 100 mM NaCl, 2 mM dithiothreitol, pH 7.6. Fractions were kept if their A_{390}/A_{280} ratio was greater than 50 % of the maximum.

In total the purification procedure for *Pf* Fd was carried out on three separate occasions. No differences were observed between any of the three different preparations. The typical yield was 25 mg ferredoxin per 100 g of *Pf* cells.

---

[a] All stages of the primary purification of *Pf* Fd were carried out aerobically. Although it was known that this would lead to degradation of some of the 4Fe clusters, a complete anaerobic purification was impractical. This 'mixture' of 4Fe and 3Fe protein obtained after the primary purification was separated into pure samples by the secondary purification stage using FPLC (*Section 2.1.4.2*).

2.1.4.2 Secondary Purification of *Pf* Fd

Degradation of the 4Fe cluster to the 3Fe cluster was found to have occurred as a result of the aerobic preparation of the protein, hence a mixture of products was isolated.[b] It was thus necessary to perform a second purification step, by FPLC, to ensure a homogeneous protein sample. This step was carried out under anaerobic conditions.

In the initial preparation the retained fractions obtained from the gel filtration column were concentrated and dialysed into 50 mM Tris-HCl buffer pH 7.6 and loaded onto a Mono-Q anion exchange column (Pharmacia). The protein was then eluted with a linear 0-1.0 M NaCl gradient. Two major fractions were collected. On the basis of their UV/Vis spectra, Fraction 1 (λ_{max} = 390 nm) and Fraction 2 (λ_{max} = 408 nm) comprised, respectively, the [4Fe-4S] and [3Fe-4S] forms of the ferredoxin (Figure 2.1). Approximately 60 % degradation of the 4Fe cluster to the 3Fe cluster occurred as a direct result of the aerobic purification.

[b] This was determined by a preliminary cyclic voltammetry experiment (see *Chapter 6*).

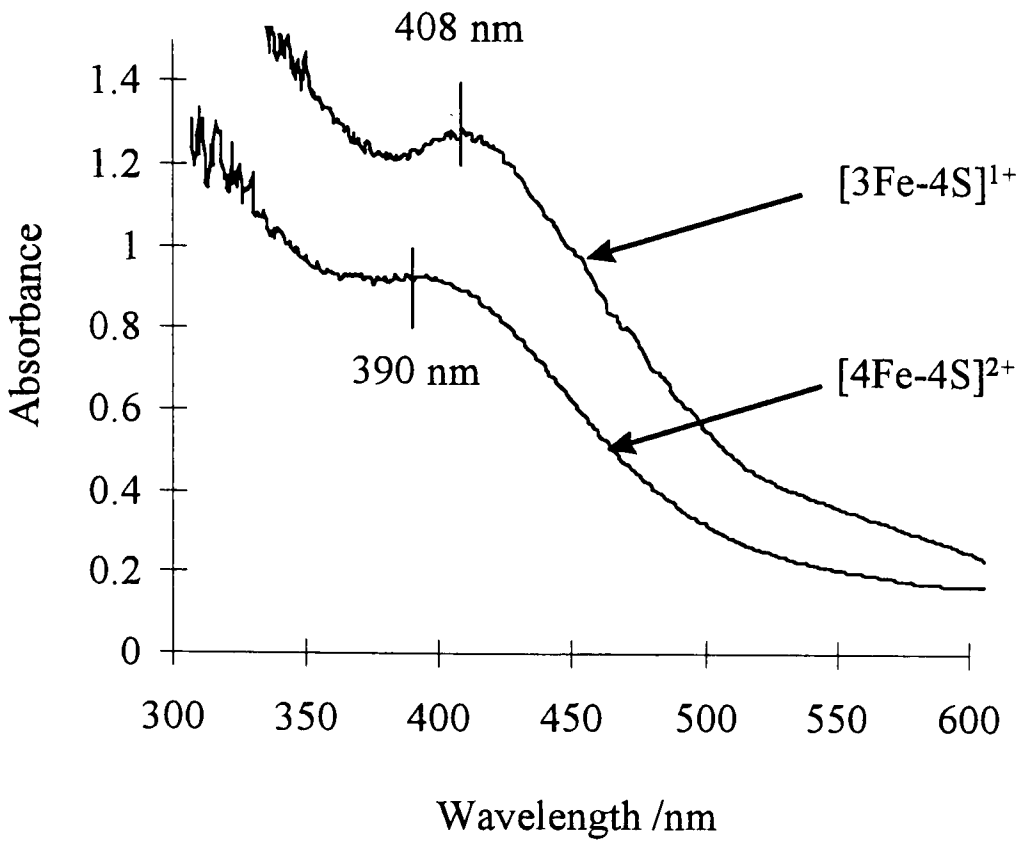

Figure 2.1 UV/Vis spectra of *Pyrococcus furiosus* ferredoxin (oxidised)

Spectra recorded using a MG-6000 diode-array spectrometer unit (Hi-Tech Scientific, Salisbury, UK). Both the [4Fe-4S]$^{2+}$ and [3Fe-4S]$^{1+}$ forms of the ferredoxin are shown, protein concentrations are 56 μM and 70 μM respectively. Peak maxima for each species are marked.

The secondary purification stage was then further refined to collect a minimum of 95 % of the Fd in one form. This was achieved by pre-oxidising the combined Fd sample obtained from the gel filtration column, before loading onto the Mono-Q column. Pre-oxidation was achieved by heating the sample to 60 °C for 30 minutes in the presence of a five-fold molar excess of ferricyanide (Aldrich). This ensured that almost all of the protein was subsequently in the 3Fe form before loading onto the Mono-Q column. Thus, maximum yields of the Fd in only the 3Fe Fd state were obtained. Manipulation of the 3Fe Fd form could then be carried out to generate the other forms of *Pf* Fd, (see *Chapter 6* for a full description of these methods). *Pf* Fd also contains a disulfide bridge[9] and so the final stage of purification was to determine the status of the disulfide bridge.

2.1.5 Determination of the Disulfide Bridge Status (see also *Section 6.2.3*)

The free thiol content of the various protein preparations was determined spectrophotometrically by their reaction with Ellman's reagent, 5,5'-dithio*bis*(2-nitrobenzoic acid) (DTNB; Aldrich) as described by Riddles *et al.*[10] This reagent is water-soluble, may be used at neutral pH with few side-reactions and its reaction with thiols is fast.[c] It is a very sensitive test - the sensitivity originates from the high molar absorption co-efficient of the 2-nitro-5-thiobenzoate anion (TNB^{2-}), which is produced together with the mixed disulfide from the reaction of a thiolate anion (RS^-) with $DTNB^{2-}$ (Figure 2.2).

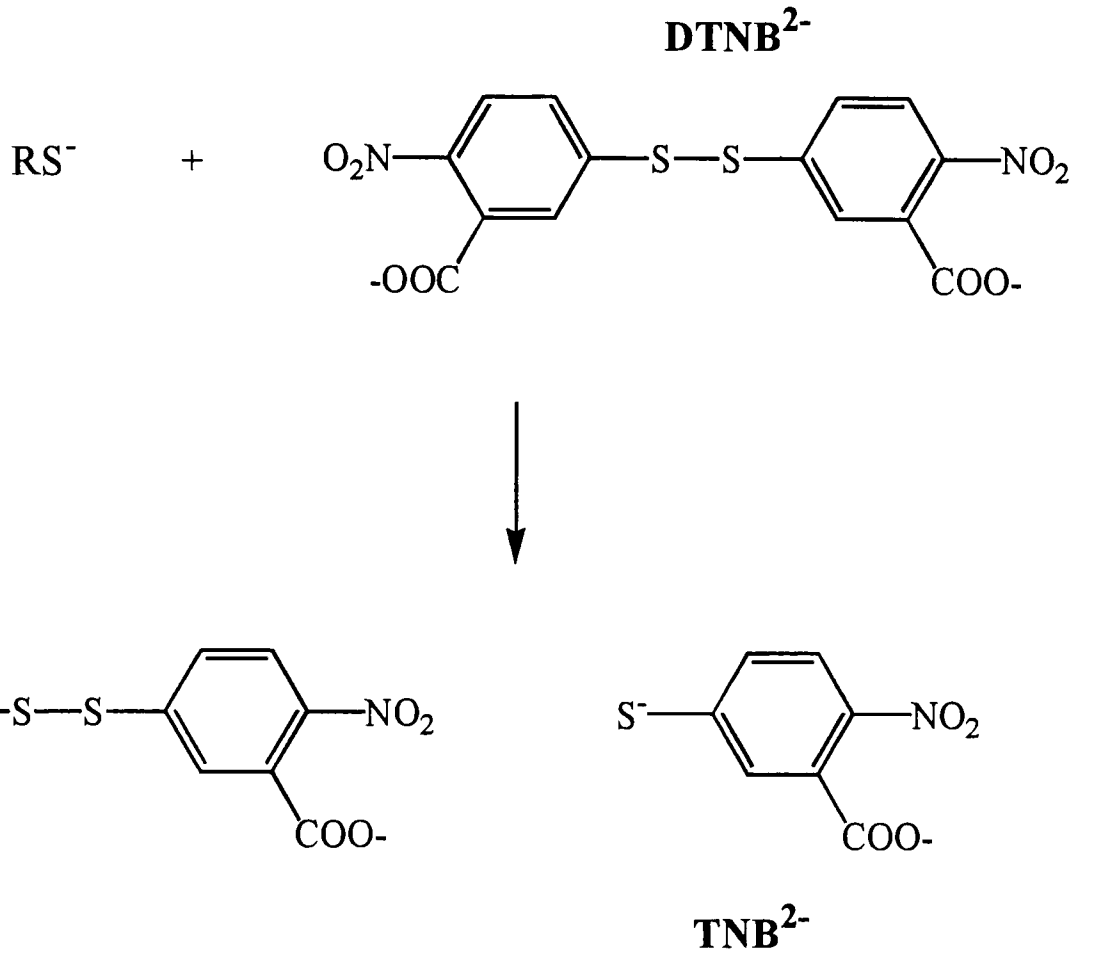

Figure 2.2 The reaction of free thiol with DTNB

The stock buffer for the spectroscopic assay was 0.1 M phosphate, 1 mM EDTA at pH 7.27. The stock solution of DTNB was 7 mM DTNB, made up in the stock buffer. To measure the free thiol content of a protein, the following procedure was used. In a

[c] Reaction may be slower for proteins which have their thiol groups 'buried' so making them less accessible to DTNB.

cuvette a known amount of the protein solution[d] was added to the stock buffer and the absorbance at 412 nm was recorded for 1- 2 minutes to ensure a steady baseline. An aliquot of the 7 mM DTNB reagent was added (total volume 1.0 ml), the cuvette was stirred well to ensure complete mixing of the reactants, and the absorbance at 412 nm monitored until no further change was observed (generally no longer than 30 minutes). The ΔA_{412} allowed the concentration of the free thiol in the protein to be calculated using a value of $\varepsilon_{412} = 14{,}150\ M^{-1}\,cm^{-1}$ for TNB^{2-}.[10]

$$\Delta A_{412} = A_{final} - A_{initial} - A_{DTNB} \qquad \textbf{Equation 2.1}$$

$$\Delta A_{412} = \varepsilon_{412}\,[\text{R-SH}] \qquad \textbf{Equation 2.2}$$

Where $A_{initial}$ is the absorbance at 412 nm of the buffer and protein solution, A_{final} is the final absorbance at 412 nm after reaction is complete and A_{DTNB} is the absorbance contribution at 412 nm of the added DTNB reagent.

Knowing the concentration of free thiol in the solution allows the ratio of free thiol:protein to be calculated because a *known* amount of protein was added to the cuvette. A typical titration of the protein with the disulfide bridge broken, $\mathbf{Fd_B}$, gave a free thiol content of 2 ± 0.1 moles of -SH per protein molecule. Samples of $\mathbf{Fd_A}$ did not show any reactivity when the reagent DTNB was added (i.e. increase in A_{412} was negligible). A scheme for the various interconversions of *Pf* Fd, in either the 4Fe or 3Fe Fd, is given in *Chapter 6*.

[d] Concentration of the protein solution was determined prior to the experiment, using the molar absorption co-efficient as listed in Table 2.1.

2.2 BUFFERS AND CO-ADSORBATES

The vast majority of electrochemical experiments in this thesis were carried out in an anaerobic glove box (Belle Technology, Dorset, UK) under an inert nitrogen atmosphere ($O_2 < 2$ ppm). For the few experiments which were carried out aerobically, the electrolyte solution in the electrochemical cell was thoroughly degassed by passing argon through it immediately prior to commencing a voltammetric scan. For bulk electrolysis experiments, the catalysts in the Belle Technology glove box were freshly regenerated to obtain a very low partial pressure of O_2 (< 1 ppm). All buffers were thoroughly degassed with argon before introduction into the glove box.

Previous electrochemical investigations of proteins have shown that metal ion contamination must be kept to a minimum for optimal results,[11] consequently, deionised water of resistivity 18 MΩm (Millipore) was used for preparing all solutions and washing glassware. Throughout this thesis all the chemicals used were of at least analytical reagent grade. Glassware was rinsed thoroughly with the chelator EGTA (ethene glycol-*O,O'-bis*(2aminoethyl)-*N,N,N',N'-tetra*-acetic acid; Aldrich) before use and electrochemical cells were stored containing a solution of approximately 25 mM EGTA.

2.2.1 pH Measurement

The pH of solutions were recorded at the temperature at which the experiments were performed, using an Accumet 950 pH-meter (Fisher), equipped with a combination glass pH electrode (BDH). The pH-meter was calibrated at the required temperature with three standard buffers (BDH) immediately before use.

2.2.2 Buffer-electrolyte solutions

Buffers were selected to cover a pH range of approximately ± 0.5 pH units either side of their pK_a. The supporting electrolyte was generally 0.1 M NaCl (BDH). Buffers used are listed in Table 2.2.

Buffer	Chemical name	pK_a	Supplier
Acetic acid	Glacial acetic acid	4.8	BDH
Mes	2-[*N*-morpholino]ethanesulfonic acid	6.1	Sigma
Hepes	N-[2-hydroxyethyl]piperazine-*N*-[2-ethanesulfonic acid]	7.4	Sigma
Tris	tri[hydroxymethyl]aminomethane, Trizma base	8.1	Sigma
Taps	*N*-tris[hydroxymethyl]methyl-3-amino-propanesulfonic acid	8.4	Sigma

Table 2.2 Biochemical buffers

For studies covering a wide pH range, a 'mixed buffer' was used, containing 5 mM each of acetic acid, Mes, Hepes, Taps and 0.1 M NaCl. The pH of a buffer solution was adjusted by adding aliquots of aqueous NaOH (BDH) or HCl (BDH). Care was taken to record the final pH of the buffers only after all additions had been made to the buffer, e.g. after addition of any co-adsorbate which may have caused a shift in the pH. To ensure accuracy of electrolyte solutions, the pH values were checked routinely after each experiment. All solutions were retained after experiments for subsequent inspection if needed.

2.2.3 Co-adsorbates

Co-adsorbates were prepared as concentrated stock solutions and adjusted to pH 7.0 with aqueous NaOH or HCl as required. They were stored as concentrated stock 'pellets' in liquid nitrogen and added to buffer-electrolyte solutions as required.

Common name	Chemical name	Concentration of stock	Supplier
Polymyxin	Polymyxin B sulfate	20 mg/ml ≈ 15 mM	Sigma
Neomycin	Neomycin sulfate	0.2 M	Sigma

Table 2.3 Stock concentrations of co-adsorbates

Polymyxin was used for film experiments (see *Section 2.3.1*) since it was found to induce a stronger adsorption than neomycin, probably because polymyxin has a larger $-NH_3^+$ array.[4] Neomycin was used preferentially for bulk solution voltammetry and bulk electrolysis (see *Section 2.3.2*) because neomycin is known to promote a weaker adsorption response than polymyxin, this allows greater/more efficient diffusional exchange at the electrode.

2.2.4 Metal Ion Salts

Investigation of metal ion interaction with both *Desulfovibrio africanus* Fd III and *Pyrococcus furiosus* Fd was a significant aspect of the work described in this thesis, and therefore metal ion solutions of accurate concentrations were critical. To avoid disturbance of the composition of the buffered electrolyte solution, small aliquots (ca. 5-50 μl) of concentrated stock solution of metal ion were added to the buffer-electrolyte in order to achieve the required concentration. Stock solutions of the metal ions were prepared in a glove box (Belle Technology) and used immediately.

Metal Ion	Salt	Supplier
Fe^{2+}	$(NH_4)_2Fe(SO_4)_2.6H_2O$	BDH
Zn^{2+}	$ZnSO_4.7H_2O$ or $Zn(NO_3)_2.6H_2O$	BDH
Co^{2+}	$CoCl_2.6H_2O$	BDH
Tl^{1+}	$TlOOC.CH_3$	BDH
Cd^{2+}	$Cd(NO_3)_2$	BDH
Cu^{2+}	$CuSO_4.5H_2O$	BDH

Table 2.4 Metal ion solutions used

2.2.5 Ligand Solutions

Aliquots of concentrated stock solution of ligand were added to the buffered electrolyte to give the required concentration in bulk solution. Solutions of ligands were made up and used immediately.

Ligand	Concentration of Stock Solution/M	Supplier
Mercaptoethanol	0.20	Fluka
Glutathione	0.20	Sigma
L-cysteine	0.20	Sigma
Coenzyme M	0.20	Sigma
Thioacetic acid	0.20	Sigma
Thiomalic acid	0.20	Sigma
Thioglycolic acid	0.30	Sigma
Catechol	0.18	Sigma
Oxalacetic acid	0.20	Sigma
Oxalic acid	0.20	Sigma

Table 2.5 Ligand solutions

2.3 Electrochemical Apparatus

2.3.1 Film experiments

The pyrolytic graphite edge (PGE) electrodes used in this thesis were constructed according to the following method. Cuboid pieces of pyrolytic graphite (Le Carbone, France) were cut to expose the 'edge' plane surfaces. A piece of graphite (ca. 4 x 4 x 8 mm) was then affixed, using conducting silver epoxy glue (RS Components; Northants), to the end of a brass rod so that the upper most surface (4 x 4 mm) (i.e. the finished electrode surface) was 'edge' plane. The brass rod was then glued into a Teflon sleeve. A mould was placed over the top of the extending piece of graphite and Epoxy resin (Araldite™; Ciba Geigy) poured into the mould to seal the surface. When the glue was dry the mould was removed and the excess Epoxy filed down with sandpaper to expose the edge plane graphite. Electrodes were polished immediately prior to use with an aqueous alumina slurry (Buehler Micro-polish; 1.0 μm), and then sonicated extensively to remove traces of Al_2O_3.

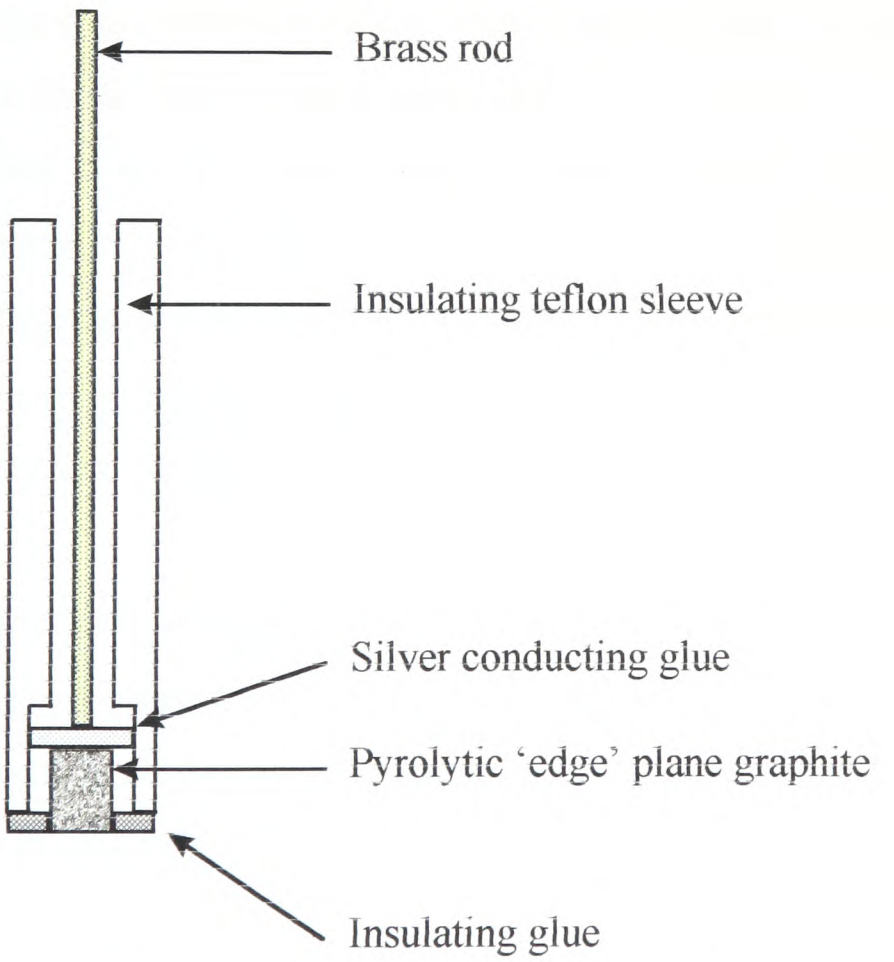

Figure 2.3 Pyrolytic graphite edge plane working electrode

The electrochemical cells used were based on a 'three-electrode cell' arrangement[12] with a working, reference and counter electrode. The precise design of the cells used was based on one developed by Armstrong *et al.*[13] The working electrode was inserted into the sample pot which also contained the platinum wire counter electrode. The reference electrode, a saturated calomel electrode (SCE), was housed in a separate compartment from the working solution, connected via a 0.1 mm Luggin capillary, which prevented mass transfer between the chambers. This arrangement allows the reference electrode to be at a minimum distance from the working electrode, thereby reducing any potential drop across the solution.[12] The sample compartment was enclosed in a water jacket which was held at the desired temperature using a water circulator (Neslab). The reference electrode was allowed to equilibrate to the ambient room temperature and a note of this temperature was taken. At 22 °C the correction factor used was +243 mV to convert the measured potential (SCE) to a potential versus the **S**tandard **H**ydrogen **E**lectrode (SHE).[12] All potentials quoted in this thesis are versus SHE.

In the majority of experiments, especially those investigating metal exchange or ligand binding, where sequential exposure of the protein film to different solutions was required and hence the electrode was required to be moved, a 'multipot' cell was used (Figure 2.4). This differs from the typical 'single' electrochemical cell in that it has four separate compartments, for different experimental solutions, which are connected radially to one central reference compartment, as described by Armstrong *et al.*[14] The addition of an interconnecting water jacket around each of the working electrode compartments was added as a modification for the experiments in this thesis.

The protein films were formed by application of the protein solution (typically 100 μM), with a capillary glass pipette, directly onto the electrode surface. It was noted that careful and adequate polishing of the electrode was a factor which strongly influenced the quality of the protein film.

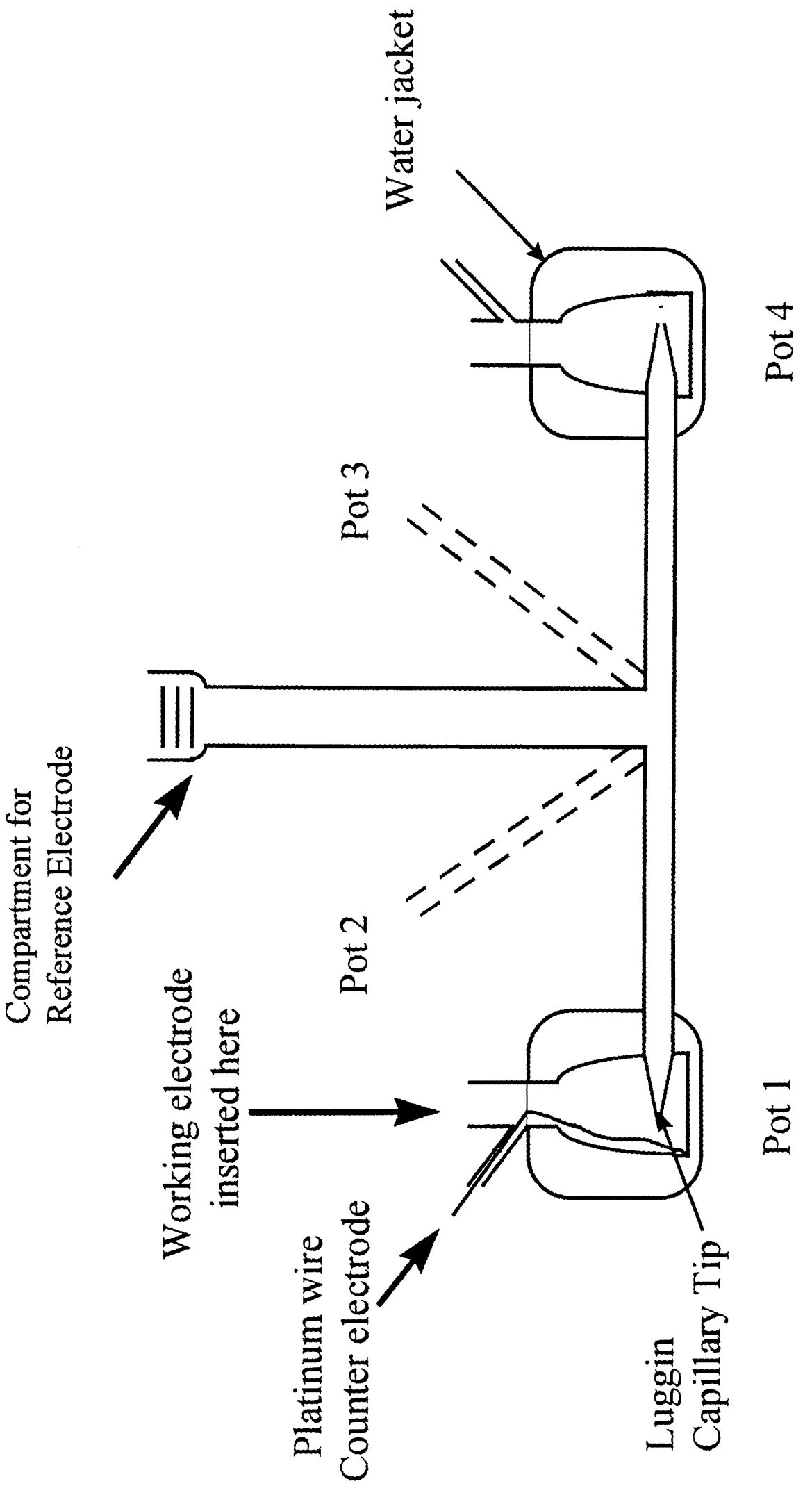

Figure 2.4 Electrochemical 'multipot' cell used in film experiments

RE: saturated calomel electrode as reference electrode, WE: working electrode, CE: platinum wire counter-electrode.

2.3.2 Bulk electrochemistry and bulk electrolysis

The electrochemical cell used for bulk solution electrochemistry and bulk electrolysis was based on that previously used by Armstrong *et al.*[13] This design has undergone various modifications,[11] and the working electrode used in this thesis (Figure 2.3) was found to be highly efficient for carrying out bulk electrolysis.[3] The working electrode consisted of a small graphite pot, with a capacity of 200-600 μl. It was constructed in such a way as to give a maximal surface area of graphite in contact with the protein solution.

The version of the working electrode used in this thesis was developed by J.L.C. Duff.[15] The working electrode was constructed from a cylindrical block of pyrolytic graphite, which had been bored out to give a hole (1 cm in diameter) such that the inside walls were 'edge' surface. This block was then glued onto a graphite base, (using insulating epoxy) which also projected an 'edge' plane surface into the pot. The walls and the base were connected to the potentiostat independently using silver wire (diameter: 0.127 mm) glued with conducting silver epoxy (RS Components) and dried in an oven at 60 °C for 3 hours. The graphite surface was then filed down and polished with 1 μm Al_2O_3 until the surface was smooth. The graphite pot was glued into a Teflon housing and the connections of silver wire attached to electrical plugs on the circumference of the housing. These were then covered with epoxy glue for protection. The pot was rigorously polished with 0.3 μm Al_2O_3 (Buehler) slurry before each experiment.

The Teflon housing containing the graphite pot was placed inside a glass circulating jacket which was part of an all-glass cell supporting the reference (SCE, Luggin capillary junction) and auxiliary (Pt, salt-bridge 'Vycor' junction) side arms, each projecting into the sample solution (Figure 2.5). The entire cell was set up in an anaerobic glove box (Belle Technology), $O_2 < 2$ppm. For typical cyclic voltammetry of the protein solution in the graphite pot only the base of the pot was connected. For bulk electrolysis all parts of the electrode were connected (both walls and base) and the solution was stirred with a magnetic micro-flea to ensure all the solution was in contact with the surface. If experiments required additions to be made to the protein solution in the working

electrode pot, this was easily accomplished by adding liquid *via* a syringe, fitted with a cannula, through an opening at the top of the glass cell.

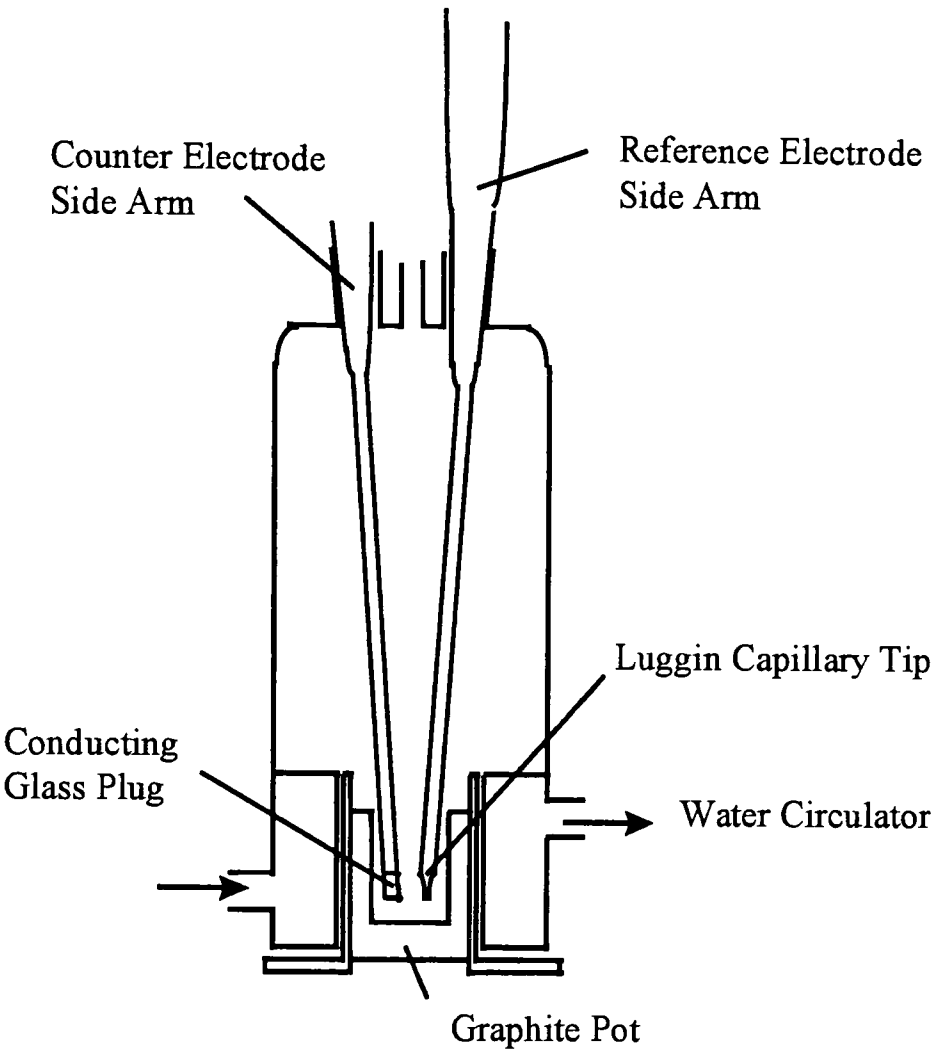

Figure 2.5 Bulk cell apparatus

2.3.3 Potentiostats and recorders

Cyclic voltammetry was carried out using either an analogue potentiostat (Ursar Instruments) or digital AutoLab potentiostat (Eco-Chemie, Utrecht, The Netherlands). Voltammograms were recorded on a Kipp and Zonen BD90 XY recorder or using a 486 PC running Eco-Chemie GPES3 software. Bulk electrolysis was monitored on a Kipp and Zonen BD41 YT recorder. The output of the potentiostats was calibrated by measuring the potential difference between working and reference electrodes of the electrochemical cells using a Beckman Industrial 310B Digital Multimeter.

2.4 UV/VISIBLE SPECTROSCOPY

UV/Visible absorption spectra of ferredoxin solutions were measured using either a Hitachi U-3210 spectrophotometer fitted with 1 cm, 1 ml quartz cuvettes (Hellma) or a spectrometer cell-block located in the glove box and linked by fibre-optic cables to a MG-6000 diode-array spectrometer unit (Hi-Tech Scientific, Salisbury, UK). For observing the uptake of Fe^{2+} by the 3Fe $Fd_{A/B}$ of *Pf,* UV/Vis spectra were recorded using the latter system and recording spectra at equal time intervals (*Chapter 6*).

2.5 MCD SPECTROSCOPY

Low-temperature MCD spectroscopy was carried out in collaboration with Dr. Jacques Breton and Prof. Andrew Thomson at the University of East Anglia, Norwich.

Low-temperature MCD measurements were made using a Jasco J-500D dichrograph and an Oxford Instruments split-coil superconducting magnet SM-4. Procedures for measuring MCD spectra are described in detail by Thomson *et al.*[16] Protein samples were diluted with ethylene glycol to 50% v/v (to enable the formation of optical quality glasses upon freezing) and transferred using a syringe to a 1 mm pathlength MCD cell.

2.6 REFERENCES

1) Raven, N.; Ladwa, N.; Cossar, D.; Sharp, R. *Applied Microbiology and Biotechnology* **1992**, *38*, 263-267.

2) Kerscher, L.; Nowitzki, S.; Oesterhelt, D. *Eur. J. Biochem.* **1982**, 223-230.

3) Duff, J. L. C. *Ph. D. Thesis*; University of Oxford, **1996.**

4) Hatchikian, E. C.; Bruschi, M. *Biochimica Et Biophysica Acta* **1981**, *634*, 41-51.

5) Fujinaga, J.; Meyer, J. *Biochemical and Biophysical Research Communications* **1993**, *192*, 1115-1122.

6) Meyer, J.; Fujinaga, J.; Gaillard, J.; Lutz, M. *Biochemistry* **1994**, *33*, 13642-13650.

7) Bovierlapierre, G.; Bruschi, M.; Bonicel, J.; Hatchikian, E. C. *Biochimica Et Biophysica Acta* **1987**, *913*, 20-26.

8) Conover, R. C.; Kowal, A. T.; Fu, W.; Park, J. B.; Aono, S.; Adams, M. W. W.; Johnson, M. K. *Journal of Biological Chemistry* **1990**, *265*, 8533-8541.

9) Gorst, C. M.; Zhou, Z. H.; Ma, K. S.; Teng, Q.; Howard, J. B.; Adams, M. W. W.; Lamar, G. N. *Biochemistry* **1995**, *34*, 8788-8795.

10) Riddles, P. W.; Blakeley, R. L.; Zerner, B. *Methods in Enzymology* **1983**, *91*, 49-60.

11) Butt, J. N. *Ph. D. Thesis;* University of California, Irvine, **1993.**

12) Bard, A. J.; Faulkner, L. R. *Electrochemical Methods; Fundamentals and Applications*; Wiley: New York, **1980.**

13) Armstrong, F. A.; George, S. J.; Cammack, R.; Hatchikian, E. C.; Thomson, A. J. *Biochemical Journal* **1989**, *264*, 265-273.

14) Armstrong, F. A.; Butt, J. N.; Sucheta, A. *Methods in Enzymology* **1993**, *227*, 479-500.

15) Duff, J. L. C.; Breton, J. L. J.; Butt, J. N.; Armstrong, F. A.; Thomson, A. J. *Journal of the American Chemical Society* **1996**, *118*, 8593-8603.

16) Thomson, A. J.; Cheeseman, M. R.; George, S. J. *Methods in Enzymology* **1993**, 199-231.

CHAPTER 3

THE POTENTIAL DEPENDENCE OF [3FE-4S] ↔ [4FE-4S] CLUSTER TRANSFORMATIONS (M = Fe, Zn, Cd) IN FERREDOXIN III FROM *Desulfovibrio africanus*

CHAPTER 3

THE POTENTIAL DEPENDENCE OF [3FE-4S] ↔ [M3FE-4S] CLUSTER TRANSFORMATIONS (M = Fe, Zn, Cd) IN FERREDOXIN III FROM *Desulfovibrio africanus*

3.1 INTRODUCTION

In nature there are several examples of FeS clusters in proteins which undergo interconversion between the [3Fe-4S] and [M3Fe-4S] forms (Figure 3.1). The factor common to all these systems is that the clusters are co-ordinated by three cysteinyl ligands (to three of the four Fe atoms), the fourth metal being co-ordinated by a non-cysteinyl ligand. The best known example of such a cluster is undoubtedly that of aconitase,[1] but this type of chemistry is also displayed by Fd III from *Desulfovibrio africanus* (*Da* Fd III),[2-7] and the Fd from *Pyrococcus furiosus* (*Pf* Fd).[8-13] The ferredoxin from *Desulfovibrio gigas* (*Dg* Fd II) also contains a [3Fe-4S] cluster which can be converted to various [M3Fe-4S] forms, but unlike aconitase, *Da* Fd III and *Pf* Fd the [M3Fe-4S] cluster is co-ordinated by four cysteines.[a][15-17] The ligand X, co-ordinated to M in [M3Fe-4S] as shown in Figure 3.1, may be an amino acid from the protein structure, an exogenous ligand e.g. H_2O or ^-OH, or an enzyme substrate. The process of metal incorporation and its subsequent co-ordination by X is dependent on the nature of

---

[a] The [3Fe-4S] cluster of *Dg* Fd II is ligated by the cysteines at 8,14 and 50. The cysteine at position 11 was found to extend away from the cluster and is modified, most probably by a methanethiol group.[14]

both M and X, on the immediate cluster environment, the protein structure and also the cluster oxidation level. The latter determining factor, i.e. the potential dependence of [3Fe-4S] to [M3Fe-4S] cluster transformations, is the subject of this chapter.

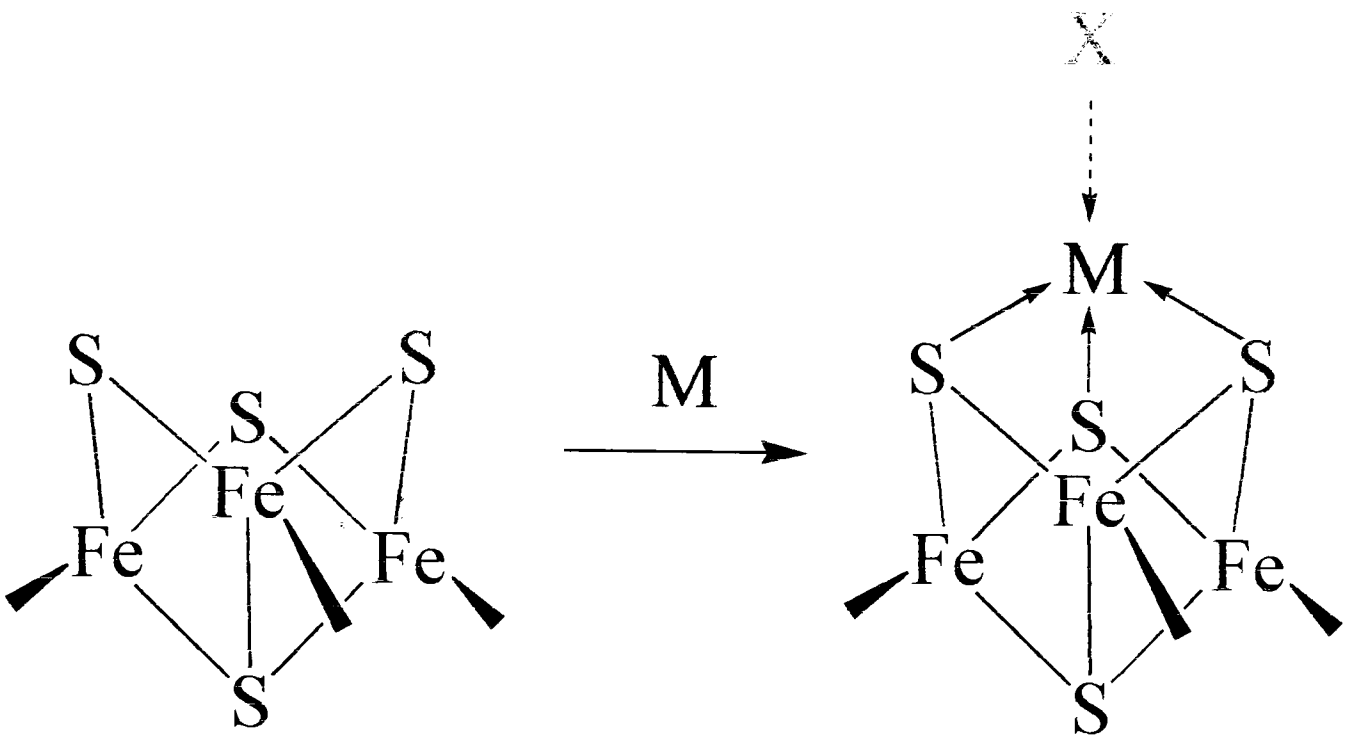

Figure 3.1 [3Fe-4S] ↔ [M3Fe-4S] cluster conversion

The effects of varying M and X and the immediate environment of the cluster can be studied both in proteins and in non-protein analogues. The most recent studies of non-protein analogues present a detailed picture of metal uptake in these systems.[18] Of all the low-nuclearity FeS clusters (2Fe, 3Fe and 4Fe) the [3Fe-4S] cluster was the last to be chemically synthesised outside a protein environment,[19,20] and this has permitted the reactions of the $[3Fe\text{-}4S]^{0}$ core with a variety of heterometals, to be studied. Consequently, this has allowed the determination of binding affinities, the relative stabilities of cluster products, and the influence of the heterometal on the reduction potential to be studied.[18] Previously the synthesis of analogue heterometal clusters had involved self-assembly systems, utilising tetrathiometalates as the source of the heterometal,[21] rather than direct reaction of M^{n+} with a preformed [3Fe-4S] cluster. Heterometal incorporation into the preformed (synthetic) [3Fe-4S] cluster has been successful for Fe, Cu, Ag, Tl, Co and Ni,[18] but the Mn, Zn and Cd heterometal clusters could not be formed by this method. Zhou *et al* ascribed this lack of conversion to the fact that the native protein [3Fe-4S] cluster has enhanced stability, due to the protein

structure, in comparison to the synthetic cluster, [3Fe-4S(LS_3)] (LS_3 = 1,3,5-tris((4,6-dimethyl-3-mercaptophenyl)thio)-2,4,6-tris(*p*-tolylthio)benzene(3-).[18] It is also suggested that subsite ligation by the protein controls affinity for Fe vs. other metals.

Although the non-protein analogue chemistry of FeS clusters has advanced considerably in recent years, these studies cannot take into account the important aspect of protein structure - to gain a more realistic picture, experiments must be carried out on clusters 'in-situ' in the protein. In *Da* Fd III and *Pf* Fd the [3Fe-4S] cluster is co-ordinated by an unconventional sequence, -C-X_2-D-X_2-C-X_n-C-, in which an aspartate (D) is found in the central position normally occupied by a cysteine (C) in a typical $[4Fe\text{-}4S]^{2+/1+}$ cluster binding motif (Figure 3.2). *Da* Fd III contains seven cysteines, and the remaining four ligate a comparatively inert [4Fe-4S] cluster in the conventional way.[22] It has been shown by ^1H NMR for *Pf* Fd that the labile Fe in the [Fe3Fe-4S] cluster is ligated by Asp14[23,24] and similarly it is postulated that in *Da* Fd III, Asp14 is the non-cysteine ligand.[2,6,22] Furthermore, the addition of M to the [3Fe-4S] core of both *Da* Fd III and *Pf* Fd produces a [M3Fe-4S] cluster which is capable of binding exogenous ligands such as ^-CN and thiolates, this topic is dealt with in detail in *Chapters 4* and *6*.[25,26]

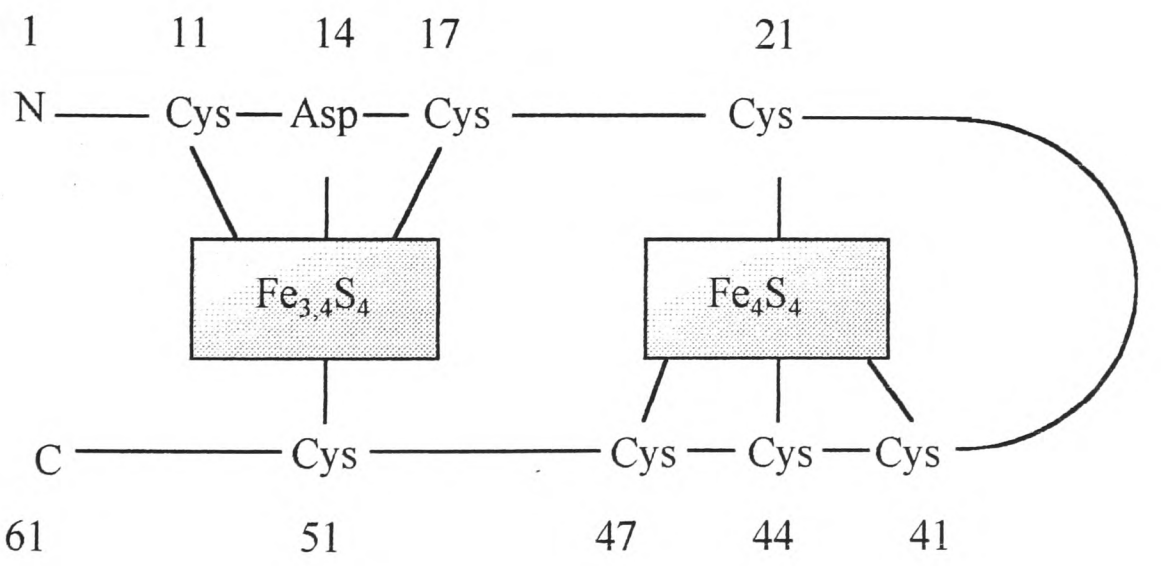

Figure 3.2 Amino acid sequence of *Desulfovibrio africanus* Fd III showing cluster binding

A wide range of metal ions have now been incorporated into the [3Fe-4S] cores of *Da* Fd III and *Pf* Fd: Fe,[3,27] Cu,[5] Zn,[3,11,13,16,27] Tl,[4,12] Co,[13,15,17,27] Ni,[10,11,17] Mn,[13]

Cd[3,17,27] and Ga,[28] and the resulting heterometal clusters characterised using, in particular, EPR, MCD and Mössbauer spectroscopies. Conventionally, heterometals are incorporated into the cluster by adding very high concentrations of the metal ion in question to a solution of the reduced protein (usually in the presence of dithionite), and a period of time is then allowed to elapse before the protein is purified, prior to analysis. The high metal concentrations used can, however, lead to partial, or complete destruction of the cluster, especially if the metal is thiophillic e.g. Pb^{2+} or Cd^{2+}. The limited stability of some of the oxidised $[M3Fe\text{-}4S]^{2+}$ clusters and their tendency to 'eject' the metal can also make subsequent characterisation difficult. Protein film voltammetry, however, offers an alternative to this procedure. The protein, adsorbed onto an electrode, can be placed into solutions containing the metal ion of interest and held at different potentials.[3,27,29] If metal uptake is favoured, heterometal cluster formation will result and a direct readout from the voltammetry can be obtained. Major attributes of this method are that it allows heterometal cluster formation and destruction to be viewed directly, in the time domain, under ambient conditions, and with the strictest control of potential.

The 7Fe Fd from *Da* (containing one 3Fe and one 4Fe cluster) is very well suited to the investigation of metal ion uptake by protein-film voltammetry and several previous studies have already exploited this fact. First, the 3Fe cluster is known to be very labile and is able to respond quickly to changes in conditions whilst adsorbed on the electrode as a protein film.[2-7] Second, metal uptake by the 3Fe cluster is easily observed in the voltammetry - the characteristic signals of the [3Fe-4S] centre, due to the $[3Fe\text{-}4S]^{1+/0}$ and $[3Fe\text{-}4S]^{0/2-}$ couples (A' and C' respectively), are replaced, upon conversion, by the new signal D' - due to the $[M3Fe\text{-}4S]^{2+/1+}$ couple. This new redox couple, D', is observed at a potential which is characteristic of the identity of the heterometal of the [M3Fe-4S] cluster (Table 3.1). The redox couple B', associated with the native $[4Fe\text{-}4S]^{2+/1+}$ cluster, remains unchanged throughout the process of metal uptake by the 3Fe cluster. All these redox couples (A', B', C' and D') are displayed and labelled in Figure 3.6. Recently the influence of pH upon metal uptake by the 3Fe cluster in *Da* Fd III has also been established.[27] The uptake of Fe, Zn and Co was found to depend upon the ionisation state of a group with a pK of 5.5 (± 0.3), which supports congruence of the products, and is also indicative of the involvement of Asp14.[27]

3.1.1 Aims of this Investigation

The aim of the work described in this chapter is to establish reactivity relationships amongst [3Fe-4S] and [M3Fe-4S] clusters, and to define more closely the conditions for their interconversion, placing particular emphasis upon the influence of the cluster's redox state. The basis of the experimental approach was to utilise the ease by which a cluster's redox state can be manipulated by altering the potential applied to a protein film adsorbed on an electrode surface. The full range of oxidation states accessible to a [3Fe-4S] core, and how these are linked by electron-transfer and metal uptake reactions, is illustrated in Figure 3.3.

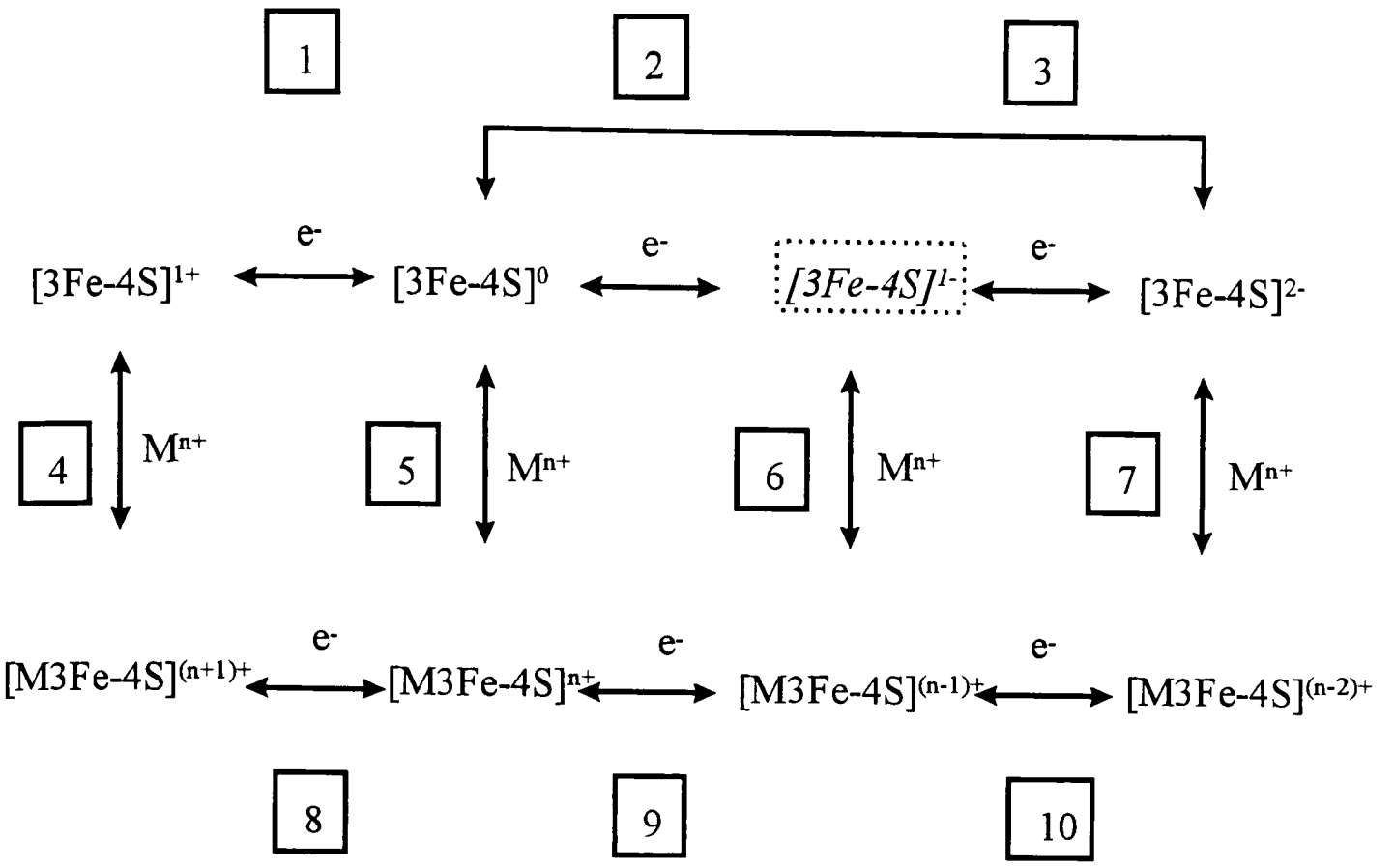

Figure 3.3 Core scheme for electron-transfer and metal uptake for [3Fe-4S]

The [3Fe-4S]$^{1-}$ state has not been directly observed in a biological system.

The reactions as defined in Figure 3.3 depict the stability of different core species as a function of metal ion and potential, although they do neglect the influence of the protein. Reaction 1 is the normal one-electron redox reaction of the [3Fe-4S]$^{1+/0}$ cluster; reactions 2 and 3 are, together, the co-operative two-electron redox reaction of the reduced cluster - the [3Fe-4S]$^{0/2-}$ couple.[30] The intermediate [3Fe-4S]$^{1-}$ has not yet been isolated in a biological system but has been generated in a non-protein analogue in aprotic solvents at very low potentials.[19,20] The [3Fe-4S]$^{2-}$ and [M3Fe-4S]$^{2-}$ states are the fully reduced forms of the 3Fe and cubane clusters respectively and have only been recently identified. Examples include the 7Fe Fd of *Sulfolobus acidocaldarius*,[30] the fully reduced state of a water soluble fragment of a Rieske protein,[31] the [3Fe-4S]^{0} cluster from the fully reduced forms of spinach and parsley 2Fe ferredoxins[32] and the [4Fe-4S]^{0} cluster from the Fe protein of nitrogenase.[33] Reaction 9 is the [4Fe-4S]$^{2+/1+}$ one-electron redox reaction of the standard cubane-type 4Fe cluster, whilst Reaction 8 is the one-electron redox reaction of a high potential iron protein (HiPIP), the [4Fe-4S]$^{3+/2+}$ couple.[34,35] There are thus three possible, reversible pathways for metal uptake, occurring without coincident electron transfer - Reactions 4, 5 and 7. Uptake of

monovalent metal ions such as Tl^{1+} may involve Reaction 4 or 5,[4] but Reaction 4 occurs specifically for divalent metal ions such as Fe, Zn and Cd.[2,3,7] The pathway for Cu addition may be either Reaction 4 or 5, depending on whether Cu adds as the monovalent or divalent ion, Cu^{1+} or Cu^{2+} respectively.[5]

3.2 EXPERIMENTAL

All experiments were carried out as detailed in *Chapter 2*. Metal ion uptake experiments were carried out in a 'multipot' cell so that transfer of the electrode, carrying an adsorbed protein film, could be easily effected. An intermediate pot, containing only buffer electrolyte, was used in metal ejection experiments, so that any excess metal ion solution adhering to the electrode could be rinsed off, after formation of the heterometal cluster, and before poising of the electrode to promote metal ion release. It was imperative that all of the electrode transfers were carried out rapidly to avoid degradation or disruption of the protein film whilst not in the solution. All of the experiments described in this chapter were carried out at a scan rate of 500 mV s^{-1} - this was found to be the optimum scan rate since it was not fast enough to cause complications from i-R drop but was fast enough to avoid any significant changes occurring to the film composition during scanning.

3.3 RESULTS

3.3.1 Metal Uptake of the [3Fe-4S] Cluster in Different Oxidation States

3.3.1.1 Mathematical Representation

For the uptake reaction (Reaction 5 in Figure 3.3),

$$[3Fe\text{-}4S]^0 + M^{2+} \rightarrow [M3Fe\text{-}4S]^{2+}$$

K_d can be defined as,

$$K_d = \frac{C'_{[3Fe\text{-}4S]^0} C_{M^{2+}}}{C'_{[M3Fe\text{-}4S]^{2+}}} \qquad \textbf{Equation 3.1}$$

where $C'_{[3Fe\text{-}4S]}{}^{0}$ and $C'_{[M3Fe\text{-}4S]}{}^{2+}$ are surface populations on the electrode surface, and $C_M{}^{2+}$ is the concentration of M^{2+} in bulk solution.

To derive an equation taking account of the influence of the applied potential ($E_{applied}$) it is necessary to incorporate the Nernst Equation (for couples A' and D'), which governs the relative populations of oxidised and reduced species.

The total population of [3Fe-4S] clusters (without a bound heterometal) at equilibrium is

$$C'^{equil}_{[3Fe-4S]^T} = C'_{[3Fe-4S]^{1+}} + C'_{[3Fe-4S]^0} \qquad \textbf{Equation 3.2}$$

The Nernst equation for the $[3Fe\text{-}4S]^{1+/0}$ couple can be written as,

$$\theta_A = \frac{C'_{[3Fe-4S]^{1+}}}{C'_{[3Fe-4S]^0}} = \frac{C'^{equil}_{[3Fe-4S]^T} - C'_{[3Fe-4S]^0}}{C'_{[3Fe-4S]^0}} = \exp\left\{\frac{nF}{RT}\left(E_{applied} - E^{o\,\prime}{}_{A'}\right)\right\} \qquad \textbf{Equation 3.3}$$

where θ_A is the ratio of oxidised cluster to reduced cluster.

Similarly for the $[M3Fe\text{-}4S]^{2+/1+}$ cluster:

$$\theta_D = \frac{C'_{[M3Fe-4S]^{2+}}}{C'_{[M3Fe-4S]^{1+}}} = \frac{C'_{[M3Fe-4S]^{2+}}}{C'^{equil}_{[MFe\text{-}4S]_T} - C'_{[M3Fe\text{-}4S]^{2+}}} = \exp\left\{\frac{nF}{RT}\left(E_{applied} - E^{o\,\prime}{}_{D'}\right)\right\} \qquad \textbf{Equation 3.4}$$

Substituting $C'_{[3Fe\text{-}4S]}{}^{0}$ and $C'_{[M3Fe\text{-}4S]}{}^{2+}$, as derived from Equations 3.3 and 3.4, into Equation 3.1 gives,

$$K_d = C_{M^{2+}}\left(\frac{(1+\theta_D)}{\theta_D(1+\theta_A)}\right)\left(\frac{C'_{[3Fe-4S]_T}}{C'_{[M3Fe-4S]_T}}\right) \qquad \textbf{Equation 3.5}$$

where the subscript $_T$ denotes 'total' concentration.

As K_d must remain constant, when $C_{M2+} = K_d$ the ratio $C'_{[M3Fe\text{-}4S]T}/C'_{[3Fe\text{-}4S]T}$ will vary with $E_{applied}$, as described by $(1+\theta_D)/\{\theta_D(1+\theta_A)\}$. This is illustrated in Figure 3.4 for $M^{2+} = Fe^{2+}$.

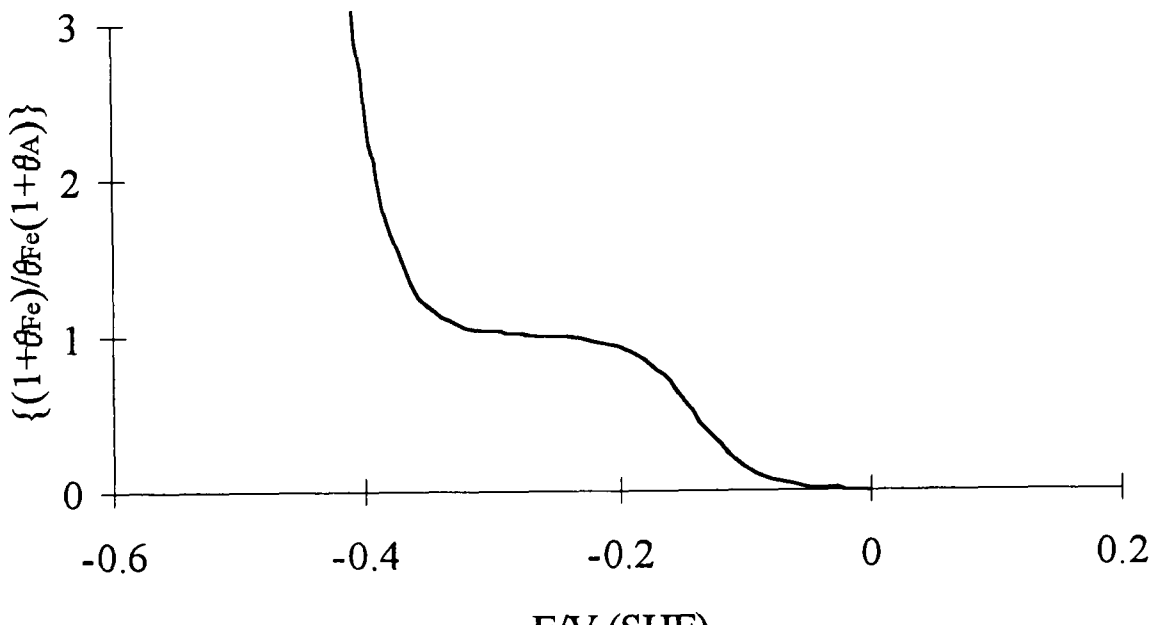

Figure 3.4 Variation of the [Fe3Fe-4S] cluster population with applied potential
Variation of the ratio $(1+\theta_{Fe})/(\theta_{Fe}(1+\theta_A))$ with applied potential. As plotted here for $C_{Fe2+} = K_d$, the ratio is equivalent to the population ratio $C'_{[M3Fe\text{-}4S]T}/C'_{[3Fe\text{-}4S]T}$ (Equation 3.5).

It is apparent that in the region $E_{applied} > E^{o\prime}_{A'}$ this ratio of cluster populations approaches zero, since all clusters are in the $[3Fe\text{-}4S]^{1+}$ state, while for $E_{applied} < E^{o\prime}_{D'Fe}$ the ratio tends to infinity since the population of [3Fe-4S] clusters is very small. At $E_{applied} = (E^{o\prime}_{A'} + E^{o\prime}_{D'Fe})/2$ the ratio is unity - since Equation 3.5 collapses to the definition of K_d given in Equation 3.1.

3.3.1.2 Established Values For K_d

During the experiments and analysis it was necessary to use the previously measured K_d values (as defined in Equation 3.1) for Fe^{2+}, Zn^{2+} and Cd^{2+}, which are listed in Table 3.1.[3] Reduction potentials for the heterometal clusters have also been previously determined,[3] and the values are in agreement with those measured during this work.

M^{2+}	$K_d/\mu M$	$E^{o'}[M3Fe\text{-}4S]^{2+/1+}$ /mV
Fe	30 ± 15	-393 ± 10
Zn	1.6 ± 1.0	-492 ± 10
Cd	0.8 ± 0.5	-569 ± 10

Table 3.1 Dissociation constants and reduction potentials for the heterometal clusters of *Da* Fd III

3.3.1.3 Experimental Protocols

Two experimental protocols used to investigate the dependence of metal uptake by the [3Fe-4S] cluster of *Da* Fd III on the applied potential are now discussed:

Method 1: A film of the 7Fe Fd was formed on the electrode, with polymyxin as co-adsorbate, and the potential was cycled until the electrochemical signal had stabilised. The electrode was then transferred to a pot containing 20 μM Fe^{2+} and the potential poised at 143 mV for 60 s, after which a scan was recorded at 500 mV s^{-1} to record any cluster transformations which may have taken place. The film was then immediately held at the new potential of 43 mV for 60 s and another scan recorded. This was repeated at 100 mV intervals until the potential had decreased to -557 mV. The extent of cluster transformation, determined by measuring the absolute peak heights of the two peaks, A' and D', was then plotted against the potential at which the film had been poised; a typical result is shown in Figure 3.5.

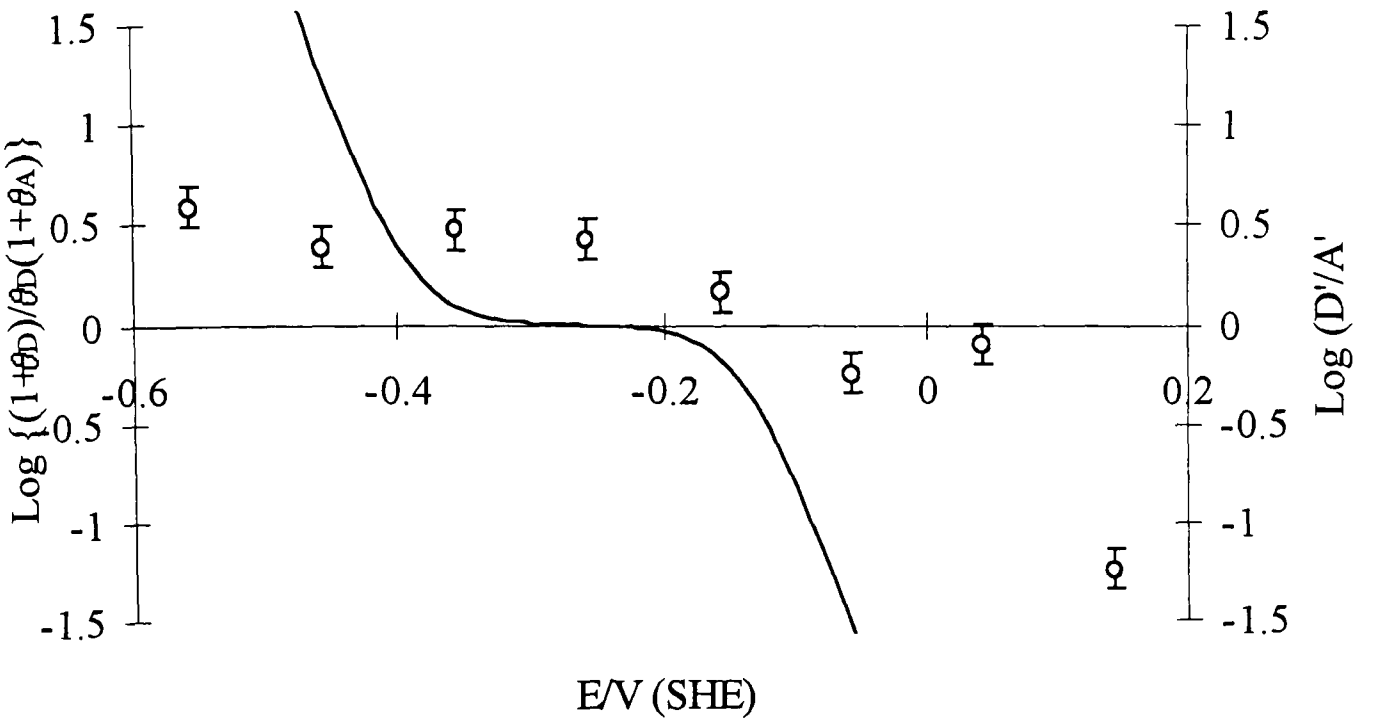

Figure 3.5 Fe uptake for [3Fe-4S] at increasingly negative potentials

Solid line (LHS Y-axis) indicates the cluster populations as calculated from Equation 3.5 with $K_d = C_{Fe2+}$ *but expressed in logarithmic form. The data shown as (●) (RHS Y-axis) are equivalent to the population of [Fe3Fe-4S] clusters after the electrode was held at various potentials for a period of 60 s, for a film of Da Fd III placed into a solution of* Fe^{2+} *(20 μM).*

It is apparent from Figure 3.5 that the population of [3Fe-4S] clusters does not significantly decrease until the applied potential is less than -150 mV (cf. $E^{o\prime}_{A'}$ = -140 mV) and that there is thereafter a gradual decrease in the A' peak, along with an increase in peak D', i.e. log(D'/A') increases. Most importantly, however, as the cluster is held at very negative potentials it is obvious that the theoretically predicted significant increase in [M3Fe-4S] (Equation 3.5 and Figure 3.4) does not occur. . At the lowest applied potentials, the ratio of D'/A' appears to reach a limiting value which was observed experimentally by the complete loss of the A' wave. This contradiction between theory and experiment could be due to either a systematic error in the experimental procedure or to neglect of one or more important equilibria involving the $[3Fe\text{-}4S]^{1-}$ or $[3Fe\text{-}4S]^{2-}$ oxidation states of the cluster (Figure 3.3). A similar set of experiments has also been carried out previously on this system, using this method, and the data obtained were in agreement with those described here (J.N. Butt, *unpublished work*). Due to this

discrepancy with the predicted results, Method 1 was only undertaken for the [Fe3Fe-4S] cluster, and the alternative method, Method 2, was used to investigate further the dependence of potential of metal uptake by [3Fe-4S].[29]

Method 2: As for Method 1, comparisons were made of the metal uptake ability of the [3Fe-4S] cluster using a range of different poising potentials. The main difference between Methods 1 and 2 was that for the latter, a new protein film was used for poising at each 'investigative' potential, this meant that no 'carry on' effects would be seen over the time course of the experiment. For Method 1, the total length of a protein film experiment was at least 10-15 minutes, and so any cumulative influence of the poising potentials (progressively more negative at each separate stage) would affect the protein film. Method 2 avoided any possible complications from cumulative effects, as each potential was investigated beginning from the same point i.e. a fresh film of *Da* Fd III. Studies using Method 2 were carried out for both Zn^{2+} and Fe^{2+}.

Experiments were carried out as follows: first a film of the 7Fe Fd was formed on the electrode and the potential was then cycled until the signals were stabilised. The film was then held at a specific potential, and transferred to a pot containing 0.5 μM Zn^{2+}, at pH 7.0 and held at potential for 60 s. Immediately, following this poising stage, the extent of any transformations which had occurred were examined by cycling at 500 mV s^{-1}. Typical results for an experiment carried out using Zn are shown in Figure 3.6 where it can be seen that little uptake of Zn^{2+} is observed after 1 minute at potentials above 43 mV, i.e. at which [3Fe-4S] exists in the 1+ level, whereas at a potential (-457 mV) favouring both $[3Fe\text{-}4S]^{0}$ and the product $[Zn3Fe\text{-}4S]^{2+}$, rapid conversion occurs, as noted previously for the $[Fe3Fe\text{-}4S]^{2+/1+}$ cluster using Method 1. However, as the potential is decreased below -750 mV, where the [3Fe-4S] core is 'locked' into the 2-state, there is again little formation of [Zn3Fe-4S]. Some attenuation of signals A' and C' is observed at this potential, but this is due to slow degradation of the [3Fe-4S] cluster in this highly reduced state - a similar decrease is observed in buffer alone. To ensure that the remaining, unreacted [3Fe-4S] cluster was still capable of metal ion uptake after being held at these low potentials the film was re-poised at -550 mV whereupon signals due to $[Zn3Fe\text{-}4S]^{2+/1+}$ appeared as expected.

Results obtained for Fe uptake (10 μM) were similar, although the results were more difficult to analyse because the new signal D', arising from that of $[Fe3Fe\text{-}4S]^{2+/1+}$, overlays that of the inert B' couple, Figure 3.7. In Figure 3.7, it can be seen that at the poising potential of -1007 mV, there is little in the way of Fe uptake as the A' and C' couples are clearly visible. At the poising potential of -257 mV, where the 3Fe cluster is in the $[3Fe\text{-}4S]^{0}$ state, Fe uptake is seen to occur, as judged by the decrease in size of the A' and C' peaks. When the 3Fe cluster is in the $[3Fe\text{-}4S]^{1+}$ state (i.e. when the potential was held at 93 mV) Fe uptake is not observed. At this positive potential a decrease in the general quality of the film is seen as positive potentials are generally disruptive to the protein film.

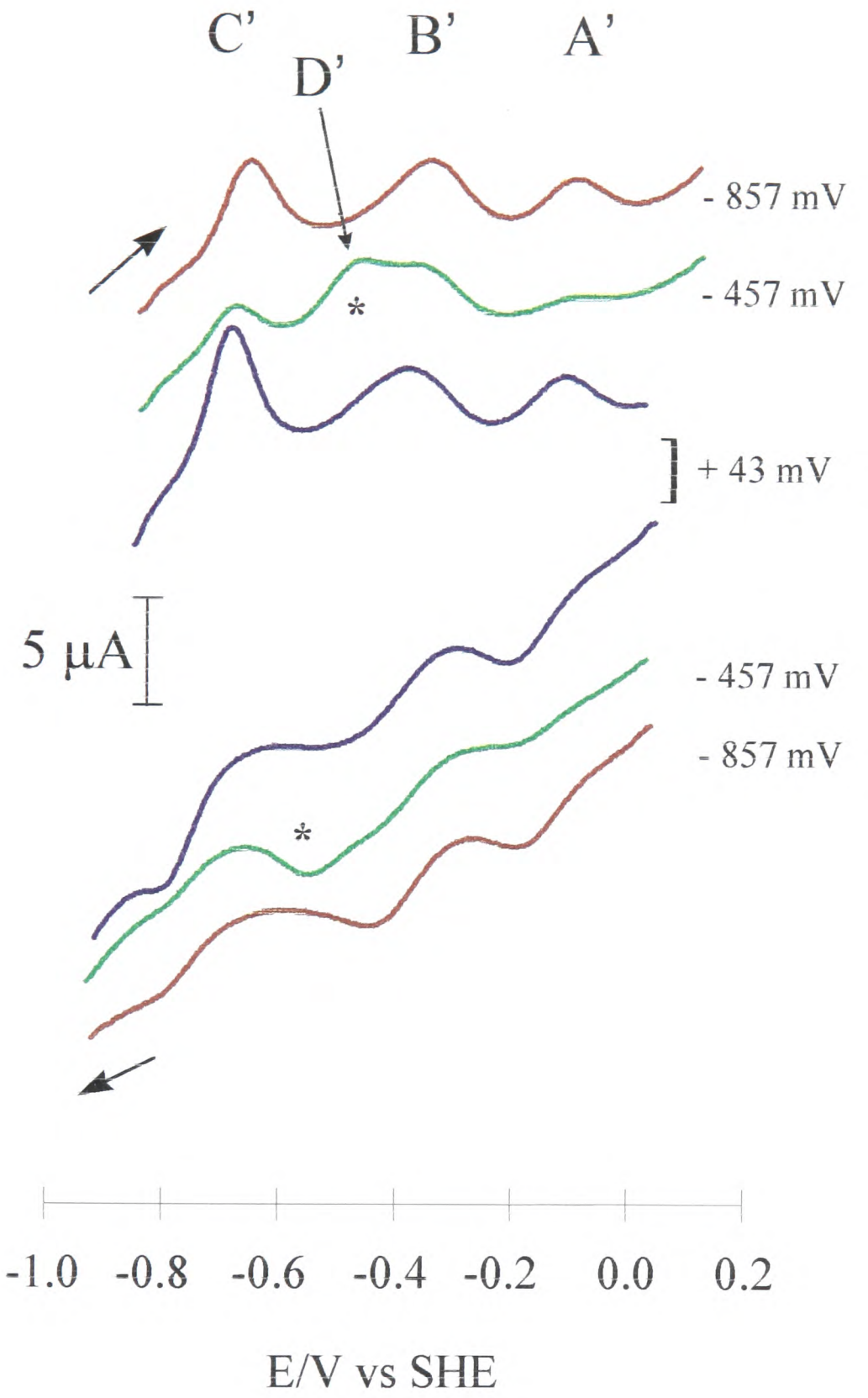

Figure 3.6 Potential dependence of zinc uptake in [3Fe-4S] from *Da* Fd III

Cyclic voltammograms showing the extent of uptake of Zn^{2+} into the [3Fe-4S] cluster at different potentials. Films of the 7Fe Fd were poised for 60 s at the potentials indicated, then a cycle was recorded at a scan rate of 500 mV s^{-1}. The signal due to $[Zn3Fe\text{-}4S]^{2+/1+}$ (D') is indicated by (*). Buffer electrolyte 20 mM Hepes, 0.1 M NaCl, pH 7.0 at 0 °C, 200 μg ml^{-1} polymyxin as co-adsorbate.

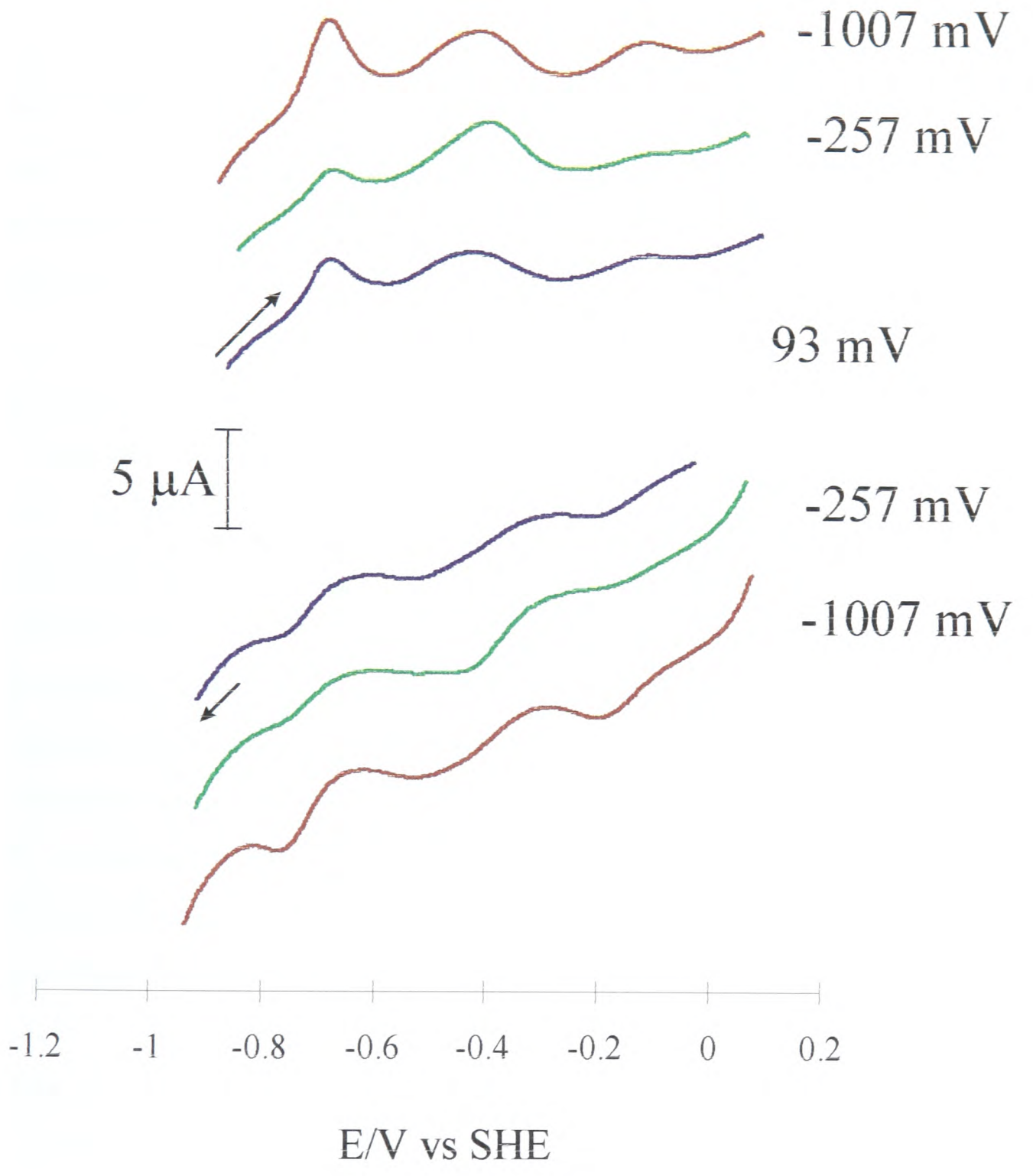

Figure 3.7 Potential dependence of iron uptake in [3Fe-4S] from *Da* Fd III

Cyclic voltammograms showing the extent of uptake of Fe^{2+} into the [3Fe-4S] cluster at different potentials. Films of the 7Fe Fd were poised for 60 s at the potentials indicated, then a cycle was recorded at a scan rate of 500 mV s^{-1}. Buffer electrolyte 20 mM Hepes, 0.1 M NaCl, pH 7.0 at 0 °C, 200 µg ml^{-1} polymyxin as co-adsorbate.

3.3.2 Potential Dependence of Metal Ejection from [M3Fe-4S]

Release of M from [M3Fe-4S], to give the original cluster [3Fe-4S], was measured as a function of electrochemical potential, in a method analogous to Method 2 for the uptake experiments. First, a film of *Da* Fd III was prepared and transferred to a pot containing an excess of metal ion ($[M^{2+}] >> K_d$). After complete formation of [M3Fe-4S] (by holding at a potential < $E^{o'}_{DFe}$) the electrode was transferred to a third pot containing no metal ions in solution and was poised at a specific potential for 60 s. A voltammogram was immediately recorded by scanning rapidly at 500 mV s^{-1} to view the cluster status. As the actual amount of metal ion ejected could not be measured directly, metal ejection was instead monitored by the return of the C' couple - and in particular the height of the C' couple oxidative wave. Couple C' is a well-defined reduction couple, typically with δ = 60 mV indicating a $2e^-$ co-operative reaction, and also involves uptake of $2H^+$ (3 with respect to the oxidised cluster) - as demonstrated for *Da* Fd III, *Sulfolobus acidocaldarius* Fd and *Azotobacter vinelandii* Fd I.[30] At scan rates > 200 mV s^{-1} the C' couple reductive wave is considerably broadened - presumably because of slow electron- or proton-transfer processes.[36] A comprehensive range of holding potentials were used in metal ejection experiments for both [Zn3Fe-4S] and [Fe3Fe-4S]. To compare metal ejection from these two clusters the percentage of the oxidative C' peak return was measured, normalised with respect to the amplitude obtained upon complete transformation and then plotted as a function of potential. An example of Fe ejection is illustrated in Figure 3.8 and similarly Zn ejection in Figure 3.9.

Considering Fe ejection: This process was barely detectable at potentials below -400 mV, where [Fe3Fe-4S] exists in the 1+ level but there were indications of a slight increase of Fe ejection at very negative potentials, perhaps owing to the stability of $[3Fe\text{-}4S]^{2-}$ as a product. As the potential was raised above -400 mV, the extent of Fe release increased and became instantaneous (on the experimental timescale) at 200 mV. No additional voltammetric signals, which might correspond to the HiPIP reduction couple $[Fe3Fe\text{-}4S]^{3+/2+}$ were observed in scans up to 500 mV.

Considering Zn ejection: Release of Zn from [Zn3Fe-4S] was found to be more rapid than that of Fe. In Figure 3.9, it can be seen that at the lower poising potential of -757 mV, the Zn ejection is marginal whereas at the higher poising potentials of -257 mV

and 243 mV Zn ejection is more noticeable - as judged from the return of the A' and C' peaks. The rate of Zn ejection accelerated noticeably above -500 mV and again, marginally, above -100 mV - as shown in Figure 3.10.

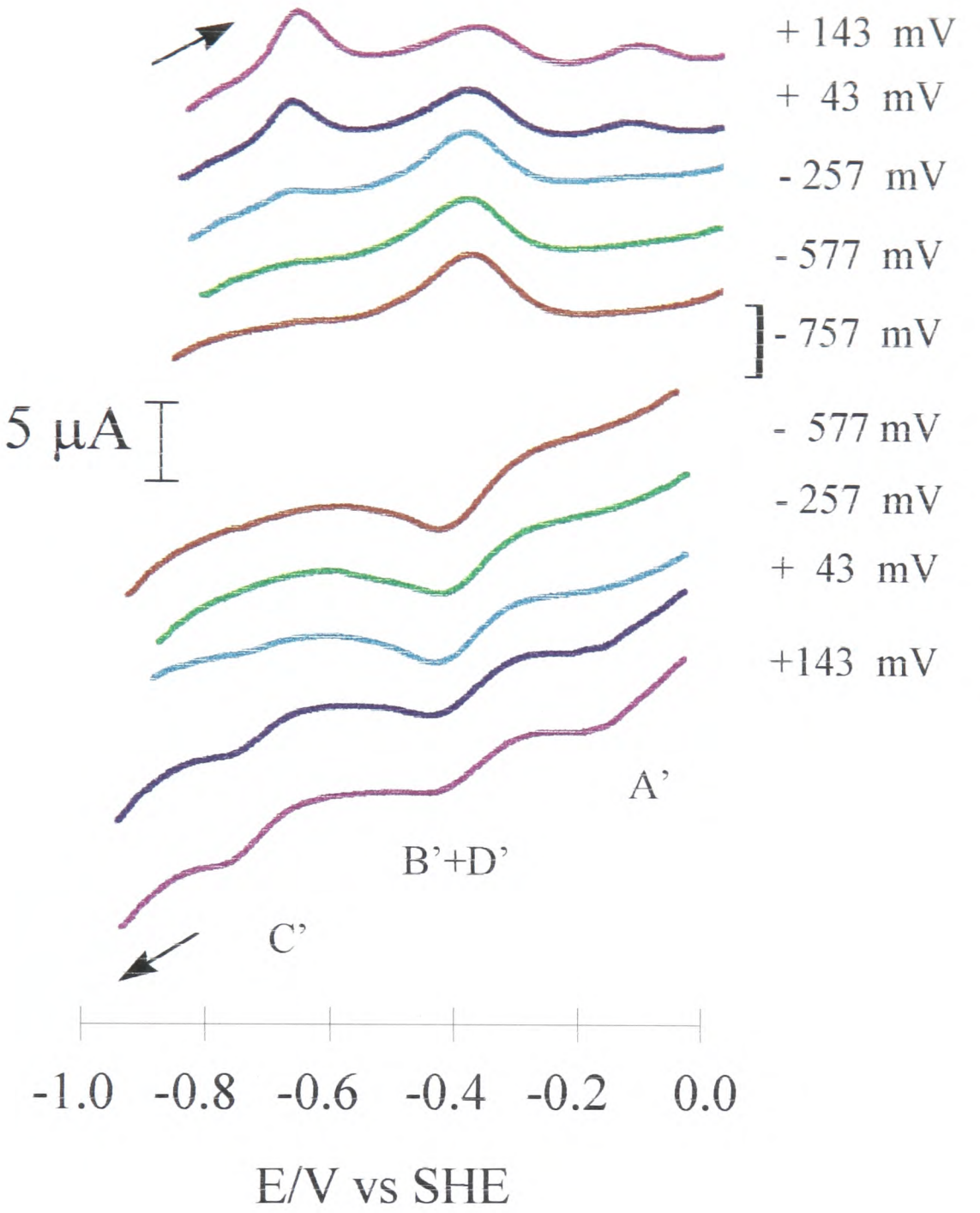

Figure 3.8 Metal Ejection from the [Fe3Fe-4S] cluster in *Da* Fd III

Cyclic voltammograms showing ejection of Fe from the [Fe3Fe-4S] cluster at different potentials. Films of the previously transformed 8Fe Fd were poised at the potentials indicated for 60 s and then the film was scanned at 500 mV s^{-1}. Buffer electrolyte 20 mM Hepes, 0.1 M NaCl, pH 7.0 at 0 °C, 200 µg ml^{-1} polymyxin as co-adsorbate. (Note the broadened reductive wave of the C' couple due to the high scan rate.)

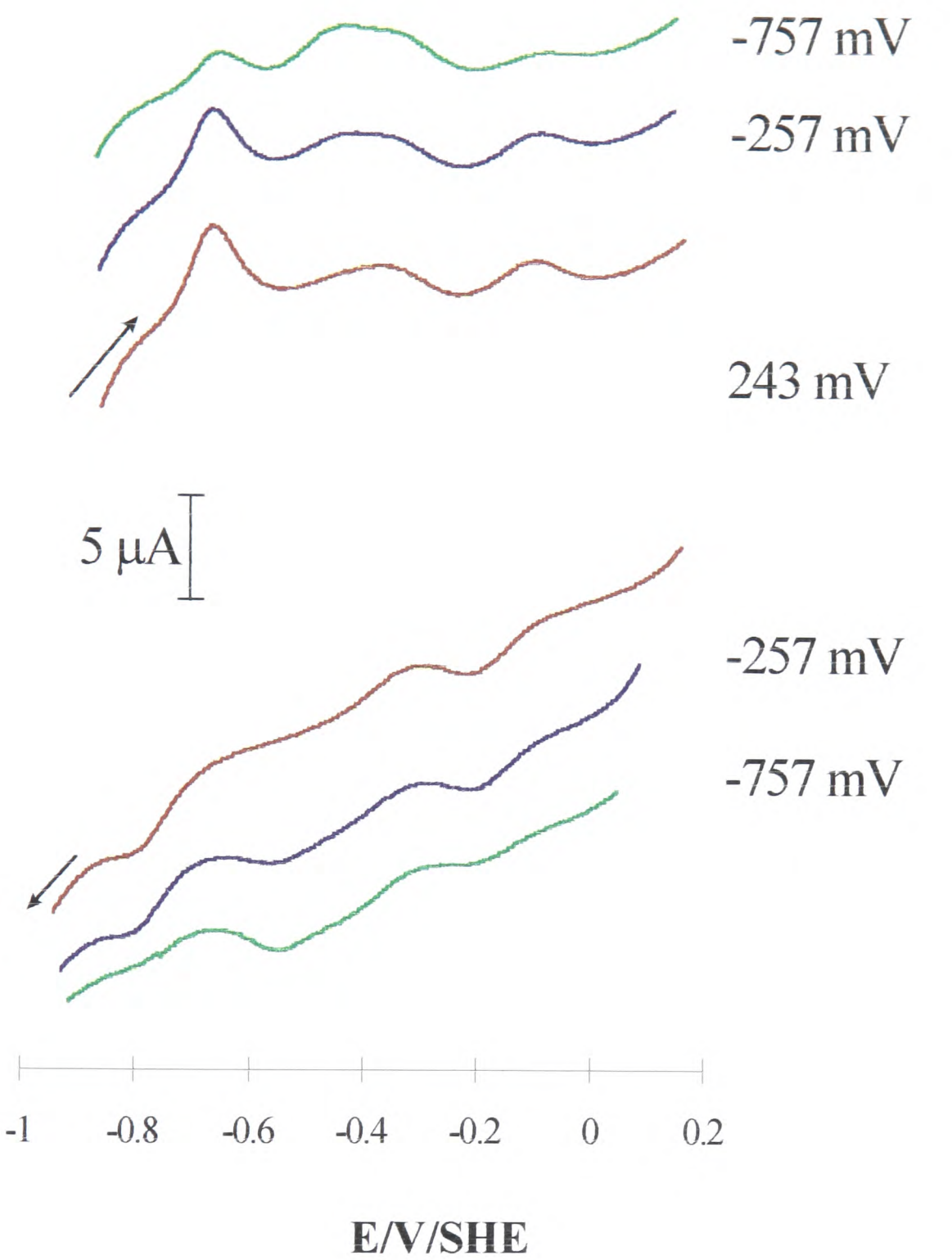

Figure 3.9 Metal ejection from the [Zn3Fe-4S] cluster in *Da* Fd III

Cyclic voltammograms showing ejection of Zn from the [Zn3Fe-4S] cluster at different potentials. Films of the previously transformed Zn Fd were poised at the potentials indicated for 60 s and then the film was scanned at 500 mV s^{-1}. Buffer electrolyte 20 mM Hepes, 0.1 M NaCl, pH 7.0 at 0 °C, 200 µg ml^{-1} polymyxin as co-adsorbate. (Note the broadened reductive wave of C' couple due to the scan rate.)

$[Zn3Fe\text{-}4S]^{1+}$	$[Zn3Fe\text{-}4S]^{2+}$	
$[3Fe\text{-}4S]^{2-}$	$[3Fe\text{-}4S]^{0}$	$[3Fe\text{-}4S]^{1+}$
$[Fe3Fe\text{-}4S]^{1+}$	$[Fe3Fe\text{-}4S]^{2+}$	

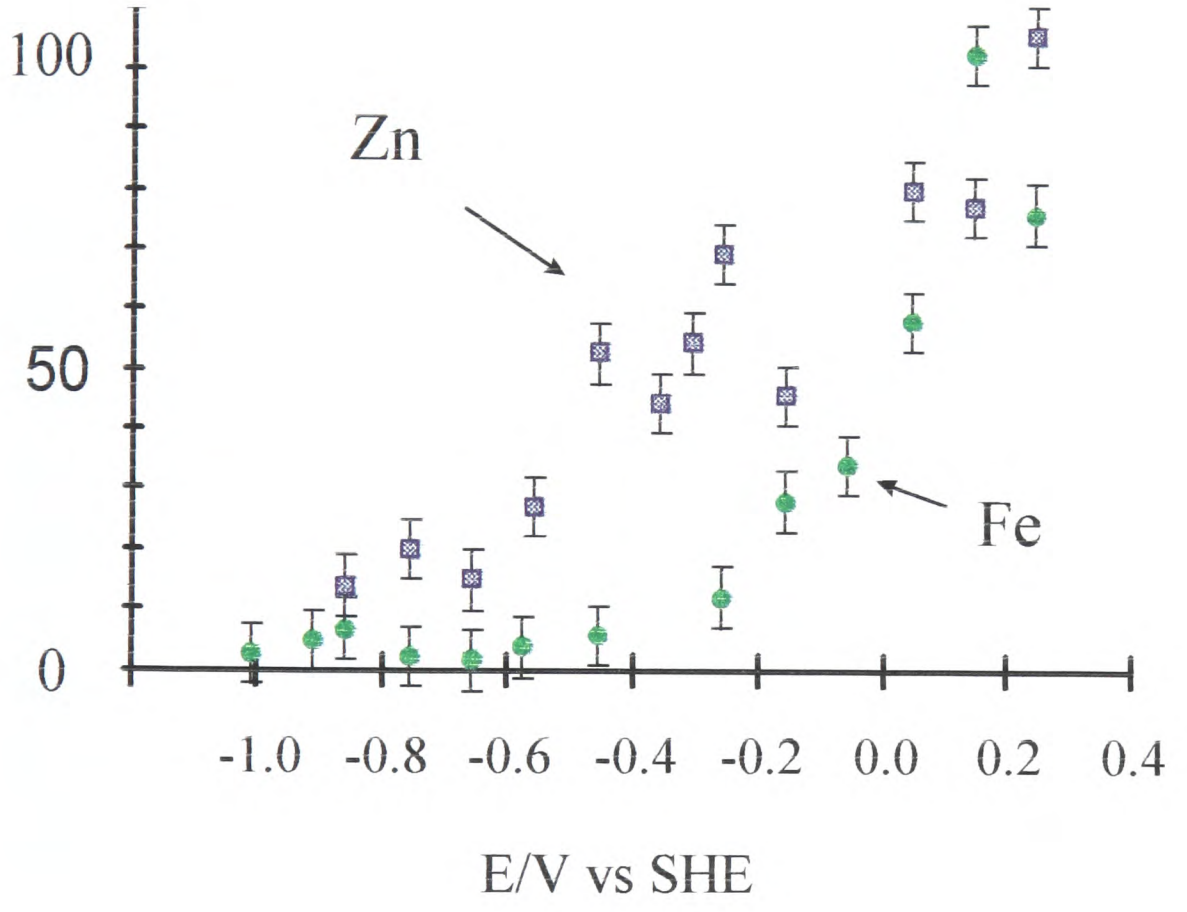

Figure 3.10 Potential dependence of the release of Fe and Zn from the [M3Fe-4S] in *Da* Fd III

Experiments were carried out as described as in the Figure 3.8 legend. The symbols for [Fe3Fe-4S] and [Zn3Fe-4S] are a green circle and blue square respectively. The percentage ejection of M was quantified by comparing the fractional extent of reappearance of the [3Fe-4S] - by measuring the height of the oxidation peak for signal C' after poising for 60 s at the potentials indicated. Above the graph is a potential phase diagram aligned to show the cluster species present at the various potentials.

3.3.3 Metal Competition Experiments

Experiments were also carried out to measure direct competition between two metals. If the reduction potential of $[M_Y3Fe\text{-}4S]^{2+/1+}$ is Y mV and is sufficiently more negative than that of $[M_X3Fe\text{-}4S]^{2+/1+}$, X mV, then application of an electrode potential midway between Y and X ought to produce a noticeably greater proportion of the M_X adduct, since this alone would be in the 1+ state. This reasoning is based on the thermodynamics of the core chemistry, $K_6 < K_5$ because M^{2+} should be bound more tightly in $[M3Fe\text{-}4S]^{1+}$ than $[M3Fe\text{-}4S]^{2+}$ (Figure 3.3) provided $E^{o'}$ for Reaction 2 << $E^{o'}$ for Reaction 9. The ideal situation would be if the two heterometal clusters had well-separated reduction potentials for $[M3Fe\text{-}4S]^{2+/1+}$ ($E^{o'}_{D'}$), in order that accurate quantitation of each peak could be easily undertaken.

The first choice for such a system was Cd vs. Fe, $[Cd3Fe\text{-}4S]^{2+/1+}$ and $[Fe3Fe\text{-}4S]^{2+/1+}$, whose reduction potentials are 180 mV apart, as shown in Table 3.1. However, the K_d for Cd binding to the cluster (0.8 μM) is much less than the K_d for Fe binding (30 μM),[3] and it was found that at whatever potential the system was poised, Cd uptake always occurred preferentially.

The second choice was Fe vs. Zn. Although Zn binds more tightly than Fe in Reaction 5, the reduction potential of the $[Zn3Fe\text{-}4S]^{2+/1+}$ couple (-492 mV) is sufficiently more negative than $[Fe3Fe\text{-}4S]^{2+/1+}$ (-393 mV) that application of a potential to the protein film midway between $[Fe3Fe\text{-}4S]^{2+/1+}$ and $[Zn3Fe\text{-}4S]^{2+/1+}$ ought to produce a noticeably greater proportion of the Fe adduct, since this alone would be in the 1+ state. To test this hypothesis a film of the Fd III was poised at either -307 mV or -457 mV in a solution at pH 7.0 containing the mixture 10 μM Fe^{2+} and 0.5 μM Zn^{2+}, each concentration approximately 1/3 of their K_d values.[3] Although a greater extent of overall transformation was apparent at -457 mV, reliable quantitation of the contributions of different species could not be achieved in this congested region of the voltammogram because of the proximity of $E^{o'}_{D'Fe}$ and $E^{o'}_{D'Zn}$. However, qualitatively, the results obtained at -457 mV did indicate, as expected, a relatively lower contribution of the more characteristic D' signal due to $[Zn3Fe\text{-}4S]^{2+/1+}$. This is shown in Figure 3.11. Use of higher Fe levels attenuated the characteristic $[Zn3Fe\text{-}4S]^{2+/1+}$ at either potential.

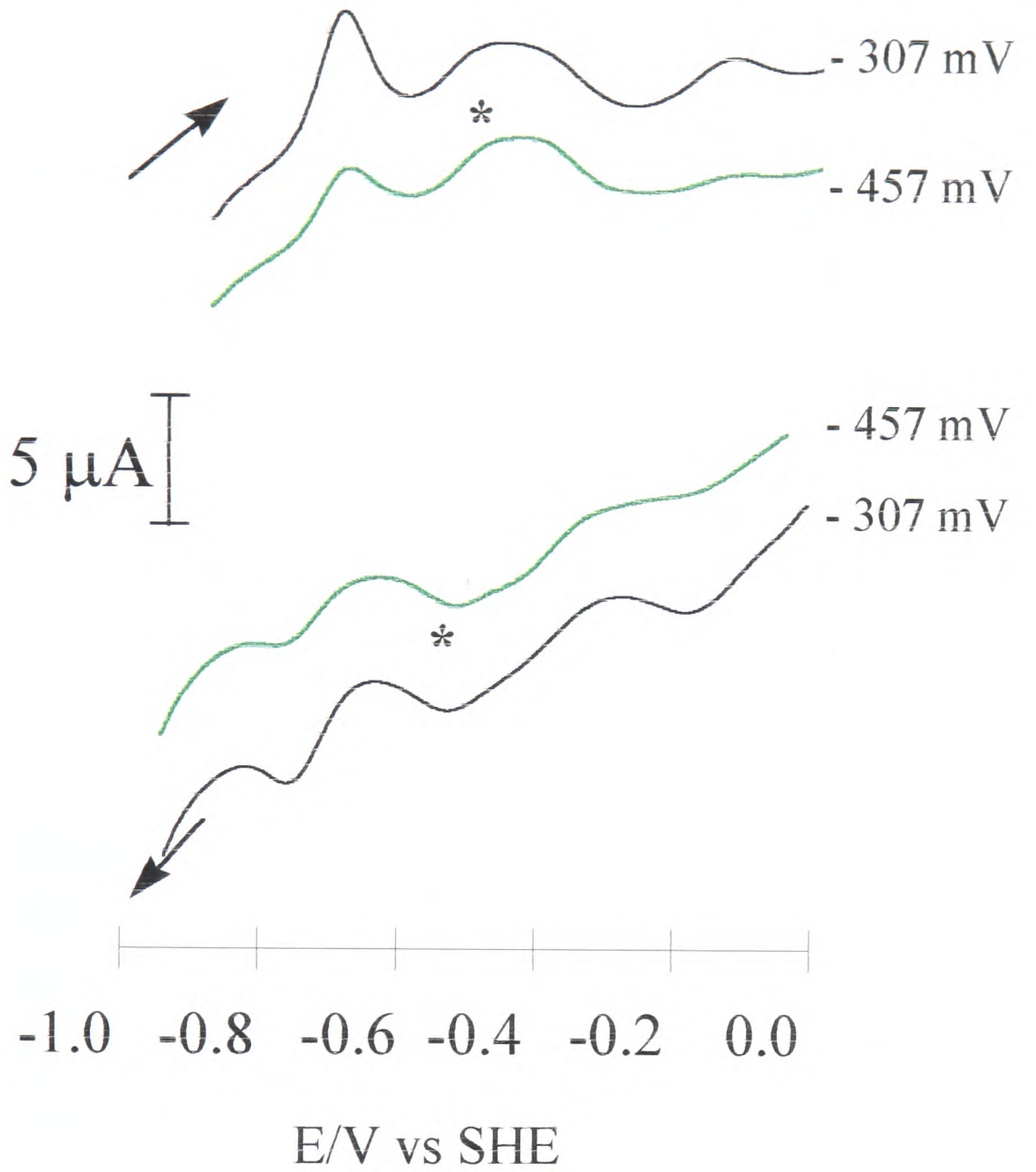

Figure 3.11 Metal Competition Experiment

Cyclic voltammograms showing the competitive metal ion uptake with a solution containing Zn^{2+} (0.5 µM) and Fe^{2+} (10 µM). Films of the Fd III were poised for 60 s at the potentials indicated, then a cycle was recorded at a scan rate of 500 mV s^{-1}. The signal due to $[Zn3Fe\text{-}4S]^{2+,1+}$ is indicated by (*****). Buffer electrolyte 20 mM Hepes, 0.1 M NaCl, pH 7.0 at 0 °C, 200 µg ml^{-1} polymyxin as co-adsorbate.

3.4 DISCUSSION

Direct potential control and the sensitivity achieved by having such a minuscule amount of protein adsorbed on the electrode, has allowed the relationship between cluster reactivity and the electrochemical potential to be explored in a very specific way. The cluster interconversions as depicted in Figure 3.3 occur in a simple and reversible manner for free metal ion, M^{2+}, via Reaction 5 only. This process occurs rapidly for a film of *Da* Fd III when it is adsorbed on the electrode surface. Therefore it is likely that only a small barrier must be overcome to accommodate the metal ion. Reaction rates of metal uptake appear to be dependent on the metal M. Previously, studies have shown that metal uptake of Tl^{1+} into the [3Fe-4S] core is very fast, and that Tl^{1+} also forms a weak complex with $[3Fe\text{-}4S]^{1+}$ (Reaction 4 in Figure 3.3). The M^{2+} ions, however, are slower with estimated rates,[4] following the approximate order, $\mathbf{Cd^{2+}>Zn^{2+}>Fe^{2+}>Co^{2+}}$ for *Da* Fd III. This order is as expected on the basis of typical ligand substitution rates, e.g. exchange of inner-sphere water molecules.[37]

Other ferredoxins for which transformation products are well characterised are the single-cluster systems *Desulfovibrio gigas* Fd and *Pyrococcus furiosus* Fd, both of these containing disulfide bridges.[38,39] *Da* Fd III is most certainly more amenable to cluster reactions than *Pf* Fd[b] when adsorbed on an electrode surface. A possible explanation is that the disulfide bridge confers extra rigidity in the protein structure of *Pf* Fd (and indeed for *Dg* Fd) which would hinder cluster interconversions. However, it is unlikely that *Da* Fd III is more reactive for this reason because it possesses instead, the inert [4Fe-4S] cluster as a cross-link. In addition, Fd III contains a glutamate in place of the proline which normally follows the remote cysteine residue[3,40] and this lack of the proline residue may result in a decrease of the rigidity in the cluster domain. Conformational flexibility is also suggested by the lack of hyperfine structure in the EPR spectra of $[Tl3Fe\text{-}4S]^{1+}$ and $[Co3Fe\text{-}4S]^{2+}$, consistent with greater M-subsite heterogeneity.[4,27] This is in contrast to the well-resolved spectra observed for $[Co3Fe\text{-}4S]^{1+}$ in *Pf* Fd[13] and *Dg* Fd.[15]

[b] See *Chapter 6* for a comprehensive examination of metal uptake for *Pf* Fd

For M^{2+} ion uptake, no significant reactivity was observed either for $[3Fe\text{-}4S]^{1+}$ or the hyper-reduced species $[3Fe\text{-}4S]^{2-}$. The former is too electron-deficient to co-ordinate a fourth divalent metal, whereas the all-Fe^{2+} cluster is likely to be extensively protonated.[30] It is not yet certain where exactly the protons bind, either on or near to the cluster, but clearly the greater electron count and/or the associated proton binding confers kinetic stability upon this state. Thus, for optimum conversion from the [3Fe-4S] cluster to the heterometal cluster, [M3Fe-4S], the potential at which the protein film had to be poised was below that of the reduction couple of $[3Fe\text{-}4S]^{1+/0}$ and at a higher potential than $E^{o'}$ for $[3Fe\text{-}4S]^{0/2-}$. This knowledge was particularly useful (i.e. for optimising conditions) when studying the metal uptake reactions of the [3Fe-4S] cluster from *Pf* Fd, which was considerably less amenable to cluster conversion when adsorbed on the film (*Chapter 6*).

For M^{2+} release, it was observed that degradation of $[Fe3Fe\text{-}4S]^{2+}$ to produce $[3Fe\text{-}4S]^{0}$ and Fe^{2+} was significantly slower than release of Zn^{2+} from $[Zn3Fe\text{-}4S]^{2+}$, for all potentials investigated. In both cases there appeared to be a 'threshold potential' for metal ejection. After poising at potentials above this value (for 60 s) voltammograms showed at least 50 % transformation to the [3Fe-4S]. For the Zn adduct this threshold potential was -400 mV and for the Fe adduct this was 0 mV. Sensitivity to the nature of the product is expected for a process in which the transition state most resembles the product, which in this case has little affinity for the leaving M. Although rates of release did increase somewhat as the potential was raised further, i.e. to 200 mV, no additional signals were observed in the voltammetry at high potentials which may have indicated formation of $[M3Fe\text{-}4S]^{3+}$. The superoxidised form of the cubane, $[M3Fe\text{-}4S]^{3+}$, is thought to be the intermediate for degradation of [M3Fe-4S] to [3Fe-4S] clusters, for example by oxidation with $Fe(CN)_6^{3-}$. In Figure 3.3 this pathway is depicted through Reactions 8 and 4. It is noted that the characteristics of M^{2+} release in *Da* Fd III are different to those of M^{2+} release observed for *Pf* Fd, which required much higher poising potentials to cause Fe to be released from the [Fe3Fe-4S] cluster (see *Chapter 6*). Thus, it can be concluded that applying a potential at which the [3Fe-4S] product is trapped in the 1+ level, i.e. pathway 5 → 1, is a viable route for metal ion release from [M3Fe-4S] in *Da* Fd III.

The potential dependence of metal uptake and ejection in *Da* Fd III shows that Reaction 5 alone provides a pathway for cluster degradation. This is particularly evident when the product is further trapped as $[3Fe\text{-}4S]^{1+}$, i.e. Reaction 5 is followed by Reaction 1 (Figure 3.3). In contrast, the [M3Fe-4S] core is conspicuously least labile in the 1+ level (i.e. < -400 mV for M = Fe, and < -500 mV for M = Zn). Significantly, this inertness extends to the low-potential region favouring the existence of hyper-reduced $[3Fe\text{-}4S]^{2-}$, a species which exhibits little activity in the uptake direction. The conclusion is that one or indeed both of these cluster species, $[M3Fe\text{-}4S]^{1+}$ and $[3Fe\text{-}4S]^{2-}$ are inert (kinetically stable) with regard to interconversion. The greater stability of $[Zn3Fe\text{-}4S]^{2+}$ versus $[Fe3Fe\text{-}4S]^{2+}$ (as inferred from the K_5 values) clearly contrasts with its relative lability, but is in accordance with the higher Zn uptake rates.

As is evident from Table 3.2, comparisons of the reduction potentials of the [3Fe-4S] clusters, and their corresponding [M3Fe-4S] products in different ferredoxins, serve to highlight the remarkable influence of just a single subsite - i.e. the M-ligand component. Notably, there is a great variation among cubanes with different M, whereas the [3Fe-4S] clusters have similar potentials in the biological examples given. With the exception of M = Mn and Ni for *Pf* Fd, reduction potentials for $[M3Fe\text{-}4S]^{2+/1+}$ (where M is a 2+ ion) are always more negative than $[3Fe\text{-}4S]^{1+/0}$. This is despite the more positive core and therefore, this reflects the importance of local protein structure and intrinsic electronic factors. Several points are apparent with regard to the complex influences of the ligand to M. Firstly, it has been reported previously that ligation by an exogenous thiolate (RS^-) causes the *Da* Fd III $[Fe3Fe\text{-}4S]^{2+/1+}$ reduction potential to decrease by nearly 200 mV due to the much tighter binding of RS^- to the oxidised cluster (see *Chapter 4*). Secondly, for M = Fe and Zn, the order of $E^{o'}$ values are reversed between Fd III and *Pf* Fd, suggesting different M-ligand co-ordination environments in the two proteins, as recently proposed by Finnegan *et al.*[13] It is probable that many thermodynamic and kinetic differences exist among cubane metal adducts formed in different proteins, reflecting either direct changes localised in the M-subsite region, or structural constraints originating elsewhere but transmitted to this region. Thirdly, and most obviously, the lability of the non-cysteine ligated metal in these proteins (and also aconitase) stems from the replacement of cysteine by oxygen-atom donors.

Several factors provide strong support for this.

1. Thiolate (RS^-) is a superior ligand for late transition- and post-transition metals, and competition with protonation is much more favourable. The corresponding K_5 values for typical S-ligation, must be $<< 10^{-8}$ since the pK for thiol/thiolate equilibrium in free cysteine is 8.4.[41]
2. It has been shown by Holm and co-workers that weak ligation ($X = CF_3SO_3^-$) to one of the Fe atoms generates a unique subsite of $[Fe_4S_4(LS_3)(X)]^{2-}$ from which it is possible to obtain the $[3Fe\text{-}4S]^0$ analogue with ease, $[Fe_3S_4(LS_3)]^{3-}$.[19,20]
3. Cowan and co-workers have investigated a mutant of *Chromatium vinosum* HiPIP, Cys77Ser, in which one cysteine is replaced by serine. Replacement of the cysteine by serine results in the oxidised cluster $[4Fe\text{-}4S]^{3+}$ being much more prone to degradation, an intermediate of which was found to be the $[3Fe\text{-}4S]^{1+}$ cluster. Thus, ligation of one of the Fe atoms by an oxygenic ligand results in destabilisation of the cluster.[42]
4. Replacement of aspartate-14 by cysteine in *Da* Fd III has recently been shown to stabilise the [M3Fe-4S] cluster compared to the [3Fe-4S] cluster (for M = Fe), as evidenced from the decrease in the observed K_5.[6]
5. Evidence has been collated which indicates that the more thiophilic metals such as Cd^{2+} or Tl^{1+} might override the need for protein ligation. It has been proposed that they need bond only to the exposed tri-μ_2-sulfido face of the [3Fe-4S] cluster, which would be sufficient to ensure metal complexation, and recruit solvent molecules to complete the co-ordination shell.

The difficulties associated with identifying and characterising possible heterometal clusters in nature depends primarily upon their detection but also on their stability and reactivity. Structural sensitivity to the ambient electrochemical potential, within biologically feasible limits, presents a natural asset to be exploited by regulatory Fe proteins, including the Iron Regulatory Protein[43] and redox sensors such as the transcription factor FNR.[c, 44] The ability to monitor and control very reactive cluster

[c] FNR (fumarate nitrate reduction) protein - a redox responsive regulator that activates and represses genes enabling anaerobic or aerobic metabolism in *Escherichia coli*, see *Chapter 1*.

species by sensitive methods such as protein film voltammetry represents an important aspect in these and other investigations.

	Da Fd III[d]	*Pf* Fd[e]	*Dg* Fd[f]	$[MFe_3S_4(X)(SR)_3]$[g]
[3Fe-4S]	-140 **-150**	-160 **-150**[h]	-130	-548[i]
Mn		>-100	-	-
Fe	-400 **-393**	-345 **-430**	-420	-1008[j] -958[k]
Co	-271 **-247**	-163	-245	-778
Ni	-	>-100	-360	-658
Cu	- **148**	190 -	-	-
Zn	-480 **-492**	-241 **-262**	-	-
Cd	-580 **-569**	-470 **-359**	-495	-
Cr	-	-440	-	-
Tl	- **80**[l]	- **152**	-	
Pb	- **-440**[m]	- -	-	-

Table 3.2 Reduction potentials for [M3Fe-4S] clusters in proteins and analogues[n]

Potentials for [M3Fe-4S] are given for the 2+/1+ redox couple, which in Figure 3.3 corresponds to Reaction 9 except for M = Cu and Tl, in which case the half-cell process is Reaction 8. Values for the [3Fe-4S] are given for the 0/1+ couple. Potentials in ***bold*** *are $E^{o'}$ values measured for protein films.* <u>References:</u> *Da Fd III*[2-5,22,27] *Pf Fd*[8,13,45] *Dg Fd*[17] *$[MFe_3S_4(X)(SR)_3]$*[20,46]

---

[d] Data are for pH 7.0, 0.1 M NaCl except where stated.

[e] Data are for pH 8.0, values determined by potentiometric EPR titrations except where stated.

[f] pH 7.6 values determined by potentiometric EPR titrations or square wave voltammetry.

[g] Values determined by cyclic voltammetry in acetonitrile, corrected to the SHE scale.

[h] Protein film method, pH 7.0, 0 °C, see *Chapter 6.*

[i] (SR) = (LS_3), no X

[j] $(SR)_3$ = LS_3 a tripodal cavitand ligand, (X) = N-methylimidodiacetate.

[k] SR = X = S-mesitylthiolate.

[l] pH 7.0, 0.5 M NaCl

[m] pH 6.0, 0.1 M NaCl

[n] For a graphical representation of this data see *Chapter 6.*

3.5 REFERENCES

1) Beinert, H.; Kennedy, M. C.; Stout, C. D. *Chemical Reviews* **1996**, *96*, 2335-2373.

2) George, S. J.; Armstrong, F. A.; Hatchikian, E. C.; Thomson, A. J. *Biochemical Journal* **1989**, *264*, 275-284.

3) Butt, J. N.; Armstrong, F. A.; Breton, J.; George, S. J.; Thomson, A. J.; Hatchikian, E. C. *Journal of the American Chemical Society* **1991**, *113*, 6663-6670.

4) Butt, J. N.; Sucheta, A.; Armstrong, F. A.; Breton, J.; Thomson, A. J.; Hatchikian, E. C. *Journal of the American Chemical Society* **1991**, *113*, 8948-8950.

5) Butt, J. N.; Niles, J.; Armstrong, F. A.; Breton, J.; Thomson, A. J. *Nature Structural Biology* **1994**, *1*, 427-433.

6) Busch, J. L. H.; Breton, J. L.; Bartlett, B. M.; Armstrong, F. A.; James, R.; Thomson, A. J. *Biochemical Journal* **1997**, *323*, 95-102.

7) Armstrong, F. A. *Advances in Inorganic Chemistry* **1992**, *38*, 117-163.

8) Aono, S.; Bryant, F. O.; Adams, M. W. W. *Journal of Bacteriology* **1989**, *171*, 3433-3439.

9) Conover, R. C.; Kowal, A. T.; Fu, W.; Park, J. B.; Aono, S.; Adams, M. W. W.; Johnson, M. K. *Journal of Biological Chemistry* **1990**, *265*, 8533-8541.

10) Conover, R. C.; Park, J. B.; Adams, M. W. W.; Johnson, M. K. *Journal of the American Chemical Society* **1990**, *112*, 4562-4564.

11) Srivastava, K. K. P.; Surerus, K. K.; Conover, R. C.; Johnson, M. K.; Park, J. B.; Adams, M. W. W.; Munck, E. *Inorganic Chemistry* **1993**, *32*, 927-936.

12) Fu, W. G.; Telser, J.; Hoffman, B. M.; Smith, E. T.; Adams, M. W. W.; Finnegan, M. G.; Conover, R. C.; Johnson, M. K. *Journal of the American Chemical Society* **1994**, *116*, 5722-5729.

13) Finnegan, M. G.; Conover, R. C.; Park, J. B.; Zhou, Z. H.; Adams, M. W. W.; Johnson, M. K. *Inorganic Chemistry* **1995**, *34*, 5358-5369.

14) Kissinger, C. R.; Sieker, L. C.; Adman, E. T.; Jensen, L. H. *Journal of Molecular Biology* **1991**, *219*, 693-715.

15) Moura, I.; Moura, J. J. G.; Munck, E.; Papaefthymiou, V.; Legall, J. *Journal of the American Chemical Society* **1986**, *108*, 349-351.

16) Surerus, K. K.; Munck, E.; Moura, I.; Moura, J. J. G.; Legall, J. *Journal of the American Chemical Society* **1987**, *109*, 3805-3807.

17) Moreno, C.; Macedo, A. L.; Moura, I.; Legall, J.; Moura, J. J. G. *Journal of Inorganic Biochemistry* **1994**, *53*, 219-234.

18) Zhou, J.; Raebiger, J. W.; Crawford, C. A.; Holm, R. H. *Journal of the American Chemical Society* **1997**, *119*, 6242-6250.

19) Zhou, J.; Holm, R. H. *Journal of the American Chemical Society* **1995**, *117*, 11353-11354.

20) Zhou, J.; Hu, Z. G.; Munck, E.; Holm, R. H. *Journal of the American Chemical Society* **1996**, *118*, 1966-1980.

21) Cen, W.; Lee, S. C.; Li, J. G.; Macdonnell, F. M.; Holm, R. H. *Journal of the American Chemical Society* **1993**, *115*, 9515-9523.

22) Armstrong, F. A.; George, S. J.; Cammack, R.; Hatchikian, E. C.; Thomson, A. J. *Biochemical Journal* **1989**, *264*, 265-273.

23) Gorst, C. M.; Yeh, Y. H.; Teng, Q.; Calzolai, L.; Zhou, Z. H.; Adams, M. W. W.; Lamar, G. N. *Biochemistry* **1995**, *34*, 600-610.

24) Calzolai, L.; Gorst, C. M.; Zhao, Z. H.; Teng, Q.; Adams, M. W. W.; Lamar, G. N. *Biochemistry* **1995**, *34*, 11373-11384.

25) Butt, J. N.; Sucheta, A.; Armstrong, F. A.; Breton, J.; Thomson, A. J.; Hatchikian, E. C. *Journal of the American Chemical Society* **1993**, *115*, 1413-1421.

26) Telser, J.; Smith, E. T.; Adams, M. W. W.; Conover, R. C.; Johnson, M. K.; Hoffman, B. M. *Journal of the American Chemical Society* **1995**, *117*, 5133-5140.

27) Butt, J. N.; Fawcett, S. E. J.; Breton, J.; Thomson, A. J.; Armstrong, F. A. *Journal of the American Chemical Society* **1997**, *119*, 9729-9737.

28) Surerus, K. K. *Ph.D. Thesis*; University of Minnesota:, **1989**.

29) Butt, J. N. *Ph.D. Thesis* University of California, Irvine, **1993**.

30) Duff, J. L. C.; Breton, J. L. J.; Butt, J. N.; Armstrong, F. A.; Thomson, A. J. *Journal of the American Chemical Society* **1996**, *118*, 8593-8603.

31) Verhagen, M. F. J. M.; Link, T. A.; Hagen, W. R. *FEBS Lett.* **1995**, 75-78.

32) Im, S. C.; Kohzuma, T.; McFarlane, W.; Gaillard, J.; Sykes, A. G. *Inorganic Chemistry* **1997**, *36*, 1388-1396.

33) Angove, H. C.; Yoo, S. J.; Burgess, B. K.; Munck, E. *Journal of the American Chemical Society* **1997**, *119*, 8730-8731.

34) Cammack, R. *Advances in Inorganic Chemistry*, **1992**; Vol. 38.

35) Johnson, M. K. *Encyclopedia of Inorganic Chemistry*; Wiley: Chichester:, **1994**; Vol. 4.

36) Hirst, J.; Duff, J. L. C.; Jameson, G. N. L.; Kemper, M. A.; Burgess, B. K.; Armstrong, F. A. *Journal of the American Chemical Society* **1998**, *120*, 7085-7094.

37) Cotton, F. A.; Wilkinson, G. *Advanced Inorganic Chemistry*; Fith ed., **1988.**

38) Macedo, A. L.; Moura, I.; Surerus, K. K.; Papaefthymiou, V.; Liu, M. Y.; Legall, J.; Munck, E.; Moura, J. J. G. *Journal of Biological Chemistry* **1994**, *269*, 8052-8058.

39) Gorst, C. M.; Zhou, Z. H.; Ma, K. S.; Teng, Q.; Howard, J. B.; Adams, M. W. W.; Lamar, G. N. *Biochemistry* **1995**, *34*, 8788-8795.

40) Hatchikian, E. C.; Bruschi, M. *Biochimica Et Biophysica Acta* **1981**, *634*, 41-51.

41) *CRC Handbook of Chemistry and Physics*; CRC Press: Boca Raton, **1996**, 77th Edition.

42) Agarwal, A.; Li, D. W.; Cowan, J. A. *Journal of the American Chemical Society* **1996**, *118*, 927-928.

43) Rouault, T. A.; Haile, D. J.; Downey, W. E.; Philpott, C. C.; Tang, C.; Samaniego, F.; Chin, J.; Paul, I.; Orloff, D.; Harford, J. B.; Klausner, R. D. *Biometals* **1992**, *5*, 131-140.

44) Green, J.; Bennett, B.; Jordan, P.; Ralph, E. T.; Thomson, A. J.; Guest, J. R. *Biochem.J.* **1996**, *316*, 887-892.

45) Staples, C. R.; Dhawan, I. K.; Finnegan, M. G.; Dwinell, D. A.; Zhou, Z. H.; Huang, H. S.; Verhagen, M.; Adams, M. W. W.; Johnson, M. K. *Inorganic Chemistry* **1997**, *36*, 5740-5749.

46) Zhou, J.; Scott, M. J.; Hu, Z. G.; Peng, G.; Munck, E.; Holm, R. H. *Journal of the American Chemical Society* **1992**, *114*, 10843-10854.

CHAPTER 4

INVESTIGATION OF EXOGENOUS LIGAND BINDING TO HOMO- AND HETEROMETAL CLUSTERS, [M3FE-4S], IN FERREDOXIN III FROM *Desulfovibrio africanus*

CHAPTER 4

INVESTIGATION OF EXOGENOUS LIGAND BINDING TO HOMO- AND HETEROMETAL CLUSTERS, [M3FE-4S], IN FERREDOXIN III FROM *Desulfovibrio africanus*

4.1 INTRODUCTION

Initial interest in biological iron-sulfur centres focused upon their electron-transfer characteristics, and their role in maintaining protein structure. However, as research progressed and several new types of metal clusters were discovered, it became apparent that they play a much wider role in biochemical processes.[1-5] Clusters with the ability to interconvert between [3Fe-4S] and [M3Fe-4S] have been discovered (*Chapter 3*) and, contrary to the initial assumption that ligation was exclusively by cysteine, it has been found that clusters may be co-ordinated by a variety of ligands (*Chapter 1*). The nature and lability of the ligating residues is a rapidly expanding area of research in metallo-sulfur cluster chemistry.

Cubane-type [4Fe-4S] clusters are ubiquitous in biological systems and are found in ferredoxins (simple redox proteins) and also in a wide range of cytoplasmic and membrane-bound enzymes.[4] There are two main strategies through which these simple metallo-sulfur clusters may access a greater variation of physical and chemical properties and reactivity - these are *metal uptake* of the cluster [6-23] and *ligand binding* (either *ligand exchange* or *ligand addition*).[24] Metal uptake can result in significant changes in the electron density and hence the redox characteristics of the cluster - two detailed

investigations of metal uptake (and also metal release) are contained in this thesis. Metal uptake by Fd III from *Desulfovibrio africanus* (*Da*) is considered in *Chapter 5* and metal uptake by the ferredoxin from the hyperthermophile *Pyrococcus furiosus* (*Pf*) is considered in *Chapter 6*. A schematic cartoon of ligand binding is shown in Figure 4.1.

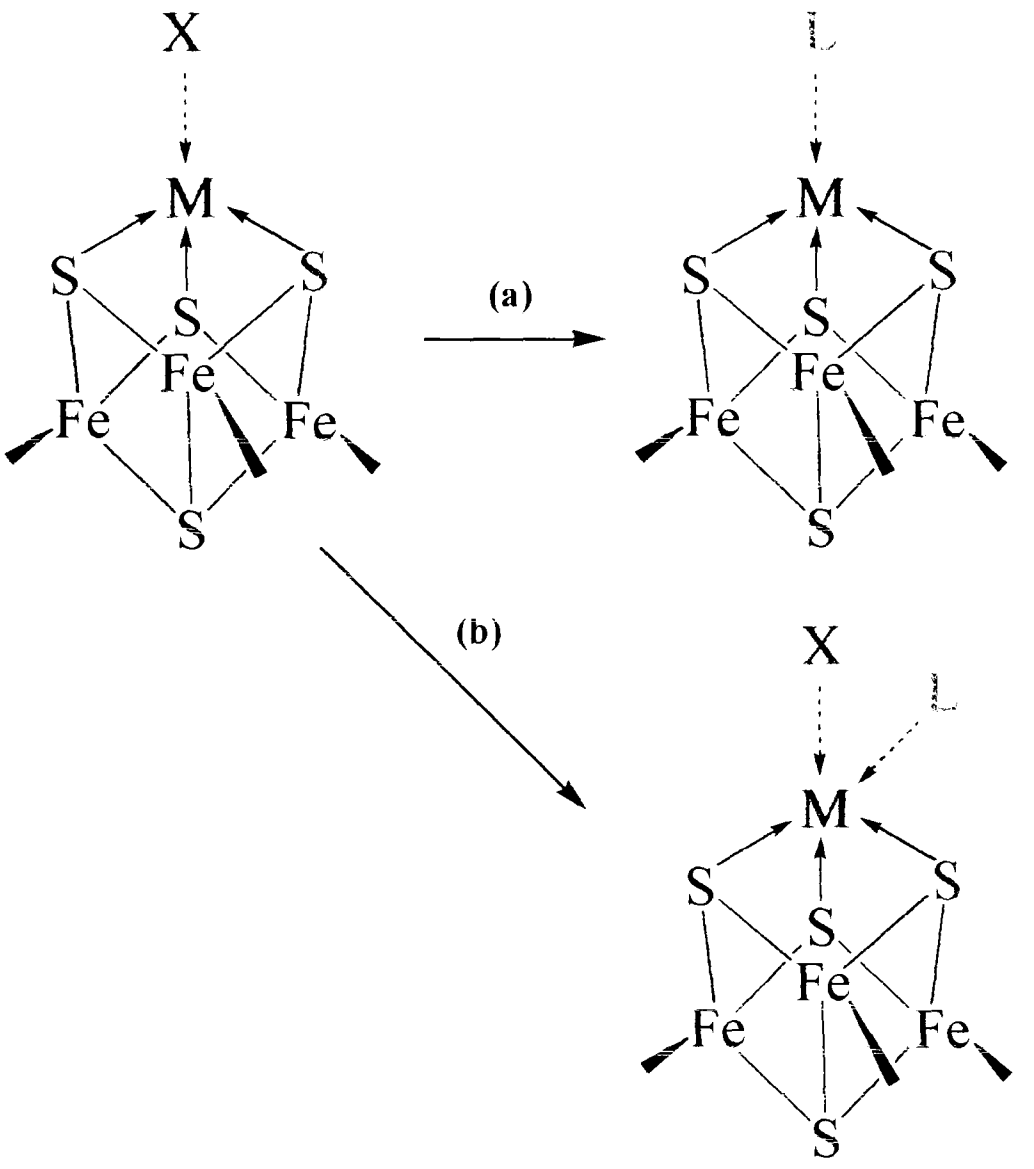

Figure 4.1 Cartoon showing ligand binding in *Da* Fd III

The above cartoon shows the two options for ligand binding to the transformed cluster [M3Fe-4S] from Da Fd III. (a) ***Ligand exchange****, if the X ligand is displaced by L from the M co-ordination sphere; (b)* ***ligand addition*** *if both X and L co-ordinate M.*

Ligand exchange, whereby the native ligating residue of the cluster is exchanged for another ligand, can be either *internal* or *external*. Internal ligand exchange - in which the replacement ligand originates from the protein's primary structure, can be accomplished using site directed mutagenesis.[25] However, this chapter is based upon the substitution,

or augmentation, of a native protein ligand for a ligand originating externally. For examples of internal ligand exchange see *Chapter 5*.

For ligand exchange to be a useful 'property' of a metallo-sulfur cluster, for example as in the enzyme aconitase (see *Chapter 1*), it is essential that ligand exchange be *specific* to a certain atom in the cluster. This is essential in order to avoid competing reactions at other sites in the cluster during catalysis and the atom in question must, therefore, be in some way differentiated from the other atoms in the cluster. If the atom is the same chemical element as the other metal atoms in the cluster, then the direct environment of this atom must be such that it differentiates between them. That is to say the particular atom must be *subsite-differentiated*. For example, aconitase contains an FeS cluster which is able to bind substrate at the 'fourth' iron atom of the cluster - this Fe atom is predisposed for substrate binding because it is ligated by an aspartate ($^{-}$OH), unlike the three other Fe atoms, which are more conventionally ligated by cysteine.[26]

Holm and co-workers have successfully synthesised a non-biological analogue of a subsite differentiated [4Fe-4S] cluster, in which the subsites are differentiated in the ratio 3:1. This has been achieved by using tridentate trithiolate ligands to co-ordinate three of the four atoms, while the fourth Fe is co-ordinated by an exchangeable ligand such as chloride.[27] This labile ligand may then be replaced by a wide range of alternative ligands which may be monodentate, bidentate or tridentate - the resultant products are four-, five-, and six-co-ordinate with respect to the unique fourth Fe.[28] The clusters thus formed have been characterised by NMR and electrochemistry, most significantly there is a considerable negative shift in the reduction potential of the 2+/1+ and 3+/2+ redox couples of the cluster, and asymmetry is introduced into the electron density of the cluster. In a related study Barclay *et al* have reacted the site-differentiated [4Fe-4S] cores with a series of amino acid methyl esters.[29] These 3:1 site-differentiated clusters $[Fe_4S_4(L)(SEt)]^{2-}$ (where L is tridentate ligand)[a] react with Cys-OMe, Tyr-OMe, Ser-OMe or HHis-OMe to give $[Fe_4S_4(L)(AA\text{-}OMe)]^{2-}$ or $[Fe_4S_4(L)(HHis\text{-}OMe)]^{-}$.

---

[a] L = L^1 or L^2; where H_3L^1 = 1,4,7-tris(4-sulfanylbenzoyl)-1,4,7-triazacyclononane, H_3L^2 = 1,5,9-tris(4-sulfanylbenzoyl)-1,5,9-trizazcyclododecane)[29]

The non-biological analogues discussed above mimic behaviour which has long been thought to occur in biological systems such as aconitase. Aconitase was one of the first examples of an FeS cluster-containing protein which performed a function other than electron transfer. Aconitase has been known for over 50 years, but was only found to contain an FeS cluster in the 1970's.[30] The enzyme catalyses the stereospecific conversion of citrate to isocitrate via the intermediate *cis*-aconitate,[26] and is part of a larger group of enzymes known as (de)hydratases. The active form of aconitase contains a [4Fe-4S] cluster, one Fe of which is co-ordinated by a hydroxide ion, and not a cysteine, as in more conventional [4Fe-4S] clusters. Thus, there is a 'subsite-differentiated' Fe atom which acts as a Lewis acid catalyst and which is able to bind a substrate molecule reversibly - on binding the substrate the Fe becomes six-co-ordinate (see Figure 1.7, *Chapter 1*).[26] The inactive state, resulting from exposure to O_2, is a [3Fe-4S] cluster which is unable to bind the substrate due to lack of the fourth iron. Reactivation of the enzyme is effected by the addition of Fe^{2+} under reducing conditions. This ability of the cluster to exchange its ligating groups thus allows it to 'communicate' with the external media.

A further example of ligand exchange has been observed in the small ferredoxin from *Pyrococcus furiosus*. This ferredoxin is similar to aconitase in that it contains a [4Fe-4S] cluster with one non-cysteinyl ligand.[11,31] Recent ^{1}H-NMR[32,33] and ^{1}H-ENDOR[34] results indicate that the cluster is ligated by three cysteines and an aspartate, which replaces cysteine in the characteristic -C-X_2-C/D-X_2-C-X_n-C- arrangement of co-ordinating cysteines. This produces a subsite differentiated Fe atom in the cluster which can be reversibly removed from the cluster by oxidation with ferricyanide, and may be subsequently reintroduced by addition of Fe^{2+} under reducing conditions.[11] Spectroscopic methods have been used to examine exogenous ligand binding to various adducts of the [3Fe-4S] cluster of *Pf* Fd.[12,13,15,34] Mercaptoethanol and cyanide binding have been examined using EPR and variable temperature magnetic circular dichroism (VTMCD). Incubation of the [Zn3Fe-4S] form of the protein with a 250 fold excess of mercaptoethanol resulted in reversible spectral changes indicating formation of a mercaptoethanol adduct - the ground and excited state properties of the thiolate-bound $[Zn3Fe\text{-}4S]^{1+}$ cluster in *Pf* Fd were very similar to those of the equivalent $[Zn3Fe\text{-}4S]^{1+}$

cluster in *Desulfovibrio gigas* Fd II.[15] Binding of cyanide to the cluster in *Pf* Fd was observed upon incubation in a 50 fold excess of potassium cyanide. In this case control experiments on reduced 8Fe Fd from *Clostridium pasteurianum* (where all Fe atoms are co-ordinated by cysteine residues), and also on the [3Fe-4S] form of *Pf* Fd, gave no change in the EPR spectra, thus showing that cyanide binding occurs at the subsite-differentiated site of *Pf* 4Fe Fd.[34]

The ability of clusters to exchange or add ligands leads us to ask a number of questions, most importantly:

(i) What are the determining factors in a protein structure which facilitate ligand exchange?

(ii) Which species are able to co-ordinate to a cluster?

It is possible to formulate answers by using a range of different ligands and a biological system which has a proven ligand exchange tendency[24] - in this case the atypical 7Fe ferredoxin from *Desulfovibrio africanus* (*Da* Fd III), described in detail in *Chapter 3*. It is worth reiterating that it contains both a [4Fe-4S] cluster and a [3Fe-4S] cluster. The [3Fe-4S] cluster may undergo conversion to [M3Fe-4S],[16-20] but the native [4Fe-4S] cluster is inert under the conditions employed in this chapter. The [3Fe-4S] core is co-ordinated by three cysteine residues, with an aspartate residue in what would normally be the central co-ordination position of a typical 4Fe cluster i.e. -C-X_2-C/D-X_2-C-X_n-C-.

As described in *Chapter 3*, protein film electrochemistry of the native 7Fe Fd III gives rise to three separate redox couples, A', B' and C' (Figure 3.6; *Section 3.3.1*) These are due to the couples $[3Fe\text{-}4S]^{1+/0}$, $[4Fe\text{-}4S]^{2+/1+}$ and $[3Fe\text{-}4S]^{0/2-}$ respectively.[18] As also described in *Chapter 3*, metal uptake to form new [M3Fe-4S] clusters is facile in Fd III.[16-19,35] The heterometal clusters formed have been examined both electrochemically and using spectroscopic techniques. The redox couple $[M3Fe\text{-}4S]^{2+/1+}$ is denoted D', and has a reduction potential which is dependent on the identity of M (Table 3.1; *Section 3.3.1*), although for *Da* Fd III when M = Fe^{2+}, couple D' overlays couple B'. More recently, it has been shown electrochemically that the ability to incorporate metal ions depends also on the cluster's redox state.[20] Once a metal ion has

been incorporated into the [3Fe-4S] cluster the transformed Fd III is similar to aconitase and *Pf* Fd, in that it has a subsite-differentiated metal atom in the FeS cluster. *Da* Fd III is then able to undergo exogenous ligand binding, although it should be noted that a subsite-differentiated metal substituent of a cluster is not likely to be the *only* prerequisite for ligand binding.

Electrochemistry has already been used to demonstrate that exogenous ligand binding can occur to the transformed 8Fe Fd from *Da* Fd III. When an adsorbed protein film containing the [Fe3Fe-4S] cluster is introduced into a solution of mercaptoethanol a distinct change is observed in the voltammetry and a new redox couple is observed.[24] In the absence of an exogenous ligand a single redox signal is observed, which is assigned to the superposition of two couples: the native $[4Fe\text{-}4S]^{2+/1+}$ cluster (B') and the $[Fe3Fe\text{-}4S]^{2+/1+}$ cluster (D'), Figure 4.2(a).[18] Upon introduction of the protein into a solution of mercaptoethanol this single signal (observed at slow scan rate) splits into two smaller ones, having approximately equal areas, Figure 4.2(b). One of the new couples remains in a position close to that of the original (B' only), the other is shifted to a more negative potential. The position of the new redox couple ($E^{o\prime}_{obs}$) is dependent upon the concentration of mercaptoethanol, see Figure 4.2(b) and (c). No voltammetric change is observed when an adsorbed film of *only* the 7Fe Fd is placed into the mercaptoethanol containing electrolyte. From this it is concluded that it is the subsite differentiated Fe atom that is the site of interaction. On returning the adsorbed film to a pot containing only buffer/electrolyte the A' and C' couples reappear indicating that the reaction is reversible. A scheme for reversible ligand binding is shown in Figure 4.3.

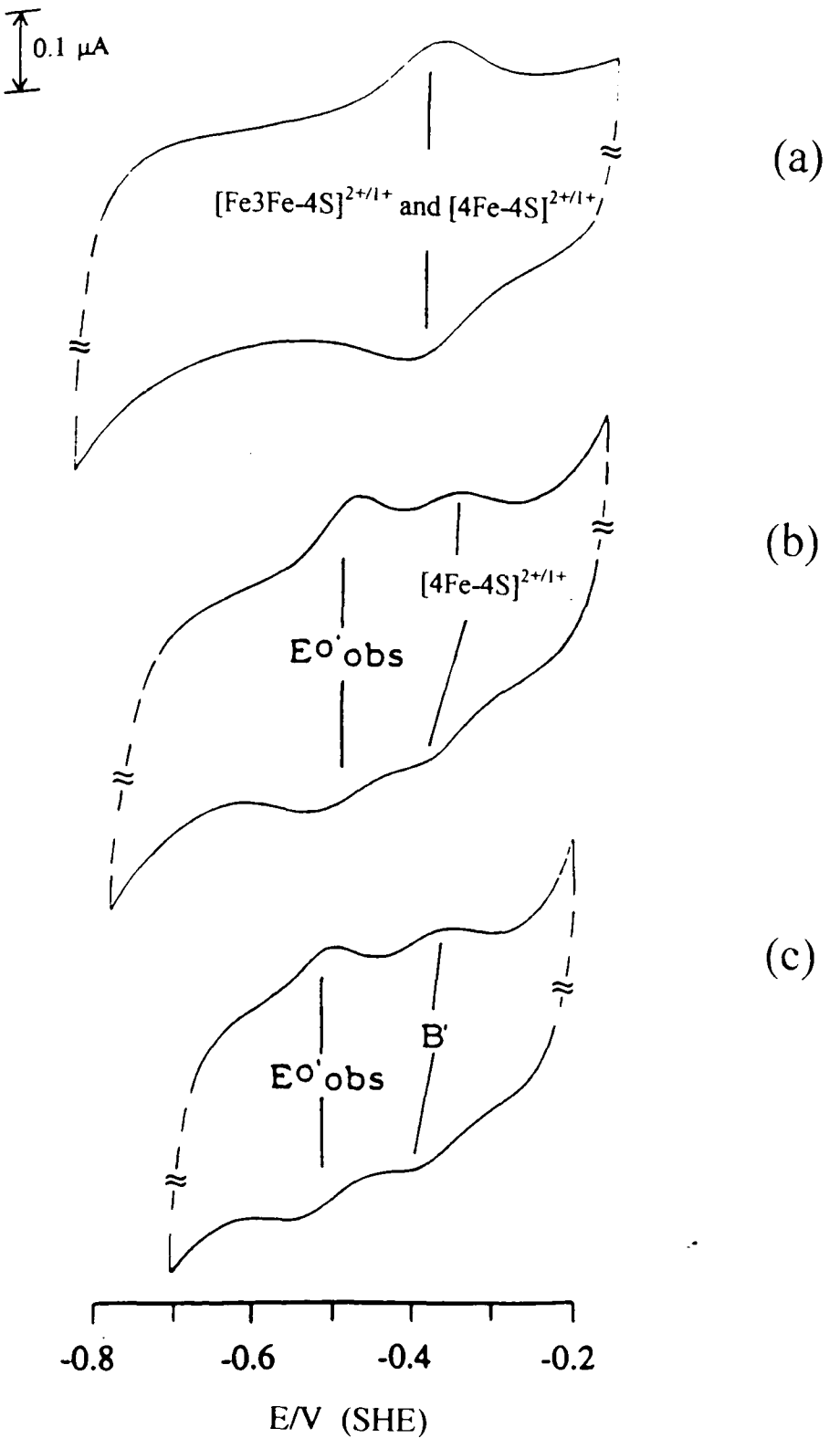

Figure 4.2 Mercaptoethanol and 8Fe Fd III

Mercaptoethanol concentrations (thiolate concentrations in parentheses) are: (a) 0 mM; (b) 168 (2.6) mM; (c) 536 (8.4) mM. $E^{o'}_{obs}$ indicates the position of the new couple and B' represents the $[4Fe\text{-}4S]^{2+/1+}$ couple. All solutions contained 180 μM Fe^{2+}, 0.2 M NaCl, 20 mM Tris, pH 8.0 at 0 °C, 10 mV s^{-1}.

4.1.1 Mathematical Representation of Ligand Binding

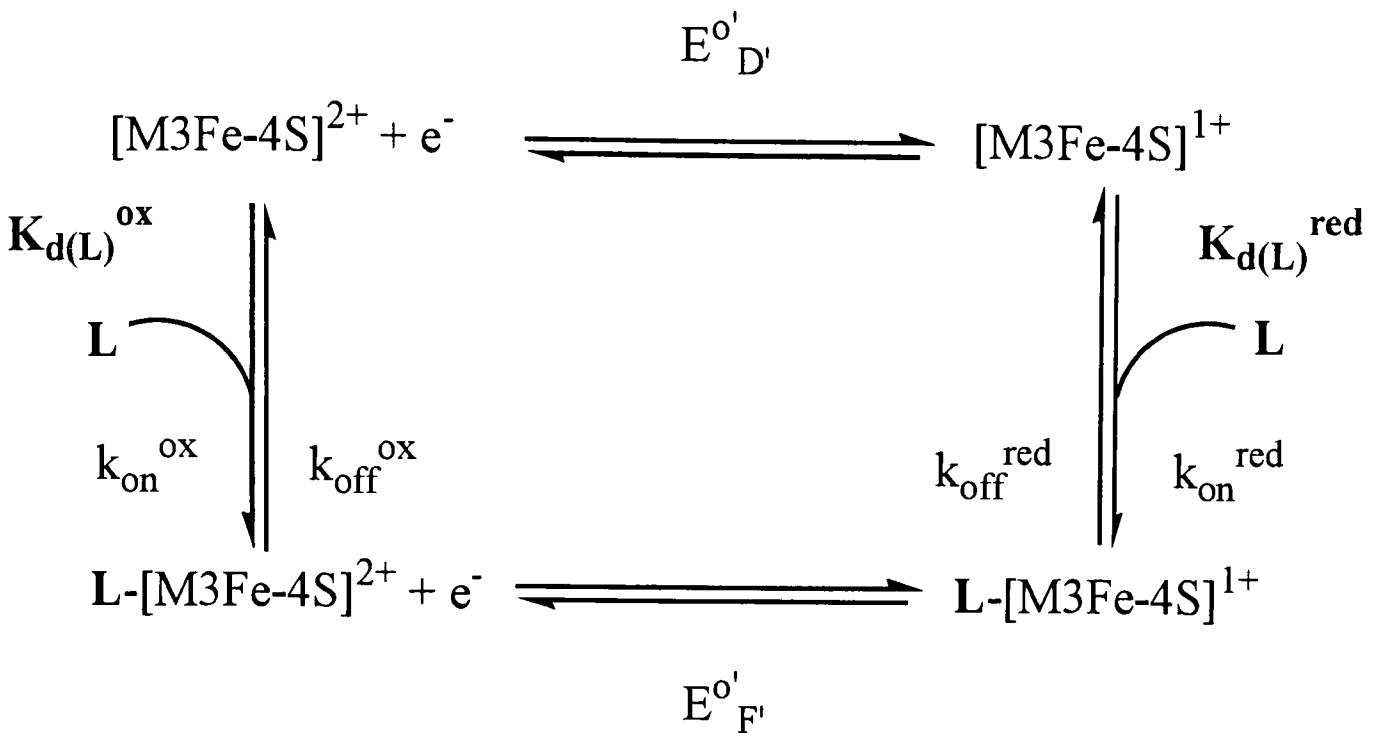

Figure 4.3 Scheme of ligand binding in *Da* Fd III

Electrochemically, the reversible exogenous ligand binding is coupled to electron transfer - a schematic overview of the reactions which occur is shown in Figure 4.3.[24] The dissociation constants $K_{d(L)}^{ox}$ and $K_{d(L)}^{red}$ are defined in Equations 4.1 and 4.2. In the following equations populations of the various clusters, denoted for example by [[M3Fe-4S]$^{2+}$], are confined to the electrode surface and [L] represents the concentration of ligand in the solution.

$$K_{d(L)}^{ox} = [[M3Fe-4S]^{2+}][L]/[L-[M3Fe-4S]^{2+}] \qquad \textbf{Equation 4.1}$$

$$K_{d(L)}^{red} = [[M3Fe-4S]^{1+}][L]/[L-[M3Fe-4S]^{1+}] \qquad \textbf{Equation 4.2}$$

At slow scan rates changes in cluster ligation will be rapid on the experimental timescale - and conditions will therefore approach electrochemical equilibrium. The observed reduction potential at equilibrium, $E^{o'}_{obs}$, is dependent upon ligand concentration (Equation 4.3). All terms are as defined in Figure 4.3.

$$E^{\circ\prime}_{obs} = E^{\circ\prime}_{D} + (2.303RT/F)\log\{(1+[L]/K_{d(L)}^{red})/(1+[L]/K_{d(L)}^{ox})\}$$

Equation 4.3

At low ligand concentration, $[L] << K_{d(L)}^{ox,red}$, thus $[L]/ K_{d(L)}^{ox,red} \rightarrow 0$. Hence, $E^{o\prime}_{obs}$ tends asymptotically towards $E^{o\prime}_{D}$ (the reduction potential of the unligated cluster). At high ligand concentration $[L] >> K_{d(L)}^{ox,red}$, thus $[L]/ K_{d(L)}^{ox,red} >> 1$ and $E^{o\prime}_{obs}$ tends asymptotically towards $E^{o\prime}_{F}$ (the reduction potential of the ligated cluster), as defined by Equation 4.4:

$$E^{\circ\prime}_{F} = E^{\circ\prime}_{D} + (2.303RT/F)\log(K_{d(L)}^{ox} / K_{d(L)}^{red}) \qquad \textbf{Equation 4.4}$$

A plot of $E^{o\prime}_{obs}$ versus log [L] is thus sigmoidal with limits at $E^{o\prime}_{D}$ for $[L] << K_{d(L)}$ and at $E^{o\prime}_{F}$ for $[L] >> K_{d(L)}^{red}$ as shown below in Figure 4.4.

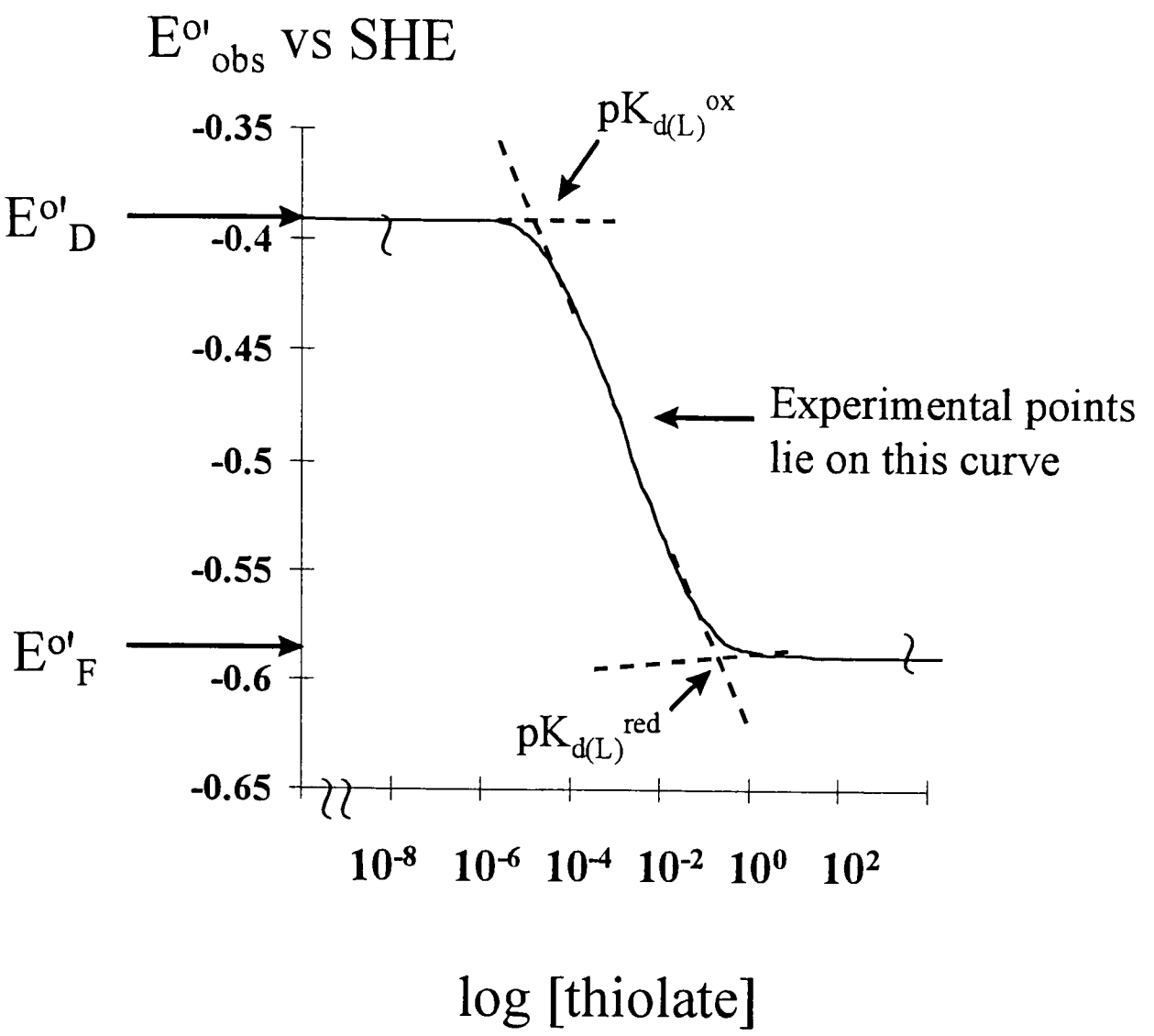

Figure 4.4 $E^{o'}_{obs}$ as a function of thiolate concentration, according to Figure 4.3

4.1.2 Aims of this Investigation

The work described in this chapter aims to define what controls the binding of an exogenous ligand to a metal cluster, within a defined protein environment. Specifically, the binding of a wide range of ligands (as detailed in Table 4.1) to the [Fe3Fe-4S], [Zn3Fe-4S] and [Co3Fe-4S] clusters produced in *Da* Fd III are studied. In this way the effects of varying the heterometal (the subsite-differentiated metal atom) are investigated in the absence of major changes in the local protein environment, and the binding properties of sets of ligands are used to shed light upon, for example, the differences between thiolate and oxygenic co-ordination. Clusters are commonly ligated by thiolate species, whereas ligation by oxygen species is relatively rare, although examples include aconitase,[26] the 4Fe Fd from *Pf* [32,36] and the [2Fe-2S] cluster in succinate dehydrogenase from *E. coli*.[37] Additional ligands, such as glutathione, were also chosen

because they are already know to function biologically either alone or as part of more complex systems.

The experimental foundation for this work was set down by J.N. Butt,[38] who studied addition of Fe to the [3Fe-4S] cluster of *Da* Fd III and subsequent ligand exchange with the mercaptoethanoate anion, determining the dissociation constants, $K_{d(L)}^{ox}$ and $K_{d(L)}^{red}$, for mercaptoethanoate binding.[24] This work was also extended to include mercaptoethanoate binding to the transformed [M3Fe-4S] clusters, M = Zn and Co, the results of these experiments are presented below in Table 4.2. The discussion at the conclusion of this chapter is thus based upon work carried out over a considerable length of time. Every attempt has been made to ensure continuity and thus allow a valid comparison of results.

Ligand	Structure
Mercaptoethanol (1-hydroxyethane-2-thiol) pK_H of thiol group = 9.8[b]	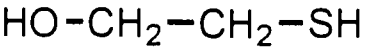
L-Cysteine pK_H of thiol group = 10.6[b]	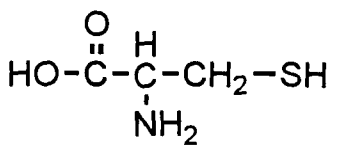
Glutathione (γ-Glutamylcysteinyl-glycine) pK_H of thiol group = 9.8[b]	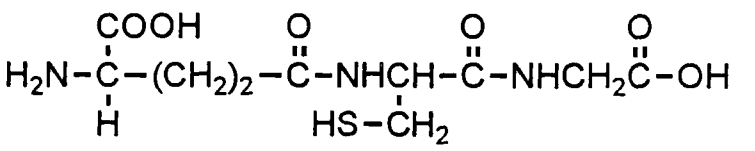
Coenzyme M (2-mercaptoethane sulfonic acid) pK_H of thiol group = 9.0[b]	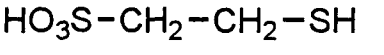
Thioacetic acid (ethanethioic acid)	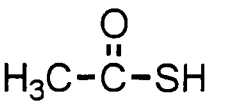
Thiomalic acid (mercaptosuccinic acid)	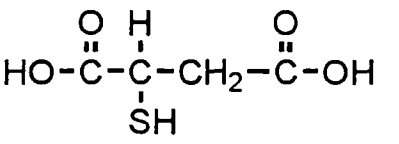
Thioglycolic acid (mercaptoacetic acid)	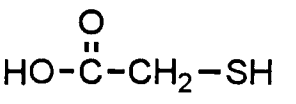
3-Mercaptopropionic acid pK_H of thiol group = 10.4[b]	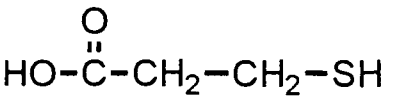
Cysteamine (2-aminoethanethiol) pK_H of thiol group = 8.9[b]	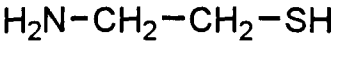

Table 4.1 Exogenous ligands investigated

...continued on following page...

[b] The pK of the thiol group was found by titration against a solution of NaOH (itself previously standardised against a solution of oxalic acid) under the experimental conditions (J.N. Butt).

Catechol (1,2-benzenediol)	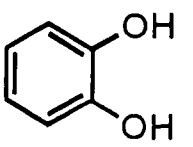
Oxalic acid (ethanedioic acid)	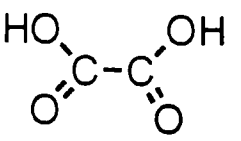
Oxalacetic acid (oxo-butanedioic acid)	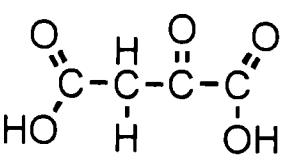

Table 4.1 Exogenous ligands investigated

4.2 EXPERIMENTAL

Electrochemical experiments were carried out in a multi-pot cell as described in *Chapter 2*, which allowed fast and efficient transfer of a protein film, adsorbed on an electrode, between solutions. All solutions were maintained at 0 °C using a thermostatted water circulator (Neslab).

Thiolate concentrations in stock solutions were determined by measuring the pH of the solution and using the following equation:

$$[\text{thiolate}] = [\text{thiol}]_{\text{total}} / (1 + [H^+] / K_H) \qquad \textbf{Equation 4.5}$$

where K_H is the dissociation constant of the thiol group on the ligand

As the majority of the experiments were carried out qualitatively, the exact concentration of the thiolate anion was not always known. For the species which a pK of the thiol group was not known, the concentration of the stock solution was generally 0.2 M (thiol). At the experimental pH (pH > 8.0) sufficient percentage of the thiol was assumed to be ionised to provide a population of thiolate molecules for reaction with the protein film. This is one of the major advantages of the protein film method - only minute quantities of the protein are used in each individual experiment and thus it is easy to have more than a 1:1 stoichiometric ratio of ligand to cluster, even at very low ligand concentrations.

Experiments were then carried out in three stages:

(1) A film of *Da* Fd III was formed on the electrode surface, and the voltammetric signals allowed to stabilise whilst the potential was cycled between -100 and -600 mV. This pot (Pot 1) contained the buffer system and EGTA (100 μM). The EGTA was in the buffer to prevent the cluster reacting with any unwanted metal prior to conversion with the selected metal ion in Stage (2).

(2) The film was then transferred to a second pot (Pot 2) containing the metal ion of interest, M^{2+}. The potential was then cycled, and the complete conversion of [3Fe-4S] to [M3Fe-4S] was monitored by observing the disappearance of the A' and C' couples and the concomitant appearance of the new D' signal.[c]

(3) The film was finally transferred to a pot (Pot 3) containing the ligand of interest, again whilst holding at a negative potential. A negative potential was used as this had previously been found to aid the stability of the heterometal cluster. The potential was then scanned to determine whether a reaction had occurred (a scan rate of 0.5 V s^{-1} was generally employed, which was found to be fast enough to see transient reactions occurring).

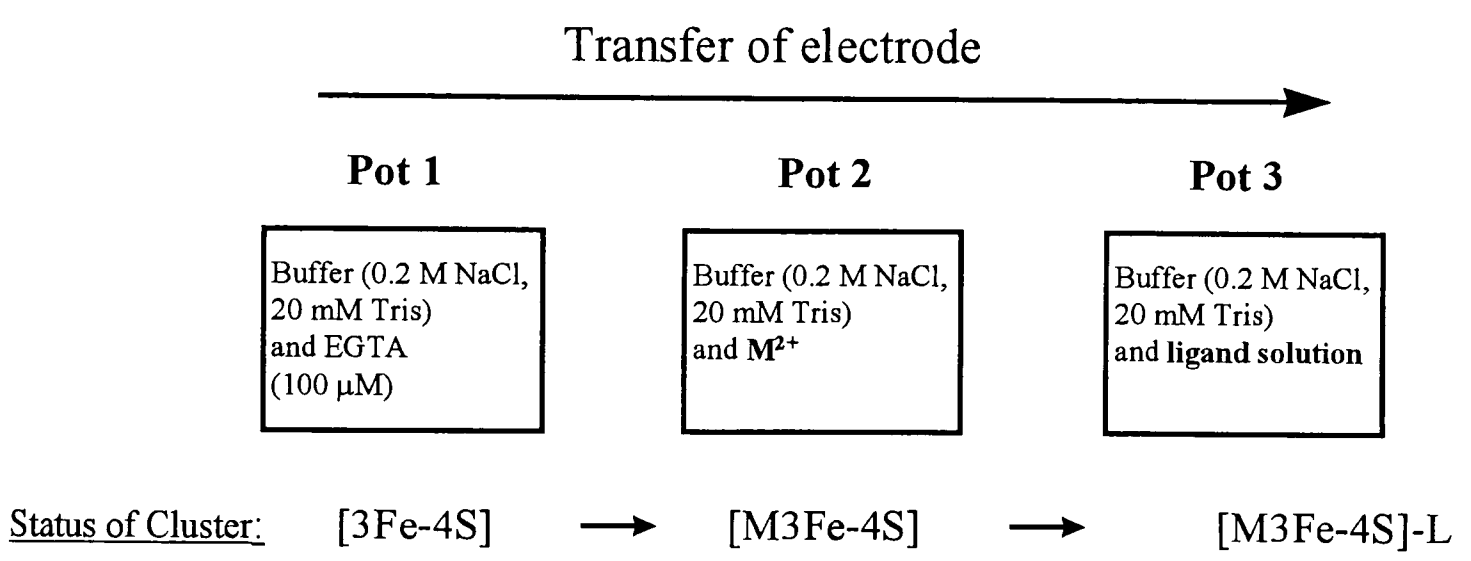

Figure 4.5 Scheme of the experimental method used for the ligand binding experiments

A number of experimental conditions were varied from those described in *Chapter 2*. In all cases the buffer used was 20 mM Tris, 0.2 M NaCl (to minimise changes in ionic strength when the thiol concentrations was changed) at pH 8.0. Each ligand solution was made up in this buffer, the pH of 8 was chosen to maximise the concentration of thiolate in the buffer-electrolyte solution. It was noted that the reduction potentials of the A', B' and C' redox couples were not significantly affected by the 0.2 M salt concentration (-129, -382 and -750 mV respectively in 0.2 M NaCl at pH 8.0 and -138,

[c] Optimum methods for the conversion [3Fe-4S] to [M3Fe-4S] in *Da* Fd III have been previously determined as described in *Chapter 3*.

-393 and -757 mV at pH 8.1 in 0.1 M NaCl electrolyte[39]). The nature of these experiments - using a potentially disruptive[d] ligand in solution together with the reactive protein - required the majority of scans to be recorded at higher scan rates, > 200 mV s^{-1}. Using a higher scan rate allowed changes in cluster ligation to be observed before molecules of the proposed ligand species could interfere and/or destroy the protein film. Furthermore, since the metal ion could generally not be contained in the same solution as the ligand, due to complexation of the free metal in solution with the ligands, rapid voltammetry was necessary to observe the [M3Fe-4S] cluster before M^{2+} was lost.

Control experiments, of which Figure 4.6 shows a typical example, were carried out using the 7Fe Fd for each ligand under investigation. In no case was there any difference between the voltammetry observed in a ligand or a non-ligand solution, therefore ruling out the possibility that the ligands interact with anything other than the additional metal, M, in the transformed cluster, [M3Fe-4S].

[d] Many of the ligands formed strong complexes with M^{2+} in solution and thus were able to extract M from the cluster [M3Fe-4S].

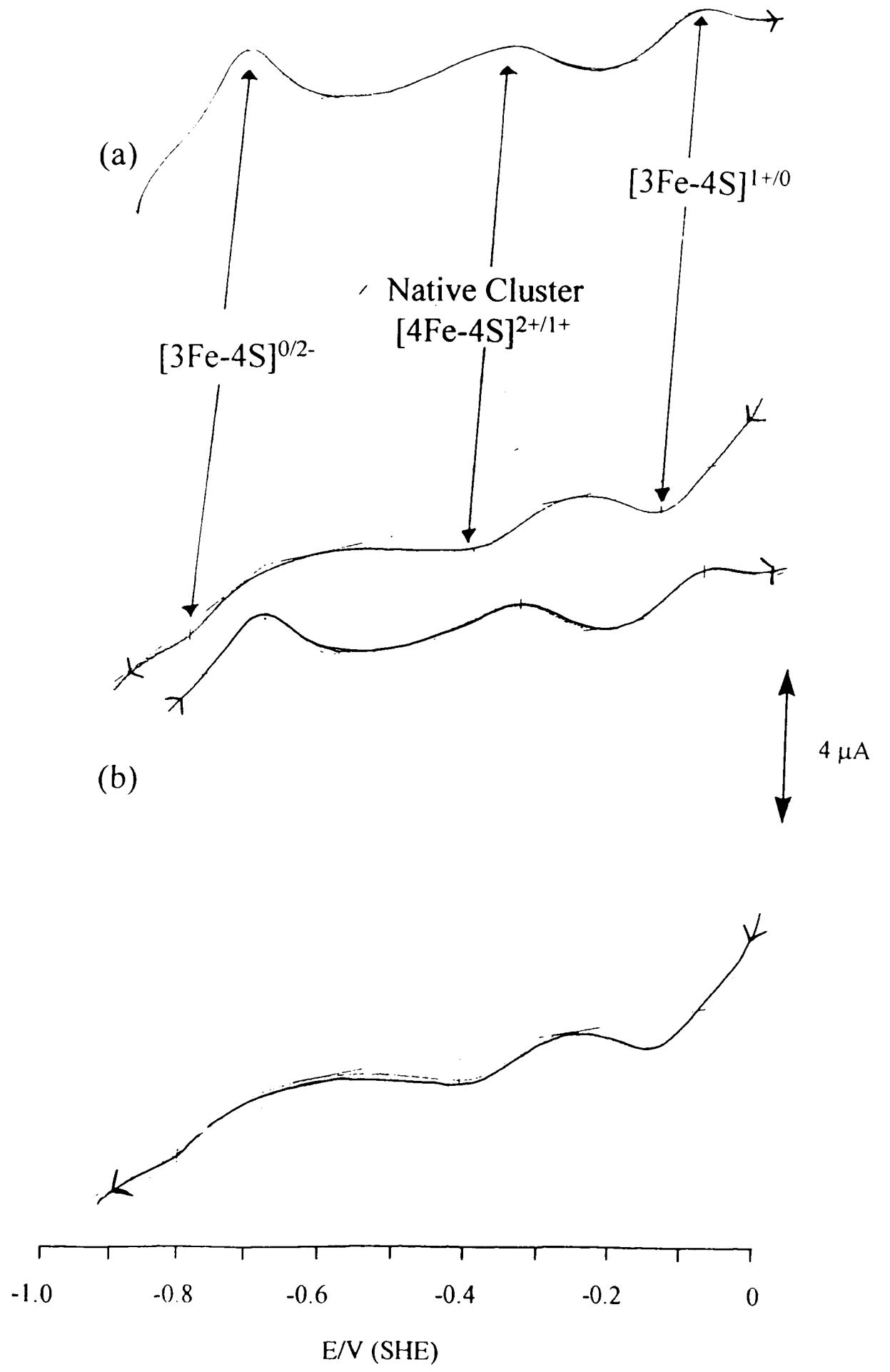

Figure 4.6 Control experiment, 7Fe Fd III and glutathione

(a) 7Fe Fd III in 20 mM Tris, 0.2 M NaCl, pH 8.0, $\nu = 200$ mV s^{-1}

(b) 7Fe Fd III in 20 mM Tris, 0.2 M NaCl, pH 8.0, 0.2 M glutathione, $\nu = 200$ mV s^{-1}

4.3 DISCUSSION OF PREVIOUS WORK

The experiments described in this chapter were carried out as a logical continuation of work conducted upon the *Da* Fd III system by J.N. Butt.[24] Before presenting my own results I therefore first describe briefly this work, in order to gain a more comprehensive overview of the subject area.

4.3.1 Mercaptoethanol

$$HO-CH_2-CH_2-SH$$

As described in earlier published work,[24] mercaptoethanoate anion binding occurs specifically at the subsite-differentiated Fe atom of the [Fe3Fe-4S] cluster of *Da* Fd III (Figure 4.2) and, in addition, co-ordination to the oxidised cluster occurs more rapidly, and more tightly, than to the reduced cluster. So far it is not known whether the thiolate ligand displaces a former ligand from the cluster (most likely the ^-OH of Asp 14) or whether binding is additive so that the co-ordination number of the Fe increases from 4 to 5. Analogous experiments were also carried out for the Zn and Co systems.

As shown in Table 4.2, thiolate binding to the [M3Fe-4S] cluster causes a negative shift in the reduction potentials in each case, consistent with an expected increase in core electron density. For all the [M3Fe-4S] clusters the tightest binding was observed for the cluster when it was in the oxidised state, as can be seen from the relative values of the dissociation constants, K_d^{ox} and K_d^{red} (Table 4.2). Furthermore, the relative magnitudes of $K_{d(L)}^{ox}$ are indicative that Fe and Co have greater affinity for the exogenous thiolate ligand, having greater trivalent character than Zn^{2+}.[38] Since it was not found to be possible for the Zn and Co adducts to define the limiting potential under high thiolate conditions, the corresponding parameters in Table 4.2 are subject to larger errors.[38] This inability to obtain a reversible signal for the ligand bound [M3Fe-4S] cluster (even at high thiolate concentrations and/or high scan rates) is indicative of the ligand exchange process for these [M3Fe-4S] clusters being faster than that of the [Fe3Fe-4S] cluster.

	$E^{o'}_D$	$E^{o'}_F$	$\Delta E^{o'}$	$K_{d(L)}^{ox}$/M	$K_{d(L)}^{red}$/M
[Fe3Fe-4S]	-393	-585	-192	$28 \pm 9 \times 10^{-6}$	$97 \pm 17 \times 10^{-3}$
[Zn3Fe-4S]	-492	-593	-101	$169 \pm 20 \times 10^{-6}$	$13 \pm 5 \times 10^{-3}$
[Co3Fe-4S]	-247	-389	-142	$20 \pm 2 \times 10^{-6}$	$9 \pm 5 \times 10^{-3}$

Table 4.2 Equilibrium constants for mercaptoethanoate binding

4.3.2 L-Cysteine

An obvious question to ask is whether the [M3Fe-4S] cluster is capable of binding L-cysteine, the physiological ligand to the vast majority of Fe-S clusters. Experiments analogous to those discussed above for mercaptoethanol (*Section 4.3.1*) showed that in all cases the $[M3Fe\text{-}4S]^{2+/1+}$ (M = Fe, Zn and Co) reduction couple moved to a more negative potential. That is to say, the oxidised form is stabilised relative to the reduced by ligand binding, dependent upon the concentration of cysteine in solution. A clear interaction of cysteine and the protein film can be seen in Figure 4.7, where the signal attributable to the both the native [4Fe-4S] cluster and the transformed [Fe3Fe-4S] cluster (B' and D') can be seen to split into two components on introduction to the ligand solution. For the Fe and Zn clusters the proximity of these two couples (ca. 80 mV) meant that analysis of data to yield values for $K_{d(L)}^{ox,red}$ and D'_{Fe} was complex. Results were ill-defined for the [Co3Fe-4S]-cysteine system and errors in $E^{o'}_{obs}$ were considerable. Table 4.3 details the thermodynamic parameters for this system.

	$E^{o'}_{D'}$	$E^{o'}_{F'}$	$\Delta E^{o'}$	$K_{d(L)}^{ox}$/M	$K_{d(L)}^{red}$/mM
[Fe3Fe-4S]	-393	-489	-84	$68 \pm 7 \times 10^{-6}$	$2.4 \pm 0.7 \times 10^{-3}$
[Zn3Fe-4S]	-498	-618	-120	$7.2 \pm 1 \times 10^{-6}$	$1.2 \pm 0.3 \times 10^{-3}$
[Co3Fe-4S]	-273	-	-	-	-

Table 4.3 Equilibrium constants for L-cysteinate binding

As with mercaptoethanol the magnitudes of $K_{d(L)}^{ox}$ and $K_{d(L)}^{red}$ are consistent with tighter binding to the oxidised form of the cluster, although the difference is less marked - most probably because of the lower electron density on the thiol group in cysteine. However, the binding affinity of cysteine to the oxidised Fe and Zn clusters is the reverse of that observed for mercaptoethanol. It has been postulated that this may be because of the charged residues of the amino and carboxylate groups on cysteine, or because of the steric bulk of these two groups.[38]

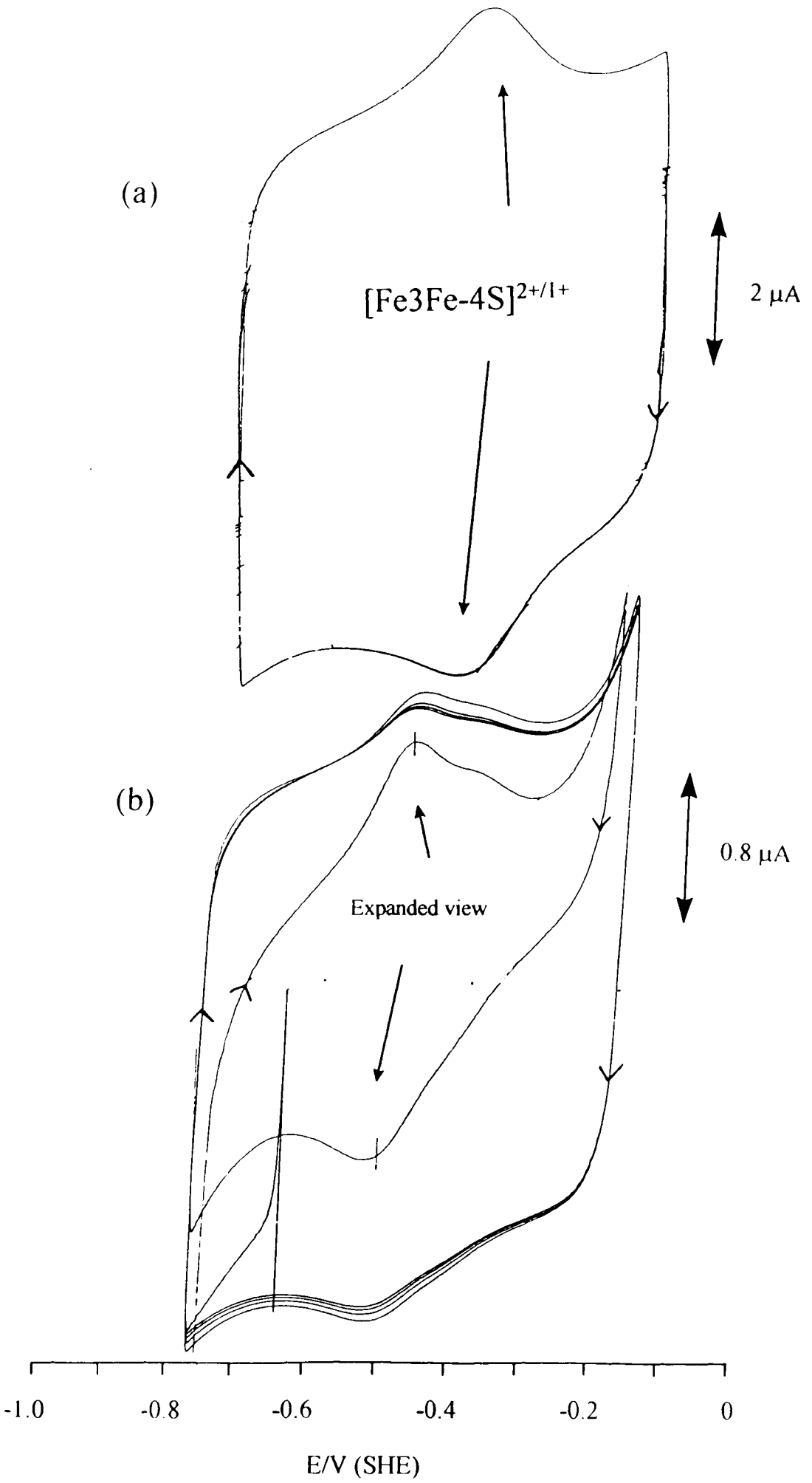

Figure 4.7 L-Cysteine and 8Fe Fd III

(a) Voltammogram of 8Fe Fd III, pH 8.0, ν = 200 mV s^{-1}, 2 mM neomycin as co-adsorbate.

(b) Film transferred to pot containing 0.4 M L-cysteine, otherwise conditions as (a)

4.3.3 Mercaptopropionic acid

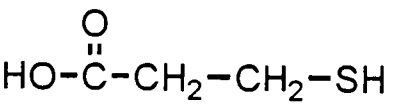

The binding of mercaptopropionic acid to the [Fe3Fe-4S] transformed cluster was investigated in ~ 250 μM thiolate solution (concentration of mercaptopropionic acid was 33 mM, using a pK of the thiol group of 10.4, as measured by J.N. Butt) and there were weak indications of binding, since a negative shift of ca. 150 mV in the potential was observed. However, difficulties in measuring the position of the oxidative wave were encountered since the ligand was found to dissociate rapidly from the reduced cluster (faster than from the oxidised cluster). These results indicate that this acidic thiol may be binding very weakly to the cluster, and it certainly shows much weaker binding than mercaptoethanol.[40]

4.3.4 Cysteamine

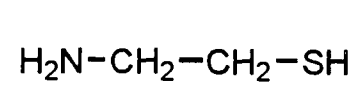

This thiol ligand differs in that it does not contain any acidic or alcoholic groups, but instead contains an amino and a thiol group. At a concentration of 463 mM cysteamine (which under the experimental conditions is ~80 mM thiolate) the total negative shift of $E^{o'}_{obs}$ was ca. 70 mV. Data were obtained which allowed $K_{d(L)}^{ox}$ and the $K_{d(L)}^{red}$ to be calculated as $1.52 \pm 0.3 \times 10^{-3}$ M and $36 \pm 19 \times 10^{-3}$ M respectively, using the analysis as demonstrated in *Section 4.1.1.* As observed for all the thiolate ligands the higher $K_{d(L)}^{red}$ indicates that the affinity of the thiolate ligand has a greater affinity for the oxidised form of the cluster. A typical result showing the extent of cysteamine interaction with the 8Fe Fd is shown in Figure 4.8.

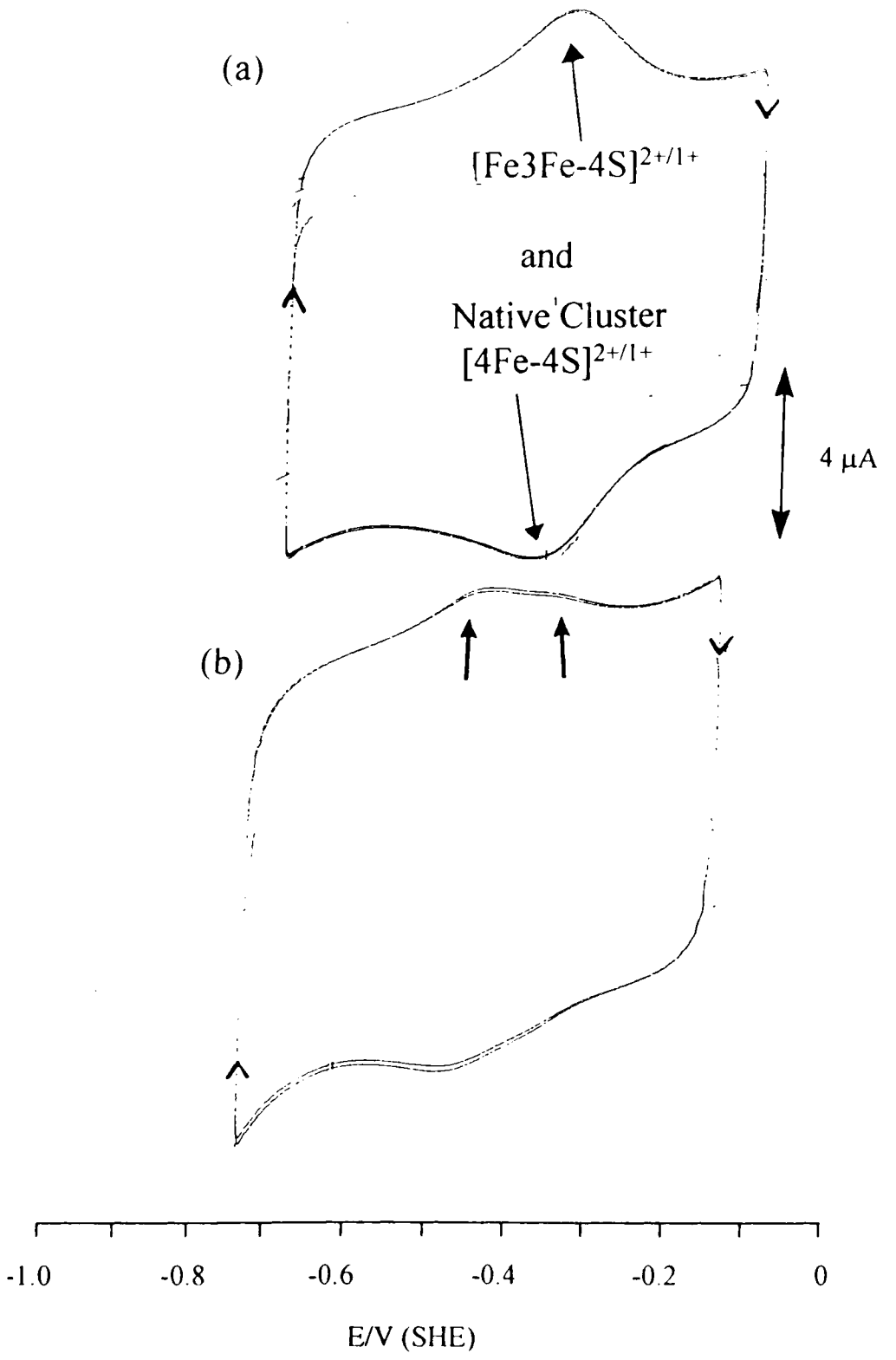

Figure 4.8 Cysteamine and 8Fe Fd III

(a) *Voltammogram of transformed 8Fe Fd III, showing the redox couple for* $[Fe3Fe\text{-}4S]^{2+/1+}$ *and native* $[4Fe\text{-}4S]^{2+/1+}$, *pH 8.0,* $\nu = 200\ mV\ s^{-1}$, $200\ \mu g\ ml^{-1}$ *polymyxin as co-adsorbate.*

(b) Film transferred to pot containing 0.16 M cysteamine, otherwise conditions as (a). The oxidative peak can be seen to split into two components (marked by arrows), indicating that there is a ligand interaction with the [Fe3Fe-4S] cluster. For the reductive peak the definition of the two components is harder to observed.

4.3.5 Imidazole / Histidine

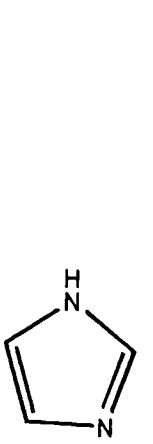

Imidazole

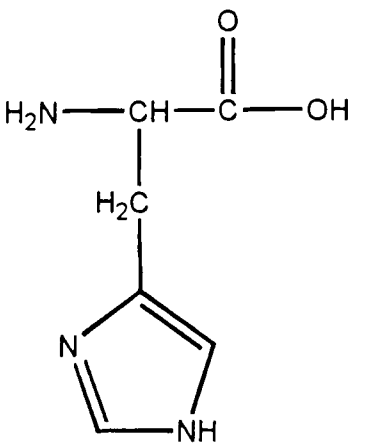

Histidine

A brief experimental survey was also carried out using the transformed 8Fe Fd and two possible nitrogen donor ligands, imidazole and histidine. When the 8Fe Fd protein film was introduced to a solution of imidazole (1.0 M) the oxidative and reductive waves (for $[Fe3Fe\text{-}4S]^{2+/1+}$ and $[4Fe\text{-}4S]^{2+/1+}$) were split into two components, with a shift in the potential of ca. 50 mV. However, when the same experiment was carried out with the 7Fe Fd the $[3Fe\text{-}4S]^{1+/0}$ couple was shifted by ca. 30 mV thus making it difficult to conclude whether the imidazole was interacting solely with the subsite-differentiated Fe or with the cluster and/or protein. No reaction was observed with either the 7Fe Fd or 8Fe Fd in the presence of 0.1 M histidine.

4.4 RESULTS

4.4.1 Glutathione

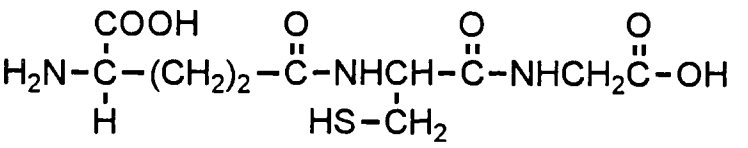

The tripeptide, glutathione, is a very important biologically active molecule, and is essential for maintaining the redox status of the cytoplasm. It is both a protective and homeostatic redox device, maintaining the potential balance between various metabolic pathways at -0.1 V.[41] It was chosen for this study since, firstly, it is biologically available and, secondly, has a pendant thiol, making it a possible thiolate donor.

Control experiments with the untransformed 7Fe Fd did not show an observable reaction when the protein film was introduced to a solution of glutathione (a typical example is shown above in Figure 4.6). Similarly, a film of transformed 8Fe Fd was introduced into a solution of glutathione and, again (as shown in Figure 4.8), no changes were observed in the voltammetry at concentrations of up to 0.2 M glutathione (thiolate concentration = 6 mM).

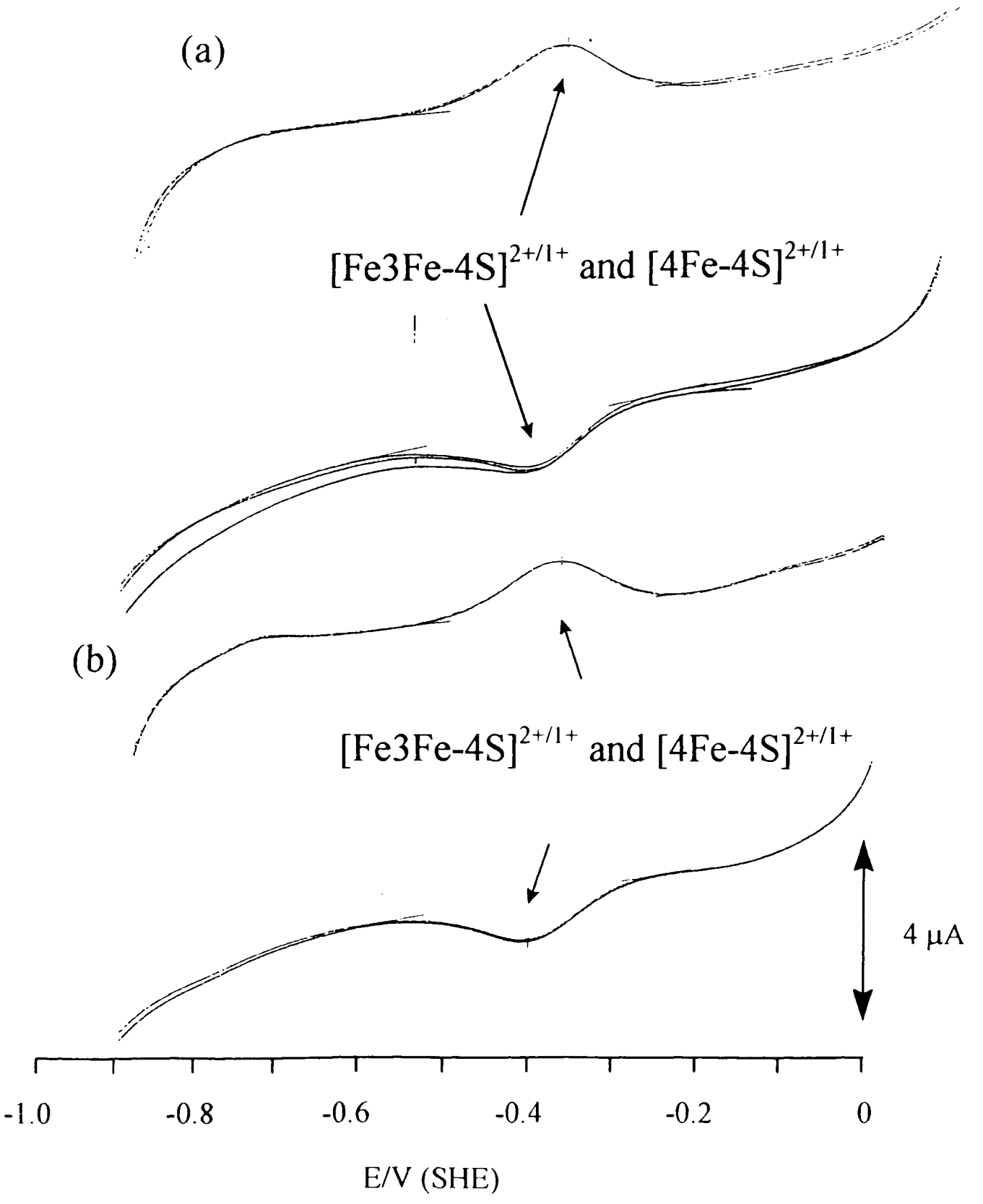

Figure 4.9 Glutathione and 8Fe Fd

(a) Voltammogram of 8Fe Fd III, 20 mM Tris, 0.2 M NaCl, pH 8.0, ν = 100 mV s^{-1}, 200 µg ml^{-1} polymyxin as co-adsorbate.

(b) Film transferred to pot containing 0.1 M glutathione, otherwise conditions as (a)

In contrast, definite negative shifts in the reduction potential of both the [Zn3Fe-4S] and the [Co3Fe-4S] peaks (Figure 4.10) were observed when these proteins were introduced to a solution of glutathione (concentrations ranging from 0.02 - 0.2 M). For the highest concentrations of glutathione used the negative shift in $E^{o'}_{obs}$ was approximately 30 mV in both cases. However, under these conditions the reductive peak for [Co3Fe-4S] was broadened and became convoluted with the reductive peak of the [4Fe-4S] cluster, there were thus considerable difficulties in determining the reduction potentials accurately. The dependence of $E^{o'}_{obs}$ on the glutathione concentration, for the [Co3Fe-4S] cluster, is shown in Figure 4.11.

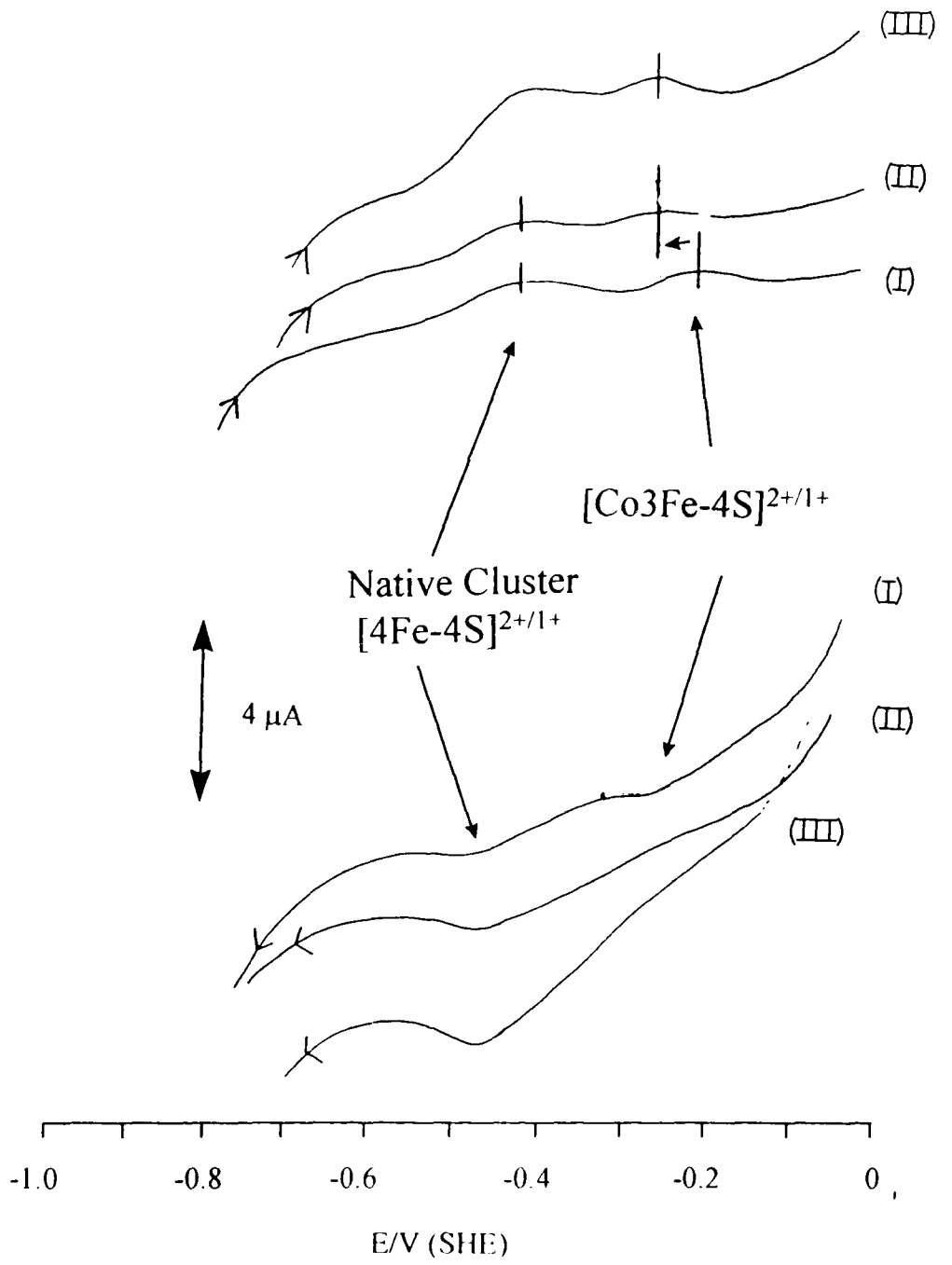

Figure 4.10 Glutathione and cobalt transformed Fd III

(I) Voltammogram of cobalt transformed Da Fd III, showing the redox couples for $[Co3Fe\text{-}4S]^{2+/1+}$ *and native* $[4Fe\text{-}4S]^{2+/1+}$*, pH 8.0,* $\nu = 100\ mV\ s^{-1}$*, 200* $\mu g\ ml^{-1}$ *polymyxin as co-adsorbate.*

(II) Film transferred to a pot containing 0.12 M glutathione, otherwise conditions as (I), a small negative shift of the oxidative $[Co3Fe\text{-}4S]^{1+/2+}$ *peak can be seen.*

(III) Expanded view of (II), the difficulty in determining the positions of two reductive waves can be seen.

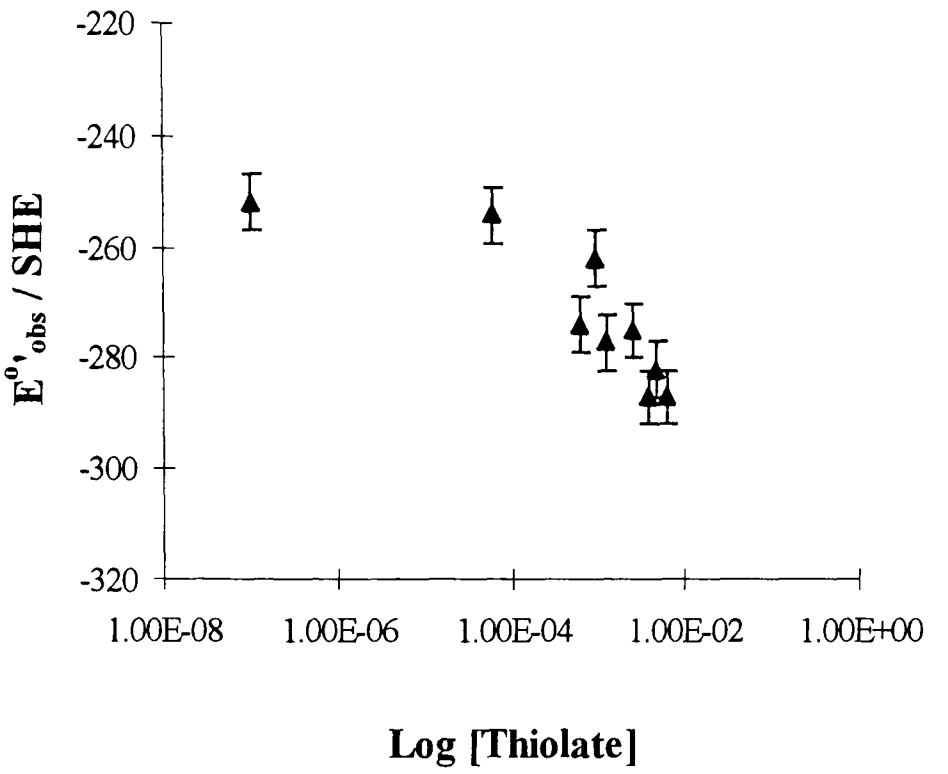

Figure 4.11 Graph showing thiolate concentration (glutathione) against $E^{o'}_{obs}$ for [Co3Fe-4S]

Continued scanning with a film containing the [Zn3Fe-4S] cluster in a solution of glutathione resulted in the Zn being extracted from the cluster i.e. the D' signal decreased in height, with a concomitant increase in A' and C'. Thus glutathione, as well as having an interaction with the zinc *in situ* in the protein, also has a high enough affinity for the Zn to extract it from the cluster. ($K = [ML_2]/[M][L]^2 = 10^{12.5}$ for Zn^{2+} and glutathione.[42])

Cluster	$E^{o'}_D$	$E^{o'}_F$	$\Delta E^{o'}$	$K_{d(L)}^{ox}$/M	$K_{d(L)}^{red}$/M
[Fe3Fe-4S]	-393	not observed	-	Very weak binding to the cluster, if at all.	
[Zn3Fe-4S]	-492			Zinc extracted from the cluster	
[Co3Fe-4S]	-247			ca. 10^{-6}	n.d.

Table 4.4 Data for glutathione binding

4.4.2 Coenzyme M

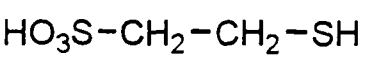

When protein films of the transformed [M3Fe-4S] clusters (M = Fe, Zn and Co) were introduced to a solution of coenzyme M, a negative shift in the reduction potential of the redox couple for $[M3Fe\text{-}4S]^{2+/1+}$ was observed. This was a positive indicator that the small thiolate molecule, coenzyme M was interacting with the transformed cluster, [M3Fe-4S].

As the electrochemical signal of the inert 4Fe cluster, B', is co-incident with the signal for the transformed [Fe3Fe-4S] cluster, D', any ligand interaction with the cluster must be observed via this co-incident signal. Of the three metal clusters the reaction of coenzyme M with the [Fe3Fe-4S] cluster gave the best resolution of data, an example of the voltammetry observed is shown in Figure 4.12. The first complete cycle, starting from a negative potential of -650 mV, at which the [Fe3Fe-4S] cluster is in the reduced form, showed no change in the single oxidative peak - hence no binding of the exogenous ligand to the reduced cluster had occurred. However, as the potential is cycled (scan rate 1 V s^{-1}) and the [Fe3Fe-4S] cluster was oxidised, the reductive peak was split into two components, indicating binding of coenzyme M to the *oxidised* cluster. On the second cycle the oxidative peak was seen to be split into two components - demonstrating that some of the cluster has remained bound during cycling.

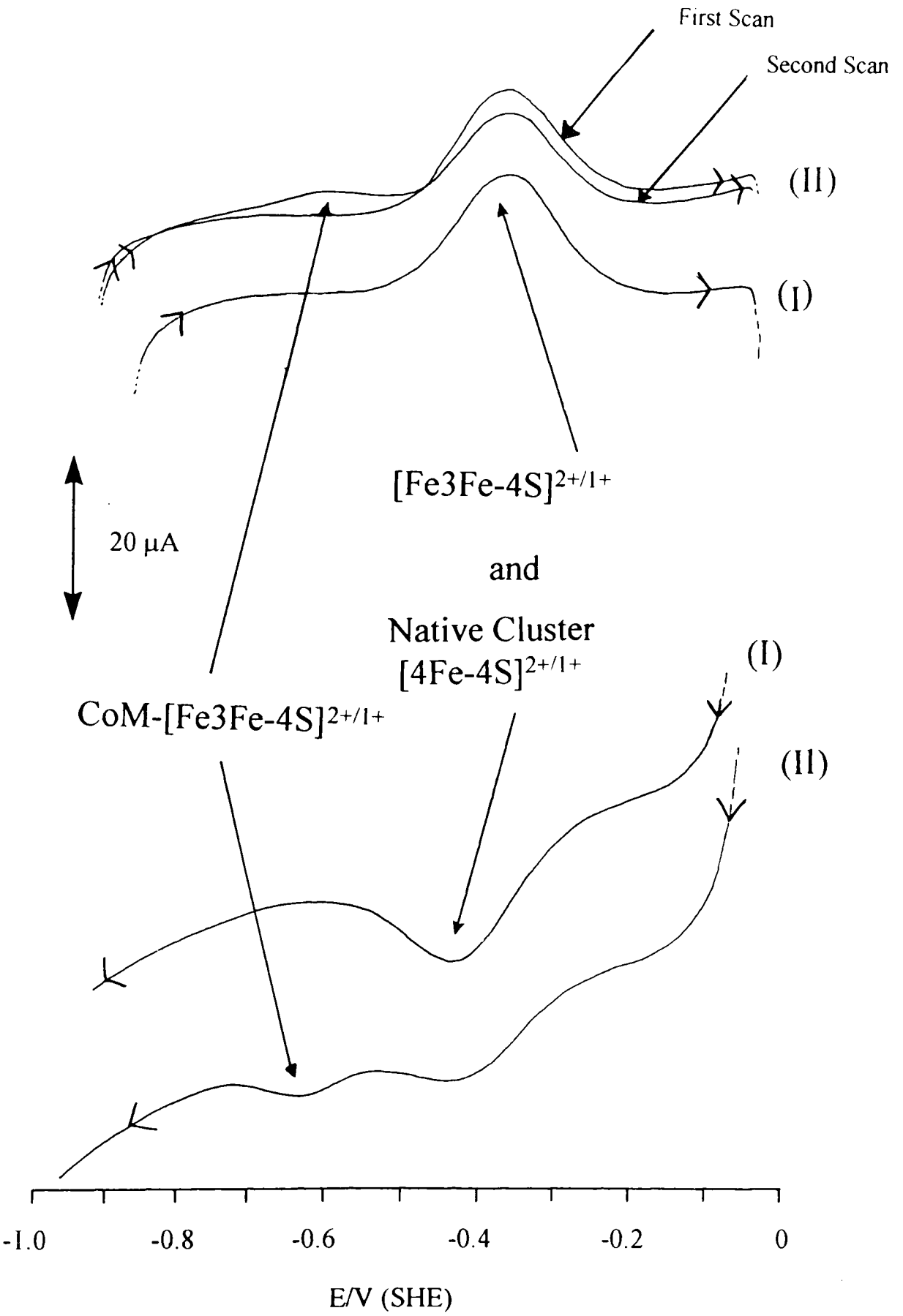

Figure 4.12 Coenzyme M and 8Fe Fd III

(I) *Voltammogram of Da Fd III, 8Fe Fd showing the (overlaying) redox couples for* $[Fe3Fe\text{-}4S]^{2+/1+}$ *and native* $[4Fe\text{-}4S]^{2+/1+}$, *pH 8.0,* $\nu = 1000\ mV\ s^{-1}$, $200\ \mu g\ ml^{-1}$ *polymyxin as co-adsorbate.*

(II) Film transferred to a pot containing 0.1 M coenzyme M (CoM), the first scan in the CoM solution shows no change to the voltammetry, until the cluster is oxidised $[Fe3Fe\text{-}4S]^{1+}$, *whereupon the ligand interacts with the cluster and a new redox couple is seen -* ***CoM-[Fe3Fe-4S]***$^{2+/1+}$

Changes in the voltammetry, though less definitive, were also seen for both the zinc and cobalt transformed clusters upon introduction to a solution of coenzyme M. However, only small negative shifts in the potential of the oxidative peaks were observed - in both cases the reductive peaks were broadened and it was not feasible to determine a specific value for the position of the reductive peak. An example of this behaviour can be seen in Figure 4.13 for the reaction of the Zn-transformed cluster and coenzyme M. Hence, although an interaction with coenzyme M was seen for all three of the metals investigated, approximate values for $K_{d(L)}^{ox}$ and $K_{d(L)}^{red}$ were only calculated for CoM-[Fe3Fe-4S][40] and these were $567 \pm 78 \times 10^{-6}$ M and 2.38 ± 0.6 M respectively.

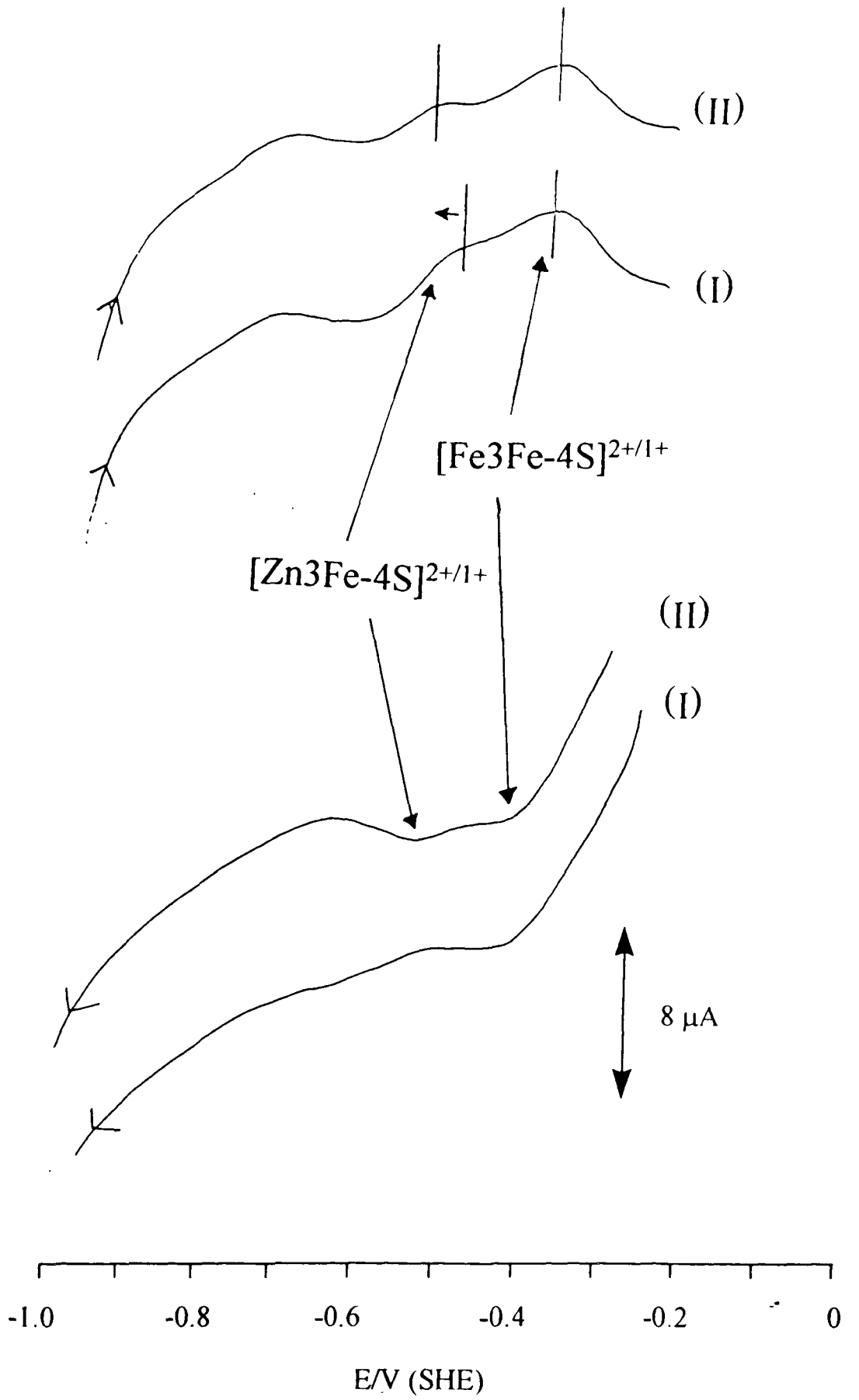

Figure 4.13 Coenzyme M and zinc transformed Fd III

(I) Voltammogram of zinc transformed Da Fd III, showing the redox couples for $[Zn3Fe\text{-}4S]^{2+/1+}$ *and native* $[4Fe\text{-}4S]^{2+/1+}$*, pH 8.0,* $\nu = 500\ mV\ s^{-1}$*, 200* $\mu g\ ml^{-1}$ *polymyxin as co-adsorbate.*

(II) Film transferred to a pot containing 0.1 M coenzyme M, otherwise conditions as (I). A small negative shift of the oxidative $[Zn3Fe\text{-}4S]^{1+/2+}$ *peak is marked by an arrow.*

4.4.3 Thioacetic Acid

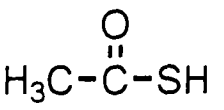

For thioacetic acid, although tentative signs of binding to the cluster were apparent under the applied experimental conditions, this potential ligand was found to be disruptive to the integrity of the protein film. On introduction to a solution of thioacetic acid, the [Co3Fe-4S] cluster showed only a small shift in potential of the oxidative peak, and it was found that the Co was removed from the [Co3Fe-4S] cluster by complexation as observed by the clear reappearance of the A' and C' couples, associated with the [3Fe-4S] cluster, and the disappearance of the D' couple.

As has been described in *Chapter 3*, the removal of M from [M3Fe-4S] is dependent upon the oxidation level of the cluster, but additionally, in the presence of thioacetic acid, removal of Co was also dependent on the concentration of thioacetic acid in solution. It was possible to observe the time-dependence of Co extraction by using the reappearance of the C' signal as a sign of the return of the [3Fe-4S] cluster, at 500 mV s^{-1}. The reaction was assumed to have reached completion when the C' peak attained a constant height, and it was shown that the removal of Co was dependent upon the ligand concentration.

When introduced to a solution of thioacetic acid the [Zn3Fe-4S] cluster exhibited a negative shift in its oxidative peak of ca. 25 mV and the reductive wave broadened considerably, as shown in Figure 4.14. Upon placing a film of ferredoxin containing the [Fe3Fe-4S] cluster into a solution of thioacetic acid at a concentration of 0.2 M, no changes in the reduction potential of the $[Fe3Fe\text{-}4S]^{2+/1+}$ couple were apparent from the voltammetry. However, over a 5 - 10 minute period of continuous scanning the signals attributed to the A' and C' couples increased, indicating the extraction of Fe from the cluster. There was no observable interaction between thioacetic acid and the [Fe3Fe-4S] cluster prior to this.

The main characteristic of this ligand is thus its ability to extract the metal from the cubane cluster, presumably because of the strength of its metal complexation in free solution. Hence, the properties of thioacetic acid interacting with the cluster remain largely uninvestigated, although some ligand binding tendency is apparent.

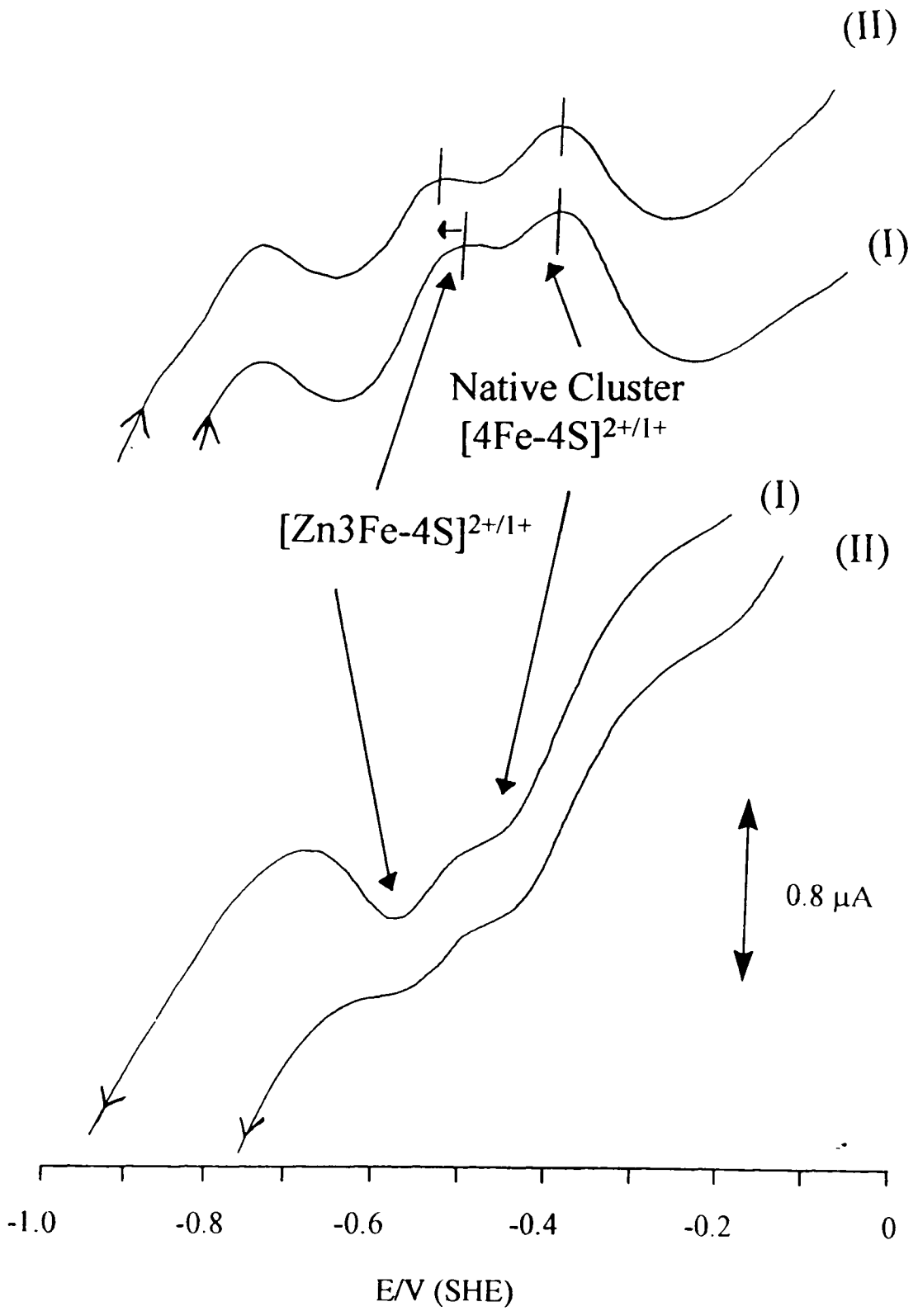

Figure 4.13 Thioacetic acid and zinc transformed Fd III

(I) Voltammogram of zinc transformed Da Fd III, showing the redox couples for $[Zn3Fe\text{-}4S]^{2+/1+}$ *and native* $[4Fe\text{-}4S]^{2+/1+}$*, 20 mM Tris, 0.2 M NaCl, pH 8.0,* ν = *100 mV* s^{-1}*, 200 µg* ml^{-1} *polymyxin as co-adsorbate.*

(II) Film transferred to a pot containing 0.1 M thioacetic acid, otherwise conditions as (I). A small negative shift of the oxidative $[Zn3Fe\text{-}4S]^{1+/2+}$ *peak is marked by an arrow.*

4.4.4 Thiomalic Acid

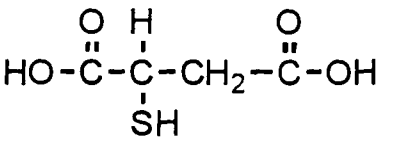

When a film of [Fe3Fe-4S] was introduced to a solution containing thiomalic acid at concentrations of 0.05 M and 0.1 M, the subsite-differentiated Fe was very quickly complexed out from the cluster, as the return of the A' and C' couples was immediately observed. Hence, no potential shift in either the oxidative or reductive peaks of the [Fe3Fe-4S] cluster was observed. In the case of the [Zn3Fe-4S] transformed cluster and 0.05 M and 0.1 M concentrations of thiomalic acid, the Zn^{2+} ion was completely removed from the cluster within 2/3 cycles (ν = 100 mV s^{-1}). The cluster itself was not destroyed, as indicated by the return of the A' and C' signals, characterising the [3Fe-4S] cluster.

In the case of [Co3Fe-4S] the situation was a little more complex. High concentrations of thiomalic acid in solution (0.2 M) did appear to cause a negative shift (ca. 25 mV) of the oxidation wave of the transformed cluster, Figure 4.15, however, this species appeared to be short-lived. Not only did the thiomalic acid appear to complex out the Co atom from the cluster, but it also appeared to destroy the protein film/[3Fe-4S] cluster itself, because no return of the A' and C' peaks were observed. At lower concentrations of thiomalic acid (0.04 M) the A' and C' signals did reappear, (signs of the A' couple reappearing at 0.1 M thiomalic acid, see Figure 4.15) although the Co atom was pulled out of the cluster as before, indicating that the [3Fe-4S] cluster remained intact.

In conclusion, although the Co cluster exhibited tentative signs that thiomalic acid was weakly binding to the cluster (there was a small shift in reduction potential) it appeared that this ligand was much more likely to disrupt and/or destroy the protein film and/or cluster.

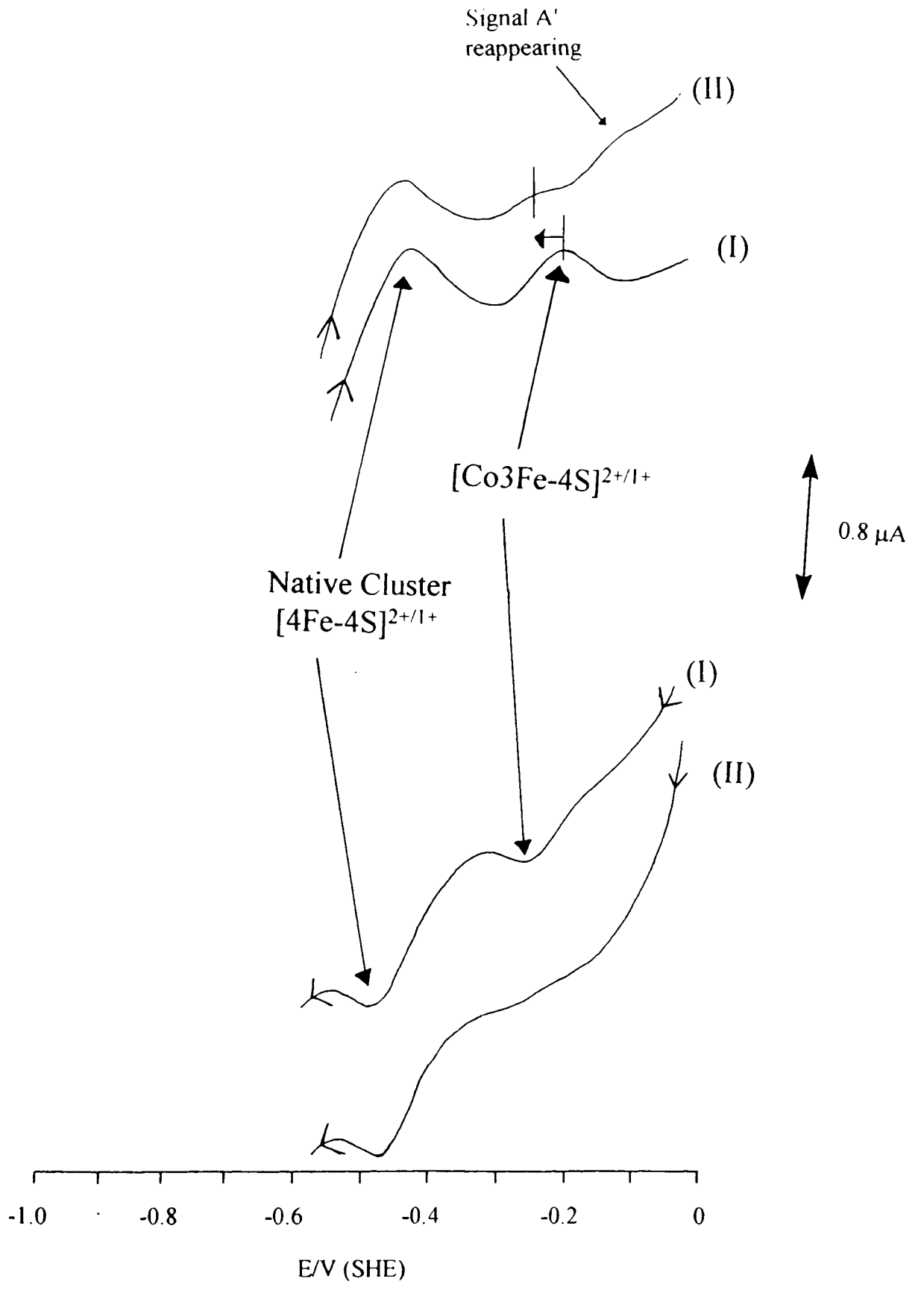

Figure 4.15 Thiomalic acid and cobalt transformed Fd III

(I) Voltammogram of cobalt transformed Da Fd III, showing the redox couples for $[Co3Fe\text{-}4S]^{2+/1+}$ *and native* $[4Fe\text{-}4S]^{2+/1+}$*, 20 mM Tris and 0.2 M NaCl, pH 8.0,* $\nu = 100\ mV\ s^{-1}$*,* $200\ \mu g\ ml^{-1}$ *polymyxin as co-adsorbate.*

(II) Film transferred to a pot containing 0.1 M thiomalic acid, otherwise conditions as (I). A small negative shift of the oxidative $[Co3Fe\text{-}4S]^{1+/2+}$ *peak is marked by an arrow. The reductive wave is broadened and a shift in the reductive peak of [Co3Fe-4S] was not able to be determined.*

4.4.5 Thioglycolic acid

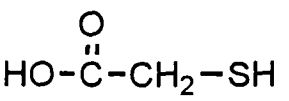

When the [Zn3Fe-4S] cluster was introduced into a solution of 0.1 M thioglycolic acid there was a negative shift in potential of ca. 35 mV for the oxidative wave of the D' signal, associated with the [Zn3Fe-4S] cluster. However, the reductive wave was broadened and so it was not possible to determine with any reliability the dependence of $E^{o'}_{obs}$ upon thiolate concentration. Little information was obtained when the [Co3Fe-4S] cluster was introduced to the solution of mercaptoacetic acid, as the Co atom was immediately extracted from the cluster, as evidenced from the immediate loss of the $[Co3Fe\text{-}4S]^{2+/1+}$ couple, Figure 4.16.

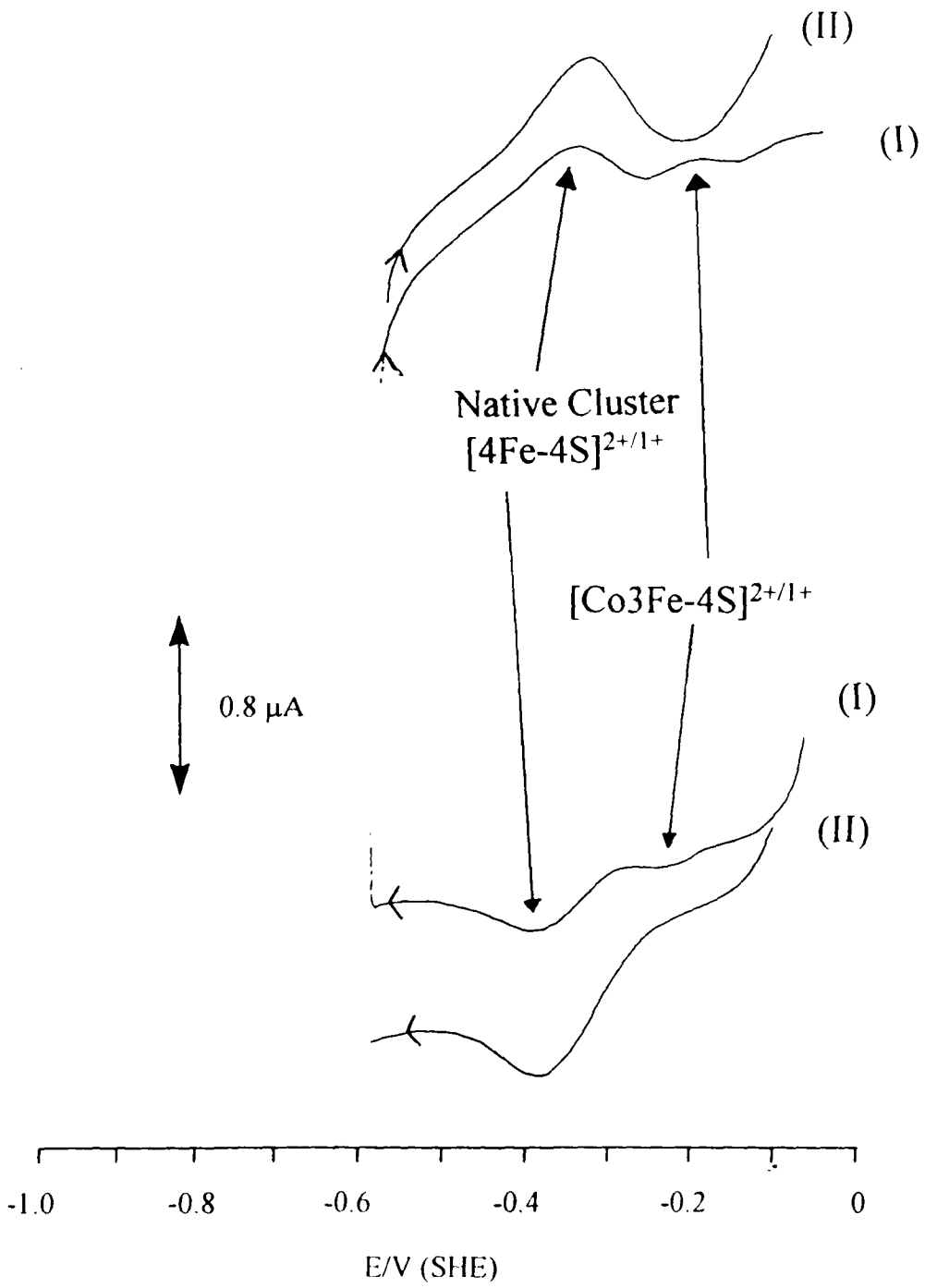

Figure 4.16 Thioglycolic acid and cobalt transformed Fd III

(I) Voltammogram of cobalt transformed Da Fd III, showing the redox couples for $[Co3Fe\text{-}4S]^{2+/1+}$ *and native* $[4Fe\text{-}4S]^{2+/1+}$*, pH 8.0,* $\nu = 500\ mV\ s^{-1}$*, 200* $\mu g\ ml^{-1}$ *polymyxin as co-adsorbate.*

(II) Film transferred to a pot containing 0.1 M thioglycolic acid, otherwise conditions as (I). No interaction between the ligand and the [Co3Fe-4S] is evident due to the immediate removal of Co from the cluster. The second voltammogram shows only the $[4Fe\text{-}4S]^{2+/1+}$ *redox couple.*

4.4.6 Catechol, oxalic acid and oxalacetic acid

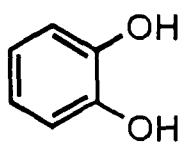
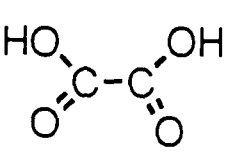
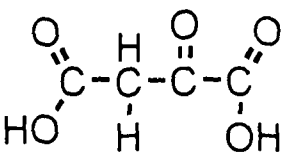

These ligands were chosen in order to test the hypothesis that the proposed oxygenic ligand to the cluster of *Da* Fd III (from either the aspartate or possibly a water molecule) could be replaced by an alternative O ligand, either a mono- or bi-dentate ligand. Exogenous ligand exchange from a mono- to a bi-dentate oxygenic ligating system is not unprecedented - this is observed in aconitase: the substrate (citrate) binds to the 4Fe form, increasing the co-ordination at the Fe site from 4 to 6.[26] Similar behaviour is observed in the non-biological analogues of FeS clusters synthesised by Holm *et al.* In these instances it has been shown that mono-dentate ligands to the subsite differentiated Fe can be replaced by bi- or even tri-dentate ligands.[27]

Experiments were carried out for a range of different concentrations for all three oxygenic ligands and no changes, or shifts of reduction potential, for any of the [M3Fe-4S] redox couples, were observed. This can be seen in Figures 4.17 - 4.19, the only substantial effect that these ligands had on the voltammetry was that on continued cycling the M^{2+} was gradually complexed out of the cluster.

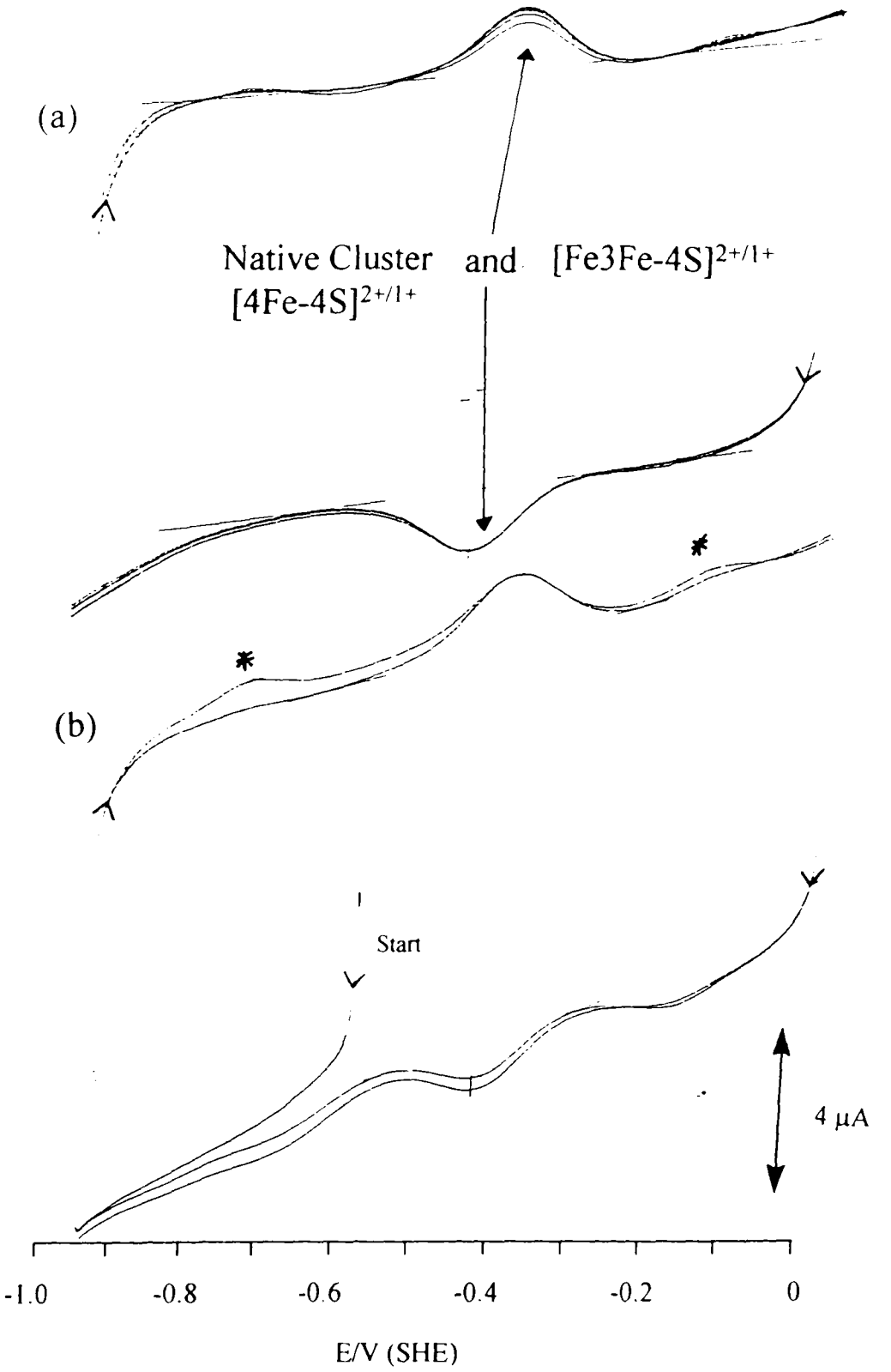

Figure 4.17 Catechol and 8Fe Fd III

(a) Voltammogram of 8Fe Fd III, showing the redox couple for $[Fe3Fe\text{-}4S]^{2+/1+}$ *and native* $[4Fe\text{-}4S]^{2+/1+}$*, 20 mM Tris, 0.2 M NaCl, pH 8.0,* $\nu = 200\ mV\ s^{-1}$*,* $200\ \mu g\ ml^{-1}$ *polymyxin as co-adsorbate.*

(b) The transformed protein film was then transferred to a pot containing 0.1 M catechol. The return of the A' and C' couples, $[3Fe\text{-}4S]^{1+/0}$ *and* $[3Fe\text{-}4S]^{0/2-}$*, can be clearly seen (*), indicating that the catechol solution causes the release of Fe from [Fe3Fe-4S]. No changes or shifts in potential are seen for the* $[Fe3Fe\text{-}4S]^{2+/1+}$ *redox couple.*

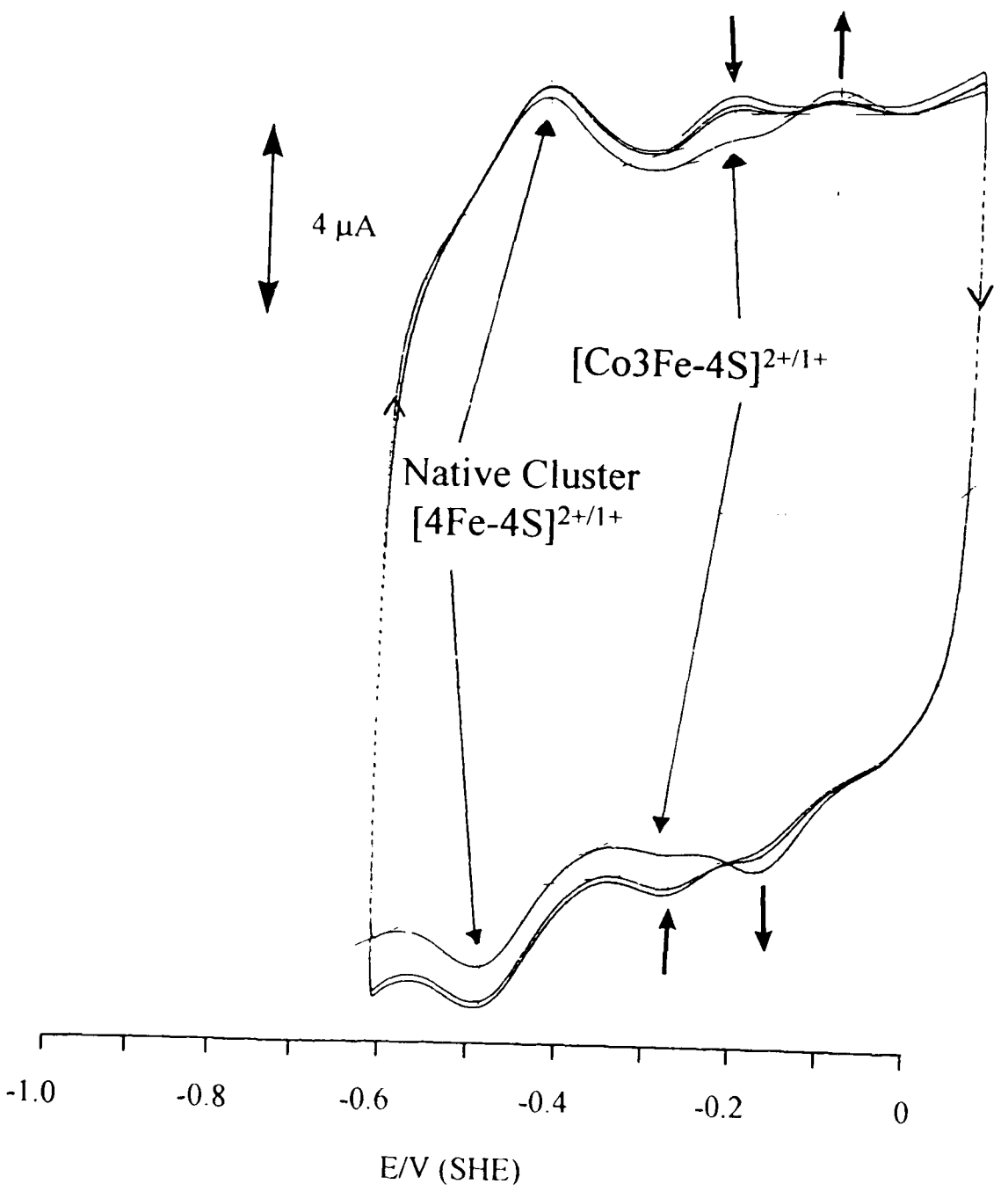

Figure 4.18 Catechol and cobalt transformed Fd III

Voltammogram of cobalt transformed Da Fd III, showing the redox couples for $[Co3Fe\text{-}4S]^{2+/1+}$ *and native* $[4Fe\text{-}4S]^{2+/1+}$, *pH 8.0, 0.1 M catechol,* $\nu = 200\ mV\ s^{-1}$, $200\ \mu g\ ml^{-1}$ *polymyxin as co-adsorbate. The return of the A' couple,* $[3Fe\text{-}4S]^{1+/0}$ *can be clearly seen, concomitant with the decrease in the [Co3Fe-4S] cluster signals. No potential shifts of the [Co3Fe-4S] redox couple are visible.*

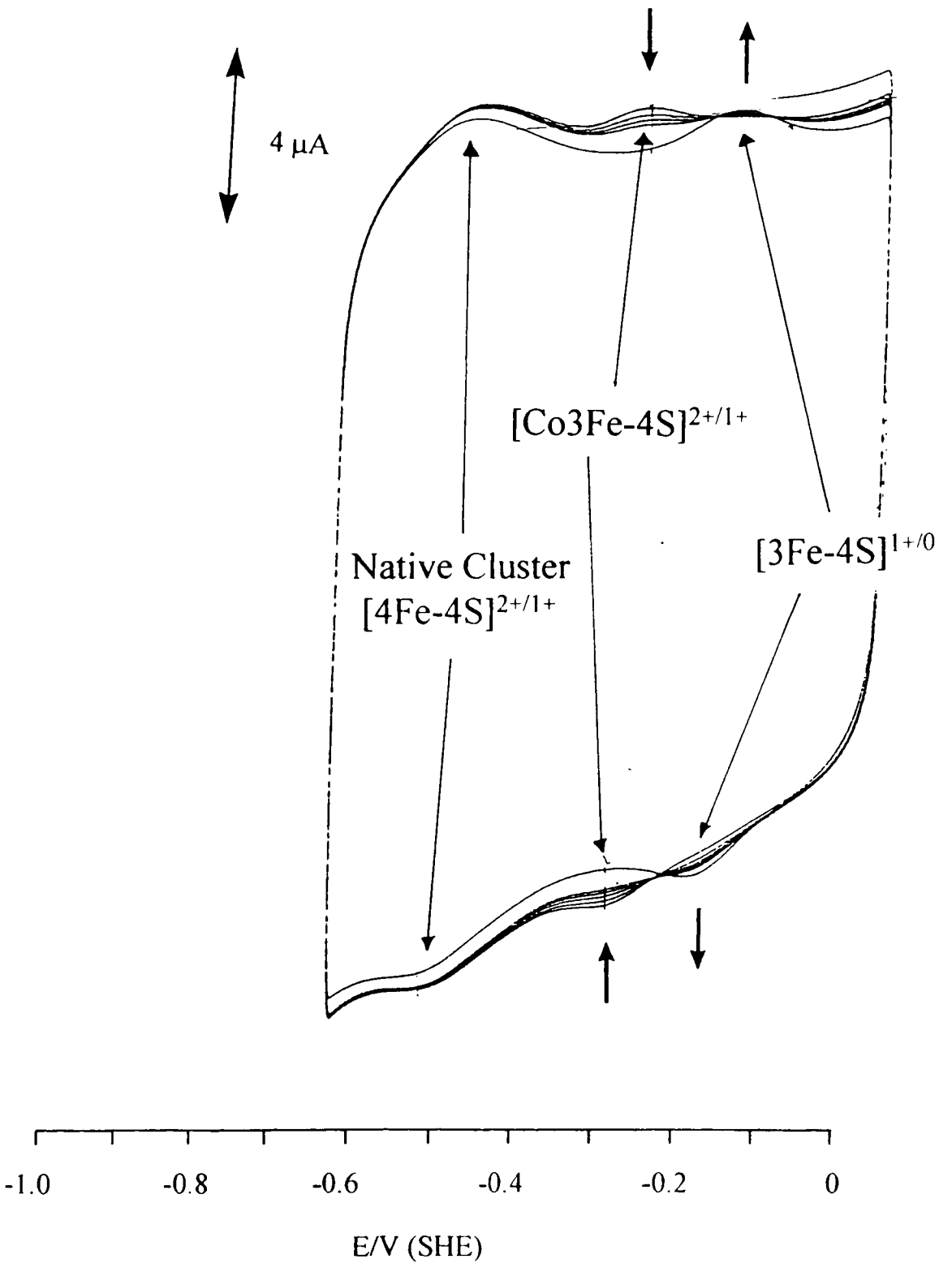

Figure 4.19 Oxalic acid and cobalt transformed Fd III

Voltammogram of cobalt transformed Da Fd III, showing the redox couples for [Co3Fe-4S]$^{2+/1+}$ and native [4Fe-4S]$^{2+/1+}$, pH 8.0, 0.1 M oxalic acid, v = 200 mV s^{-1}, 200 μg ml^{-1} polymyxin as co-adsorbate. The return of the A' redox couple, [3Fe-4S]$^{1+/0}$ can be clearly seen, concomitant with the decrease in the [Co3Fe-4S] cluster signals. No potential shifts of the [Co3Fe-4S] redox couple are visible.

4.5 SUMMARY

LIGAND	Fe	Zn	Co	COMMENTS
THIOLATE LIGANDS				
Mercaptoethanol	✓	✓	✓	-OH on α-carbon Strong binding
$Kd_{(L)}^{ox}$	28 μM	169 μM	20 μM	
$Kd_{(L)}^{red}$	97 mM	13 mM	9 mM	
L-Cysteine	✓	✓	✓	$-NH_2$ on α-carbon
$Kd_{(L)}^{ox}$	68 μM	7 μM	-	Strong Binding
$Kd_{(L)}^{red}$	2 mM	1 mM	-	
Glutathione	×	✓	✓	-NH on α-carbon Weak binding only to the Co
$Kd_{(L)}^{ox}$	-	-	~1 μM	and Zn adducts
$Kd_{(L)}^{red}$	-	-	-	
Coenzyme M	✓	✓	✓	$-SO_3^-$ on α-carbon
$Kd_{(L)}^{ox}$	0.5 mM	-	-	Weak binding
$Kd_{(L)}^{red}$	2.4 M	-	-	
Thioacetic acid	╬	✓	✓	$-CH_3$ α-carbon Small shift for Co and Zn adducts, complexes all 3 metals out after a short time
Thiomalic acid	╬	╬	╬	$-CH_2$ or -COOH on α-carbon Complexes out Fe, Co and Zn very quickly
Thioglycolic acid	-	✓	╬	-COOH group on α-carbon
Mercaptopropionic acid	✓			-COOH on α-carbon
Cysteamine	✓	-	-	$-NH_2$ on α-carbon
$Kd_{(L)}^{ox}$	1.5 mM	-	-	Very weak binding
$Kd_{(L)}^{red}$	36 mM	-	-	
OXYGEN LIGANDS				
Catechol/ Oxalic acid/ Oxalacetic acid	×	×	×	No changes in the voltammetry were observed.

Table 4.5 Summary of results for exogenous ligand binding to [M3Fe-4S]

Key:

× No reaction detected

╬ Exogenous ligand complexes metal out

✓ Positive interaction seen

Table 4.5 presents a summary of all the information gained on ligand binding to the [M3Fe-4S] clusters in *Da* Fd III. There are three distinct situations which may be observed when a protein film containing such a cluster is introduced to a solution of a potential ligand. These three situations are: no change in the voltammetry; changes that indicate ligand binding; or disruption of the heterometal clusters - either totally, or by removal of the heterometal. It is unlikely that every cluster in such a sample will behave in exactly the same way - the overall situation will finally be represented by a number of equilibria, it is the interplay of these different events which govern the observed response. The complete picture will, however, take into account other processes such as protonation equilibria, particularly of potential ligands, and co-ordination of the protein (aspartate) residue. The simplest picture is shown in Figure 4.20.

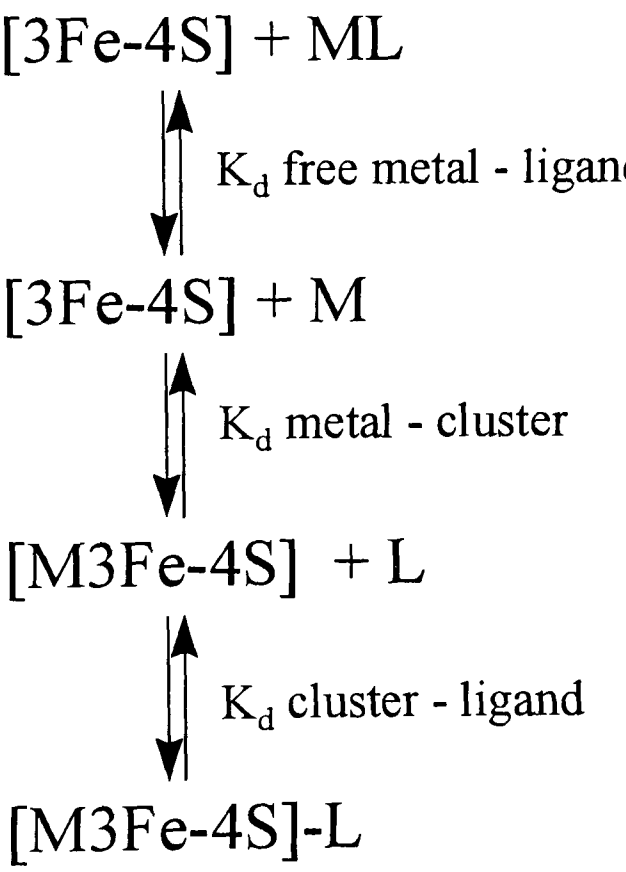

Figure 4.20 Scheme of equilibria for ligand interaction with [M3Fe-4S]

Initially, the simplest case is where the exogenous ligand causes removal of M from the [M3Fe-4S] cluster, and it is these cases which are discussed first.

4.5.1. Removal of M from the [M3Fe-4S] Cluster

As shown in Table 4.5 the ligands which caused removal of the heterometal centre from the cluster were thiomalic acid (Fe, Zn and Co), thioacetic acid (Fe) and thioglycolic acid (Co), respectively:

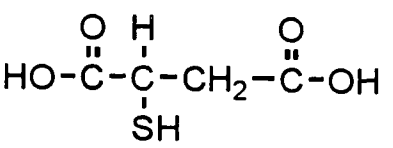

Thiomalic acid

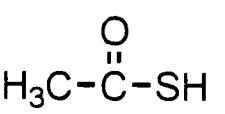

Thioacetic acid

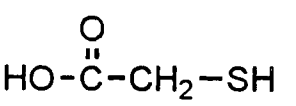

Thioglycolic acid

By referring to the scheme in Figure 4.20, metal abstraction is thermodynamically likely to result from the fact that the ligand in free solution forms very strong complexes to the metal ion, whilst binding in the protein interior is weaker. Reasons for the latter could include steric hindrance and constraint, the electronic structure of the cluster, or because of the ligating protein residue. In the case of thiomalic acid, there are two carboxylic groups available for metal complexation - the possibility for multi-dentate chelation which exists in solution may explain the tendency of this ligand to bind in solution, rather than in the protein interior. For thioacetic and thioglycolic acids, whether the ligand complexes the metal in the protein, or in solution, is dependent on the identity of the metal and the thermodynamics are thus finely balanced. In the case of thioacetic acid the electron-withdrawing carbonyl functionality decreases the electron density on the thiol - probably the major factor bringing about the marked difference between this ligand and a more general thiol ligand. Thioglycolic acid also possesses a carbonyl group, but this is separated by an sp^3 carbon centre, and it is also present as a carboxylic acid functionality - thus it is unclear why the strength of ligand binding is affected in this case. One possibility is that the proximity of this group to the thiol is less favourable within the hydrogen bonding structure around the cluster - this is discussed further below.

4.5.2 No Evidence for Ligand Binding, the Voltammetry is Unchanged

There are three situations discussed in which it can be said that the voltammetry does not change in the presence of the ligand. First, however, it is useful to note that ligand binding will only be observed if there is differential binding to one oxidation level - hence a situation of ligand binding but without voltammetric change is conceivable, but unlikely.

i) The Oxygenic Ligands : catechol, oxalic acid and oxalacetic acid

Although several attempts were made, no positive indications of ligand interaction were observed when a transformed film was introduced to an oxygenic ligand. It should be noted however, that an added reason why no voltammetric change may be observed on binding is that if a direct replacement of one oxygenic ligand for another similar oxygenic ligand (in this case we propose Asp14) were to occur, the change in the electronic structure of the cluster may be limited and thus, the reduction potential relatively invariant. However, ligand *addition* may also occur at the cluster, as for aconitase, and this would be more likely to cause changes in the physical properties of the cluster. Exogenous ligand exchange from a mono- to a bi-dentate oxygenic ligating system (all three ligands have the capability of bidentate co-ordination) is not unprecedented - indeed it is observed in aconitase where the substrate (citrate) binds to the 4Fe form, increasing the co-ordination at the Fe site from 4 to 6.[26] Similar behaviour is observed in the non-biological analogues of FeS clusters synthesised by Holm *et al.* In these instances it has been shown that mono-dentate ligands to the subsite differentiated Fe can be replaced by bi- or even tri-dentate ligands.[27]

Oxygenic ligation does occur to native FeS clusters, but it is unusual. As well as aconitase, examples include the 4Fe Fd from *Pyrococcus furiosus*,[32,36] and the 2Fe cluster from succinate dehydrogenase from *E. coli*.[37] Oxygenic ligands have also been introduced to protein sequences (using site directed mutagenesis) and have been incorporated as ligands to FeS clusters. Examples include the C56S and C60S mutants of *Clostridium pasteurianum* 2Fe Fd (*Chapter 5*), the FrdB subunit of *E. coli* fumarate reductase[43,44] and the vegetative cell ferredoxin from *Anabaena* sp. 7120.[45] However, there are also examples where, despite a serine being inserted in the spatially correct location for a cluster ligand, proteins have undergone rearrangement to utilise an

alternative cysteine - for example, the C20S mutant of *Azotobacter vinelandii* [46] and the C24S mutant of *Cp* 2Fe Fd (*Chapter 5*).

As seen from these examples, oxygenic co-ordination to Fe-S clusters is unusual and, indeed, is often actively 'chosen against' by the protein. It is perhaps thus not surprising that the ligands discussed here do not co-ordinate to the metal centre.

ii) Nitrogenous Ligands - imidazole and histidine

As described in *Section 4.3.5* there is little evidence that imidazole and histidine can be induced to bind to the Fe-S centre in *Da* Fd III. This is not surprising in light of the lack of known examples of nitrogenous co-ordination to FeS centres - in Nature, nitrogenous ligation of FeS clusters is rare, with the exception of the subgroup of 2Fe Fds - the Rieske subclass. Rieske clusters are ligated by two histidine and two cysteine ligands and have reduction potentials noticeably higher than all-cysteine ligated 2Fe Fds, at 140 mV to 350 mV.[4] Ligation of a [4Fe-4S] cluster by a nitrogenous ligand was unprecedented, until the discovery that one of the [4Fe-4S] clusters in *Desulfovibrio gigas* hydrogenase is ligated by a histidine side chain[47] - it is believed that the imidazole ring is located on the surface of the molecule, where it could participate in electron transfer to and from the reported redox partner of hydrogenase, cytochrome c_3.

iii) Glutathione binds to the Zn and Co centres, but not to [4Fe-4S]

The case of glutathione is the only example where the identity of the metal is crucial to determining whether the ligand binds to the cluster and not withstanding the very likely delocalisation of electrons throughout the cluster, the reason for this is not clear in simple terms. It could be postulated that the trend of decreasing stability of the 3+ oxidation state - Fe^{3+} is stable, more so than Co^{3+} and obviously far more than Zn^{3+} - means that Fe^{3+} would preferentially bind anionic ligands when the cluster is in the oxidised state. Thus, the observation that glutathione does not react with the [Fe3Fe-4S] cluster is not readily explained and would seem to contradict conventional reasoning.

4.5.3 Ligand Binding to the Cluster

When a reaction between the ligand and the cluster was observable, it was generally true that a negative shift in the reduction potential occurred - thus the oxidised cluster has a greater affinity for the exogenous ligand. In cases where the reduction potential could not be recorded unambiguously, because of broadening of the reduction wave, the oxidative wave - taken as an 'indicator' of the reduction potential - was still shifted to a more negative potential. The negative shifts in reduction potential varied greatly from one ligand to another, the largest being for the [Fe3Fe-4S] and mercaptoethanoate system (200 mV). Finite shifts in the reduction potentials (the end value $E^{o'}{}_{F}$) for some ligands were impossible to determine - this was particularly the case if the ligand was only weakly bound to the cluster. Further complications in determining the shift were brought about by $E^{o'}{}_{obs}$ being coincident with the potential of the native [4Fe-4S] cluster, this was an especial problem for ligand reactions with the [Co3Fe-4S] cluster.

Preferential binding to the oxidised form of the cluster can be explained if the binding affinity depends upon the extent of electron delocalisation across the cluster. For example, Figure 4.12 clearly shows for the reaction between [Fe3Fe-4S] and coenzyme M that at the starting point of the scan at a negative potential, ($[Fe3Fe\text{-}4S]^{1+}$) there is no detectable interaction between the ligand and the cluster. The strong donor ligand S^{-} is of course expected to form a stronger bond with the more electron-deficient oxidised cluster.

Ligand	$Kd_{ox}^{(L)}$	$Kd_{red}^{(L)}$	Comments
Glutathione	~ 1 μM	-	This value is for the [Co3Fe-4S] cluster, no reaction was seen with the [Fe3Fe-4S] cluster and glutathione
Mercaptoethanol	28 μM	97 mM	// *Decreasing affinity*
L-Cysteine	68 μM	2 mM	// *for the*
Coenzyme M	0.5 mM	2.4 M	// *oxidised [Fe3Fe-4S]$^{2+}$*
Cysteamine	1.5 mM	36 mM	// *cluster*

Table 4.6 Ligands which showed a positive interaction with the [Fe3Fe-4S] cluster
Only the K_d values of the [Fe3Fe-4S] cluster are considered. The ligands are placed in increasing order of their $Kd_{(L)}^{ox}$ values.

Of the ligands which show the most consistent evidence of interacting with the cluster (mercaptoethanol, cysteine, glutathione, coenzyme M and cysteamine) there is an obvious common feature - the thiol group, which must be ionised to ligate the cluster atom.

Additionally, there is a possible role for groups which can donate hydrogen bonds - this may be important for construction of a 'network' around the cluster. There is a suitable H-bond donor on mercaptoethanol (OH), cysteine (NH_2), glutathione (NH), and cysteamine (NH_2). In each case this group is on the 'vicinal' carbon to the thiol group (the α-carbon of the molecule). This H-bond donor may form an intrinsic link to the protein at residues proximal to the cluster. This extra stability may therefore favour interaction of these particular ligands with the cluster. In the case of mercaptopropionic acid, the carboxylic acid group is further removed, by an additional carbon centre, and although the OH of this functional group (the H-bond donor) may be a positive influence on binding to the cluster, it is possible that the increased distance to the thiol is the reason for the apparently poorer binding capacity. (An opposite effect is seen for the molecules in *Section 4.5.1* - which contain a proximal carbonyl group to the thiolate, it is

possible that the carbonyl both aids metal abstraction from the cluster and does not interact so favourably with the protein network.)

4.5.4 Conclusion

Protein film voltammetry is an extremely sensitive method of observing the very subtle reactions of iron-sulfur proteins - as well as allowing measurements in real time it allows an integrated picture of both the thermodynamics and kinetics of processes to be gained. An obvious example of this capability is the picture of exogenous ligand binding which has been built up, particularly for mercaptoethanol.[24] While in many of the above cases such a detailed analysis was not possible, it is hoped that by taking a wider overview some progress has been made toward rationalising the factors which govern the outcome of a possible exogenous ligand binding event.

From these studies it is difficult to draw all-encompassing conclusions about small molecule ligand binding to FeS clusters but two determining factors are apparent. Firstly the overall preference of the cluster for thiolate ligands cannot be ignored. Although the variety of ligands in this study was by no means exhaustive, the results obtained (Table 4.5) show that non-thiolate ligands appear to have no significant affinity for the cluster, in contrast to thiolate ligands. This is mirrored in Nature: thiolate ligands i.e. cysteinate ligation is the universally acknowledged *major* ligand of FeS clusters - although there are a few significant exceptions to this (*Chapter 1*).[4,5] Secondly the presence of an available thiolate on the proposed ligand is not a guarantee for binding, this also depends on the neighbouring groups in the molecule.

4.6 REFERENCES

1) Beinert, H.; Kennedy, M. C. *European Journal of Biochemistry* **1989**, *186*, 5-15.

2) Beinert, H. *Faseb Journal* **1990**, *4*, 2483-2491.

3) Cammack, R. *Advances in Inorganic Chemistry*, 1992; Vol. 38.

4) Johnson, M. K. *Encyclopedia of Inorganic Chemistry*; Wiley: Chichester:, 1994; Vol. 4.

5) Beinert, H.; Holm, R. H.; Munck, E. *Science* **1997**, *277*, 653-659.

6) Kent, T. A.; Dreyer, J. L.; Kennedy, M. C.; Huynh, B. H.; Emptage, M. H.; Beinert, H.; Munck, E. *Proceedings of the National Academy of Sciences of the United States of America-Biological Sciences* **1982**, *79*, 1096-1100.

7) Moura, J. J. G.; Moura, I.; Kent, T. A.; Lipscomb, J. D.; Huynh, B. H.; Legall, J.; Xavier, A. V.; Munck, E. *Journal of Biological Chemistry* **1982**, *257*, 6259-6267.

8) Moura, I.; Moura, J. J. G.; Munck, E.; Papaefthymiou, V.; Legall, J. *Journal of the American Chemical Society* **1986**, *108*, 349-351.

9) Surerus, K. K.; Munck, E.; Moura, I.; Moura, J. J. G.; Legall, J. *Journal of the American Chemical Society* **1987**, *109*, 3805-3807.

10) Moreno, C.; Macedo, A. L.; Moura, I.; Legall, J.; Moura, J. J. G. *Journal of Inorganic Biochemistry* **1994**, *53*, 219-234.

11) Conover, R. C.; Kowal, A. T.; Fu, W.; Park, J. B.; Aono, S.; Adams, M. W. W.; Johnson, M. K. *Journal of Biological Chemistry* **1990**, *265*, 8533-8541.

12) Conover, R. C.; Park, J. B.; Adams, M. W. W.; Johnson, M. K. *Journal of the American Chemical Society* **1990**, *112*, 4562-4564.

13) Srivastava, K. K. P.; Surerus, K. K.; Conover, R. C.; Johnson, M. K.; Park, J. B.; Adams, M. W. W.; Munck, E. *Inorganic Chemistry* **1993**, *32*, 927-936.

14) Fu, W. G.; Telser, J.; Hoffman, B. M.; Smith, E. T.; Adams, M. W. W.; Finnegan, M. G.; Conover, R. C.; Johnson, M. K. *Journal of the American Chemical Society* **1994**, *116*, 5722-5729.

15) Finnegan, M. G.; Conover, R. C.; Park, J. B.; Zhou, Z. H.; Adams, M. W. W.; Johnson, M. K. *Inorganic Chemistry* **1995**, *34*, 5358-5369.

16) George, S. J.; Armstrong, F. A.; Hatchikian, E. C.; Thomson, A. J. *Biochemical Journal* **1989**, *264*, 275-284.

17) Butt, J. N.; Sucheta, A.; Armstrong, F. A.; Breton, J.; Thomson, A. J.; Hatchikian, E. C. *Journal of the American Chemical Society* **1991**, *113*, 8948-8950.

18) Butt, J. N.; Armstrong, F. A.; Breton, J.; George, S. J.; Thomson, A. J.; Hatchikian, E. C. *Journal of the American Chemical Society* **1991**, *113*, 6663-6670.

19) Butt, J. N.; Niles, J.; Armstrong, F. A.; Breton, J.; Thomson, A. J. *Nature Structural Biology* **1994**, *1*, 427-433.

20) Butt, J. N.; Fawcett, S. E. J.; Breton, J.; Thomson, A. J.; Armstrong, F. A. *Journal of the American Chemical Society* **1997**, *119*, 9729-9737.

21) Staples, C. R.; Dhawan, I. K.; Finnegan, M. G.; Dwinell, D. A.; Zhou, Z. H.; Huang, H. S.; Verhagen, M.; Adams, M. W. W.; Johnson, M. K. *Inorganic Chemistry* **1997**, *36*, 5740-5749.

22) Zhou, J.; Raebiger, J. W.; Crawford, C. A.; Holm, R. H. *Journal of the American Chemical Society* **1997**, *119*, 6242-6250.

23) Fawcett, S. E. J.; Davis, D.; Breton, J. L.; Thomson, A. J.; Armstrong, F. A. *Biochemical Journal* **1998**, *335*, 357-368.

24) Butt, J. N.; Sucheta, A.; Armstrong, F. A.; Breton, J.; Thomson, A. J.; Hatchikian, E. C. *Journal of the American Chemical Society* **1993**, *115*, 1413-1421.

25) Moulis, J. M.; Davasse, V.; Golinelli, M. P.; Meyer, J.; Quinkal, I. *Journal of Biological Inorganic Chemistry* **1996**, *1*, 2-14.

26) Beinert, H.; Kennedy, M. C.; Stout, C. D. *Chemical Reviews* **1996**, *96*, 2335-2373.

27) Holm, R. H. *Advances in Inorganic Chemistry* **1992**, *38*, 1-71.

28) Ciurli, S.; Carrie, M.; Weigel, J. A.; Carney, M. J.; Stack, T. D. P.; Papaefthymiou, G. C.; Holm, R. H. *Journal of the American Chemical Society* **1990**, *112*, 2654-2664.

29) Barclay, J. E.; Diaz, M. I.; Evans, D. J.; Garcia, G.; Santana, M. D.; Torralba, M. C. *Inorganica Chimica Acta* **1997**, *258*, 211-219.

30) Kennedy, C.; Rauner, R.; Gawron, O. *Biochem.Biophys.Res.Commun.* **1972**, *47*, 740.

31) Park, J. B.; Fan, C. L.; Hoffman, B. M.; Adams, M. W. W. *Journal of Biological Chemistry* **1991**, *266*, 19351-19356.

32) Calzolai, L.; Gorst, C. M.; Zhao, Z. H.; Teng, Q.; Adams, M. W. W.; Lamar, G. N. *Biochemistry* **1995**, *34*, 11373-11384.

33) Gorst, C. M.; Zhou, Z. H.; Ma, K. S.; Teng, Q.; Howard, J. B.; Adams, M. W. W.; Lamar, G. N. *Biochemistry* **1995**, *34*, 8788-8795.

34) Telser, J.; Smith, E. T.; Adams, M. W. W.; Conover, R. C.; Johnson, M. K.; Hoffman, B. M. *Journal of the American Chemical Society* **1995**, *117*, 5133-5140.

35) Thomson, A. J.; Breton, J.; Butt, J. N.; Hatchikian, E. C.; Armstrong, F. A. *Journal of Inorganic Biochemistry* **1992**, *47*, 197-207.

36) Gorst, C. M.; Yeh, Y. H.; Teng, Q.; Calzolai, L.; Zhou, Z. H.; Adams, M. W. W.; Lamar, G. N. *Biochemistry* **1995**, *34*, 600-610.

37) Werth, M. T.; Sices, H.; Cecchini, G.; Schroder, I.; Lasage, S.; Gunsalus, R. P.; Johnson, M. K. *Febs Letters* **1992**, *299*, 1-4.

38) Butt, J. N. *Ph.D. Thesis* University of California, Irvine, **1993.**

39) Duff, J. L. C.; Breton, J. L. J.; Butt, J. N.; Armstrong, F. A.; Thomson, A. J. *Journal of the American Chemical Society* **1996**, *118*, 8593-8603.

40) Butt, J. N., Unpublished Observation.

41) Frausto da Silva, J. J. R.; Williams, R. J. P. *The Biological Chemistry of the Elements*; Oxford University Press: Oxford, **1993.**

42) Martell; Smith *Critical Stability Constants* .

43) Kowal, A. T.; Werth, M. T.; Manodori, A.; Cecchini, G.; Schroder, I.; Gunsalus, R. P.; Johnson, M. K. *Biochemistry* **1995**, *34*, 12284-12293.

44) Werth, M. T.; Cecchini, G.; Manodori, A.; Ackrell, B. A. C.; Schroder, I.; Gunsalus, R. P.; Johnson, M. K. *Proceedings of the National Academy of Sciences of the United States of America* **1990**, *87*, 8965-8969.

45) Cheng, H.; Xia, B.; Reed, G. H.; Markley, J. L. *Biochemistry* **1994**, *33*, 3155-3164.

46) Shen, B.; Jollie, D. R.; Diller, T. C.; Stout, C. D.; Stephens, P. J.; Burgess, B. K. *Proceedings of the National Academy of Sciences of the United States of America* **1995**, *92*, 10064-10068.

47) Volbeda, A.; Charon, M.-H.; C., P.; Hatchikian, E. C.; Frey, M.; Fontecilla-Camps, J. C. *Nature* **1995**, 580-587.

CHAPTER 5

ELECTROCHEMICAL INVESTIGATION OF THE [2FE-2S] FERREDOXIN FROM *Clostridium pasteurianum* AND SEVERAL MUTANT FORMS

CHAPTER 5

ELECTROCHEMICAL INVESTIGATION OF THE [2FE-2S] FERREDOXIN FROM *Clostridium pasteurianum* AND SEVERAL MUTANT FORMS

5.1 INTRODUCTION

Two iron, two sulfur clusters, [2Fe-2S], constitute a structural-functional motif that is widely used in proteins. These [2Fe-2S] clusters serve as a site for either one-electron oxidation or reduction. Factors which influence the ability to transfer electrons, aside from the cluster itself, are the cluster ligation sphere i.e. which amino acid residues are ligating the cluster, and also the protein structure surrounding the cluster. The 2Fe clusters are usually co-ordinated by four cysteine residues from the protein which complete pseudo-tetrahedral co-ordination around the iron atoms, see Figure 5.1. The notable exception is the 'Rieske' cluster, which are co-ordinated by two cysteines and two histidines.

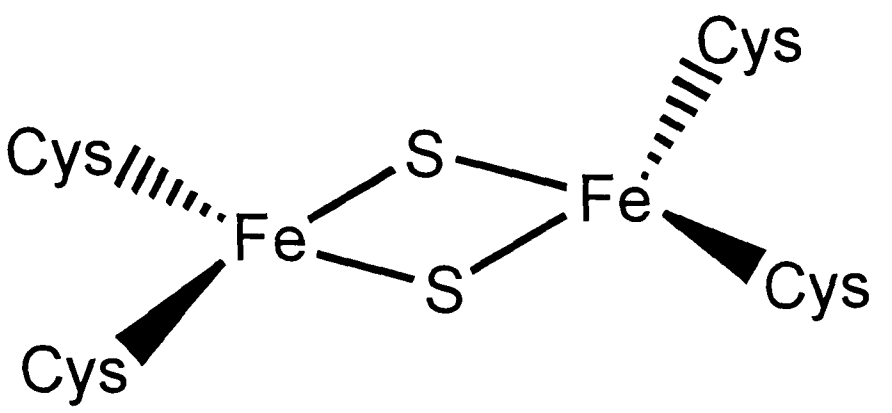

Figure 5.1 Core structure of a [2Fe-2S] cluster

Proteins which contain only a [2Fe-2S] cluster are known as two-iron ferredoxins and are widely dispersed in nature. They were first identified as photosynthetic electron-transfer proteins in chloroplasts, and have been since found in a large variety of different organisms and environments. However, [2Fe-2S] clusters exist as electron-transfer agents in a wider range of multi-component redox enzymes such as succinate dehydrogenase, xanthine oxidase, some dioxygenases and hydrogenases.[1,2]

A number of [2Fe-2S] ferredoxins have been sequenced, of which the majority possess a common theme to the ligation motif, the -Cys-X-X-Cys- sequence, repeated twice in the protein structure.[3] Examples of such ligand sequences (usually -Cys-X-X-Cys- but in some cases -Cys-X-X-His-) for [2Fe-2S] clusters are shown in Table 5.1. However, the amino acid sequence for *Clostridium pasteurianum* (*Cp*) 2Fe Fd was found to have an anomalous amino acid sequence,[4] containing five cysteines, and thus the co-ordinating residues could not be identified by sequence analogy alone.[5] It is for this reason that the 2Fe Fd from *Clostridium pasteurianum* was investigated further, using a combination of site-directed mutagenesis experiments together with spectroscopy and electrochemistry. The subsequent results and discussion are the subject of this chapter.

LIGATING SEQUENCE	FERREDOXIN
NH_3^+-X_n-Cys-X_2-Cys-X_9-Cys-X_{31}-Cys-X_3-Cys-X_n-CO_2^-	*Clostridium pasteurianum* Fd[6]
NH_3^+-X_n-**Cys** -X_4-**Cys**-X_2-**Cys** -X_{29} -**Cys** -X_n-CO_2^-	Plant-type Fds[1]
NH_3^+-X_n-**Cys**-X_5-**Cys**- X_2-**Cys**-$X_{36/37}$-**Cys**-X_n-CO_2^-	Hydroxylase-type Fds[1]
NH_3^+-X_n-Cys-X_3-Cys-X_2-Cys-X_{36}-Cys- $X_{30/31}$-Cys-X_{59}-Cys-X_n-CO_2^-	Biotin synthases[7]
NH_3^+-X_n-**Cys**-X-**His**-X_{16} -**Cys**-X_2-**His**-X_n-CO_2^-	Benzene dioxygenase Fd[8]
NH_3^+-X_n-**Cys**-X-**His**-X_{17}-**Cys**-X_2-**His**-X_n-CO_2^-	Dioxygenases[8]
NH_3^+-X_n-**Cys**-X-**His**-X_2-Cys-X_{14}-**Cys**-X-Cys-**His**-X_n-CO_2^-	Rieske proteins[8]

Table 5.1 Ligating sequences of [2Fe-2S] clusters

Residues in red indicate those which are thought to be ligands, based on X-ray structure, sequence homology, site-directed mutagenesis or spectroscopic evidence. The five cysteines of Clostridium pasteurianum 2Fe Fd are highlighted in green. NH_3^+ *and* CO_2^- *are the terminal amino and carboxylic ends of the protein chain.*

An increasingly ubiquitous tool in the characterisation and identification of iron-sulfur clusters is site-directed mutagenesis (SDM), which enables the researcher to generate point mutational proteins. Commonly for iron-sulfur proteins, cysteine is mutated because of its almost universal role in ligating the Fe atoms in these proteins.[9] Site-directed mutagenesis is an extremely useful method for determining which cysteines are actually ligating the clusters. This is especially the case for very large enzymes, which contain more than one iron-sulfur cluster (and the clusters are also distinguishable by EPR). Changes in the ligating residues of an FeS cluster are likely to have a fundamental impact on all characteristics of the cluster (see *Section 5.1.1* (1)-(5)). Research has shown that substituting only one cysteine, even for a functionally similar ligand like serine, can cause disruption of cluster assembly and, in extreme cases, will prevent cluster assembly altogether, thus terminally affecting the protein structure.[9] In general, success in this field has occurred when residues in either one- or two-iron centred

proteins have been involved, noticeably rubredoxin and the [2Fe-2S] cluster proteins.[9] With larger clusters, changes of the cluster nuclearity or 'poaching' of a proximal free cysteine are often preferred by the protein, instead of utilisation of the introduced ligand.[10] Importantly, the success of mutating a ligand of the cluster not only depends on the ability of the cluster to co-ordinate the new ligand, but depends on the local flexibility of the polypeptide chain, the accessibility of the solvent and the electronic distribution on the active centres.

Experiments to elucidate the co-ordinating ligands of [2Fe-2S] centres using SDM have included the Rieske subunit of *Rhodobacter capsulatus* bc1 complex,[11] the FrdB subunit of *Escherichia coli* fumarate reductase,[12-14] the vegetative cell ferredoxin from *Anabaena* sp. 7210[15] and the NQO2 subunit of *Paracoccus denitrificans* NADH-quinone oxidoreductase.[16]

5.1.1 Site-directed Mutagenesis Experiments

Specific site-directed mutagenesis experiments can produce a number of scenarios, dependent upon the protein *and* the number of mutations undertaken for each mutant. With site-directed mutagenesis experiments involving proteins containing FeS clusters, the primary target is usually to identify the cysteine residues of the cluster. This is carried out by replacing each cysteine residue individually and observing changes in the protein and/or the cluster characteristics. A summary of the possible outcomes of site-directed mutagenesis on a protein containing an FeS cluster are listed below.

(1) In the simplest and trivial case, the protein is successfully expressed in a host, without alteration of the normal gene sequence; this produces what is known as the wild-type (WT) protein. This is thus the 'control' experiment and no change in any of the biophysical or chemical properties of either the protein or the redox centre (the cluster) should be observed.

(2) If a one-point mutational protein is constructed, with no subsequent changes to any of the biophysical or chemical properties, of either the protein or the redox centre, this suggests that the replaced residue is *not* a ligand to the cluster.

(3) The protein is successfully expressed complete with redox centre, but in some way, the biophysical and/or the chemical properties of the cluster are altered. This suggests that the replaced residue may be a cluster ligand. The protein must have compensated for this disruption, in some way, to have successfully incorporated a cluster. If the inserted residue is of a chemically similar nature to the replaced ligand, then *ligand exchange* may have occurred. Alternatively if the residue replacing the original ligand is very different to that of the replaced ligand, then the protein may undergo a *structural rearrangement* to utilise a nearby residue, similar to the one which has been removed. Alternatively, as for a number of [4Fe-4S] clusters, replacement of a co-ordinating cysteine ligand may result in loss of one of the corners of the cubane and a [3Fe-4S] cluster is the resultant product.[17]

(4) The cluster is not detectable, although the apoprotein is successfully expressed and purified. This implies, almost certainly, that the replaced residue is a co-ordinating ligand of the cluster. The protein may not be able to substitute a suitable proximal residue, as a result of one not being available, or rearrangement may be sterically hindered. If the expression system is using a foreign host then this will have little or no impact on the organism's viability. Alternatively, if the expression system is utilising the native host this may have consequences upon the organism's viability.

(5) The most serious consequence is that the protein, containing the mutation, is not detected at all in the host, and thus it can be concluded that the mutated residue is a ligand of the cluster. This is unlikely to be due to problems with the transcription-translation processes, but instead to post-translational events, i.e. when the correct folding of a protein is dependent on the correct insertion of the iron-sulfur cluster. If the protein is unfolded it is possible that it will be destroyed by the gene-host. Once again the viability of the organism will depend on which expression system was used, i.e. native or foreign, and how critical the protein is to the native host, if used.

In cases (4) and (5) above, the protein might be destabilised by other factors other than the involvement of the residue in cluster co-ordination. It is important to note that definite conclusions should not be made for site directed mutagenesis experiments until

all suspect residues have been investigated and the corresponding data for each mutant collected.

5.1.2 *Clostridium pasteurianum* Ferredoxin

As previously stated, work in this chapter investigates the unusual [2Fe-2S] ferredoxin from *Clostridium pasteurianum*, together with a number of specifically chosen site-directed mutants which are listed in Table 5.2.[6,18]

Mutant	Comments	Reference
C14A[□]	Identical UV/Vis spectra to WT	6
C24A[□]	UV/Vis spectrum shows small bandshifts (< 5 nm) and slight variations in the relative intensities of the bands at 420 nm and 460 nm compared to WT	6
H6A/H7A/H90A[□]	All histidine residues in amino acid sequence mutated to alanine, identical UV/Vis spectra to WT	19
C11S[□]	Low content of chromophore, as observed from UV/Vis spectra	6
C24S	Identical UV/Vis spectra to C24A	6
C14S	Identical UV/Vis spectra to WT	6
C14A/C24A[□]	UV/Vis spectra differs from WT, C14A and C24A by displaying a single maximum at 442 nm and has a lower A_{450}/A_{280} absorbance ratio	6
C14S/C24A	Identical UV/Vis spectra C14A/C24A and C14A/C24S	6
C14A/C24S	Identical UV/Vis spectra C14S/C24A and C14A/C24A	6
C60S[□] **and C56S**[□]	Hypsochromic shifts of the spectra, from that of the WT, in the 10-80 nm range for the serine mutants i.e. (blueshifts)	18
C56S/C14A/L16C /Δ19-30[□]	Identical UV/Vis spectrum to the C56S mutant	20
C60S/S61A[□]	Similar UV/Vis spectrum to C60S	21

Table 5.2 Mutants of *Clostridium pasteurianum* ferredoxin

Δ19-30 denotes that the residues 19 to 30 have been removed

[□]*Mutants characterised by electrochemical methods in this chapter.*

Clostridium pasteurianum is a nitrogen-fixing saccharolytic anaerobe and contains a [2Fe-2S] ferredoxin, first isolated in 1965.[22] The protein is homodimeric in solution,[23] each subunit containing one [2Fe-2S] cluster.[4] The presence of binuclear iron-sulfur clusters in *Cp* Fd has been confirmed using spectroscopy. The biochemical[23,24] and spectroscopic features of the iron-sulfur chromophore,[23-26] together with the complete amino acid sequence have also been determined.[4] Furthermore, electrospray ionisation mass spectra (ESI-MS) of this protein found two components with masses of 11 428 Da (monomeric apoprotein) and 11 600 Da holoprotein (apoprotein plus 2 sulfur and 2 iron atoms, minus 4 cysteinyl protons).[27]

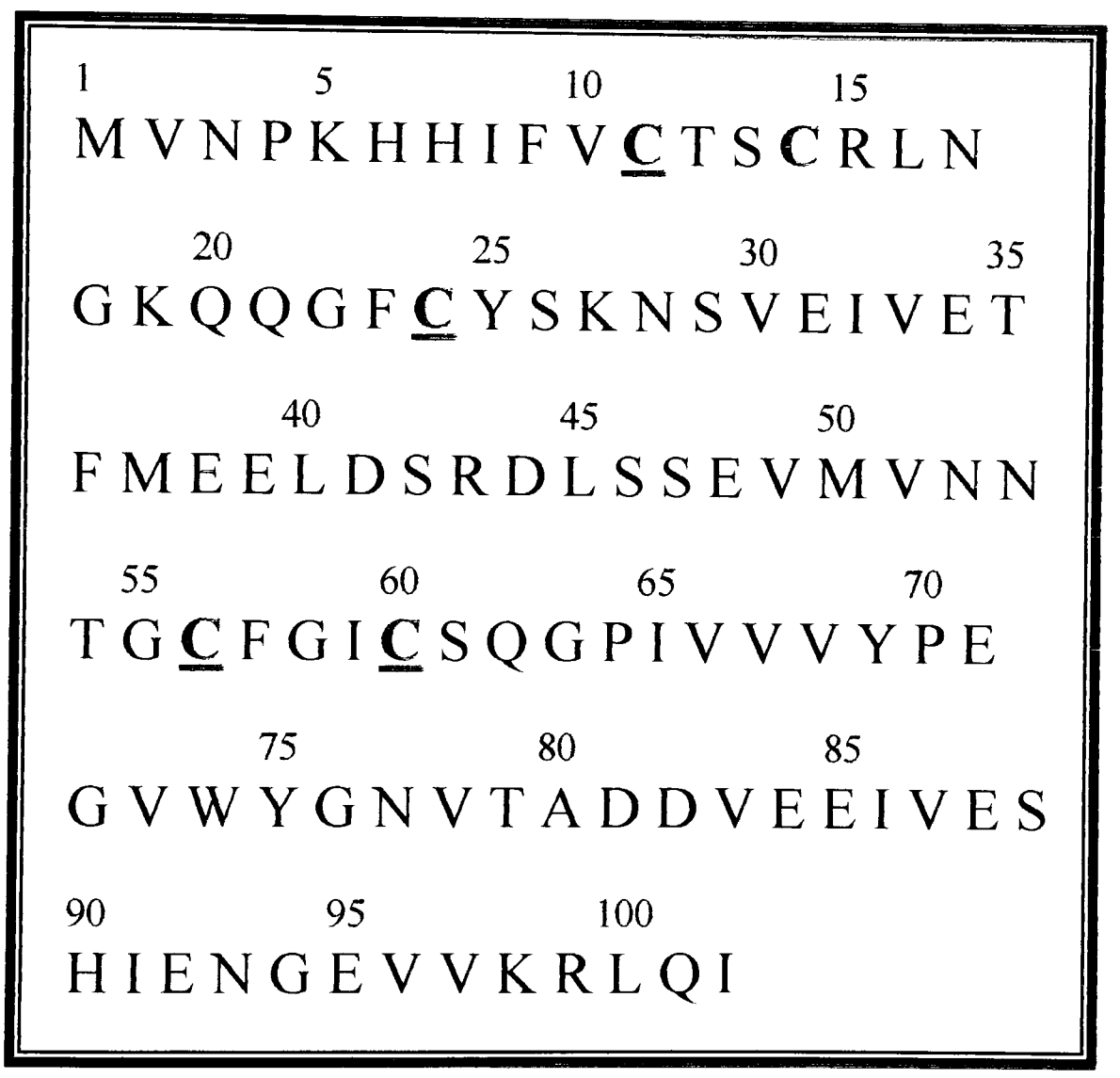

Figure 5.2 Amino acid sequence of the 2Fe ferredoxin from *Clostridium pasteurianum*[28]

*The underlined cysteine residues (**C**) are ligands to the native [2Fe-2S] cluster, the cysteine at position 14 (**C**) is not a ligand to the cluster but can be recruited as a cluster ligand, as for the mutant C24A - see text. Amino acid single letter codes are given in the Abbreviations section of this thesis.*

It was found that *Cp* 2Fe Fd has an unusual amino acid sequence of five cysteines at positions 11, 14, 24, 56 and 60, see Figure 5.2. The primary structure prevents a straightforward identification of the co-ordinating residues of the ferredoxin by initial sequence homology, because the sequence is unique.[5] Until a complete three dimensional structure is determined, SDM experiments represent a promising path towards identifying the co-ordinating residues since the gene encoding the [2Fe-2S] *Cp* Fd has been overexpressed in *Escherichia coli*,[28] allowing the critical mutations to be carried out.

A large number of mutants were constructed[a] with either serine[18] alanine or histidine replacing one, two or three cysteines in the original protein structure, (Table 5.2). Initial spectroscopic screening (UV/Vis, EPR and resonance Raman) of the mutants was carried out by Meyer *et al.*[6,18,19] Of those mutants which had almost identical spectra to each other e.g. C14A and C14S, only one was investigated (Table 5.2).

The mutants C56S and C60S were considered for electrochemical investigation because a combination of EPR, VTMCD spectra, and magnetisation studies revealed that the $[2Fe\text{-}2S]^{1+}$ clusters in the C56S and the C60S mutants are present as $S = 1/2$ and $S = 9/2$ spin mixtures.[29] The $S = 1/2$ species, in both mutants, is indicative of a localised valence Fe^{3+}/Fe^{2+} cluster with serinate ligation at the Fe^{2+}.[29] The VTMCD spectrum of the $S = 9/2$ species is marked by an intense positive band at 700 nm, which is tentatively attributed to the valence-delocalised intervalence band. Further studies using Mössbauer spectroscopy have demonstrated that the $S = 9/2$ state is valence-delocalised.[30]

The mutant C60S/S61A was studied as part of an investigation on the novel $S = 9/2$ ground state for the mutant C60S.[29]

The mutant C56S/C14A/L16C/Δ19-30 was investigated, but was part of a larger study on cysteine ligand swapping on a deletable loop of the [2Fe-2S] ferredoxin from *Cp*.[20]

---

[a] Standard notation is used for identifying mutations of proteins. For example, C24A denotes that the cysteine residue at position 24 on the amino acid chain has been replaced by an alanine residue in the mutant form.

The electrochemical investigations were carried out with ongoing collaboration from the Meyer group (Grenoble, France) the Cammack group (London, UK) and the Johnson group, (Georgia, USA). All wild-type protein and mutants used were prepared by the Meyer group.

From the initial spectroscopic investigation, it was concluded that the cysteines at 11, 24, 56 and 60 were ligands to the 2Fe Fd, as inferred from the significant spectral changes in the UV/Vis spectra.[6] Formation of an FeS cluster in the double mutant C14A/C24A, which only contained three cysteines, proved to be more difficult to explain, suggesting that H_2O or ^-OH ligation was occurring, although this has not been confirmed.

The C24S mutant had practically an identical UV/Vis spectrum to the C24A mutant, indicating that the same co-ordinating ligands were utilised in both cases.[6] The likely proximity of C14 to the cluster suggested that ligand exchange had occurred, with C14 replacing C24. To investigate this further, the double mutants containing only three cysteines were constructed as listed in Table 5.2. All of these mutants had identical UV/Vis characteristics, containing an FeS chromophore, and so only C24A/C14A was investigated. The initial study, by Meyer *et al*, although proving that a cluster was contained in the double mutant protein, did not conclusively identify the fourth ligand to the cluster.[6]

5.1.3 Aims of this Investigation

The aim of this investigation was to characterise, electrochemically, the wild-type and various mutants of *Cp* 2Fe Fd, in particular to examine how the serine ligands to the cluster alter the electrochemical characteristics of the ferredoxin. Furthermore, the aim was to investigate the ferredoxin in the double mutant, C24A/C14A, and to try and elucidate the fourth ligand and/or its characteristics.

5.2 EXPERIMENTAL

Experiments were carried out as detailed in *Chapter 2*. Any significant changes to these procedures are detailed in this Chapter. All experiments were carried out at 0 °C.

5.3 RESULTS AND DISCUSSION

5.3.1 Wild-type Ferredoxin

Film Voltammetry

Prior to this study, no electrochemical investigations had been carried out on this particular ferredoxin and so the optimum conditions for direct electrochemistry were unknown.

Initially a film was applied to the electrode, consisting of ca. 100 μM protein solution, with no co-adsorbate in either electrolyte solution or protein solution. This elicited hardly any observable signal and so co-adsorbate, polymyxin at 200 μg ml^{-1}, was added to the protein solution and the electrolyte solution, both separately and then simultaneously. The best response, as previously documented,[31] was achieved when the co-adsorbate was present in *both* the protein solution and the electrolyte solution.

The wild-type [2Fe-2S] ferredoxin exhibited a single redox couple with a reduction potential of -262 ± 10 mV at pH 7.0, 0 °C, which was assigned to the $[2Fe\text{-}2S]^{2+/1+}$ couple (Figure 5.3). This is the redox couple that is normally associated with 2Fe ferredoxins. Typical values of the reduction potential of $[2Fe\text{-}2S]^{2+/1+}$ clusters range from 90 mV to -450 mV.[2] The average half-life of the films were found to be of the order of 10 minutes. Half-height peak widths (δ) were of the order of 115 ± 10 mV and a typical film gave a coverage of 1.3×10^{-10} moles cm^{-2}, which approximates to that of a densely packed monolayer.

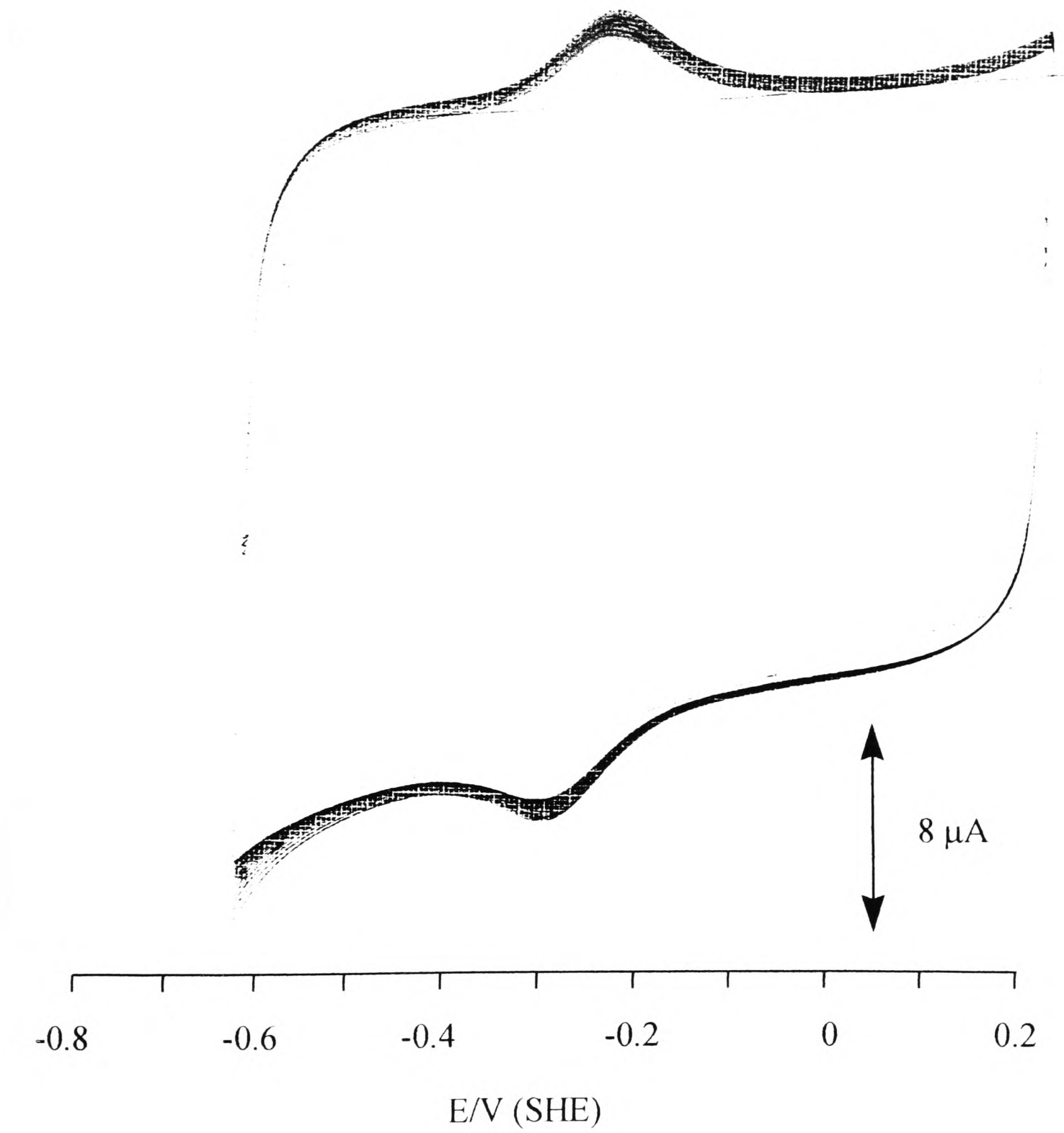

Figure 5.3 Film voltammogram of wild-type *Cp* 2Fe Fd

pH 7.0, 50 mM Hepes buffer, 0.1 M NaCl, 200 μg ml^{-1} polymyxin (as co-adsorbate), ν = 50 mV s^{-1}. As can be seen above, subsequent scans upon continued cycling demonstrate the stability of the protein film.

An investigation of the pH dependence of the reduction potential of the wild-type ferredoxin over the pH range 4 to 9 showed that there was no significant variation in $E^{o'}$ with pH. At the more extreme values of pH the film stability did deteriorate, but this is a normal observation for protein film experiments, with the exception of some proteins from the acidophilic bacteria (*Chapter 6*). The results are shown below in Figure 5.4.

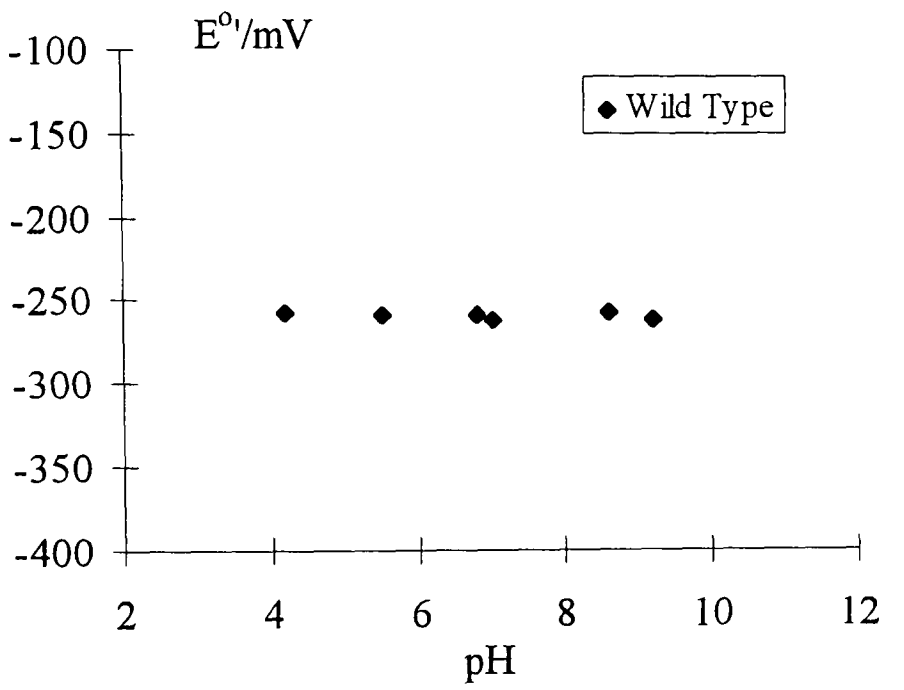

pH	4.2	5.5	6.8	7.0	8.6	9.2
$E^{o'}$/mV	-257	-259	-258	-261	-257	-262

Figure 5.4 pH Dependence for the wild-type *Cp* 2Fe Fd

Bulk Electrochemistry

Bulk electrochemistry of the wild-type 2Fe Fd was carried out at pH 7.0 and a single diffusion-controlled peak was observed at a potential of -282 ± 10 mV at 0 °C, which is in good agreement (i.e. within 20 mV) of the reduction potential obtained from the adsorbed films. The voltammetry was known to be diffusion controlled because of the linear dependence of the peak current with (scan rate)$^{1/2}$, up to 50 mV s^{-1}. A bulk solution voltammogram of wild-type 2Fe ferredoxin is shown in Figure 5.5. Neomycin (2 mM) was successfully used as the co-adsorbate for the bulk solution voltammetry, favouring exchange of molecules in the protein layer.

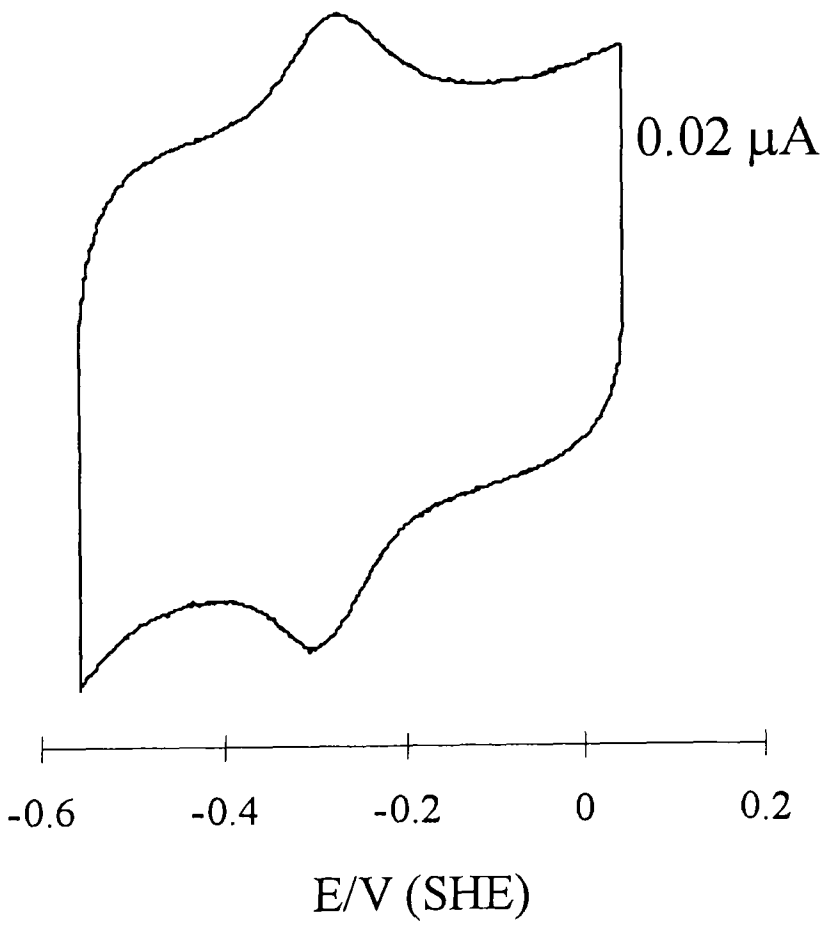

Figure 5.5 Bulk voltammogram of wild-type *Cp* 2Fe Fd

pH 7.4, 20 mM mixed buffer, 0.1 M NaCl, co-adsorbate 2mM neomycin, $v = 2\ mV\ s^{-1}$.

Protein concentration 80 μM

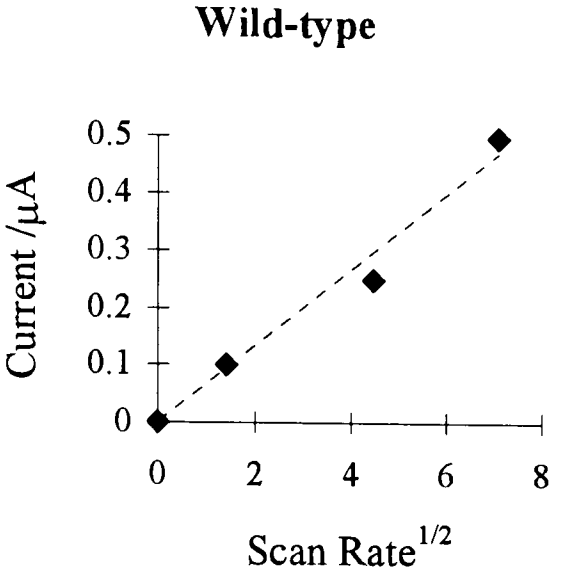

Figure 5.6 Linear dependence of (scan rate)$^{1/2}$ vs. current for bulk diffusional voltammetry of wild-type 2Fe Fd

5.3.2 THE ALANINE MUTANTS - Replacement of -CH_2SH for -CH_3

The alanine mutants investigated were **C14A**, **C24A**, the double mutant (DM) **C14A/C24A** and the triple mutant **H6A/H7A/H90A**. Films of the mutants C14A, C24A and H6A/H7A/H90A were all found to have a similar stability on the electrode as the wild-type protein. However, this was not the case for the double mutant, C14A/C24A, films of which were found to be considerably less stable (*Section 5.3.2.3*). The conditions for all the film experiments were ca. 100 μM protein with 200 μg ml^{-1} polymyxin in *both* the protein solution and the electrolyte solution, as for the wild-type protein. Variations were attempted with higher and lower concentrations of polymyxin, and the co-adsorbate neomycin (2 mM), in both the protein and the electrolyte, but there was no further improvement of the voltammetry for any of the alanine mutants investigated.

5.3.2.1 C14A

The mutant C14A was found to contain an FeS chromophore, the spectroscopic data of C14A were similar to the wild-type protein.[6] The electrochemical data obtained for the C14A mutant were also consistent with the electrochemical data of the wild-type ferredoxin. The mutant C14A exhibited reversible film voltammetry, and the average half-life of the film was 10 minutes. A single redox couple was observed with a reduction potential of -267 ± 10 mV at pH 7.0 and 0 °C, and the half-height peak width was 115 mV ± 10 mV (Figure 5.7).

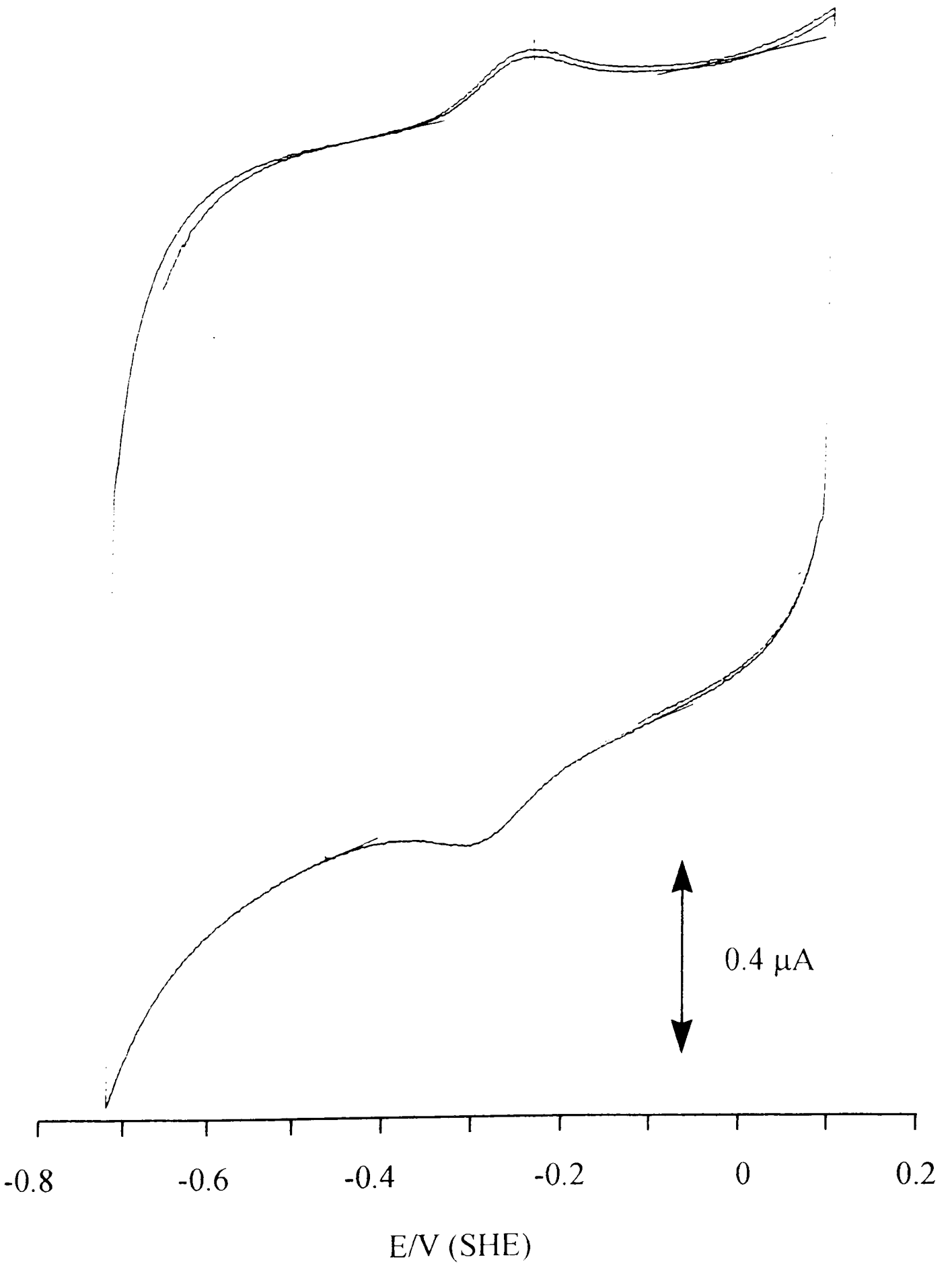

Figure 5.7 Film voltammogram of C14A *Cp* 2Fe Fd

pH 7.0, 50 mM Hepes buffer, 0.1 M NaCl, 200 μg ml^{-1} polymyxin (as co-adsorbate), $\nu = 20\ mVs^{-1}$

A pH dependence study was carried out over the pH range 5.1 to 9.0: little variation of the reduction potential was observed (Figure 5.8).

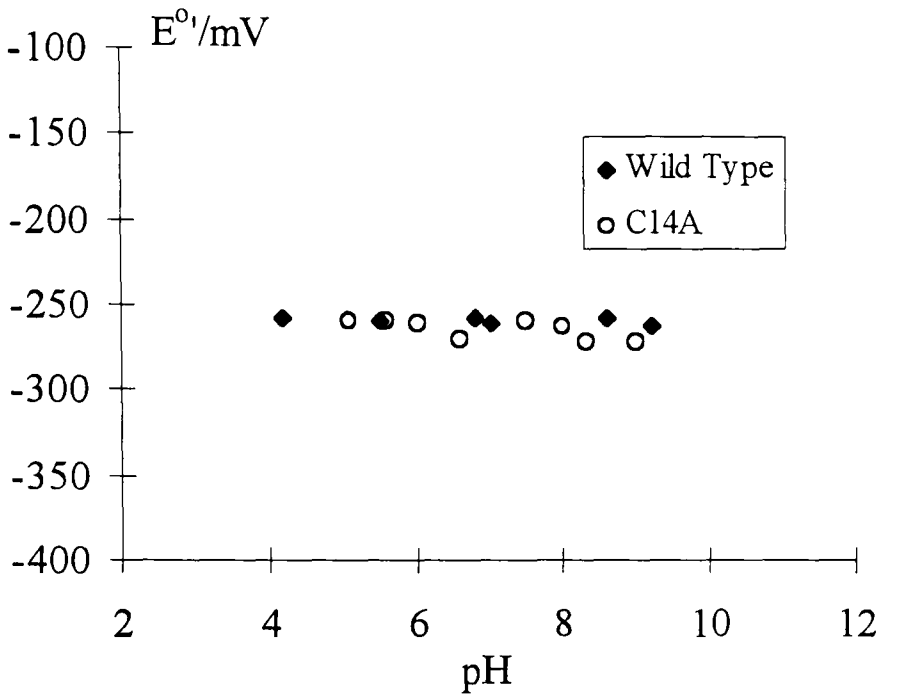

pH	5.1	5.6	6.0	6.6	7.0	7.5	8.0	8.3	9.0
E°'/mV	-260	-260	-261	-270	-267	-260	-263	-272	-272

Figure 5.8 pH Dependence for the C14A mutant of *Cp* 2Fe Fd

Bulk solution voltammetry was carried out at pH 7.0, using neomycin as co-adsorbate. A diffusion-controlled peak was observed with a potential of -265 ± 10 mV; this was within 10 mV of the result obtained with protein film experiments, Figure 5.9. A linear dependence of the peak current with (scan rate)$^{1/2}$, was observed, Figure 5.10.

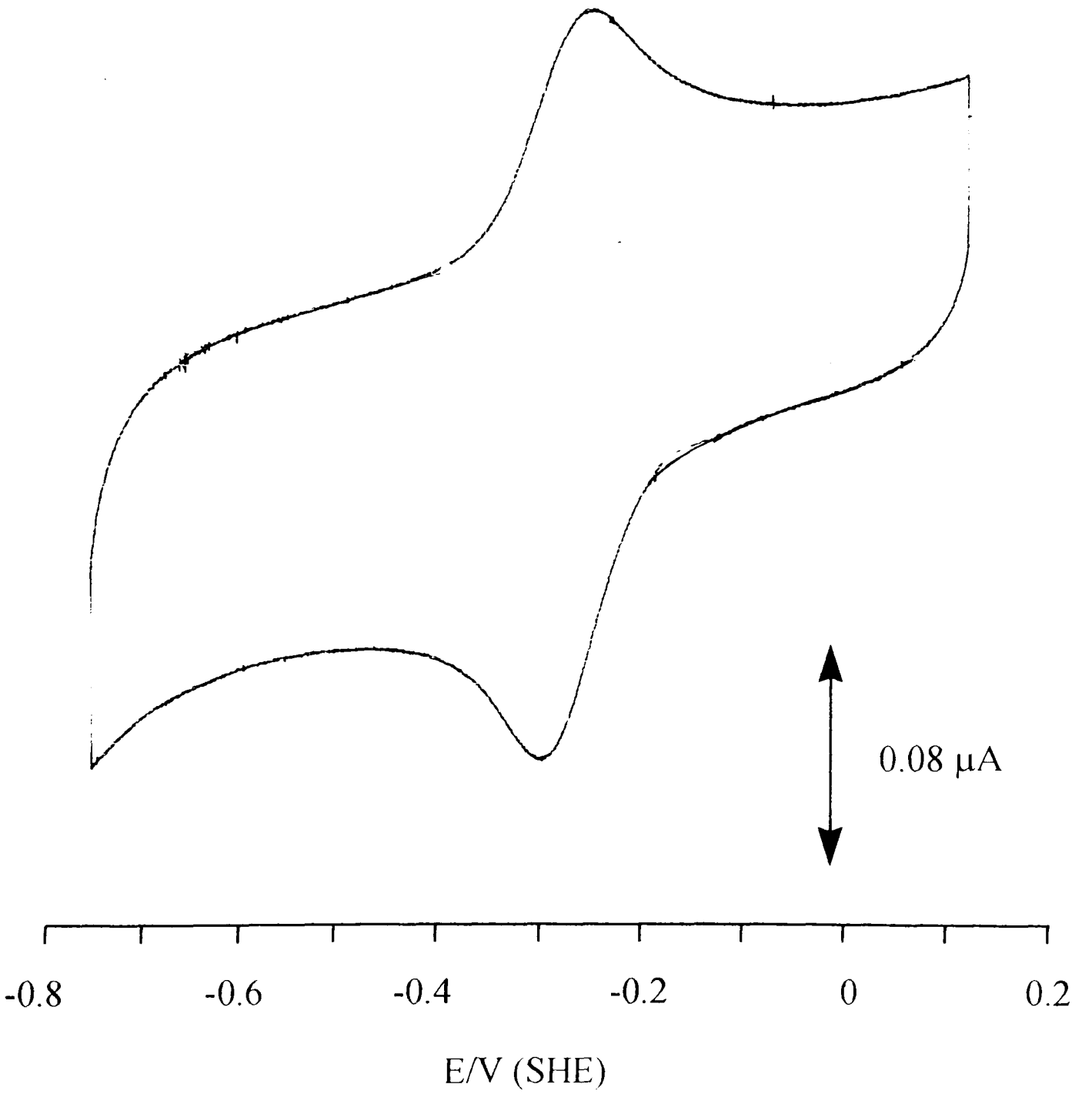

Figure 5.9 Bulk voltammogram of C14A *Cp* 2Fe Fd

pH 7.0, 50 mM Hepes buffer, 0.1 M NaCl pH 7.0, 2 mM neomycin (as co-adsorbate),

$\nu = 2\ mV\ s^{-1}$

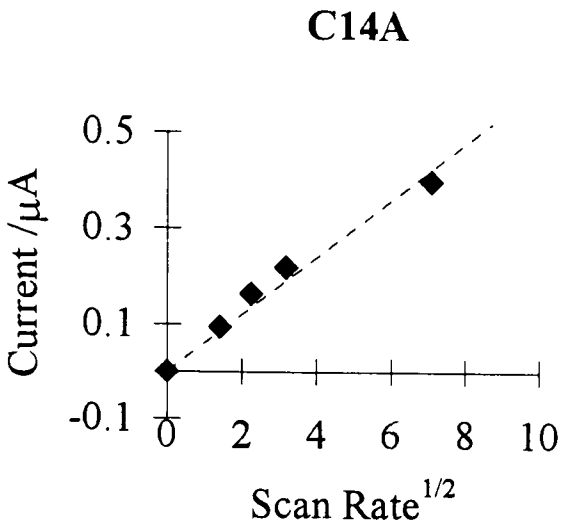

Figure 5.10 Linear dependence of (scan rate)$^{1/2}$ vs. current for bulk diffusional voltammetry of C14A

The reduction potentials were -265 ± 10 mV and -261 ± 10 mV for the C14A mutant and the wild-type ferredoxin respectively, which, together with their lack of variation of the $E^{o'}$ with pH, shows that the electrochemical behaviour of both these ferredoxins is similar. This similarity implies that the cysteine at position 14 is not likely to be a ligand of the [2Fe-2S] cluster. Additional support for this conclusion stems from the spectroscopic investigation by Meyer *et al*, whereby the UV/Vis, EPR and Resonance Raman spectra of these two proteins were found to be identical.[6] Thus, the non-ligating cysteine at position 14 opposes the observation made by Matsubara and Saeki, which proposes that a -Cys-X-X-Cys- ligand sequence is a universal feature of 2Fe Fds.[3] The two cysteines at positions 11 and 14 are ideally placed to be the ligands in the primary sequence of *Cp* 2Fe Fd. However, from the almost identical spectroscopic and electrochemical behaviour of both the C14A mutant and the wild-type, the hypothesis can be discounted in this case and we therefore have corroborative evidence of the unique primary structure of *Cp* 2Fe Fd.

5.3.2.2 C24A

The adsorbed film voltammetry of the mutant C24A showed one reversible redox couple at a potential of -337 ± 10 mV, which represents a negative shift of 75 mV with respect to the reduction potential ($E^{o'}$) of the wild-type protein. The oxidative and reductive half-height peak widths were slightly broader than that of the wild-type, typically 120 ± 10 mV at low scan rates i.e. < 20 mV s^{-1}, Figure 5.11.

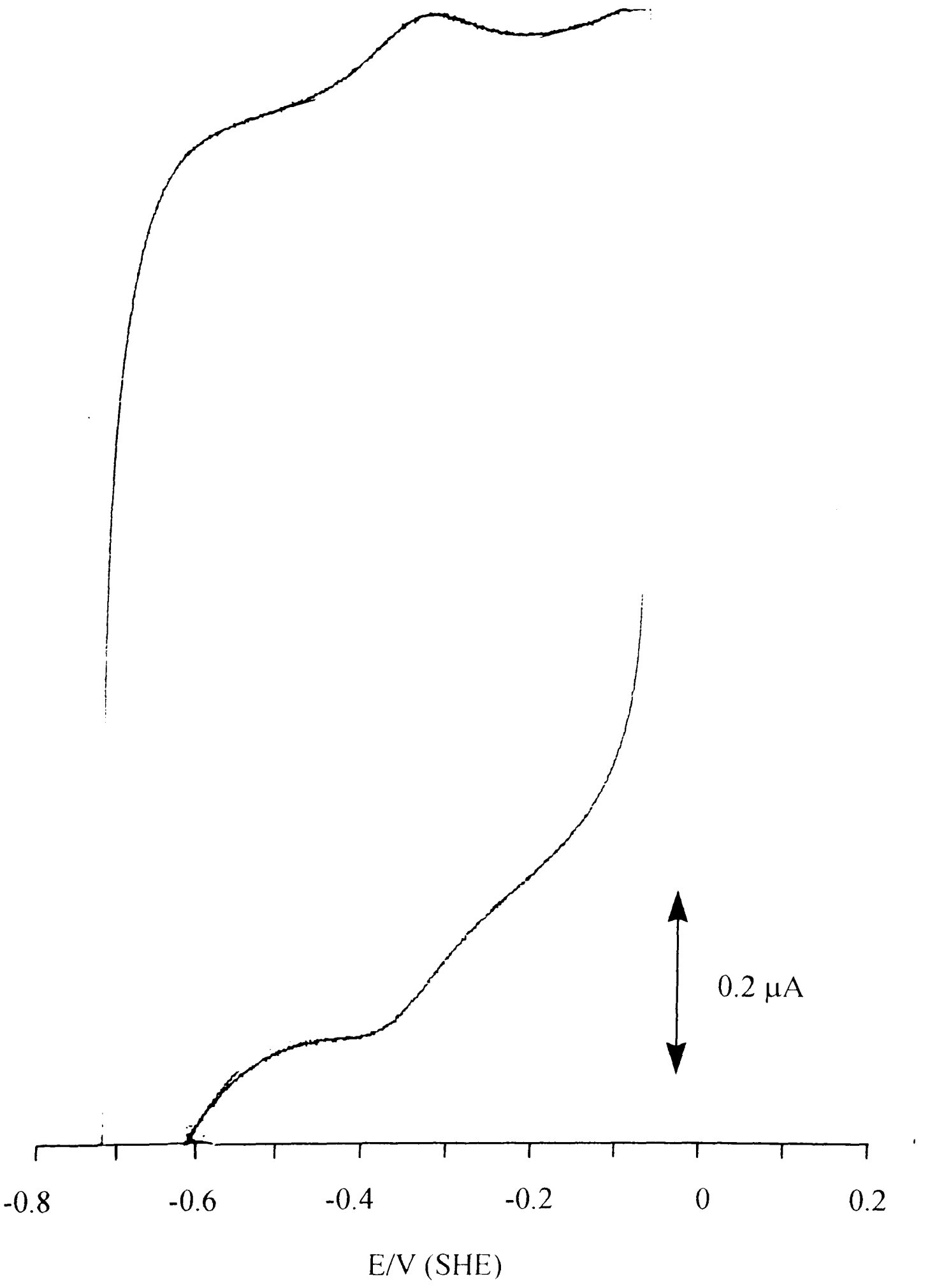

Figure 5.11 Film voltammogram of C24A *Cp* 2Fe Fd

pH 7.0, 50 mM Hepes, 0.1 M NaCl, 200 μg ml^{-1} polymyxin (as co-adsorbate),

ν = 10 mV s^{-1}

The corresponding pH dependence study (Figure 5.12) showed just a small variation in reduction potential over the pH range investigated.

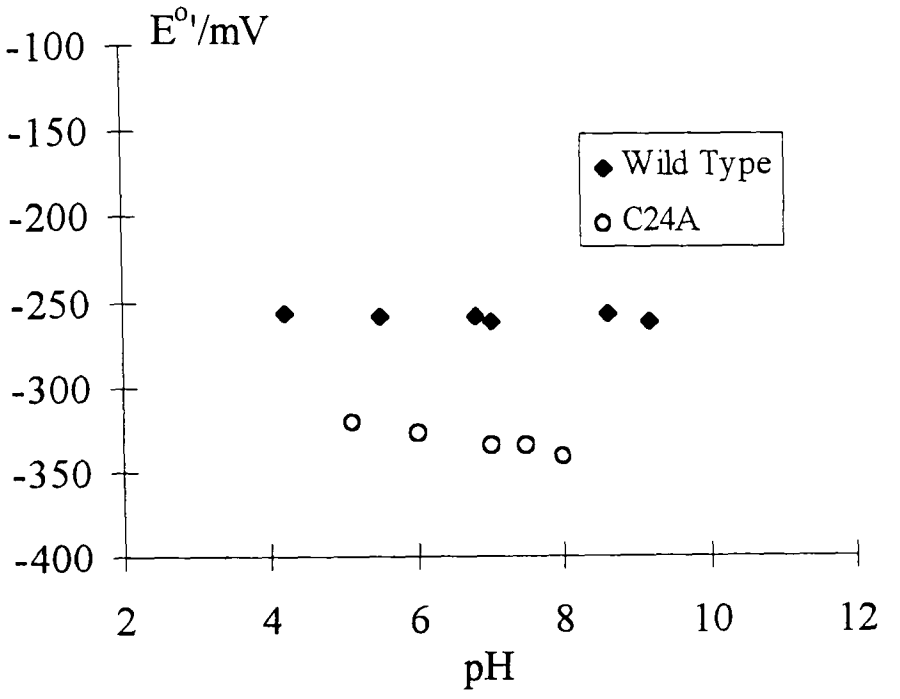

pH	5.1	6.0	7.0	7.5	8.0
$E^{o'}$/mV	-321	-327	-334	-335	-341

Figure 5.12 pH Dependence for the C24A mutant of *Cp* 2Fe Fd

The bulk solution electrochemistry at pH 7.4 produced a signal with a reduction potential of -340 ± 10 mV at 0 °C, (Figure 5.13) which correlates well (within 10 mV) with the value determined from the protein film experiments. A linear dependence of the peak current with (scan rate)$^{1/2}$ was observed for the oxidative and reductive peaks, up to 100 mV s^{-1}, indicating that the voltammetry was diffusion controlled, Figure 5.14.

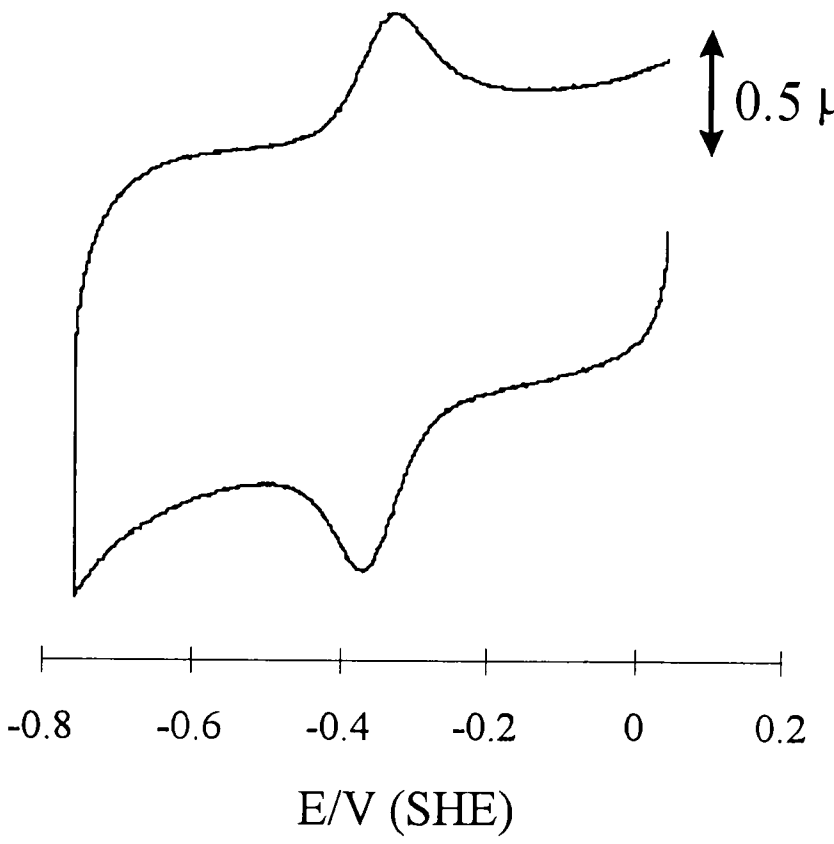

Figure 5.13 Bulk voltammogram of C24A *Cp* 2Fe Fd

pH 7.4, 20 mM mixed buffer, 0.1 M NaCl, neomycin 2 mM (as co-adsorbate), ν = 2 mV s^{-1}, protein concentration 80 μM

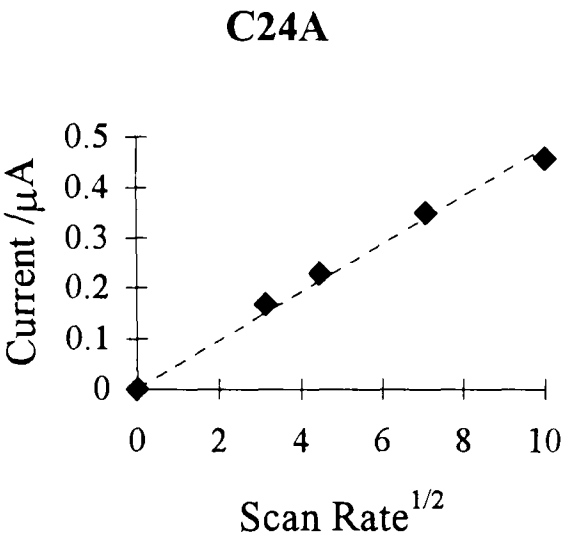

Figure 5.14 Linear dependence of (scan rate)$^{1/2}$ vs. current for bulk diffusional voltammetry of C24A

The mutant C24A, like C14A, also contained an FeS chromophore, which suggests that C24 either was not a ligand to the cluster, or it was replaced by some other residue upon mutation of cysteine to alanine.[6] In contrast to the C14A mutant, there were noticeable differences, both spectroscopic and electrochemical, between the C24A mutant and the wild-type Fd, indicative of significant changes in the cluster co-ordination sphere.[6] Thus it can be inferred that the residue C24 is likely to be one of the co-ordinating ligands of the 2Fe cluster, and therefore in the mutant C24A the cysteine at position 24 must be replaced by an alternative ligand. The UV/Vis absorption spectra of C24A is very similar to the wild-type protein, but there are small differences e.g. small shifts in the spectrum (5 nm or less) and slight variations in the relative intensities of the bands at 420 nm and 460 nm.[6] Electrochemically, the most noticeable difference was the negative shift in the reduction potential (ca. 75 mV) of the C24A mutant, compared to the wild-type protein. Additionally, the film's half-life was noticeably shorter than a typical film of the wild-type ferredoxin, under the same conditions.

The electrochemical evidence documented here, together with the spectroscopic evidence found by Meyer *et al*, shows that the substitution of this particular cysteine for an alanine changes the redox properties of the [2Fe-2S] cluster, and indicates that *either*

the C24 is a co-ordinating ligand of the cluster (hence in this mutant C24 must be replaced by another residue) *or* is in very close proximity to the cluster.[6]

Assuming that C24 is replaced by an alternative residue, it follows that the pH electrochemical dependence study of this mutant should yield information about the replacement residue. The pH dependence study showed little response to pH in the reduction potential of C24A; the variation was just ca. 20 mV over 3 pH units (Figure 5.12). In addition, it was found that the reversible signal associated with $[2Fe\text{-}2S]^{2+/1+}$ was more difficult to obtain at extreme values of pH, but this was also the case for the wild-type ferredoxin. As the reduction potential of the cluster was not found to be dependent upon pH, the ligand replacing C24 is not a serine or histidine as these ligands would be likely to impose a pH dependence on the reduction potential of the FeS cluster. It is documented that all-cysteine ligated [2Fe-2S] clusters are pH independent, unlike the Rieske clusters[32,33] which are ligated by two cysteine and two histidine residues (*Chapter 1*). The ligating histidine residues in Rieske clusters are able to be protonated, and hence the reduction potential of these clusters is pH dependent. An excellent example of a co-ordinating serine residue imposing a pH dependence on an FeS cluster is seen with the serine mutants of *Cp* 2Fe Fd (*Section 5.3.3*).

Drawing from these observations, it can be concluded that the ligand to the cluster of the mutant C24A is likely to be the proximal cysteine at position 14. A rearrangement of the protein structure is therefore necessary to replace the cysteine at position 24 with cysteine 14. Although this cannot be emphatically proven without X-ray crystallography data, the pH independence of the reduction couple and the proximity of C14 to the cluster make C14 a strong contender to be a ligand of the cluster. The mutant C24S of *Cp* Fd, which was investigated spectroscopically by Meyer *et al*, has an identical UV/Vis spectrum and A_{450}/A_{280} ratio to those of the C24A mutant.[6] Thus, whatever protein rearrangement occurs in the mutant C24A probably occurs for the mutant C24S, hence their identical spectra, implying that C14 must also be a co-ordinating ligand for C24S. Rearrangement of the protein structure is evidently preferred over ligation of the cluster by a serine ligand, in place of the original cysteine.

A similar example of a protein rearrangement occurring to replace a co-ordinating ligand, removed by a SDM experiment, was observed for the C20A mutant of Ferredoxin I of *Azotobacter vinelandii* (*Av*).[10] When one of the ligating cysteines to the [4Fe-4S] cluster of *Av* Fd I was mutated to alanine, it was shown, by X-ray crystallography, that formation of the cluster was subsequently achieved by the protein rearranging to accommodate the nearby free cysteine residue at position 24. In addition, a further crystallographic study of *Av* Fd I showed that if the cysteine at position 20 was mutated to a serine residue, the same protein rearrangement still occurred.[34] This shows that structural rearrangement to achieve cysteine ligation to the cluster is preferred over serinate ligation, despite the serine ligand being in the position of the original cysteine ligand. This example of protein rearrangement being preferred over serinate ligation in *Av* Fd I is mirrored in *Cp* 2Fe Fd.

5.3.2.3 C14A/C24A

The C14A/C24A mutant has the two cysteines at position 14 and 24 both replaced by alanine, which is not able to co-ordinate the cluster. Thus, because the C14A/C24A protein contains an iron-sulfur chromophore, and contains only three cysteines, this mutant utilises non-cysteinyl ligation to the cluster. The identity of the fourth ligand was therefore the primary focus in the study of this mutant protein.

Protein films of the mutant C14A/C24A were found to be significantly less stable than the wild-type. The typical half-life of a film on the electrode was less than 1 minute as compared to > 10 minutes for the wild-type protein. There were a number of inconsistencies with different samples of the mutant and consequently the results obtained varied erratically. The instability of the films and their short lifetime was improved marginally by carrying out experiments under an inert atmosphere in a glovebox (O_2 < 2 ppm).

The first sample (Sample I) from the Meyer group (Grenoble) gave poor electrochemistry, but none the less exhibited just the expected single redox couple, of which the oxidative scan was broad (typically 150 mV) and the reductive scan was even broader. Consequently difficulties were found in estimating a peak position for the reductive wave and the margin of error in the reduction potential is therefore high, in the order of 20 mV. The reduction potential at pH 7.0 was estimated at -331 ± 20 mV. A pH dependence study was attempted and although the results were difficult to analyse, there was a variation of $E^{o'}$ with pH, of 23 mV/pH unit see Figure 5.15.

Bulk solution electrochemistry was attempted, but poor signal quality, even with the presence of neomycin, which had successfully worked for other mutants, prevented any reproducible bulk voltammetry being obtained.

A second sample (Sample II) of the same mutant, C14A/C24A, was received from the Meyer group, and direct film electrochemistry was repeated as above, with a more

extensive pH dependence study being undertaken. Although the UV/Vis spectra of both samples were almost identical, Sample II of the C14A/C24A mutant proved to have a more positive reduction potential (-222 ± 20 mV at 0 °C, pH 7.0), and the pH dependence of the reduction potential was considerably greater than for Sample I (Figure 5.15). A linear 'best fit' was plotted for Sample II to obtain an 'approximate' pH dependence value (-46 mV/pH unit). A simple linear fit was used because there was insufficient evidence to indicate that the data might be fitted to a 'curve' and so obtain a reliable pK_a value (see *Section 5.3.3*). A linear 'best fit' was not carried out for Sample I, as the data obtained were limited and too erratic, due to the instability of the protein films.

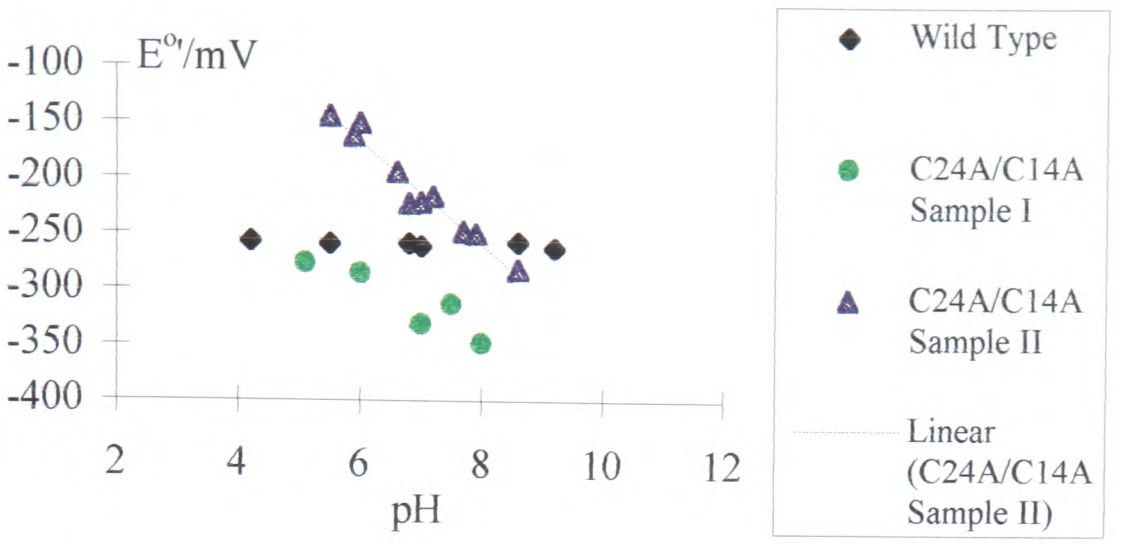

Sample I

pH	5.1	6.0	7.0	7.5	8.0
$E^{o'}$/mV	-277	-286	-331	-313	-348

Sample II

pH	5.5	5.9	6.0	6.6	6.8	7.0	7.2	7.7	7.9	8.6
$E^{o'}$/mV	-145	-163	-152	-195	-223	-222	-217	-248	-250	-282

Figure 5.15 pH Dependence of the C14A/C24A mutant of *Cp* 2Fe Fd

As a result of these differences between the two independent samples sent from France, it was decided to purify the proteins using FPLC in order to:

(a) discover if there were one or more components which were separable by their different binding behaviour on the anion exchange column

(b) purify the proteins - since apoprotein or another contaminant may be responsible for the discrepancy in the electrochemical results

The procedure used for the purification of the proteins was the general procedure used for ferredoxins as described in *Chapter 2*, and was carried out under anaerobic conditions. The protein was eluted using a 0 to 1.0 M NaCl gradient with 50 mM Tris at pH 7.4, using an anion exchange column, Mono-Q (Pharmacia).

Despite their different electrochemical behaviour, the proteins behaved very similarly during FPLC. During the elution of the protein, with a gradient of 0 - 1 M NaCl, a major fraction comprising more than 95 % of the total protein content eluted at 0.51 M NaCl, and a smaller peak, 2 - 4 % of the total protein content, was eluted at 0.55 M NaCl (Figures 5.16 and 5.17). Only the centre of the band of the largest protein peak was used for the subsequent electrochemistry.

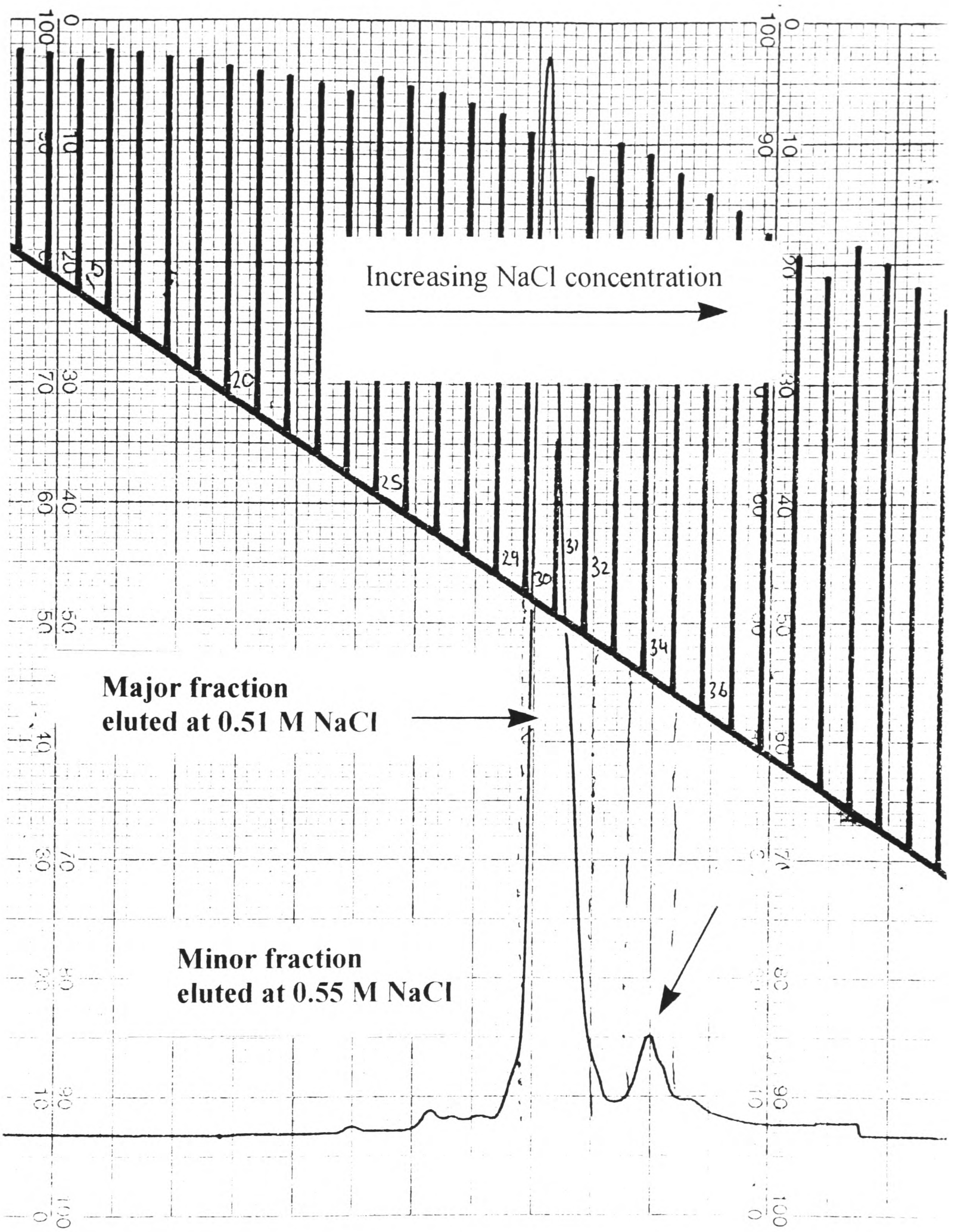

Figure 5.16 FPLC elution profile of Sample I of C14A/C24A

50 mM Tris pH 7.4, concentration gradient 0-1.0 M NaCl , flow rate 1 ml min^{-1}, chart speed 10 mm min^{-1}

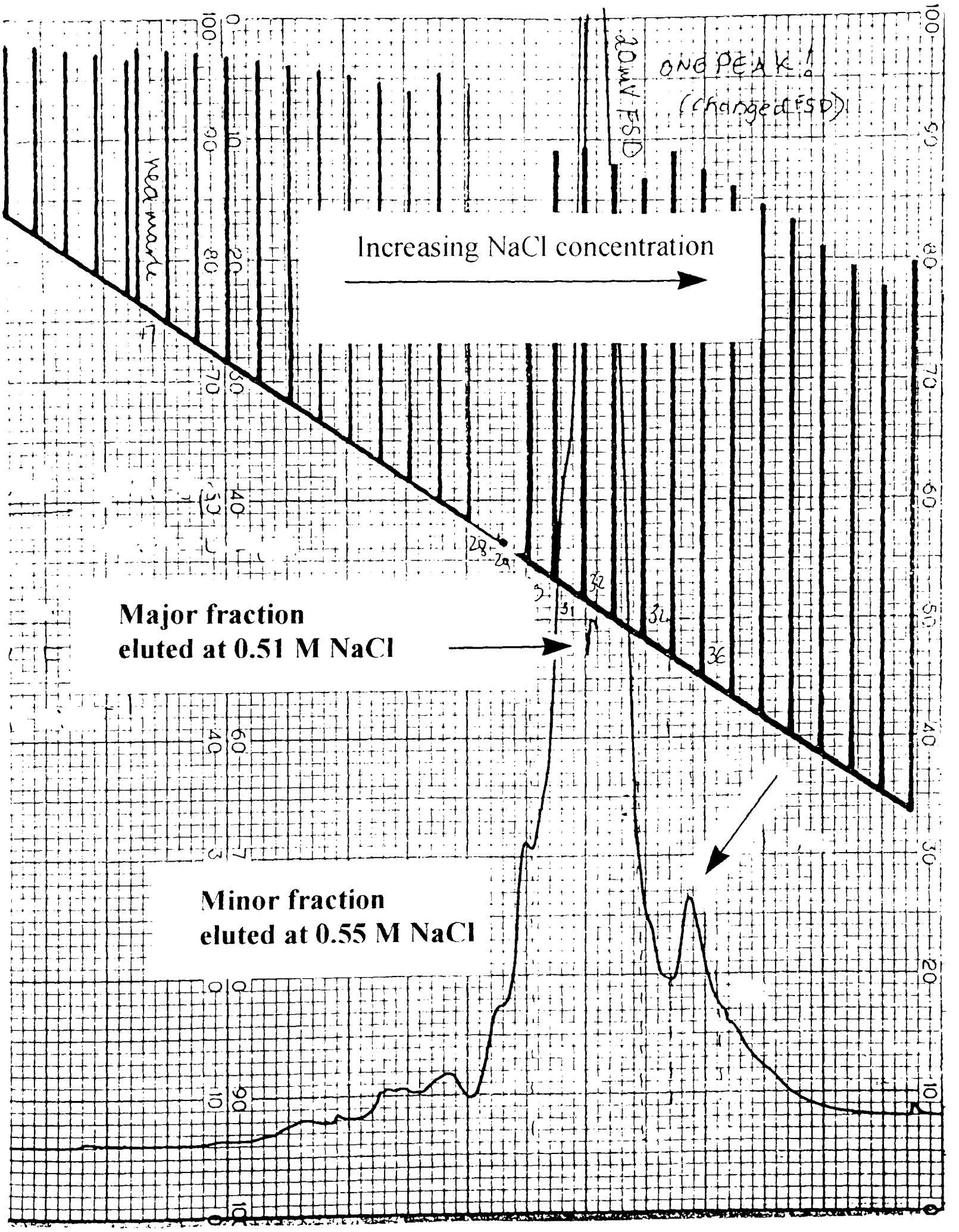

Figure 5.17 FPLC elution profile of Sample II of C14A/C24A

50 mM Tris pH 7.4, concentration gradient 0-1.0 M NaCl, flow rate 1 ml min^{-1}*, chart speed 10 mm* min^{-1}

After the additional purification step, the two proteins were found to exhibit the same electrochemical behaviour i.e. the reduction potentials of each sample and pH dependence behaviour were almost identical. However, the general quality of the electrochemistry was still poor, i.e. poor peak resolution and short half-life of ca. 1 minute, despite the FPLC stage.

From adsorbed film experiments Sample I was found to have a reduction potential of -288 ± 10 mV while Sample II showed a reduction potential of -292 ± 10 mV at pH 7.6, 0 °C. A pH dependence study was carried out with both samples of the mutant (Figure 5.18). The variation of $E^{o'}$ with pH for both samples of the C14A/C24A mutant was -22 mV/pH unit.

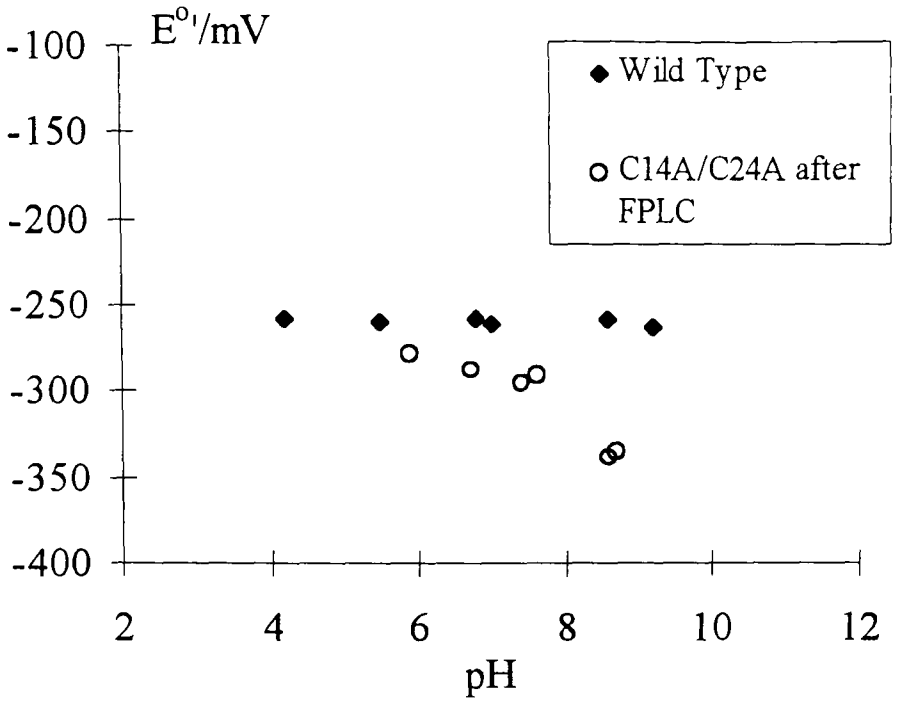

pH	5.9	6.7	7.4	7.6	8.7
$E^{o'}$/mV Sample I after FPLC	-283	-289	-288	-293	-323
$E^{o'}$/mV Sample II after FPLC	-278	-287	-295	-290	-335

Figure 5.18 pH Dependence of the C14A/C24A mutant of *Cp* 2Fe Fd after FPLC

After FPLC purification, both Samples I and II exhibited an additional electrochemical feature at low potential. A second reversible redox couple was observed at a significantly lower potential than the $[2Fe\text{-}2S]^{2+/1+}$ redox couple (Figure 5.19). For ease of writing, this second couple, not previously observed for *Cp* Fd variants, is called the low potential couple (LPC). The peak was similar in size to that of the formal $[2Fe\text{-}2S]^{2+/1+}$ redox couple, i.e. comparisons showed that the LPC area was ca. 70-75 % of the peak area of the 2+/1+ redox couple. The pH dependence of this new redox couple was found to be -44 mV/pH unit (Figure 5.20). The protein films were too unstable to obtain data below pH 5.9 or above pH 8.7, and so the limited data obtained

were not sufficient to indicate if there were any turning points in the pH dependence plot which would have indicated a pK_a value.

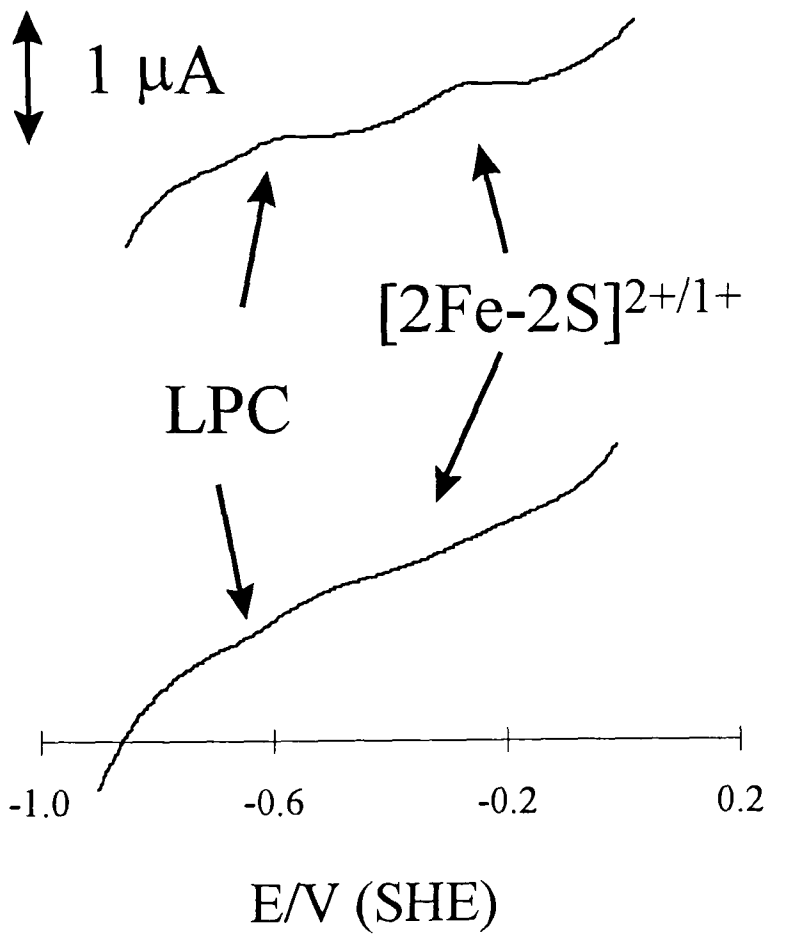

Figure 5.19 Film voltammogram of the FPLC purified C14A/C24A *Cp* 2Fe Fd

LPC = low potential couple. pH 7.6, 20 mM mixed buffer, 0.1 M NaCl, polymyxin 200 μg ml^{-1} (as co-adsorbate), ν = 50 mV s^{-1}

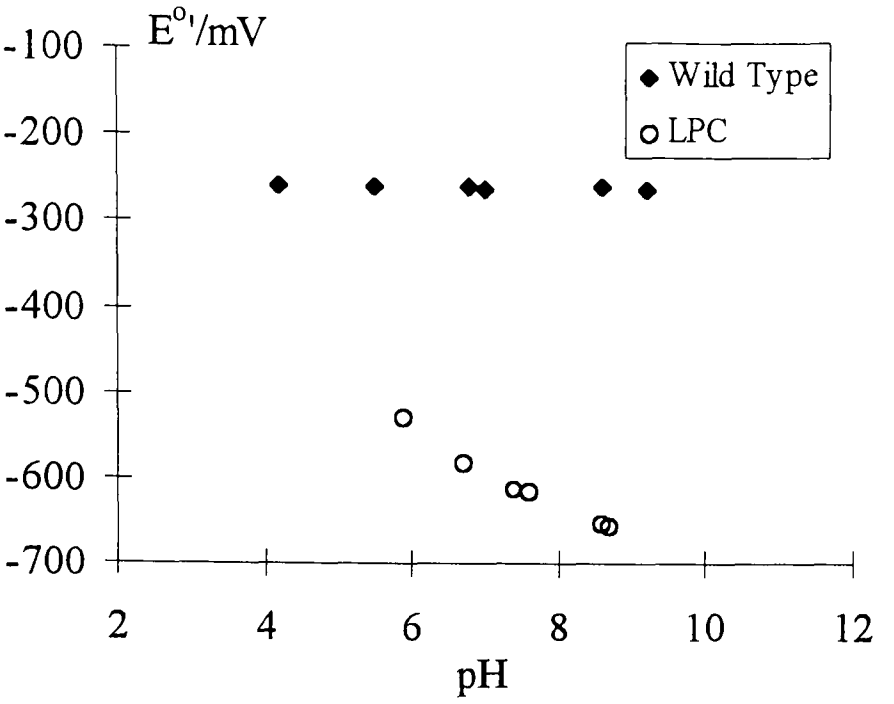

pH	5.9	6.7	7.4	7.6	8.6	8.7
E°'/mV	-530	-583	-613	-617	-654	-658

Figure 5.20 pH Dependence of the 'LPC' of C14A/C24A *Cp* 2Fe Fd

Bulk Electrochemistry

Bulk electrochemistry was carried out with both Sample I and Sample II, after they had been purified. Before FPLC purification, bulk solution electrochemistry had been unsuccessful, with Sample I or II, i.e. no reproducible voltammetry had been obtained.

After purifying the double mutant, using FPLC, the same conditions were employed, as had been used to obtain bulk electrochemistry for other mutants, to investigate the bulk electrochemistry. A redox couple was observed for both Sample I and II, however the characteristics of the peak and its dependence upon scan rate were not that of a bulk diffusional system, as described in *Chapter 1*. The voltammogram was more like that of an adsorbed film with the ip_{ox} directly proportional to the scan rate and not (scan rate)$^{1/2}$, Figure 5.22. Voltammograms at different scan rates of Sample II in bulk solution voltammetry are shown in Figure 5.21 (at 50 and 5 mV s^{-1}). The potential of this peak was -261 mV ± 20 mV which was ca. 20 mV more positive than the redox couple of $[2Fe\text{-}2S]^{2+/1+}$ when measured using film voltammetry. No indication of the second couple was observed at any of the scan rates investigated. The anomalous behaviour during bulk electrochemistry of this protein is likely to be a factor of the instability of the cluster in this case.

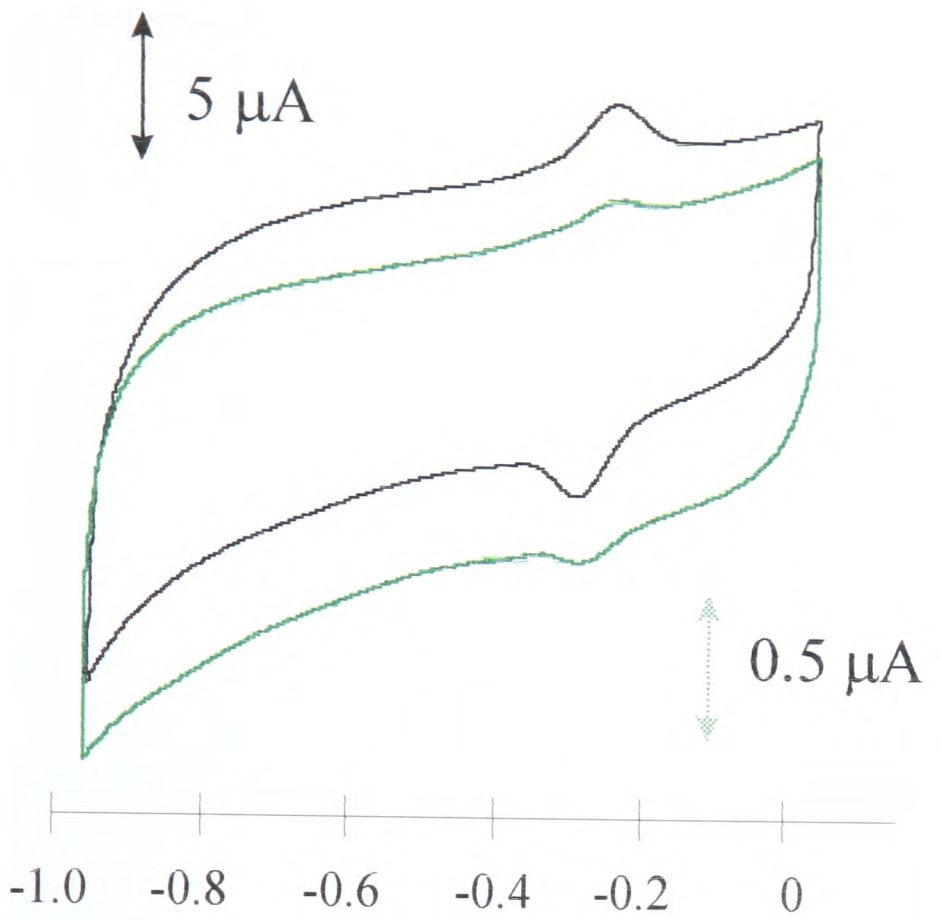

Figure 5.21 Bulk voltammogram of C14A/C24A after FPLC purification

pH 7.0, 50 mM Hepes buffer, 0.1 M NaCl, 2 mM neomycin.

Black voltammogram, v = 50 mV s^{-1}, green voltammogram v = 5 mV s^{-1}

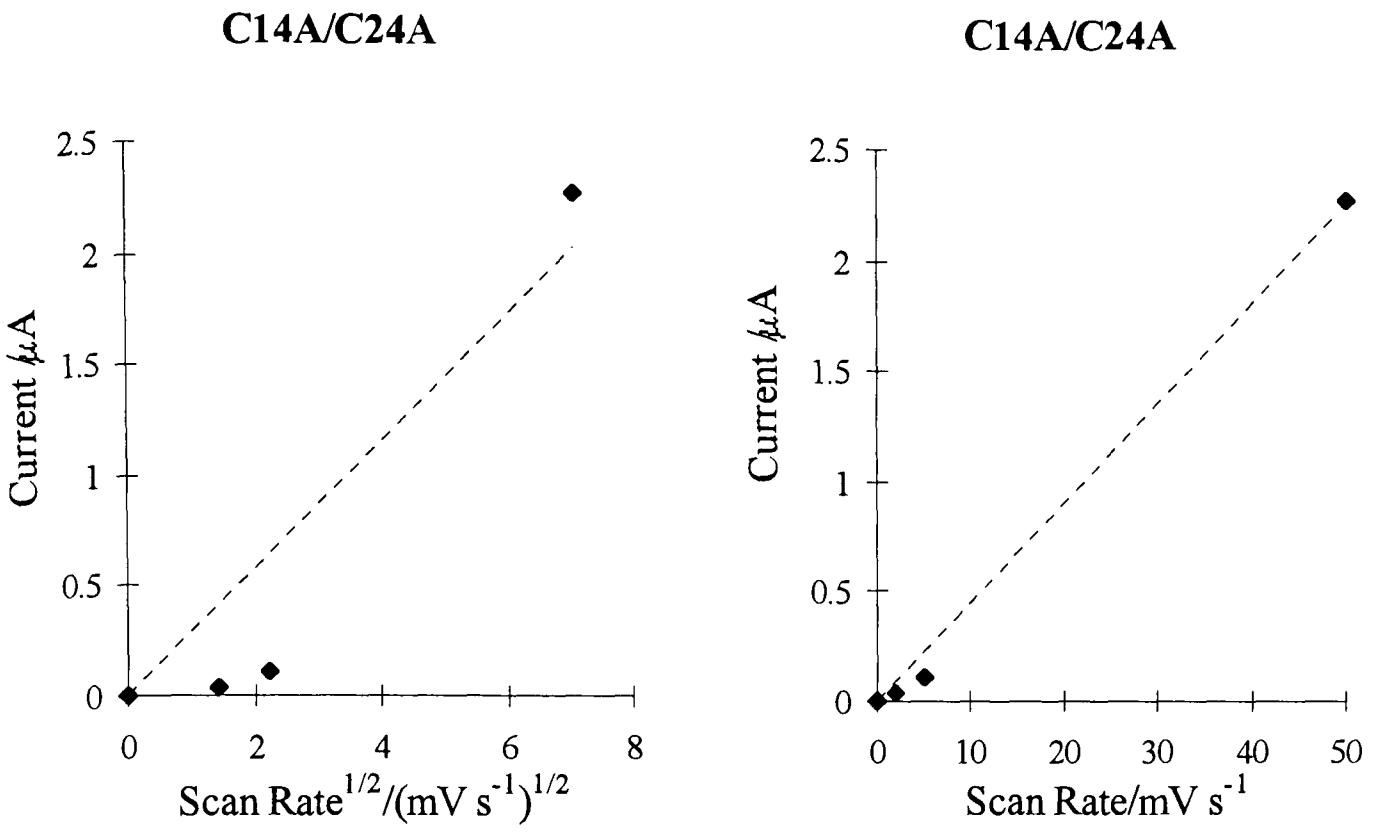

Figure 5.22 Dependence of (scan rate)$^{1/2}$ and scan rate vs. current (ip_{ox}) for bulk diffusional voltammetry of C14A/C24A

From above it can be seen the voltammetry obtained under conditions used to obtain bulk diffusional electrochemistry for the other mutants produced voltammograms indicative of adsorbed film electrochemistry, i.e. i_p proportional to scan rate NOT (scan rate)$^{1/2}$.

These experiments can be used to help gain an insight into the nature of the fourth ligand in C14A/C24A. The double mutant, C14A/C24A has an important significance among all of the other mutants studied, because it only has three possible cysteines which are available to co-ordinate the cluster. Despite the incomplete cysteinyl co-ordination, the cluster is still assembled *in vivo* and hence there must be *non*-cysteinyl ligation to the cluster. Possibilities for the fourth ligand include a proximal non-cysteinyl residue from the protein structure or a ligand from an external source.

It had been thought that histidine was a likely candidate for the fourth ligand, in lieu of a cysteine, because of the sequence homology between the 25 kDa subunit of the NADH-quinone oxidoreductase (NDH-1) from *Paracoccus denitrificans*, which also contains a [2Fe-2S] cluster, and the amino acid sequence of *Cp* Fd.[16] Although their amino acid

sequences are not identical, the spacing of the conserved cysteine and histidine residues are similar: when they are aligned (Figure 5.23) it can be seen that the histidine at position 7, in the amino acid sequence of *Cp*, is a possible candidate for cluster ligation. However an extensive ESEEM spectroscopy study was carried out by Shergill *et al* and no direct evidence for either cysteinyl, histidyl or alternative nitrogenous co-ordination of the [2Fe-2S] cluster of the DM of *Cp* Fd was found.[19]

- H^{92} - X_3 - C^{96} - X_4 - C^{101} - X_{35} - C^{137} - X_3 - C^{141} -	25 kDa subunit of NDH-1
- H^{7} - X_3 - C^{11} - X_2 - C^{14} - X_{41} - C^{56} - X_3 - C_{60} -	*Cp* Fd

Figure 5.23 Binding motifs of the 25 kDa subunit of NDH-1 and *Cp* 2Fe Fd

Other alternatives for the fourth ligand in C14A/C24A include methionine, aspartic or glutamic acid and serine. Since no known examples have ever been found of methionine co-ordination to a FeS cluster it is likely that this can be ruled out. Direct evidence for aspartate co-ordination has recently emerged for *Pyrococcus furiosus* [4Fe-4S] Fd,[35] and has also been proposed for the Cluster I, $[2Fe\text{-}2S]^{2+/1+}$, in succinate dehydrogenase from *E. coli*.[13] Serine co-ordination to Fe-S clusters has been recorded in a number of examples, both engineered and wild-type; examples include the fumarate reductase from *E. coli*,[12] a mutant of the 2Fe Fd from *Cp*[18] and *Anabaena* Fd.[15] Until the exact protein structure is known, none of these possibilities can be completely ruled out. Alternatively an oxygenic ligand from the solvent may be binding to the cluster, either H_2O or HO^-, as found for aconitase.[36] If either H_2O or HO^- is binding to the cluster in the C14A/C24A mutant, it is likely that the cluster's reduction potential would be pH dependent to some degree, which is indeed as observed experimentally.

A striking feature of the electrochemistry of this double mutant, when adsorbed on a film, is that, unlike every other mutant investigated, *two* redox couples were observed. The similarity of both redox couples, in area and half-height peak width, suggests that the new couple, the 'low potential couple' (LPC), is also a one-electron redox couple. It

was therefore tentatively assigned to the 1+/0 electron step, thus the LPC is associated with the double reduction of the $[2Fe\text{-}2S]^{2+}$ cluster to give the $[2Fe\text{-}2S]^{0}$ state.

All Fe^{2+} Biological Clusters

Until a few years ago, although it was thought to be theoretically feasible, the fully reduced[b] state of any biological FeS cluster was considered to be too reactive to be experimentally observed, and was therefore uncharacterised in biological iron-sulfur clusters. However more recently, a number of biological examples have been partially characterised, including the fully reduced state of a water soluble fragment of a Rieske protein,[37] the $[3Fe\text{-}4S]^{2-}$ cluster from the 7Fe Fd of *Sulfolobus acidocaldarius*,[38] the fully reduced forms of spinach and parsley 2Fe ferredoxins[39] and the $[4Fe\text{-}4S]^{0}$ cluster from the Fe protein of nitrogenase.[40] It is also highly likely that more examples are yet to be discovered.

Typically the iron centres in 2Fe Fds cycle between the $[2Fe\text{-}2S]^{2+/1+}$ states as below,

$$Fe^{3+}/Fe^{3+} \rightarrow Fe^{2+}/Fe^{3+}$$

The LPC observed in the film voltammetry of the double mutant of *Cp* Fd is tentatively assigned to $[2Fe\text{-}2S]^{1+/0}$ thus,[c]

$$Fe^{2+}/Fe^{3+} \rightarrow Fe^{2+}/Fe^{2+}$$

This fully reduced state, which notably is *not* seen in the *Cp* wild-type or any of the other mutants of *Cp* Fd, may be favoured in C14A/C24A because of the modified co-ordination sphere of the cluster. Importantly there are no other possible sources of electrons which are available in the protein. As previously discussed, it is likely that the fourth co-ordination ligand to the C14A/C24A cluster is water or ^{-}OH. The limited number of reports in the literature of fully reduced biological FeS clusters is probably due

[b] In this context, 'super-reduced' is used for a one-electron step to the all Fe^{2+} state and 'hyper-reduced' is used for the two-electron step to the all Fe^{2+} state, more commonly seen for 7Fe Fds.

[c] There are no other possible sources of electrons which are available in the protein e.g. S^{0} which would undergo a redox reaction.

to the destabilising effect of the excess negative charge at the cluster, hence the highly reactive nature of these states. The possible ways in which the negative charge could be offset, and so render the fully reduced state more stable, are an ongoing subject of investigation. A major influencing factor upon the stability of super-reduced clusters is likely to be the co-ordination sphere of the cluster and how this can dissipate the negative charge, and the nature of the proximal residues and protein structure. For the mutant C14A/C24A, replacement of the second cysteine in the cluster binding domain (i.e. C14 or C24) by an alternative ligand results in the observation of a fully reduced state, using protein film voltammetry. The alternative ligand is presumably able to dissipate the negative charge from the cluster and so increase the stability of the fully reduced state.

Two situations which could help stabilise fully reduced FeS clusters are,

(i) proton binding at or near to the cluster *or*

(ii) influence of the cluster co-ordination sphere by external ligands i.e. swap an anionic for a neutral ligand.

Considering 7Fe Fds which contain [3Fe-4S] clusters: these are readily reduced to the $[3Fe\text{-}4S]^{2-}$ state during film experiments, and the negative charge localised on the cluster is thought to be counterbalanced, to some degree, by the uptake of three protons at, or near to the cluster.[38] This is demonstrated by the significant pH dependence of the $[3Fe\text{-}4S]^{0/2-}$ reduction couple, which is equal to $1H^+$ per electron (at least). Similarly the reduction potential of the LPC shows a notable pH dependence ca. -44 mV/pH unit.[d] A report detailing the reduction of spinach and parsley $[2Fe\text{-}2S]^{2+}$ ferredoxin with the complex, 1,4,8,12-tetraazacyclopentadecane $[Cr(15\text{-ane}N_4)(H_2O)_2]^{2+}$ ($Cr^{2+}L$) provides evidence for two equivalent steps to give the $[2Fe\text{-}2S]^0$ product. Notably the $Cr^{3+}L$ formed in the first step, remains attached to the $[2Fe\text{-}2S]^{1+}$ product and presumably is able to perturb the protein active site sufficiently to make the second reduction step

[d] However, this is not thought to be the case for the Fe protein from nitrogenase, and its fully reduced form, $[4Fe\text{-}4S]^0$.[40] An initial report states that this reduction potential is not dependent upon the pH and so presumably the negative charge on the cluster is stabilised in some other way.[41]

possible. The square wave voltammetric study upon modified spinach ferredoxin[e] (the $Cr^{3+}L$ bound form) measured two reduction potentials at -273 mV and -410 mV.[39] The latter reduction potential for the 1+/0 reduction step is not as negative as the LPC measured for *Cp* Fd (-613 mV) indicating that the fully reduced form of the spinach ferredoxin is more stable than that of the fully reduced form of C14A/C24A. In contrast, an alternative investigation by Verhagen *et al* used direct unmediated electrochemistry to investigate the possibility of generating the fully reduced state in spinach ferredoxin, *Spirulina platensis* ferredoxin and the water soluble fragment of the Rieske protein.[37] In only one case, the Rieske fragment, was a voltammetric signal observed which could be interpreted as the formation of a fully reduced state. A voltammetric signal was observed at -840 mV which was approximately 1100 mV from the $[2Fe\text{-}2S]^{2+/1+}$ reduction potential (300 mV). The fully reduced couple $[2Fe\text{-}2S]^{1+/0}$ of the Rieske subunit was observed to be pH independent, unlike the first transition. The first transition, $[2Fe\text{-}2S]^{2+/1+}$, was observed to be pH dependent because the Fe atom which is reduced, is co-ordinated by two histidines which are able to be protonated.[33] The second Fe atom is co-ordinated by two cysteines and this reduction potential was not found to be pH dependent. This is in contrast to the reduction couples of C14A/C24A which both show a definite pH dependence (Figure 5.18 and Figure 5.20). However, as noted earlier, no reproducible bulk electrochemistry was observed for this mutant and so generation of this fully reduced state could not be verified in bulk solution. This could indicate that the fully reduced state is not stable enough to exist in 'free' bulk solution and protein film voltammetry thus helps to stabilise the fully reduced form.

Exogenous Ligand Binding

An alternative method of probing the fourth ligand of C14A/C24A and its chemical reactivity, is to investigate the lability of the ligand and examine if the *in vivo* ligand can be replaced by an external ligand. The prevalent example of exogenous binding to an FeS cluster is aconitase,[42] but examples include other non-cysteinyl ligated clusters, e.g. the [3Fe-4S] cluster from *Desulfovibrio africanus* Fd III,[43] and further examples, as seen in *Chapters 1* and *4*. The C14A/C24A mutant of *Cp* 2Fe Fd has only 3 cysteines in the protein chain and therefore must have a non-cysteinyl ligand in order for co-ordination of

[e] Square wave voltammetric measurements for the native spinach ferredoxin, in the same study, gave a

the [2Fe-2S] cluster to be complete. One of the iron atoms is therefore 'subsite-differentiated' which is one of the prerequisites for ligand exchange (*Chapter 4*) - thus, it was decided to investigate whether ligand exchange was a viable possibility for the C14A/C24A mutant. Preliminary evidence suggested that the fourth ligand was oxygenic in nature, most likely either H_2O or ^-OH. If an exogenous thiolate ligand could be included in the co-ordination sphere of the cluster, this would result in a cluster co-ordination sphere more closely resembling that of the original wild-type Fd. Changes in the voltammetry should therefore become apparent on introducing the protein film to a buffer solution containing thiolate. Two noteworthy examples of exogenous ligand binding are the reversible binding of a thiolate ligand to the transformed [Fe3Fe-4S] cluster in *Da* Fd III[f] and reversible thiolate or cyanide binding to the subsite differentiated metal atom in the [4Fe-4S] cluster from *Pyrococcus furiosus* Fd.[43,44] In both these two examples the exogenous ligand may either substitute for the co-ordinating ligand, or it may add to the co-ordination sphere of the metal atom, so increasing the co-ordination number of the Fe atom. It is not certain which of these two scenarios is correct for *Da* Fd III or *Pf* Fd because of a lack of structural evidence about the form of the cluster in these proteins.

When an adsorbed film of the FPLC purified C14A/C24A protein was transferred at a negative potential (ensuring that the cluster was in the $[2Fe\text{-}2S]^{1+}$ state) to a pot containing 200 mM mercaptoethanol at pH 8.0, changes in the voltammetry were observed. The two redox couples were replaced by a *single* 'new' redox couple which was shifted negatively, with respect to the $[2Fe\text{-}2S]^{2+/1+}$ reduction couple (Figure 5.24). The reduction potential of the new couple was -391 ± 20 mV, compared to the previous reduction potentials of -287 and -613 mV. The reduction peak, which was generally broader than the oxidative wave for adsorbed films of C14A/C24A, was now found to be of a similar peak width as the oxidative wave; the half-height peak width of the transformed C14A/C24A voltammetry was ca. 120 mV compared to ca. 115 mV for the wild-type ferredoxin.

---

value of -462 mV for the single redox process observed, i.e. $[2Fe\text{-}2S]^{2+/1+}$.[39]

[f] The investigation in *Chapter 4* showed that an adsorbed film of *Da* Fd III exhibits a definite change in its voltammetry when introduced to a number of different thiolate ligands, but not with oxygenic ligands.

On returning the adsorbed protein film to a pot containing no mercaptoethanol, the voltammetry reverted to that seen before addition of mercaptoethanol, i.e. two reduction couples were observed within a few minutes of cycling in the new buffer, without mercaptoethanol (Figure 5.24). It was observed that the return to the original voltammetry was slower if traces of mercaptoethanol were not removed from the electrode by rinsing in an intermediary pot between transfers.

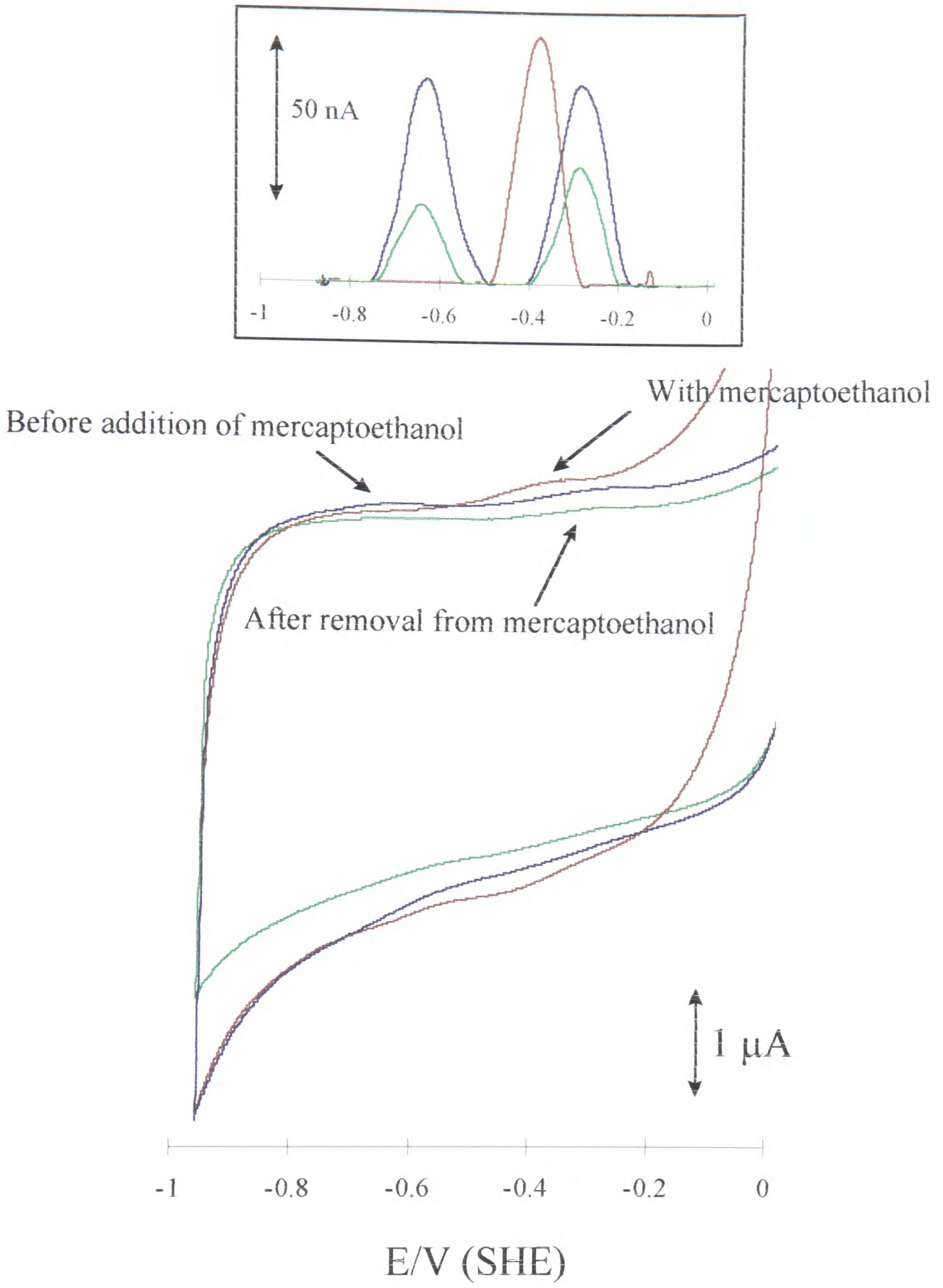

Figure 5.24 Reaction of mercaptoethanol with the double mutant C14A/C24A

Blue: adsorbed film of C14A C24A, pH 8.6, 200 mM Tris, 0.2 M NaCl, 200 µg ml^{-1} polymyxin (as co-adsorbate)

Red: Protein film transferred to pot containing 200 mM mercaptoethanol

Green: Protein film returned to buffer only pot (after rinsing in an intermediary pot)

This behaviour can be explained by either proposing ligand addition or substitution. It is possible that the mercaptoethanoate anion is binding to the cluster and replacing the unknown non-cysteinyl ligand and, hence, returning the cluster to a pseudo 'wild-type' state i.e. four thiolates co-ordinating the 2Fe Fd. Alternatively the ligand could be adding to the co-ordination sphere of the iron, thus making a five-co-ordinate atom. However, which scenario is prevalent cannot be easily determined without a structural determination e.g. X-ray crystallography or the right type of spectroscopic experiment. With mercaptoethanoate ligated to the cluster, the extra stability associated with the super-reduced state may be lost, due to a disruption of the co-ordination sphere of the cluster because the fourth ligand of C14A/C24A is replaced/added to by the thiolate ligand. For example, if the unknown fourth ligand is in some way stabilising the fully reduced state, by counter balancing the negative charge at the cluster, replacement of the fourth ligand with a thiolate, which is less able to counterbalance the negative charge at the cluster, would explain the loss of the LPC.

As an alternative to the proposed super-reduced form of *Cp* Fd, it is also possible that there are two forms of the protein adsorbed; each with different potentials, with one form of the $[2Fe\text{-}2S]^{2+/1+}$ cluster having a much lower reduction potential. The way in which these two options could be differentiated would be to use the ligand binding experiment with mercaptoethanol. If the sum of the two peaks, prior to introduction of the protein film to mercaptoethanol, was equal to the area of the 'new' peak, after placing the protein film into mercaptoethanol, it would mean the protein was indeed in two forms. However, if the 'new' peak observed after the protein was introduced into the mercaptoethanol solution, was the same area as only *one* of the previous peaks, this would then indicate that the two redox couples seen were for the *same* protein, i.e. subsequent electron-transfer reactions. Quantitatively this could not be reliably carried out because of the generally poor signals of the C14A/C24A protein and also the significant loss of the protein film upon transferral of the electrode between different solution using the 'multipot' cell. (Seen in Figure 5.24, as the loss in peak height between the 'before' and 'after' mercaptoethanol voltammograms.)

In summary, the electrochemistry of the C14A/C24A mutant demonstrates chemical reactivity which is not immediately apparent from conventional spectroscopic

experiments. The electrochemistry data shows that the differences in protein/cluster characteristics of the [2Fe-2S] cluster, due to the unknown fourth ligand, can help stabilise the fully reduced form of the [2Fe-2S] cluster, and the fourth ligand is labile enough, or sufficiently accommodating (space-wise), to promote ligand exchange/addition at the cluster. As a result of the observed experimental pH dependence, either the fourth ligand must be able to undergo protonation, or the cluster must be close to ligands which can be protonated. However the former is more likely to be the case, since a pH dependence of the reduction couples is not seen for the C14A or C24A mutants. Thus the question of the fourth ligand to the [2Fe-2S] cluster of the C14A/C24A mutant is still unanswered and is subject to ongoing spectroscopic investigation. The evidence gathered here from electrochemical experiments suggests that the fourth cluster ligand is oxygenic in nature. It is unlikely to be a serinate ligand because the serine mutants did not react with exogenous ligands, unlike C24A/C14A (see *Section 5.3.3*).

5.3.2.4 H6A/H7A/H90A

The mutant H6A/H7A/H90A was originally constructed to investigate the possibility that non-cysteinyl co-ordination of the 2Fe Fd was prevalent as a result of the FeS cluster persisting in the double mutant C14A/C24A, which only contains three cysteines. Histidine is a possible substitute for cysteinyl ligands, as found in the Rieske proteins.[45,46]

Each histidine in the sequence (three in total) was individually and then collectively replaced by alanine or valine. Each mutant was found to incorporate the [2Fe-2S] cluster, and they all had identical UV/Vis, EPR and ESEEM spectra to that of the wild-type protein.[19] Thus only one mutant, the triple histidine mutant was investigated electrochemically.

The triple histidine mutant exhibited good reversible electrochemistry when adsorbed as a film on the electrode surface. The quality of the electrochemistry was extremely similar to that of the wild-type Fd, with one redox couple being observed at a reduction

potential of -260 ± 10 mV. Half-height peak widths were ca. 120 mV (in each case) and both the oxidative and reductive peaks were of a comparable peak height i.e. symmetrical. A typical voltammogram is shown in Figure 5.25. The similarity of this mutant to that of the wild-type Fd indicated that no gain would be made by further electrochemical investigations of this mutant. Concomitantly, it was proved using EPR and ESEEM, by Shergill *et al*, that the fourth ligand of the cluster was neither a histidine nor another nitrogenous ligand.[19]

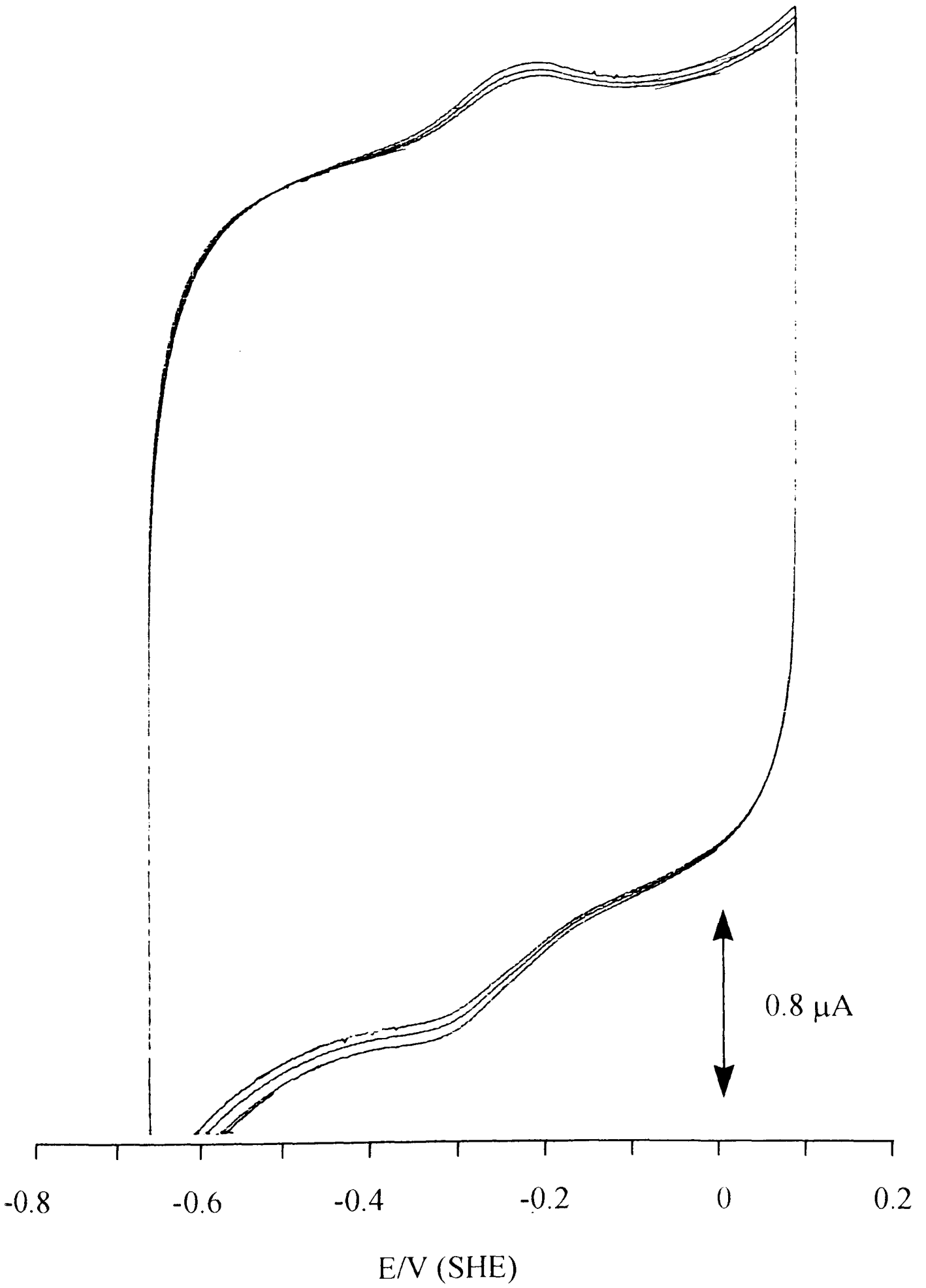

Figure 5.25 Film voltammogram of H6A/H7A/H90A *Cp* 2Fe Fd

pH 7.0 50 mM Hepes buffer, 0.1 M NaCl, 200 μg ml^{-1} polymyxin (as co-adsorbate), $\nu = 50$ mV s^{-1}

5.3.3 THE SERINE MUTANTS -Replacement of -CH_2SH for -OH

The serine mutants investigated were the singly mutated **C11S**, **C56S**, **C60S**, the double mutant **C60S/S61A** and also **C56S/C14A/L16C/Δ19-30** (also written as **C56S***). For all the serine mutants, with the exception of C11S (*Section 5.3.3.1*) the protein films were poorly resolved, i.e. broad δ and short film half-lives, compared to the single alanine mutants, but were of comparable quality to the C14A/C24A mutant.

Replacing a cysteine ligand for a serine ligand is a very common procedure in FeS proteins - frequently used to discover more about a protein's active site and ligation sphere etc.[9] It is a procedure not restricted to iron-sulfur centres and there are many examples in the literature.[14,15,17,47-55] For iron-sulfur centres it is an interesting exchange because it opens the door to non-cysteinyl ligation of the iron-sulfur core, which in the majority of proteins, although not impossible, is atypical - although examples of non-cysteinyl co-ordination to FeS clusters are increasing e.g. aconitase,[42] serine hydratase,[56] hydrogenase[57] and Rieske clusters (*Chapter 1*).[45,46]

5.3.3.1 C11S

For the C11S mutant, protein yields were very low, with a high content of apoprotein present after purification. Meyer *et al* observed that typically the pure protein content per litre of culture was only 20 % of that obtained for the other mutants.[6] Although a number of attempts were made to observe an electrochemical signal, using the same methodology as had been previously used for the alanine mutants, none were observed. The lack of electrochemical signal may either be explained by the protein not adsorbing to the electrode, or the protein adsorbing to the electrode but with a redox centre which was electroinactive or dysfunctional. Previously, however, protein adsorption was not found to be a limiting factor with the wild-type or alanine mutants. That is, for all the mutants, with the one exception of C11S, application of a drop of the protein/co-adsorbate solution onto the electrode surface always produces an electrochemical signal - even if this is weak. Additionally, the pure protein was found to be very unstable when compared to the other mutant proteins, and additional purification stages, which for the other mutants yielded pure ferredoxin, were unsuccessful in increasing the A_{450}/A_{280} ratio of the C11S Fd.[28]

Thus, as judged from the instability of the chromophore of this particular mutant and the likelihood of decomposition, cysteine at position 11 is likely to be a ligand of the cluster. In addition C11S was far more unstable than C56S, C60S and the other serine mutants (*Section 5.3.3.2*). There is therefore a stability order for the serine mutants of *Cp* Fd. It can be postulated that the cysteine residue at position 11 must be critical to the formation of the cluster: it cannot be successfully replaced by serine and is possibly the first ligand to co-ordinate the cluster in the cluster formation process. The cysteine at position 11 is evidently more important than the cysteines at 24, 56 and 60, because when these were replaced by serine the cluster was formed, albeit with some modification to the cluster's properties.[6,18]

5.3.3.2 C56S and C60S

Throughout the electrochemical investigation the results for C56S and C60S were extremely similar and their behaviour, both in film and bulk solution experiments, was almost identical and so the results are reported together.

Both C56S and C60S exhibit one reduction couple, which is at a more negative potential than that of the wild-type Fd. The reduction potentials are -372 ± 10 mV and -369 ± 10 mV, respectively, at pH 7.0 and 0 °C (Figure 5.26). This is a negative shift of ca. 100 mV with respect to the wild-type ferredoxin. Both of these mutants gave poor quality adsorbed film voltammetry; the films were very poorly resolved at intermediate scan rates ($\nu = 100$ mV s^{-1}) and at pH 7 their lifespan was greatly decreased to that of the wild-type Fd (half-life was less than one minute).

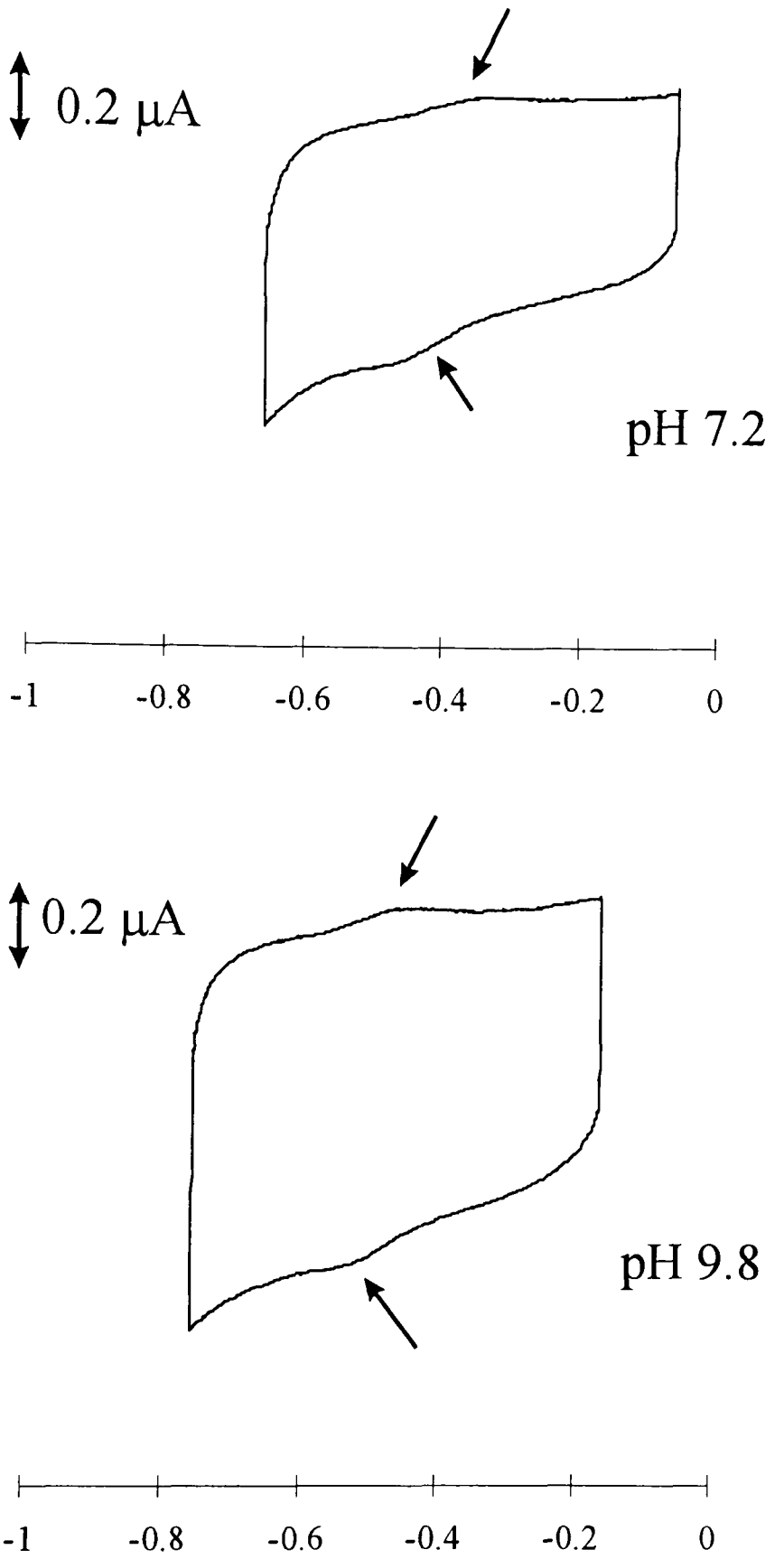

Figure 5.26 Film voltammograms of C56S *Cp* 2Fe Fd

pH as above, 20 mM mixed buffer, 0.1 M NaCl, 200 μg ml^{-1} polymyxin (as co-adsorbate), ν = 10 mV s^{-1}

A pH dependence study was carried out, at slow scan rates, for both C56S and C60S. The reduction potentials of the mutants were found to be markedly dependent on pH (Figures 5.27 and 5.28). This is also clearly demonstrated in Figure 5.26; the reduction potential of the couple at pH 9.8 is -487 ± 10 mV, compared with -382 ± 10 mV at pH 7.2.

As a result of the reduction potentials of both mutants being strongly dependent on pH, the data were plotted with a non-linear regression fit using Equation 5.1 (with no fixed parameters). The slope and the turning point of the line, the pK_{red} were found for each mutant. The slope and pK_{red} values, determined using this method, for all the serine mutants are tabulated in Table 5.4. The theoretical limiting slope for a one electron/one proton reaction is -54 mV at 0 °C; the values found for C56S and C60S were consistent with this, although the value for C60S was slightly lower, most likely this is a direct result of the poor-quality electrochemistry seen for all the serine mutants.

$$E^{o\prime} = E^{o\prime}{}_{alk} + \frac{RT}{nF} \ln\left[1 + \frac{\left(a_{H^+}\right)^y}{K_{red}}\right] \qquad \textbf{Equation 5.1}$$

Equation 5.1 *$E^{o\prime}{}_{alk}$ is the reduction potential in the limit of high pH, a_{H+} is the H^+ activity, n is the number of electrons transferred, y is the number of protons transferred, and K_{red} is the H^+-dissociation constant of the reduced species. In the limit $(a_{H+})/K_{red} >> 1$, a plot of $E^{o\prime}$ as a function of pH should be linear with a slope of -54 mV per pH unit ($n = y = 1$, 0 °C)*

The results shown in Figure 5.27 when fitted with a non-linear regression equation give a pH dependence of -53.6 and -43.1 mV/pH unit and pK_{red} of 8.7 and 9.3 for C56S and C60S respectively. The former value in particular is close to the theoretical value of -54 mV for a one proton/one electron reaction - while the value for C60S is slighter lower and this is probably due to the spread of results obtained for this mutant. It was observed that the voltammetry was improved at higher pH (i.e. > 8.5), especially at intermediate scan rates, where the reductive wave was noticeably less broad (Figure 5.30).

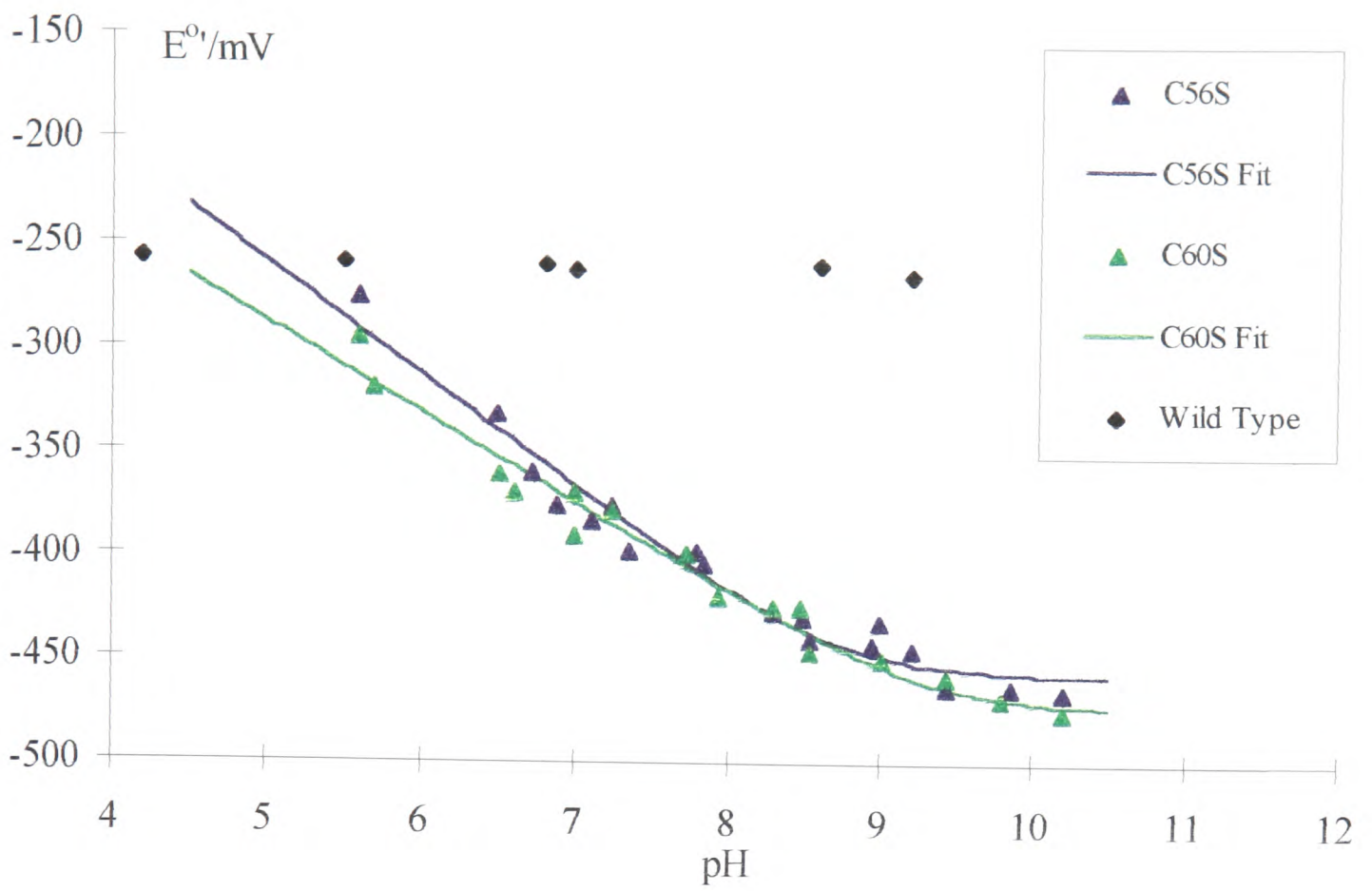

Figure 5.27 pH Dependence of the C56S and C60S mutants of *Cp* 2Fe Fd

20 mM mixed buffer, 0.1 M NaCl, 200 μg ml^{-1} polymyxin (as co-adsorbate), 0 °C, v = 20 mV s^{-1}

(a)

pH	5.6	6.5	6.7	6.9	7.0	7.1	7.2	7.4	7.8	8.3
$E^{o'}$/mV	-275	-332	-360	-375	-370	-383	-375	-397	-397	-427

pH	8.5	8.6	9.0	9.2	9.9	10.2
$E^{o'}$/mV	-429	-440	-443	-445	-463	-466

(b)

pH	5.6	5.7	6.5	6.6	7.0	7.2	7.7	7.9	8.3	8.5	8.3
$E^{o'}$/mV	-295	-320	-361	-370	-369	-378	-399	-419	-424	-424	-427

pH	9.0	9.4	9.8	10.2
$E^{o'}$/mV	-450	-459	-470	-475

Figure 5.28 pH Dependence of (a) C56S and (b) C60S of *Cp* 2Fe Fd

A more rigorous investigation of the scan rate dependence was carried out for C56S at two different pH values, both above and below the pK_{red} value.

pH 9.8: At higher pH (pH 9.8) above the pK_{red} half-height peak widths (δ) of the oxidative and reductive waves were very similar. That of the oxidative wave varied from 112 $\pm$ 10 mV to 163 $\pm$ 10 mV, while values for the reductive wave varied from 91 $\pm$ 10 mV to 142 $\pm$ 10 mV, over the scan rate range 5 to 500 mV s^{-1}. At very slow scan rates, i.e. 20 mV s^{-1} or lower, the voltammetry at pH 9.8 showed half-height peak widths of 100 $\pm$ 10 mV i.e. approaching idealised parameters. At this pH the broadening of the oxidative and reductive waves was symmetrical and there was no significant variation in the reduction potential over this range of scan rates (Figure 5.29).

pH 7.2: At pH 7.2, i.e. below the pK_{red}, values of δ for the oxidative peak ranged from 93 ± 10 mV to 142 ± 10 mV over the scan rate range 5 to 500 mV s^{-1}. For the reductive peak wave δ was much more dependent upon scan rate; at 5 mV s^{-1} the δ was 114 mV but the reductive wave was so broad at $\nu > 100$ mV s^{-1} that the peak was imperceptible and it was impossible to obtain any quantitative information. The scan-rate dependence of the reductive wave is shown in Figures 5.29 and 5.30.

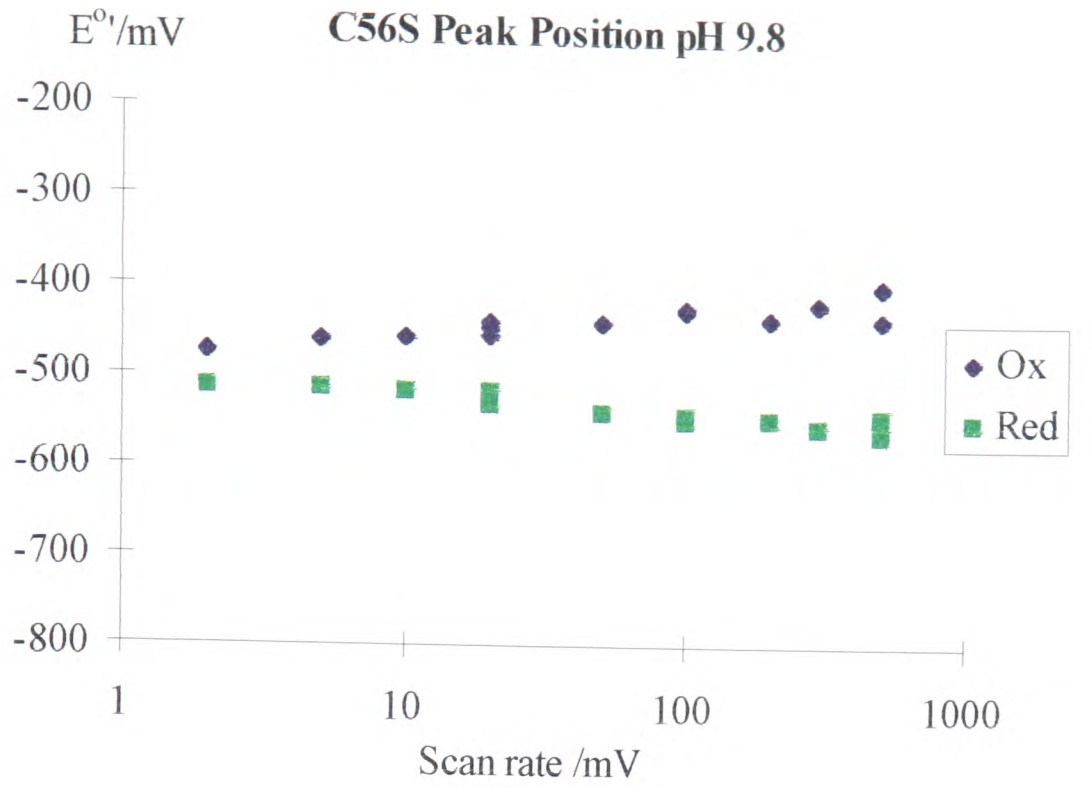

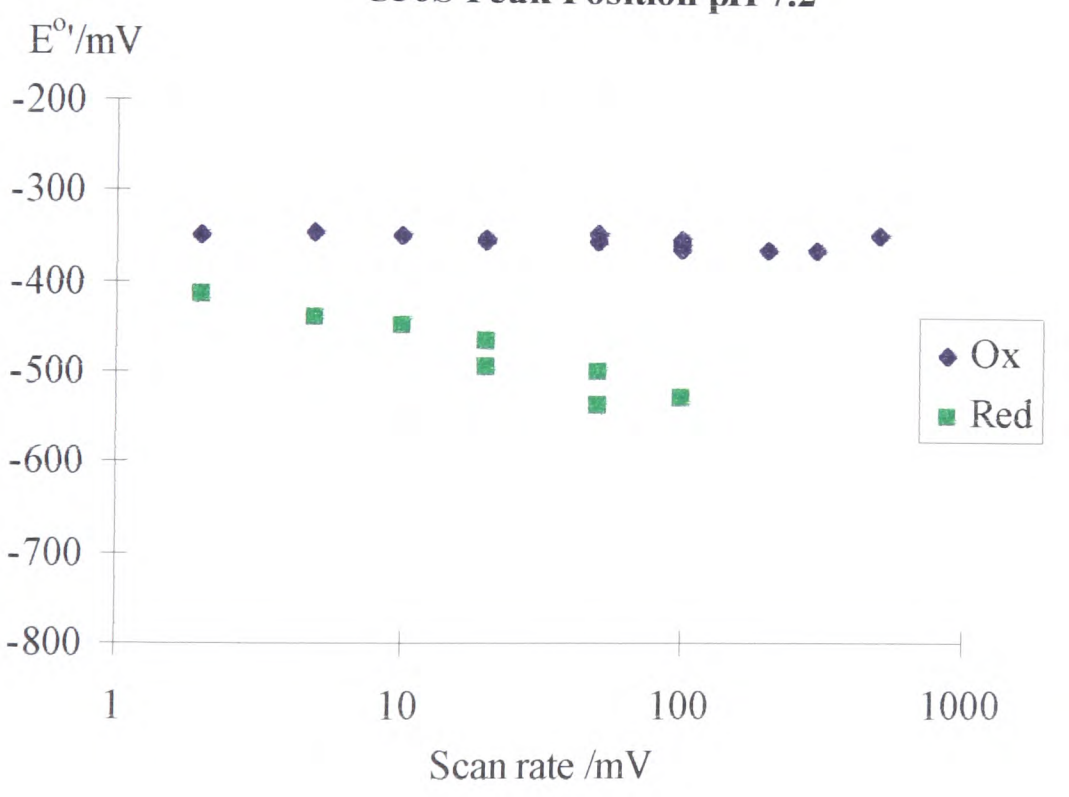

Figure 5.29 Oxidative and reductive peak positions for C56S

20 mM mixed buffer, 0.1 M NaCl, 0 °C, pH as indicated above. Protein films were 100 μM with 200 μg ml^{-1} polymyxin as co-adsorbate.

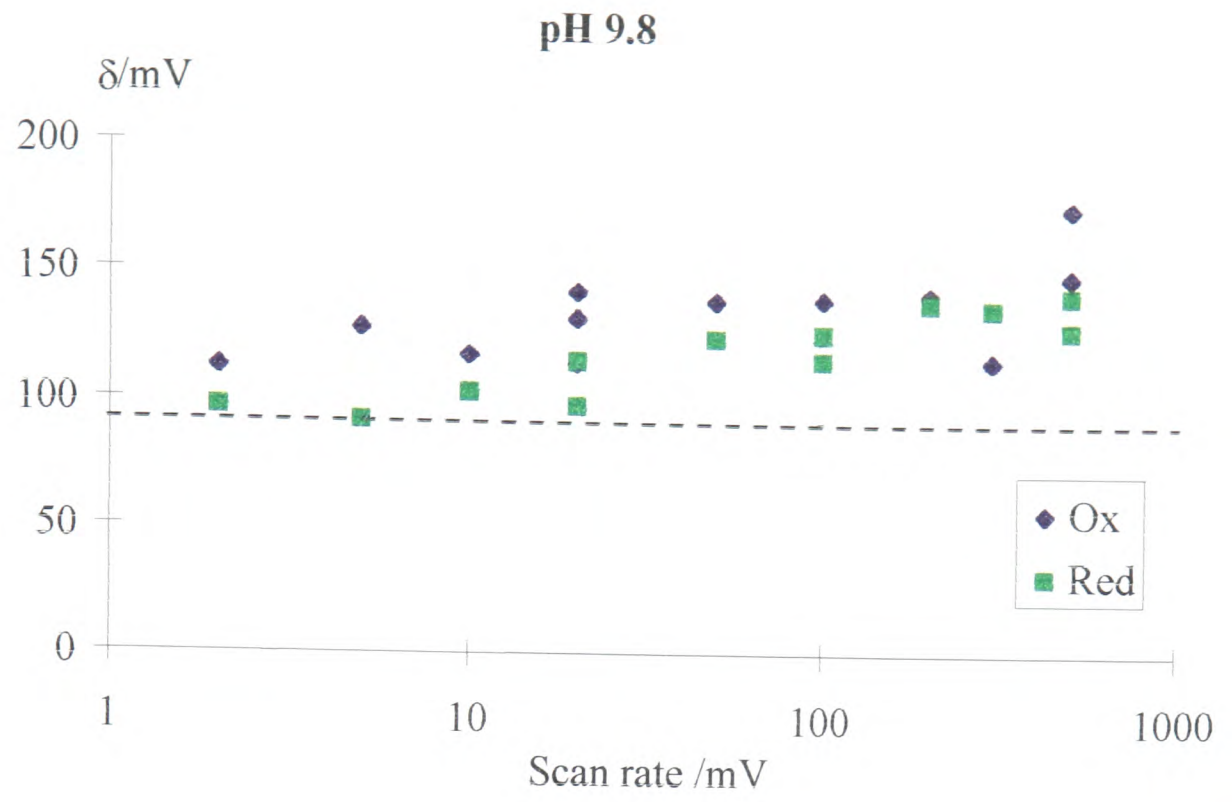

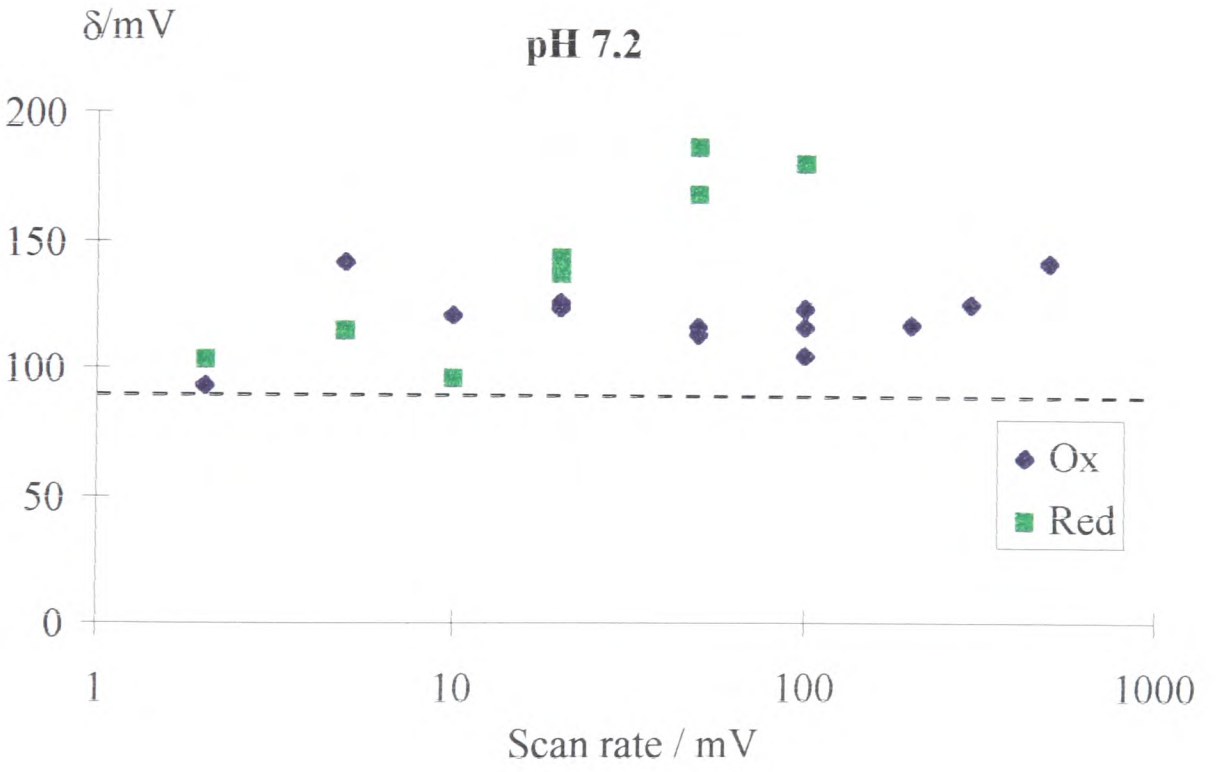

Figure 5.30 Oxidative and reductive half-height peak widths (δ) for C56S

20 mM mixed buffer, 0.1 M NaCl, 0 °C, pH as indicated above. Protein films were 100 μM with 200 μg ml^{-1} polymyxin (as co-adsorbate).

Dashed line indicates ideal value of δ = 84 mV.

Bulk Electrochemistry

In direct contrast to the poor quality film voltammetry, the bulk electrochemistry at pH 7.0 for both of these two mutants was exceptionally well resolved and reproducible over a range of scan rates. Figures 5.31 and 5.32 show bulk diffusional voltammetry of the C56S and C60S mutants respectively. The reduction potentials of the proteins in bulk were found to be -364 ± 10 mV and -370 ± 10 mV for C56S and C60S respectively, which compare well with the values found in adsorbed films, i.e. within 10 mV. They were judged to be diffusion-controlled from the linear dependence of the current against $(\text{scan rate})^{1/2}$ (Figures 5.33 and 5.34).

Exogenous Ligand Binding

Experiments were carried out on both the C56S and C60S mutants to see if an exogenous thiolate ligand would interact with the cluster, as had been previously observed for C14A/C24A (*Section 5.3.2.3*). The experiments were performed with mercaptoethanol, exactly as they had been for the C14A/C24A mutant. A film of the serine mutant was formed and the signal allowed to stabilise, before transfer into a pot containing mercaptoethanol. The electrode transfer was carried out at a potential $< E^{o\prime}_{\text{C56S or C60S}}$. Two concentrations of mercaptoethanol were used (200 mM and 400 mM). No changes in the observed voltammetry were seen for either C56S or C60S, i.e. no reduction potential shifts or a change in the shape of the waves were apparent.

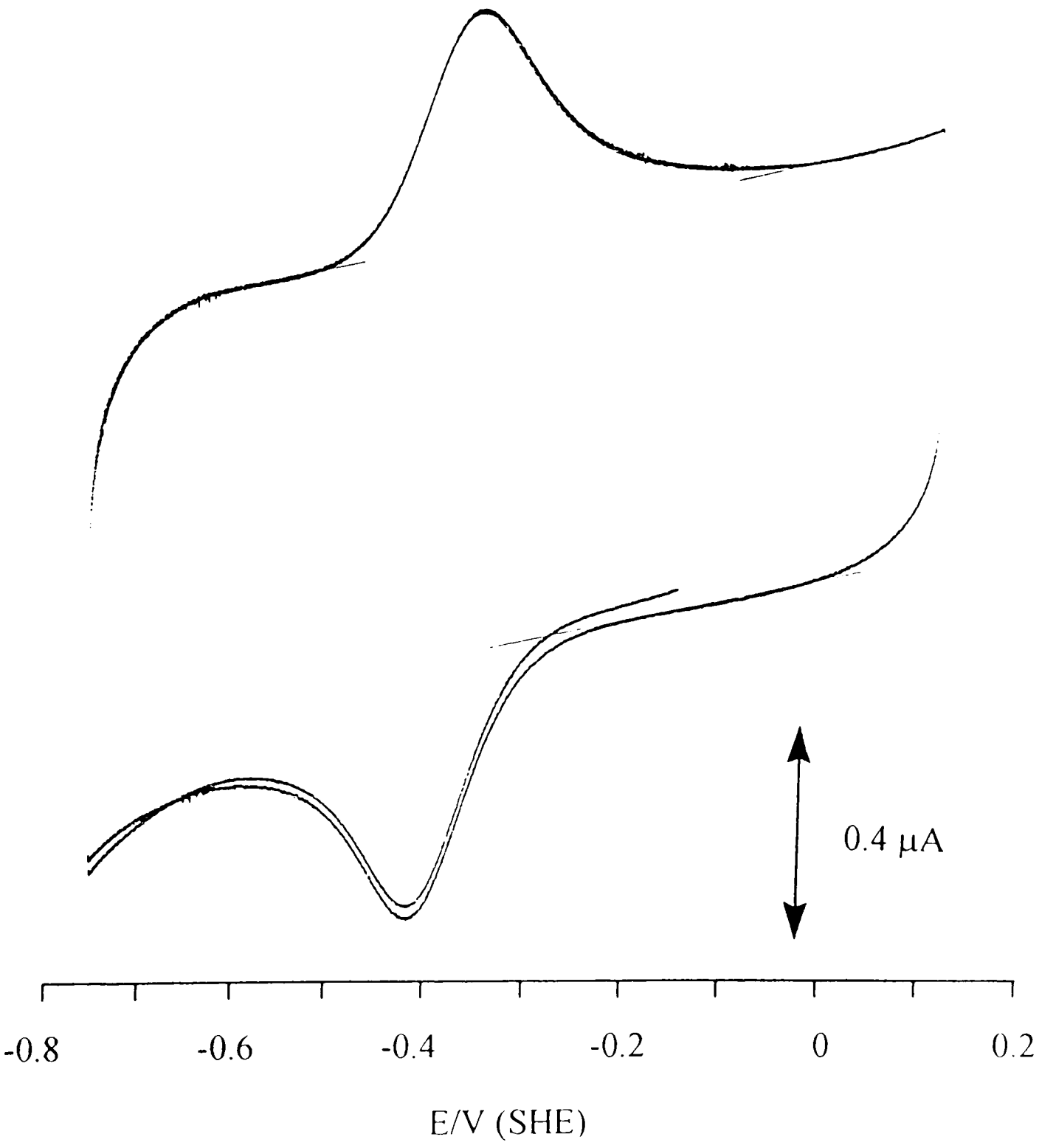

Figure 5.31 Bulk voltammograms of C56S *Cp* 2Fe Fd

pH 7.0, 50 mM Hepes buffer, 0.1 M NaCl, 2 mM neomycin (co-adsorbate),

$\nu = 10\ mV\ s^{-1}$

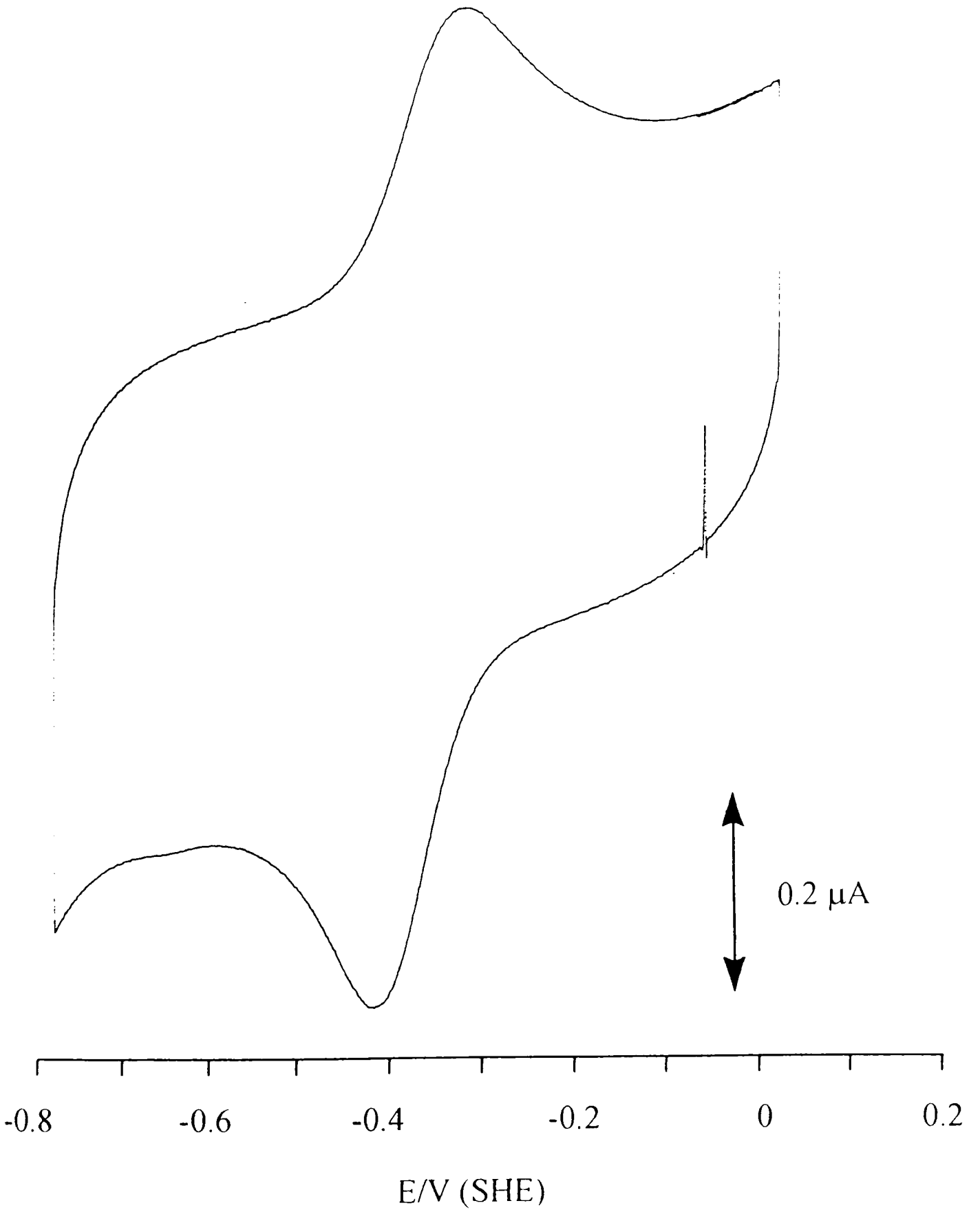

Figure 5.32 Bulk voltammograms of C60S *Cp* 2Fe Fd

pH 7.0, 50 mM Hepes buffer, 0.1 M NaCl, 2 mM neomycin (as co-adsorbate),

$\nu = 5\ mV\ s^{-1}$

C56S

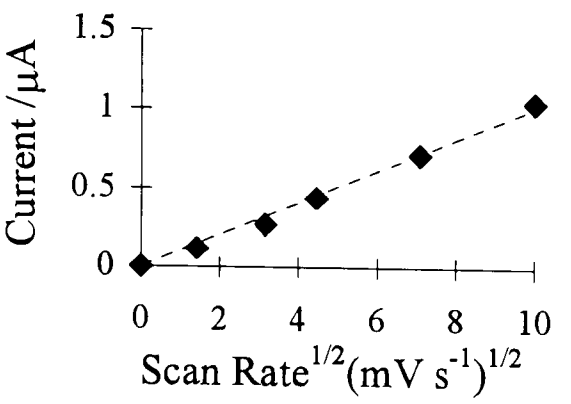

Figure 5.33 Linear dependence of (scan rate)$^{1/2}$ vs. current for bulk diffusional voltammetry of C56S

C60S

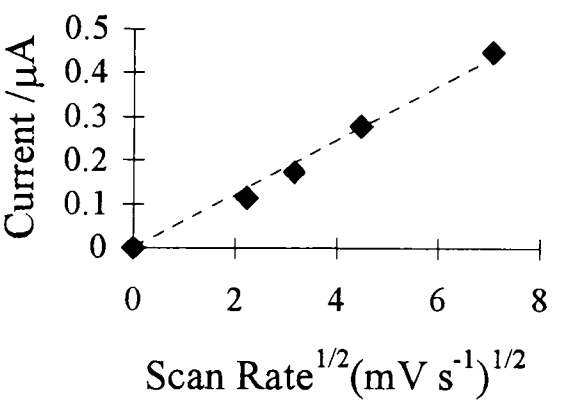

Figure 5.34 Linear dependence of (scan rate)$^{1/2}$ vs. current for bulk diffusional voltammetry of C60S

Both the mutants C56S and C60S contain a [2Fe-2S] chromophore, but the UV/Vis spectra and the electrochemistry of these mutants were noticeably different from the wild-type ferredoxin.[6,18] The ca. 20 nm blueshifts in the 400-500 nm region of the spectrum, from the spectrum of the wild-type protein,[18] were consistent with the replacement of a sulfur by an oxygen ligand.[58] From Figures 5.27 and 5.28 it can be seen that the results for these two proteins were found to be very similar, both in their reduction potentials and the pH dependence of the latter. The negative 100 mV shift of the reduction potential of C56S and C60S, from that of the wild-type, is indicative that a

major change has occurred in the co-ordination sphere of the FeS cluster. An additional observation, which reinforces the theory that a serinate is a ligand to the cluster,[g] is the variation of reduction potential with pH, an attribute which was entirely absent from the wild-type Fd. The negative shift in reduction potential for the serine mutants, compared to the wild-type ferredoxin, suggests serine replacement for a cysteine at the reducible Fe site, there are further examples in the literature (Table 5.3).[9] (An exception is the mutant of *Anabaena* vegetative ferredoxin, C49S, which was found to have a positive shift in reduction potential for the serine mutant, with respect to the wild-type protein.[55])

Oxygen co-ordination, from a serinate, preferentially stabilises the oxidised form of the cluster because of the higher electronegativity of O^- than the S^- from a cysteinate ligand. Therefore, without considering any macroscopic effect of the protein structure, the reduction potentials of all cysteine to serine mutations would be expected to be shifted to a more negative potential because of the stabilisation of the oxidised form. For the cysteine-to-serine mutants of *Escherichia coli* fumarate reductase, C148S and C151S, the 60 and 72 mV decrease in reduction potential respectively, from the wild-type protein, is consistent with serinate co-ordination.[14,54] Stabilities of cysteine to serine mutants are typically found to be lower than that of the wild-type cluster, as expected from the relative pK_a values of cysteine to serine. Differences in the pK_a values; 10.8 for the sulfhydryl of cysteine and ca. 16 for the hydroxyl of serine, mean that it is energetically more costly to produce a serinate rather than a cysteinate ligand; the energy difference being about 7 kcal mol^{-1} at 298 K but this will depend on the competition between metal (ion) and a proton.[53]

[g] However, it should be remembered that *if* the fourth co-ordinating ligand of the C56S and C60S mutants is a serinate, this cannot be exclusively proved through electrochemical experiments alone and other experimental data is required for absolute verification e.g. X-ray crystallography or ^1H NMR.

FeS Cluster	Reduction Potential of Mutant /mV	Reduction Potential of Wild-type /mV
Escherichia coli fumarate reductase $[4Fe\text{-}4S]^{2+/1+}$ of FrdB [14]		
C148S	-360	-300
Escherichia coli fumarate reductase $[4Fe\text{-}4S]^{2+/1+}$ of FrdB [14]		
C151S	-372	-300
Escherichia coli fumarate reductase $[2Fe\text{-}2S]^{2+/1+}$ [12] **C57S**	-182	-79
C62S	-322	
C65S	-49	
C77S	-110	
Chromatium vinosum HiPIP [50] $[4Fe\text{-}4S]^{3+/2+}$		
C77S	330	355
Anabaena 7120 Vegetative Ferredoxin[55]		
C49S	-329	-384
C46S	-381	
Clostridium pasteurianum Rubredoxin **(C42S)**[51] $Fe^{3+/2+}$	ca. -270	ca. -70
$[Fe_2S_2(OAr)_4]^{2-}$ (I, Ar = phenyl: II, Ar = *p*-tolyl: III, Ar = *p*-C_6H_4Cl)	Negative shift of approximately 200 mV, for the first and second reduction potentials of the $[Fe_2S_2]^{2+}$ core.[58]	

Table 5.3 The effect on reduction potentials of cysteine to serine mutations, for both biological and non-biological examples

The voltammetry of both mutants was poorly resolved at intermediate scan rates, and the pH dependence of the reduction potentials was therefore only measured at slow scan rates, ideally < 20 mVs^{-1} to ensure greatest approach to equilibrium. The reduction potentials of both mutants were strongly dependent on pH. The data were plotted with a non-linear equation, (Equation 5.1) and the slope and pK_{red} were determined for each mutant (Table 5.4). The reduction potential at pH 7.0 was verified with the bulk solution experiment.

Mutant	mV/pH (limit)	pK
C56S	53.6	8.7
C60S	43.1	9.3
C56S*	47.6	9.6
C60S/S61A	As for C60S	As for C60S

Table 5.4 pH Dependence data for the serine mutants of the 2Fe Fd from *Cp*

Two consistent traits were noted when examining the film voltammetry.

(1) The oxidative peak has greater definition than the reductive wave at pH values below the pK, i.e. the reductive peak is always broader than the oxidative peak. This is very much in evidence at scan rates above 200 mV s^{-1}, indicating asymmetry in the reversibility of the system (Figures 5.29 and 5.30).

(2) At higher pH values (typically > 9.0) the voltammetric peaks intensify considerably and the half-height peak widths, especially for the reductive waves, are significantly narrower than at the same scan rates at lower pH values (Figures 5.29 and 5.30).

For C56S and C60S the situation became more complex with an increase in the scan rate. At pH 9.9, above the pK_{red}, although the value of δ increased for both the oxidative and reductive peaks, the peaks broadened symmetrically and the $E^{o'}$ was found to be fairly constant over the scan range investigated (2-500 mV s^{-1}). Above the pK_{red}, the behaviour of the reduction couple is as expected for a reaction which is *not* dependent

upon protonation. The reaction is simply an electron-transfer reaction, from 2Fe Fd_{ox} to 2Fe Fd_{red} and the return reaction, Reaction **1**, (Figure 5.35).[h]

At pH 7.5, below the pK_{red}, the oxidative peak shape behaved very similarly to that found in experiments at pH 9.9; however the reductive wave at this pH was found to broaden with increasing scan rates. Above 100 mV s^{-1} the peaks were too broad for accurate analysis. This more complex behaviour, below the pK_{red}, for the serine mutants could result from a number of factors. One possible reason is that the oxidised form of the protein may exist in two or more slowly interconverting states, either protonated (2Fe Fd_{ox}) or unprotonated (2Fe Fd_{ox}-H^+). Thus conversion of the oxidised cluster into a 'second' oxidative state may prevent the reappearance of the reduction wave at higher scan rates. (Equally the proposed interconverting states could be *either* conformational changes in the protein *or* two different orientations of the protein on the electrode surface).

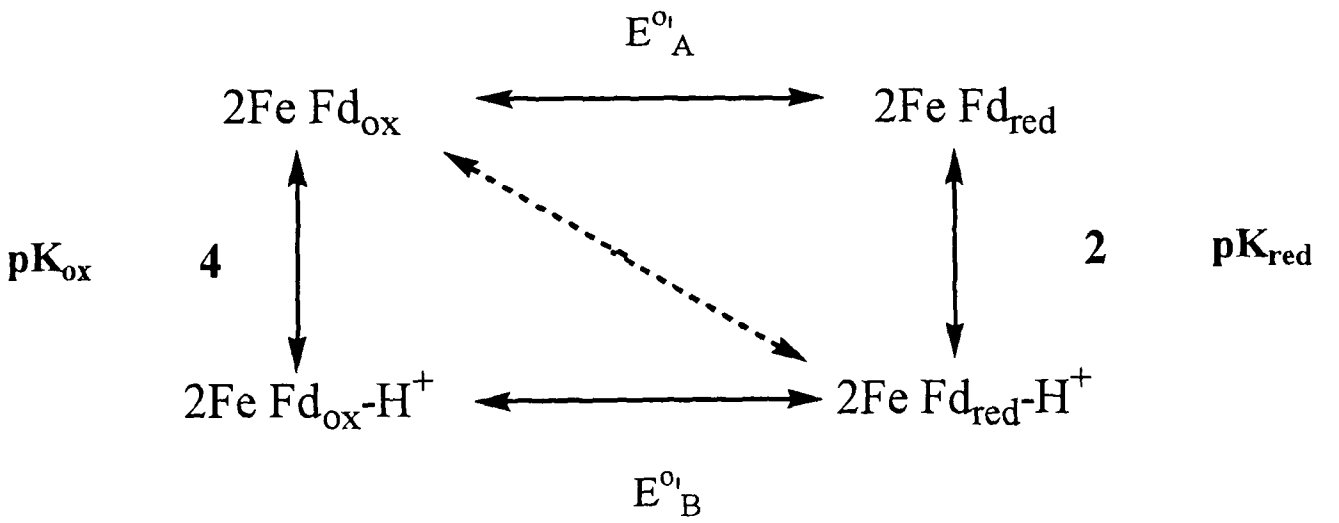

Figure 5.35 Proposed square scheme for the serine mutants

See Chapter 1 for a description of square schemes.

An alternative explanation for the complex voltammetry, is that the serinate, which ligates the cluster, may be protonated at pH < pK_{red} which may induce structural changes

[h] Where 2Fe Fd_{ox} is the $[2Fe\text{-}2S]^{2+}$ state and 2Fe Fd_{red} is the $[2Fe\text{-}2S]^{1+}$ state of the cluster.

in the protein or alter the cluster ligation. Protonation of the oxygenic bond of the serinate may cause a partial or complete breaking of the oxygen bond between the serinate and the $Fe^{2+/3+}$ of the cluster, resulting in electron transfer being impeded. However, the complexity of the voltammetry, indicating that it is the *oxidative* form which consists of more than one form is in direct contrast to the pK_{red} which suggests that it is the reduced form which uptakes a proton below the pK_{red}.[59]

A further explanation may be that the broad reductive wave could be composed of more than one oxidised component i.e. two species with similar reduction potentials. This would be the case if there was only slow interconversion between two (or more) oxidised forms, Reaction **4**, Figure 5.35, and there was fast interconversion between the two reduced forms, Reaction **2**, Figure 5.35. Hence only one oxidative peak would be observed but this would give rise to two (or more) reductive peaks, due to there always being a heterogeneous and slowly interconverting population of oxidised forms of the cluster on the electrode surface.

Ultimately, the data obtained in this study for the C56S and C60S mutants gives us a glimpse of the more complex reactions which are occurring due to electron and proton transfer reactions, but the data acquired are not of sufficient quality to completely deconvolute the exact reactions. Though what is known: replacing a cysteinate for a serinate ligand to this cluster imparts significant changes to the properties of the cluster, can be in no doubt. The previous suggestions and discussion are just that - they can only be taken as proposals of what might actually be occurring, it may be that other factors must also be taken into account.[i]

The argument for proposed serine co-ordination, rather than $H_2O/^-OH$ co-ordination, is aided by observations which were made during experiments carried out on the serine mutants with mercaptoethanol. Previously it had been noted that changes in the voltammetry were observed when an adsorbed protein film of the C14A/C24A mutant

[i] Recently it has become apparent through low temperature studies (as low as -40 °C), that protein film voltammetry is dependent not only on the protein-electrode interface but also on the 'movement' of the adsorbed protein molecules on the electrode surface. This was observed through an increase in the half-height peak width as the temperature was lowered, presumably movement of the protein molecules was attenuated, and the voltammetry became more like that of a dispersion of different species.[60]

was introduced to a solution of mercaptoethanol, see *Section 5.3.2.3.* In contrast the same experiments were carried out with both of the serine mutants and no changes were observed in the voltammetry. This demonstrates that the non-cysteinyl ligand in C56S and C60S compared to C14A/C24A does not have the same chemical reactivity with respect to mercaptoethanol, and in all likelihood the non-cysteinyl ligands are not the same. It could be that C56S or C60S are more stable, with respect to ligand exchange/ligand addition to the cluster co-ordination sphere, because the proposed co-ordinating ligand, serine, is part of the amino acid backbone. If the fourth ligand is either H_2O or ^-OH, as has been proposed for C14A/C24A, it may be more labile because it is not directly attached to the protein's polypeptide chain.

An additional observation, which must be taken into account, concerns the bulk solution electrochemistry. For both C56S and C60S (and also for C56S/C14A/L16C/Δ19-30, see *Section 5.3.3.3*) the bulk solution electrochemistry at slow and intermediate scan rates was well defined at pH 7.0. Both reductive and oxidative waves were of a similar magnitude and no asymmetry in the peaks was observed at a pH < pK_{red}, unlike the adsorbed film experiments. Thus, under bulk electrochemical conditions the 'pH effect', i.e. the asymmetry of the oxidative and reductive waves at a pH below the pK_{red}, was not seen. It is difficult to explain the reasons behind the difference in protein film voltammetry and the bulk solution voltammetry. One possible hypothesis is that adsorption of the protein molecules on the electrode surface (in protein films) may align the protein molecule in different ways depending on the pH. In bulk solution the contact with the electrode surface is only transitory. It is not yet fully understood how exactly protein molecules are confined to the electrode surface, but presumably in bulk solution the protein molecules interact differently with the electrode surface and/or they are not adsorbed as strongly to the electrode surface. This feature of protein electrochemistry, i.e. different behaviour observed for the serine mutants when the species are either adsorbed as a protein film or in a bulk electrochemical solution, is also seen for some 7Fe Fds. The very low reduction couple which is associated with $[3Fe\text{-}4S]^{0/2-}$ for *Desulfovibrio africanus* Fd III and for *Azotobacter vinelandii* Fd I is readily seen using protein film techniques but is not seen in the bulk electrochemistry. Conversely this reduction couple is readily observed using *both* electrochemical techniques for the 7Fe Fd from *Sulfolobus acidocaldarius*.[38,61] Formation of the hyper-reduced state has been

proposed to be dependent on the concomitant uptake of $2e^-$ and $3H^+$ and thus the length of time and how (directionally) the protein molecules interact with the electrode may be important.

5.3.3.3 C56S/C14A/L16C/Δ19-30

The mutant, C56S/C14A/L16C/Δ19-30, was constructed as an extension to a study investigating the effect of deleting a flexible loop of *Cp* Fd and its subsequent influence on the chemical and physical characteristics of the Fd.[20] This research illustrated that a cysteine ligand positioned at either C14, C16 or C24 was able to co-ordinate the [2Fe-2S] cluster as a result of a likely protein rearrangement. The 'parent' mutants used in the study by Golinelli *et al* were: wild-type, C14A/L16C/C24A and C14A/L16C, all with various length deletions in the region 15-32. Thus as an extension to the electrochemical study of the singly mutated serine ferredoxins, C56S/C14A/L16C/Δ19-30 was also included in the electrochemical investigation of the serine mutants.

The C56S/C14A/L16C/Δ19-30 mutant was very similar to both the C56S and C60S mutants with respect to its behaviour in adsorbed protein films and bulk electrochemistry. That is to say, protein film electrochemistry was generally poor, i.e. low resolution of the oxidative and reductive waves, and the film had a half-life of less than one minute. A voltammogram is shown in Figure 5.36. At pH 7.0, 0 °C, an adsorbed film of the C56S/C14A/L16C/Δ19-30 showed a reduction potential of -464 ± 10 mV, representing a further negative shift of ca. 90 mV for the $E^{o'}$ of the C56S/C14A/L16C/Δ19-30 mutant, compared to -372 ± 10 mV for the C56S mutant. There is therefore an overall negative shift of ca. 200 mV, relative to the reduction potential of the wild-type ferredoxin. A pH dependence study was carried out on this mutant (Figure 5.37). The pH dependence study was used to determine the slope and pK for this mutant. These were determined using Equation 5.1; the slope was -47.6 mV/pH and the pK 9.6 (Table 5.4).

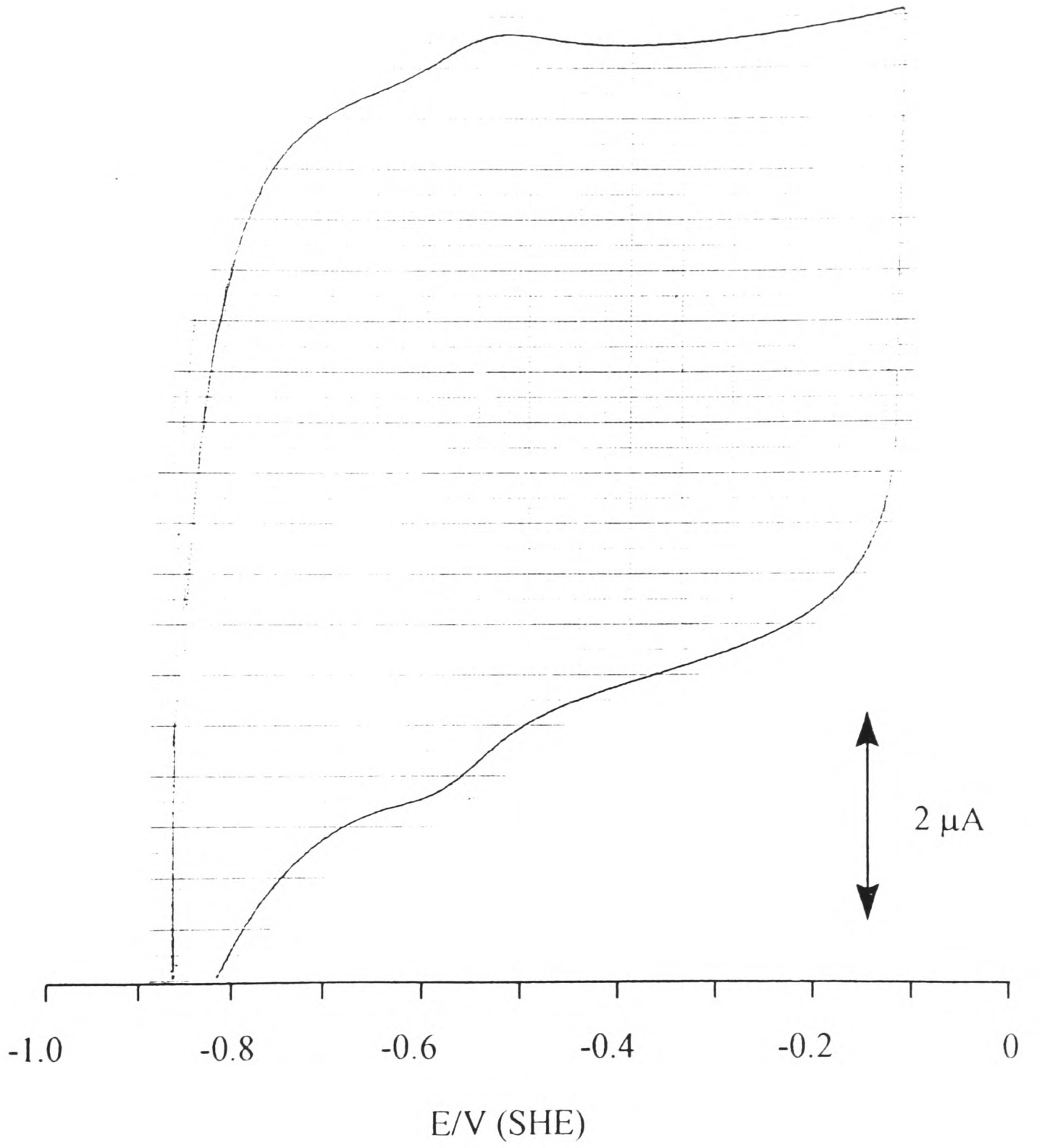

Figure 5.36 Film voltammogram of C56S/C14A/L16C/Δ19-30 *Cp* 2Fe Fd

pH 10.0, 20 mM mixed buffer, 0.1 M NaCl , 200 μg ml^{-1} polymyxin (as co-adsorbate), 0 ^{o}C, ν = 100 mV s^{-1}

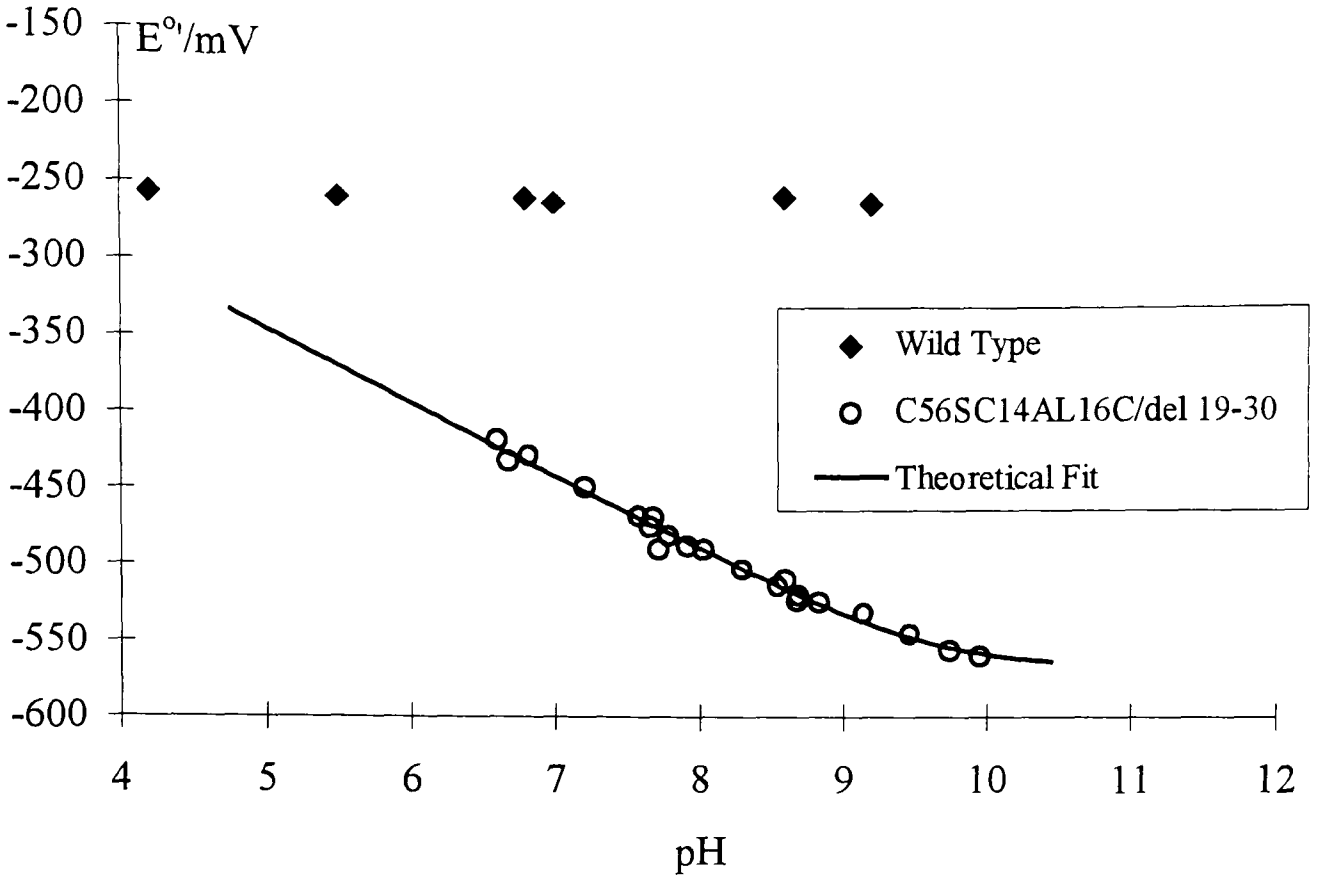

pH	6.6	6.8	7.0	7.2	7.6	7.7	7.9	8.0	8.3	8.6	8.7
$E^{o'}$/mV	-417	-427	-464	-448	-467	-477	-487	-489	-502	-509	-521

pH	8.8	9.1	9.5	9.7	10.0
$E^{o'}$/mV	-524	-531	-545	-556	-560

Figure 5.37 pH Dependence of the C56S/C14A/L16C/Δ19-30 mutant of *Cp* 2Fe Fd

Bulk Electrochemistry

The bulk solution electrochemistry was similar to that of the single serine mutants C56S and C60S, namely the diffusion controlled voltammetry was well-defined as shown in Figure 5.38. The voltammetry was determined to be diffusion controlled from the linear relationship of the current with the (scan rate)$^{1/2}$, Figure 5.39. Moreover, the same negative shift in reduction potential for C56S/C14A/L16C/Δ19-30 as compared to the single serine mutants, and also the wild-type, was also observed in bulk solution. The $E^{o'}$ of C56S/C14A/L16C/Δ19-30 was determined as -454 ± 10 mV, compared to -469 ± 10 mV when measured in a protein film.

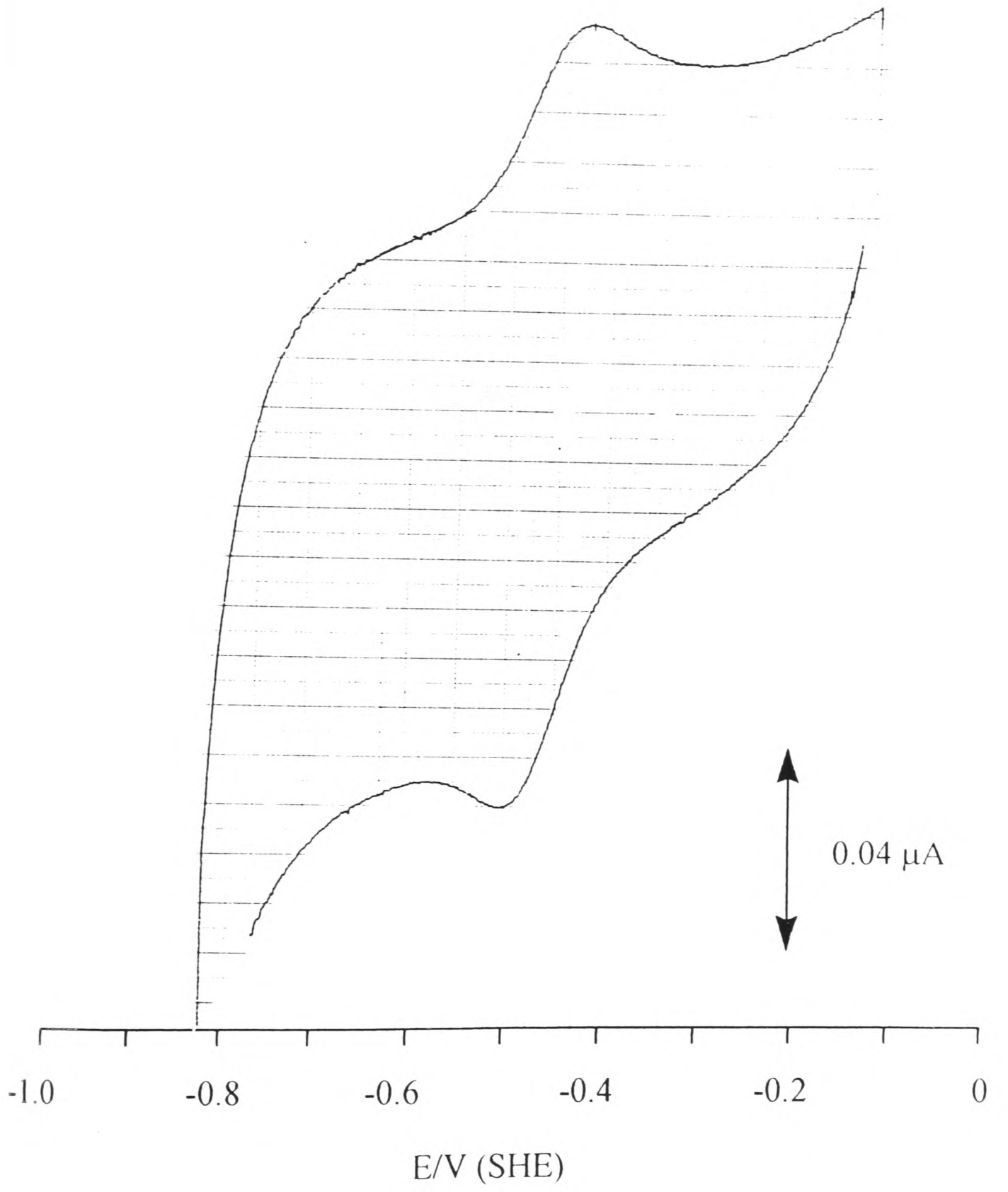

Figure 5.38 Bulk solution voltammogram of C56S/C14A/L16C/Δ19-30

pH 7.0, 50 mM Hepes buffer, 0.1 M NaCl , 2 mM neomycin (as co-adsorbate),

$\nu = 5\ mV\ s^{-1}$

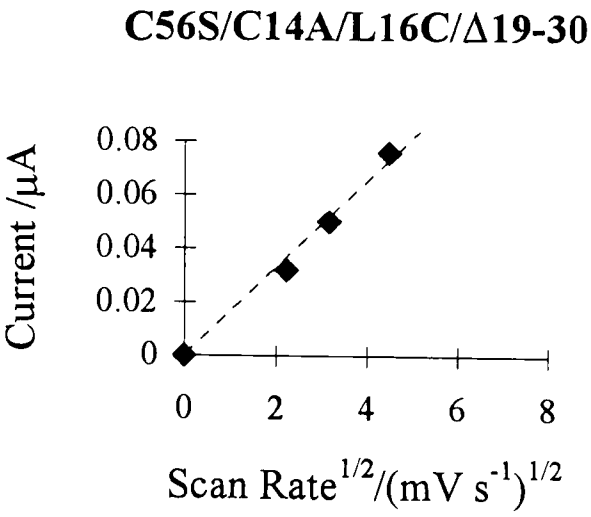

Figure 5.39 Linear dependence of (scan rate)$^{1/2}$ vs. current for bulk diffusional voltammetry of C56S/C14A/L16C/Δ19-30

In general, the electrochemical characteristics of the mutant C56S/C14A/L16C/Δ19-30, were found to be similar in many respects to C56S and C60S. The major difference was that the reduction potential was shifted negatively by ca. 90 mV with respect to the C56S and C60S mutants, over the whole pH range investigated. This negative shift in reduction potential can be clearly seen in Figure 5.37. The quality of adsorbed film signals and the bulk solution electrochemistry were very similar to that of C56S and C60S.

In the C56S/C14A/L16C/Δ19-30 mutant, the [2Fe-2S] cluster is ligated by C11, C16, S56 and C60; thus there are two major differences in the co-ordination of the cluster in the C56S/C14A/L16C/Δ19-30 mutant and C56S or C60S and these must contribute to the further negative shift in reduction potential.[20] These are:

(a) The change in position of the second co-ordinating cysteine, from C24 to C16
(b) Deletion of the loop i.e. residues 19 to 30

In *Section 5.3.2.2* it was shown that movement of the second cysteine in the binding motif, i.e. from C24 to C14, resulted in a negative shift of the reduction potential of ca. 80 mV for the C24A mutant. It is therefore likely that a similar change in position of the ligand, from C24 to C16, would also induce a shift in the reduction potential of the

protein. The second contributing factor to a change in the reduction potentials, deletion of the loop i.e. residues 19 to 30, has precedence in the literature.[20] Consequently it is difficult to decide whether the negative shift in reduction potential of C56S/C14A/L16C/Δ19-30 is due to (a) or (b) as written above. However, it is most probable that the negative shift of the reduction potential of C56S/C14A/L16C/Δ19-30 is a combination of both (a) and (b).[j]

Spectroscopic evidence has recently shown that the C56S/C14A/L16C/Δ19-30 mutant can also exist with the unusual spin state, $S = 9/2$, routinely seen for both the C56S and C60S mutants.[62] Preliminary data indicates that ca. 60 % of this protein contains a cluster with $S = 9/2$.[62] Changes in the co-ordination sphere of the cluster and hence the co-ordination sphere of the individual Fe atoms, through the deletion of a loop from the protein structure or the change in co-ordinating residue from C24 to C16, may both affect the cluster spin state. However this is very speculative, more work is required to understand these subtle changes in protein structure and how they can affect the spin states of the metallocentres.

5.3.3.4 C60S/S61A

The mutant C60S/S61A was constructed as an extension to the study of the C56S and C60S mutants and their unusual ground spin state, $S = 9/2$.[21] The C60S/S61A mutant was constructed to discover if subtle differences in the environment of the cluster would affect the spin state of the cluster; in this case a serine proximal to the cluster replaced by an alanine.

The C60S/S61A mutant showed almost identical electrochemical behaviour to that of the C60S mutant. The only difference between the C60S/S61A mutant and C60S, is one point mutation in the vicinity of the cluster, and this small change in the protein structure was not found to result in a difference in electrochemical properties. Thus, adsorbed films were poorly resolved and bulk solution voltammetry was comparably better than the film voltammetry. The reduction potential of this mutant, determined with protein

[j] The redox potentials measured by Golinelli *et al* indicate that when going from WT to C14A/L16C/Δ19-30 the displacement of the cysteine ligand contributes -20 mV to the total -100 mV shift (cysteine displacement and deletion).[20]

film voltammetry was -369 ± 10 mV while with bulk diffusional voltammetry, the reduction potential was -387 ± 10 mV, both at 0 °C and pH 7.1 and pH 7.0 respectively. Only a limited pH dependence study was carried out, due to the similarity of C60S/S61A and the C60S mutant. When compared to the C60S data, as shown in Figures 5.40 and 5.43, it can be seen that the pH dependence data mirrors that of the C60S, and indeed the C56S mutant.

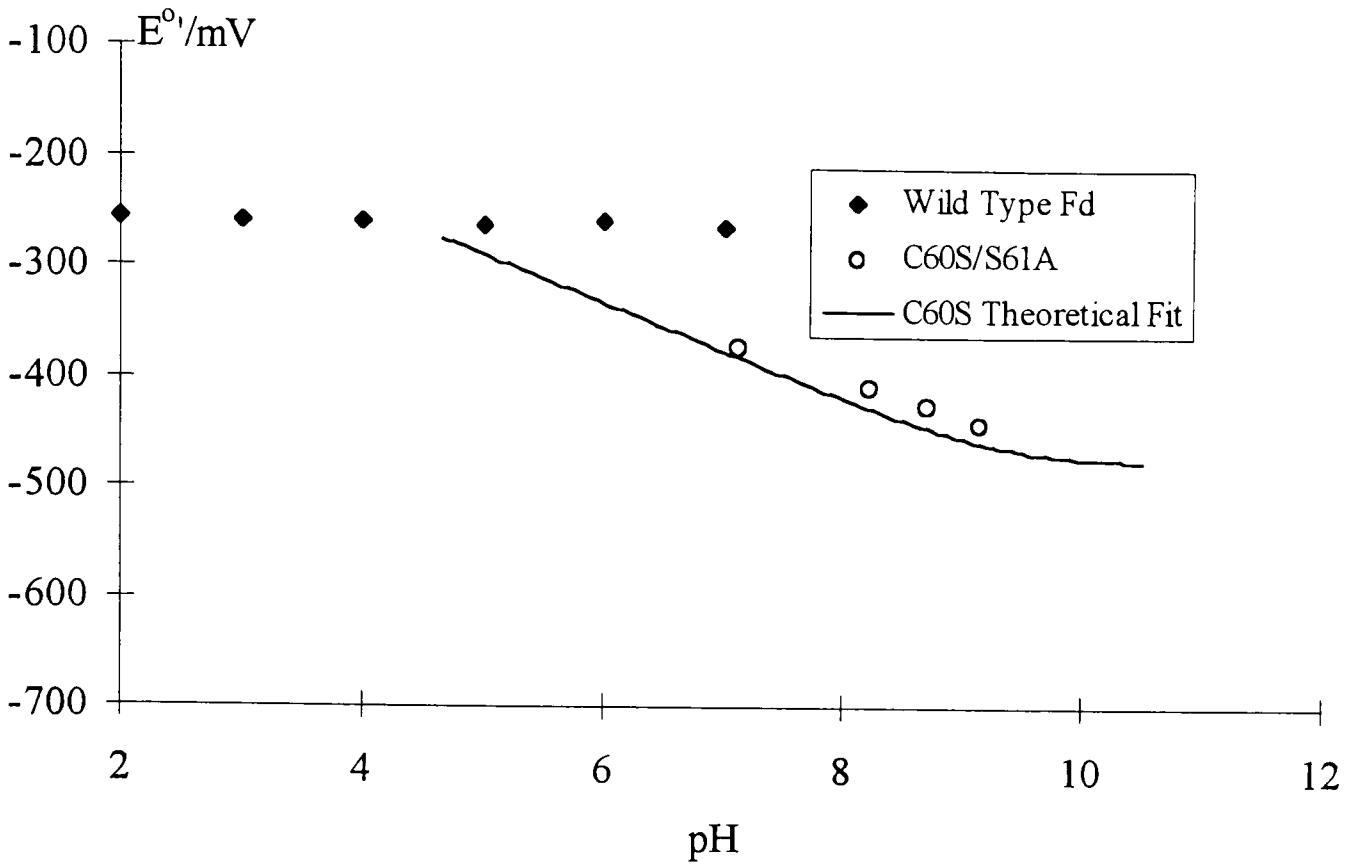

pH	7.1	8.2	8.7	9.1
$E^{o'}$/mV	-369	-407	-424	-440

Figure 5.40 pH Dependence of the C60S/S61A mutant of *Cp* 2Fe Fd

NB The limited pH dependence data of C60S/S61A is plotted against the theoretical fit obtained for C60S for comparison purposes only.

Cysteine-to-Serine Mutants in FeS biological clusters

Precedence for serinate co-ordination of biological FeS clusters comes from the X-ray crystal structures of the nitrogenase P cluster,[63] the C49S mutant of *Anabaena* [2Fe-2S] clusters.[64] and the [2Fe-2S] cluster in succinate dehydrogenase from *E. coli*.[13] The implications of substituting serine for cysteine in a protein can be difficult to predict, and the results will be dependent on the individual protein. Serine can be substituted in place of cysteine without greatly changing the electronic structure of a cluster, as observed for the mutant C77S from *Chromatium vinosum* (*Cv*), a HiPIP FeS cluster. It was found that there were only slight differences between the wild-type and the C77S mutant of *Chromatium vinosum*.[49] The reduction potential of C77S is only 25 mV lower than that of the wild-type HiPIP - this lack of difference in the $E^{o'}$ of the two mutants thus supports the idea that the polypeptide surrounding the prosthetic group can be a very important factor in determining the reduction potentials of metalloproteins.[50]

Other examples of cysteine to serine mutations can involve much more significant changes to the redox-active centre. The serine mutants of *Anabaena* 7120 vegetative ferredoxin,[15,55] and the rubredoxin from *Cp*,[51] all have a significant impact on the reduction potential and other biophysical attributes of the FeS cluster (Table 5.3). Differences in the stability of the mutants, depending on which cysteine is replaced by a serine, are also noted in most proteins. An example is seen in the ferredoxin from *Anabaena, a*mong the four cysteine-to-serine mutants constructed, C46S and C49S were more stable than the other two serine mutants, C41S and C79S.[15] Notably the two most stable cysteine-to-serine mutants have one of the cysteines in the sequence -C-X-X-C- replaced, and this has also been noted for the serine mutants of Human Fd.[53] Similarly in *Cp* 2Fe Fd, C11S was found to be less stable than either C56S or C60S. The cysteines at positions 56 and 60 are spaced by only one more residue than in the typical 'bidentate' motif often found in 2Fe Fds ($-C^{56}$-X-X-X-C^{60}-). The stability difference among cysteine-to-serine mutants may provide some insight into protein folding and cluster formation. For example, among the cysteine-to-serine mutants of *Chromatium vinosum* HiPIP, the mutant C77S is much more stable than the other three serine mutants.[49] For the mutant C77S of *Cv* HiPIP, the cluster formation may be initiated and indeed almost completed by the first three cysteines and so serine (at position 77) simply finalises co-

ordination at an almost complete polymetallic centre. Additional factors which influence protein stability and may also influence position-sensitive effects of S-to-O substitutions include: changes in strain energy of the cluster; differences in protein flexibility; differences in H-bonding to the cluster, and alterations in solvent accessibility to the cluster.[12,53]

5.4 SUMMARY

As a result of this study, a series of mutants of a unique [2Fe-2S] ferredoxin have been investigated and a range of answers and, indeed, a number of further questions have emerged (Table 5.5). It has been successfully shown that voltammetric experiments, together with SDM and spectroscopic techniques can be used collectively in an investigation of the active site and reactivities of an FeS protein. Using a combination of these techniques has enabled the four cysteine ligands of the 2Fe Fd from *Cp* to be determined: C11, C24, C56 and C60. Importantly this is one of the first 2Fe Fds not to contain a -C-X-X-C- ligand sequence to co-ordinate the FeS cluster and, as such, *Clostridium pasteurianum* contains a 2Fe Fd which forms a unique subclass of 2Fe ferredoxins.

Although voltammetry was not used as a stand-alone technique, it has been able to highlight a number of features which might not have been so easily observed using alternative methods. Most importantly it is a dynamic technique, and although equilibrium properties, e.g. reduction potentials can be measured by other means, (which are generally more sample intensive) coupled reactions such as the exogenous ligand interaction of the double mutant, C14A/C24A, would remain unresolved.

The pH dependencies and the chemical reactivities of the mutants were investigated, and subsequently pK_{red} values for the serine mutants were measured (Table 5.4). A more in-depth study of the pH dependence data of C56S and C60S implied that coupled proton/electron reactions were occurring, but unfortunately the data were insufficient to deconvolute these reactions. This is in contrast to systems where coupled proton and electron transfer have been successfully deconvoluted in a ferredoxin system.[59,65] The double mutant, C14A/C24A was found to exhibit a number of unusual features, including co-ordination of a non-cysteinyl ligand to the cluster, exogenous ligand interaction of the cluster with a thiolate ligand and the proposed formation of the all-Fe^{2+} state, previously identified in very few [2Fe-2S] clusters.

One of the limiting factors found in this study was the lack of stability of the protein films of some of the mutants, during the electrochemical experiments. The extent of this loss

of stability was dependent upon each individual mutant. It was noted for all the mutants, except C14A and H6A/H7A/H90A,[k] that the general electrode coverage of the protein was less than the wild-type. This led to problems in measuring the reduction potentials and observing subsequent chemical reactions i.e. exogenous ligand binding. Qualitatively the following order of stability was found (decreasing film stability): wild-type > C14A > H6A/H7A/H90A > C24A > C56S and C60S and C60S/S61A > C56S/C14A/L16C/Δ19-30 > C14A/C24A. Thus, from this study it can be concluded that even though the FeS cluster may still be formed in the mutated proteins, alterations of the cluster's co-ordination sphere may also affect the ability of the cluster to communicate with the electrode. It is not possible to say whether this was a macroscopic protein effect i.e. the point mutation(s) lead to a general protein change and so affected the overall adsorption of the protein and its stability, or the point mutation(s) just affected the redox centre and hence electrode response.[l]

The lack of stability was especially noticeable for the serine mutants of *Cp* 2Fe Fd (*Section 5.3.3.2*)[6,18] and a similar lack of stability has been reported for serine mutants of *Anabaena* ferredoxin[15] and Human ferredoxin.[53] The differences in stability between various serine mutants of one particular ferredoxin could lead to information on the structural formation of the ferredoxin. The fact that C11S was so unstable, which prevented any voltammetry being carried out on this protein, may indicate that this cysteine is the anchor of the FeS cluster formation process i.e. without cysteine at position 11, cluster formation is unlikely to proceed.

The formation of an FeS cluster in the mutant C56S/C14A/L16C/Δ19-30 demonstrated that a number of amino acid deletions can be carried out in the region of residues 17 to 32 of *Cp* 2Fe Fd, without significant loss of the iron-sulfur cluster and/or its redox function (*Section 5.3.3.3*).[20][*This work*] From structure predictions and site-directed mutagenesis experiments it has been postulated that the region between cysteines 14 and 24 is a flexible loop, because cysteines at positions 14, 16 or 24, depending on the

---

[k] Cysteine-14 was not found to be an *in vivo* ligand of the [2Fe-2S] cluster, nor too any of the histidine residues.

[l] A similar phenomenon has also been recorded for the W51F mutant of cytochrome *c* peroxidase, whereby the mutant becomes partially inactive on adsorption at the electrode, unlike the more stable wild-type protein.[66]

mutated protein, are able to ligate the cluster. Deletion of this protein loop does not markedly affect the protein and its interaction with the electrode, i.e. no more so than for the one point mutations, e.g. C56S, but it does have a considerable impact on the reduction potential of the mutant.

Further experiments in the future ideally would include a pH dependence of the serine mutants in bulk electrochemical conditions, and an investigation of the EPR spectra at pH values above and below the pK_{red} for C56S and C60S, to investigate if more than one form of the protein could be observed.[m] The fully reduced state of the C14A/C24A mutant also needs to be further investigated, the ability to generate this state in solution would greatly simplify any spectroscopic study. The ability to form the fully reduced state of the [2Fe-2S] cluster in this mutant shows how, with only the alteration of two amino acids, the redox states of the cluster can be manipulated.

[m] Spectroscopic data (EPR) has been recently obtained for both the C56S and C60S mutants both above and below the pK_{red} (pH 6.0 and pH 11.0).[62] Subtle changes are observed in the EPR spectra at the two different pH values, but further work is planned using ENDOR to see if changes can be detected which are due to (de)protonation and/or changes in ligands.[62]

5.5 DATA SUMMARY

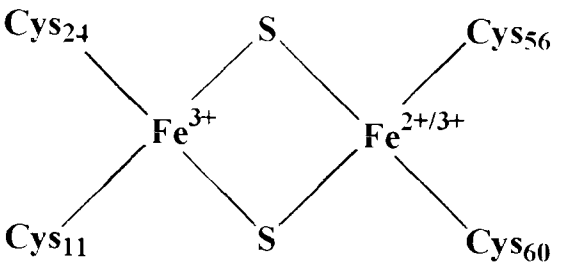

WT

C14A

H6A/H7A/H90A

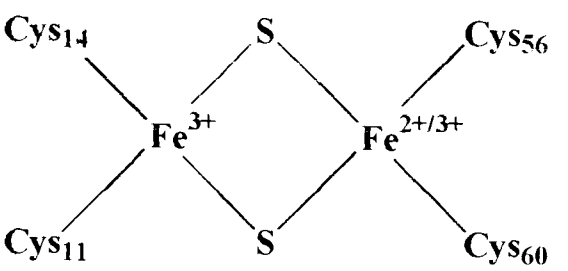

C24A

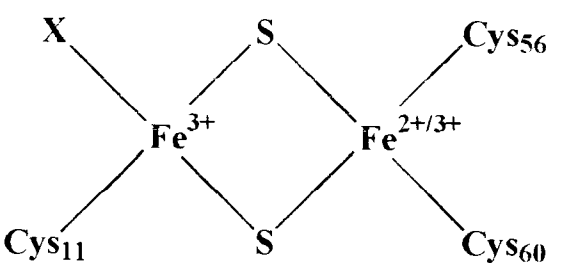

C14A/C24A
X = $^{-}$OH or H_2O ?

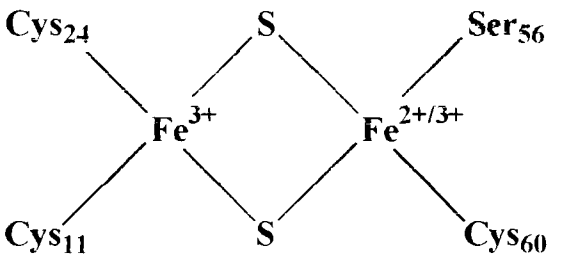

C56S
and also similarly
C60S

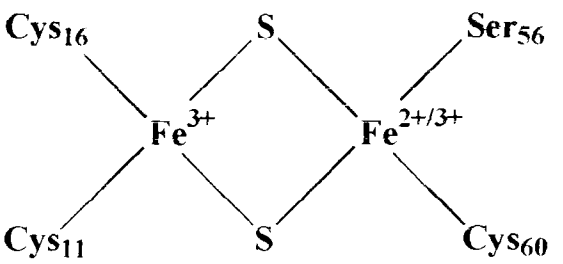

C56S/C14A/L16C/Δ19-30

Figure 5.41 Cartoon showing the [2Fe-2S] cluster and putative ligands of the mutants of *Clostridium pasteurianum* 2Fe Fd

Ferredoxin	Film $E^{o'}$/ mV	Bulk $E^{o'}$/ mV	mV/pH	pK	Comment	Ligands of [2Fe-2S]
Wild-type	-261	-262	No pH dependence			**C11,C24,C56,C60**
ALANINE MUTANTS						
C14A	-265	-265	No pH dependence		Identical to wild-type	**C11,C24,C56,C60**
C24A	-337	-340	No pH dependence			**C11,C14,C56,C60**
C14A/C24A	-287	Ø	~ 25		Reduction couple at $E^{o'}$ = -613mV	**C11,?,C56,C60**
H6A/H7A/ H90A	-260	-	-	-	Identical to wild-type	**C11,C24,C56,C60**
SERINE MUTANTS						
C11S	Protein expressed but mainly as apoprotein, no electrochemistry observed					**S11,C24,C56,C60**
C56S	-372	-364	53.6	8.7		**C11,C24,S56,C60**
C60S	-369	-370	43.1	9.3		**C11,C24,C56,S60**
C56S/C14A/ L16C/ Δ19-30	-464	-454	47.6	9.6		**C11,C16,S56,C60**
C60S/S61A	-369	-387	As for C60S			**C11,C24,C56,S60**

Table 5.5 Summary of all the electrochemical results for the alanine and serine mutants of *Cp* 2Fe Fd

? = unknown ligand

Ø = not observed as pure bulk diffusion voltammetry see Section 5.3.2.3

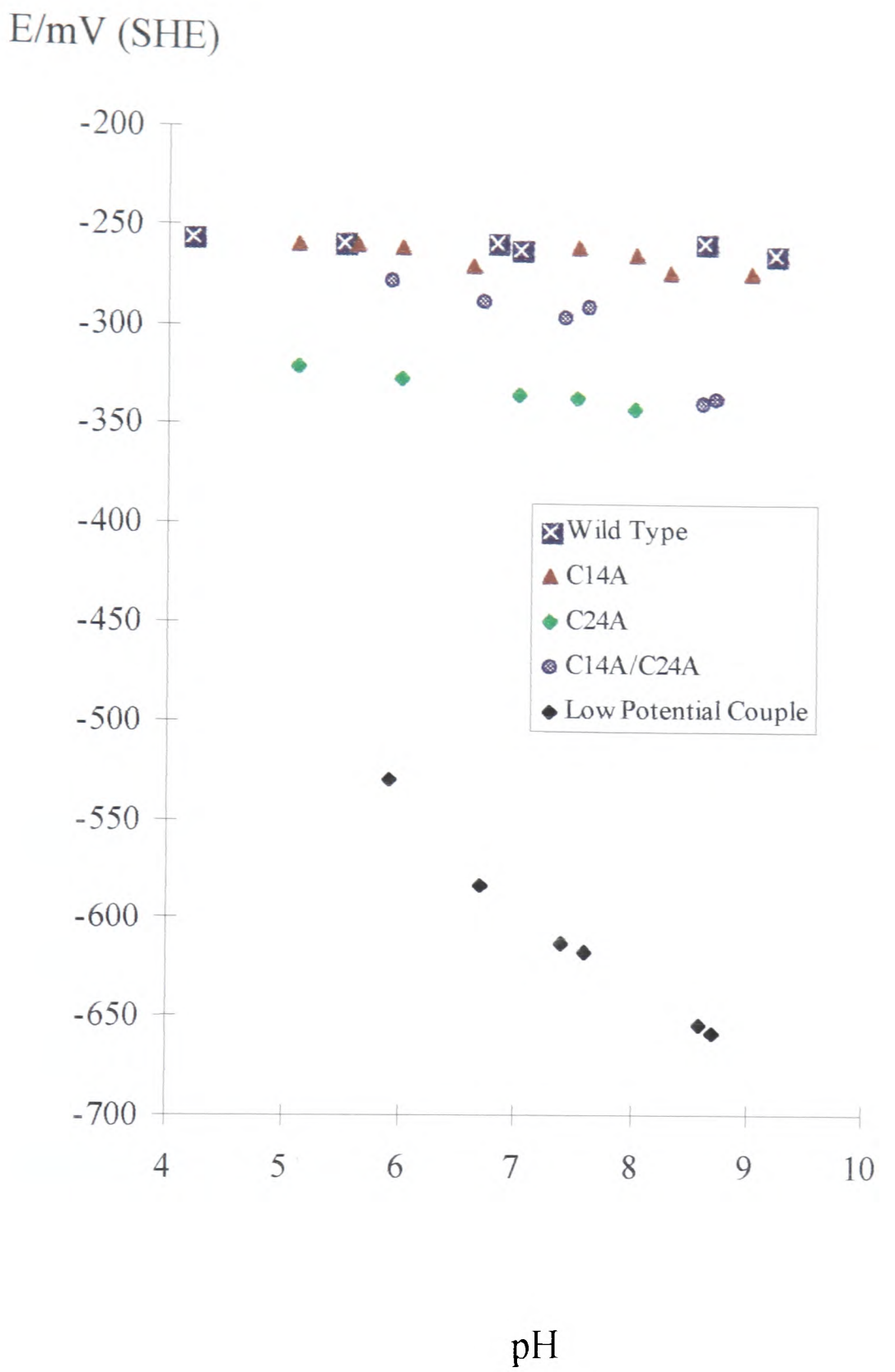

Figure 5.42 pH Dependence for the alanine mutants

The wild-type data are plotted on the graph for comparison. Data were collected at 0 °C, and at slow scan rates i.e. 20 mV s^{-1}. (The data for C14A C24A is that obtained after FPLC purification)

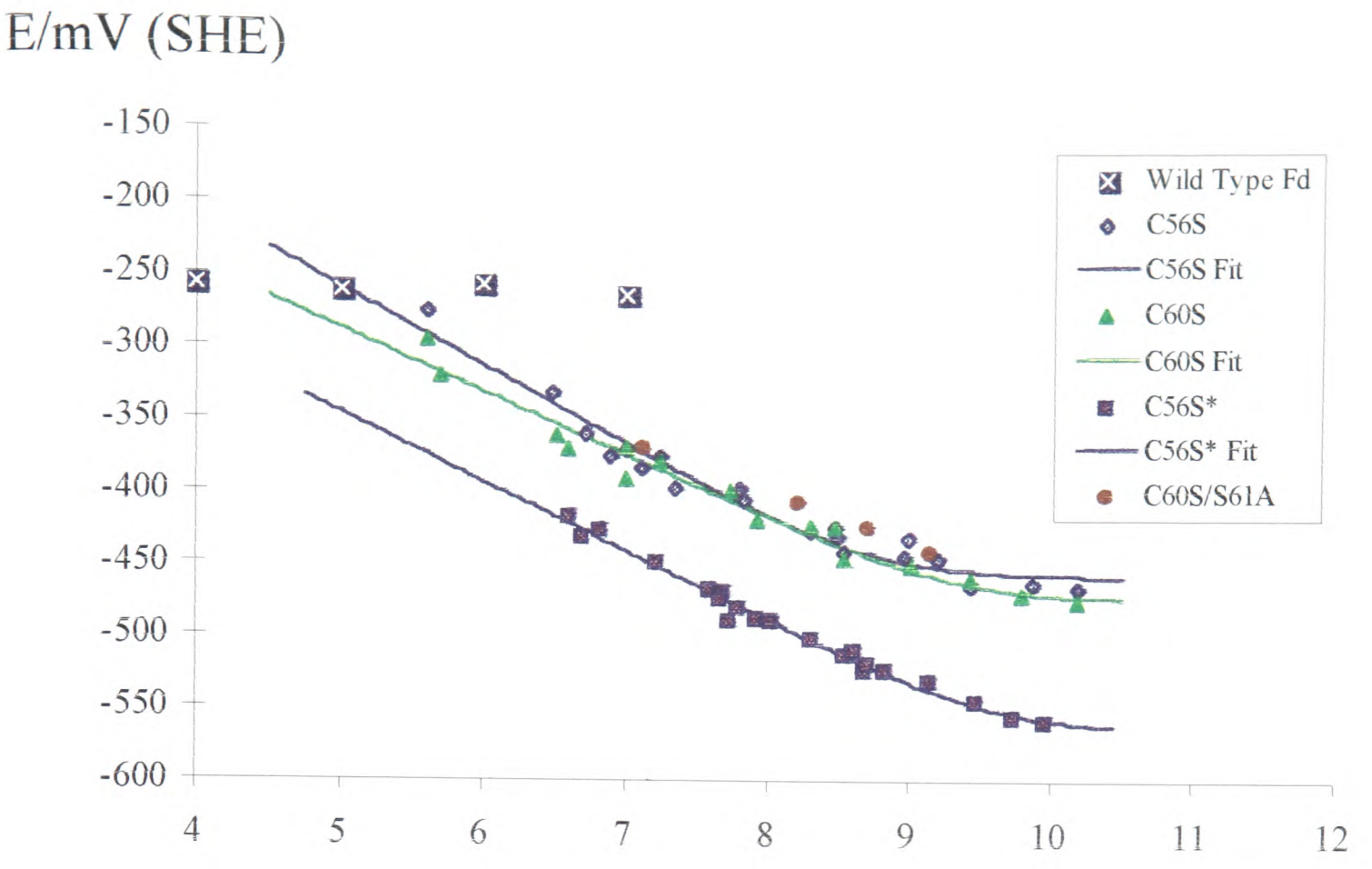

Figure 5.43 pH Dependence for the serine mutants

The wild-type data are plotted on the graph for comparison purposes. Data were measured at 0 °C, and at slow scan rates i.e. 20 mV s^{-1}

5.6 REFERENCES

1) Cammack, R. *Advances in Inorganic Chemistry*, 1992; Vol. 38.

2) Johnson, M. K. *Encyclopedia of Inorganic Chemistry*; Wiley: Chichester:, 1994; Vol. 4.

3) Matsubara, H.; Saeki, K. *Adv. Inorg. Chem.* **1992**, *38*, 223-280.

4) Meyer, J.; Bruschi, M. H.; Bonicel, J. J.; Bovier-Lapierre, G. E. *Biochemistry* **1986**, *25*, 6054-6061.

5) Meyer, J. *Trends Ecol. Evol.* **1988**, *3*, 222-226.

6) Meyer, J.; Fujinaga, J.; Gaillard, J.; Lutz, M. *Biochemistry* **1994**, *33*, 13642-13650.

7) Ohsawa, I.; Speck, D.; Kisou, T.; Hayakawa, K.; Zinsius, M.; Gloeckler, R.; Lemoine, Y.; Kamogawa, K. *Gene* **1989**, *80*, 39.

8) Davidson, E.; Ohnishi, T.; Atta-Asafo-Adjei, E.; Daldal, F. *Biochemistry* **1992**, *31*, 3342.

9) Moulis, J. M.; Davasse, V.; Golinelli, M. P.; Meyer, J.; Quinkal, I. *Journal of Biological Inorganic Chemistry* **1996**, *1*, 2-14.

10) Martin, A. E.; Burgess, B. K.; Stout, C. D.; Cash, V. L.; Dean, D. R.; Jensen, G. M.; Stephens, P. J. *Proc. Nat. Acad. Sci. USA* **1990**, 598-602.

11) Davidson, E.; Ohnishi, T.; Atta-Asafo-Adjei, E.; Daldal, F. *Biochemistry* **1992**, *31*, 3342-3351.

12) Werth, M. T.; Cecchini, G.; Manodori, A.; Ackrell, B. A. C.; Schroder, I.; Gunsalus, R. P.; Johnson, M. K. *Proceedings of the National Academy of Sciences of the United States of America* **1990**, *87*, 8965-8969.

13) Werth, M. T.; Sices, H.; Cecchini, G.; Schroder, I.; Lasage, S.; Gunsalus, R. P.; Johnson, M. K. *Febs Letters* **1992**, *299*, 1-4.

14) Kowal, A. T.; Werth, M. T.; Manodori, A.; Cecchini, G.; Schroder, I.; Gunsalus, R. P.; Johnson, M. K. *Biochemistry* **1995**, *34*, 12284-12293.

15) Cheng, H.; Xia, B.; Reed, G. H.; Markley, J. L. *Biochemistry* **1994**, *33*, 3155-3164.

16) Yano, T.; Sled, V. D.; Ohnishi, T.; Yagi, T. *FEBS Lett.* **1994**, *354*, 160-164.

17) Rothery, R. A.; Weiner, J. H. *Biochemistry* **1991**, *30*, 8296-8305.

18) Fujinaga, J.; Gaillard, J.; Meyer, J. *Biochemical and Biophysical Research Communications* **1993**, *194*, 104-111.

19) Shergill, J. K.; Golinelli, M. P.; Cammack, R.; Meyer, J. *Biochemistry* **1996**, *35*, 12842-12848.

20) Golinelli, M. P.; Akin, L. A.; Crouse, B. R.; Johnson, M. K.; Meyer, J. *Biochemistry* **1996**, *35*, 8995-9002.

21) Meyer, J., *Personal Communication.*

22) Hardy, R. W. F.; Knight, E. J.; McDonald, C. C.; D'Eustachio, A. J. *Non-Heme Iron Proteins: Role in Energy Conversion* **1965**, 275-282.

23) Meyer, J.; Moulis, J. M.; Lutz, M. *Biochemical and Biophysical Research Communications* **1984**, *119*, 828-835.

24) Cardenas, J.; Mortenson, L. E.; Yoch, D. C. *Biochimica et Biophysica Acta* **1976**, *434*, 244-257.

25) Meyer, J.; Moulis, J.-M.; Lutz, M. *Biochim. Biophys. Acta* **1986**, *873*, 108-118.

26) Fu, W.; Drozdzewski, P. M.; Davies, M. D.; Sligar, S. G.; Johnson, M. K. *J.Biol.Chem.* **1992**, *267*, 15502-15510.

27) Petillot, Y.; Golinelli, M. P.; Forest, E.; Meyer, J. *Biochemical and Biophysical Research Communications* **1995**, *210*, 686-694.

28) Fujinaga, J.; Meyer, J. *Biochemical and Biophysical Research Communications* **1993**, *192*, 1115-1122.

29) Crouse, B. R.; Meyer, J.; Johnson, M. K. *Journal of the American Chemical Society* **1995**, *117*, 9612-9613.

30) Achim, C.; Golinelli, M. P.; Bominaar, E. L.; Meyer, J.; Munck, E. *Journal of the American Chemical Society* **1996**, *118*, 8168-8169.

31) Butt, J. N. *Ph.D. Thesis* University of California: Irvine, **1993**

32) Anemuller, S.; Schmidt, C. L.; Schafer, G.; Bill, E.; Trautwein, A. X.; Teixeira, M. *Biochemical and Biophysical Research Communications* **1994**, *202*, 252-257.

33) Link, T. A.; Hagen, W. R.; Pierik, A. J.; Assmann, C.; Vonjagow, G. *European Journal of Biochemistry* **1992**, *208*, 685-691.

34) Shen, B.; Jollie, D. R.; Diller, T. C.; Stout, C. D.; Stephens, P. J.; Burgess, B. K. *Proceedings of the National Academy of Sciences of the United States of America* **1995**, *92*, 10064-10068.

35) Calzolai, L.; Gorst, C. M.; Zhao, Z. H.; Teng, Q.; Adams, M. W. W.; Lamar, G. N. *Biochemistry* **1995**, *34*, 11373-11384.

36) Werst, M. M.; Kennedy, M. C.; Beinert, H.; Hoffman, B. M. *Biochemistry* **1990**, *29*, 10526-10532.

37) Verhagen, M. F. J. M.; Link, T. A.; Hagen, W. R. *FEBS Lett.* **1995**, 75-78.

38) Duff, J. L. C.; Breton, J. L. J.; Butt, J. N.; Armstrong, F. A.; Thomson, A. J. *Journal of the American Chemical Society* **1996**, *118*, 8593-8603.

39) Im, S. C.; Kohzuma, T.; McFarlane, W.; Gaillard, J.; Sykes, A. G. *Inorganic Chemistry* **1997**, *36*, 1388-1396.

40) Angove, H. C.; Yoo, S. J.; Burgess, B. K.; Munck, E. *Journal of the American Chemical Society* **1997**, *119*, 8730-8731.

41) Watt, G. D.; Reddy, K. R. N. *Journal of Inorganic Biochemistry* **1994**, *53*, 281-294.

42) Beinert, H.; Kennedy, M. C.; Stout, C. D. *Chemical Reviews* **1996**, *96*, 2335-2373.

43) Butt, J. N.; Sucheta, A.; Armstrong, F. A.; Breton, J.; Thomson, A. J.; Hatchikian, E. C. *Journal of the American Chemical Society* **1993**, *115*, 1413-1421.

44) Telser, J.; Smith, E. T.; Adams, M. W. W.; Conover, R. C.; Johnson, M. K.; Hoffman, B. M. *Journal of the American Chemical Society* **1995**, *117*, 5133-5140.

45) Gurbiel, R. J.; Batie, C. J.; Sivaraja, M.; True, A. E.; Fee, J. A.; Hoffman, B. M.; Ballou, D. P. *Biochemistry* **1989**, *28*, 4861-4871.

46) Gurbiel, R. J.; Ohnishi, T.; Robertson, D. E.; Daldal, F.; Hoffman, B. M. *Biochemistry* **1991**, *30*, 11579-11584.

47) Chernaik, M. L.; Huang, P. C. *Proceedings of the National Academy of Sciences of the United States of America* **1991**, *88*, 3024-3028.

48) George, G. N.; Garrett, R. M.; Prince, R. C.; Rajagopalan, K. V. *Journal of the American Chemical Society* **1996**, *118*, 8588-8592.

49) Bentrop, D.; Bertini, I.; Capozzi, F.; Dikiy, A.; Eltis, L.; Luchinat, C. *Biochemistry* **1996**, *35*, 5928-5936.

50) Babini, E.; Bertini, I.; Borsari, M.; Capozzi, F.; Dikiy, A.; Eltis, L. D.; Luchinat, C. *Journal of the American Chemical Society* **1996**, *118*, 75-80.

51) Meyer, J.; Gaillard, J.; Lutz, M. *Biochemical and Biophysical Research Communications* **1995**, *212*, 827-833.

52) Warren, P. V.; Smart, L. B.; McIntosh, L.; Golbeck, J. H. *Biochemistry* **1993**, *32*, 4411-4419.

53) Xia, B.; Cheng, H.; Bandarian, V.; Reed, G. H.; Markley, J. L. *Biochemistry* **1996**, *35*, 9488-9495.

54) Manodori, A.; Cecchini, G.; Schroder, I.; Gunsalus, R. P.; Werth, M. T.; Johnson, M. K. *Biochemistry* **1992**, *31*, 2703-2712.

55) Hurley, J. K.; WeberMain, A. M.; Hodges, A. E.; Stankovich, M. T.; Benning, M. M.; Holden, H. M.; Cheng, H.; Xia, B.; Markley, J. L.; Genzor, C.; GomezMoreno, C.; Hafezi, R.; Tollin, G. *Biochemistry* **1997**, *36*, 15109-15117.

56) Grabowski, R.; Hofmeister, A. E. M.; Buckel, W. *TIBS* **1993**, 297-300.

57) Volbeda, A.; Charon, M.-H.; C., P.; Hatchikian, E. C.; Frey, M.; Fontecilla-Camps, J. C. *Nature* **1995**, 580-587.

58) Cleland, W. E.; Averill, B. A. *Inorg.Chem.* **1984**, *23*, 4192-4197.

59) Hirst, J.; Duff, J. L. C.; Jameson, G. N. L.; Kemper, M. A.; Burgess, B. K.; Armstrong, F. A. *Journal of the American Chemical Society* **1998**, *120*, 7085-7094.

60) Macevoy, J. *Unpublished Observation* **1998**.

61) Breton, J. L.; Duff, J. L. C.; Butt, J. N.; Armstrong, F. A.; George, S. J.; Petillot, Y.; Forest, E.; Schafer, G.; Thomson, A. J. *European Journal of Biochemistry* **1995**, *233*, 937-946.

62) Johnson, M. K.; Duin, E. *Unpublished Data* **1998**.

63) Peters, J. W.; Stowell, M. H. B.; Soltis, S. M.; Finnegan, M. G.; Johnson, M. K.; Rees, D. C. *Biochemistry* **1997**, *36*, 1181-1187.

64) Holden, H. M.; Jacobson, B. L.; Hurley, J. K.; Tollin, G.; Oh, B. H.; Skjeldal, L.; Chae, Y. K.; Cheng, H.; Xia, B.; Markley, J. L. *Journal of Bioenergetics and Biomembranes* **1994**, *26*, 67-88.

65) Armstrong, F. A.; Heering, H. A.; Hirst, J. *Chemical Society Reviews* **1997**, *26*, 169-179.

66) Mondal, M. S.; Goodin, D. B.; Armstrong, F. A. *J. Am. Chem. Soc.* **1998**, *120*, 6270-6276.

CHAPTER 6

REACTIONS OF THE FERREDOXIN FROM THE HYPERTHERMOPHILE *Pyrococcus furiosus*

CHAPTER 6

℘ REACTIONS OF THE FERREDOXIN FROM THE HYPERTHERMOPHILE *Pyrococcus furiosus*

6.1 INTRODUCTION

It has been shown earlier in this thesis (*Chapters 3*, *4* and *5*) that the ligands of FeS clusters (especially when different from cysteine) and the protein structure surrounding the cluster, are extremely important and influencing features of these biological clusters. As a reply to the diversity of clusters, many attempts have been made to mimic the range of FeS clusters by synthesising inorganic model compounds. These inorganic model compounds are useful in many ways, but are unable to reproduce or mimic the extrinsic factors of protein structure, or the interactions between more than one reaction centre (catalytic or redox). As a direct result of this, a common search amongst research workers in this area has been for a well-behaved protein model system. A frequently quoted example of a biological organism, which has been a source of several interesting and 'model' proteins, is the hyperthermophilic archaeon *Pyrococcus furiosus* (*Pf*).[1] This is a strict anaerobe which grows optimally at 100 °C by a fermentative mechanism in which H_2 and CO_2 are the only detectable products.[1] Many proteins have now been purified from this organism and a large number of these have been purified in order to compare them specifically with their mesophilic counterparts. The ultimate aim of this type of work is to identify features which are responsible for the remarkable thermostability of the proteins themselves. In addition, it is likely that understanding of

---

℘ The majority of this chapter is published in the *Biochemical Journal*, **1998**, Vol 335, pp 357-368

hyperthermostability may lead to an increased number of industrial applications for biological systems.

Pyrococcus furiosus contains a 4Fe ferredoxin, a monomeric protein of 66 amino acids (7.5 kDa),[2,3] which plays a central role in the primary metabolism of *Pf.* The ferredoxin is the electron acceptor for oxidoreductases involved in carbohydrate fermentation, including pyruvate ferredoxin oxidoreductase[4] and a novel tungsten-iron containing oxidoreductase.[5] Reduced ferredoxin is oxidised by ferredoxin:NADP oxidoreductase[6] and NADP serves as the electron donor to the H_2-evolving hydrogenase of *Pf.*[7] *Pf* ferredoxin is ideal to study as a model biological protein for a number of reasons:

1. The protein contains only one [4Fe-4S] cluster, and as such, potential complications from other clusters are avoided, e.g. unwanted spectroscopic contributions.

2. The ligating motif of the cluster is based upon that of a typical [4Fe-4S] cluster (see *Chapter 1*). However, like Fd III from *Desulfovibrio africanus* (*Chapter 3*), the second cysteine in the motif is replaced by aspartic acid (*Section 6.1.1*). It is known that incomplete cysteinyl ligation of a cubane cluster leads, in some cases, to a 4Fe cubane cluster which is able to undergo a reversible interconversion to a 3Fe cluster. The ferredoxin from *Pf* [2,3] is one such example, in that the cluster is readily and reversibly interconverted between the [4Fe-4S] and [3Fe-4S] forms.

3. The [3Fe-4S] cluster from *Pf* can also be converted to different [M3Fe-4S] forms, where M is a heterometal atom.[3,8-12] Thus, the differences in the physical and chemical characteristics of heterometal clusters can be examined.

4. The protein is from a hyperthermophilic organism and therefore it is useful to compare and contrast its reactivities with other similar clusters from non-hyperthermophilic organisms.

5. The Fd is present in a relatively high concentrations in the cells of *Pf* and is therefore easily obtained.

6.1.1 Structure and Reactivity

The amino acid sequence of *Pf* Fd contains five cysteine residues, three of which are involved in ligation of the cluster,

$$\mathbf{Cys^{11}\text{-}X_2\text{-}Asp^{14}\text{-}X_2\text{-}Cys^{17}\text{-}X_{38}\text{-}Cys^{56}}$$

There is well documented spectroscopic evidence indicating that the labile Fe in *Pf* Fd is co-ordinated by the aspartate residue.[13-15] As previously described (*Chapter 3*) there are other proteins with a similar amino acid sequence which also co-ordinate a cubane cluster, and where one of the ligands is an aspartic acid residue. One of the most remarkable features of aspartate ligation is the facile interconversion of the cubane 4Fe form to the 3Fe form of the FeS cluster. Following this, addition of other metals, M, can also be accomplished to give [M3Fe-4S] adducts. Metal cluster interconversions have been extensively examined for the 7Fe Fd from *Desulfovibrio africanus* Fd III[16-20] and also for *Desulfovibrio gigas* Fd II.[a] [22-25] Importantly it was noted that although aspartate co-ordination of an Fe atom is one of the determinants of 3Fe to 4Fe cluster conversion, this is not always the case e.g. *Sulfolobus acidocaldarius* Fd.[26]

It can be surmised that aspartate ligation has several consequences:

1. It labilises the cluster towards the release of the O-bound Fe[27] and subsequent binding of exogenous ligands.[28-30]

2. The reduced $[4Fe\text{-}4S]^{1+}$ clusters exist completely (*Da* Fd III) or partially (*Pf* Fd) in the unusual S = 3/2 spin ground state.[3,16]

3. The O-ligation (RCO_2^-) does not markedly alter the reduction potential relative to conventional all-cysteine (RS^-) ligated clusters.[31,32]

Although *Pf* ferredoxin is a simple example of a protein containing an interconvertable 4Fe/3Fe cluster, it additionally contains a disulfide bridge located in the region of the

---

[a] The [3Fe-4S] cluster of *Dg* Fd II is ligated by the cysteines at 8,14 and 50. The cysteine at position 11 was found to extend away from the cluster and is modified, most probably by a methanethiol group.[21]

amino acid sequence which would normally contain the second cluster in a 8Fe or 7Fe Fd (*Chapter 1*). The influence of this disulfide bridge upon redox characteristics or biochemical behaviour of the primary cluster is uncertain.[14,33] Samples of the Fd can be prepared which have the disulfide bridge intact (oxidised form - Fd_A) and broken (reduced form - Fd_B).[33] The notation Fd_A and Fd_B for the oxidised and reduced disulfide bridge, has been used previously in the literature by Gorst *et al*,[33] and is also used here. The ability of *Pf* Fd to interconvert between both the 3Fe and 4Fe forms means that in total there are eight different forms of the ferredoxin as shown in Figure 6.1.

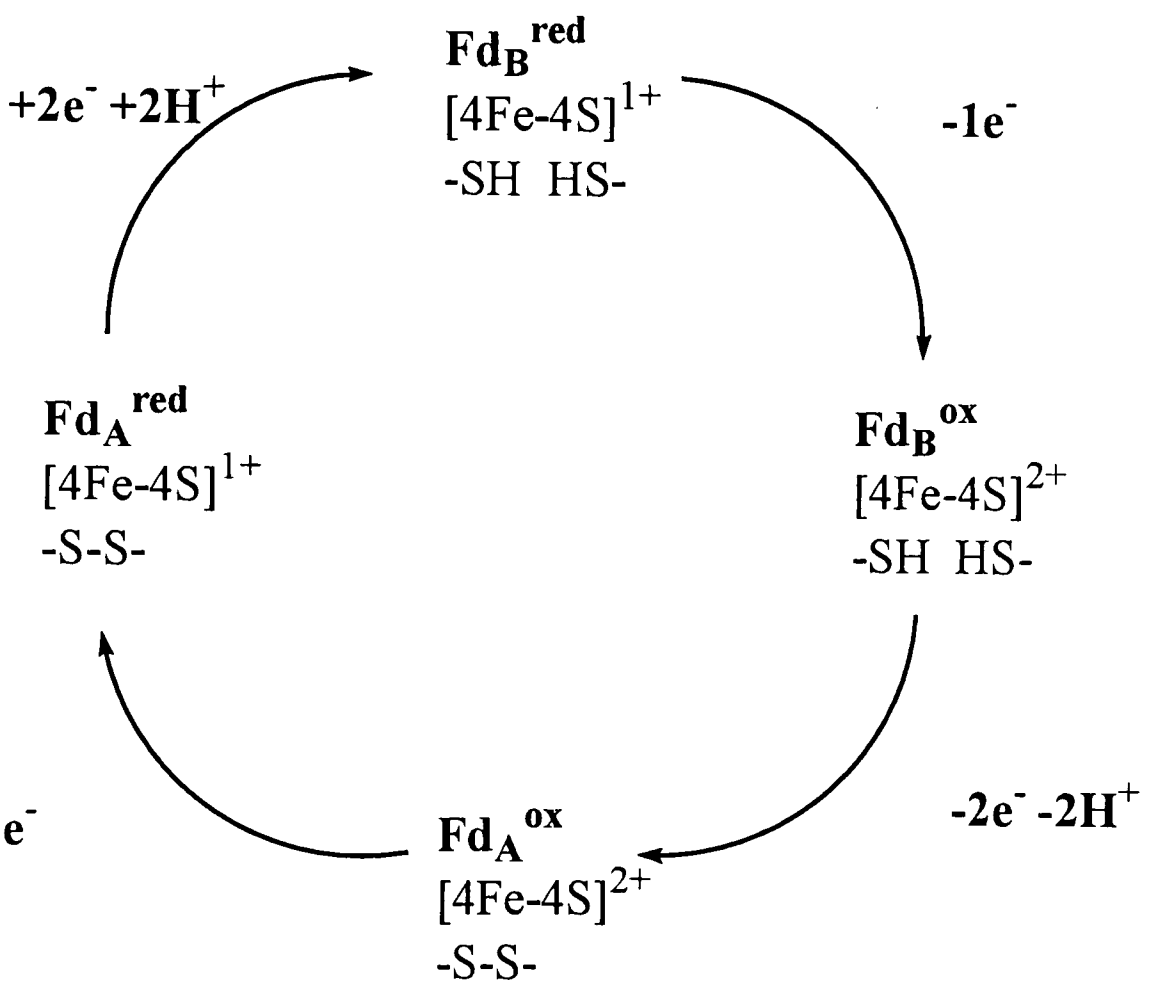

Figure 6.1 Proposed cycle for the redox states of *Pf* Fd (4Fe form)
*The $[4Fe\text{-}4S]^{2+/1+}$ could equally be replaced by the $[3Fe\text{-}4S]^{1+/0}$ cluster resulting in **eight** different redox states for the cluster in Pf Fd.*

The 3Fe clusters, [3Fe-4S], are able to exhibit a wide variety of different chemical and redox transformations compared to the less complex 2Fe and 4Fe clusters. Reactions of 3Fe clusters not only include electron transfer but also proton transfer (*Chapter 1*). The unusual $2e^-/2\text{-}3H^+$ coupled reaction, which results in the hyper-reduced state, $[3Fe\text{-}4S]^{2-}$, observed in some 3Fe ferredoxins, has only recently been identified and partially

characterised.[26,34,35] The likely reason this state has only recently been identified may be due to the potential of the $2e^-$ reaction being outside the boundaries of the traditional redox dyes normally used for EPR redox titrations - the usual method of measuring a biological reduction potential. Instead, the hyper-reduced state, $[3Fe\text{-}4S]^{2-}$, has been generated in bulk, under anaerobic conditions, using electrochemical methods and then studied spectroscopically. The best characterised example of the hyper-reduction of a [3Fe-4S] cluster is for the 7Fe Fd from *Sulfolobus acidocaldarius (Sa)*. This $[3Fe\text{-}4S]^{2-}$ species has been successfully generated in bulk solution and characterised by EPR and MCD.[34,35] Other examples of hyper-reduction of [3Fe-4S] clusters are known, but they have been observed only during adsorbed film experiments and only with proteins containing [3Fe-4S] clusters as part of a 7Fe Fd. If a protein such as *Pf* Fd, which contains only a single [3Fe-4S] cluster, can also undergo this reaction, then characterisation of the $[3Fe\text{-}4S]^{2-}$ state would be less complex, since it would be without the added spectroscopic complication of an additional [4Fe-4S] cluster, as is the case for 7Fe Fds.

6.1.2 Aims

This chapter focuses on using protein film voltammetry, in conjunction with other methods, to undertake an extensive study of the reactions of the Fd from *Pf*. Firstly, it was necessary to establish the complex pH-dependent redox chemistry of this ferredoxin - both in the 3Fe and 4Fe forms. Until now only [3Fe-4S] clusters from 7Fe Fds have been investigated for pH dependence.[b] Secondly, a comparison was undertaken of the thermodynamic characteristics and kinetics of reversible metal ion uptake and release for *Pf* with results from a recent study on *Desulfovibrio africanus* Fd III.[16-20] The metals chosen (M = Fe, Zn, Cd, Tl) bind to $[3Fe\text{-}4S]^0$ in *Da* Fd III and the products have been spectroscopically characterised in *Pf* Fd.[9-12] Hence, knowledge of the relationships existing between properties such as [M3Fe-4S] cluster stabilities and reduction potentials can be extended. Metal uptake experiments were also carried out for Fe^{2+} using spectrophotometry to record more detailed information about the solution kinetics, as opposed to the kinetics of metal uptake when the protein is adsorbed on the electrode.

[b] Very recently a study has been completed on the pH dependence of the [3Fe-4S] cluster and a number of site-directed mutants of *Pf* Fd.[36] The results of this study are compared to the results in this chapter in *Section 6.4.1*.

The influence of the disulfide bridge upon electrochemical and chemical reactivity has also been investigated. Finally the differences between bulk solution and film electrochemistry for this ferredoxin were investigated.

6.2 EXPERIMENTAL

General experimental procedures for the electrochemical experiments were as described in *Chapter 2*. Further details specific to the *Pf* Fd purification and the spectrophotometric experiments are described in the following sections.

6.2.1 Protein Purification

On completing the primary purification (*Chapter 2*) of *Pyrococcus furiosus* ferredoxin, the initial voltammetry obtained resembled that observed for a 7Fe Fd, i.e. three poorly resolved reduction couples were observed, at approximately -160, -350 and -690 mV. As it is known that *Pf* Fd is composed of only one cluster, which can interconvert between 4Fe and 3Fe forms, it was apparent that degradation of some clusters had occurred, and that the protein sample was a mixture of both [3Fe-4S] and [4Fe-4S] Fds. Hence the similarity to the voltammetry of a 7Fe Fd, although the stoichiometry would be expected to be variable. Typical voltammetry of a 7Fe Fd shows three redox couples, A', B' and C' corresponding to the $[3Fe\text{-}4S]^{1+/0}$, $[4Fe\text{-}4S]^{2+/1+}$ and $[3Fe\text{-}4S]^{0/2-}$ states, with integrations ideally in ratios 1:1:2.[35] This partial degradation of the *Pf* Fd sample was to be expected[3] due to the primary purification taking place under aerobic conditions, because of practical limitations.

A secondary purification step, using FPLC with a Mono-Q column (*Chapter 2*) was carried out on this sample, and two major fractions were collected. On the basis of their UV/Vis spectra, Fraction 1 (λ_{max} = 390 nm) and Fraction 2 (λ_{max} = 408 nm) were deduced to comprise, respectively, the [4Fe-4S] and [3Fe-4S] forms of the ferredoxin. Approximately 60 % of the 4Fe clusters had degraded to the 3Fe form as a direct result of aerobic purification. Protein concentrations were calculated using ε_{390} = 17, 000 and ε_{408} = 18, 000 M^{-1} cm^{-1} for the 4Fe and 3Fe forms respectively.[3]

The need for sample homogeneity prior to starting experiments meant that all subsequent samples of the Fd had to be purified by FPLC. After chemical oxidation with a five-fold molar excess of ferricyanide for 30 minutes at 60 °C, the major fraction recovered was the 3Fe Fd_A. This method of bulk oxidation of the sample thus ensured that ca. 95 % of the protein sample applied to the Mono-Q column was already 3Fe Fd_A. Additional

peaks, (ca. 5 %) when examined by UV/Vis spectroscopy, were found to be non-coloured and were likely to be apoprotein. All subsequent manipulations began with $[3Fe\text{-}4S]_A$.

6.2.2 Determination of Disulfide Bridge Status

Disulfide bridge status was determined spectrophotometrically by the reaction of free thiol groups in the protein with 5,5'-dithio*bis*(2-nitrobenzoic acid) (DTNB).[37] The protocol used is described in *Chapter 2*. A typical titration of the protein with the disulfide bridge broken, Fd_B, gave a free thiol content of 2 ± 0.1 moles per protein molecule, and samples of Fd_A did not show any reactivity when the reagent was added.

It was found that once the two forms, Fd_A or Fd_B, were prepared and identified, the rate of interchange between the disulfide bridge oxidised or reduced form was negligible throughout the course of the experiments. This was checked by additional titrations on protein samples, where possible, after an experiment. All experiments were carried out anaerobically, under which conditions the Fd_B form would be unlikely to oxidise.

6.2.3 Interconversion Between the Four Redox States

To generate the 3Fe Fd_B form of the ferredoxin, a sample of 3Fe Fd_A was incubated for a minimum of 48 hours with a 5-fold molar excess of dithiothreitol, at 25 °C, in an anaerobic glovebox (O_2 < 2ppm). The protein was then extensively dialysed into a buffer containing 50 mM Tris, pH 7.4, 0.1 M NaCl, 100 μM EGTA.

To generate the 4Fe Fd_A, a sample of 3Fe Fd_A was incubated with a 5 fold excess of sodium dithionite and a 5 fold excess of Fe^{2+} for approximately 15 minutes under anaerobic conditions, the sample was then extensively dialysed into buffer as above. It was important to check that incubation with dithionite and Fe^{2+}, for these time periods, did not reduce the disulfide bond and this was verified by a DTNB titration.

The 4Fe Fd_B was produced by incubating 3Fe Fd_B with sodium dithionite and Fe^{2+} as for 4Fe Fd_A. A summary of these interconversions is shown schematically in Figure 6.2.

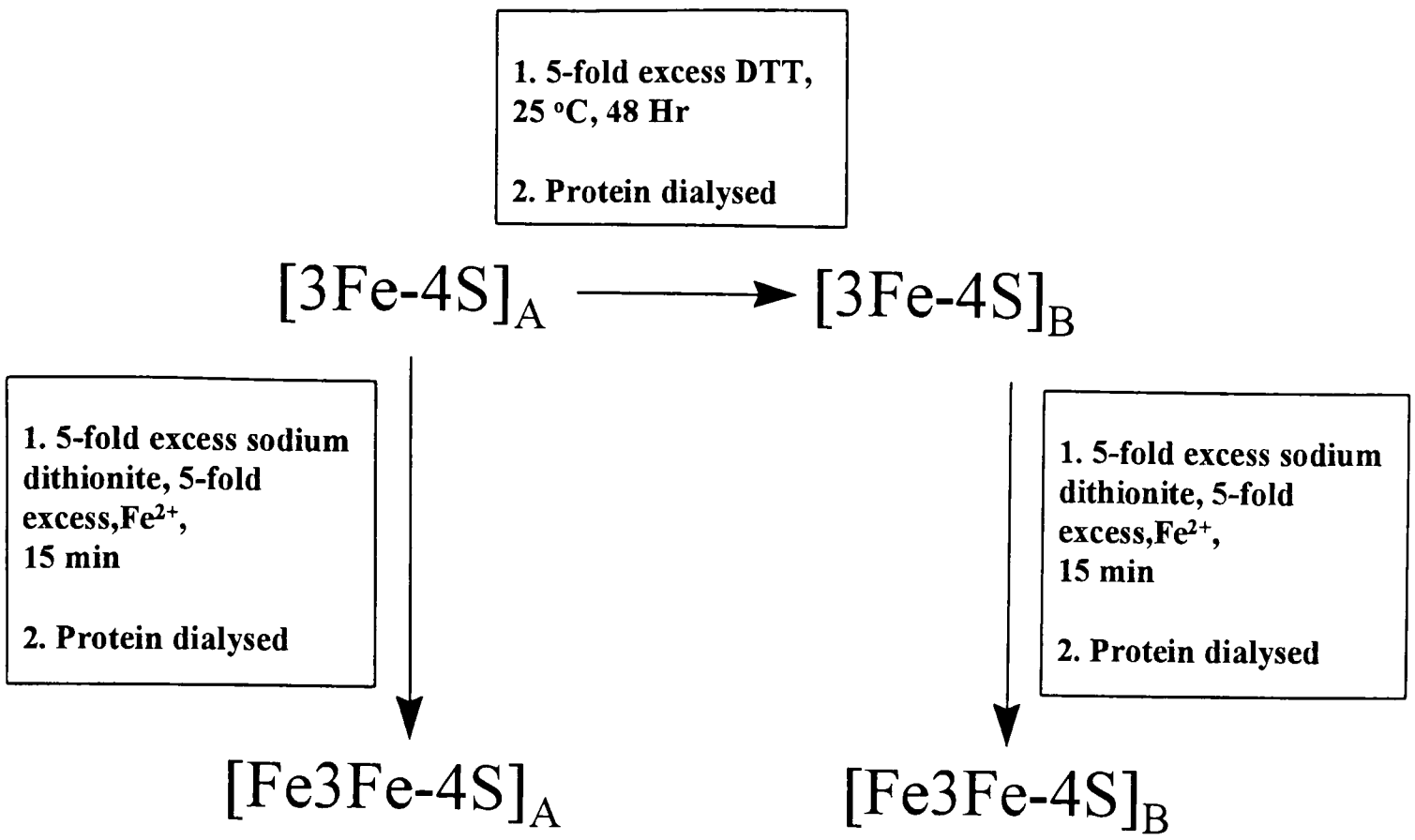

Figure 6.2 Schematic representation of 3Fe/4Fe and disulfide bridge interconversions for *Pf* Fd

6.2.4 Spectrophotometric Observation of Fe Uptake by [3Fe-4S]

An alternative method to protein film voltammetry, used to observe the uptake of Fe^{2+} into the [3Fe-4S] cluster, is spectrophotometric solution kinetics. The experiments were carried out in an anaerobic glovebox using a spectrometer cell-block and linked by fibre-optic cables to a MG-6000 diode-array spectrometer unit (Hi-Tech Scientific, Salisbury, UK). A solution of the [3Fe-4S] protein was placed in a cuvette, under anaerobic conditions, and the UV/Vis spectrum recorded. The protein was then reduced, by the addition of dithionite in the presence of methyl viologen, and the subsequent spectrum of the reduced protein was recorded. An aliquot of Fe^{2+} solution was then added to the cuvette and the resultant spectral changes were recorded. The theory of these experiments depends on an important assumption, that the rate of metal uptake is the only *rate determining* step: as shown in Figure 6.3. To confirm that this was the case it was important to ensure that the reduction of the product, the $[Fe3Fe\text{-}4S]^{2+}$ cluster, was fast.

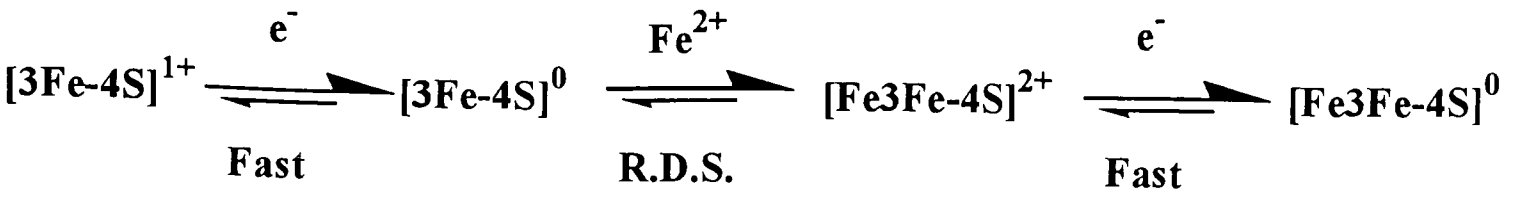

Figure 6.3 Schematic addition of Fe^{2+} to [3Fe-4S]

Optimisation

Although the rate of the reduction of the [3Fe-4S] cluster was not important, as this was a preliminary stage to the experiment, it was essential that complete reduction had occurred before the experiment was initiated. If the sodium dithionite was not sufficient to reduce the [3Fe-4S] cluster, it followed that there would be no excess available to reduce the $[4Fe\text{-}4S]^{2+}$ cluster when formed. Checks were therefore made on the rate of reduction of the [3Fe-4S] cluster and it was found that an excess of sodium dithionite was not sufficient to reduce the cluster in any reasonable time. Quantities of up to 20-fold excess of dithionite were added to the [3Fe-4S] cluster and the reduction was not instantaneous - the reduction took ca. 5 minutes to go to completion. As a result it was decided to use methyl viologen as a catalyst to aid the reduction of the cluster.

Sodium dithionite is known to reduce methyl viologen, generating the radical of methyl viologen, and this radical acts as a mediator in the reduction of the $[3Fe\text{-}4S]^{1+}$ cluster. Reduced methyl viologen has a very characteristic absorption spectrum including a λ_{max} at 604 nm (ε_{604} = 13,600 M^{-1} cm^{-1}), but this was not found to hinder the spectroscopic experiment, as the amount of methyl viologen required to catalyse the reduction of the protein was only 1 μM. A final concentration of 1 μM methyl viologen and 1 mM sodium dithionite in the spectroscopic cell caused instantaneous reduction of the $[3Fe\text{-}4S]^{1+}$ protein - i.e. bleaching of the brown ferredoxin colour was immediately visible upon addition of the methyl viologen to the protein and sodium dithionite solution. Checks were made to ensure that when the reduction of the $[3Fe\text{-}4S]^{1+}$ cluster was performed it did not also reduce the disulfide bridge of the $[3Fe\text{-}4S]_A$ form, when the Fe^{2+} uptake of this form was being investigated.

The sequence of additions to the protein solution, in order to observe the addition of Fe^{2+} to the clusters, was as follows:

1. Record spectrum of 3Fe Fd_A (typically 200 µl of 25 µM protein)
2. Add 1.5 µl of 70 mM sodium dithionite (ca. 20 fold excess)
3. Add 1 µl of 200 µM methyl viologen solution (final concentration approximately 1 µM)
4. Add a known aliquot of Fe^{2+} (typical volume 2 µl, concentration varied with experiment), stir solution in cuvette.
5. Simultaneously record a spectrum (300 nm to 600 nm) and start stopwatch, recording spectra at regular time intervals. The intermediate time between spectra measurements depended upon the amount of Fe added, i.e. rate of reaction.

6.3 RESULTS

6.3.1 Protein film voltammetry

Protein film voltammetry was carried out as described in *Chapter 2*, on both the 3Fe and 4Fe forms, with the disulfide bridge either oxidised or reduced using polymyxin as a co-adsorbate.

The $[4Fe\text{-}4S]_A$ form shows a single signal (a pair of oxidation and reduction waves) with $E^{o'} = -428 \pm 5$ mV at pH 7.0. The $[3Fe\text{-}4S]_A$ form shows two signals (two pairs of oxidation and reduction waves) which is the characteristic voltammetric pattern observed for other proteins containing the [3Fe-4S] cluster (Figure 6.4).[26,34,35] The higher potential couple, is denoted A', and the narrow, more intense signal at lower potential is denoted C'. Signal A' has a reduction potential with $E^{o'} = -150 \pm 5$ mV at pH 7.0, and is assigned to the redox couple $[3Fe\text{-}4S]^{1+/0}$, the value being similar to that reported by Adams and co-workers.[2,11] Signal C' has a reduction potential $E^{o'} = -695 \pm 5$ mV at pH 7.0. Integration of the areas under signals A' and C' gave C'/A' ratios of 2.0 ± 0.3 for all samples examined. By analogy with recent studies[35] on [3Fe-4S] clusters in several other proteins, signal C' is therefore assigned to the novel proton-linked two-electron redox couple $[3Fe\text{-}4S]^{0/2-}$. All the voltammetric waves observed in these two forms of the protein were broader than had previously been found for other ferredoxins, even at the slowest scan rates, thus suggesting dispersion arising from some inhomogeneity in the adsorbed sample. Voltammograms of both the 3Fe and 4Fe clusters are shown in Figure 6.4.

Analogous experiments were carried out on samples in which the disulfide bridge was reduced (Fd_B). The results were essentially indistinguishable. For $[3Fe\text{-}4S]_B$, also at pH 7.0, signal A' has $E^{o'} = -159 \pm 5$ mV and signal C' has $E^{o'} = -714 \pm 5$ mV. The $[4Fe\text{-}4S]_B$ form has a reduction potential of $E^{o'} = -428 \pm 5$ mV.

A number of investigations have been previously carried out upon the ferredoxin from *Pf*. The vast majority of these have been concerned with the characterisation of this protein by EPR and NMR spectroscopy, together with MCD. Only one report on the direct electrochemistry of this protein has been published.[38] In that experiment, direct

electrochemistry was achieved using differential pulse voltammetry, together with a temperature controlled cell, with pyrolytic graphite as the working electrode (sample volumes of either 250 µl or 25 µl). The authors reported the reduction potential of the $[4Fe\text{-}4S]^{2+/1+}$ cluster as -370 mV and that of the $[3Fe\text{-}4S]^{1+/0}$ cluster[c] as -190 mV. An additional signal was observed at -700 mV for the [3Fe-4S] cluster which was tentatively assigned to a one-electron reduction: $[3Fe\text{-}4S]^{0/1-}$ (based merely upon the observed half height peak width).

[c] Some confusion was evident as to the use of co-adsorbates: neomycin (1 mM) was only required for observing the signal of the $[3Fe\text{-}4S]^{1+/0}$ cluster and not for the $[4Fe\text{-}4S]^{2+/1+}$ cluster.[38]

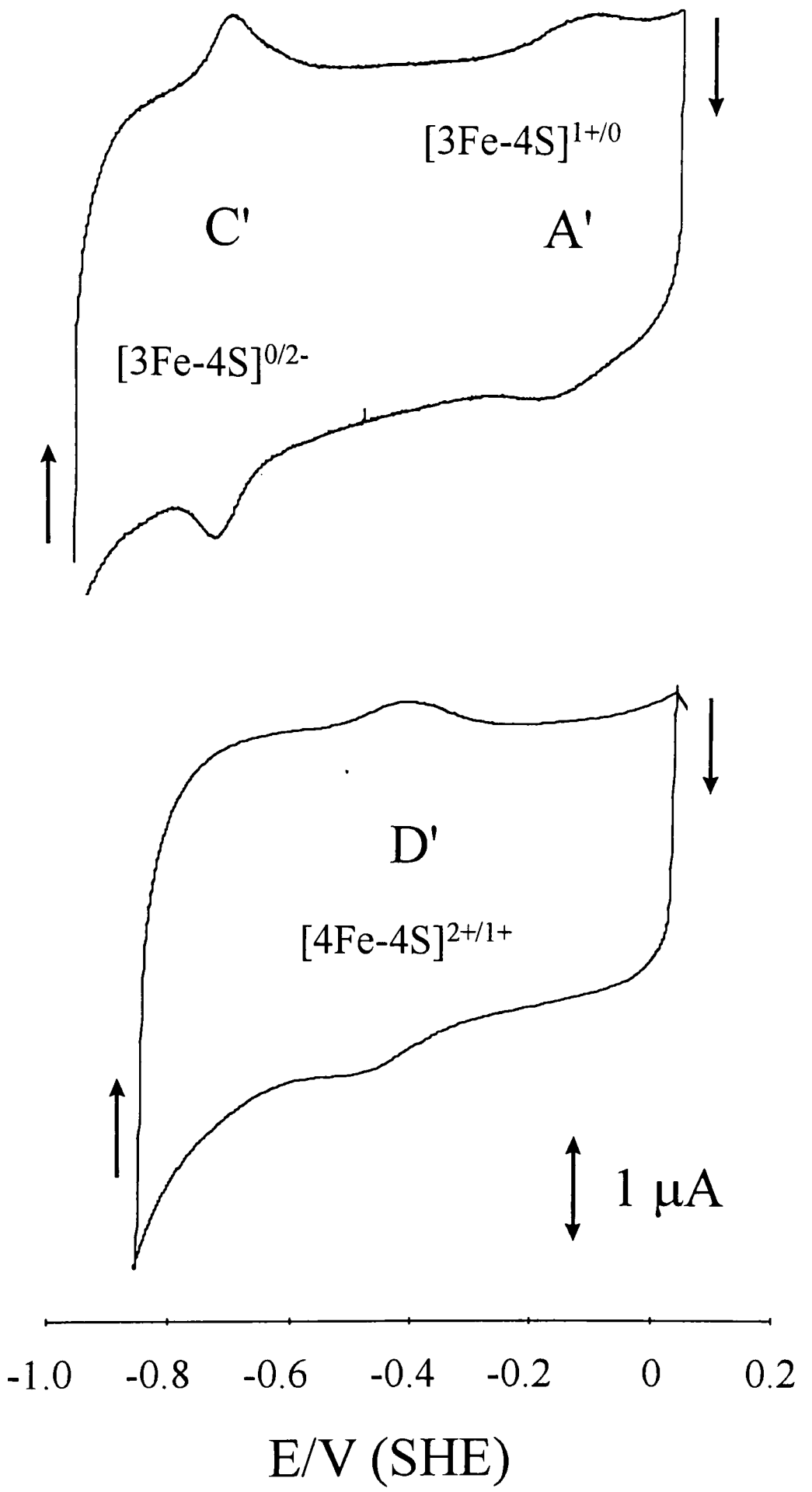

Figure 6.4 Film voltammograms of the 3Fe Fd_A and 4Fe Fd_A forms of *Pyrococcus furiosus* Fd

20 mM mixed buffer, 0.1 M NaCl, pH 7.0, 0 °C, scan rate 50 mV s^{-1}, 200 μg ml^{-1} polymyxin as co-adsorbate. A', D' and C' are the film adsorbed reduction couples $[3Fe\text{-}4S]^{1+/0}$, $[4Fe\text{-}4S]^{2+/1+}$ and $[3Fe\text{-}4S]^{0/2-}$ respectively.

6.3.2 Bulk Solution Voltammetry

Bulk voltammetry was carried out at 0 °C, pH 7.4, 20 mM Hepes, 0.1 M NaCl, on both the 4Fe and 3Fe forms of the protein, either Fd_A and Fd_B, at concentrations of typically 50 - 100 μM. The reduction potential for the $[3Fe\text{-}4S]^{1+/0}$ cluster was -215 ± 10 mV for the 3Fe Fd_A form and -219 ± 10 mV for the 3Fe Fd_B form. These reduction potentials are 60 - 65 mV more negative than the values obtained from direct adsorbed film voltammetry. The low-potential (C) couple in the potential region expected for $[3Fe\text{-}4S]^{0/2-}$ (i.e. corresponding to signal C' for the film) appeared only at very slow scan rates (2 mV s^{-1}) and was always much more prominent on the first scan. On successive cycles the oxidative wave (C) was attenuated (as can be seen in Figure 6.5) and the reduction wave gradually disappeared. The reduction potentials for the $[4Fe\text{-}4S]_A$ and $[4Fe\text{-}4S]_B$ clusters were -361 ± 10 mV and -365 ± 10 mV respectively when measured using bulk solution voltammetry. This is ca. 65 mV more *positive* than the reduction potential obtained from film experiments. A summary of film and bulk solution experiments is shown in Table 6.1.

	Disulfide Bridge Oxidised (Fd_A)		**Disulfide Bridge Reduced (Fd_B)**	
	Film	**Bulk**	**Film**	**Bulk**
$[3Fe\text{-}4S]^{1+/0}$	-150	-215	-159	-219
$[3Fe\text{-}4S]^{0/2-}$	-713	-718	-714	-711
$[Fe3Fe\text{-}4S]^{2+/1+}$	-430	-361	-428	-365

Table 6.1 Reduction potentials of 3Fe and 4Fe clusters in *Pyrococcus furiosus* Fd

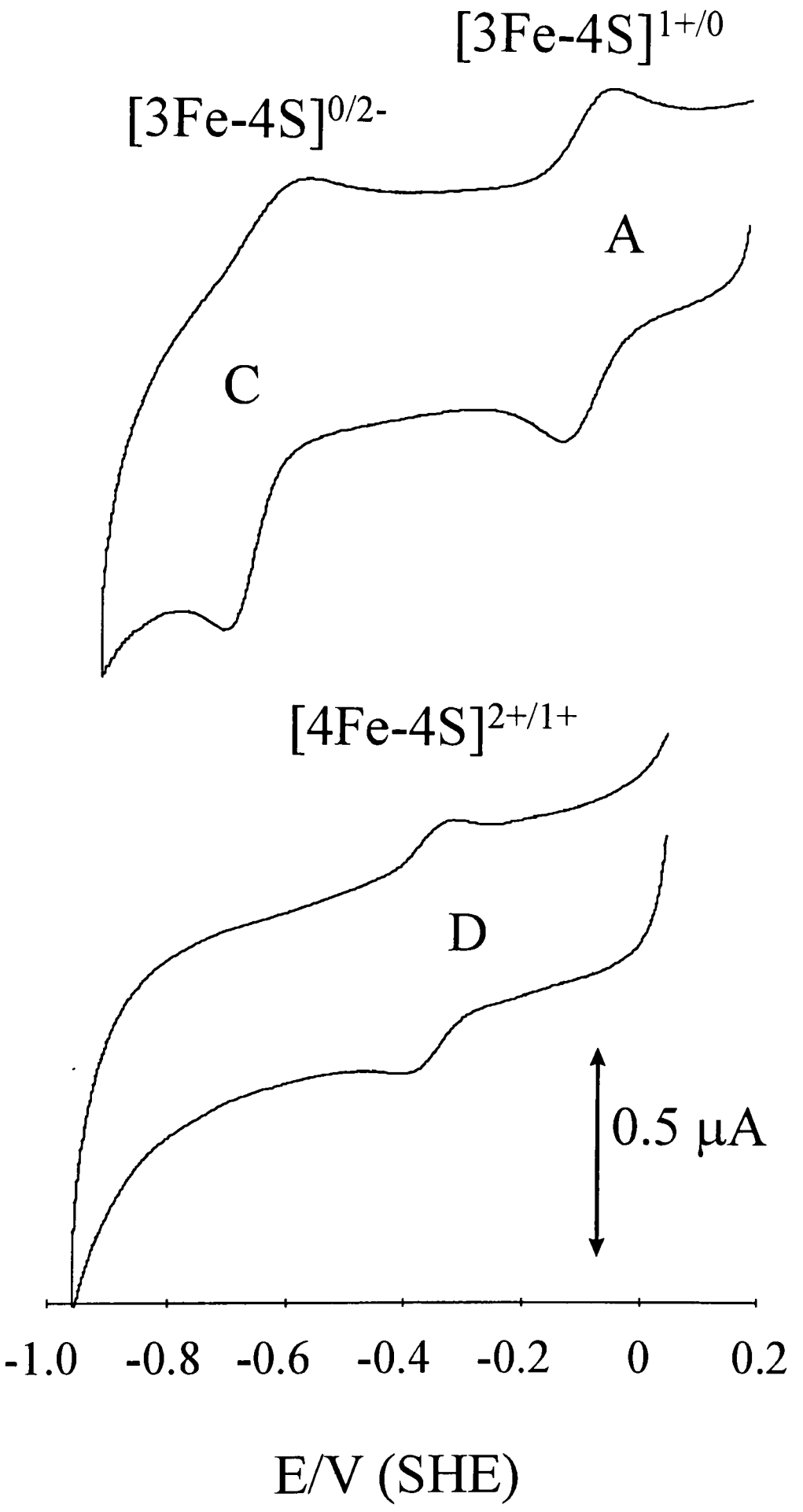

Figure 6.5 Bulk voltammograms of the 3Fe Fd_A and 4Fe Fd_A forms of *Pyrococcus furiosus* Fd

Protein concentrations of 42 μM and 40 μM respectively, at pH 7.4, 20 mM Hepes, 0.1 M NaCl, 0.1 mM EGTA, 2 mM neomycin, 0 °C. Scan rate 2 mV s^{-1}.

6.3.3 pH Dependence

By transferring an adsorbed film of the protein between solutions of differing pH, the pH dependence of the reduction potentials for signals A', D' and C', could be directly observed. This is an extremely rapid and efficient method of recording the pH dependence of a redox couple. Extreme pH conditions, otherwise inaccessible with conventional experimental methods, can be investigated using this method - in this case as low as pH 1.7. Thus numerous data points were obtained, to enable a thorough examination of the pH dependence profile of all three redox couples.

The reduction potentials of both forms of the 4Fe Fd, i.e. $[4Fe\text{-}4S]_A$ and $[4Fe\text{-}4S]_B$, were virtually pH independent over the pH range 2.5 - 9.0, the variation was < 40 mV over this range. Data for the $[4Fe\text{-}4S]_A$ form are plotted in Figure 6.7.

The reduction potentials of the A' and C' couples from the $[3Fe\text{-}4S]_A$ and $[3Fe\text{-}4S]_B$ forms were highly dependent upon pH, with the pH dependence of either the disulfide bridge oxidised or reduced forms of the 3Fe Fd being identical. It was found that the A' couple varied by ~ 180 mV and the C' couple varied ~ 450 mV over the pH range 2 - 8. Figure 6.6 shows the excellent voltammetry which is observed at pH values as low as 2.7. It can be clearly seen (Figure 6.7) that the C' couple is *more* dependent upon pH (i.e. a greater positive shift is observed as the pH is increased) than the A' couple. Data for the 3Fe Fd_A or the 3Fe Fd_B forms have been labelled accordingly.

Considering the A' couple: in Figure 6.7 there is a well-defined region corresponding to protonation of the reduced form, but it is not possible to fit the curve to a simple scheme involving a single pK. There is clearly a pK_{red} at approximately pH 7, but the slope of the best *straight* line extending to the acid region is much less than predicted for a $1H^+/1e^-$ reaction, thus the pH properties of couple A' are complex. The best fit to the data for couple A' was obtained using Equation 6.1.

$$E^{o\prime} = E^{o\prime}_{alk} + \frac{RT}{nF} \ln \left[\frac{\left(a_{H^+}\right)^2 + \left(a_{H^+}\right)K_{red1} + K_{red1}K_{red2}}{\left(a_{H^+}\right) + K_{ox}} \right] \quad \textbf{Equation 6.1}$$

In Equation 6.1, $E^{o'}_{alk}$ is the reduction potential in the limit of high pH, a_{H^+} is the H^+ activity, n is the number of electrons transferred, y is the number of protons transferred, and K_{red2}, K_{ox} and K_{red1} are successive H^+-dissociation constants of reduced and oxidised species, appearing as the pH is decreased. In Figure 6.7, the corresponding line obtained for couple C' appears to mirror that for couple A', with the steeper portions approximately coinciding with the shallower sections of the couple A' line and *vice versa* of C'. It was found that data above pH 8.0 were less reliable because the peak size and reversibility were diminished.

The overall proton uptake for the A' and C' couples was determined in the same way as previously carried out for the 7Fe ferredoxins from *Desulfovibrio africanus*, *Sulfolobus acidocaldarius* and *Azotobacter vinelandii*.[35] The total H^+/e^- ratio was found by calculating (2A' + C')/3 for each point in the acidic/slightly neutral range of the graph, and this was then plotted as a function of pH. The gradient of this line is $(dE^{o'}/dpH)_{av}$ and for *Pf* Fd this value is 51.9. This is close to what would be expected for the case when the net ratio H^+/e^- is close to 1.0, the theoretical value is -54.2 mV/pH unit at 0 °C. This demonstrates that an overall uptake of $3H^+$ accompanies the 3-electron reduction of the $[3Fe\text{-}4S]^{1+}$ cluster.

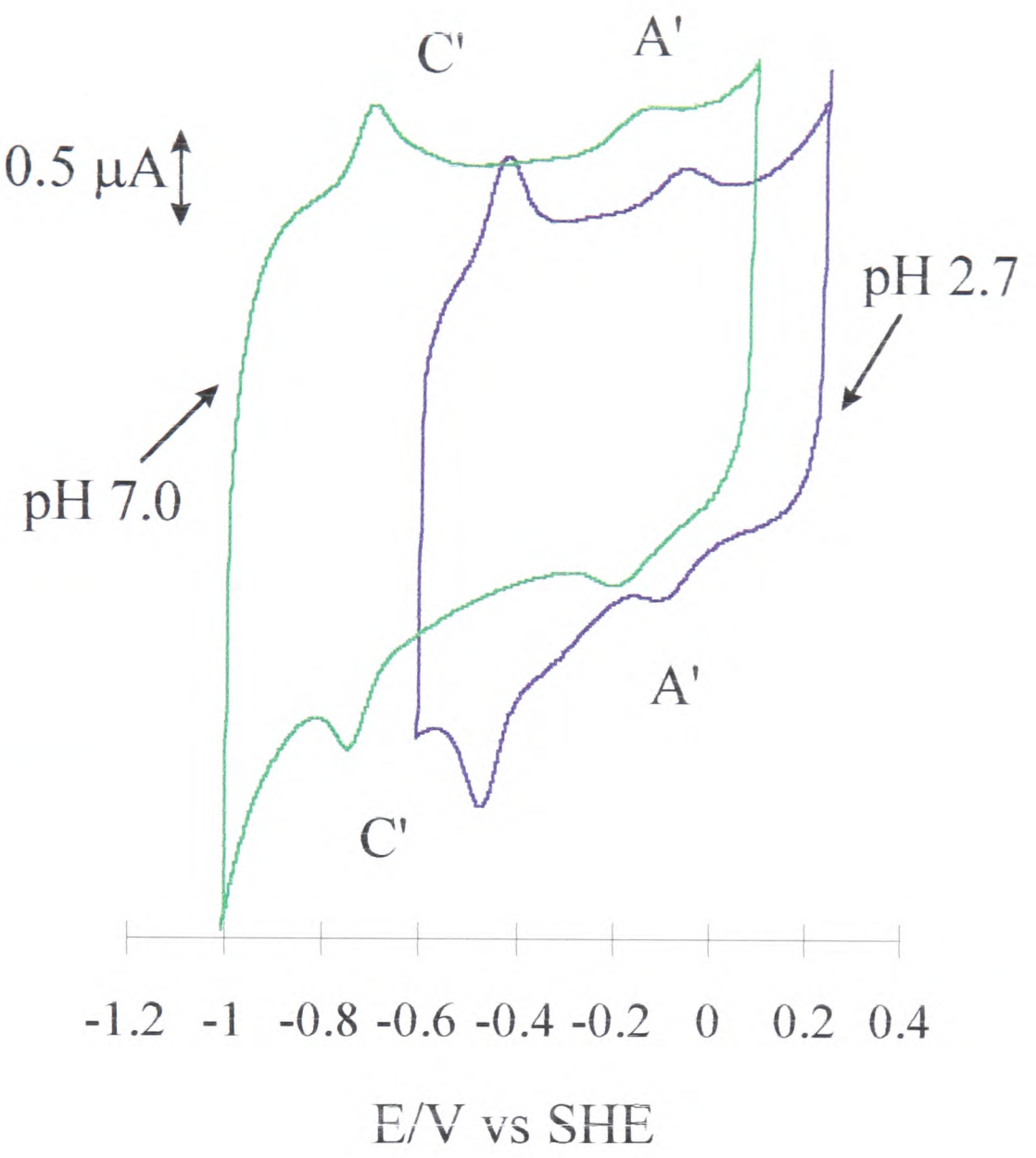

Figure 6.6 Voltammograms showing the pH dependence of the $[3Fe\text{-}4S]_A$ cluster from *Pyrococcus furiosus* Fd

20 mM mixed buffer, 0.1 M NaCl, 100 μM EGTA, 0 °C, scan rate 50 mV s^{-1}, 200 μg ml^{-1} polymyxin as co-adsorbate, pH as denoted above.

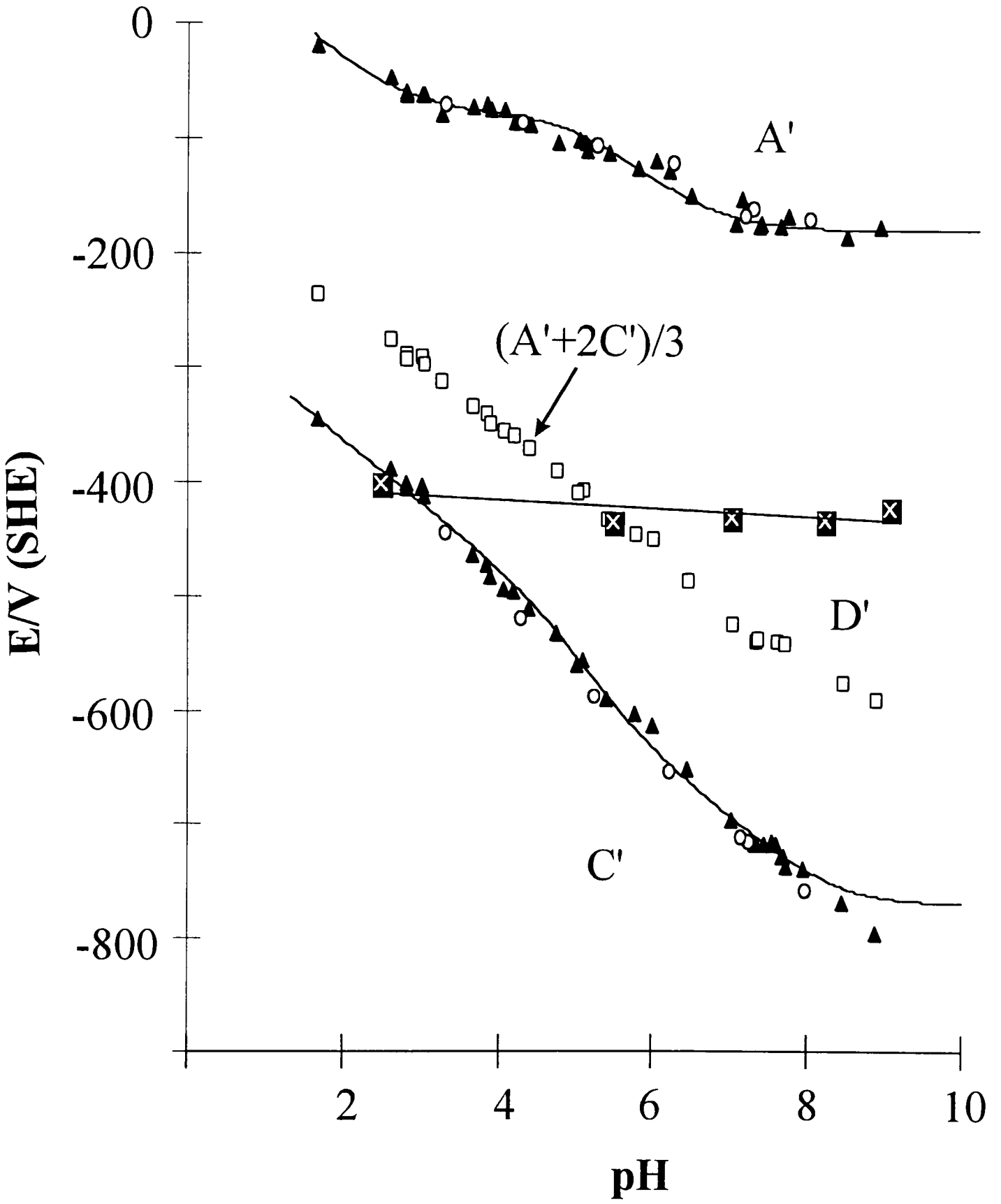

Figure 6.7 The pH dependence of reduction potentials for the Fd from *Pyrococcus furiosus*

Data obtained by adsorbed film electrochemistry using 20 mM mixed buffer, 0.1 M NaCl, co-adsorbate 200 μg ml^{-1} polymyxin, 0 °C. Closed triangles are data for the $[3Fe\text{-}4S]_A$ form, open circles are data for the $[3Fe\text{-}4S]_B$ form. Filled squares with crosses are data for the $[4Fe\text{-}4S]_A$ form. The open squares show the weighted average of the A' and C' couples to give the overall number of protons per electron for the three electron reduction of $[3Fe\text{-}4S]^{1+}$.

6.3.4 MCD[d]

The MCD spectra of the dithionite reduced *Pf* Fd $[3Fe\text{-}4S]^0$ cluster were recorded in the pH range 1.0 to 8.25. Partial cluster loss occurred at the more acidic pH values, resulting in some uncertainty in the final concentration, and, therefore, in the final calculated intensity of the spectra. To compensate for this, the samples were reoxidized after the MCD spectra were recorded, and the final cluster concentration was determined again by UV/Vis spectroscopy. At least 50 % of the clusters were still present after 15 minutes incubation at pH 1.0, thus confirming the extreme resistance of *Pf* Fd under acidic conditions.

The MCD spectrum of $[3Fe\text{-}4S]^0$ *Pf* Fd prepared at various pH values, is shown in Figure 6.8. The spectrum at pH 8.25 is essentially identical to the spectrum reported by Conover *et al.*[3,12] This spectrum is characteristic of the $[3Fe\text{-}4S]^0$ cluster, having a $S = 2$ ground spin state with negative axial zero-field splitting.[39] It is very intense ($\Delta\varepsilon_{max} \approx$ 250-300 $M^{-1}cm^{-1}$ at 1.6 K and 5 Tesla), with characteristic positive peaks around 370 nm, 445 nm and 700 nm, and a crossover at 550 nm. The EPR spectrum of the sample, at low field, showed only a broad trough (g = '12' signal). The MCD spectrum undergoes a continuous series of changes as the pH is lowered, and at pH 3.0 the pattern of transitions is similar to the 'acid form' observed for other ferredoxins containing a protonated 3Fe cluster. Shown in Figure 6.9 are spectra for *Azotobacter chroococcum* Fd (pK_{red} = 7.8 [40,41]) and *Sulfolobus acidocaldarius* Fd (pK_{red} = 5.8 [34]) while the spectrum of *Azotobacter vinelandii* Ferredoxin I (pK_{red} = 7.8 [42] is identical to that of *Azotobacter chroococcum*. Another spectrum of *Pf* Fd was recorded at pH 1.0 and although this suffered extensive cluster destruction, the characteristic peak-to-trough distance (400 to 450 nm) was similar to that of the pH 3.0 sample. Thus the pK for protonation of the reduced $[3Fe\text{-}4S]^0$ cluster of *Pf* Fd in bulk solution lies in the region of 3 - 4, and probably coincides with pK_{red1} as determined by protein film voltammetry, although comparisons between samples at 4.2 K in glycerol/buffer solution and protein films are difficult to make. The spectrum divides into two parts, with two sets of positive MCD bands ($\Delta\varepsilon_{max} \approx 200\ M^{-1}cm^{-1}$ at 1.6 K and 5 Tesla) separated by a trough at 450 nm in the 300 to 550 nm region, and less intense transitions at lower energy (550 nm

[d] EPR spectra were recorded as a diagnostic tool, prior to carrying out MCD spectra.

to 850 nm). Comparisons of the spectra of the three ferredoxins in this region show that upon protonation of the cluster the intense 710 nm band splits into several less intense constituents with positive signs. There is some spectral variability among the different ferredoxins, although this may be due to the difficulty of determining the cluster concentration at the very acid pH values required for the experiment.

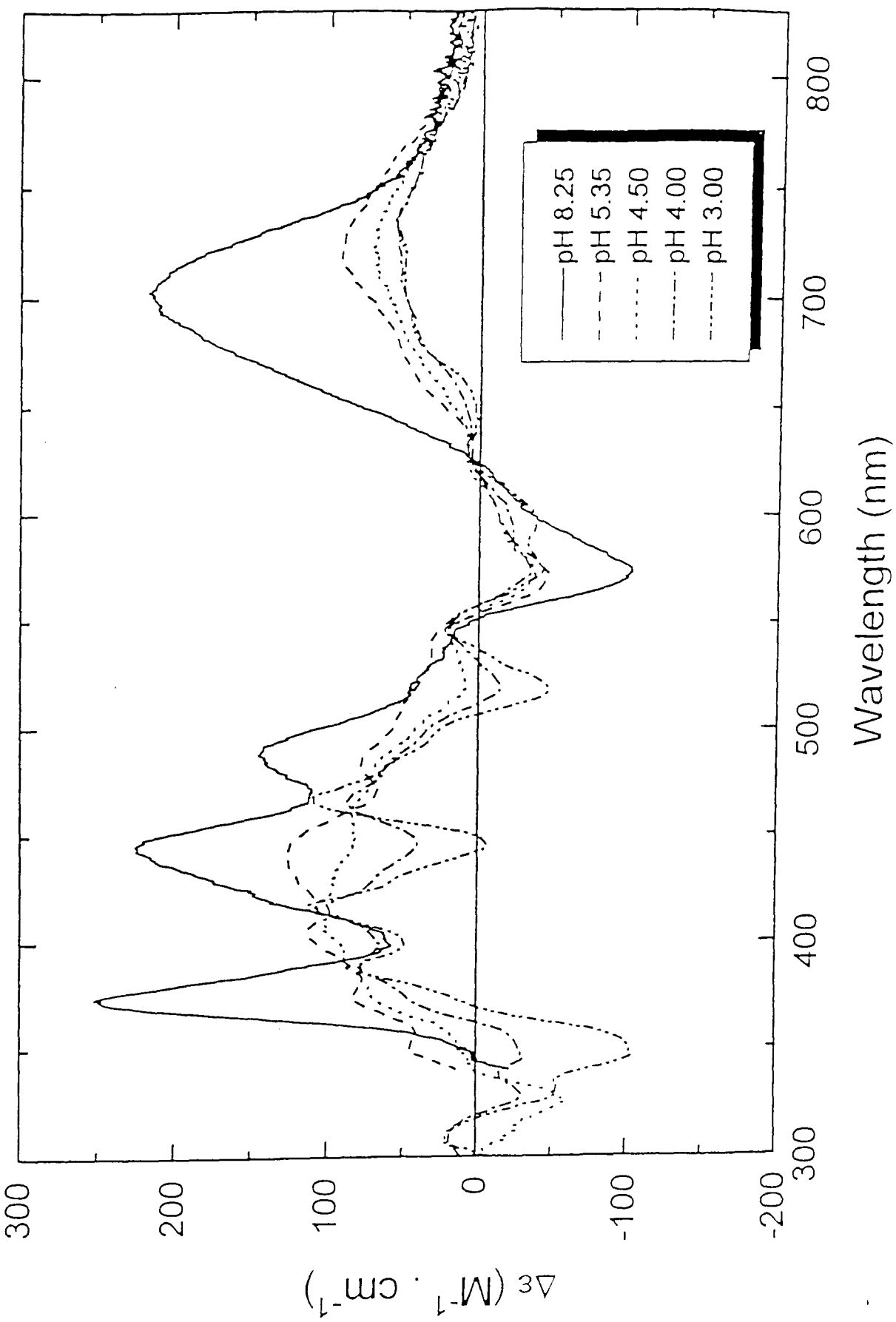

Figure 6.8 Low-temperature MCD spectra of *Pyrococcus furiosus* [3Fe-4S]^0 Fd at various pH values

Ferredoxin concentrations were 150-200 μM in 50 % (vol/vol) glycerol/water, containing 40 mM acetate, and 0.4 mM EDTA. The spectra were measured at a temperature of 1.6 K and magnetic field 5 Tesla, pathlength 1 mm.

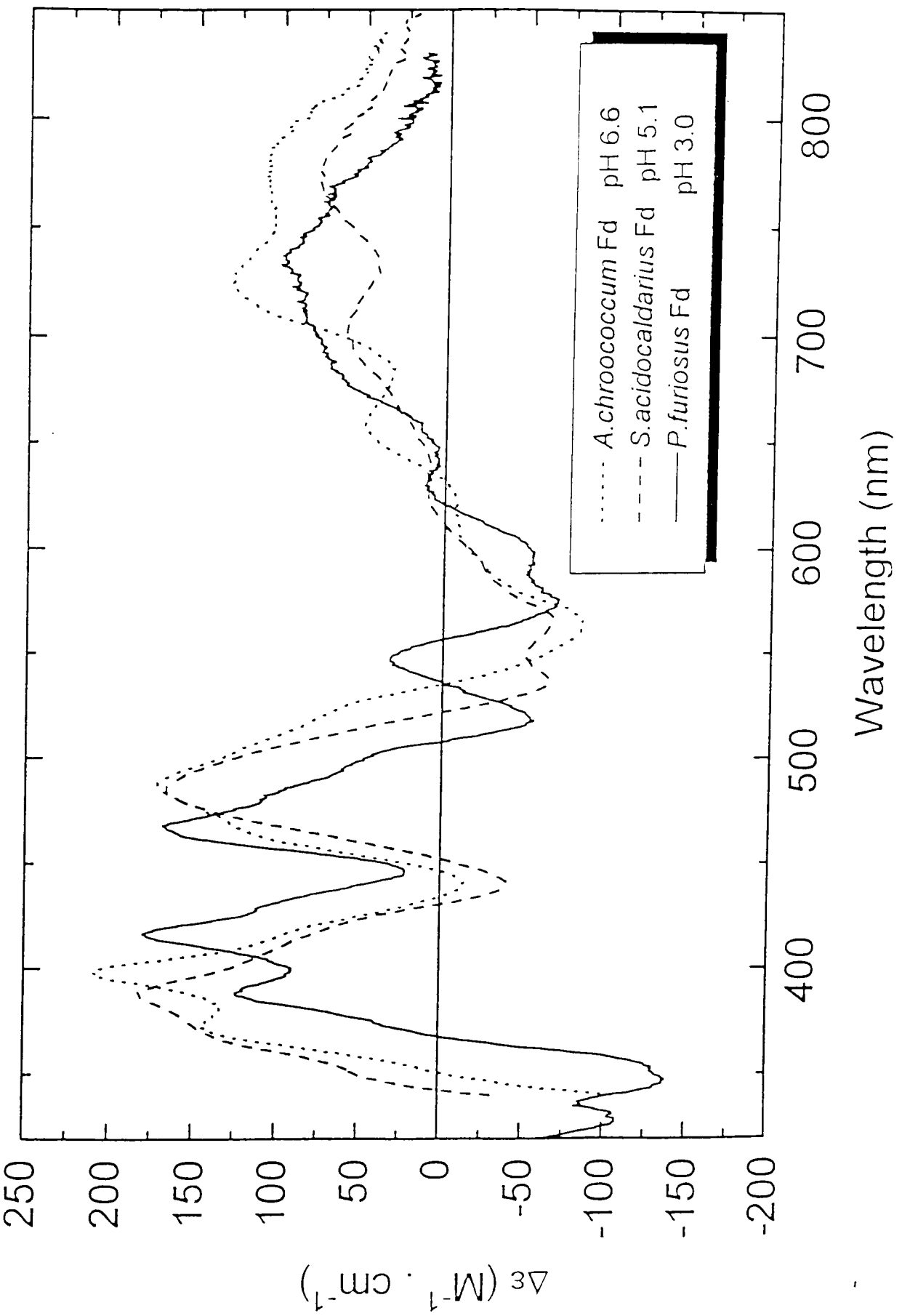

Figure 6.9 Comparison of the MCD spectra of the acid form of three Fds at low temperature

Pyrococcus furiosus [3Fe-4S]^{0} ferredoxin (------) with Azotobacter chroococcum Fd (·····) and Sulfolobus acidocaldarius Fd (- - - -). Spectra were measured at 4.2 K and 5 Tesla. The spectrum of Pf Fd has been multiplied by 2.0 to normalise the comparison with the other two spectra (Sa Fd spectrum taken from Breton et al, (1995)[34]Ac Fd spectrum taken from George et al, (1984).[40]

6.3.5 Metal Uptake[e]

Three different methods were used to study the conversion of the [3Fe-4S] cluster to [M3Fe-4S], as shown schematically below:

$$[3Fe\text{-}4S]^{1+} + 1e^- + M^{2+} \longrightarrow [M3Fe\text{-}4S]^{2+}$$

Method 1: The first method was similar to that carried out by Finnegan *et al.*[11] A solution of the 3Fe ferredoxin, either 3Fe Fd_A or 3Fe Fd_B (100 μM), was placed in an Eppendorf tube together with sodium dithionite and a large excess of metal (M) solution. Typically this solution was stirred anaerobically for 15 minutes (25 °C). The products were examined electrochemically by applying a small amount of protein to the electrode and scanning the film in pH 7.0 buffer electrolyte. No further purification was necessary, as the excess dithionite and metal contaminants were released and diluted into the bulk solution once cycling of the potential was begun. This method of metal uptake proved to be successful for Fe, Zn and Cd. With this method the observation that the A' and C' couples, characteristic of the [3Fe-4S] cluster, had disappeared to be replaced by a new couple, D', was taken as an indication that metal uptake into the cluster to form [M3Fe-4S] had occurred. It was found that samples of the Cd adduct had to be used within 2-3 hours since the excess Cd, in contact with the protein solution, resulted in the eventual loss of the protein signals, presumably due to degradative reactions.

Method 2: The second method utilised the protein film method of metal uptake. This has previously worked extremely well for *Desulfovibrio africanus* Fd III,[17-20,43,44] with numerous heterometal clusters being formed and studied. Conventionally this method involves transferring an adsorbed protein film (at a specific holding potential) to a pot containing metal ions in solution. The oxidation-level dependence of transformations was ascertained by holding the electrode potential at particular values, then cycling rapidly to view the products that have formed.[17,20] (See *Chapter 3*) Continued cycling for several minutes results in the A' and C' signals decreasing, concomitant with the D' signal increasing (the signal attributable to $[M3Fe\text{-}4S]^{2+/1+}$).

---

[e] The slow reaction rates meant that equilibrium constants of metal uptake could not be measured and this was in contrast to *Da* Fd III, see *Section 6.4.2*.[17]

Method 3: A bulk solution of either Fd_A or Fd_B was reduced electrochemically (0 °C), inside a small graphite pot which formed the working electrode for this experiment.[31,45] To reduce the protein sample, the potential was held at a value sufficient to ensure complete reduction of the $[3Fe\text{-}4S]^{1+/0}$ couple, i.e. $E_{app} < E^{o'}_{[3Fe\text{-}4S]1+/0}$ and the protein was continuously stirred whilst the current was monitored. Electrochemical reduction was continued until no further current output was observed, at which point the cluster was fully reduced; this was verified by calculating the total charge passed, by integrating the current trace recorded by the YT recorder. Knowing the concentration and volume of the initial protein sample, a calculation of the theoretical value of the charge required to reduce the cluster could be made; this was then compared to the value found by integration. It was found that the measured value was typically > 95 % of the theoretical value. With the cluster in the $[3Fe\text{-}4S]^0$ form, a solution of M^{2+} was then quantitatively titrated into the solution and the current output recorded after each addition.

6.3.5.1 Uptake of iron, zinc and cadmium

Method 1: When a sample of either 3Fe Fd_A or 3Fe Fd_B was reduced with dithionite and a solution of M^{2+} was added to the mixture, conversion to the [M3Fe-4S] form was found to occur. Confirmation that conversion had taken place was found in the cyclic voltammogram: the signals A' and C' had disappeared and a new signal, D', was observed at different potentials depending on the heterometal used. This method was found to work for Fe, Zn and Cd (Figure 6.10). For Fe, 100 % conversion was readily obtainable after the protein had been incubated with the dithionite and Fe^{2+} for 15 minutes. After incubation with Zn^{2+} and Cd^{2+} the protein film was still found to show traces of the C' couple after 15 minutes, and therefore a slightly longer incubation time, i.e. 30 minutes, was required for 100 % conversion. Typically, using 100 μM protein, the concentration of sodium dithionite and the metal ion used were 0.4 mM and 0.6 mM respectively. The reduction potentials of the Fe, Zn and Cd heterometal clusters (with the disulfide bridge oxidised, i.e. Fd_A) were -430 ± 10 mV, -262 ± 10 mV and -359 ± 10 mV respectively. Identical values, within experimental error, were obtained for the Fd_B forms, i.e. 428 ± 10 mV, -261 ± 10 mV and -353 ± 10 mV respectively for the Fe, Zn and Cd adducts (Table 6.2).

Method 2: The investigation of *Pf* Fd metal uptake on a film, using the identical experimental protocol which had been successfully used for *Da* Fd III,[16-20] produced mixed results with *Pf* Fd. It was found that the optimum way to achieve metal uptake into the [3Fe-4S] cluster of *Pf,* when the protein was adsorbed onto the electrode, was to poise at a negative potential for long periods of time, e.g. 60 minutes. (For *Da* Fd III, as noted in *Chapter 3*, this method of observing metal uptake into a [3Fe-4S] cluster was rapid, changes were instantaneous when the protein film was introduced into a metal ion solution.) The chosen potential was dependent on two factors; the potential below which the 3Fe cluster was reduced to the $[3Fe\text{-}4S]^0$ state and the relevant M^{2+}/M stripping potential. The concentration of M^{2+} used in the buffer electrolyte solution was typically around 200 μM. Film stability of the untransformed [3Fe-4S] cluster under these experimental conditions was found to be excellent, despite the long poising time required. After one hour, the new signal attributable to $[M3Fe\text{-}4S]^{2+/1+}$ (the D' signal) was clearly visible (Figure 6.10). The reduction potential of the $[Zn3Fe\text{-}4S]^{2+/1+}$ cluster was -275 ± 10 mV and for $[Cd3Fe\text{-}4S]^{2+/1+}$ it was -354 ± 10 mV. There was no noticeable difference in the reduction potentials for either the disulfide bridge oxidised or reduced forms of the heterometal protein.

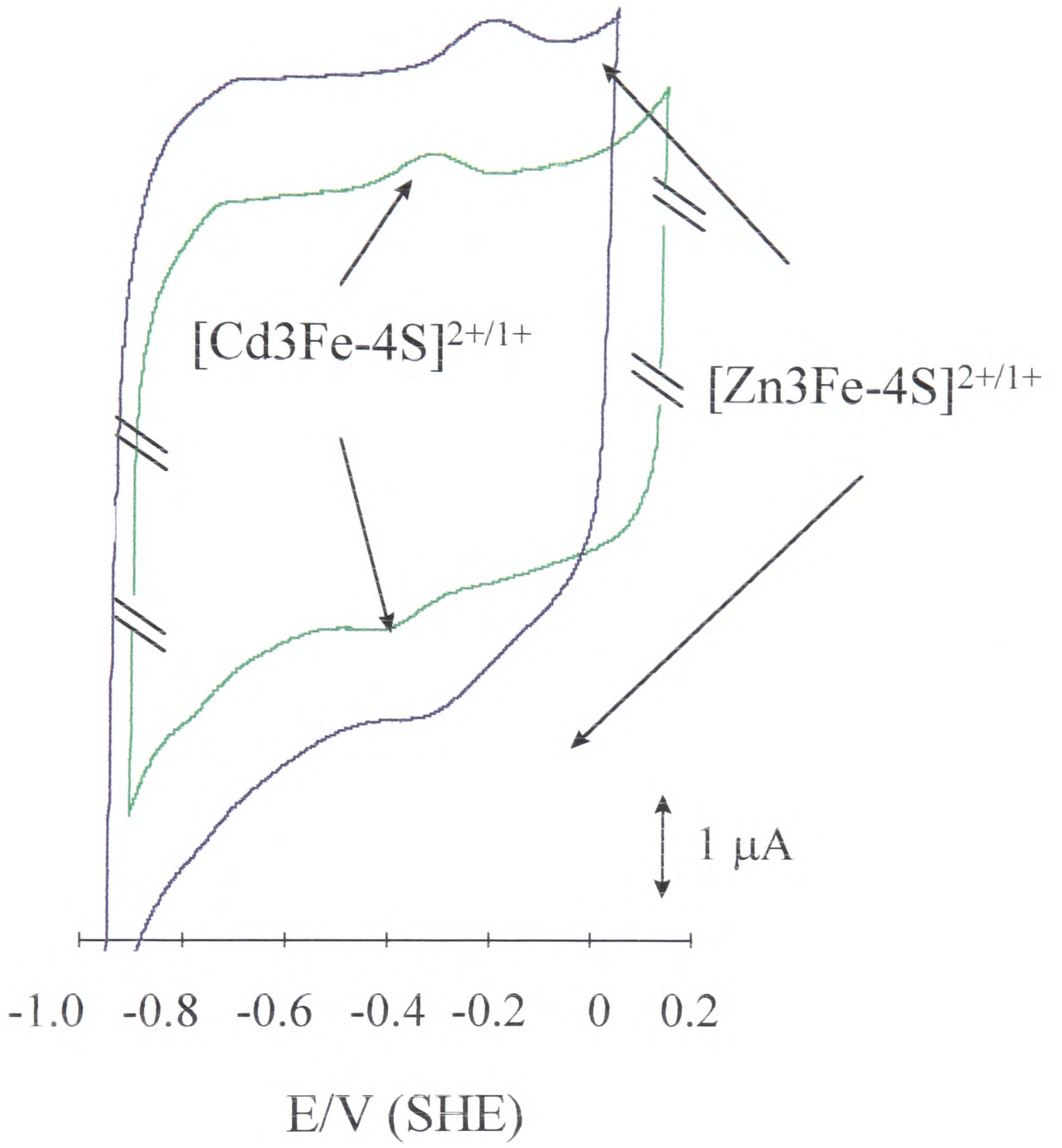

Figure 6.10 Film voltammograms of $[Zn3Fe\text{-}4S]_A$ and $[Cd3Fe\text{-}4S]_A$ forms of *Pyrococcus furiosus* Fd

The Cd adduct was prepared by poising a film of $[3Fe\text{-}4S]_A$ at -540 mV for 60 minutes (Method 2). The Zn adduct was prepared by adding excess Zn^{2+} and excess sodium dithionite to a 100 μM solution of $[3Fe\text{-}4S]_A$ protein, in solution (Method 1). Conditions were pH 7.0, 20 mM mixed buffer, 0.1 M $NaNO_3$, 0 °C, 200 μg ml^{-1} polymyxin as co-adsorbate, scan rate 50 mV s^{-1}.

In contrast, the addition of Fe^{2+} to the [3Fe-4S] cluster, to form [Fe3Fe-4S], was not observed during the lifetime of the film (viable for 90 minutes at 0 °C).

The same reaction was then carried out at 25 °C with the concentration of Fe^{2+} being 0.4 and 2.0 mM Fe^{2+}. Despite the film stability being less at 25 °C than at 0 °C, it was possible to poise the film for up to 60 minutes and still be able to detect voltammetric signals from the protein. It was determined that approximately 50 % conversion to [4Fe-4S] had occurred after 60 minutes at 25 °C (Figure 6.11).

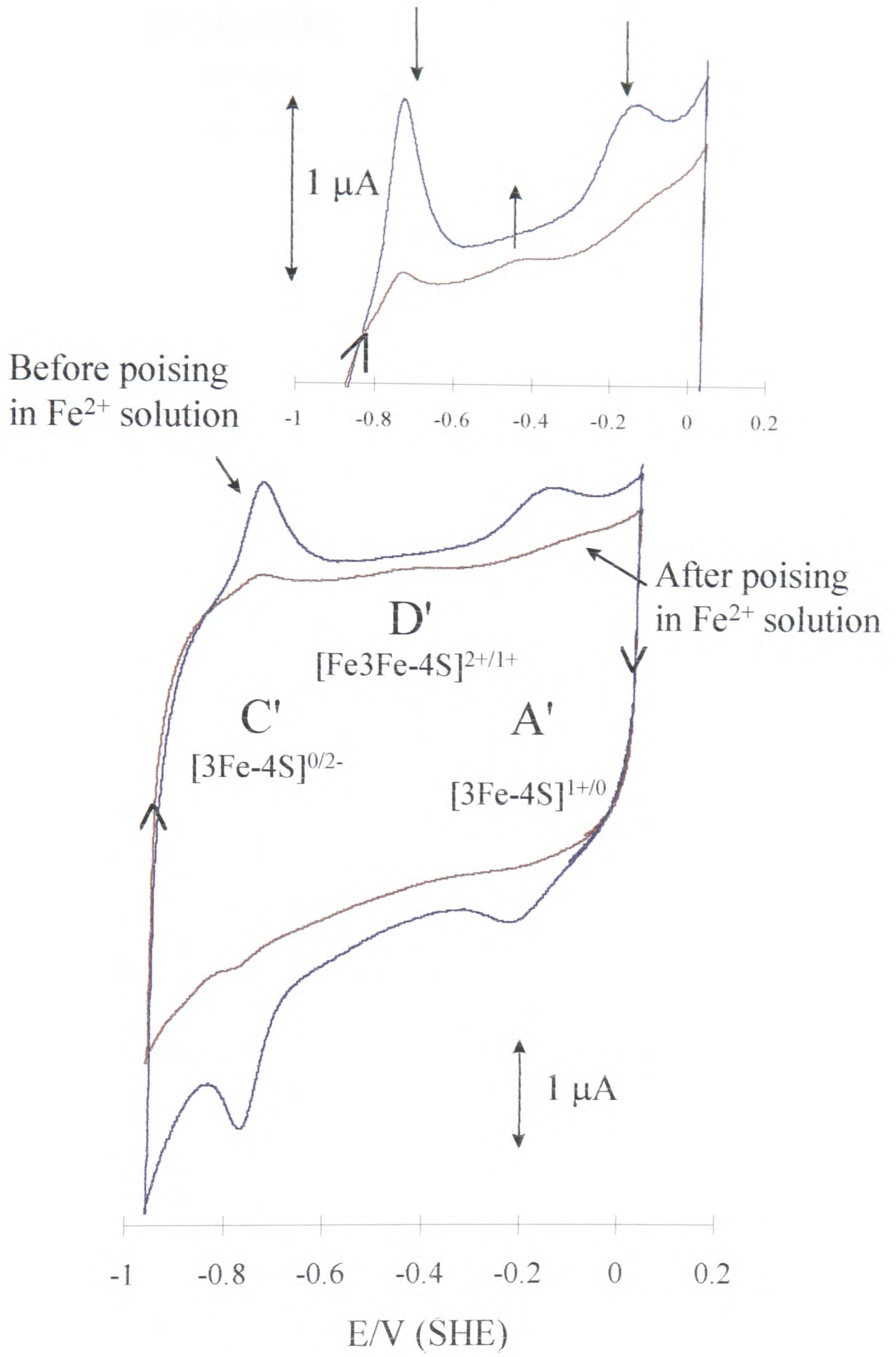

Figure 6.11 Fe uptake of $[3Fe\text{-}4S]_A$ at 25 °C

A film of $[3Fe\text{-}4S]_A$ was held at -500 mV for 60 minutes in the presence of 200 µM Fe^{2+}, pH 7.0, 20 mM mixed buffer, 0.1 M NaCl, 200 µg ml^{-1} polymyxin as co-adsorbate. An expanded view is shown in the top right hand corner. The film deterioration after 60 minutes at 25 °C is in contrast to that observed at 0 °C, see Figure 6.10.

Method 3: A sample of ca. 300 µl of protein (100 µM) was electrochemically reduced using a large surface area electrode, in a small graphite pot (illustrated in *Chapter 2*). Aliquots of Fe^{2+} were then added to the reduced protein and the electrochemical changes were monitored. This method had been previously used to quantitatively observe the conversion of the [3Fe-4S] to the [4Fe-4S] cluster from *Da* Fd III.[16]

The 3Fe Fd was reduced by poising at a potential low enough to reduce the cluster to the $[3Fe\text{-}4S]^{0}$ state (-300 mV), recording the current response of the reduction on a Y-T chart recorder. When all of the sample was reduced, aliquots of Fe^{2+} (typically 10 µl of 1 mM) were titrated into the pot containing the protein and the current response monitored after each addition, following which a voltammogram was recorded to view the status of the clusters.

(i) 3Fe Fd_A

Samples of this form of the protein were electrochemically reduced, as above, and aliquots of Fe^{2+} were added to the reduced protein. Initial additions of Fe^{2+} did not cause an increase in current, but continued addition of Fe^{2+} caused an immediate increase in the cell current. Addition of Fe^{2+} was continued until no further increase in current was observed. A voltammogram was then recorded of the resultant protein solution - this exhibited one reduction couple at a potential of -361 mV, which was attributed to the $[Fe3Fe\text{-}4S]^{2+/1+}$ redox state. A lag phase for the increase in current was observed at the start of the experiment due to initial uptake of the Fe^{2+} by EGTA. EGTA (0.1 mM) was present in the solution to ensure that there was no 4Fe form of the protein present before the experiment was started.[f]

The current increases correspond to Fe^{2+} adding into the cluster. Each increase was accompanied by a gradual decrease as the product was reduced; $[M3Fe\text{-}4S]^{2+} \rightarrow [M3Fe\text{-}4S]^{1+}$. When sufficient Fe^{2+} had been added for total conversion to the [Fe3Fe-4S] form, i.e. no further current increases were observed, a voltammogram of the

[f] It was found that a solution of protein in the 3Fe form would gradually interconvert to the 4Fe form over a period of time. The extraneous Fe^{2+} presumably originates from the degradation of some of the 3Fe clusters. All the protein solutions used in the *Pf* Fd experiments contained 0.1 mM EGTA to scavenge excess Fe from the degradation of the 3Fe clusters, and thus prevent interconversion.

product was recorded. With the $[3Fe\text{-}4S]_A$ form, conversion to 100 % 4Fe Fd ($[4Fe\text{-}4S]_A$) was achieved with the addition of between 1 and 2 fold excess of Fe^{2+}, with respect to the initial protein concentration. Voltammograms before and after Fe^{2+} addition are shown in Figure 6.11.

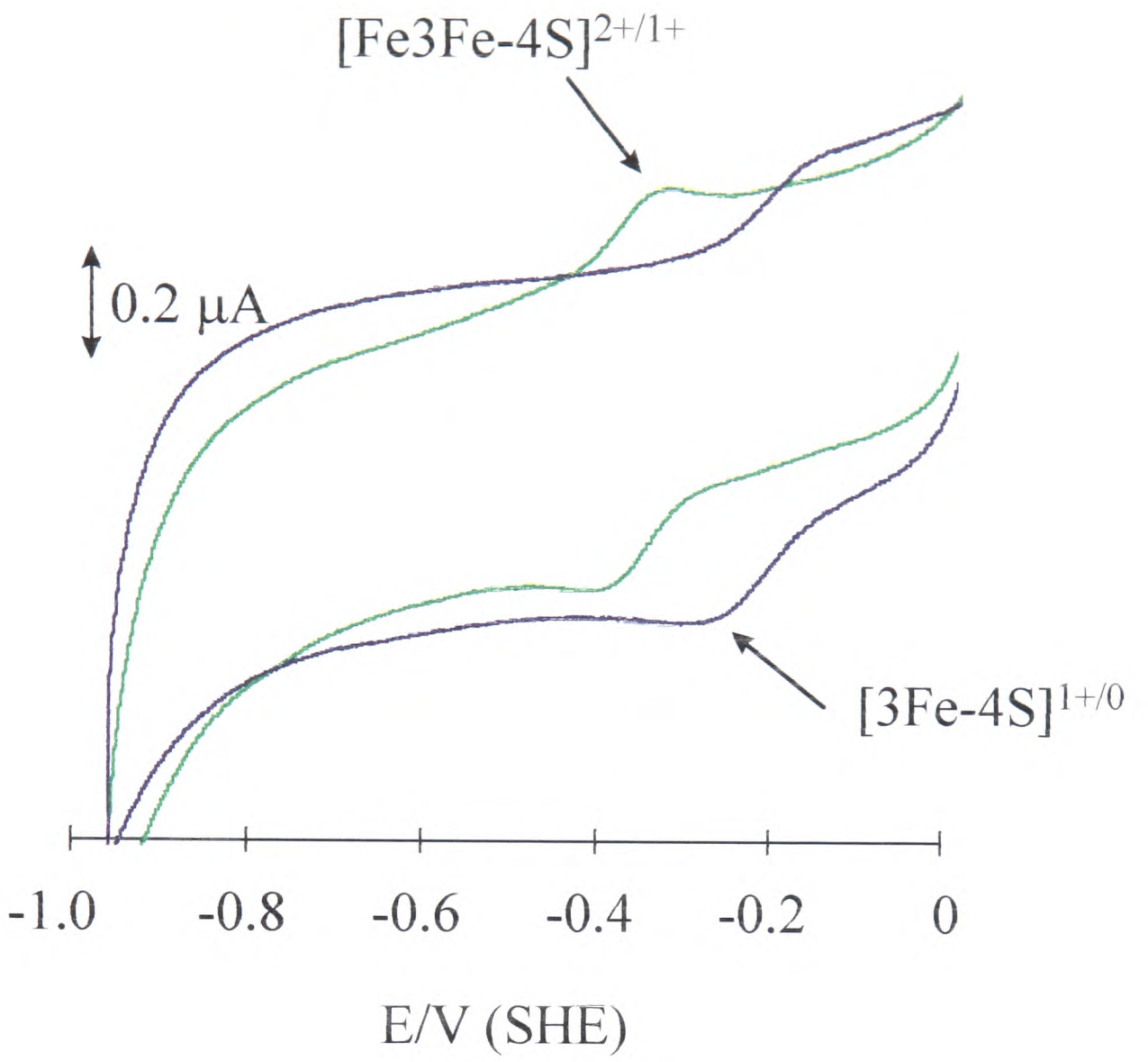

Figure 6.12 Bulk voltammograms showing the addition of Fe^{2+} to 3Fe Fd_A

(Metal uptake using Method 3 - see text) Cyclic voltammograms recorded at 2 mV s^{-1}, of Fd_1 before (blue) and after (green) addition of aliquots of Fe^{2+} to a solution of 46 µM protein solution at pH 7.0 in 20 mM mixed buffer at 0 °C, 2 mM neomycin.

(ii) 3Fe Fd_B

When a sample of 3Fe Fd_B was electrochemically reduced, and Fe^{2+} was titrated quantitatively into the mixture, (i.e. as for 3Fe Fd_A) no increases in current were observed. This surprising result was reproduced on a number of occasions, with Fe^{2+} concentrations of up to 6 fold excess added to the reduced protein solution. However, when the same sample of 3Fe Fd_B, together with the added Fe^{2+} solution, was left overnight in the cell (24 h) under anaerobic conditions, up to 50 % conversion to the $[4Fe\text{-}4S]_B$ form was observed (Figure 6.13).

The Fe uptake in bulk for 3Fe Fd_B, as with the 3Fe Fd_A, was repeated a number of times for the 3Fe Fd_B form. Immediate Fe addition was never observed to occur in any significant amount for the 3Fe Fd_B form in the electrochemical cell. If any Fe uptake was observed, directly after the addition, to form the $[4Fe\text{-}4S]_B$ cluster, this was never more than 5 % of the overall cluster population. As mentioned above, if the protein solution was left overnight in contact with the excess Fe solution, significantly more conversion to the 4Fe Fd_B form was observed. The status of the disulfide bridge was checked after both types of bulk uptake experiments, to ensure that interconversion of the disulfide bridge had not occurred, which was found to be the case.

Notably, this was the *only* experiment which showed a difference in the behaviour between the 3Fe Fd_A and 3Fe Fd_B forms of the protein.

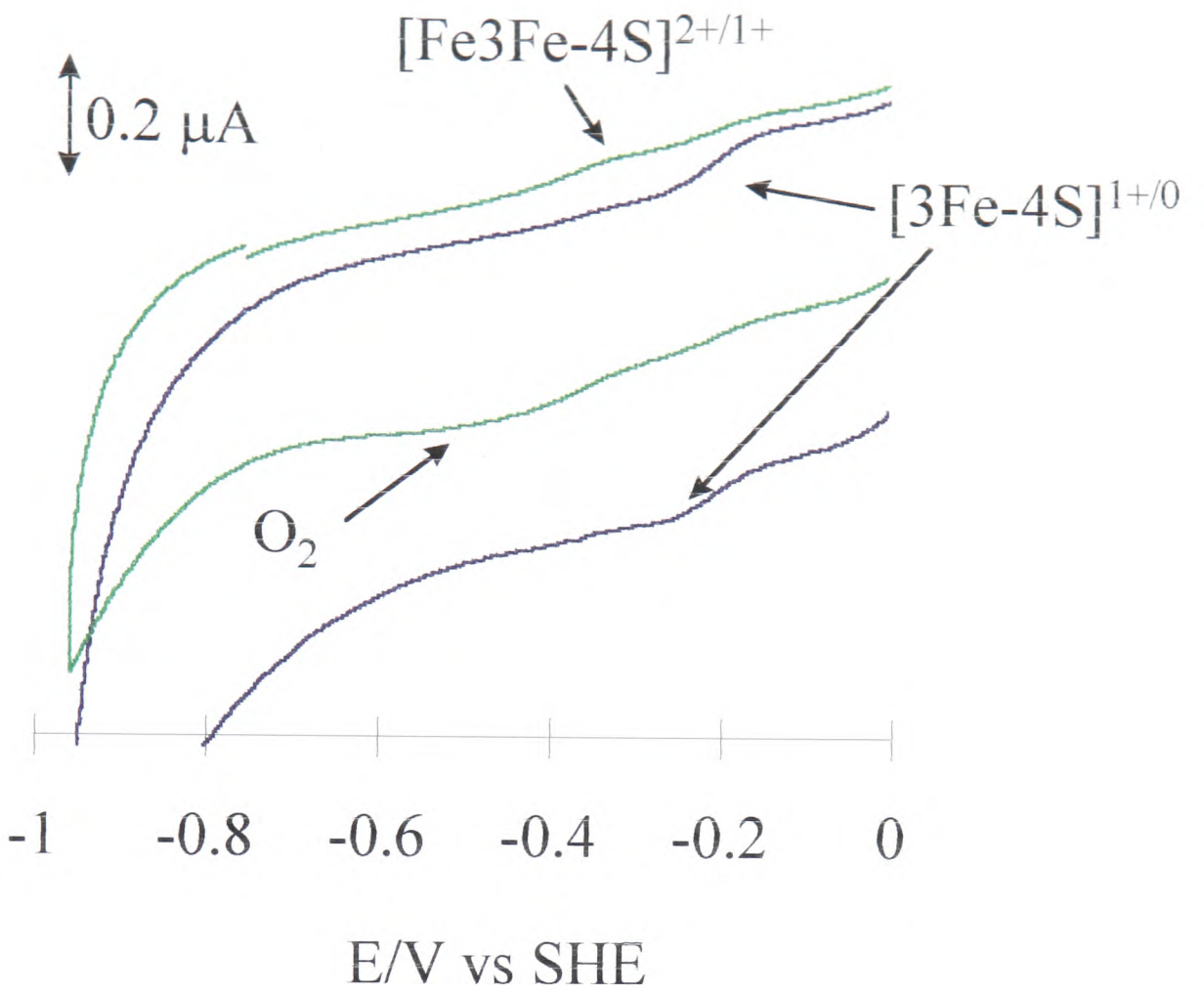

Figure 6.13 Bulk voltammograms showing the addition of Fe^{2+} to 3Fe Fd_B

Cyclic voltammograms recorded at 2 mV s^{-1}, of Fd_B after reduction and addition of Fe^{2+} as described in the text. As seen above, less than 5 % conversion to the [Fe3Fe-4S] form was observed. The green cyclic voltammogram is the same protein solution left overnight in the presence of Fe^{2+}. From the voltammogram it is possible to estimate that 50 % conversion to the [Fe3Fe-4S] form has occurred. The solution contained 42 µM protein at pH 7.0 in 20 mM mixed buffer at 0 °C, 2 mM neomycin.

(iii) Bulk Uptake of Zn

As reported in *Section 6.3.2*, there were noticeable differences between the reduction potentials of the 3Fe and 4Fe forms, when measured in a protein film or in bulk. It was thus decided to investigate if there were similar differences in the reduction potential of an alternative heterometal cluster, when measured in a protein film or in bulk. The zinc heterometal cluster was chosen because transformation from the 3Fe Fd_A cluster to the zinc adduct was straightforward using Method 1 - and the resultant product was stable, unlike the cadmium cluster, which was susceptible to cluster degradation.

It was first decided to try Method 3 to generate the Zn product, to see if the quantitative uptake of Zn could be observed as had been accomplished for Fe. As the quantitative uptake of Fe^{2+} in bulk had been electrochemically observed only for 3Fe Fd_A, 3Fe Fd_B was not investigated.

A sample of protein was reduced at -507 mV for 30 minutes. Verification that the protein had been reduced by one electron equivalent was performed by calculating the area underneath the current trace. Aliquots of Zn^{2+} were added to the reduced protein but no current increases were observed upon making these additions. After a 10 fold excess of Zn (with respect to the protein concentration) had been added, a voltammogram was recorded, but no signs of any Zn adduct were present, i.e. couple A was still visible. The voltammogram was very similar to the initial voltammogram measured before the addition of Zn and it could be concluded that no transformation had occurred.

A further check was made on the protein solution, in case the bulk reduction potential of the [Zn3Fe-4S] cluster, was at an overlapping potential with the $[3Fe\text{-}4S]^{0/1+}$ couple (A). A portion of the protein solution was taken from the bulk electrochemical pot and a film voltammetry experiment was carried out. The product, after Zn addition, was found to possess voltammetric signals identical to that shown in Figure 6.4, i.e. two couples were clearly seen corresponding to the A' and C' couples. As a final check, this film was then held at an oxidising potential (0.2 V for 30 s) and a voltammogram recorded. No change was observed in the voltammetry after poising at a positive potential. If there had been any Zn^{2+} in any of the clusters, then poising at this potential would have released the Zn^{2+}

ions (see *Section 6.3.6* for a complete description of this technique) and there would have been a subsequent increase in both the A' and C' couple peak heights, but this was not observed.

A second attempt was made to record the potential of the Zn heterometal cluster in bulk solution. A 200 µl sample of the Zn adduct was prepared, using Method 1. Conversion to the Zn form was verified by performing film voltammetry on a small sample of the product. The sample showed ca. 90 % conversion to the [Zn3Fe-4S] form, as identified by the decrease in the A' and C' couples, and by the appearance of the D' couple at the expected potential of -262 mV. This transformed protein sample was then dialysed using the small volume Amicon apparatus (*Chapter 2*), to remove impurities i.e. sodium dithionite. The whole sample was then placed into the large working electrode pot and a bulk diffusional voltammogram was recorded (Figure 6.14).

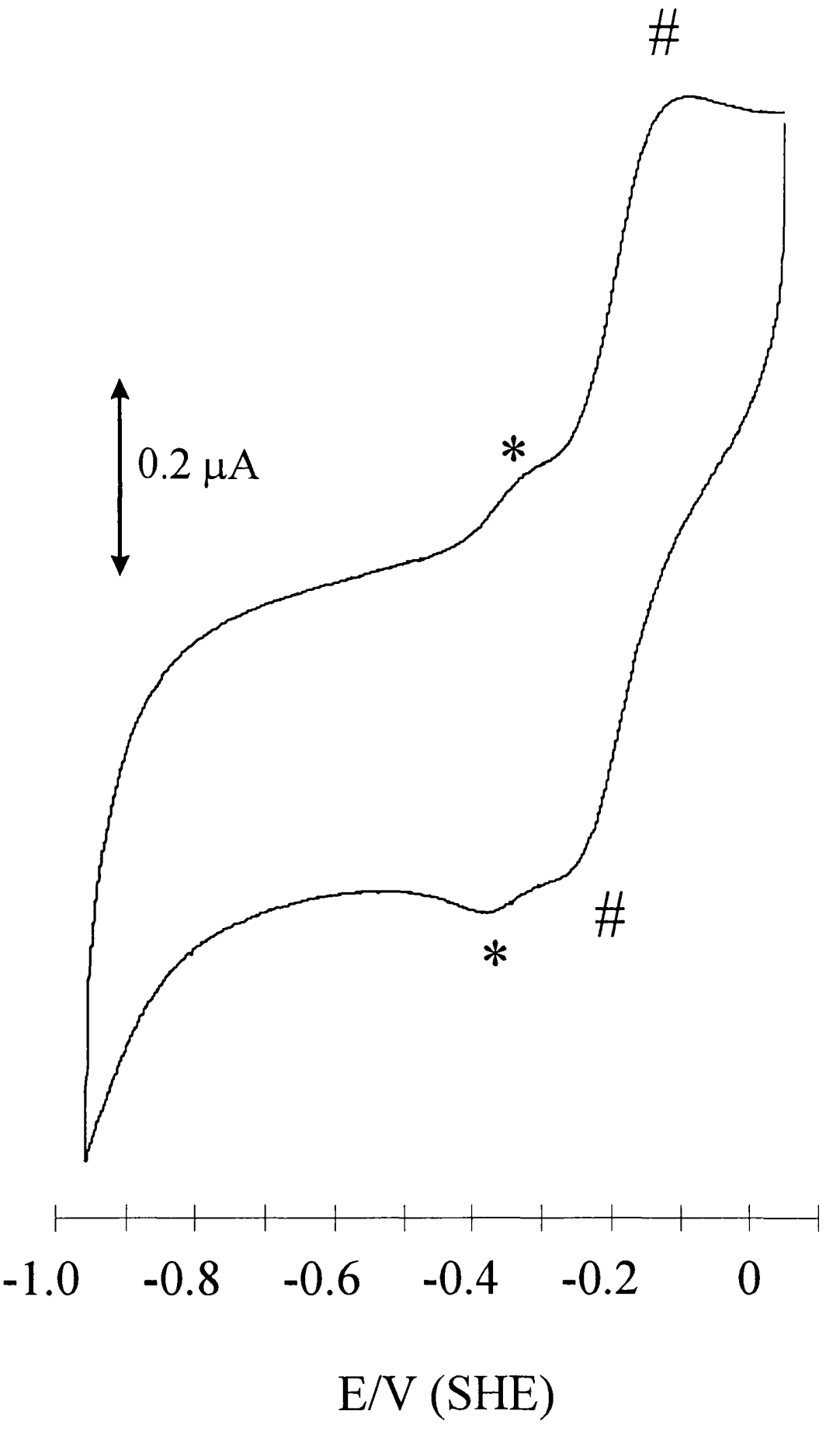

Figure 6.14 A bulk voltammogram of the Zn product

*The Zn product was formed by incubating a sample of 3Fe Fd_A with a 15-fold excess of Zn^{2+} and a 5-fold excess of sodium dithionite. This was then dialysed and a bulk voltammogram was recorded at scan rate 2 mV s^{-1}, in 50 mM Hepes, pH 7.0, 0.1 M NaCl, 2 mM neomycin. Explanation of the reduction couples, marked * and # is given in the text.*

The bulk voltammogram exhibited two separate reduction couples, a small signal at -363 ± 10 mV (*) and a more prominent signal at -196 ± 10 mV (#). The lower reduction couple was at the potential of the [4Fe-4S] cluster (see Table 6.2). Presumably degradation and reassembly of some of the clusters, to incorporate Fe, had occurred thus explaining this lower potential couple. The higher potential reduction couple was expected to be the reduction couple attributed to the [Zn3Fe-4S] cluster. However the potential, at -196 mV, is ca. 60 mV more positive than the reduction potential of the Zn cluster when the potential was measured using the protein film method (Table 6.2). From Table 6.2 it is also noted that the reduction potential of the [4Fe-4S] form is ca. 60 mV more positive when measured using bulk voltammetry than when measured with the film method. Thus, the higher reduction couple at -196 ± 10 mV may be the Zn bulk reduction couple. Equally so, the higher reduction potential couple is in the region of the $[3Fe\text{-}4S]_A$ reduction couple (which is -215 ± 10 mV) when measured in bulk solution. Alternatively, the higher potential couple could be a composition of both the reduction couples A' and D'. It is thus evident from this situation that it is difficult to identify, without doubt, the observed cluster species using bulk solution voltammetry alone.[g] Thus, the issue of the heterometal cluster potentials in bulk solution was not satisfactorily concluded.

	Disulfide Bridge Oxidised (Fd_A)		**Disulfide Bridge Reduced (Fd_B)**	
	Film	**Bulk**	**Film**	**Bulk**
[3Fe-4S]	-150	-215	-159	-219
[Fe3Fe-4S]	-430	-361	-428	-365
[Zn3Fe-Fe]	-262	*-196 (?)*	-261	-
[Cd3Fe-4S]	-359	-	-353	-

Table 6.2 Comparison of reduction potentials of heterometal clusters of *Pf* Fd
Film vs. bulk, disulfide bridge oxidised vs. reduced, for [3Fe-4S] and [M3Fe-4S] clusters in Pyrococcus furiosus ferredoxin

[g] In this case an alternative technique such as EPR would have aided the identification of the cluster species.

6.3.5.2 Thallium

Observations have been made previously on the interaction between Tl^+ and [3Fe-4S] clusters for both *Da* Fd III[18] and *Pf* Fd.[10] It is almost certain that Tl^+ interacts to form a heterometal cluster, [Tl3Fe-4S], similar to the previous examples of heterometal clusters. More recently, the synthetic analogue $[TlFe_3S_4(LS_3)]^{3-}$, has been synthesised by Holm and co-workers.[46]

Formation of the Tl^+ adduct has not been observed in *Pf* Fd using the protein film method. Previous studies have been carried out upon a bulk sample of the [Tl3Fe-4S] cluster, which was produced by incubation with a 1-1000 fold excess of $Tl(OOCCH_3)$ for 30 minutes.[10] No previous studies have been carried out on the kinetics of formation of the Tl adduct of the 3Fe form from *Pf* Fd.

Method 2, as described previously, was used for observing the transformation of the 3Fe cluster to the Tl adduct. A number of experimental modifications had to be used for the Tl experiments. All voltammetry was carried out at 7 °C to avoid precipitation of Tl^+ acetate when used at very high concentrations. A restricted voltage range was used because of the rather positive stripping potential of Tl^+, this meant that the C' couple was not observable throughout the course of these experiments. The experimental cell compartments were rinsed frequently (a maximum of three film experiments were made before all the solutions were changed) to avoid cross contamination of Tl^+ into the 'buffer only' pot.

A film of *Pf* Fd [3Fe-4S] was prepared, and the characteristic signal (the A' reduction couple) was stabilised in the 'buffer only' pot before transferral to the pot containing Tl^+, transferral was carried out at a potential to ensure the 3Fe cluster was in the $[3Fe\text{-}4S]^0$ state. An alteration in the voltammetry was *immediately* noted upon resuming scanning in the pot containing the Tl^+, in complete contrast to the previously explored reactions between the cluster and other metal ions, when adsorbed on a film.

Thus, a rapid and reversible reaction was observed when an adsorbed protein film was placed into a solution of Tl^+. The extent of this reaction depended on both scan rate and the concentration of Tl^+ used. Experiments at slow scan rates (~ 10 mV s^{-1}) showed

that the signal A' shifted to increasingly positive potentials as the thallium concentration was raised. It was not possible to examine the properties of couple C' because of thallium metal deposition at negative potentials.[h] As the scan rate was increased (> 0.5 V s^{-1}) marked changes occurred in the voltammetry. The reduction wave of couple A' shifted back towards its original potential in the absence of Tl^{+}, whereas the oxidation peak remained at a higher potential. At very fast scan rates (> 30 V s^{-1}) a second reduction wave appears in the voltammetry, the reduction wave of which is just discernible. Voltammograms at scan rates of 20 mV s^{-1}, and 30 V s^{-1} are shown in Figure 6.15.

[h] Below -600 mV the voltammogram was totally dominated by the stripping wave, $Tl^{+/0}$

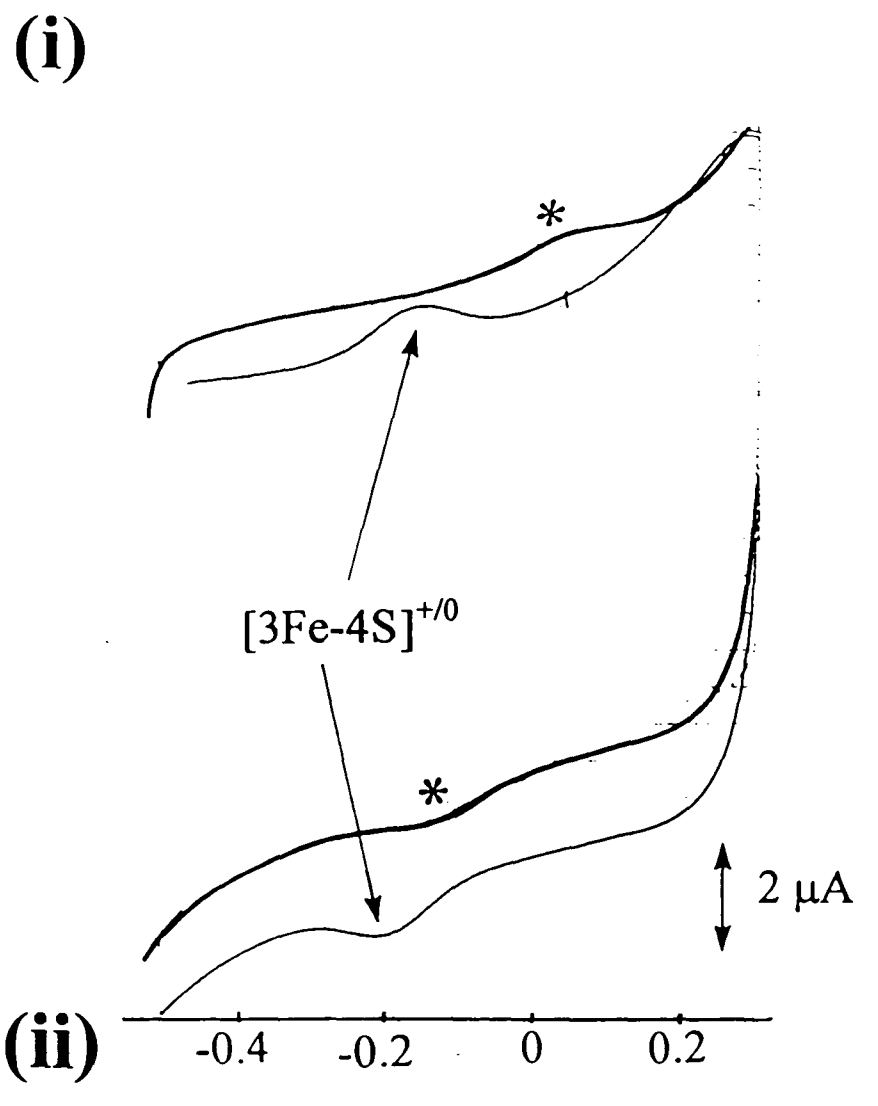

Figure 6.15 Film voltammetry of $[3Fe\text{-}4S]_A$ in the presence of 1 mM Tl^+

(i) Scan rate 20 mV s^{-1} (ii) scan rate 30 V s^{-1}. Conditions pH 6.8, 0.1 M acetate, 200 μg ml^{-1} polymyxin as co-adsorbate, 7 ^oC. In both cases the film voltammetry of $[3Fe\text{-}4S]^{1+/0}$ is shown, for comparison.

The inherent dependence of the voltammetry upon scan rate is indicative of a fast coupled reaction occurring between the [3Fe-4S] cluster and Tl^+. The results obtained with $[3Fe\text{-}4S]_A$ in the presence of Tl^+ can be interpreted in terms of a rapid equilibrium, involving Tl^+ binding to both the $[3Fe\text{-}4S]^{1+}$ and the $[3Fe\text{-}4S]^0$ forms. This system can be represented as a square scheme, shown in Figure 6.16.

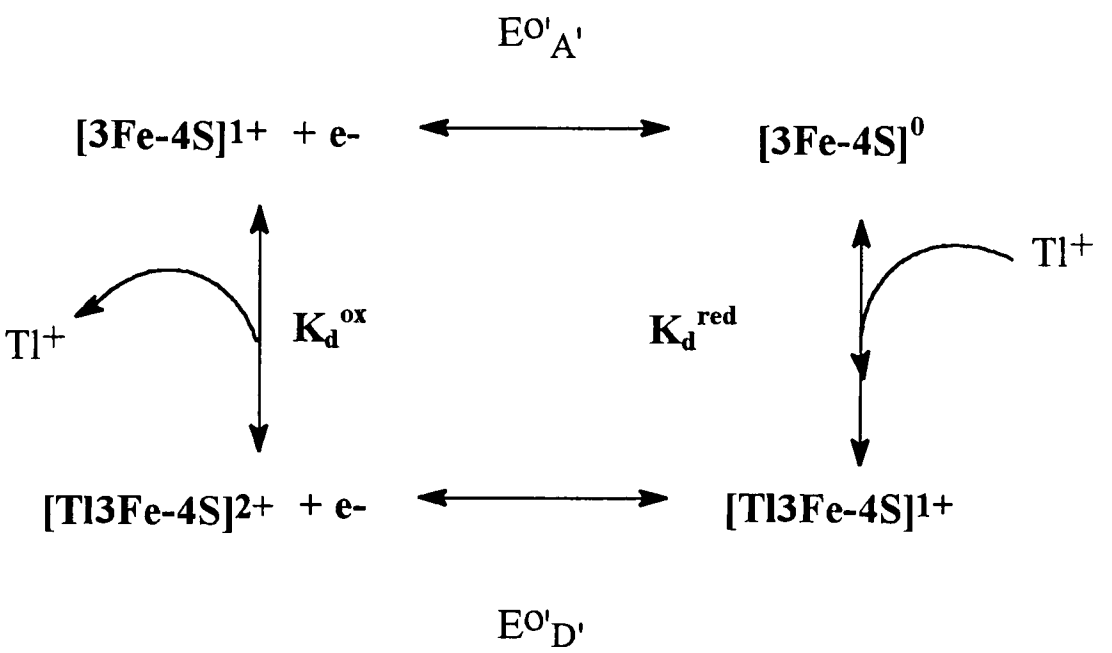

Figure 6.16 Square scheme for Tl^+ binding to $[3Fe\text{-}4S]^{1+/0}$

The above scheme represents a thermodynamic cycle, with the observed variation in reduction potential explained in terms of the variation of Tl^+ concentration and timescale. At slow scan rates the system equilibrates between the populations of the four species, shown in Figure 6.15, and hence only one reduction couple is observed with a reduction potential dependent upon the concentration of Tl^+. At $E^{o'}$ the surface populations of both the oxidised and reduced species must be equal thus,

$$\{[3Fe\text{-}4S]^{1+}\} + \{[Tl3Fe\text{-}4S]^{2+}\} = \{[3Fe\text{-}4S]^{0}\} + \{[Tl3Fe\text{-}4S]^{1+}\}$$

Equation 6.2

{} denotes concentration of species

The surface populations of $[Tl3Fe\text{-}4S]^{2+}$ and $[Tl3Fe\text{-}4S]^{1+}$ can be defined in terms of the dissociation constants K_d^{ox} and K_d^{red} thus,

$$K_d^{ox} = \frac{[[3Fe-4S]^{1+}][Tl^+]}{[Tl3Fe-4S]^{2+}} \qquad \textbf{Equation 6.3}$$

$$K_d^{red} = \frac{[[3Fe-4S]^{0}][Tl^+]}{[Tl3Fe-4S]^{1+}} \qquad \textbf{Equation 6.4}$$

From this an expression for the ratio of $[3Fe\text{-}4S]^{1+}/[3Fe\text{-}4S]^{0}$ can be obtained. Substitution into the Nernst equation gives,

$$E^{o'}_{obs} = E^{o'}_{A'} + \frac{2.303RT}{nF}\log\frac{1+\frac{[Tl^+]}{K_d^{red}}}{1+\frac{[Tl^+]}{K_d^{ox}}} \qquad \textbf{Equation 6.5}$$

The reduction potential of the $[Tl3Fe\text{-}4S]^{2+/1+}$ couple, $E^{o'}_{D'Tl}$ is given by Equation 6.6, in the limit that $[Tl^+]/K_d^{ox} >> 1$ and $[Tl^+]/K_d^{red} >> 1$,

$$E^{o'}_{D'Tl} = E^{o'}_{A'} + \frac{2.303RT}{nF}\log\frac{K_d^{ox}}{K_d^{red}} \qquad \textbf{Equation 6.6}$$

$E^{o'}_{obs}$ is the experimentally observed reduction potential, which is dependent on the concentration of Tl^+. The sigmoidal shaped curve, shown in Figure 6.17, is defined by the lower limit (the reduction potential of $[3Fe\text{-}4S]^{1+/0}$) and the upper limit (152 ± 5 mV) is the reduction potential of $[Tl3Fe\text{-}4S]^{2+/1+}$ ($E^{o'}_{D}$), as measured at 30 V s^{-1}. The equilibrium constants K_d^{ox} and K_d^{red} were calculated as 740 mM and 1.9 μM respectively.

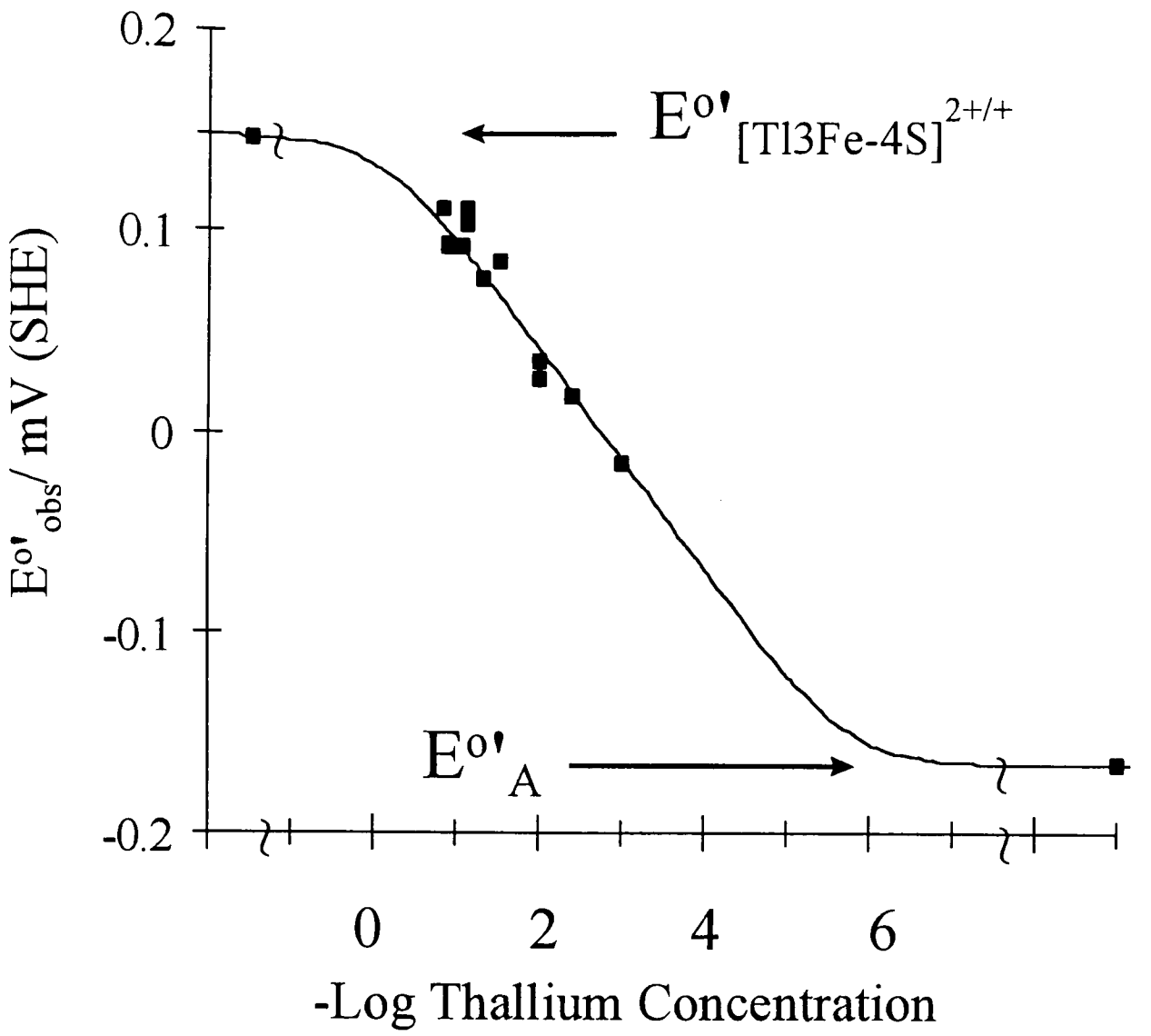

Figure 6.17 Dependence of $E^{o'}_{obs}$ with Tl^+ concentration for the $[3Fe\text{-}4S]_A$ cluster

As the scan rate is increased, equilibration of the species does not occur. The oxidation wave is still clearly visible, i.e. Tl^+ is bound to the reduced 3Fe cluster, but Tl^+ is easily lost from the oxidised cluster and so the reduction wave observed is representative of the original A' reduction wave. This is because the affinity of Tl^+ for the oxidised 3Fe cluster is much less than the affinity of Tl^+ for the reduced 3Fe cluster - the more electron-rich species. As the scan rate is increased to very high scan rates the experiment can 'outrun' the disassociation of Tl^+ from the oxidised 3Fe cluster and hence the reduction peak observed is that of couple D', $[Tl3Fe\text{-}4S]^{2+/1+}$.

Figure 6.16 shows how binding of Tl^+ to the $[3Fe\text{-}4S]^0$ cluster results in the stabilisation of the reduced species and, hence, $E^{o'}$ is shifted to a more positive potential. Co-ordination of Tl^+ to the reduced cluster is of a similar magnitude to Tl^+ binding to the 3Fe cluster in *Da* Fd III (1.5 ± 1 μM for *Da* Fd III compared to 1.9 ± 1 μM for *Pf* Fd). In

contrast binding of Tl^+ to the oxidised cluster in *Pf* Fd is very much weaker than for the 3Fe cluster in Fd III (34 ± 1 mM compared to 740 mM for *Pf* Fd). Thus for *Da* Fd III the potential of $E^{o'}_D$ could be determined from relatively slow cycles at high concentrations of Tl^+, whereas fast scan voltammetry is required for *Pf* Fd.

6.3.6 Spectroscopic Observation of Fe Uptake by $[3Fe\text{-}4S]_{A/B}$

This section describes an alternative method of measuring the rate of Fe uptake into the 3Fe cluster of *Pf* Fd. This particular method was explored because,

1. There was a notable difference in the rate of metal uptake into the [3Fe-4S] cluster depending on whether the protein was adsorbed on the electrode surface or free in solution.

2. Fe uptake into the cluster, when the protein was directly adsorbed onto the electrode, was not observed at 0 °C and was only ca. 50 % complete at 25 °C. This was in direct contrast to Zn and Cd, which were both found to be incorporated into the cluster at 0 °C, when the protein was adsorbed on the electrode surface.

3. When the protein sample was reduced electrochemically, there was a difference in the rate of Fe^{2+} uptake reactivity for the disulfide bridge oxidised or reduced forms of *Pf* Fd. The 3Fe Fd_A form of the protein was found to take up Fe^{2+} readily from solution, in contrast the same reaction was much slower for the 3Fe Fd_B form.

Thus the slower reaction for metal uptake by *Pf* Fd was be exploited in order to measure the rate of metal uptake, using an alternative methodology to protein film voltammetry.

Although FeS proteins do not have very characteristic visible absorption spectra, there are characteristic spectroscopic differences between the oxidised or reduced forms of the [3Fe-4S] and [4Fe-4S] proteins. As *Pf* Fd only contains one cluster it is an ideal system to study spectrophotometrically because there are no additional signals in the spectrum from other clusters. This is a problem for 7Fe Fds because they contain a [4Fe-4S] cluster which always provides additional contributions to the spectrum.

It is therefore possible to study the metal uptake kinetics of divalent metals with the reduced 3Fe Fd in bulk solution, using spectrophotometry and utilising the difference between the absorbance spectra of the $[3Fe\text{-}4S]^{0}$ form and the $[4Fe\text{-}4S]^{1+}$ form. An example is shown in Figure 6.18.

As shown in *Chapter 3*, the [3Fe-4S] cluster must be reduced in order to facilitate metal uptake. Reduction of the 3Fe cluster at the start of these experiments was carried out with sodium dithionite and methyl viologen. Addition of Fe^{2+} to the reduced cluster results in cluster conversion to $[Fe3Fe\text{-}4S]^{2+}$, and with sufficient reductant present, the product is immediately reduced to $[Fe3Fe\text{-}4S]^{1+}$, a process which causes significant bleaching of the solution. Thus if reduction of the $[Fe3Fe\text{-}4S]^{2+}$ product is fast, the kinetics will be only controlled by the rate of metal ion uptake. This reaction, observed spectrophotometrically, provides an additional method to explore the differences in metal uptake of the 3Fe Fd_A and 3Fd Fd_B forms of the protein, which were indicated in the bulk reduction and metal uptake experiments.

The UV/Vis spectra of the [3Fe-4S] forms of Fd_A or Fd_B were recorded before and after reduction with a 25-fold excess of dithionite, in the presence of 1 μM methyl viologen as mediator. The spectrum was remeasured to ensure reduction was complete, and then a known quantity of Fe^{2+} was added and spectra were recorded at regular time intervals until there was no further absorbance change. In each case, addition of Fe^{2+} and subsequent reduction to $[Fe3Fe\text{-}4S]^{1+}$ was found to result in a decrease in absorbance. A typical data set, from one experiment, recording the absorption spectra of the 3Fe Fd_B oxidised and reduced forms, and progress through to the converted 4Fe Fd_B reduced cluster are shown in Figure 6.18. The wavelength at which there was the greatest difference in absorbance was determined to be 426 nm. Plots of ln ΔA against time, at 426 nm, were plotted and found to be linear for at least two half lives, giving pseudo first-order rate constants k_{obs}. Reactions were first order in $[Fe^{2+}]$ according to Equation 6.7, which is appropriate provided removal of $[Fe3Fe\text{-}4S]^{2+}$, by its reduction, is fast.[47]

$$\text{Rate} = k_f[3Fe\text{-}4S]\,[Fe^{2+}] \qquad \textbf{Equation 6.7}$$

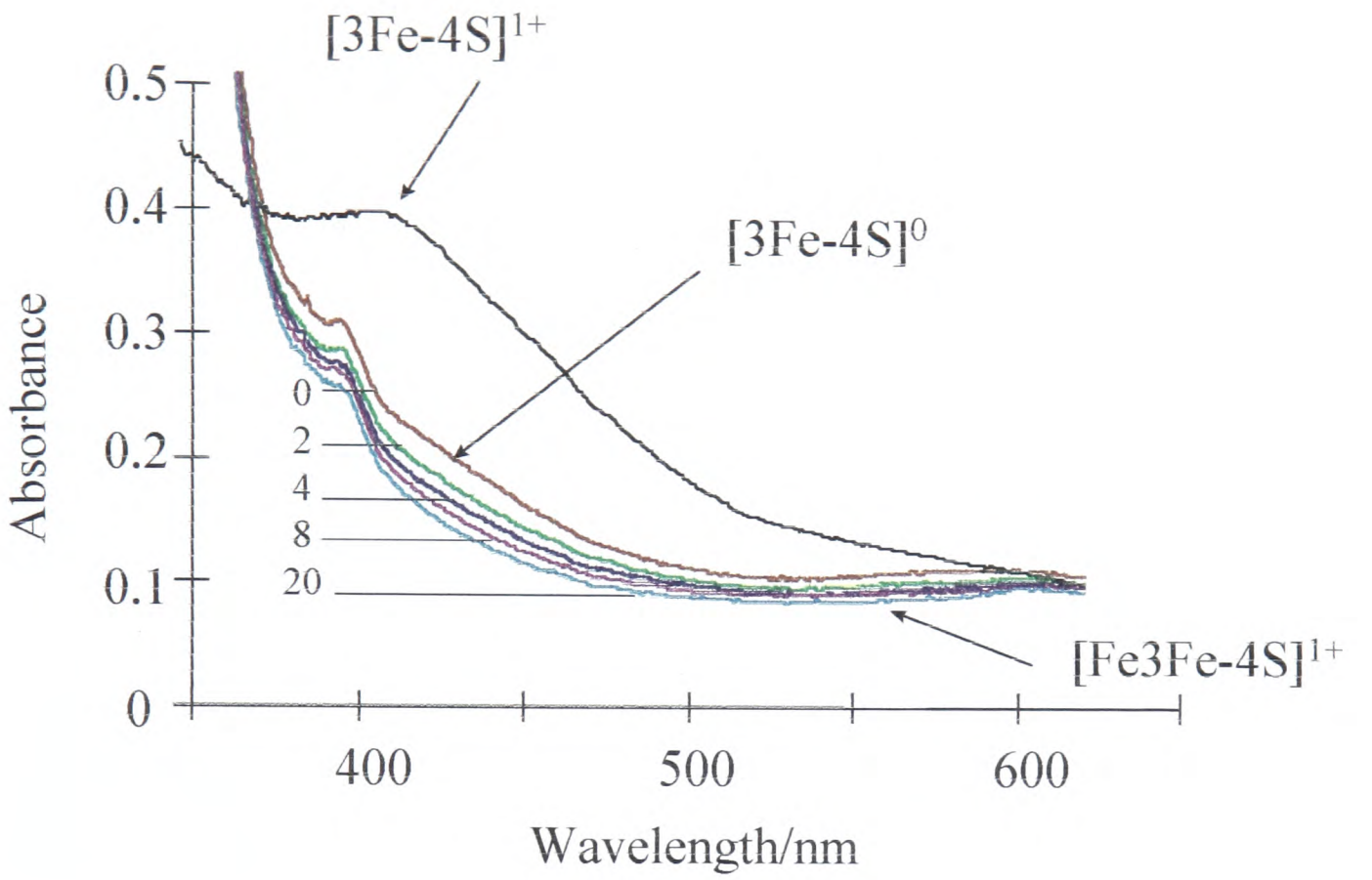

Figure 6.18 UV/Vis spectra monitoring the uptake of Fe^{2+} into the $[3Fe\text{-}4S]^0$ cluster of *Pf* Fd.

Results shown are for the $[3Fe\text{-}4S]_B$ protein. The first two spectra (black and red) correspond respectively to the $[3Fe\text{-}4S]^{1+}$ cluster and the product of reduction by sodium dithionite in the presence of methyl viologen (0 minutes). Subsequent spectra were recorded at intervals (times in minutes indicated) after addition of Fe^{2+}. Temperature 25 °C.

Graphs of ln ΔA against time for three different concentrations of Fe^{2+}, for both the Fd_A and Fd_B forms, are shown in Figures 6.19 and 6.20. The pseudo first-order rate constants, k_{obs}, are as tabulated in Table 6.3.

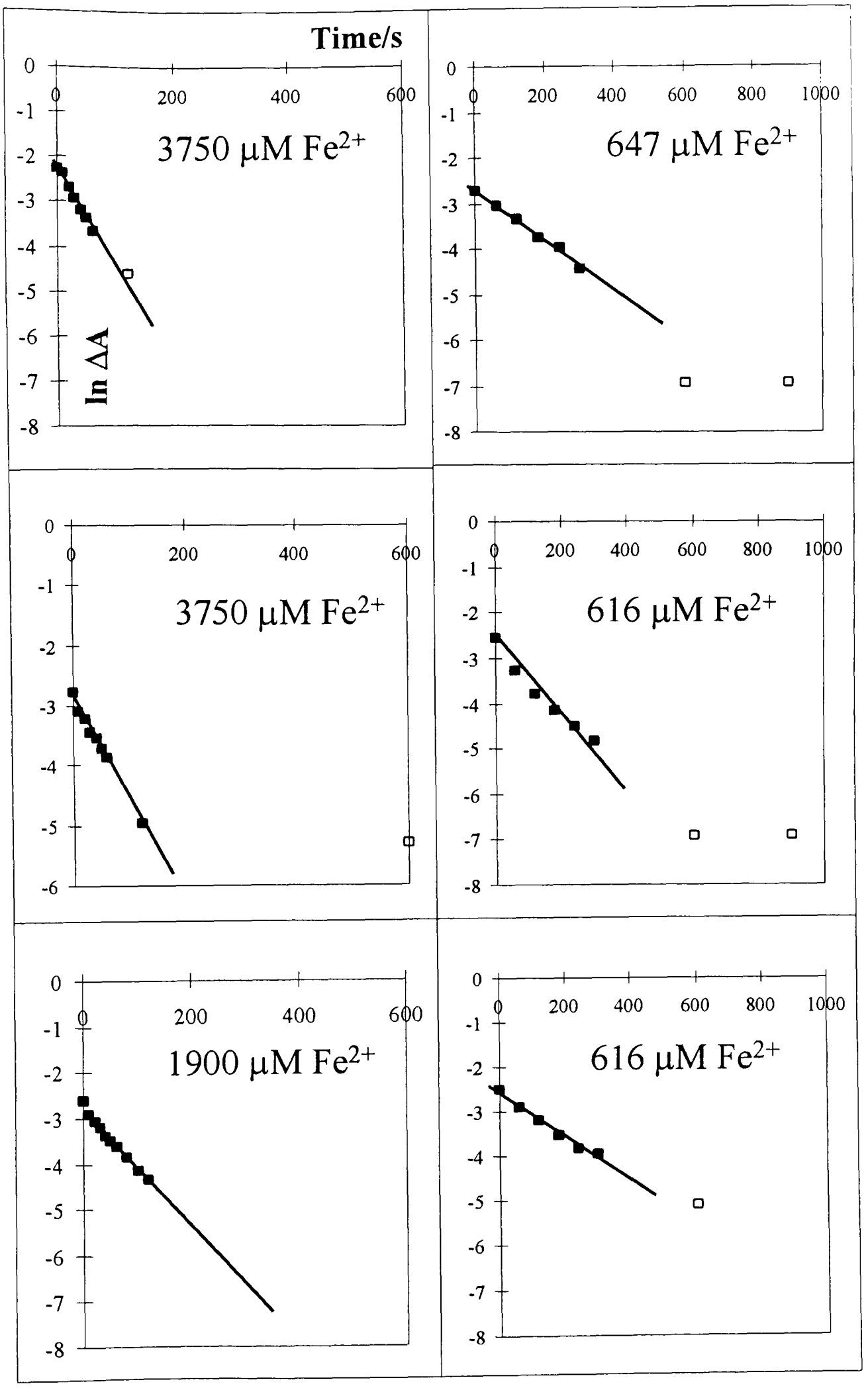

Figure 6.19 Spectroscopic observation of Fe uptake by 3Fe Fd_A

Graphs of ln ΔA against time as recorded at 426 nm. Open squares denote data which were not used when calculating the slope of the lines. Conditions were as described in the text, 25 °C, pH 7.0. Pseudo first-order rate constants are as tabulated in Table 6.3.

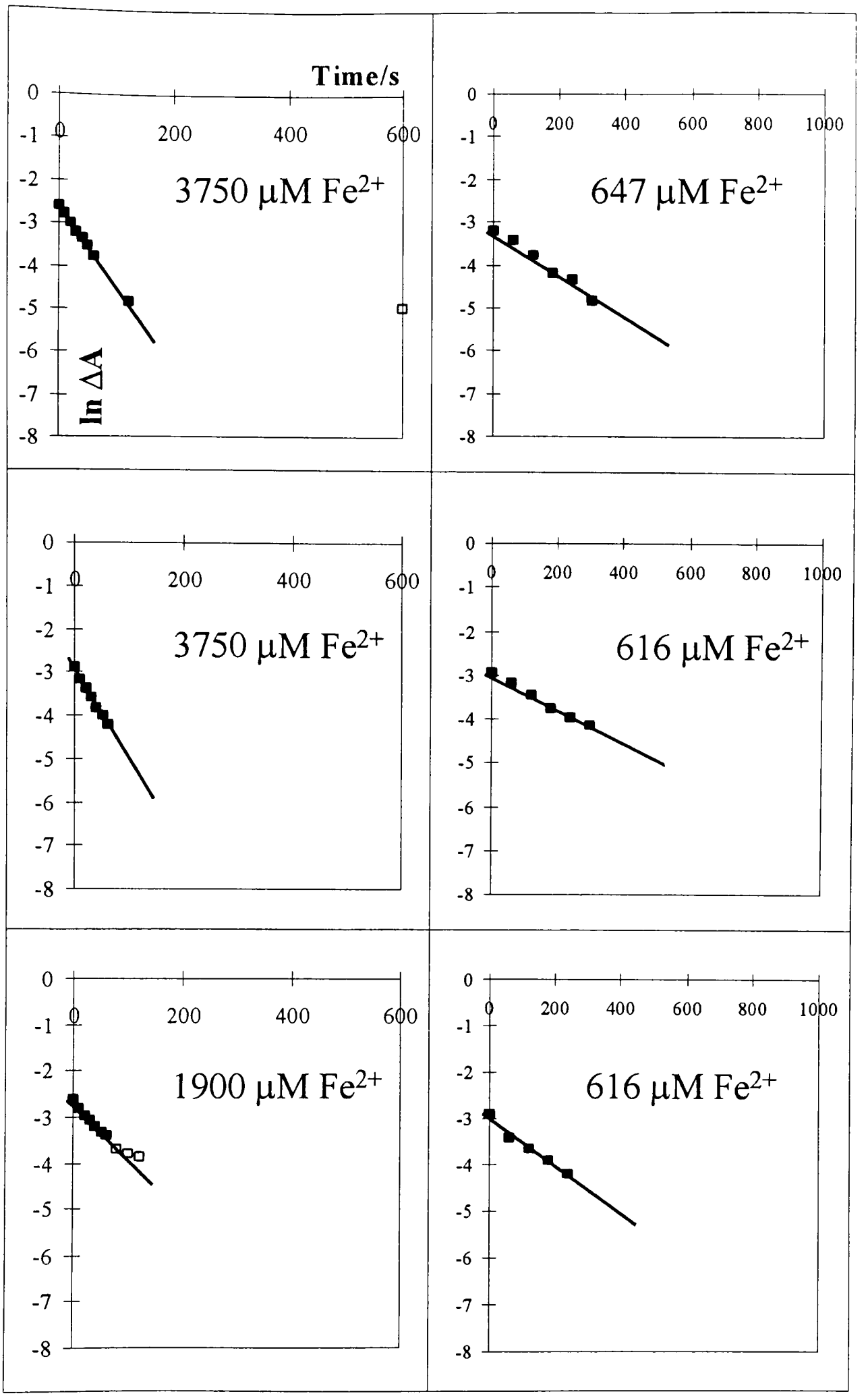

Figure 6.20 Spectroscopic observation of Fe uptake by 3Fe Fd_B

Graphs of ln ΔA against time as recorded at 426 nm. Open squares denote data which were not used when calculating the slope of the lines. Conditions were as described in the text, 25 °C, pH 7.0. Pseudo first-order rate constants are as tabulated in Table 6.3.

The slopes of each of these plots (k_{obs}) were then plotted against the corresponding Fe concentrations (Figure 6.21).

$Fe^{2+}/\mu M$	$Fe^{2+}/\mu M$ [i]	k_{obs}/s^{-1}
716	616	-0.0043
716	616	-0.0050
747	647	-0.0052
2000	1900	-0.0126
3850	3750	-0.0202
3850	3750	-0.0175

Table 6.3 Dependence of k_{obs} on Fe^{2+} concentration for $[3Fe\text{-}4S]_A$

$Fe^{2+}/\mu M$	$Fe^{2+}/\mu M$[f]	k_{obs}/s^{-1}
716	616	-0.0052
716	616	-0.0043
747	647	-0.0054
2000	1900	-0.0094
3850	3750	-0.0186
3850	3750	-0.0217

Table 6.4 Dependence of k_{obs} on Fe^{2+} concentration for $[3Fe\text{-}4S]_B$

As can be seen from the plots of k_{obs} against Fe^{2+} (Figure 6.21) the plot is linear passing through the origin and the determined values for the rate, k_{uptake}, can be seen in Table 6.5.

[i] The Fe^{2+} concentrations shown in this column take into account the complexation of Fe^{2+} by EGTA. EGTA was present in the protein solution at all times. (It was necessary to have EGTA in the protein solution because it has been observed that extraneous iron in the buffer/protein solution results in partial conversion of some [3Fe-4S] clusters to [Fe3Fe-4S] clusters.) It was therefore necessary to subtract the concentration of EGTA (100 μM) from each Fe^{2+} concentration.

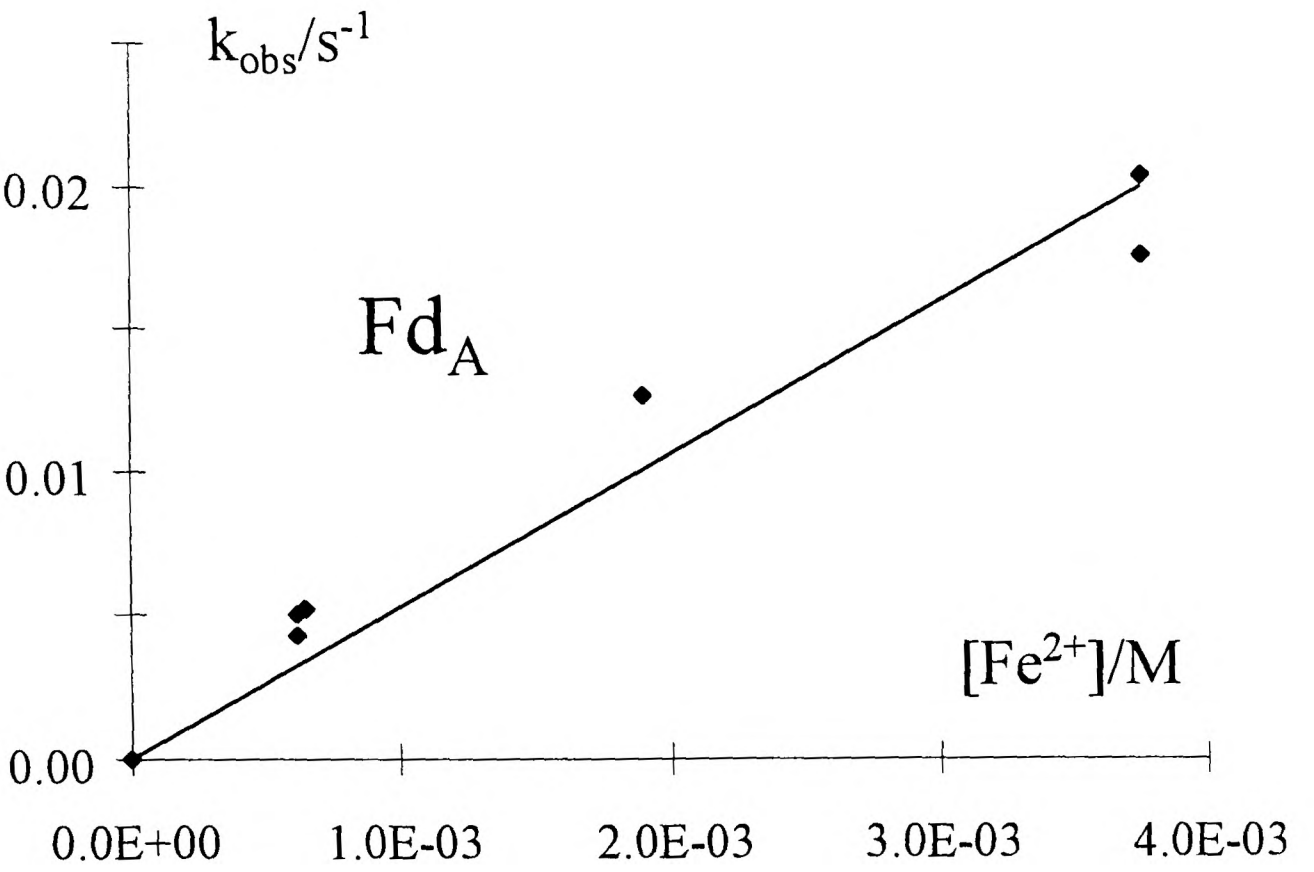

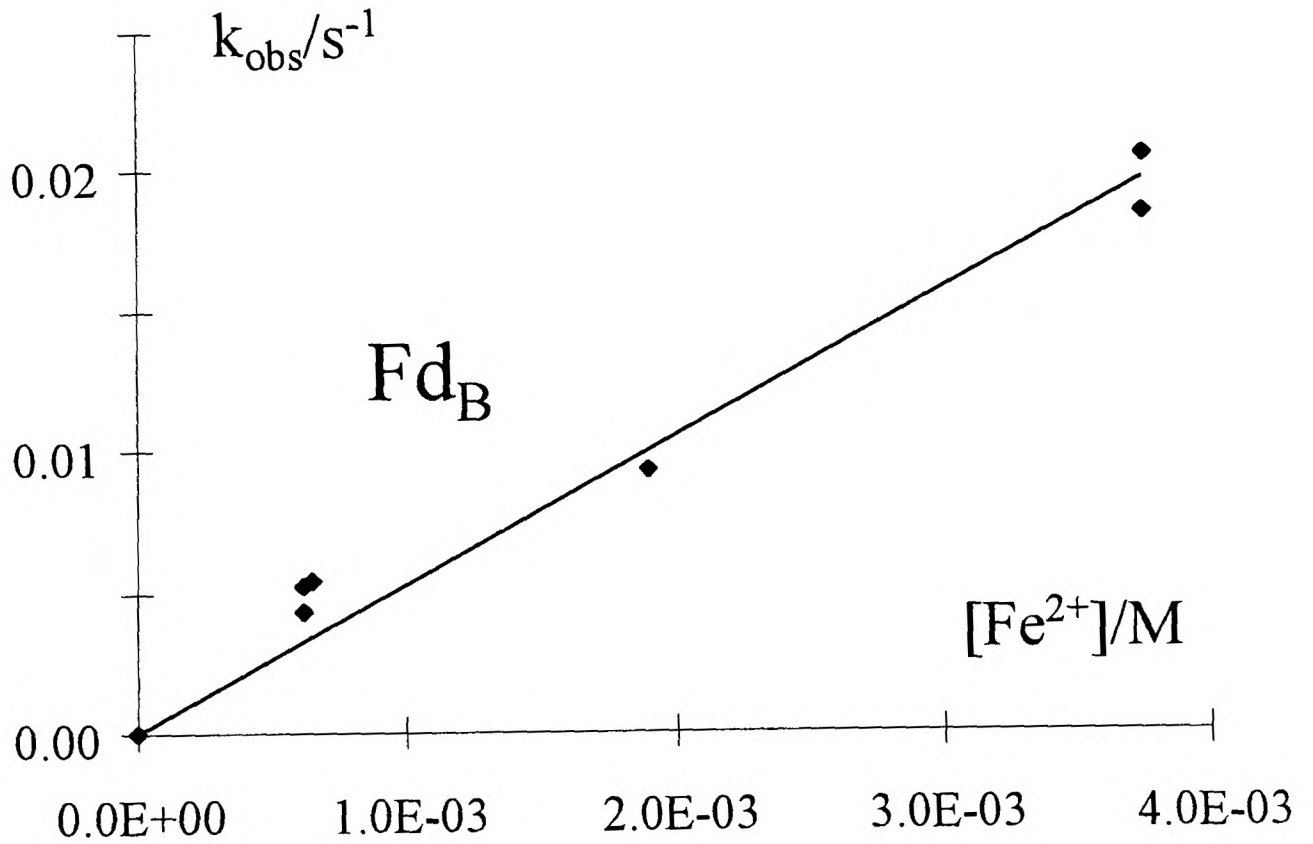

Figure 6.21 Pseudo first-order rate constants as a function of Fe^{2+} concentration for Fe^{2+} uptake by $[3Fe\text{-}4S]_A$ (upper) and $[3Fe\text{-}4S]_B$ (lower)

Variation of pseudo first-order rate constants (ordinate = k_{obs}/sec^{-1}) with Fe^{2+} concentration.

	$[3Fe\text{-}4S]_A$	$[3Fe\text{-}4S]_B$
k_{uptake} / s^{-1} M^{-1}	5.28	5.23

Table 6.5 Rate constants (second order) for Fe uptake in the $[3Fe\text{-}4S]_{A/B}$ clusters from *Pf* Fd

6.3.7 Metal Ejection

The complementary method of studying heterometal clusters and the characteristics of cluster formation, is to observe cluster disassembly. This method has been utilised for *Da* Fd III to explore the stabilities of various heterometal clusters, (*Chapter 3*) and is here used once again, to study the stabilities of three heterometal clusters of *Pf* Fd.

Experiments were carried out to determine the characteristics and traits of metal ion ejection for the metal adducts, [Fe3Fe-4S], [Zn3Fe-4S] and [Cd3Fe-4S] of *Pf* Fd. The experiments were carried out with samples of the heterometal clusters which had been produced in bulk solution using Method 1, i.e. chemical reduction with dithionite. A film was made of the heterometal cluster and allowed to equilibrate in buffer (2-3 complete cycles of the potential scanning range). Two techniques were employed - the first method is known as the 'poise and sample' method. The electrode was held at a fixed potential, then transferred to a second pot where it was poised at a specific potential for increasing amounts of time - a voltammetric scan was then recorded at each time interval. The second method involved cycling the pre-transformed cluster over a defined scan range and on each subsequent scan the positive scan limit was increased by a set interval e.g. 100 mV. In all cases the unique signature of the [3Fe-4S] cluster, namely the C' couple and its characteristic $2e^-$ reduction peak was an excellent indicator of cluster status.

6.3.7.1 Zinc

A sample of the [Zn3Fe-4S] cluster was poised at different potentials for time intervals of 60 s, following which a cyclic voltammogram was recorded. In all cases, no formation of the [3Fe-4S] cluster was observed at negative potentials (-757 mV or -457 mV), even after holding for 10 minutes. Subjecting a protein film containing the Zn cluster to more positive potentials than that of the Zn cluster's reduction potential (i.e. -262 mV) resulted in some cluster degradation. The amount of degradation depended upon both the time and the potential at which the cluster was poised. When the poising potential was -207 mV, i.e. midway between the $[Zn3Fe\text{-}4S]^{2+/1+}$ and $[3Fe\text{-}4S]^{1+/0}$ reduction potentials, slight signs of Zn ejection were observed. It was not until the film was poised at a potential where the [3Fe-4S] cluster was in the oxidised (1+) state, that considerable ejection of the Zn from the cluster was observed. Examples

of poising at different potentials for the Zn cluster are shown in Figure 6.22. Since the potential of the Zn cluster is -262 mV and that of the A' couple is -150 mV, the two signals overlap somewhat and as a result only one composite peak is visible. This one peak can clearly be seen to shift in potential, concomitant with the increase in the C' couple. That is, as the Zn ion is ejected from the heterometal cluster, the contribution to the composite peak of the A' couple increases, and therefore the peak shifts to a more positive value. The results of poising at different potentials are shown in Table 6.6.

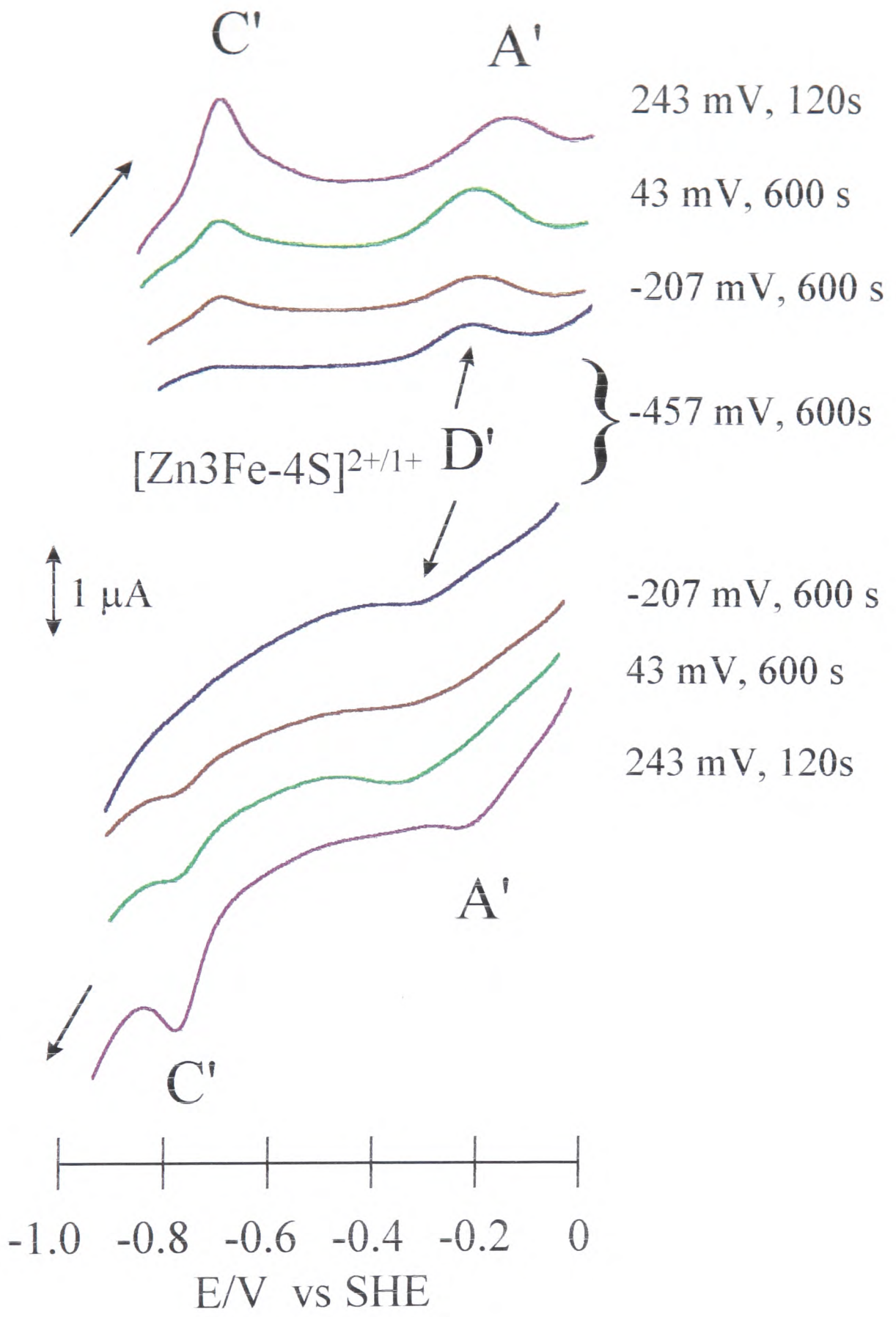

Figure 6.22 Film voltammetry showing ejection of Zn from [Zn3Fe-4S]

The Zn cluster was prepared as Method 1 (see text). The protein film, prepared using polymyxin as co-adsorbate, was held at the potential and times indicated and then a scan was recorded. Conditions were 20 mM mixed buffer, 0.1 M NaCl, 0.1 mM EGTA, pH 7.0, 200 µg ml^{-1} polymyxin as co-adsorbate, 0 °C, scan rate 500 mV s^{-1}.

Potential	% of Zn Ejected
-457	0 after 600 s
-207	< 10 after 600 s
43	50 after 600 s
143	75 after 600 s
243	100 after 120 s
343	100 after 60 s

Table 6.6 Zinc ejection from the [Zn3Fe-4S] core

The percentage of Zn ejected is quantified as follows:

***0 % ejected**: no observed appearance of the C' couple height, i.e. [M3Fe-4S] remains intact.*

***100 % ejected**: no sign of the D' couple in the voltammetry, together with no further increase in the C' couple height after further poising at this potential.*

6.3.7.2 Cadmium

The pattern of cadmium ejection was extremely similar to that of zinc. Ejection of Cd from the cluster was not observed at potentials below that of the [Cd3Fe-4S] reduction potential, -359 mV. Ejection of Cd was notably faster when the potential at which the film was poised was above the reduction potential of the $[3Fe\text{-}4S]^{1+/0}$ cluster (-150 mV). The rate subsequently increased as the potential was raised. Holding at a potential of 343 mV was found to cause release of the Cd within 20 s. Scans of the Cd cluster poised at different potentials are shown in Figure 6.23. Additionally the marked dependence upon potential can be clearly seen in Figure 6.24, where the positive switching potential of the scan is increased by 100 mV. Here, looking at the whole scan, the D' couple can be clearly seen decreasing together with the increase of the A' and C' couples.

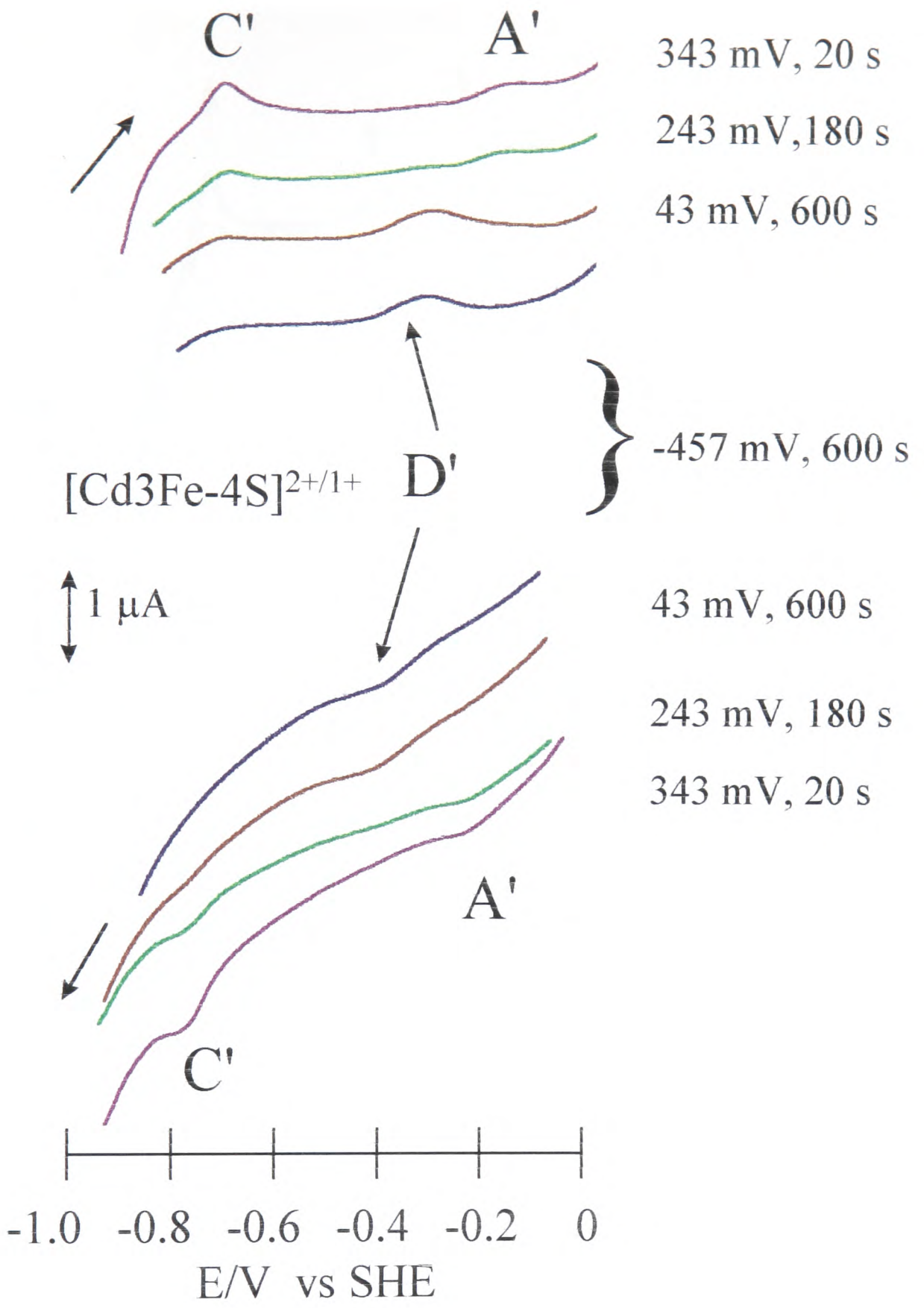

Figure 6.23 Film voltammetry showing ejection of Cd from [Cd3Fe-4S]

The Cd cluster was prepared as Method 1 (see text). The protein film, prepared with polymyxin as co-adsorbate, was held at the potential and times indicated and then a scan recorded. Conditions were 20 mM mixed buffer, 0.1 M NaCl, 0.1 mM EGTA, pH 7.0, 200 µg ml^{-1} polymyxin as co-adsorbate, 0 °C, scan rate 500 mV s^{-1}.

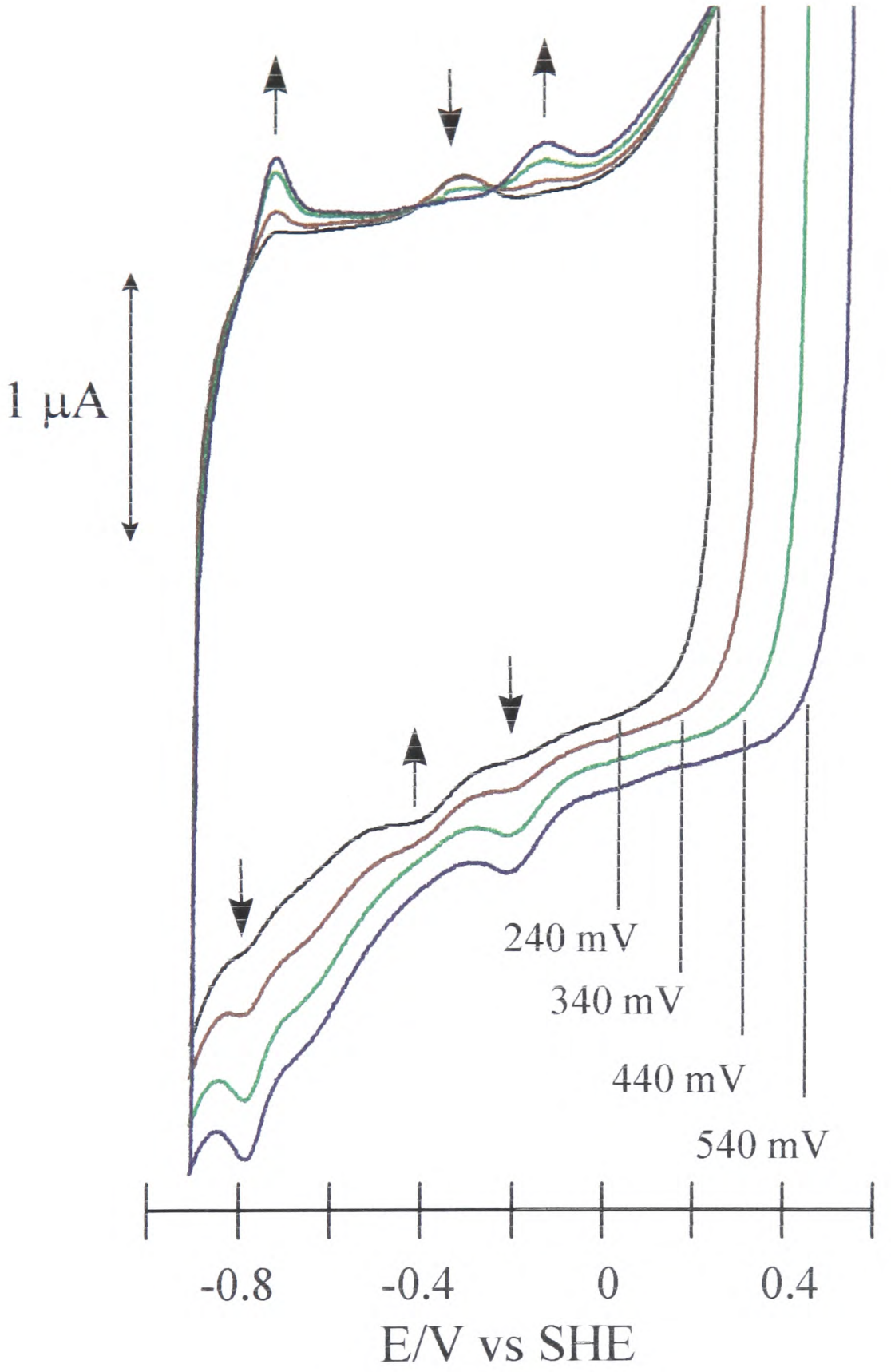

Figure 6.24 Film voltammetry showing sequential ejection of Cd from [Cd3Fe4S]

The [Cd3Fe-4S] cluster was prepared from the [3Fe-4S]$_{ox}$ form by poising a film at -540 mV in the presence of Cd (Method 2 - see text). Voltammograms (50 mV s^{-1}) were then recorded at increasingly positive switching potentials, after transfer to a pot containing 20 mM mixed buffer, pH 7.0, 0.1 M $NaNO_3$, with 0.1 mM EGTA, 200 µg mg^{-1} polymyxin as co-adsorbate, 0 °C.

Potential	% Cd Ejected
-757	0 after 600s
-242	0 after 600s
43	< 10 after 600s
143	50 after 600s
243	100 after 180 s
343	100 after 20 s

Table 6.7 Cadmium ejection from the [Cd3Fe-4S] core

6.3.7.3 Fe Ejection

Experiments were carried out on the [Fe3Fe-4S] cluster as had been carried out for the Zn and Cd adducts. It was found that the [Fe3Fe-4S] cluster was much less reactive when the cluster was subjected to oxidising potentials, compared with the Zn or Cd adducts. This cluster had to be poised at potentials as high as 500 mV for at least 60 s before any sign of the [3Fe-4S] product was observed. The stability of the [Fe3Fe-4S] cluster, when poised at different potentials, is evident from the results shown in Figure 6.25, where it can be seen that after 10 minutes at 243 mV the voltammogram was essentially unchanged, i.e. still that of the [Fe3Fe-4S] form. It was not until the film was poised at 543 mV for 300 s that there were signs of Fe ejection i.e. the A' and C' couples became visible. Tabulated results of oxidative poising and the subsequent percentage Fe ejected from the cluster are shown in Table 6.8. Complete removal of Fe from the [Fe3Fe-4S] cluster was found to be difficult using this method, requiring very positive oxidising potentials (> 500 mV). However, such high potentials were also found to cause more widespread film degradation as evidenced from the loss of total signal intensity.

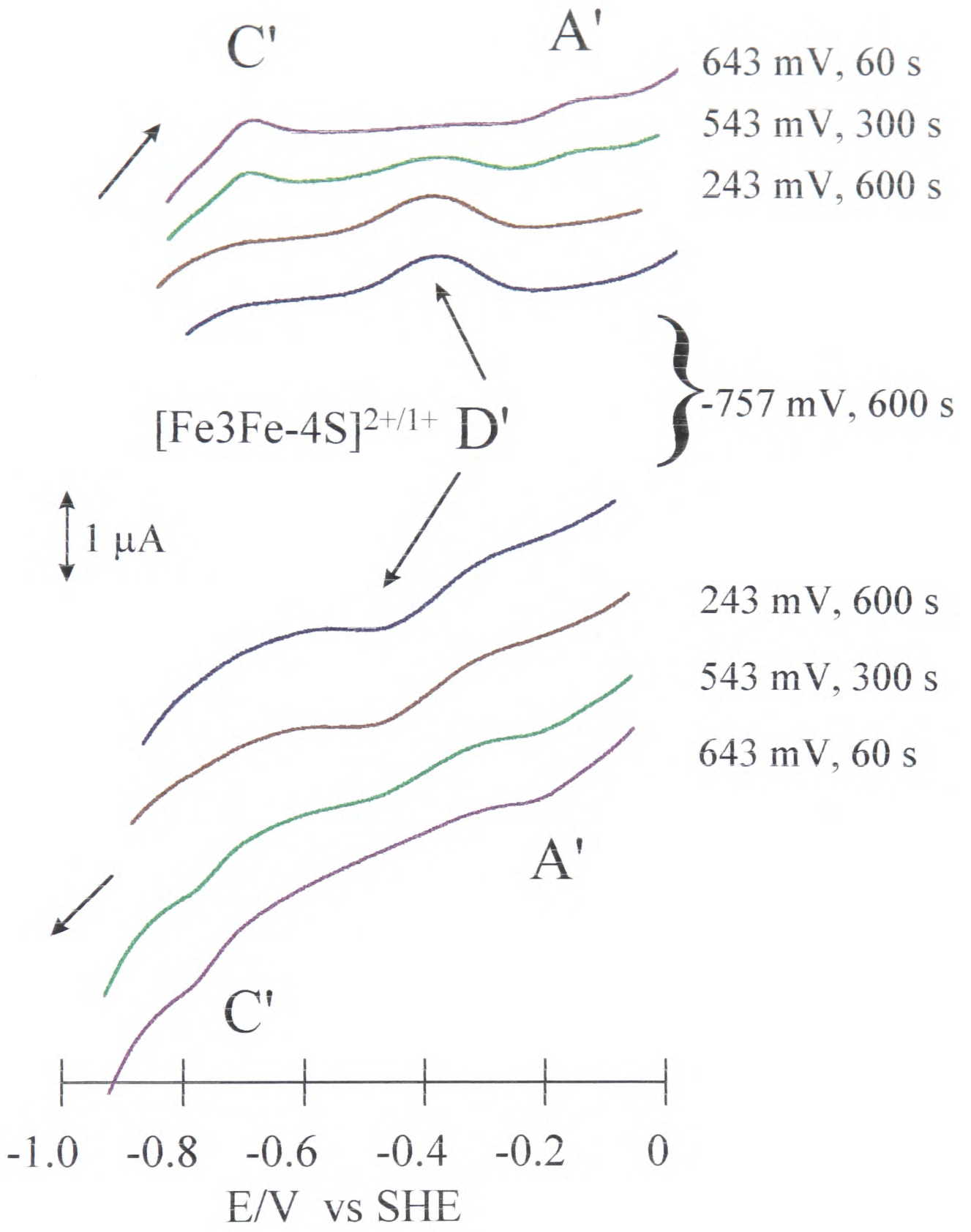

Figure 6.25 Film voltammetry showing ejection of Fe from [Fe3Fe-4S]

The Fe cluster was prepared by Method 1 (see text). The protein film, prepared with polymyxin as co-adsorbate, was held at the potential and times indicated and then a scan recorded. Conditions were 20 mM mixed buffer, 0.1 M NaCl, 0.1 mM EGTA, pH 7.0, 200 µg ml^{-1} polymyxin as co-adsorbate, 0 °C, scan rate 500 mV s^{-1}.

Poising Potential/mV	% Fe Ejected from [Fe3Fe-4S]
-757	0 after 600 s
243	0 after 300 s
343	0 after 300 s
443	0 after 300 s
543	50 after 300 s
643	100 (Partial film destruction)

Table 6.8 Iron ejection from the [Fe3Fe-4S] core

Although it had been found that poising at potentials more positive than $E^{o'}$ of the [3Fe-4S] cluster facilitated ejection of the Zn or Cd adducts, this was not the case for the [Fe3Fe-4S] cluster. In the latter case, the potential at which the protein film had to be held to facilitate Fe ejection was considerably more positive. This stability of the [Fe3Fe-4S] cluster towards oxidative degradation may be indicative of the cluster's preferred co-ordination of Fe as the fourth metal of the cubane. The Zn and Cd adducts behaved very similarly when subjected to oxidising potentials, with respect to the potential at which they were ejected, although the Cd adduct was marginally more stable. It is likely that this is due to the enhanced binding of the softer Cd to the tri-μ_2-S core and its higher thiophilicity. Thus, each heterometal cluster was found to have a different stability with respect to electrochemical oxidation.

Disulfide Bridge Considerations

For each of the aforementioned studies on the ejection of the fourth metal from the cluster, Zn, Cd and Fe, experiments were carried out with both the disulfide bridge oxidised, $[M3Fe\text{-}4S]_A$ and reduced $[M3Fe\text{-}4S]_B$, forms. No differences were observed between the two different states for any of the heterometal clusters.

6.4 DISCUSSION

6.4.1 pH Dependence

From the electrochemical investigation which was carried out over a wide pH range, it was found that the reduction potential of the [4Fe-4S] cluster is pH-independent. This is in contrast to the [3Fe-4S] form, which was found to exhibit a marked pH dependence and can be compared with *Av* Fd I, *Da* Fd III and *Sa* Fd.[35] By analogy with all the [3Fe-4S] clusters so far examined by direct electrochemical means, *Pf* Fd also undergoes hyper-reduction to the all-ferrous cluster: $[3Fe\text{-}4S]^{2-}$. Thus, significantly, the hyper-reduced state $[3Fe\text{-}4S]^{2-}$, which has been partially characterised in *Sa* Fd, has been identified in a protein containing only a [3Fe-4S] cluster. This hyper-reduced state has now been identified in [3Fe-4S] clusters from both mesophilic and hyperthermophilic organisms although *in vivo* function of this very low potential couple (if any) has yet to be identified. The electrochemical experiments clearly show that the overall proton uptake for the A' and C' couples in the neutral/weakly acidic region can be calculated by averaging the n $E^{o'}$ values for A' and C', to give a value $(dE^{o'}/dpH)_{av}$ of -51.9 mV/pH unit which equates to a net ratio for H^+/e^- close to 1.0. Similar values have been found for *Av* Fd I, *Da* Fd III, *Sa* Fd[35] and *Thermoplasma acidophilum* (*Ta*) Fd, data for which are shown in Table 6.9. This result reinforces conclusions drawn previously, that reduction of the well-characterised oxidised $[3Fe\text{-}4S]^{1+}$ cluster to the hyper-reduced state $[3Fe\text{-}4S]^{2-}$ requires net transfer of three protons from bulk solution.[35] Above pH 8.0 this relationship breaks down, and it was seen that the complex reaction is suppressed. This was observed in the voltammetry - film experiments showed a marked attenuation of the C' couple at pH > 8.0, but not of the A' couple. Throughout the wide pH range, ionisations of $[3Fe\text{-}4S]^{0}$ complement those for $[3Fe\text{-}4S]^{2-}$, thus yielding a straight line for the overall reaction (Figure 6.7). The electroneutrality of the overall reduction is probably responsible for the straight line of the corresponding A' and C' pH dependencies. The ionisation of a nearby residue such as aspartate will be relatively sensitive to cluster oxidation level and its influence on the reduction potential is largely quenched, c.f. the A' couple in the region where an electron but not a proton is added.

Ferredoxin	$(dE^{o'}/dpH)_{av}$/ mV/pH [#]
Pyrococcus furiosus Fd	51.9
Azotobacter vinelandii Fd I	50.1
Sulfolobus acidocaldarius Fd	49.8
Desulfovibrio africanus Fd III	51.4
Thermplasma acidophilum Fd	55.1

Table 6.9 Comparison of $(dE^{o'}/dpH)_{av}$ for the three electron reduction of $[3Fe\text{-}4S]^{1+}$ clusters from different ferredoxins

[#] *Where $(dE^{o'}/dpH)_{av} = (dE/dpH)\{1/3[A'+2C']\}$ calculated for all individual data points A' and C'*

In addition, it was possible to observe the reduction couple C in molecules diffusing freely between the solution and the electrode interface, but only at very low scan rates (2 mV s^{-1} - see Figure 6.5). Experiments which have been carried out with solutions of *Av* Fd I and *Da* Fd III have consistently shown that the reduction couple $[3Fe\text{-}4S]^{0/2-}$ is not observed during bulk solution voltammetry.[26,45] This suggests that the reaction only occurs when the molecules are adsorbed on the electrode surface.[31,48] This restriction is likely to be due to kinetic complications for the timing of the multielectron and multiproton transfer reaction. However, this was not found to be the case for *Sa* Fd, the protein in bulk solution undergoes hyper-reduction, and the C couple is readily observed. This readiness for *Sa* 7Fe Fd to undergo hyper-reduction in bulk allowed larger samples to be generated, and the $[3Fe\text{-}4S]^{2-}$ state could be investigated with EPR and MCD.[35]

Pf Fd, however, seems to be an intermediate case; signs of the hyper-reduction couple were seen in bulk solution but only under certain conditions. The scan rate had to be very slow and the C couple was only seen on the first scan. The disappearance with continued slow cycling may reflect instability of the $[3Fe\text{-}4S]^{2-}$ state in this ferredoxin or

it may reflect subtle changes on the electrode surface which occur during continued cycling.[j]

The MCD spectra indicate that the pH dependence of the $[3Fe\text{-}4S]^{1+/0}$ couple can be rationalised in a complex series of changes, culminating at pH < 3. The final form is similar to that generated in other Fds at low pH.[34,40-42,50,51] Thus protonation can be considered as a characteristic property of $[3Fe\text{-}4S]^{0}$ centres, but noticeably there is a large difference in pK values, with the cluster in *Azotobacter* ferredoxins being particularly basic. [41,42,50] The observation that the [4Fe-4S] cluster in Fd_A or Fd_B shows little pH dependence of reduction potential suggests strongly the involvement of aspartate-14 which becomes ligated upon metal ion addition. Reported pK values for aspartate in proteins cover a wide range, with 5.5 being typical.[52] However, the carboxylate pK will be sensitive to the oxidation level of the $[3Fe\text{-}4S]^{1+/0}$ cluster due to the introduction of a nearby negative charge, and since invariably $pK_{red} > pK_{ox}$, pK_{ox} = 4.9 and pK_{red2} = 6.7 were assigned to deprotonations of aspartate-14 in reduced and oxidised forms respectively. Although these ionisations occur within the sequence of spectral changes in the MCD, and leave the pK_{red1} at 2.8 as the formal value for $[3Fe\text{-}4S]^{0}$ protonation, it is probable that the stepwise addition of two protons to the cluster region will involve anti-cooperative interactions between the aspartate and the cluster, thus giving rise to the complex, drawn-out titration profile.

---

[j] Recent film experiments with *Sa* 7Fe Fd, have shown that at low scan rates the voltammetry of the C' couple ($[3Fe\text{-}4S]^{0/2-}$ appears simple and reversible, but as the scan rate is increased, the reductive peak separates into two components (C1 and C2) whilst the oxidation peak remains as a single entity. Ultimately, the reductive peak is composed entirely of the C2 wave and the reduction potential of this new couple is more positive than the original C couple. The new couple is associated with a $2H^+/2e^-$ reaction and it has been proposed that disulfide coupling (of the cluster S atoms) could form the basis of this new phenomenon.[49]

A recent publication by Brereton *et al* explores a number of mutants of *Pf* Fd - D14X where X = C, S, H, N, V and Y.[36] It was found that only in the D14S and D14C mutants was a $[4Fe\text{-}4S]^{2+/1+}$ cluster present, the other mutants only contained a $[3Fe\text{-}4S]^{1+/0}$ centre. The reduction potentials of the D14C and the D14S mutants were decreased by 58 and 133 mV respectively, compared to the wild-type (WT) ferredoxin, which has a reduction potential of -368 mV (this compares well with the bulk electrochemical value measured at -361 mV for the native 4Fe Fd (*Section 6.3.5.1*)). While the reduction potentials of the WT or D14C mutants were not significantly dependent upon pH, the reduction potential of the D14S mutant, showed a marked dependence with pH; a slope of -55 mV/pH unit and a pK of 4.75 were calculated.[36] This was proposed to be arise from protonation of the co-ordinating serinate, though it is not known if serine remains as a ligand or is replaced by $H_2O/^-OH$ when protonation occurs. This is similar to the situation found for the C56S and C60S mutants of the 2Fe Fd from *Clostridium pasteurianum* - although in the latter case the pK values for the protonation are much higher ($pK_{red} \sim 9$), see *Chapter 5*.

The mutants containing the 3Fe form had reduction potentials varying between 15 and 118 mV more positive than that of WT 3Fe form. The mutants, D14N, D14V and D14Y were all found to have a single pK in their pH titration profile, and this pK (3.3, 4.5 and 3.8 respectively) was proposed to be for cluster protonation.[k] The WT 3Fe form and the D14H were found to have a complex pH titration curve with two pK values, the pK_{ox} and pK_{red} values were 4.7 and 5.9 for the D14H mutant and 4.2 and 5.9 for the WT form respectively. The pK_{red} found for the WT 3Fe form and D14H is at pH 5.9 and was proposed to be due to the ionisable side chains of the Asp14 (WT) or His14, which must be influencing the properties of the cluster. Clearly this pH dependence data does not reflect the observations made in this chapter for the native 3Fe Fd, i.e. that the complex pH titration profile contains three pK values: pK_{ox} = 4.9 and pK_{red2} = 6.7 to deprotonations of Asp14 in the oxidised and reduced forms respectively; and the pK_{red1} at 2.8 as the formal value for $[3Fe\text{-}4S]^0$ protonation.

[k] This pK is not clearly defined - in the paper it is implied that this is the pK_{ox} of the cluster, but if this were the case the curvature of the graph would be opposite to that which is seen in the data.

6.4.2 Metal Uptake

6.4.2.1 Cluster Transformations

Transformations between the [3Fe-4S] and [M3Fe-4S] clusters of *Pf* Fd can be discussed with reference to the framework shown in Figure 6.26. Additionally comparisons can be made with similar studies carried out with *Da* Fd III.[20]

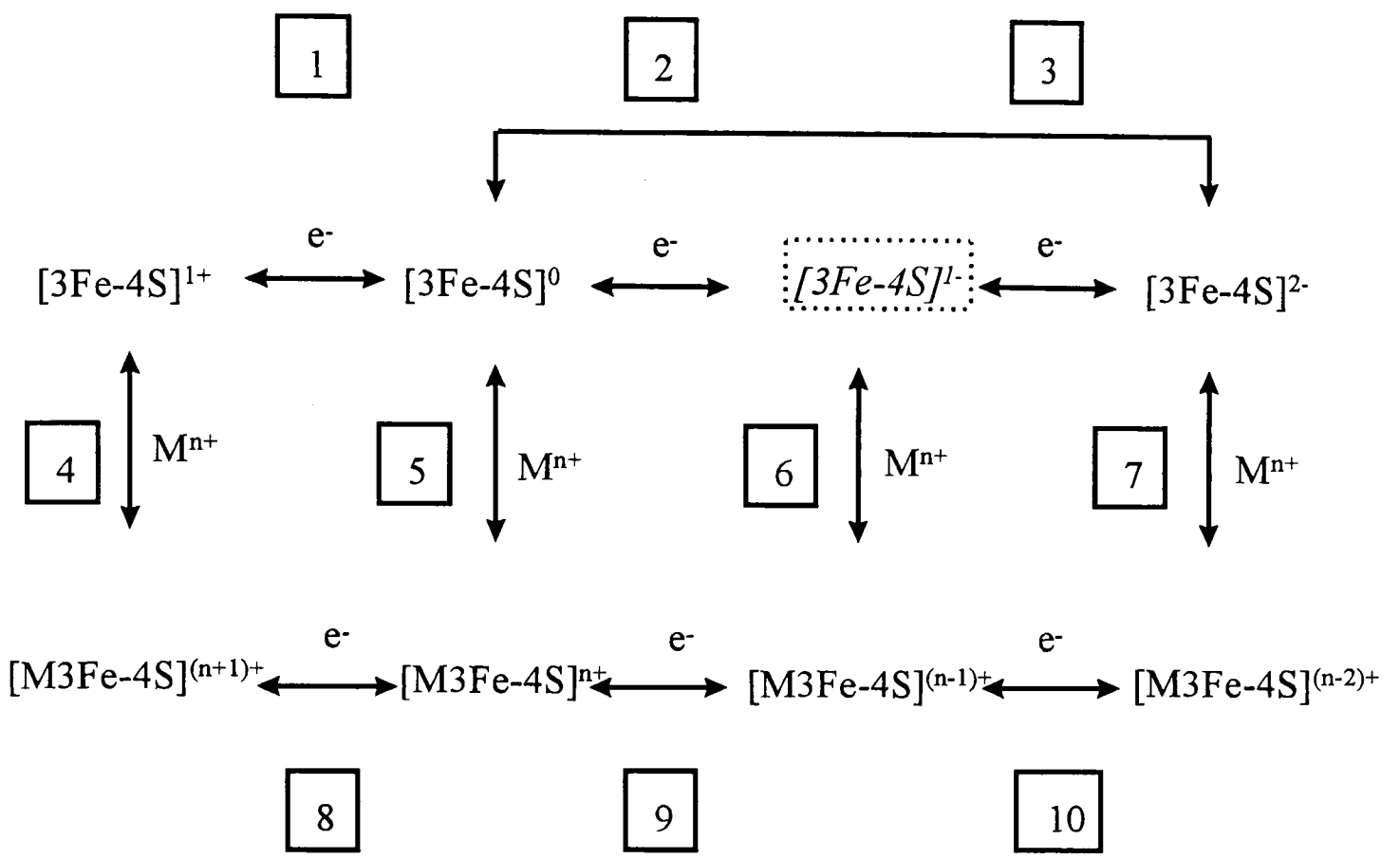

Figure 6.26 Core model for cluster transformations of [3Fe-4S] clusters

As mentioned previously, it is evident that the rates of metal uptake, [3Fe-4S] → [M3Fe-4S], (Reaction 5) measured under potential control in the film, are much slower for *Pf* Fd than for *Da* Fd III.[17,20] For M = Fe, reaction with *Pf* Fd at 25 °C was estimated to be only 50 % complete after 60 minutes, compared to less than one minute at 0 °C for *Da* Fd III, under comparable Fe levels. Due to these slow reaction rates, equilibrium constants for Reaction 5 were not measured for M^{2+}. In contrast, uptake and release of Tl^{+} was fast for *Pf* Fd with changes occurring on rapid voltammetric timescales, and appearing only a little slower than observed for *Da* Fd III at the same temperature of 0 °C.[18]

The most significant observations from the metal uptake experiments of the [3Fe-4S] cluster of *Pf* Fd are as follows. Firstly, there is a considerable difference in the rates of metal uptake between Tl^{+} and the M^{2+} ions (Fe, Cd and Zn). Secondly, when the [3Fe-4S] cluster is adsorbed on the electrode surface (Method 2) Fe uptake is slower than Cd or Zn uptake. Thirdly, in addition, when a bulk sample of protein was electrochemically reduced, and quantitative amounts of Fe were added to the protein, the rate of metal uptake was observed to be faster for the 3Fe Fd_A form than for the 3Fe Fd_B form.

As can be seen from the comparative data in Table 6.10, there was no difference in the reduction potentials of the Zn and Cd adducts depending on whether they were formed using Method 1 or Method 2. Therefore, it was concluded that the method of formation does not have a significant affect upon the reduction potentials of the heterometal cluster, because the product in each case is believed to be identical.

	Protein film voltammetry			**Protein bulk solution voltammetry**		**Values measured by EPR titration**
	Method 1		*Method 2*			
	Fd_A	**Fd_B**	**Fd_A**	**Fd_A**	**Fd_B**	-
[3Fe-4S]	-150	-159	-150	-215	-219	-160[11]
[Fe3Fe-4S]	-430	-428	-419*	-361	-365	-345[11]
[Zn3Fe-Fe]	-262	-261	-274	-196 (?)	-	-241[11]
[Cd3Fe-4S]	-359	-353	-347	-	-	-470[12]

Table 6.10 Reduction potentials of heterometal clusters of *Pf* Fd, obtained using different experimental methods

All results are ± 10 mV

** [Fe3Fe-4S] formed at 25 °C, as Fe^{2+} uptake on film at 0 °C not observed*

6.4.2.2 Iron, Zinc and Cadmium

Successful incorporation of Fe, Zn and Cd was achieved with the addition of a M^{2+} solution to the dithionite reduced [3Fe-4S] cluster (Method 1). In general the samples were left for 15 minutes at 25 °C (after addition of the M^{2+} and dithionite) and the resultant solution was then investigated. After this length of time, the percentage conversion to the metal adduct was ca. 95-100 %. This was estimated by observing the peak height of any remaining C' couple. No further purification was required to remove excess metal ions or sodium dithionite, as the agents for metal addition were diluted in the buffer electrolyte solution when the electrode was placed into the cell.

Metal uptake into the [3Fe-4S] cluster, when adsorbed in the protein film (Method 2) was not as straightforward as the chemical reduction method. The most noticeable feature was that at 0 °C, uptake of Fe^{2+} by the [3Fe-4S] cluster was not observed. This was despite poising for periods of up to 90 minutes, together with a large excess of Fe^{2+}. The 'poise method' of metal ion uptake was relatively straightforward for Zn and Cd, although long periods of time (t = 60 minutes) were required before 100 % conversion to the [M3Fe-4S] cluster was observed. This time dependence for metal ion uptake for the 3Fe Fd is in direct contrast to the results for *Da* Fd III.[17,20]

It is difficult to readily explain this major difference in metal uptake ability between the clusters in the two proteins. However, it can be proposed that it is the protein structure which has the major influence over the cluster reactivity as all the other experimental conditions for the two proteins were the same. The slow reactivity of *Pf* Fd could be as a direct result of the protein originating from a highly stable hyperthermophilic organism and thus its protein structure is more rigid than that of similar proteins from mesophilic organisms. It is extremely likely that all of the proteins contained within *Pf* are specially adapted to the extreme conditions under which they must function. Therefore, at the temperature at which this study was undertaken, 0 °C, it is possible that the *Pf* Fd is in a 'semi-frozen' state and therefore the protein conformation is not as flexible as it would be at 100 °C, hence slowing down these metal uptake reactions, optimal growth temperature for *Pf* is ca. 100 °C.[1]

Da Fd III and *Pf* Fd are mesophilic and hyperthermophilic proteins respectively, and their different structures may well influence their behaviour on the electrode surface. *Da* Fd III is likely to be considerably more conformationally labile than *Pf* Fd, and this may be the reason why *Da* Fd III appears more reactive when adsorbed as a protein film. Neither structures are known, but two possible contributing factors are evident from the amino-acid sequences that co-ordinate the [3Fe-4S] or [M3Fe-4S] cluster.[13,31]

***Da* Fd III**	**C** - T - G - **D** - G - E - **C**----------**C** - E
***Pf* Fd**	**C** - I - G - **D** - A - I - **C**----------**C** - P

Figure 6.27 Cluster amino acid sequence for *Da* Fd III and *Pf* Fd
Greater mobility in the cluster region of Da Fd III ought to be favoured by the presence of glycine either side of the putative ligand aspartate, and from the unusual presence of glutamate(E) instead of proline (P) following the remote cysteine.

The hypothesis that the reactivity of a protein film depends, to some extent, upon the interactions between the *different* protein structures and the electrode surface may explain the differences in reactivity between *Da* Fd III and *Pf*. It does not however, explain the differences in rates of metal uptake for one particular protein. For *Pf* Fd the rate of Fe^{2+} uptake is significantly slower than the rate of uptake of Zn^{2+} and Cd^{2+}; whereas the variation in metal uptake for *Da* Fd III, for different M^{2+} ions, was less marked (Fe < Zn < Cd).[17] This observation therefore implies that the different rates of metal uptake for *Pf* Fd are due to specific metal-protein interactions. When comparing the film experiments with the spectrophotometric determinations of the rates of Fe^{2+} uptake at the $[3Fe\text{-}4S]^0$ cluster in solution they clearly show,

a) the protein is more reactive in solution than in the film[1]
b) the uptake of Fe^{2+} follows simple second-order kinetics up to 4 mM Fe^{2+}
c) the presence or absence of the disulfide bridge makes no difference to the rates

[1] Film instability prevented experiments being performed at high temperatures where higher reactivity would be expected.

6.4.2.3 Thallium

In contrast to Fe, Zn and Cd uptake, reaction with thallium was found to be very fast, with electrochemical equilibration occurring on voltammetric timescales, only slightly longer than found for *Da* Fd III.[18] The mode of thallium binding to the [3Fe-4S] cluster of *Pf* Fd is therefore proposed to differ from the mode of M^{2+} binding.

From the non-linear regression fit to Equation 6.6, the parameters of thallium binding i.e. the dissociation constants for Tl^+ binding to the oxidised or reduced form of the [3Fe-4S] cluster, (K_d^{ox} and K_d^{red}) were determined. The values of 740 ± 40 mM and 1.9 ± 1.0 μM for K_d^{ox} and K_d^{red} respectively, show clearly that the thallium has a higher affinity for the reduced cluster $[3Fe\text{-}4S]^0$, than for the oxidised cluster $[3Fe\text{-}4S]^{1+}$. The K_d^{red} value is very similar to the value obtained for *Da* Fd III (1.5 ± 1 μM) but the K_d^{ox} of Tl^+ for *Pf* Fd is much greater than for *Da* Fd III (340 ± 40 mM).[18] Estimation of the Tl^+ 'on' rate gives a value of 10^8 M^{-1} s^{-1}, which is in the realm of a diffusion limited reaction[m] and this suggests that co-ordination of thallium does not require a substantial protein conformational change. This value is based on an estimation of k_{off} as 10^2 s^{-1}, from observing voltammetry and the release of Tl^+ at high scan rates.

Since Tl^+ still reacts so rapidly with $[3Fe\text{-}4S]^0$ we can conclude that the slow rate of M^{2+} uptake is not due to the cluster domain being obscured in the protein film. An alternative explanation is that Tl^+ and the M^{2+} ions are not co-ordinated in the same way by the protein, and make different demands on the mobility of residues. One possibility is that the tri-μ_2-sulfido face of the cluster is the only ligand required for thallium co-ordination, i.e. a protein ligand is not needed.[18] A similar example of Tl^+ being co-ordinated by three sulfido ligands is seen in the inorganic complex $[Tl([9])aneS_3)]^{1+}$, produced by reacting a solution of $TlNO_3$ with an excess of the ligand [9]aneS$_3$, (the trithia crown 1,4,7-trithiacyclononane).[54] It has been shown by X-ray crystallography that the thallium is co-ordinated by three Tl-S bonds in this complex. Secondary interactions are observed with the counter-ions, PF_6^-, and a neighbouring S atom - the Tl^+ ion is therefore

[m] A reaction is said to be diffusion-controlled if its rate constant is of the order of 10^9 M^{-1} s^{-1}.[53]

classed as formally 8-co-ordinate, however the main inner-sphere co-ordination is to the three S groups of a single [9]aneS_3.[54]

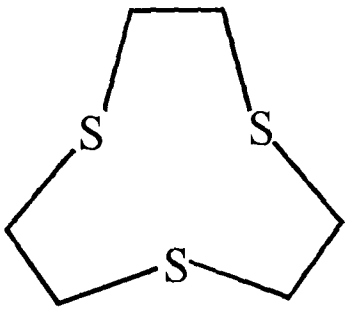

Figure 6.28 [9]aneS_3

The trithia crown 1,4,7-trithiacyclononane

The proposal that Tl^+ only requires the tri-μ_2-sulfido face of the cluster for co-ordination is also supported by the recent work of Zhou *et al* who prepared a Tl^+ adduct of the cuboidal [3Fe-4S] analogue. The pure product $(Et_4N)_2$ $[TlFe_3S_4(LS_3)]$ reveals no additional ligand to the thallium ion.[46] The fast interaction between the [3Fe-4S] cluster and Tl^+ ions for *Pf* Fd implies that in this scenario at least, the [3Fe-4S] cluster is sufficiently exposed to solvent to enable unhindered binding to the cluster.

6.4.2.4 Other Metals Investigated

There are further reports in the literature of incorporation of both Co and Ni into the [3Fe-4S] cluster of *Pf* Fd.[9,11] Formation and investigation of these heterometal clusters was attempted electrochemically with *Pf* Fd.

The Ni incorporation experiment was attempted by both Method 1 (chemical reduction) and Method 2 (electrochemical reduction). Method 2 proved to be unsuccessful even when a protein film was poised at -537 mV for up to 60 minutes. After 60 minutes, apart from the general quality of the film having deteriorated, no changes were observed in the voltammogram i.e. no new couples were seen.[n] Using the methodology as

[n] For the Ni investigation, an oxidative wave at 90 ± 10 mV was observed. However, on more careful inspection, this wave was also observed when there was no protein film on the electrode. This was therefore attributed to a surface wave of the pyrolytic graphite electrode. Unfortunately this region (ca. -50 to + 200 mV) of a graphite electrode is susceptible to surface waves.

described in Method 1 to produce a Ni adduct also resulted in no changes to the voltammetry of the protein. Similar experiments were also carried out for Co with no signs of any Co incorporation being seen.

6.4.3 Metal Ejection

The oxidative stability of each heterometal cluster was investigated using the 'poise and sample' method as previously described (*Section 6.3.7*). From the experiments carried out, it was observed that each of the heterometal adducts had a different lability with respect to oxidation stability. The order of stability to oxidative poising was,

[Fe3Fe-4S] >> [Cd 3Fe-4S] > [Zn3Fe-4S] >> [Tl3Fe-4S]

most stable.....least stable

This potential dependence of metal ion ejection provides strong evidence for the release of Fe, Zn and Cd via the 'superoxidised' level, equivalent to the oxidised HiPIP protein i.e. $[M3Fe\text{-}4S]^{3+}$. This is illustrated in Figure 6.26 via the pathway 8 → 4. All of the threshold potentials (apart from Tl^{+}) are well above that required to promote metal release from $[M3Fe\text{-}4S]^{2+/1+}$ by trapping the product as $[3Fe\text{-}4S]^{1+}$, i.e. utilizing the pathway 5 → 1. Furthermore, the Fe, Zn and Cd adducts show different threshold potentials, with Fe requiring the most forcing conditions. However, in none of the cases examined, was a discrete signal observed at higher potential, which could be attributable to a reversible redox couple, $[M3Fe\text{-}4S]^{3+/2+}$. In contrast, for *Da* Fd III rapid metal ion ejection from [M3Fe-4S] is induced merely by applying a potential at which the [3Fe-4S] product is trapped in the 1+ level, thus identifying pathway 5 → 1 as a viable route.[20]

Other examples can be found in the literature describing evidence for the superoxidised state $[M3Fe\text{-}4S]^{3+}$ as a precursor for metal ejection from cubane clusters. In a square-wave voltammetric study of aconitase[o] at a PGE electrode, Tong and Feinberg reported a reduction potential of 100 mV (SHE) for the $[4Fe\text{-}4S]^{3+/2+}$ couple, and its subsequent conversion to the $[3Fe\text{-}4S]^{1+}$ form was followed directly by EPR.[55] A similar example is seen for mutants of the HiPIP from *Chromatium vinosum* (*Cv*) in which the conserved

[o]citrate (isocitrate) hydrolase - see *Chapter 1*

aromatic residue phenylalanine 66 is replaced e.g. Phe66Asn, -Cys and -Ser. The 4Fe cluster of each of these *Cv* mutants showed a decrease in stability, compared to the recombinant WT form, when in the oxidised state, $[4Fe\text{-}4S]^{3+}$. The clusters were found to degrade via a transient $[3Fe\text{-}4S]^{1+}$ state, as recorded and characterised by EPR.[56] The instability of the oxidised clusters of the mutants was proposed to originate from an increase in solvent accessibility to the cluster core - a direct result of the phenylalanine being replaced by a more polar residue. This instability was not seen with the hydrophobic mutant Phe66Tyr. Much higher potentials than those required to cause metal ejection in aconitase are needed to cause destruction of [4Fe-4S] clusters in *Clostridium pasteurianum* 8Fe Fd.[57] Model studies also provide evidence that the [4Fe-4S] clusters degrade to [3Fe-4S] via the 3+ level.[58] Roth *et al* concluded that the higher the reduction potential, the more stable the core will be with respect to oxidative degradation; hence a 4Fe to a 3Fe conversion will be less likely to occur. Also, the local environment of the 4Fe cluster will have an influence on the oxidative stability. The more accessible the 4Fe cluster is to water, the more easily it will destabilise and convert into a 3Fe centre. Thus, ferredoxins which have more aliphatic groups surrounding the prosthetic centre than the HiPIP environment, (which includes more aromatic side chains) will be only moderately protected from oxidative degradation.

6.4.4 A Comparison of Reduction Potentials

The metal adducts, [M3Fe-4S] of *Pf* Fd, (where M = Fe, Zn, Co, Ni, Mn, Tl) have been characterised previously using spectroscopy and their reduction potentials recorded using dye-mediated EPR titrations.[11,12] With the exception of the [Fe3Fe-4S] adduct, they had not been previously characterised by direct electrochemistry. The reduction potentials obtained by direct electrochemistry compare well (within 30 mV) to the previously measured values of the reduction potentials (EPR dye-mediated titrations) with the exception of the cadmium adduct (see Table 6.11). As can be seen in Table 6.11 there are now sufficient examples of $[M3Fe\text{-}4S]^{2+/1+}$ cubane clusters in both synthetic and biological systems to compare the order of reduction potentials as a function of the metal ion, M.

Cluster	Reduction Potentials for[M3Fe-4S] *(Arranged in ascending order of reduction potential)*
Pf Fd[#]	Cd < Fe < Zn < Co < Ni, Mn < Tl
Dg Fd II	Cd < Fe < Ni < Co
Da Fd III	Cd < Zn < Fe < Co <Tl < Cu
[§]$[MFe_3S_4(SR)_4]^{2-/3-}$ & [¶]$[(Smes)\ MFe_3S_4(LS_3)]^{2-/3-}$	Fe < Co < Ni
[¶]$[(Ph_3P)MFe_3S_4(LS_3)]^{2-/3-}$	$(Fe)^*$ < Co < Ni < Cu ≤ Ag < Tl

Table 6.11 A comparison of reduction potentials in both protein and synthetic clusters

[#] *The values for Pf Fd are those found using protein film electrochemistry with the exception of $E^{o\prime}$ for [Fe3Fe-4S]. This value was determined by bulk solution voltammetry and is a similar value to that found using EPR titrations.*[11] *The order of $E^{o\prime}$ would be* ***Fe < Cd < Zn < Co < Ni, Mn <Tl****, if the $E^{o\prime}$ obtained using the film method for $[Fe3Fe\text{-}4S]^{2+/1+}$ was used.*

[§] *R = Et, mes (Smes is mesitylenethiolate ($^{1-}$))*

[¶] *LS_3 = 1,3,5-tris((4,6-dimethyl-3-mercaptophenyl)thio)-2,4,6-tris(p-tolythio)benzene($^{3-}$)*

[*] *Fe is tentatively placed in this order of reduction potentials, on the basis of its position in the order* **Fe < Co < Ni**.[46]

It can be seen from Table 6.11 that the order of heterometal cubane reduction potentials in different proteins is difficult to predict, although immediate trends can be found. For the proteins investigated in Table 6.11, the general trend can be written as,

Fe < Co < [3Fe-4S] < Tl

and Cd < Zn

These differences in the order are likely to be due to one or a combination of the following: terminal ligation, local protein charge, protein structure and environmental

considerations. Although there are small variations between the values as determined by different methods i.e. protein electrochemistry and EPR titrations, these are insignificant when the differences between the different metals are examined. A schematic figure of the overall trends of heterometal cluster reduction potentials in proteins is shown in Figure 6.29.

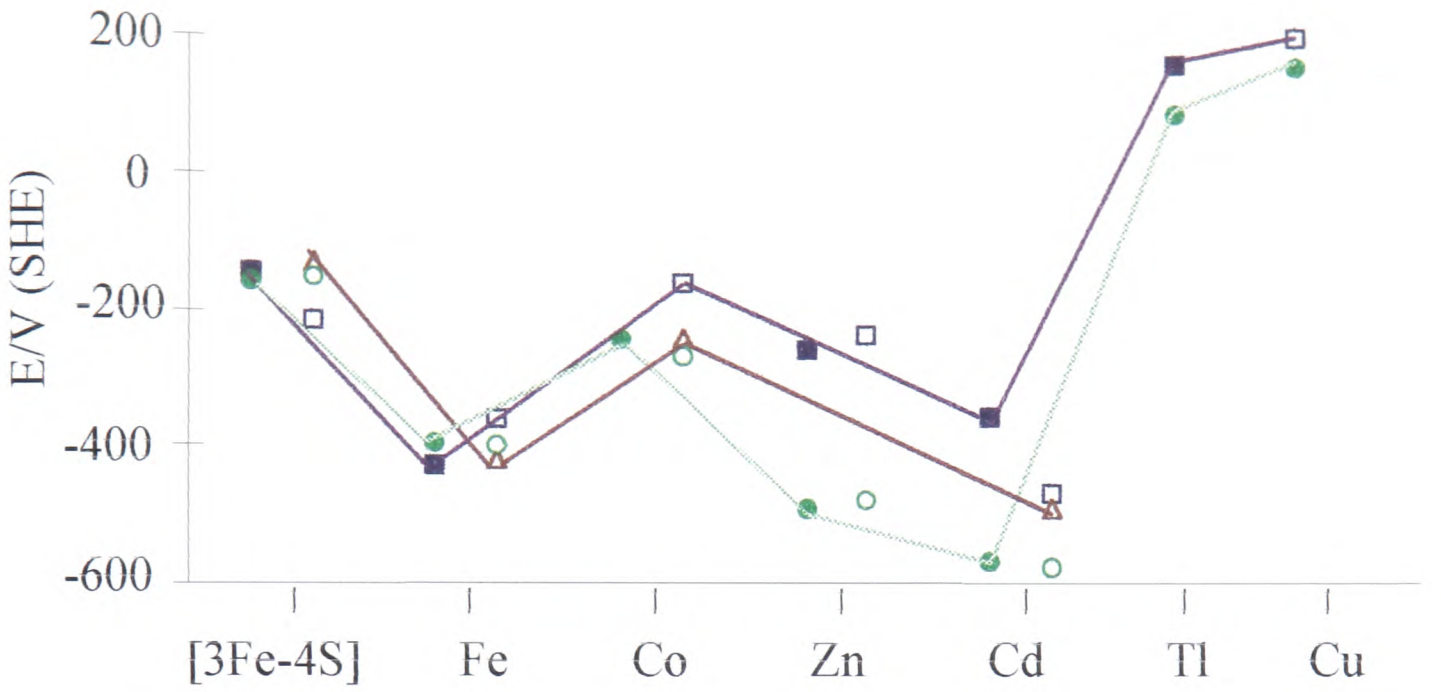

Figure 6.29 Schematic comparison of the reduction potentials of [3Fe-4S] clusters and heterometal adducts of the clusters from *Pf* Fd, *Dg* Fd and *Da* Fd III

Pyrococcus furiosus Fd (—— squares), Desulfovibrio africanus Fd III (—— circles) and Desulfovibrio gigas (—— triangles). Data taken from Butt et al (1997) and Staples et al (1997).[12,20] *Closed symbols displaced to left represent voltammetric values measured for protein films; open symbols displaced to right represent values for bulk solution measurements (voltammetry or EPR monitored potentiometry). In most cases pH 7.0, temperature 0 °C or 25 °C.*

The only major contravention of the similarity between the heterometal cluster potentials, measured with different techniques, is for the Cd adduct. The reduction potential (-470 mV) as determined by Staples *et al*,[12] for the cadmium adduct in bulk solution, using a potentiometric EPR titration, is lower than the value obtained in this study (-359 mV). As described previously, there were variations between the reduction potentials for both the [3Fe-4S] and [Fe3Fe-4S] clusters depending on whether bulk solution or film methods were employed. This is further evidence that binding of M^{2+} involves specific conformational changes and this is likely to result in variations in the energy of protein binding to the electrode. Unfortunately a direct comparison of the bulk and protein bound reduction potentials of the Cd adduct was not possible, due to the interference from excess Cd^{2+}, required to form the cluster in solution.

As we have seen, the reduction potential of a cubane, [M3Fe-4S], depends critically upon which heterometal (M) is incorporated into the cluster. If a biological system depends on this reduction potential of the cubane cluster, it is important that the correct metal is incorporated into the 3Fe core. If extraneous metals are present in the cell, it therefore becomes very important that these are *not* added to the 3Fe core, so conferring the incorrect reduction potential upon the cluster. This selection process could be carried out in either of three ways:

1. The cluster is not able to incorporate the foreign metal for structural reasons, e.g. the [3Fe-4S] cluster in *Av* Fd I, is not surrounded by a typical motif for binding a cubane cluster and so addition of Fe or any other M does not result in a formed cubane cluster.

2. Alternatively, any 'incorrect' heterometal cluster which forms, has only a limited stability, when compared to the 'correct' cubane. For example, the stability of the [Fe3Fe-4S] cluster in *Pf* Fd when subjected to oxidative degradation, is much greater than the stability of the more labile [Cd3Fe-4S] or [Zn3Fe-4S] clusters.

3. Other metal ions are controlled by the cell (homeostasis) and do not become available.

6.4.5 Disulfide Bridge Considerations

In *Chapter 1*, a typical 8Fe Fd was described with eight cysteine residues co-ordinating the two 4Fe clusters - cluster 1 and cluster 2. The binding of the cluster (designated cluster 1) which is common to both one and two-cluster Fds is the sequence Cys^1-X_2-Cys^2-X_2-Cys^3-X_n-Cys^4, where Cys^{1-3} are near the N-terminus and Cys^4 is close to the C-terminus.[59] The two-cluster containing Fds possess an additional four cysteines for the second cluster (designated cluster 2) and the ligating pattern is identical, but with three cysteines near the C-terminus. The single cluster ferredoxins have been proposed to evolve from these two-cluster proteins, by the mutation of two or more of the cysteines in the consensus sequence for the second cluster.[59] The prototypical examples, both of which have been characterised by X-ray crystallography, are the 4Fe Fd from *Bacillus thermoproteolyticus*, *Bt*, for which all four cysteines in the second cluster have been replaced[60] and the 3Fe Fd from *Desulfovibrio gigas*, *Dg*, which lacks two cysteines of the cluster sequence required for the second cluster.[21] In these proteins, an α-helix was found in the environment of the deleted second cluster and it has been proposed that such an α-helix will be present in all one-cluster bacterial ferredoxins.[60] Solution ^1H NMR studies of several such one-cluster ferredoxins support this hypothesis.[61,62]

In the Fd II from *Dg*, the two cysteines that remain from the consensus sequence of the second cluster form a disulfide bridge, as revealed in the crystal structure of the oxidised 3Fe form of this protein and also from ^1H NMR/Mössbauer spectroscopic studies.[21,63] This observation was first viewed with scepticism since disulfide bridges are rarely found in intracellular proteins. However, since the discovery that there is also a disulfide bridge in *Pf* Fd which can undergo redox reactions,[33] the disulfide bridge must be considered as an alternate or additional redox site. This site is thus capable of electron transfer and is likely to have an influence upon the redox cycle of single cluster ferredoxins.

Experimentally, no differences for *Pf* Fd were found between the disulfide bridge oxidised or reduced forms (for both 3Fe and 4Fe) in any of the reactions investigated (*Section 6.3*). Similarly Gorst *et al* reported that the cluster's reduction potential was not significantly perturbed by the different redox states of the disulfide bridge.[33] Indeed, no signs were ever seen of an additional reduction couple in the voltammetry of *Pf* Fd

(over a wide range of experimental conditions) which may have been signatory of a disulfide bridge reduction/oxidation reaction. The only occasion where a difference was observed between the disulfide bridge oxidised and reduced forms of *Pf* Fd, was the bulk electrochemical reduction and addition of Fe^{2+} (using Method 3). The 3Fe Fd_A was found to readily react with Fe^{2+} in solution and 100 % conversion to the 4Fe Fd_A was subsequently observed. However the 3Fe Fd_B form was found not to react immediately with the Fe^{2+} and only 50 % conversion to the 4Fe Fd_B form was observed but this was only after leaving the protein solution in contact with Fe^{2+} for 24 hours (*Section 6.3.5.1*).

It is difficult to explain the differences in the rate of Fe uptake between Fd_A and Fd_B when the sample was electrochemically reduced in bulk. Attempts to investigate this difference in reactivity with another metal ion, Zn^{2+}, were unsuccessful (*Section 6.3.5.1*). The reluctance of the Fd_B form to take up Fe^{2+} may be linked to the generally slow reaction of Fe^{2+} uptake when the protein was present as a film on the electrode. The faster reaction of the 3Fe Fd_A to insert Fe^{2+}, after bulk reduction, may be due to the oxidised disulfide bridge being able to hold the protein in an 'optimum' confirmation for Fe^{2+} uptake. The 3Fe Fd_B form of the protein is likely to be more flexible than the 3Fe Fd_A form, and therefore, although Fe uptake still occurs at a much slower rate, it is not optimal. However, the latter reasoning does *not* explain why the apparent rates of Fe uptake are identical for both 3Fe Fd_A and 3Fe Fd_B, when the protein is in solution and reduced with sodium dithionite and the reaction is observed spectrophotometrically (*Section 6.3.6*). In conclusion, when looking at the total picture of *Pf* Fd reactivity, the one and only difference between the disulfide bridge oxidised and reduced forms of the protein (bulk reduction and subsequent Fe^{2+} uptake) is more than likely to be an artefact of the experiment than a real difference between the two forms, because of the contradictory evidence from the film and spectrophotometric experiments.

6.5 SUMMARY

Pf Fd is an excellent protein to study the complex reactions of reactive [3Fe-4S] clusters without the spectral complications of a second [4Fe-4S] cluster, which is present in the class of 7Fe Fds. It has been demonstrated that the behaviour of the single [3Fe-4S] cluster is similar, in terms of proton binding ability and metal binding affinity, to previously studied [3Fe-4S] clusters from other 7Fe Fds. However, the biological use for these functions, (if any) have not yet been fully identified.

Protonation of the one-electron reduced cluster $[3Fe\text{-}4S]^{1+}$ is observed, and produces a form which is spectroscopically similar to other reduced [3Fe-4S] clusters from other proteins. More importantly it has been shown that the hyper-reduced state, $[3Fe\text{-}4S]^{2-}$, is also generated in *Pf* Fd, together with the overall uptake of three protons, as has been observed in several other [3Fe-4S] cluster containing proteins. Metal uptake experiments have shown that although rates of exchange for the M^{2+} ions are slower in *Pf* Fd than for *Da* Fd III, the rates of uptake for Tl^{+} are comparable. Tl^{+} uptake is therefore determined to be dependent only on the core cluster structure and not on the protein structure, unlike M^{2+} uptake. It has been postulated that rapid Tl^{+} interchange might therefore provide a diagnostic test for [3Fe-4S] clusters which are able to present a solvent-exposed face. Metal uptake experiments showed a distinct dependence upon the external environment (free solution *versus* bound to electrode surface) but not to the presence or absence of the disulfide bridge. Ejection of M^{2+} is slow and is greatly accelerated at oxidising potentials - well in excess of that required to trap the $[3Fe\text{-}4S]^{1+}$ product, thereby revealing the participation of a labile super-oxidised state, most likely $[M3Fe\text{-}4S]^{3+}$.

6.6 REFERENCES

1) Fiala, G.; Stetter, K. O. *Archives of Microbiology* **1986**, *145*, 56-61.

2) Aono, S.; Bryant, F. O.; Adams, M. W. W. *Journal of Bacteriology* **1989**, *171*, 3433-3439.

3) Conover, R. C.; Kowal, A. T.; Fu, W.; Park, J. B.; Aono, S.; Adams, M. W. W.; Johnson, M. K. *Journal of Biological Chemistry* **1990**, *265*, 8533-8541.

4) Blamey, J. M.; Adams, M. W. W. *Biochimica Et Biophysica Acta* **1993**, *1161*, 19-27.

5) Mukund, S.; Adams, M. W. W. *Journal of Biological Chemistry* **1990**, *265*, 11508-11516.

6) Ma, K.; Adams, M. W. W. *Journal of Bacteriology* **1994**, *176*, 6509-6517.

7) Ma, K.; Zhou, Z. H.; Adams, M. W. W. *FEMS Microbiol.Lett.* **1994**, *122*, 263-266.

8) Conover, R. C.; Park, J. B.; Adams, M. W. W.; Johnson, M. K. *Journal of the American Chemical Society* **1990**, *112*, 4562-4564.

9) Srivastava, K. K. P.; Surerus, K. K.; Conover, R. C.; Johnson, M. K.; Park, J. B.; Adams, M. W. W.; Munck, E. *Inorganic Chemistry* **1993**, *32*, 927-936.

10) Fu, W. G.; Telser, J.; Hoffman, B. M.; Smith, E. T.; Adams, M. W. W.; Finnegan, M. G.; Conover, R. C.; Johnson, M. K. *Journal of the American Chemical Society* **1994**, *116*, 5722-5729.

11) Finnegan, M. G.; Conover, R. C.; Park, J. B.; Zhou, Z. H.; Adams, M. W. W.; Johnson, M. K. *Inorganic Chemistry* **1995**, *34*, 5358-5369.

12) Staples, C. R.; Dhawan, I. K.; Finnegan, M. G.; Dwinell, D. A.; Zhou, Z. H.; Huang, H. S.; Verhagen, M.; Adams, M. W. W.; Johnson, M. K. *Inorganic Chemistry* **1997**, *36*, 5740-5749.

13) Gorst, C. M.; Yeh, Y. H.; Teng, Q.; Calzolai, L.; Zhou, Z. H.; Adams, M. W. W.; Lamar, G. N. *Biochemistry* **1995**, *34*, 600-610.

14) Calzolai, L.; Gorst, C. M.; Zhao, Z. H.; Teng, Q.; Adams, M. W. W.; Lamar, G. N. *Biochemistry* **1995**, *34*, 11373-11384.

15) Calzolai, L.; Zhou, Z. H.; Adams, M. W. W.; Lamar, G. N. *Journal of the American Chemical Society* **1996**, *118*, 2513-2514.

16) George, S. J.; Armstrong, F. A.; Hatchikian, E. C.; Thomson, A. J. *Biochemical Journal* **1989**, *264*, 275-284.

17) Butt, J. N.; Armstrong, F. A.; Breton, J.; George, S. J.; Thomson, A. J.; Hatchikian, E. C. *Journal of the American Chemical Society* **1991**, *113*, 6663-6670.

18) Butt, J. N.; Sucheta, A.; Armstrong, F. A.; Breton, J.; Thomson, A. J.; Hatchikian, E. C. *Journal of the American Chemical Society* **1991**, *113*, 8948-8950.

19) Butt, J. N.; Niles, J.; Armstrong, F. A.; Breton, J.; Thomson, A. J. *Nature Structural Biology* **1994**, *1*, 427-433.

20) Butt, J. N.; Fawcett, S. E. J.; Breton, J.; Thomson, A. J.; Armstrong, F. A. *Journal of the American Chemical Society* **1997**, *119*, 9729-9737.

21) Kissinger, C. R.; Sieker, L. C.; Adman, E. T.; Jensen, L. H. *Journal of Molecular Biology* **1991**, *219*, 693-715.

22) Moura, J. J. G.; Moura, I.; Kent, T. A.; Lipscomb, J. D.; Huynh, B. H.; Legall, J.; Xavier, A. V.; Munck, E. *Journal of Biological Chemistry* **1982**, *257*, 6259-6267.

23) Moura, I.; Moura, J. J. G.; Munck, E.; Papaefthymiou, V.; Legall, J. *Journal of the American Chemical Society* **1986**, *108*, 349-351.

24) Surerus, K. K.; Munck, E.; Moura, I.; Moura, J. J. G.; Legall, J. *Journal of the American Chemical Society* **1987**, *109*, 3805-3807.

25) Moreno, C.; Macedo, A. L.; Moura, I.; Legall, J.; Moura, J. J. G. *Journal of Inorganic Biochemistry* **1994**, *53*, 219-234.

26) Duff, J. L. C. *Ph. D. Thesis*; University of Oxford, **1996.**

27) Busch, J. L. H.; Breton, J. L.; Bartlett, B. M.; Armstrong, F. A.; James, R.; Thomson, A. J. *Biochemical Journal* **1997**, *323*, 95-102.

28) Butt, J. N.; Sucheta, A.; Armstrong, F. A.; Breton, J.; Thomson, A. J.; Hatchikian, E. C. *Journal of the American Chemical Society* **1993**, *115*, 1413-1421.

29) Conover, R. C.; Park, J. B.; Adams, M. W. W.; Johnson, M. K. *Journal of the American Chemical Society* **1991**, *113*, 2799-2800.

30) Telser, J.; Smith, E. T.; Adams, M. W. W.; Conover, R. C.; Johnson, M. K.; Hoffman, B. M. *Journal of the American Chemical Society* **1995**, *117*, 5133-5140.

31) Armstrong, F. A.; George, S. J.; Cammack, R.; Hatchikian, E. C.; Thomson, A. J. *Biochemical Journal* **1989**, *264*, 265-273.

32) Zhou, Z. H.; Adams, M. W. W. *Biochemistry* **1997**, *36*, 10892-10900.

33) Gorst, C. M.; Zhou, Z. H.; Ma, K. S.; Teng, Q.; Howard, J. B.; Adams, M. W. W.; Lamar, G. N. *Biochemistry* **1995**, *34*, 8788-8795.

34) Breton, J. L.; Duff, J. L. C.; Butt, J. N.; Armstrong, F. A.; George, S. J.; Petillot, Y.; Forest, E.; Schafer, G.; Thomson, A. J. *European Journal of Biochemistry* **1995**, *233*, 937-946.

35) Duff, J. L. C.; Breton, J. L. J.; Butt, J. N.; Armstrong, F. A.; Thomson, A. J. *Journal of the American Chemical Society* **1996**, *118*, 8593-8603.

36) Brereton, P. S.; Verhagen, M.; Zhou, Z. H.; Adams, M. W. W. *Biochemistry* **1998**, *37*, 7351-7362.

37) Riddles, P. W.; Blakeley, R. L.; Zerner, B. *Methods in Enzymology* **1983**, *91*, 49-60.

38) Smith, E. T.; Blamey, J. M.; Zhou, Z. H.; Adams, M. W. W. *Biochemistry* **1995**, *34*, 7161-7169.

39) Thomson, A. J.; Robinson, A. E.; Johnson, M. K.; Moura, J. J. G.; Moura, I.; Xavier, A. V.; Legall, J. *Biochimica Et Biophysica Acta* **1981**, *670*, 93-100.

40) George, S. J.; Richards, A. J. M.; Thomson, A. J.; Yates, M. G. *Biochem. J.* **1984**, 247-251.

41) Armstrong, F. A.; George, S. J.; Thomson, A. J.; Yates, M. G. *Febs Letters* **1988**, *234*, 107-110.

42) Johnson, M. K.; Bennett, D. E.; Fee, J. A.; Sweeney, W. V. *Biochim. Biophys. Acta.* **1987**, 81-94.

43) Armstrong, F. A. *Bioelectrochemistry of Biomacromolecules*; Birkhauser: Basel, **1997**; Vol. 5.

44) Armstrong, F. A.; Heering, H. A.; Hirst, J. *Chemical Society Reviews* **1997**, *26*, 169-179.

45) Butt, J. N. *Ph.D. Thesis* University of California, Irvine, **1993**.

46) Zhou, J.; Raebiger, J. W.; Crawford, C. A.; Holm, R. H. *Journal of the American Chemical Society* **1997**, *119*, 6242-6250.

47) Wilkins, R. G. *Kinetics and Mechanisms of Reactions of Transition Metal Complexes*; VCH: Weinheim, 1991, 2nd Edition.

48) Armstrong, F. A.; Butt, J. N.; George, S. J.; Hatchikian, E. C.; Thomson, A. J. *Febs Letters* **1989**, *259*, 15-18.

49) Hirst, J.; Jameson, G. N. L.; Allen, J. W. A.; Armstrong, F. A. *JACS* **1998**, *Submitted.*

50) Shen, B. H.; Martin, L. L.; Butt, J. N.; Armstrong, F. A.; Stout, C. D.; Jensen, G. M.; Stephens, P. J.; Lamar, G. N.; Gorst, C. M.; Burgess, B. K. *Journal of Biological Chemistry* **1993**, *268*, 25928-25939.

51) Hu, Z.; Jollie, D.; Burgess, B. K.; Stephens, P. J.; Münck, E. *Biochemistry* **1994**, 14475-14485.

52) Fersht, A. *Enzyme Structure and Mechanism*; W.H. Freeman: New York, **1985**, 2nd Edition.

53) Atkins, P. W. *Physical Chemistry*; Oxford University Press: Oxford, **1993**, 4th Edition.

54) Blake, A. J.; Greig, J. A.; Schroeder, M. *J. Chem. Soc., Dalton Trans.* **1991**, 529-532.

55) Tong, J. J.; Feinberg, B. A. *Journal of Biological Chemistry* **1994**, *269*, 24920-24927.

56) Bian, S.; Hemann, C. F.; Hille, R.; Cowan, J. A. *Biochemistry* **1996**, *35*, 14544-14552.

57) Armstrong, F. A.; Hill, H. A. O.; Walton, N. J. *Febs Letters* **1982**, *150*, 214-218.

58) Roth, E. K. H.; Jordanov, J. *Inorganic Chemistry* **1992**, *31*, 240-243.

59) Beinert, H. *Faseb Journal* **1990**, *4*, 2483-2491.

60) Fukuyama, K.; Nagahara, Y.; Tsukihara, T.; Katsube, Y.; Hase, T.; Matsubara, H. *J. Mol. Biol.* **1988**, 183-193.

61) Marion, D.; Guerlesquin, F. *Biochemical and Biophysical Research Communications* **1989**, *159*, 592-598.

62) Teng, Q.; Zhou, Z. H.; Smith, E. T.; Busse, S. C.; Howard, J. B.; Adams, M. W. W.; Lamar, G. N. *Biochemistry* **1994**, *33*, 6316-6326.

63) Macedo, A. L.; Moura, I.; Surerus, K. K.; Papaefthymiou, V.; Liu, M. Y.; Legall, J.; Munck, E.; Moura, J. J. G. *Journal of Biological Chemistry* **1994**, *269*, 8052-8058.

APPENDIX A

Redox-coupled proton transfer

Calculation of the pH dependence of reduction potentials

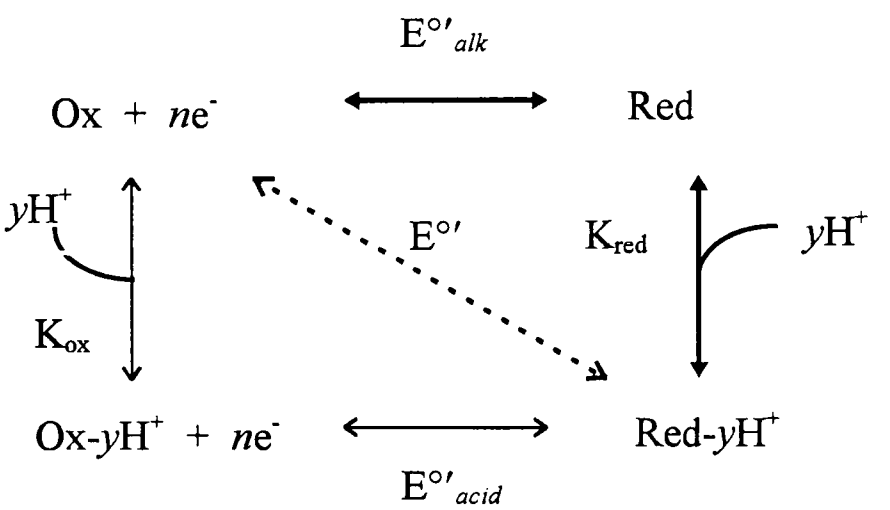

(K_{ox} and K_{red} are the equilibrium dissociation constants for proton binding to the reduced oxidised and reduced species respectively; $E^{\circ\prime}_{alk}$ and $E^{\circ\prime}_{acid}$ are the reduction potentials in the limit of high and low pH)

The potential at any point E, is given by the Nernst Equation relative to the reduction potential E°′:

$$E = E^{\circ} + \frac{RT}{nF} \ln\left(\frac{[\text{Total Oxidised Species}]}{[\text{Total Reduced Species}]}\right)$$

$$= E^{\circ} + \frac{RT}{nF} \ln\left(\frac{[Ox - yH^{+}] + [Ox]}{[Red - yH^{+}] + [Red]}\right)$$

By definition,

$$K_{red} = \frac{[Red][H^{+}]^{y}}{[Red - yH^{+}]} \qquad K_{ox} = \frac{[Ox][H^{+}]^{y}}{[Ox - yH^{+}]} \qquad (1)$$

Substituting for [Ox] and [Red] from (1) into the Nernst equation:

$$E = E^\circ + \frac{RT}{nF} \ln\left(\frac{[Ox - yH^+] + \frac{K_{ox}}{[H^+]^y}[Ox - yH^+]}{[Red - yH^+] + \frac{K_{red}}{[H^+]^y}[Red - yH^+]} \right)$$

$$= E^\circ + \frac{RT}{nF} \ln\left(\frac{[Ox - yH^+]}{[Red - yH^+]} \right) + RT \left(\frac{1 + \frac{K_{ox}}{[H^+]^y}}{1 + \frac{K_{red}}{[H^+]^y}} \right) \qquad (2)$$

Define $E = E^{\circ\prime}_{acid}$, at pH values low enough to protonate both [Red] and [Ox], *i.e.* pH « pK_{red} and pK_{ox}; or $[H^+] \gg K_{red}$ and K_{ox} then,

$$E^\circ_{acid} = E^\circ + \frac{RT}{nF} \ln\left(\frac{[Ox - yH^+]}{[Red - yH^+]} \right)$$

Substitute for E° in (2),

$$E^\circ = E^\circ_{acid} + \frac{RT}{nF} \ln\left(\frac{[H^+]^y + K_{red}}{[H^+]^y + K_{ox}} \right)$$

An alternative method involves substituting for $[Ox\text{-}yH^+]$ and $[Red\text{-}yH^+]$ from equation (1) into the Nernst equation, and in the limit of high pH, $E = E^\circ_{alk}$ and

$$E^\circ = E^\circ_{alk} + \frac{RT}{nF} \ln\left(\frac{1 + {[H^+]^y}/{K_{red}}}{1 + {[H^+]^y}/{K_{ox}}} \right)$$